PHYSICS
OF
THIN
FILMS

5
1969

PHYSICS OF
THIN FILMS

Advances in Research and Development

Edited by GEORG HASS
and
RUDOLF E. THUN

VOLUME 5 · 1969

ACADEMIC PRESS
New York and London

Physics of Thin Films

Advances in Research and Development

VOLUME 5

CONTRIBUTORS TO THIS VOLUME

Physics of Thin Films

Advances in Research and Development

Edited by

GEORG HASS

Night Vision Laboratory
U. S. Army Electronics Command
Fort Belvoir, Virginia

and

RUDOLF E. THUN

Raytheon Company
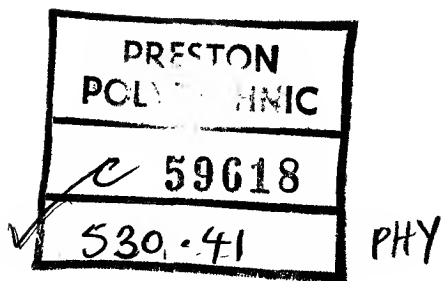*Missile Systems Division*
Bedford, Massachusetts

VOLUME 5

1969

ACADEMIC PRESS
NEW YORK AND LONDON

Contributors to Volume 5

Numbers in parentheses indicate the pages on which the authors' contributions begin.

K. DEUTSCHER (*1*), Ernst Leitz Optical Works, Wetzlar, Germany

W. M. FEIST (*237*). Research Division, Raytheon Company, Waltham, Massachusetts

M. H. FRANCOMBE (*143*), Westinghouse Research Laboratories, Pittsburgh, Pennsylvania

K. HIRSCHBERG (*1*), Ernst Leitz Optical Works, Wetzlar, Germany

J. E. JOHNSON (*143*), Westinghouse Research Laboratories, Pittsburgh, Pennsylvania

D. KOSSEL (*1*), Ernst Leitz Optical Works, Wetzlar, Germany

D. W. READEY (*237*), Research Division, Raytheon Company, Waltham, Massachusetts

H. SCHROEDER (*87*), Jenaer Glaswerk Schott & Genossen, Mainz, West Germany

S. R. STEELE (*237*), Research Division, Raytheon Company, Waltham, Massachusetts

ALFRED THELEN (*47*), Optical Coating Laboratory, Inc., Santa Rosa, California

Preface

Like the previous volumes of this serial publication, Volume 5 follows essentially the originally outlined purpose to publish comprehensive survey articles dealing with fundamental and applied research on the preparation, properties, and applications of thin films. A few years ago, vacuum deposition techniques such as evaporation and sputtering were the dominating deposition techniques. Today, new film preparation methods using predominantly chemical processes are gaining in importance and are described and discussed in various chapters of this volume.

The first article by D. Kossel, K. Deutscher, and K. Hirschberg on interference photocathodes shows that the efficiency of photoemissive materials can be increased by interference effects which improve the energy transfer from photons to electrons. This article should be of special interest to those concerned with photoemissive devices.

The article by A. Thelen describes the design of a variety of multilayer interference filters which are now widely used in the field of optics.

H. Schroeder reports on his experience of producing oxide layers from organic solutions and describes the use of such films as optical coatings and protective layers. This is followed by an extensive article by M. H. Francombe and J. E. Johnson which provides a status report on recent and current developments in the field of semiconductor films.

Volume 5 is completed by an article concerned with the preparation of films by chemical vapor deposition. In this chapter, W. M. Feist, S. R. Steele, and D. W. Readey discuss the chemical processes used in vapor deposition and give examples and applications of semiconductor, dielectric, and metallic films prepared by this technique.

M. H. Francombe and R. W. Hoffman, who have made important contributions to the field of thin films, will be guest editors for the next two volumes.

GEORG HASS

August 1969   RUDOLF E. THUN

vii

Contents

Interference Photocathodes

D. Kossel, K. Deutscher, and K. Hirschberg

Design of Multilayer Interference Filters

Alfred Thelen

Oxide Layers Deposited from Organic Solutions

H. Schroeder

The Preparation and Properties of Semiconductor Films

M. H. Francombe and J. E. Johnson

The Preparation of Films by Chemical Vapor Desposition

W. M. Feist, S. R. Steele, and D. W. Readey

Contents of Previous Volumes

Articles Planned for Future Volumes

Amorphous Films
A. K. Jonscher

Formation of Unsupported Films
E. H. Kobisk

Size Dependent Electrical Conduction in Thin Metal Films and Wires
Donald C. Larson

Thin Films in Transistor and Monolithic Circuit Technology
Arthur E. Lessor, Reinhard Glang, and Rudolf E. Thun

Electron Elastic and Inelastic Scattering Studies of Film Surfaces
T. N. Rhodin

Interactions in Multilayered Magnetic Films
Arthur Yelon

Recent Developments in Anodic Oxide Films
L. Young and D. L. Pulfrey

Physics of Thin Films

Advances in Research and Development

VOLUME 5

Interference Photocathodes

D. Kossel, K. Deutscher, and K. Hirschberg

Ernst Leitz Optical Works
Wetzlar, Germany

I. Introduction

Every photon hitting a photocathode should knock out an electron. To meet this requirement for highly sensitive photoemissive materials the object of most investigations (*1–4*) is to:

1. decrease the work function of the materials,
2. improve the energy transfer from photon to electron.

The optical aspect that only a part of the light enters the film, is absorbed, and excites electrons in a place suitable for their emission, however, has thus far attached little attention (*5–8*). Suppose 100 photons are falling onto an opaque semiconductor cathode. In the example of Fig. 1, 28 photons are reflected
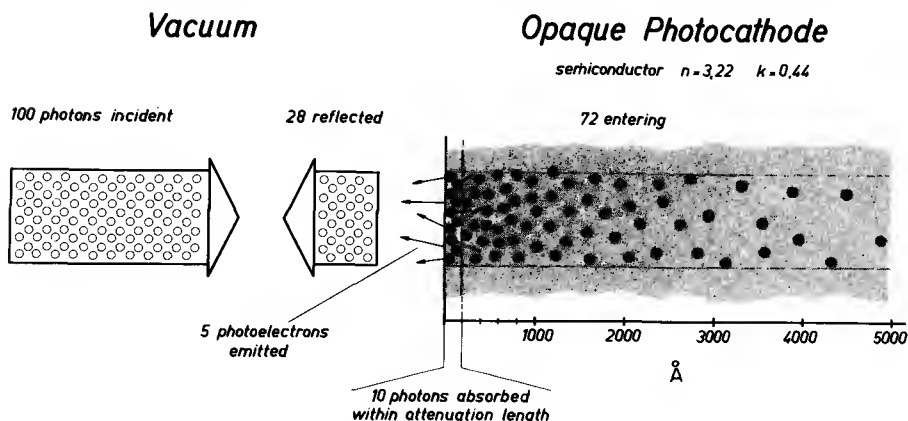
FIG. 1. Photon and photoelectron balance of a semiconductor cathode (Cs_3Sb).

according to Fresnel's equation and are therefore lost for the photoeffect; 72 photons penetrate into the material and are absorbed according to an exponential law. Because the absorption coefficient is small the medium range of the light is about 100 nm. The attenuation length of the photoelectrons— the greatest depth from which electrons can escape—for the semiconducting material cesium–antimony is about 15 nm (9–11); therefore only 10 light quanta are absorbed within the emission depth.

Assuming an isotropic starting and scattering distribution of the excited electrons only five of them can escape into the vacuum. This small yield of a semiconductor photocathode cannot be improved by using a metal cathode, such as sodium. The high absorption coefficient ($k = 55$) reduces the penetration depth of the light in Na to only 10 Å so that the penetrating light quanta are absorbed directly under the surface, but the high reflectance allows only 3 photons to enter the metal.

The optimum cathode has to comply with two requirements:

1. Photons should enter the cathode without reflection losses.

2. Photons should be completely absorbed at a depth equal to the attenuation length of the electrons.

These tasks may be treated by formulating the requirements in another way: incident light waves should be completely absorbed within the special receiver, the thin photoemissive film.

To induce a receiver to maximum absorption is a standard problem of physics. It is always solved in the same way: The receiver is adapted to the incident waves and tuned to given frequencies. Thin films capable of interference are light resonators. Properly tuned and adapted resonators are capable of maximum absorption, and if they are photosensitive they have a maximum electron output. If the films are too thin for interference effects they can be used as integrating elements in light resonators (12).

II. Light Waves and Resonators

At the boundary of two media with different refractive indices (n_0, n_1) part of the incident light is reflected. The amplitude r_1 of the reflected wave is given by Fresnel's equation, $r_1 = (n_1 - n_0)/(n_1 + n_0)$. The mean square of the resulting electric field vector E at the point z in front of the boundary is given by

$$\bar{E}^2(z) = 1 + r_1{}^2 - 2r_1 \cos[(4\pi n_0/\lambda)z] \qquad (1)$$

whereby the mean square of the amplitude of the incident wave is set equal to 1. Figure 2a shows the nodes and loops of the standing wave in front of the boundary. Since the reflectance of the surface is not equal to 1, the
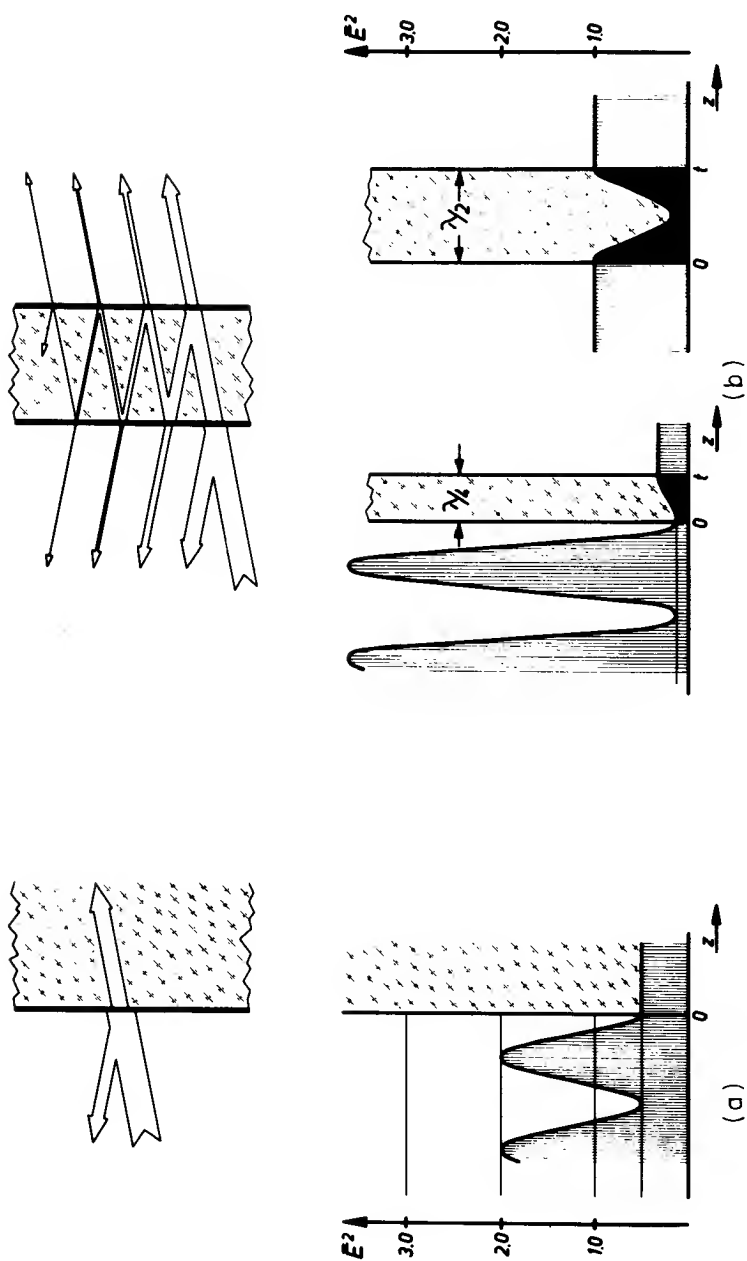
Fig. 2. (a) Wave field in front of a boundary between two different dielectric media. (b) Wave fields in and in front of thin dielectric films of different thickness ($t = \lambda/4$ = dissonance, $t = \lambda/2$ = resonance).

standing wave is superposed on a traveling one, which flows with a constant $\bar{E}^2$ into the second medium.

If light falls onto a dielectric film, the wave field changes completely, because the waves reflected at both boundaries superpose (Fig. 2b). The reflectance and the phase shift for reflection of the film towards the medium with the index n_0 are given by the well-known formulas, which are already generalized to absorbing films:

$$R \equiv r_{12}^2 = \frac{r_1^2 + r_2^2 \beta^{2t_1} + 2r_1 r_2 \beta^{t_1} \cos[(4\pi n_1/\lambda)t_1 + \Delta_1 - \Delta_2]}{1 + r_1^2 r_2^2 \beta^{2t_1} + 2r_1 r_2 \beta^{t_1} \cos[(4\pi n_1/\lambda)t_1 - \Delta_1 - \Delta_2]} \tag{2}$$

$$\Delta_{12} = \arctan \frac{(1 - r_2^2 \beta^{2t_1})r_1 \sin \Delta_1 + (1 - r_1^2)r_2 \beta^{t_1} \sin[\Delta_2 - (4\pi n_1/\lambda)t_1]}{(1 + r_2^2 \beta^{2t_1})r_1 \cos \Delta_1 + (1 + r_1^2)r_2 \beta^{t_1} \cos[\Delta_2 - (4\pi n_1/\lambda)t_{13}]} \tag{3}$$

with

$$\mathbf{r}_v = r_v \cdot e^{i\Delta^v} \qquad \text{Fresnel coefficients of boundaries,}$$
$$n_1 + iK_1 \qquad \text{complex refractive index of the film,}$$
$$t_1 \qquad \text{thickness of the film,}$$
$$\beta \equiv e^{-4\pi K_1/\lambda} \qquad \text{transmission coefficient,}$$

$$N \equiv 1 + r_1^2 r_2^2 \beta^{2t_1} + 2r_1 r_2 \beta^{t_1} \cos[(4\pi n_1/\lambda)t_1 - \Delta_1 - \Delta_2]$$

The boundary surfaces and the Fresnel coefficients are numbered starting from the vacuum-photoelectric film boundary which is emitting electrons. The mean square of the electric vector at the point z in front of, within, and behind the film is given by

$$\bar{E}^2(z) = 1 + r_{12}^2 + 2r_{12} \cos\left(\frac{4\pi n_0}{\lambda} z - \Delta_{12}\right), \qquad z < 0 \tag{4a}$$

$$= \left[1 + r_2^2 \beta^{2(t_1 - z)} + 2r_2 \beta^{(t_1 - z)} \cos\left(\frac{4\pi n_1}{\lambda}(t_1 - z) - \Delta_2\right)\right]$$

$$\times (1 - r_1^2)\beta^z/N, \qquad 0 < z < t_1 \tag{4b}$$

$$= (1 - r_1^2)(1 - r_2^2)\beta^{t_1}/N, \qquad z > t_1 \tag{4c}$$

First the wave field of a purely dielectric film will be discussed. Figure 3 illustrates the types of fields. With an optical film thickness $n_1 t_1 = \lambda/2$ the partial waves are in phase. They superpose to produce an electromagnetic eigenoscillation within the film. In the case of resonance there is no standing wave in front of the layer. The light penetrates into the film, builds up an oscillation of high amplitude, and is completely emitted.

A $\lambda/4$ film or its odd multiple is in dissonance. There is a big standing
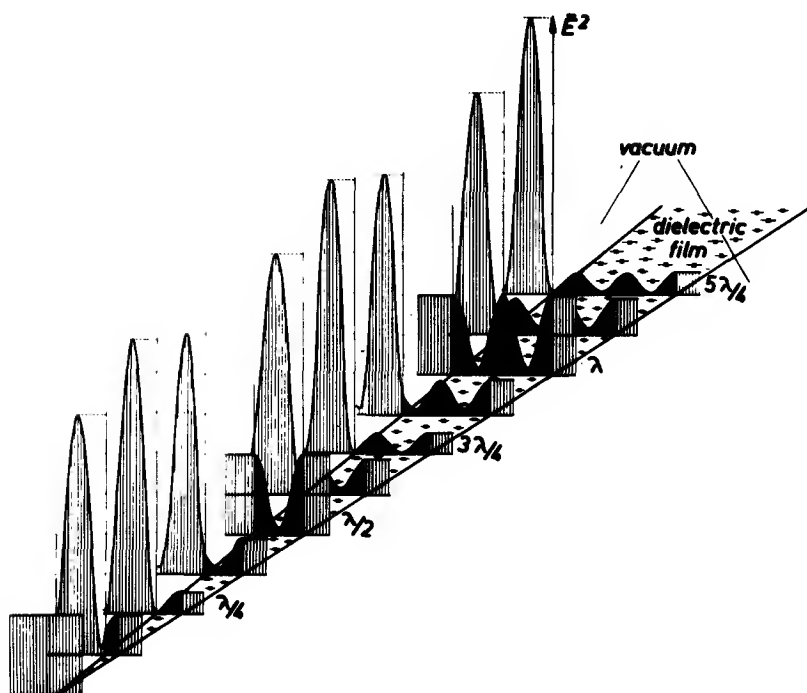
FIG. 3. Wave fields in and in front of a dielectric film versus thickness. The film is unsupported.

wave in front of the layer (high reflectance) and only a forced oscillation of a small amplitude exists in the film.

These considerations can be verified with the waves of a pendulum chain (Fig. 4). An additionally loaded pendulum simulates a partial transmissive boundary surface. In front of the boundary an elastic standing wave is formed independent of the exciting frequency of the incoming wave. In the lower part of Fig. 4 two additionally loaded pendulums simulate the boundaries of a dielectric film. If the resonator is tuned to the elastic wave (2.3 Hz), the amplitude of the resonator is high. The energy of the wave flows completely into the resonator and is emitted in the forward direction. In front of and behind the resonator only traveling waves exist. Outside the resonance condition (2.0 and 2.6 Hz) standing waves are built up in front of the resonator.

Thus far purely dielectric films have been discussed. Since the general description of light resonators was given with regard to improving photocathodes, we have to deal with weakly absorbing layers, too. The results are summarized
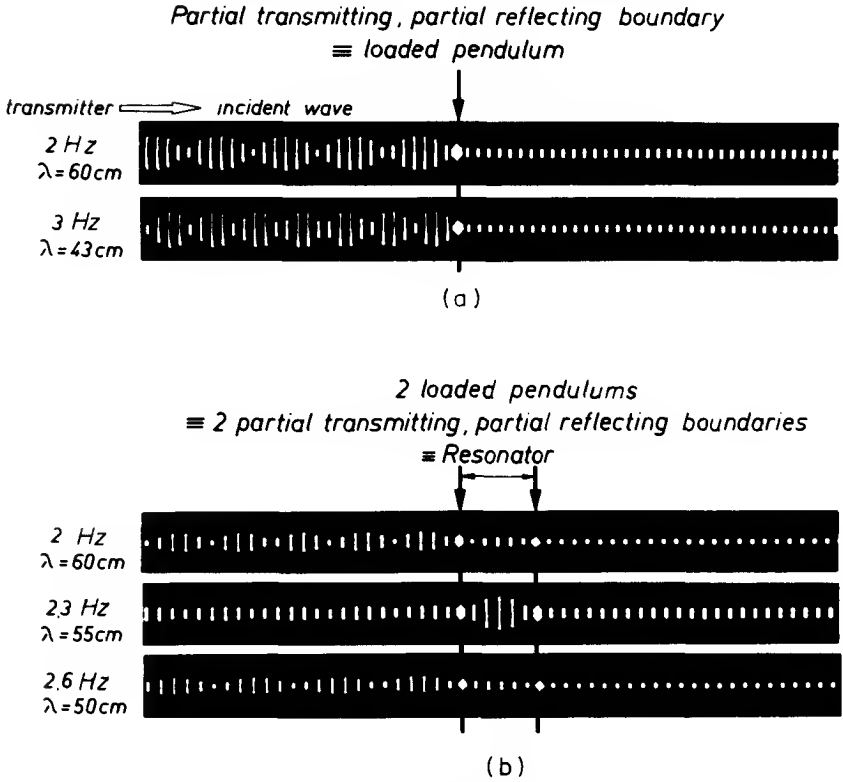
FIG. 4. Oscillations and resonance of a pendulum chain: (a) with one loaded pendulum; (b) with two loaded pendulums.

in Fig. 5. The wave fields are shown in front of, in, and behind a weakly absorbing film as a function of the film thickness t (13). The characteristic properties of the wave fields illustrated in Fig. 3 remain intact.

In contrast to the dielectric film standing waves always exist in front of the absorbing film independent of its thickness. When the thickness of the film is tuned to $\lambda/2$, the amplitude of the reflected wave has a minimum only. The amplitude condition for adaptation of a single film

$$r_1 = \beta^{t_1} \cdot r_2 \tag{5}$$

which is automatically accomplished for a dielectric film embedded into a homogeneous medium is not fulfilled for an absorbing layer.

Owing to the absorption the eigenoscillation in the film is damped; i.e., the numerical values of $\bar{E}^2$ are considerably reduced. The absorption per square
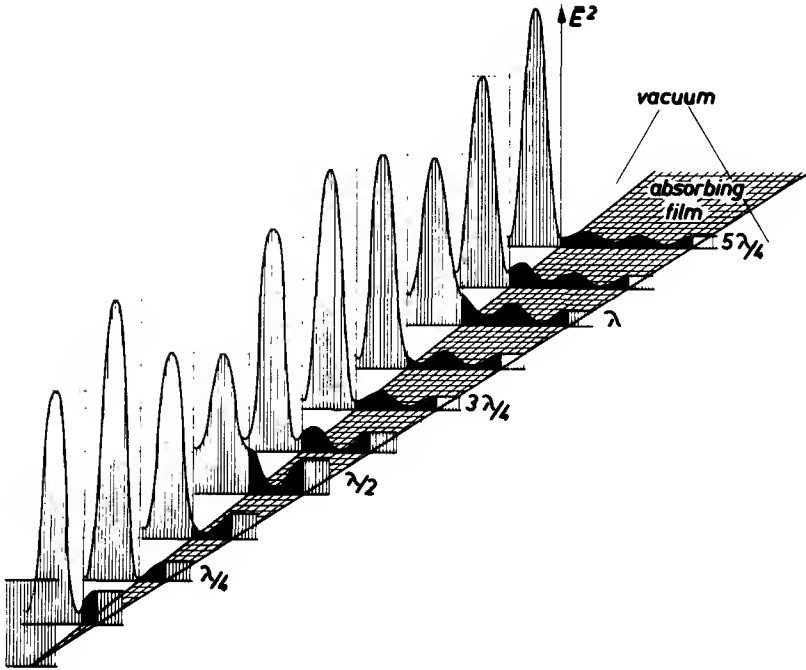
FIG. 5. Wave fields in and in front of an absorbing film versus thickness. The film ($n_1 =$ 3.5, $K_1 = 0.3$) is unsupported.

$A_L(z)$ in a lamella dz at the depth z in the film (ε_0, dielectric constant; v, frequency) is proportional to the square of the electric vector at this point

$$A_L(z) = 4\pi\varepsilon_0 n K v \, \bar{E}^2(z) \tag{6}$$

The total absorption in the film being $A = \int_0^t A_L(z) \, dz$. Instead of the absorbed energy the number of absorbed photons can be calculated which is proportional to that value. Since the excitation of the electrons in a photoemissive layer is proportional to the number of absorbed photons, the function $\bar{E}^2$ versus position z in the film directly represents the production of photoelectrons at each point.

In a $\lambda/2$ photoelectric film most of the electrons are excited in the lamellas at both boundaries, and very few in the middle of the film. Illuminated translucent films of a thickness up to $\lambda/4$ always produce more electrons in the lamellas at the back boundary than at the front boundary. The spatial distribution curve of $\bar{E}^2$ has a loop at the first boundary, as the phase shift for the reflected wave is nearly zero. The incoming and reflected waves interfere constructively. The emitted photocurrent not only depends on the

production rate of photoelectrons but also on the attenuation length of the electrons. This property will be discussed in the next section.

III. The Emission of Photoelectrons

Photoelectrons are emitted from a semiconductor by the absorption of photons with energies greater than the band gap of the photoelectric material and the electron affinity. The number of electrons emitted from a lamella dz at a distance z from the emitting surface is proportional to

1. the local photoelectron production rate, approximately the square of the electrical vector $\bar{E}^2(z)$ and
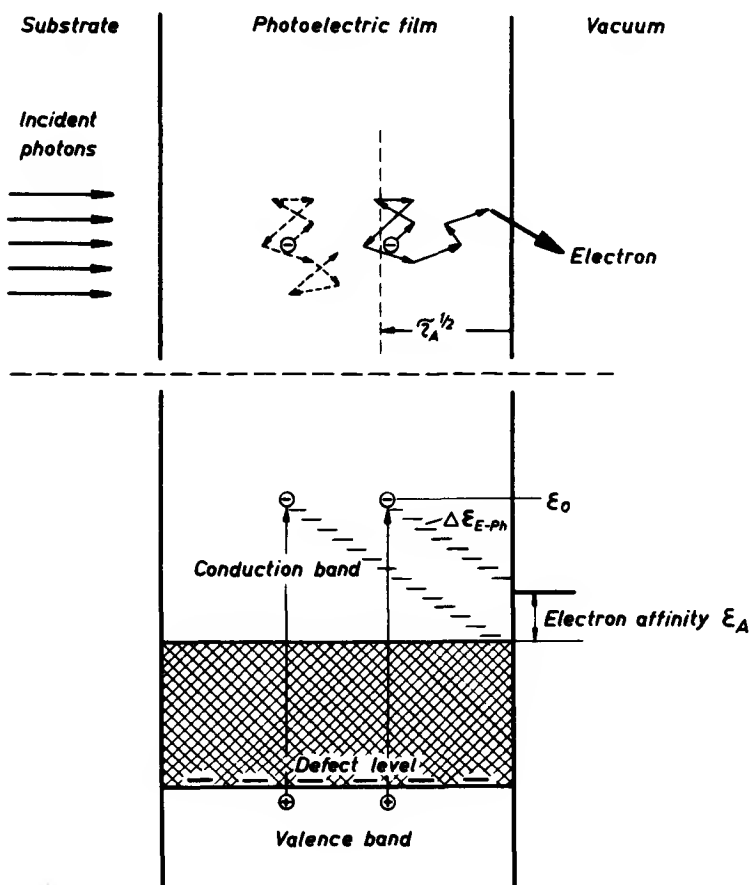
FIG. 6. Characteristic values of a semiconductor for the photoemission of electrons.

2. the transport function $f(z)$ which takes into account the scattering of the electrons of an energy ϵ traveling to the surface.*

The two possible interaction processes in a semiconductor are the electron–electron and the electron–phonon interaction. The electron–electron process is marked by a single energy loss greater than the band gap ε_G. It is described by a transport function

$$f(z) = e^{-z/l} \tag{7}$$

The parameter l defines the attenuation length of the photoelectrons.

The electron–phonon process (the energy of the excited electron above the lower edge of the conduction band is smaller than the band gap ε_G) involves a small energy loss. The mean free path between two collisions with phonons being short, the electron loses its energy in many collisions. It diffuses towards the surface. This diffusion described by Fermi's "age theory" (14) has already been applied to secondary and photoelectron problems (2, 15, 16). The transport function is of the following form:

$$f(z) = (\pi\tau_A)^{-1/2} \int_t^\infty \exp(-z^2/4\tau_A) \, dz \tag{8}$$

The parameter $\tau_A^{1/2}$ defines the attenuation length at which the electrons slow down their initial energy to the electron affinity (Fig. 6). Electrons starting from lamellas within the attenuation length with an energy corresponding
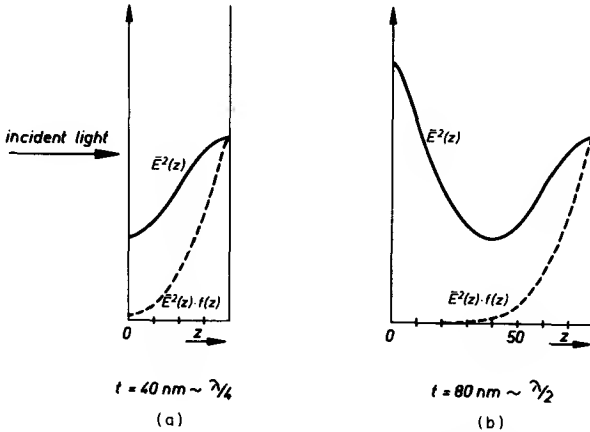
FIG. 7. Local production rate of excited electrons $(\bar{E}^2(z))$ and their contribution to photocurrent $(\bar{E}^2(z), f(z))$ for two films of different thickness: (a) $t_1 = 40$ nm, (b) $t_1 = 80$ nm ($n_0 = 1$, $n_1 = 3.20$, $K_1 = 0.44$, $n_2 = 1.5$, $\lambda = 620$ nm).

* The transport function will be discussed by assuming the same initial energy ϵ_0 of the electrons above the lower edge of the conduction band.
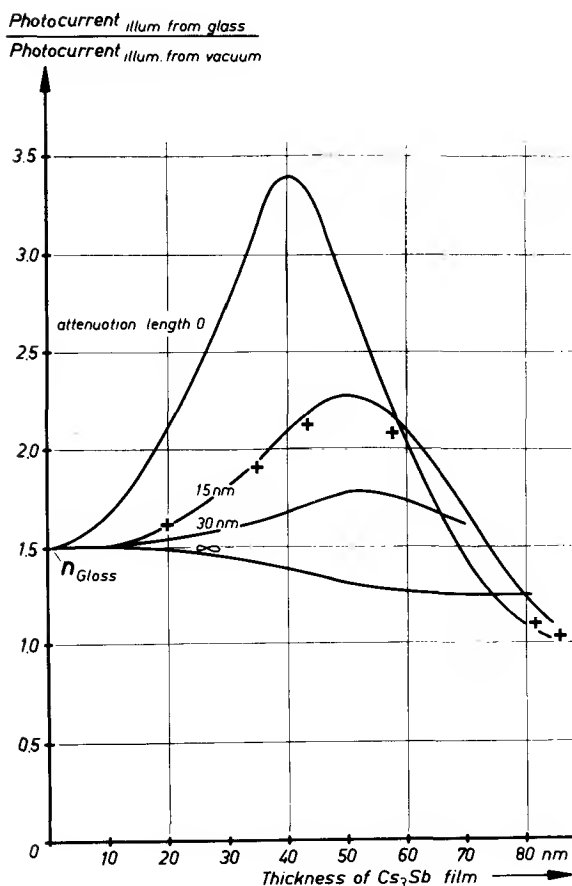
FIG. 8. Determination of the attenuation length of photoelectrons in Cs_3Sb. Measured ratios of the photocurrent (+) of a film illuminated from the glass and from the vacuum are compared with calculated ones for different values of the attenuation length as a function of thickness ($\lambda = 620$ nm).

to $\tau_A^{1/2}$ reach the surface with an energy $\varepsilon > \varepsilon_A$ (ε_A is the electron affinity) and escape into the vacuum.*

From the knowledge of the photoelectron production rate and the transport function the attenuation length can be determined. To do this we compare

* The definition of the attenuation length $\tau_A^{1/2}$ means that of 100 electrons coming out of the lamella at a depth $z = \tau^{1/2}$ and moving towards the surface 48 electrons reach the surface.

the quotient of the measured photocurrents emitted from one and the same layer by illuminating it from the glass and from the vacuum side with the quotient of the calculated photocurrents (11). The attenuation length can then be evaluated by a trial-and-error method.

As an example the procedure for determining the attenuation length in Cs_3Sb films will be shown. The photocurrents are measured from a wedge-shaped cathode for the respective exciting energies as a function of the film thickness. The spatial distribution of excited electrons and finally emitted electrons for two films of a thickness of $\lambda/4$ and $\lambda/2$ for $\lambda = 620$ nm are shown in Fig. 7. In the spectral range of 440–620 nm only electron–phonon interaction takes place in Cs_3Sb cathodes as has been shown (17). Integrating over the film thickness we get the total photocurrent.

The measured quotient of the photocurrents and the calculated ones for different values of the attenuation length are plotted versus layer thickness in Fig. 8. The function calculated for the attenuation length, $\tau_A^{1/2} = 15$ nm, coincides with the measured one. The value of the attenuation
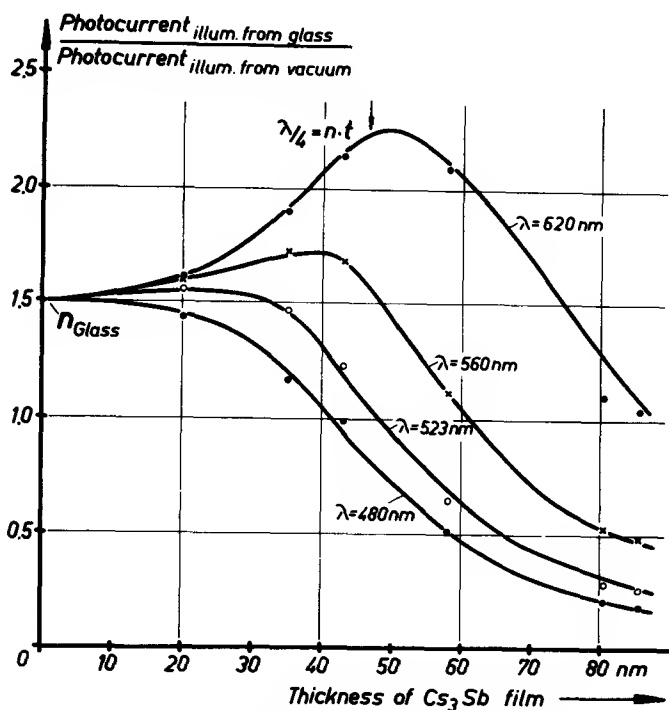
FIG. 9. Measured and calculated ratios of photocurrents for an attenuation length $\tau_A^{1/2} = 15$ nm for different wavelengths.

length, $\tau_A^{1/2} = 15$ nm, in Cs_3Sb material was also determined for the wavelengths 480, 523, 560 nm (11). See Fig. 9.

The same procedure was applied to multialkali cathodes. The attenuation length of the electrons excited by light in the visible range was determined to be about 30 nm (18).

IV. Conventional Cathodes of High Quantum Yield

Since it is our aim to improve the performance of photoelectric films by optical methods, we first have to deal with conventional cathodes of high efficiency.

The efficiency of a cathode is given by the quantum yield, i.e., the number of electrons to the number of photons. This ratio can be related either to the incident photons or to the absorbed ones. As the attenuation length of the photoelectrons is limited and the local distribution of the mean square of the electric vector depends on the film thickness, the quantum yields are functions of the thickness. Figure 10 shows the principal behavior of the yields for transmissive cathodes of the type S-11. The quantum yield per incident photon is zero for a layer of infinite thickness. With decreasing thickness more and more excited electrons emerge and the yield rises. With further decrease the vanishing absorption overrules the rising escape probability, and the photocurrent decreases. At the film thickness, $t = 0$, photons are not
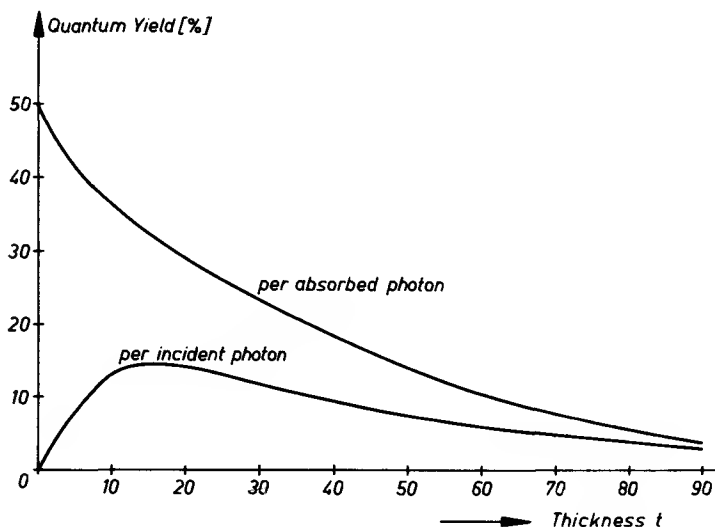
Fig. 10. Principal curve of the quantum yield per incident and per absorbed photon as a function of film thickness.

absorbed and the yield becomes zero. The declining curve of the absorption fixes the maximum of the quantum yield per incident photon for a single film at a thickness of 15 nm.

The quantum yield per absorbed photon steadily rises with decreasing thickness. From a purely optical point of view photoelectric films of smaller
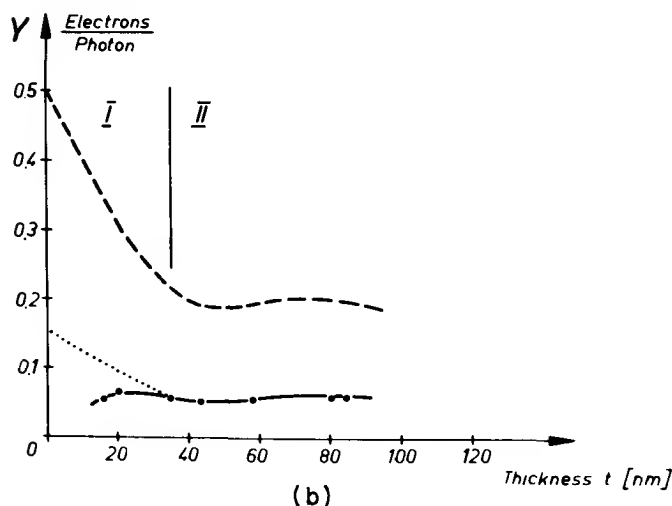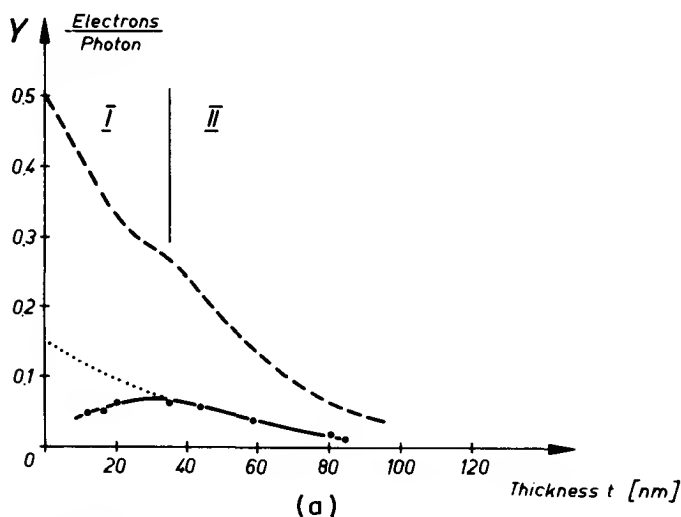
FIG. 11. Quantum yield Y (per absorbed photon) of cesium–antimony films versus thickness for $\lambda = 546$ nm: (---) upper limit $\eta = 1$, (—·—) measured values, ($\cdot \cdot \cdot$) extrapolated run: (a) light incident from the glass; (b) light incident from the vacuum.

thickness should give cathodes of higher output, if the absorption in the film could be raised by additional means.

The photocurrent depends not only on the excitation and the emission of electrons but also on their subsequent delivery. The delivery becomes more and more throttled by the rapid decrease of conductivity with decreasing film thickness (19). This explains the difference between the measured and the calculated quantum yields per absorbed photon for small film thicknesses (see Fig. 11). The rising quantum yield per absorbed photon is reduced by the declining conductivity. The maximum of the curve occurs at 25 nm for cesium–antimony films. From the optical point of view very thin cathodes would be attractive, but up to now their poor conductivity prevents their application.

The breakdown of the conductivity pushes the maximum of the quantum yield per incident photon from 15 to 25 nm.

The optical properties of a Cs_3Sb cathode, 25 nm thick, are shown in Fig. 12.

The optimum thickness of multialkali films is 25–30 nm.
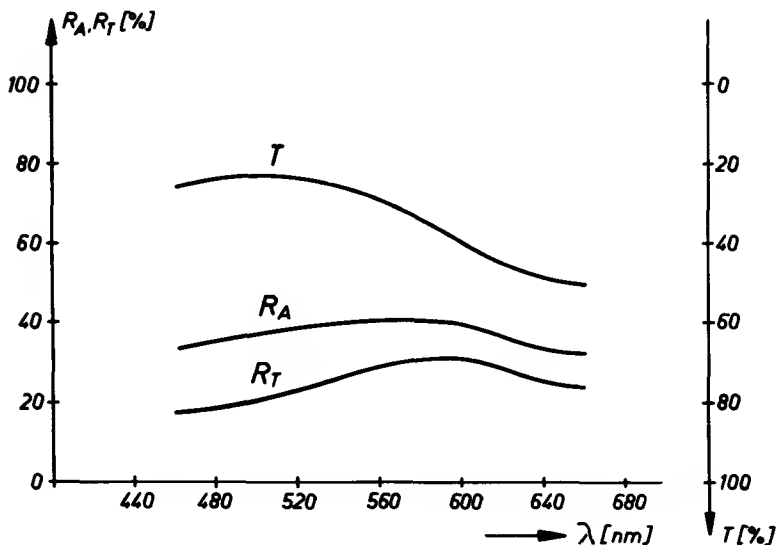
FIG. 12. Optical properties of a cesium–antimony film of optimum thickness (25 nm) versus wavelength (T is the transmittance, R_A is the reflectance from vacuum side, R_T is the reflectance from the substrate).

V. Interference Cathodes

1. TRANSMISSIVE INTERFERENCE CATHODE (TIC)

a. Principle of TIC. Cesium–antimony photocathodes (S-11) of high quantum yield with a geometrical thickness of 25–30 nm have an optical thickness between $\lambda/4$ and $\lambda/8$ for the visible light. Multialkali cathodes (S-20) of high sensitivity have a thickness in the same range. Therefore these layers are in dissonance for the incident waves as shown in Section II.

It is our aim to adapt and to tune the photoelectric films. The problem is solved by increasing the film to an optical thickness of $\lambda/2$. For cathodes of small attenuation length this matching procedure cannot be done successfully by merely enlarging the thickness of the film because the lamellas near the substrate absorb energy but do not contribute photoelectrons. Cathodes with a larger attenuation length like the multialkali films might be tuned by this
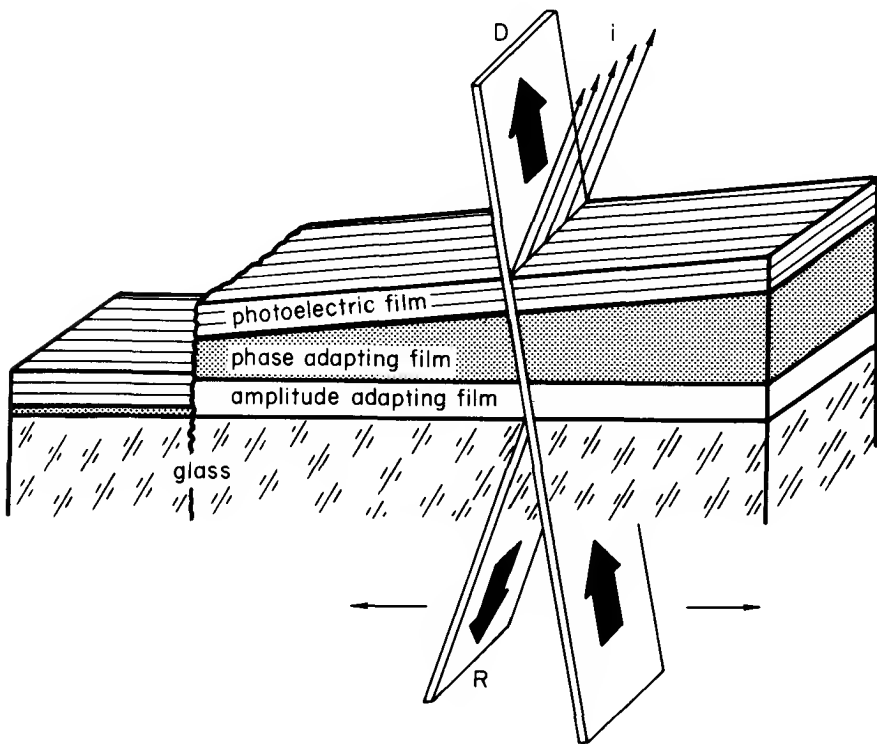
FIG. 13. Basic arrangement of a TIC with wedge-shaped phase adapting film.
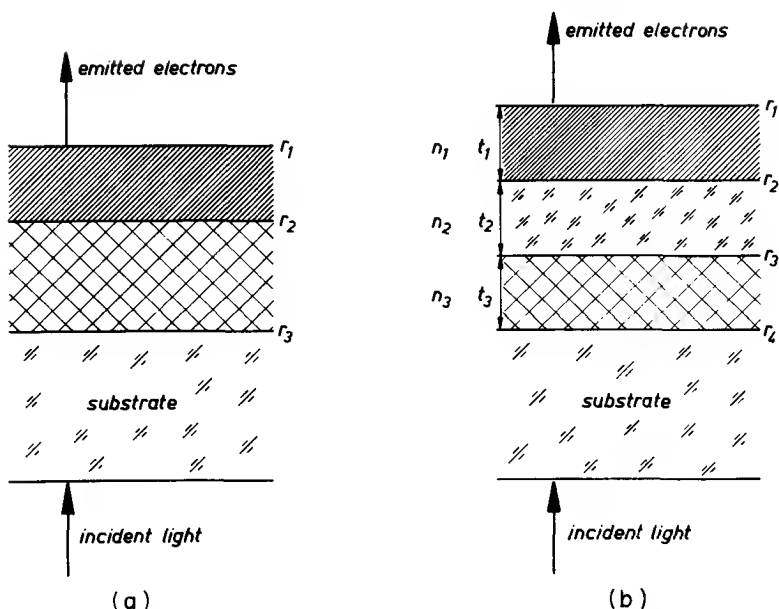
FIG. 14. Arrangement of a TIC with (a) one adapting film and (b) two adapting films.

simple method with a moderate effect. This would result in a higher absorption and a rather small current enhancement.

The right way of tuning a transmissive cathode is to extend the photoelectric film by addition of a dielectric film to a total thickness of $\lambda/2$. The refractive index and the thickness of the dielectric film have to be properly chosen to fulfill the resonance condition. In this case no reflected wave exists. The additional dielectric film acts as an antireflection coating for the photocathode. For a photocathode with the reflectance of the Cs_3Sb film a single layer of TiO_2 is suitable (Fig. 14a).

The two requirements of matching the amplitude- and the phase-condition for a TIC can experimentally be met more easily by using two dielectric films (Figs. 13 right side and 14b). A film of a suitable high index and thickness (n_3, t_3) is evaporated onto the substrate. Its reflection coefficient, r_{34}, has to match that of the photoelectric film, r_{21}, to suppress the reflection of the system:

Amplitude condition: $r_{34} = r_{21}$ (9)

In the schematically experimental setup of Fig. 13 a wedge-shaped dielectric film of low index (n_2) secures the second matching condition: The optical thickness of the system has to be a half wavelength or a multiple of it.

Phase condition: $n_1 t_1 + n_2 t_2 + n_3 t_3 = \lambda/2$ (10)

Finally the photoelectric film (n_1, t_1) completes the system.

b. *Properties of TIC's.* In Fig. 15 the reflectance, transmittance, and the photocurrent of a TIC, scanned with a light beam $(\lambda = 589$ nm), is plotted versus the thickness of the tuning film as described in Fig. 13. The amplitude
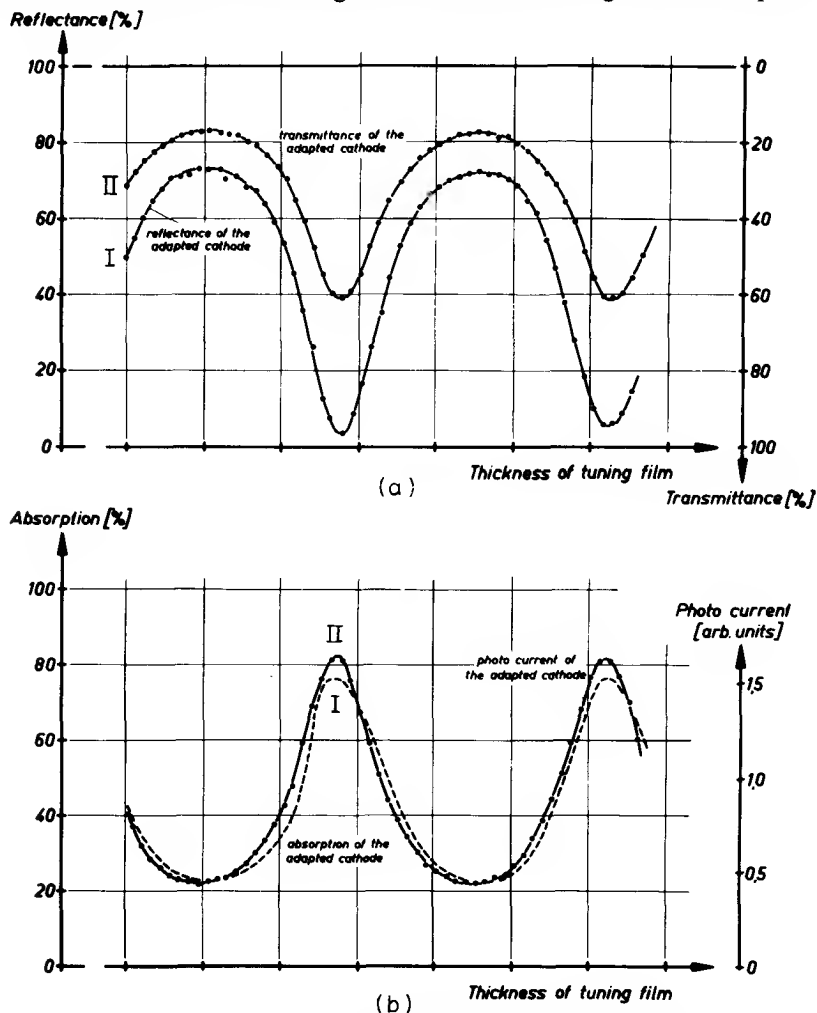
FIG. 15. (a) Reflectance (curve I) and transmittance (curve II) and (b) absorption (curve I) and photocurrent (curve II) of a TIC versus thickness of tuning film (cesium–antimony film as photoelectric device, SiO_2 as phase-adapting film, TiO_2 as amplitude-adapting film).
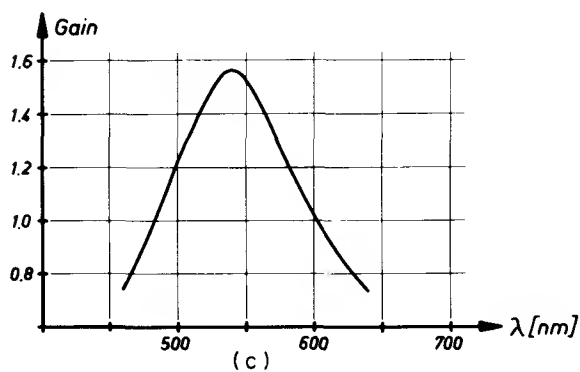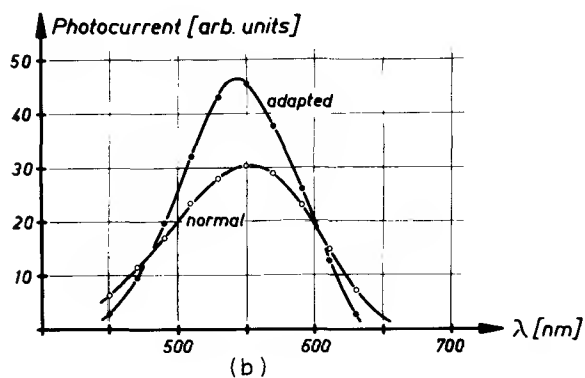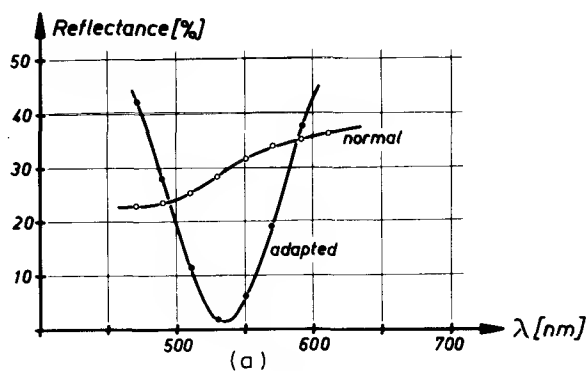
FIG. 16. Reflectance (a), photocurrent (b), and gain (c) of a second-order TIC with cesium–antimony film versus wavelength.
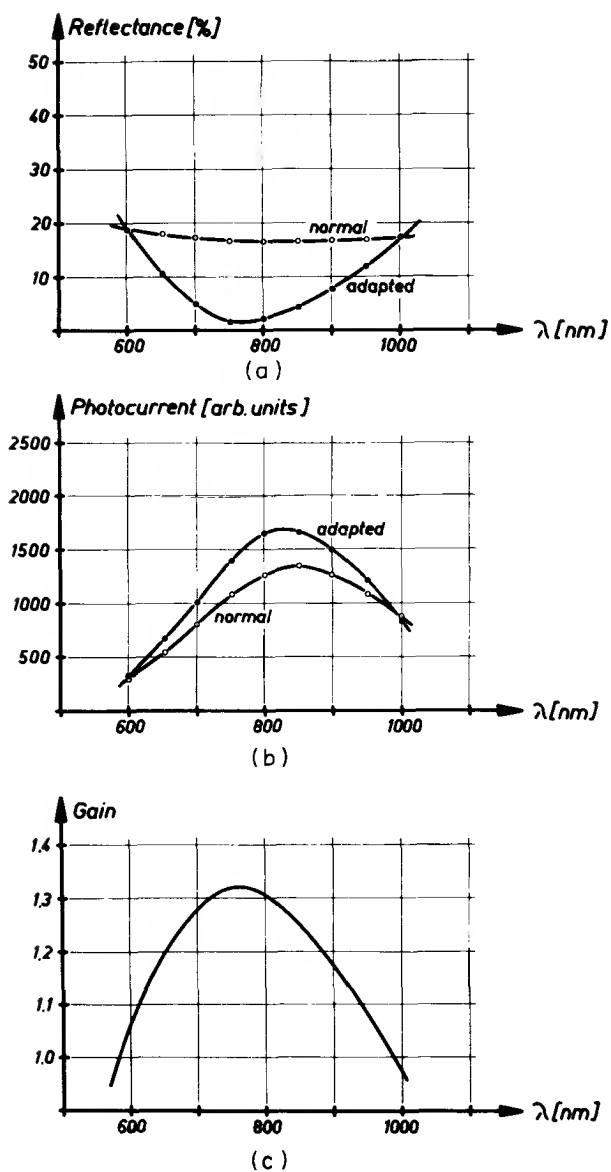
FIG. 17. Spectral dependence of reflectance (a), photocurrent (b), and gain (c) of a first-order TIC with cesium oxide film.

condition is nearly met. The minimum reflectance is still 5%. At the same thickness the absorption and the transmittance have a maximum. The light not reflected is distributed to the absorption and to the transmittance. The maximum enhancement of the induced absorption by adapting and tuning the system to zero reflectance is given by

$$A/A_{21} = 1/(1 - R_{21}) \tag{11}$$

whereby the absorption and the reflectance of the photoelectric film against the substrate are denoted by A_{21} and R_{21}. One fact has to be emphasized: There is no way to absorb completely the light energy in the photoelectric film of the TIC. The reflectance of the photoelectric Cs_3Sb film of high quantum efficiency is about 30%. Therefore the absorption can be raised by a factor 1.5. The photocurrent is exactly proportional to the absorption, as can be seen from the lower part of Fig. 15. The exact proportionality of the enhancement of the photocurrent and of the absorption is valid for the TIC. This fact becomes evident from the $\bar{E}^2$ distribution in the film. The function of the local production rate for photoelectrons is raised by the factor $(1 - R_{21})^{-1}$ but is not changed. The adaption changes the factor $(1 - r_2^2)/N$ in Eq. (4b) for the $\bar{E}^2$ distribution only.

The enhancement of the photocurrent of a TIC covers a rather broad wavelength region, depending on the tuning. Figure 16 shows the reflectance and the photocurrent of TIC with a cesium–antimony film tuned in the second order to light of the wavelength 540 nm as a function of wavelength and the respective properties of the conventional cathode. The maximum value G_m of the gain (G = photocurrent i_{TIC} of adapted film/photocurrent i_C of conventional film) is 1.6. The bandwidth of the enhancement is 120 nm.

The adaptation is not confined to photocathodes of the type S-11. Figure 17 shows the optical and photoelectric properties of an adapted and the respective conventional silver–cesiumoxide–cesium cathode (S-1). Since the reflectance of the film is smaller ($R_{21} = 20\%$) the adaptation results in a smaller maximum gain factor $G_m = 1.30$. The thickness of the tuning film is chosen for a first-order adaptation at the wavelength 700 nm. The bandwidth of the enhancement is about 400 nm, covering the red and near-infrared range. A smaller tuning thickness would result in higher photocurrents for the whole visible range with all types of photocathodes (S-1, S-11, S-20).

Technological aspects have to be regarded in preparing TIC's. A single dielectric film of high index used as an antireflection coating has to be separated by a very thin diffusion barrier of SiO_2 from the photoelectric film. It prevents any interaction between the photoelectric film and the high index coating, which usually results in a deterioration of the cathode.

The examples sufficiently show that the TIC, equipped with highly sensitive photoemissive films having a reflectance of about 30%, enhances their

photoemission by 50%. The bandwidth of the enhancement covers a range of 300–400 nm. At the same time it becomes evident that the attainable improvement of the photoemission is limited with this type of interference cathode.

2. REFLECTIVE INTERFERENCE CATHODE (RIC)

a. Principle of RIC. The adaptation of a photocathode of the transmissive type raises the absorption and the photoemission but unfortunately the transmittance too. It is impossible to achieve the total light absorption in the TIC, because the first boundary surface (film–vacuum) is permeable not only to electrons but also to light waves. The loss of light through the first boundary can be prevented by a highly reflecting surface, for instance a mirror. However the reflector blocks the emission of photoelectrons too. Electrons can only escape out of the boundary surface at which the light enters the photoelectric layer. Cathodes for which light is impinging on and electrons are emitted from the same surface are called reflective cathodes. The transmissive photoelectric film is converted to a reflective interference cathode by use of a low-index dielectric film as a tuning element and a highly reflecting mirror.

The principal arrangement of this type of cathode is shown in Fig. 18. In order to illustrate the performance of the cathode the distribution of $\bar{E}^2$ within and in front of the cathode is plotted in Fig. 19. In this example the reflectance of the backing mirror is supposed to be ideal, i.e., $r_3 = 1$. The tuning film is wedge-shaped, and the thickness of the photoelectric film is $\lambda/4$, which approximates the actual conditions. The $\bar{E}^2$ distribution in the photoelectric film—or, as we can say, the local production rate of photoelectrons—varies with the thickness of the tuning film. Most photoelectrons are produced at a tuning film thickness of 0, $\lambda/2$, or a multiple of it. The number of excited electrons (black shaded area) is impressive, but the distribution should be noticed too. Compared to a single photoelectric film the local production rate has completely changed for the same film incorporated in a RIC (Fig. 20). Nearly all photoelectrons are excited at the vacuum–film boundary. This ideal distribution favors the emission of electrons.

b. Optical Properties of RIC. The reflectance of the RIC, which is similar to the reflective interference filter of Hadley and Dennison (*20*), is given by

$$R = \frac{r_1{}^2 + r_{23}^2 \beta^{2t_1} + 2r_1 r_{23} \beta^{t_1} \cos[(4\pi n_1/\lambda)t_1 + \Delta_1 - \Delta_{23}]}{1 + r_1{}^2 r_{23}^2 \beta^{2t_1} + 2r_1 r_{23} \beta^{t_1} \cos[(4\pi n_1/\lambda)t_1 - \Delta_1 - \Delta_{23}]} \tag{12}$$
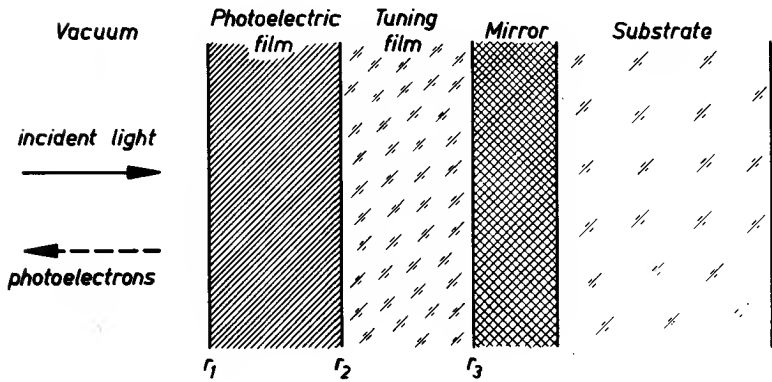
FIG. 18. Basic arrangement of a RIC.
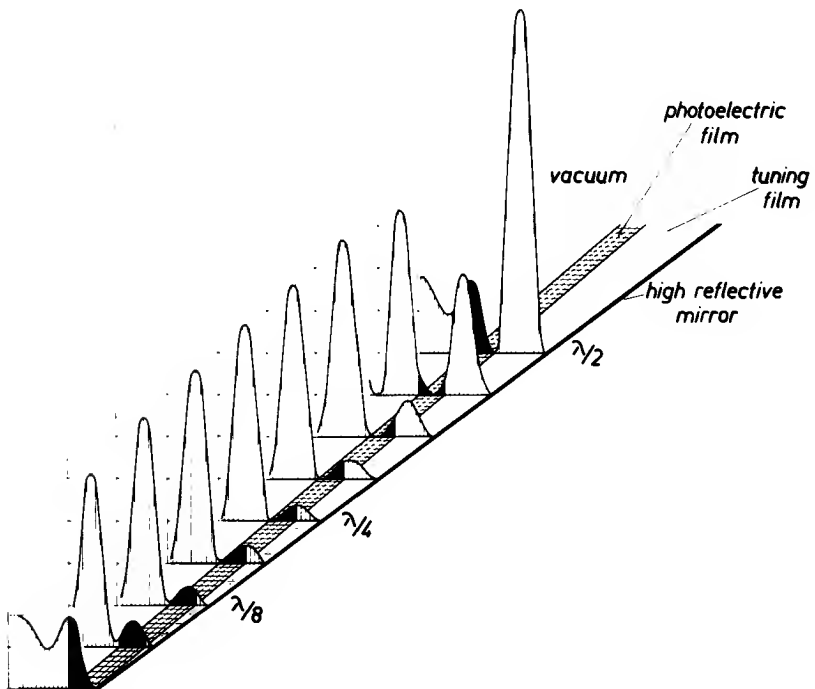
FIG. 19. Wave fields in front and in the interior of a RIC ($n_0 = 1.0$, $n_1 = 3.20$, $K_1 = 0.44$, $t_1 = 50$ nm, $n_2 = 1.50$, ideal mirror with $r_3{}^2 = 1$).
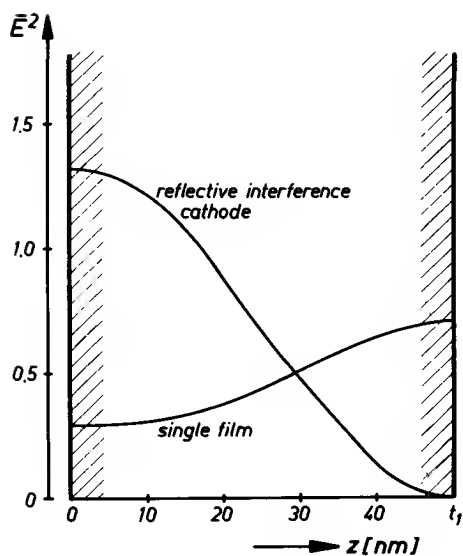
FIG. 20. Wave field in a single photoelectric film (optical thickness $\lambda/4$) and in the same film incorporated into a RIC.
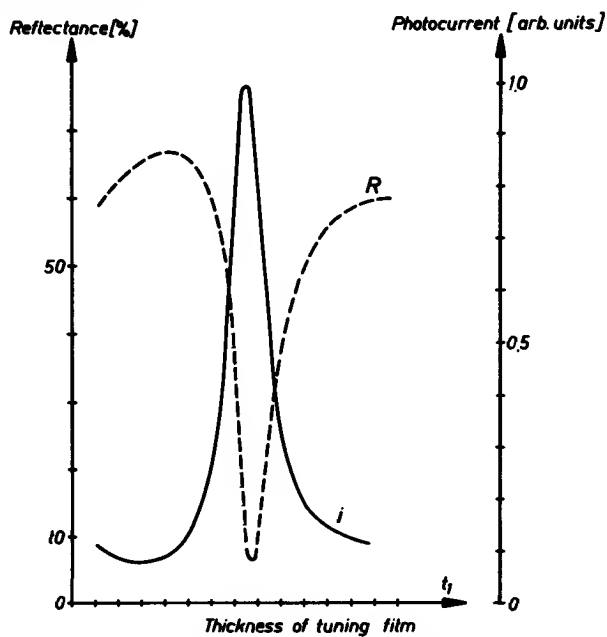
FIG. 21. Reflectance and photocurrent of a RIC with cesium–antimony film versus thickness of tuning film.

whereby

$$\mathbf{r}_1 = r_1 \cdot e^{i\Delta_1}$$ Fresnel coefficient of the boundary vacuum-film,

$$\mathbf{r}_{23} = r_{23} \cdot e^{i\Delta_{23}}$$ Fresnel coefficient of the combined boundaries photoelectric film–tuning film r_2 and tuning film–mirror r_3,

$$t_1$$ thickness of photoelectric film,

$$n_1 + iK_1$$ complex index of photoelectric film.

The minimum value of the reflectance is obtained by matching the phase condition*:

$$\frac{4\pi n_1}{\lambda} t_1 + \Delta_1 - \Delta_{23} = (2m + 1)\pi, \qquad m = 0, 1, 2, \ldots \tag{13}$$

In other words, the sum of the thickness of the photoelectric film, tuning film, and phase shift at the reflector has to be $\lambda/4$ or an odd multiple of it. The cathode is tuned to a broad spectral region, when it is tuned to the first order; i.e., the total thickness of the system is $\lambda/4$. Since the optical thickness of the photoelectric film is nearly $\lambda/4$, the thickness of the tuning film is rather small.

The amplitude condition for zero reflectance

$$r_1 = r_{23}\beta^{t_1} \tag{14}$$

cannot be realized for the RIC in general. The reflectance of the backing mirror has to be as high as possible to prevent the loss of light energy in the form of transmitted or absorbed energy. This requirement predetermines the Fresnel coefficient r_{23} to be almost one. On the other hand the photoelectric material fixes the Fresnel coefficient r and, in combination with the optimum thickness, the transmission factor β^{t_1}.

A RIC with cesium–antimony film can be adapted quite well by an aluminum backing as can be seen in Fig. 21. Here 95% of the incident light energy is absorbed in the interference system, but the energy absorbed by the mirror is already high. A multialkali film tuned in the near infrared cannot be adapted to zero reflectance as the transmission factor is too high. The remaining reflectance of an S-20 RIC tuned to 700 nm still amounts to 15% (see Fig. 22).

---

* This statement is valid for a phase shift Δ_1, which only differs slightly from π. The phase shift of photoelectric materials is about 175°.
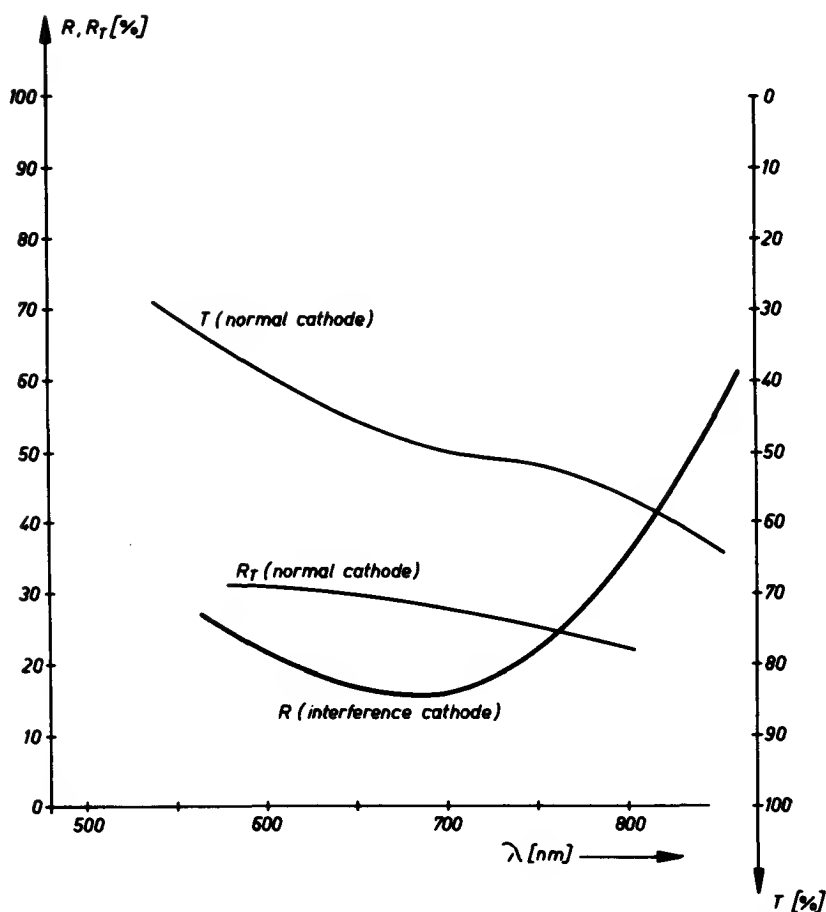
FIG. 22. Transmittance and reflectance of a single multialkali film and reflectance of the RIC versus wavelength.

There is no sense in reducing the Fresnel coefficient r_{23} just to match the amplitude condition. The high values of $\bar{E}^2$ in the tuning film of an adapted cathode considerably increase the induced absorption in the mirror. The increase is given by $A/A_3 = T_{21}/(1 - R_{21})$, where A_3 is the intrinsic absorption of the mirror and T_{21} and R_{21} are the transmittance and reflectance of the single photoelectric film. Changing the backing mirror from silver to aluminum enforces the pernicious absorption from 5 to 37%. The amplitude condition is less significant for a RIC. The requirement of a perfect reflectance of the backing mirror is more important.

c. Photoelectric Properties of RIC's. The optical properties of the photo-electric film and the induced absorption in the reflector shift the point of the highest photocurrent away from the region of lowest reflectance. In Fig. 21 the reflectance and the photocurrent of an S-11 RIC are plotted versus the thickness of the tuning film. The maximum of the photocurrent (maximum
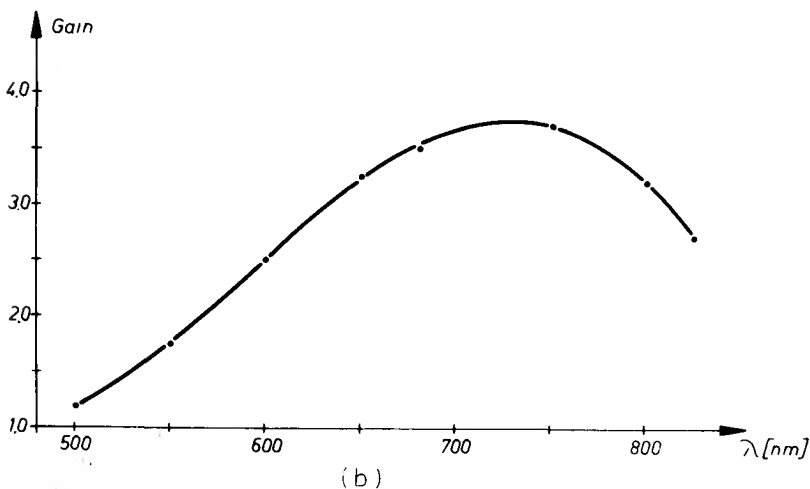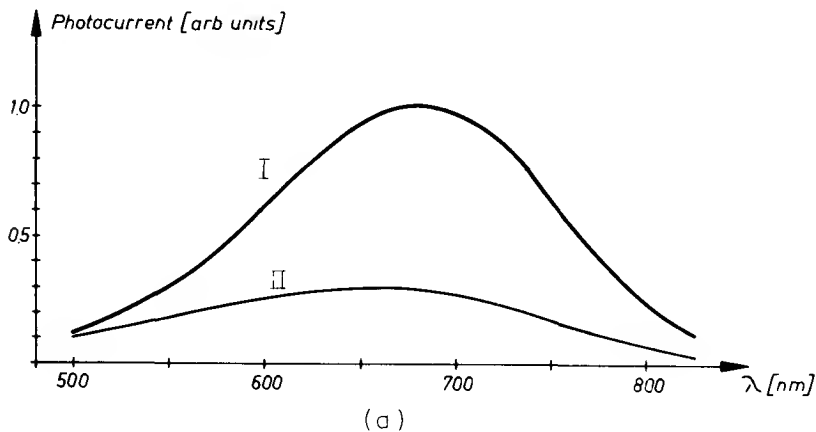
Fig. 23. (a) Photocurrents from (curve I) a RIC with multialkali film tuned to first order; curve II is the corresponding conventional film. (b) The gain *G* of the RIC versus wavelength.

of the absorption in the photoelectric film) does not coincide with the reflectance minimum (maximum of the total absorption in the system)

The photocurrent of a RIC with a multialkali film is compared with the current of the same film in the conventional transmissive arrangement (see Fig. 23). The ratio of the two currents is called the gain G ($G = i_{RIC}/i_C$). The
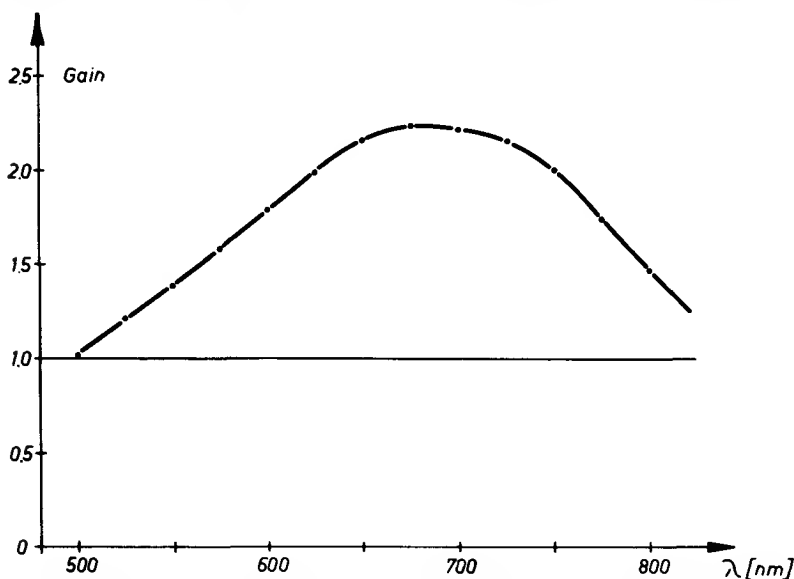
FIG. 24. Gain G of a first-order RIC with a multialkali film versus wavelength.
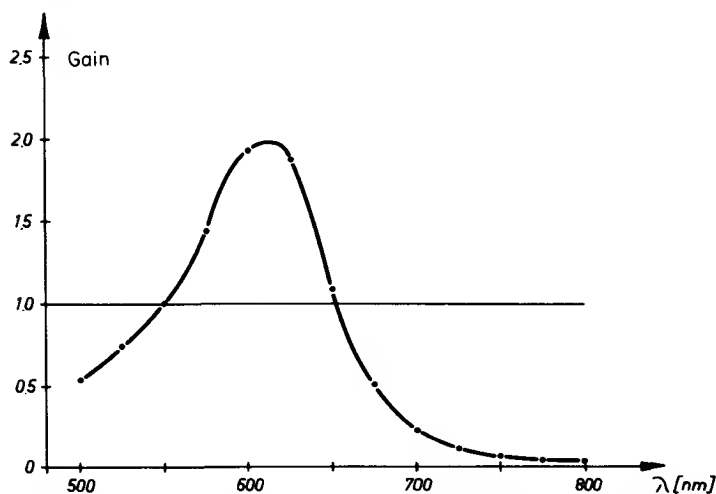
FIG. 25. Gain G of a second-order RIC with a multialkali film versus wavelength.

interference cathode is tuned with a 30-nm SiO_2 film and a silver reflector to 730 nm. The maximum value of the gain is $G_m = 3.7$ and agrees with the theoretical value. Multialkali films of conventional efficiency (180 $\mu A/lm$) used as integrating elements in RIC's tuned to 700 nm have their sensitivity increased to 450 $\mu A/lm$ (21).

The bandwidth of the current enhancement depends on the order of the tuning. A RIC tuned to the first order at 680 nm has a bandwidth of 400 nm. The cathode tuned to the second order works much more selectively. The bandwidth of the enhancement is then only 120 nm (see Figs. 24 and 25).
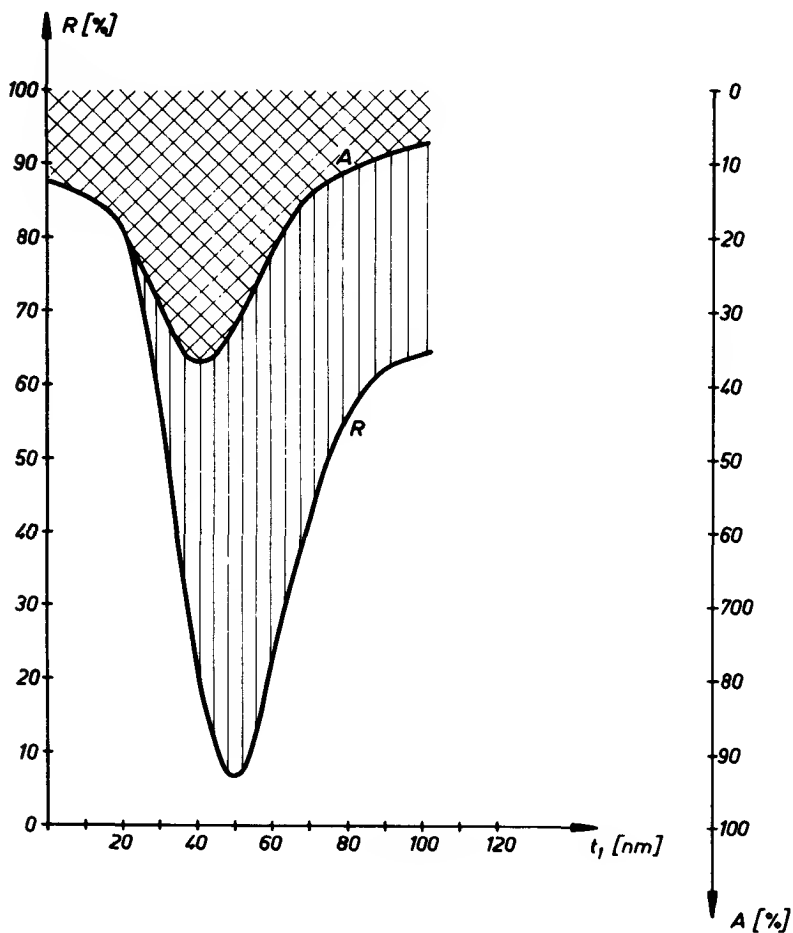
FIG. 26. Calculated reflectance and absorption of a wedge-shaped multialkali film backed by an aluminum reflector ($\lambda = 700$ nm).
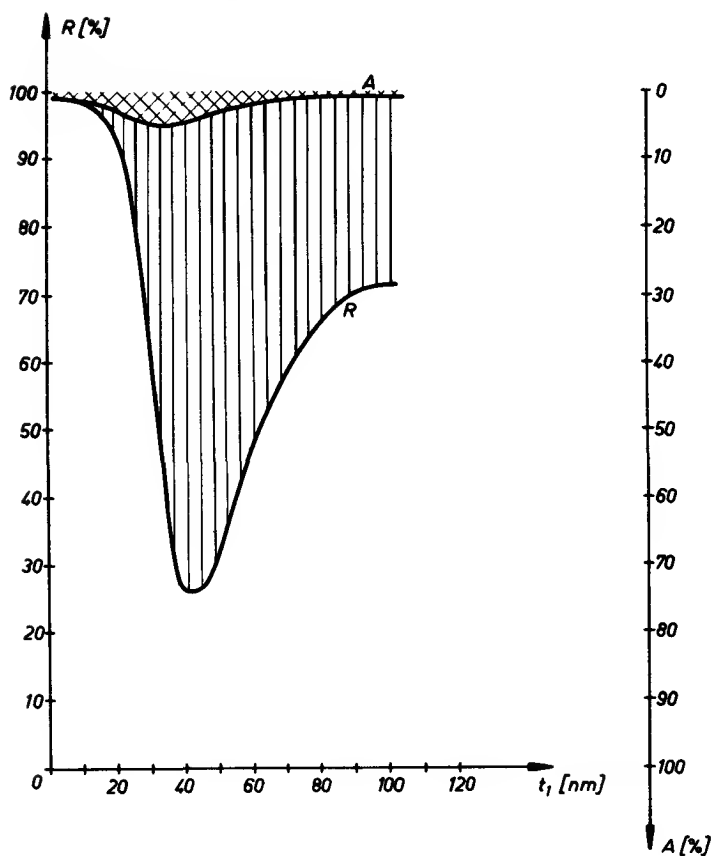
FIG. 27. Calculated reflectance and absorption of a wedge-shaped multialkali film backed by a silver reflector ($\lambda = 700$ nm).
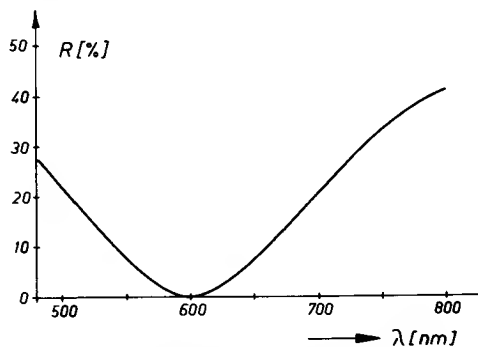
FIG. 28. Reflectance of a reflective cathode with a multialkali film and aluminum reflector versus wavelength (example for self-adaptation at 600 nm).

The maximum gain G_m slightly decreases with increasing order of tuning. That is contrary to the theoretical expectation. The decrease can be explained by the high values of $\bar{E}^2$ in the tuning film (see Fig. 19), which amplify a very small intrinsic scattering or absorption, thus reducing the energy absorbed in the photoelectric film.

A RIC tuned in the first order to the near infrared has a rather small spacer film. The thickness of the film becomes zero for a cathode tuned to the visible spectral range. Then the photoelectric film has to be evaporated directly onto the backing mirror. The performance of this reflective cathode is also determined by the interference of the waves reflected from the vacuum–film and film–backing mirror boundaries. As the phase shift at the second boundary is now fixed the cathode can only be tuned by varying the thickness of the photoelectric film. This possibility is limited as the intrinsic sensitivity of the film is affected by the variation of the thickness (see Section IV). In Fig. 26 the reflectance and the absorption in the film and in the reflector are plotted versus the thickness of the photoelectric film for one wavelength. The film acts as an absorbing antireflection coating. At a thickness of 50 nm the photoelectric film would reduce the reflectance at 700 nm to 5%, but 37% of the incident energy is then absorbed in the mirror. From an optical point of view a silver backing would be recommendable. It reduces the pernicious absorption in the mirror, and needs a smaller tuning thickness for the same wavelength (see Fig. 27). But some technological aspects prevent the use of silver as backing material for the multialkali films. Aluminum can only be used for multialkali reflective cathodes in the visible. The reflectance of a cathode tuned to 600 nm is plotted versus the wavelength in Fig. 28.

The principle of the RIC applied to multialkali films improves considerably the sensitivity of the cathodes. RIC's with conventional S-20 films have sensitivities of 450 μA/lm. Corresponding to an absorption of 70% in the photoelectric film the maximum gain could be raised to 3.7 at 700 nm. As the intrinsic absorption in the film rapidly decreases for longer wavelengths the maximum gain even increases for a tuning at a longer wavelength.

RIC prevents the high loss of light which takes place in the TIC by inserting a high reflective backing surface. In spite of this improvement the total absorption of light in the photoelectric film is not possible, since the amplitude condition for zero reflectance is not attainable with the RIC.

3. Totally Reflective Interference Cathode (TRIC)

a. Principle of TRIC. TIC and RIC comprise the partially transparent photoelectric film as an exterior element of the light resonator. In these arrangements the conditions for the complete absorption

$$R = 0, \qquad T = 0 \tag{15}$$

cannot simultaneously be realized. TIC only complies with the condition $R = 0$, and RIC with $T = 0$.

In principle the complete absorption can be obtained even in very thin films with small intrinsic absorption. The film is backed by an ideal reflector ($r_1^2 = 1$). The reflectance of this combination (r_{21}^2) is always smaller than 1. A phase adapting film and an amplitude adapting film with $r_{34}^2 = r_{21}^2$ in front of the combination always makes the reflectance of the system zero, i.e., $A = 100\%$.

Since the matching elements are dielectric films the complete absorption takes place in the weakly absorbing film.

This principle can be applied to photocathodes (22). A TIC (see Fig. 14) is illuminated under an angle of incidence $\phi > \phi_T$,

$$\phi_T = \arcsin(n_{glass})^{-1} \tag{16}$$

whereby ϕ_T denotes the angle of total reflection (Fig. 29). The totally reflecting film–vacuum boundary acts as the ideal mirror. It locks the light resonator and is transparent to photoelectrons.

The increased absorption in the TIC, the high $\bar{E}^2$ at the boundary of the cathode, is obtained at the expense of equally high $\bar{E}^2$ in the adjacent vacuum, that means with high losses of light by transmission. The continuity relation for the electric vector at the boundary of two media is valid for the TRIC too. But at total reflection the energy running over into the vacuum flows back with the boundary waves into the photoelectric film.

In case of resonance the absorption in the system is [see Eq. (11)]

$$A_{system} = A_{21}/(1 - R_{21}) \tag{17}$$
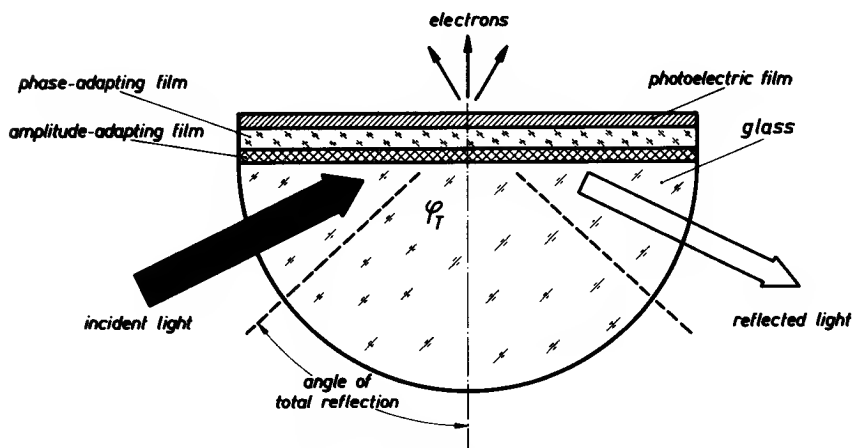
FIG. 29. Basic arrangement of a TRIC.

At angles $\phi > \phi_T$ the absorption is $A_{21} = 1 - R_{21}$. That means the absorption in the system is $A_{\text{system}} \equiv 1$. The local $\bar{E}^2$ distribution in the photoelectric film is not changed by the adaptation procedure. It is just increased by the factor $1/A_{21}$.

The totally reflective interference cathode (TRIC) can be matched for complete absorption of linear-polarized light at a given wavelength λ, a given thickness t of the photoelectric film, and a given angle $\phi > \phi_T$.

b. Optical Model of TRIC. The optical properties of a TRIC shall be verified in a model in which a Sb_2S_3 film simulates the photoelectric Cs_3Sb film (23). In Fig. 30 the reflectance versus angle of incidence is shown for films of different thickness for light vibrating perpendicularly to the plane of incidence. With increasing thickness the reflectance changes from a step function at the glass–vacuum boundary ($t = 0$) to a smooth function at the glass–Sb_2S_3 boundary ($t = \infty$).
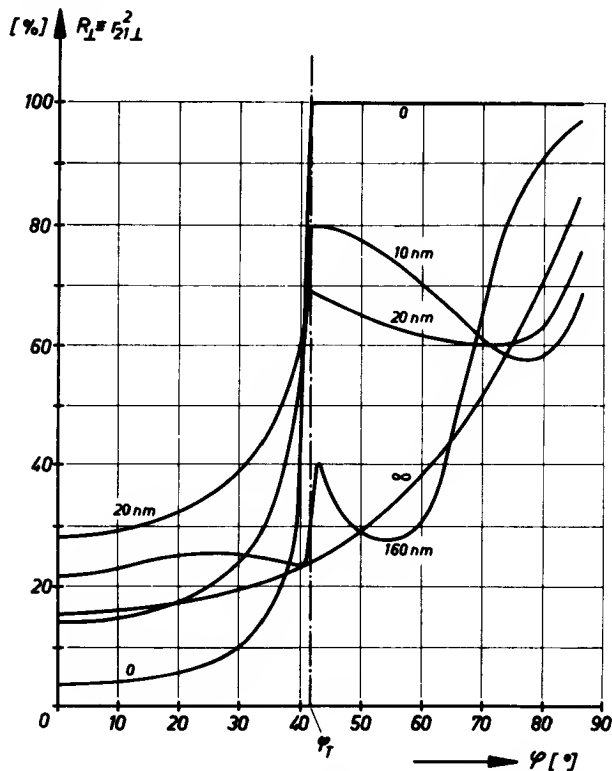
FIG. 30. Reflectance of Sb_2S_3 films of different thickness versus angle of incidence for $\lambda = 546$ nm.
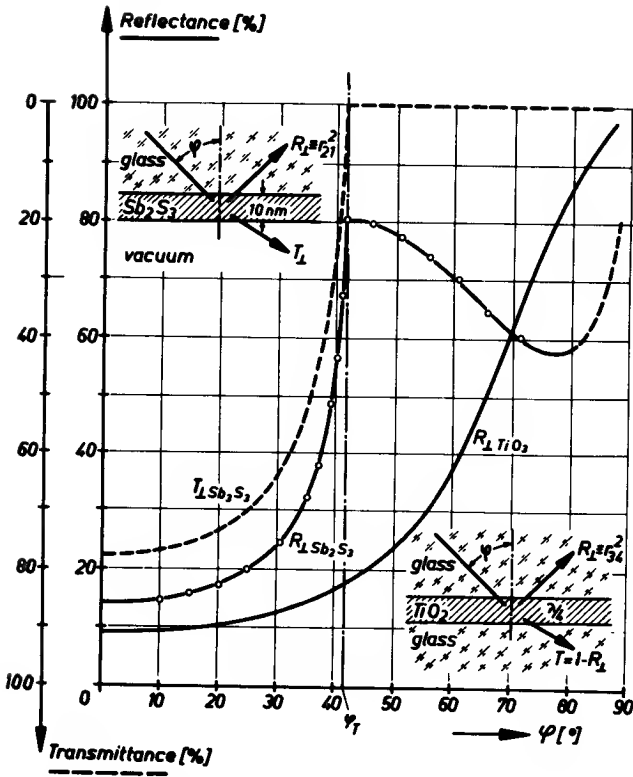
FIG. 31. Reflectance and transmittance of a 10-nm Sb_2S_3 film (light component vibrating perpendicular to the plane of incidence is denoted by the subscript $\perp$, the parallel component by $\parallel$) and reflectance of a $\lambda/4$ TiO_2 film versus angle of incidence.

The 10-nm-thick film simulates a photocathode. Its reflectance $R = r_{21}^2$ and transmittance T are plotted versus angle in Fig. 31. Furthermore the reflectance of a $\lambda/4$ TiO_2 film embedded in a medium with a refractive index 1.51 (glass or evaporated SiO_2) is shown. At an angle of 70° both films have the same reflectance. Therefore the system: Sb_2S_3 film (photoelectric film)–SiO_2-film (phase adaptation)–TiO_2 film (amplitude adaptation)–glass can be adapted at 70° to 100% absorption. In Fig. 32 the reflectance R and the transmittance T of the system are plotted versus angle of incidence. The reflectance $R(\phi)$ oscillates between the extrema of the interference function given by the limiting curves

$$R_{\substack{\max \\ \min}} = \frac{(r_{21}(\varphi) \pm r_{34}(\varphi))^2}{(1 \pm r_{21}(\varphi) \cdot r_{34}(\varphi))^2} \tag{18}$$
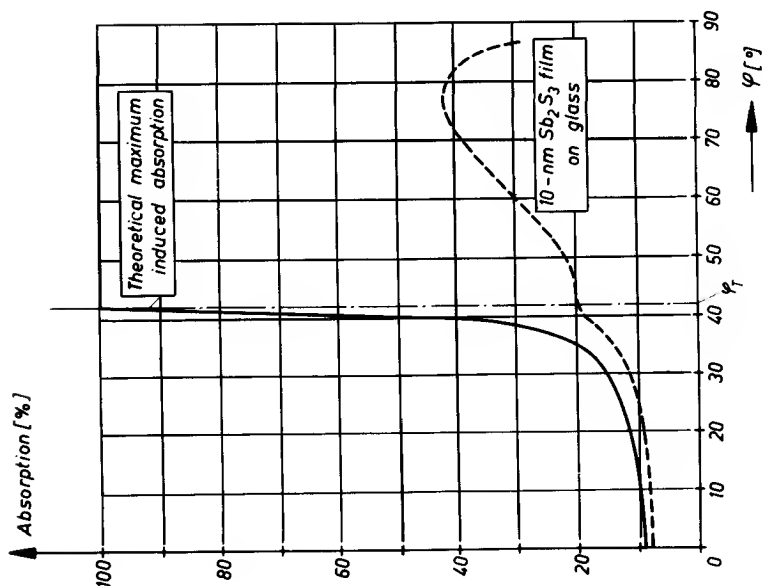
FIG. 33. Measured absorption of a single film and theoretical maximum absorption of a TRIC model versus angle of incidence ($\lambda = 546$ nm).
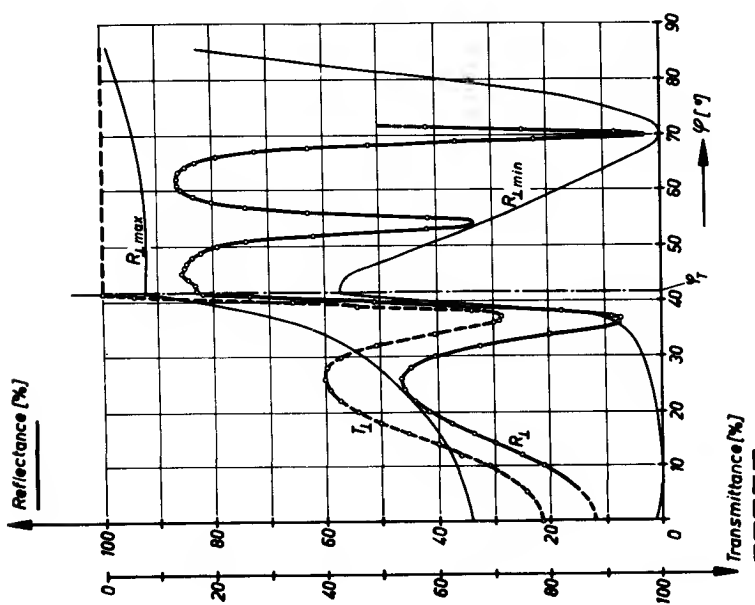
FIG. 32. Reflectance and transmittance of a TRIC model composed of an Sb_2S_3 film, an SiO_2 film, and a $\lambda/4$ TiO_2 film of Fig. 31 (perpendicular component).

FIG. 35. Absorption and photocurrent of a Cs_3Sb film (thickness = 25 nm) versus angle of incidence (λ = 546 nm).

FIG. 34. Reflectance and transmittance of a 25-nm Cs_3Sb film versus angle of incidence (λ = 546 nm).

We state the result of the experiment. The absorption in the single film at normal incidence ($\phi = 0$) $A_{21} = 8\%$ is increased to 38% by oblique illumination at $\phi = 70°$. By incorporating the film into the TRIC at the same angle the absorption is further increased to 97%. Corresponding to this statement the curves in Fig. 33 give the intrinsic absorption of the 10-nm Sb_2S_3 film (dotted curve) and the theoretically maximum attainable induced absorption in the system (solid curve). The maximum of course can be reached only in a given narrow range of the angle and for polarized light.

The photocurrent rise should be proportional to the absorption.

c. Angle Dependance of Absorption and Photocurrent of S-11 and S-1 Cathodes. The measurements of the absorption A and the photocurrent i of S-11 and S-1 cathodes versus angle of incidence provide the basic information for the construction of a TRIC.

In Fig. 34 the reflectance $R(\phi)$ and transmittance $T(\phi)$ of a conventional Cs_3Sb film of optimum thickness ($t = 25$ nm) are given for $\lambda = 546$ nm. The absorption $A_\parallel(\phi)$ and $A_\perp(\phi)$ are evaluated from these data and plotted in Fig. 35. The photocurrent $i_\parallel$ and $i_\perp$ are shown too, for which the currents are normalized at $\phi = 0$. The data of a cesium oxide film are given in Fig. 36. The results are summarized in the following statements:

1. The photocurrent roughly corresponds to the absorption. The quantum yield of the parallel component has higher values for $\phi > \phi_T$ than for normal incidence.

This behavior is unexpected since the phase change $\triangle_\parallel$ at the boundary to the vacuum remains constant with $\triangle_\parallel \approx 0°$ from normal incidence up to $\phi = \phi_T$. That means the $\bar{E}^2$ distribution within the film retains its loop at the vacuum boundary, which is the most ideal distribution for the emission of photoelectrons.

In the range $\phi_T < \phi < 90°$ the phase change $\triangle_\parallel$ increases from $0°$ to about $100°$. The increasing phase change shifts the loop of the standing wave from the boundary into the interior of the film, thus deteriorating the photoelectric effect. The quantum yield should decrease in the range $\phi > \phi_T$. Yet gold films of the thickness 3–20 nm illuminated by the parallel component also show the opposite effect. Their quantum yields always have a maximum in the range $\phi > \phi_T$. This behavior might be classified as a photoelectric vector effect. We will not specifically state that as long as the wave fields in thin absorbing films for $\phi > \phi_T$ have not been explicitly calculated.

2. Without even bothering to enhance the absorption with a TRIC, we get maxima of the absorption and of the photocurrent by merely switching from normal to oblique illumination. In the range of the principal angle of incidence the films are self-adapted. A maximum of absorption and hence of
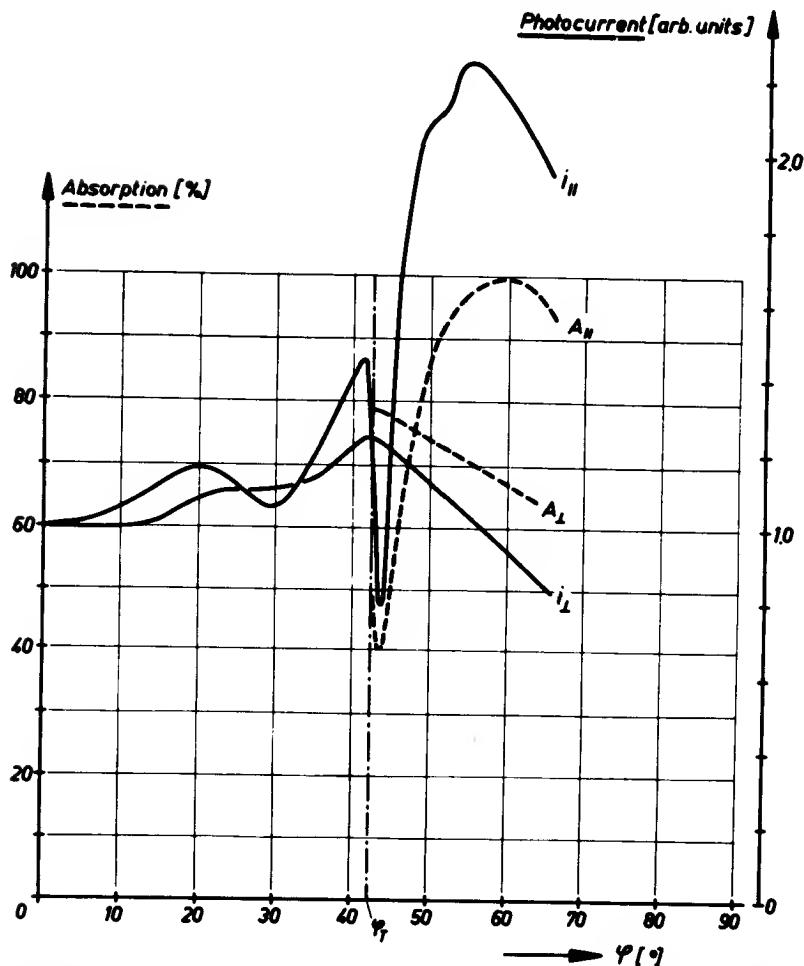
FIG. 36. Absorption and photocurrent of a cesium oxide film versus angle of incidence ($\lambda = 546$ nm).

the photocurrent corresponds to a minimum of $R_\parallel$. This maximum is further raised by the higher quantum yield in the range $\phi > \phi_T$. The main data of Figs. 35 and 36 are summarized in Table I, where the superscripts [0] and [*] denote the values at normal incidence and at the angle ϕ^* of nearly maximum absorption.

The photoemission of both cathodes can be enhanced at oblique incidence by a factor of 2.0. For unpolarized light the factor would amount to 1.6.

The nearly complete absorption and the high photoemission of S-1 and and S-11 films at oblique incidence without any adapting tricks seems to

Cathode	Thickness (nm)	A^0 (%)	i^0	φ^* (deg)	A^* (%)	i^*
Cs_3Sb	$t = 25$	50	1.0	75	86	2.00
S-1	$nt = 250$	60	1.0	55	96	2.10

leave no real chance for TRIC systems. There is a chance with thinner cathodes as will be discussed in Section V,3,e. First we have to show that a TRIC works in principle.
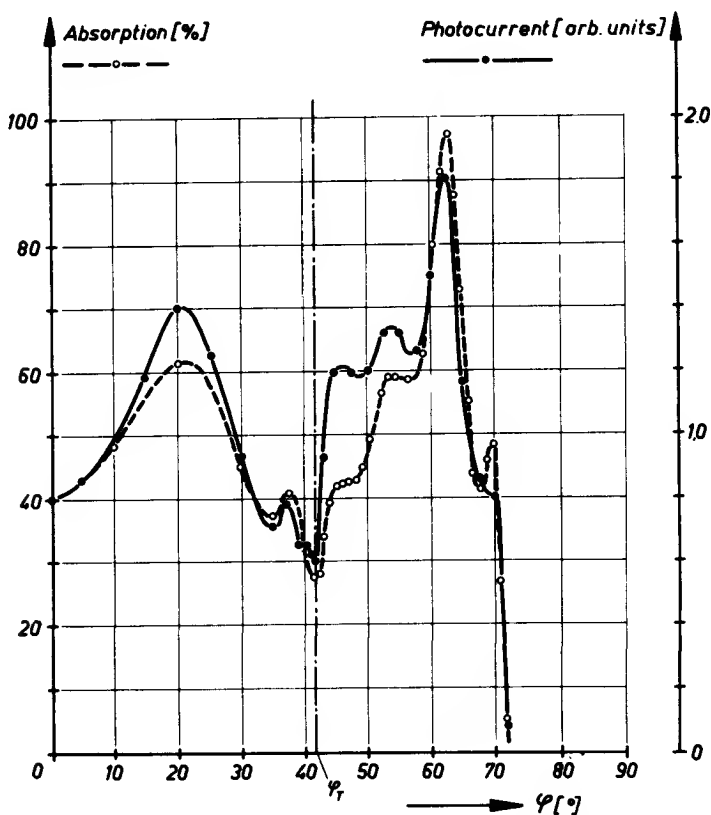
FIG. 37. Absorption and photocurrent of a TRIC with Cs_3Sb film versus angle of incidence (parallel component).
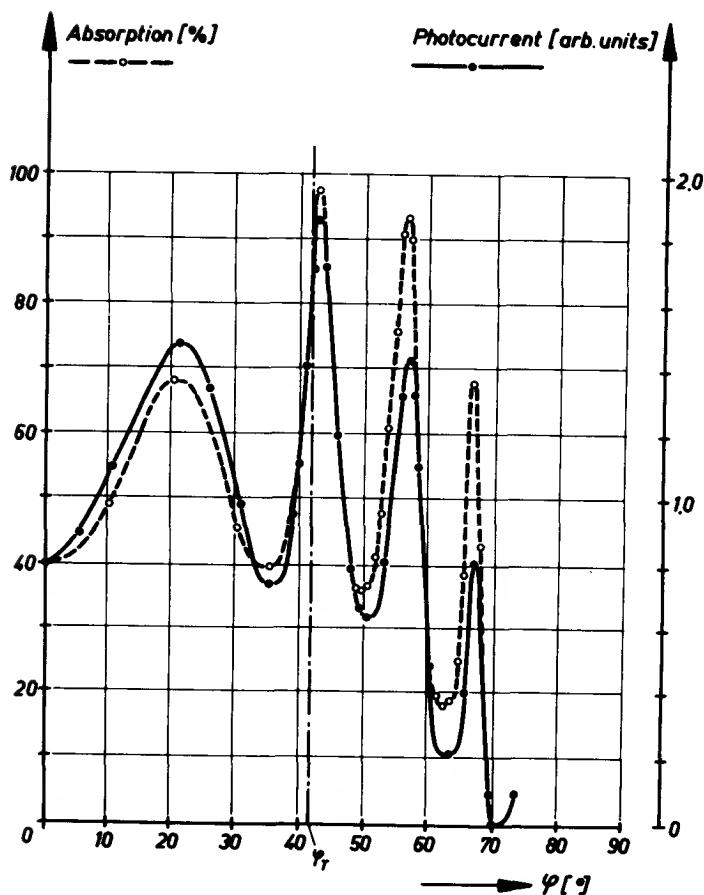
FIG. 38. Absorption and photocurrent of a TRIC with Cs_3Sb film versus angle of incidence (perpendicular component).

d. TRIC with S-11 Film. The absorption and the photocurrent of a TRIC comprising a 25 nm Cs_3Sb film–SiO_2 film (phase adaptation)–TiO_2 film (amplitude adaptation) are shown for both components in Figs. 37 and 38. In this system the functions r_{34}^2 (amplitude-adapting film) cross the functions r_1 (photoelectric film) at angles $\phi > \phi_T$. A phase-adapting film of appreciable thickness produces a close sequence of interference orders. Therefore a minimum of reflectance, a maximum of absorption, always falls in the vicinity of the crossing points. The maximum of induced absorption ($A = 97\%$) and the corresponding maximum of photoemission are observed at $\phi = 43°$ for the perpendicular component and at $\phi = 63°$ for the parallel component.

TABLE II

DATA OF CONVENTIONAL AND OF ADAPTED Cs_3Sb CATHODES

	Cs_3Sb film			TRIC		
	Angle	Absorption	Current	Angle	Absorption	Current
	φ (deg)	A (%)	i	φ (deg)	A (%)	i
Perpendicular	0	50	1.00	0	40	0.80
component	53	67	1.35	43	97	1.90
Parallel	0	50	1.00	0	40	0.8
component	75	86	2.00	63	97	1.8

The data of the adapted system are compared with those of the single photoelectric film in Table II.

Two results can be stated.

1. Complete absorption and correspondingly high photoemission can be achieved with the TRIC.

2. The quantum yield of the photoelectric film should be invariant if the film is incorporated into the adapting system and illuminated under the same angle of incidence. The absorption and the current should increase proportionally. Yet with increasing ϕ the yield of the TRIC decreases as compared to the single film. This effect is especially pronounced at the points of resonance. The high energy density strongly enhances even a very small intrinsic absorption or scattering in the phase- and amplitude-adapting films (*24*). With thinner adapting films this loss of energy would be reduced.

But the fact remains that the same or even higher emission than from a TRIC can be reached with a single film just by further tilting. For thinner cathode films a TRIC should finally dominate. However the application of very thin Cs_3Sb films seems to be blocked by their vanishing conductivity (*19*).

e. Photoemission of Thin Gold Films. Measurements of the absorption and photocurrent of gold films illuminated by ultraviolet ($\lambda = 253.7$ nm) indicate a potential use of the TRIC. In Figs. 39 and 40 the absorption and photocurrent of two Au films, 3 nm and 13.5 nm thick, are plotted versus angle of incidence. Table III sums up the results of measurements with parallel polarized light.

At normal incidence the 3-nm film emits the same photocurrent but absorbs only half the energy as the 13.5-nm film; i.e., the quantum yield is twice
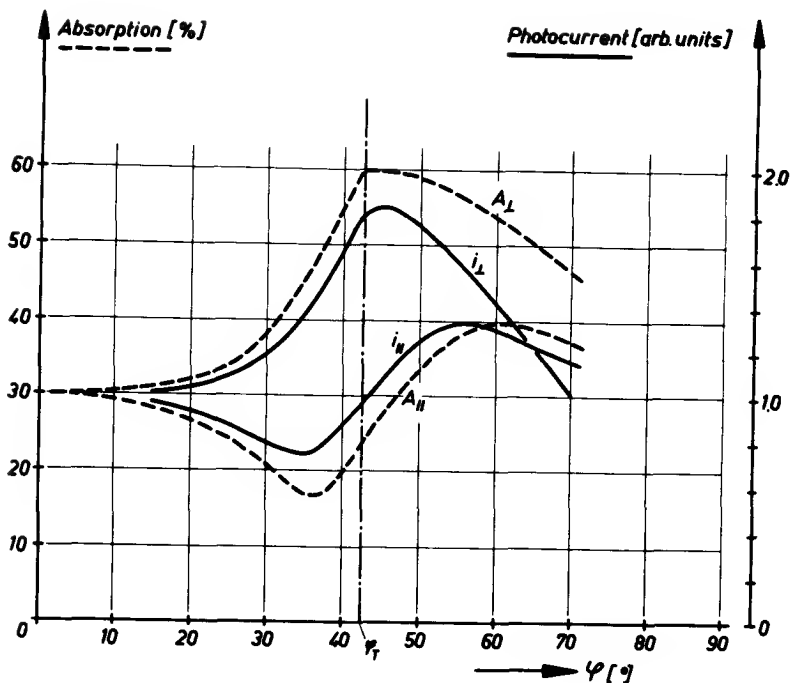
FIG. 39. Absorption and photocurrent of a gold film ($t = 3$ nm) versus angle of incidence.
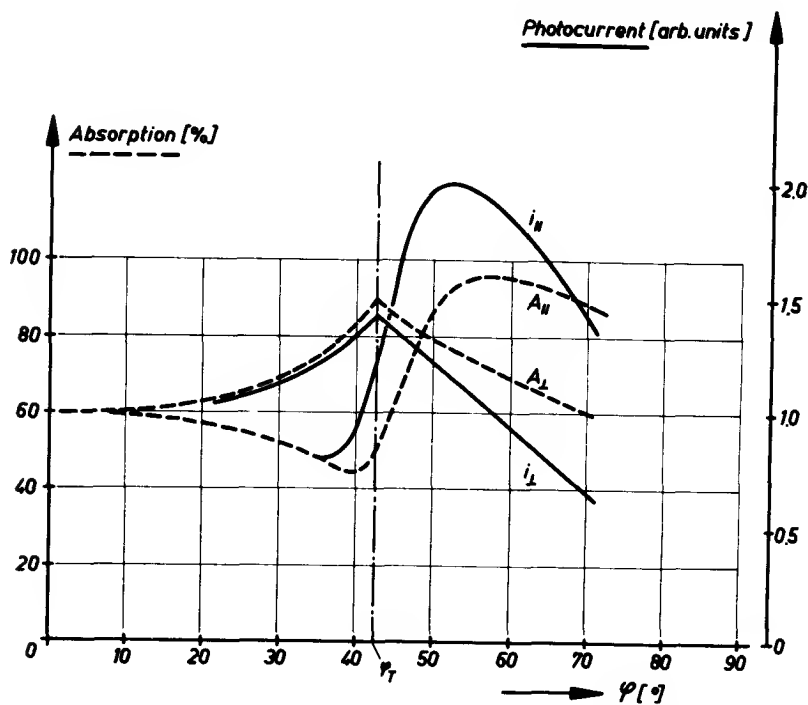
FIG. 40. Absorption and photocurrent of a gold film ($t = 13.5$ nm) versus angle of incidence.

TABLE III

DATA FOR GOLD CATHODES

Thickness of Au film (nm)	Angle φ (deg)	Absorption A (%)	Current i	Angle of max $i_\parallel \varphi^*$	Absorption $A_\parallel^*$ (%)	Current $i_\parallel^*$
3	0	30	1.0	55	37	1.33
13.5	0	60	1.0	52	96	2.0
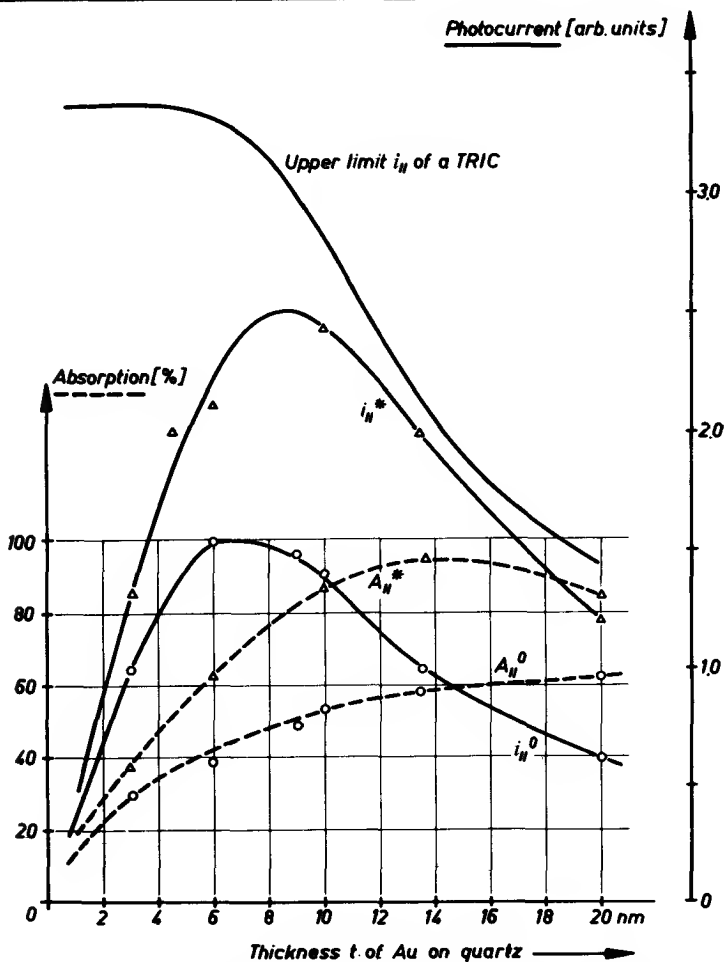
FIG. 41. Absorption (A^0) and photocurrent (i^0) of gold films at normal incidence and at the angle of maximum absorption (A^*, i^*) versus film thickness. TRIC curve represents the theoretical maximum photocurrent.

as high. At oblique incidence (ϕ^*) the maximum of the photocurrent is smaller for the thin film but the yield is still higher than that for the thick one. By adapting to form a TRIC the photocurrent of the thick film can be unessentially enhanced by the gain factor $1/A_{21} = 1.0/0.96 = 1.04$ from 2.0 to 2.08. The emission of the thin film can be increased considerably by a factor 2.7 to 3.6. To supplement this promising example measurements on Au films with parallel polarized light in the thickness range 3–200 nm are given in Fig. 41. The absorption and photocurrent at normal incidence (A_0, i_0) and at the angle ($50° < \phi^* < 55°$) of maximum photocurrent (A^*, i^*) are plotted versus film thickness. The photocurrents are normalized to the values of the films discussed in Table III.

The maxima of the photocurrent curves indicate that the attenuation length of electrons in gold is about 7 nm.

The upper curve in Fig. 41 represents the theoretical maximum photocurrent. By adapting the photoelectric film in a TRIC the photocurrent $i^*(t)$ is increased by the factor $1/A^*$. But only with films thinner than the attenuation length of electrons would the gain be attractive. Comparing the data of cesium–antimony and cesiumoxide films with gold films it is obvious that the conventional cathodes correspond to the 13.5-nm-thick gold film with its limited enhancement. These cathodes are too thick, thicker than the attenuation length of electrons. Aiming at the high photoemission of TRIC with conventional cathode materials, one has first to prepare cathodes that are thinner than conventional ones.

VI. Summary

The main object of interference cathodes is to enhance the photoemission of conventional cathodes by purely optical means. Film packets as the combination of a photoemissive film with dielectric films behave as damped light-resonators. Properly adapted and tuned to resonance these cathode systems give at the same time maxima of induced absorption and photoemission.

By varying the thickness of the system the loop of the electric vibration, the local maximum of absorption, the starting place of photoelectrons is shifted through the cathode. Due to this effect the emission depth of photoelectrons could be measured.

Yield and spectral response of three types of interference cathodes were examined:

1. the transmissive interference cathode (TIC),
2. the reflective interference cathode (RIC),
3. the totally reflective interference cathode (TRIC).

In the TIC—also in the single unadapted film on glass—the loop of the standing light wave is always positioned at the vacuum boundary. Most of the photoelectrons are produced directly under the emitting surface. The inherent high yield of the conventional transmissive cathode can be further enhanced by combining it with amplitude- and phase-adapting films into a nonreflecting TIC system. Gain factors of 1.3–1.6 for TIC's with cesium oxide, cesium–antimony, and multialkali films have been accomplished.

The high energy density at the vacuum boundary of the TIC is obtained at the expense of enhanced transmittance. This light can be arrested and used for the photoeffect, too, by illuminating the cathode in the angle range for total reflection.

For achieving a high photocurrent with monochromatic linearly polarized light, the TRIC system seems ideal. It can always be tuned to zero reflectance and zero transmittance, even with very thin cathode films, thinner than the emission depth of photoelectrons. The photoelectric films are nearly self-adapted at total reflection, giving gain factors of about 2 by switching from normal to oblique incidence. These cathodes are too thick for a further significant enhancement of photocurrents with TRIC. However experiments with Au cathodes indicate that higher gains can be achieved with cathode films thinner than the emission depth of photoelectrons.

Highest photocurrents have been reached with RIC at normal incidence. In the case of tuning the cathode to the visible spectral range one gets the loop of the enhanced resonance vibration positioned at the vacuum boundary by evaporating the conventional photoelectric film directly onto a highly reflecting mirror. The system is in this way nearly self-adapted.

A phase-adapting dielectric film between the photoelectric film and the mirror tunes the cathode to the near-infrared spectral range. Gain factors up to 3.7 were realized, increasing the sensitivity of multialkali films from 180 to 450 μA/lm. Even higher gain factors should be attainable with thinner photoelectric films.

The photoemission is governed by solid state physics and optics. Resonance phenomena of stationary light waves have to be taken into account not only with the cathodes but with all the photon–electron or photon–photon interactions in thin films.

REFERENCES

1. P. Goerlich, *Z. Physik* **101**, 335 (1936); *Phys. Status Solidi.* **3**, 963 (1963); "Photoeffekte," Vol. 1–4. Akad. Verlagsges., Leipzig, 1962.

2. W. Spicer, *Phys. Rev.* **112**, 114 (1958); *J. Appl. Phys.* **31**, 2077 (1960).

3. H. Thomas and H. Mayer, *Z. Physik* **147**, 419 (1957); *Proc. Intern. Symp., Basic Problems in Thin Film Physics, Clausthal, 1965*, p. 307 (1965); "Vandenhoek a. Ruprecht," Göttingen, 1966.
4. J. Scheer and J. van Laar, *Solid State Commun.* **3**, 189 (1965).
5. D. Kossel, D.B. Pat. 910,570 (1952); U.S. Pat. 2,972,691.
6. K. Deutscher, *Naturwissenschaften* **44**, 486 (1957); *Z. Physik* **151**, 536 (1958); *Verhandl. Phys.* **10**, 131 (1959).
7. M. Novice and J. Vine, private communication, 1966.
8. J. Love and J. Sizelove, *Appl. Opt.* **7**, 11 (1968).
9. J. Burton, *Phys. Rev.* **72**, 531A (1947).
10. B. Dyatlovitskaya, *Zh. Tekhn. Fiz.* **22**, 84 (1952).
11. K. Hirschberg and K. Deutscher, *Phys. Status Solidi.* **26**, 527 (1968).
12. D. Kossel, *J. Opt. Soc. Am.* **53**, 1355 (1963).
13. W. Schmidt, unpublished thesis, Marburg Univ., 1961.
14. E. Fermi, "Nuclear Physics." Univ. of Chicago Press, Chicago, Illinois, 1950.
15. M. Hebb, *Phys. Rev.* **81**, 707 (1951).
16. R. Lye and A. Decker, *Phys. Rev.* **107**, 977 (1957).
17. W. Spicer, *J. Phys. Chem. Solids* **22**, 365 (1961).
18. H. Hofmann, unpublished thesis, Giessen Univ., 1969.
19. K. Deutscher and K. Hirschberg, *Phys. Status Solidi.* **27**, 145 (1968).
20. L. N. Hadley and D. M. Dennison, *J. Opt. Soc. Am.* **37**, 451 (1947); **38**, 483 (1948).
21. S. Weber, "Report on Reflective Interference Cathodes," AEG-Telefunken, Berlin, 1968.
22. D. Kossel, D.B. Pat. 1,055,710 (1959); U.S. Pat. 3,043,976 (1962).
23. D. Rusch, unpublished thesis, Giessen Univ., 1965.
24. D. Kossel, *Z. Physik.* **126**, 233 (1949).
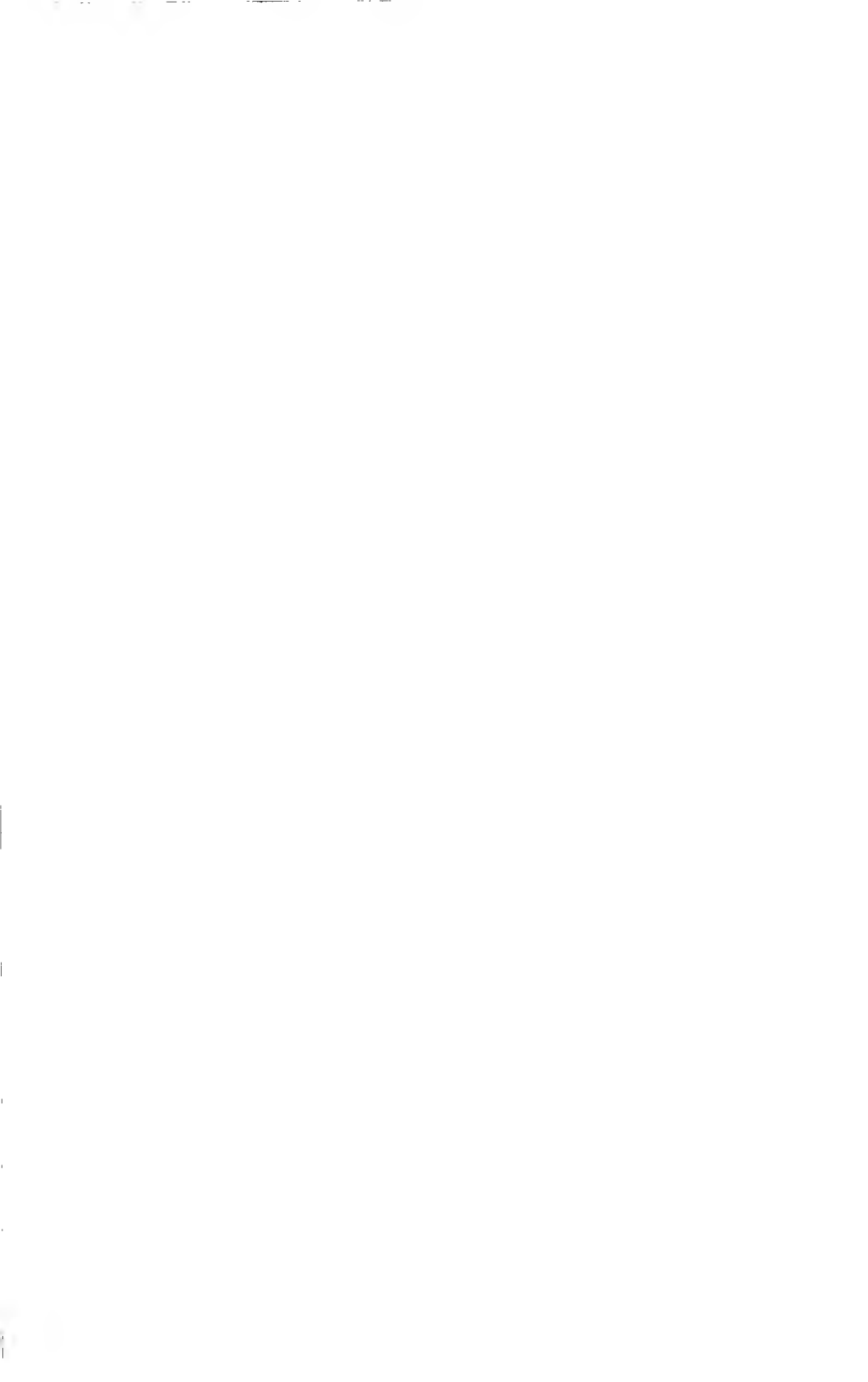
Design of Multilayer Interference Filters

Alfred Thelen

Optical Coating Laboratory, Inc.
Santa Rosa, California

I. Introduction

1. General

The manufacture of complicated multilayer interference filters has recently become a rather routine industrial process. As a result these filters are widely used in optics.

Compared to other types of filters (absorbing glass, liquid filters, gelatine filters, dispersion filters, crystal filters, etc.) their major advantages are:

1. an unlimited variety of filter characteristics can be achieved;

2. the filter characteristics can be shifted in regard to wavelength by changing the thicknesses of the individual films;

3. the losses are small (the energy which is not transmitted is virtually all reflected);

4. they can be applied to oddly shaped substrates;

5. they can be made to be mechanically rugged and environmentally stable.

Their main disadvantages are:

1. they change their characteristics with the angle between the filter and the direction of the incident energy;

2. they are very difficult to produce.

It is the purpose of this paper to describe methods for the design of long-wavelength- short-wavelength- and band-pass multilayer interference filters using nonabsorbing films. The application of interference films is of course not limited to these types of filters. Antireflection coatings, beam splitters, neutral density filters, color correction filters, and polarizing filters are examples of other coatings not discussed here. We also exclude filter coatings which use one or several metal films (metal-dielectric band-pass filters, metallic beam splitters, dark mirrors, etc.).

Figure 1 shows the construction of a typical multilayer interference filter.
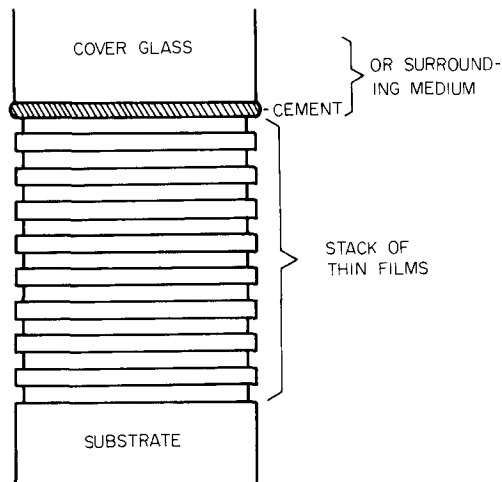
FIG. 1. Construction of a typical multilayer interference filter.

It consists of a substrate, which serves as mechanical support, and a stack of thin films. Sometimes a transparent cover is cemented to the filter for protection.

Multilayer interference filters are normally produced by vacuum deposition. The well-cleaned substrate is placed inside a vacuum chamber in which a

vacuum of at least 10^{-4} Torr can be maintained. The substrate is exposed to glow–discharge cleaning and heat to assure good adhesion and hardness of the coating. Layer after layer is deposited by thermally evaporating suitable coating materials. Elaborate schemes are used to control the thickness of each layer as precisely as possible. The substrate is normally rotated during deposition to assure uniformity of thickness over the whole filter. Although there is extensive literature available on how to produce filter coatings (*1–3*), it takes extensive experience and high technical sophistication to end up with a spectrally good filter coating which stays on the substrate and withstands handling and special environments.

2. Substrates and Media

The selection of the proper substrate for a filter coating is often a difficult compromise between optical and mechanical performance. A good substrate should:

1. withstand a vacuum environment at an elevated temperature (often up to 300°C);

2. withstand glow–discharge cleaning;

3. have a transmittance characteristic which aids the desired filter characteristic by having high transmittance in the pass band and low transmittance in as much of the rejection region as possible;

4. be compatible with the coating materials (some coating material and substrate combinations do not adhere well to each other, other combinations develop fine cracks in the coating, etc.);

5. be a material which is optically homogeneous and accepts optical polishing;

6. withstand the same handling and special environment as required of the filter.

TABLE I

Commonly Used Substrate Materials

Material	Approximate index of refraction	Usable wavelength region (μ)
Sapphire	1.7	<0.2–55
Synthetic quartz	1.45	<0.2–4.0 and from 45 on
Glass	1.5–1.7	0.35–2.5
Silicon	3.45	1.2–50
Germanium	4.0	1.8–25
MgF_2 (Irtran 1)	1.38	0.5–9
ZnS (Irtran 2)	2.2	0.7–14.5

Some commonly used substrate materials are listed in Table I. In addition to the wavelength regions of high and low transmittance the average index of refraction in the high transmittance region is given. Incidentally, the index of refraction is the only property of the substrate which enters directly into the design of the filter.

Similarly, the index of refraction of the surrounding medium enters into the design of the filter. Typically, only three cases occur: The surrounding medium is air ($n_M = 1.0$), water ($n_M = 1.33$) or a cement ($n_M = 1.45$).

3. Absorbing Filters

Very often the design of a multilayer interference filter can be simplified by using a suitable absorption-type filter as substrate or in series with the multilayer interference filter. References 4–6 contain many possibilities. It is generally easy to find good absorption-type long-wavelength-pass filters. It is much more difficult to find suitable short-wavelength-pass or band-pass filters.

4. Coating Materials

One of the greatest limitations in the applications of thin films is that only very few nonabsorbing materials are suitable for vacuum deposition. Consequently, by far the largest effort in thin film research is directed towards the search for new materials, material preparation techniques, and deposition methods. Most filter types can be realized with configurations using only two different coating materials, one material with a high index of refraction and one material with a low index of refraction. The further the two indices are apart the easier is the design. In the middle-infrared region (1.8–8 μ) the best choice available is: germanium as high-index material and silicon monoxide as low-index material. In the visual and near-infrared region (0.4–1.8 μ) zinc sulfide and titanium dioxide are used as high-index materials and magnesium fluoride and silicon oxide as low-index materials. In the near-ultraviolet (0.2–0.4 μ) and the far-infrared region (8–50 μ) some filters are possible but the available materials yield only small index spreads and are very difficult to deposit. Outside these regions no coating material combinations are available at present and consequently no interference filters can be made.

The same way as absorption in the substrate can aid a desired filter characteristic, absorption in the coating material can too. For example, the absorption of germanium below 1.8 μ eliminates the need for blocking in the visual region if a quartz substrate is used.

Table II lists some coating materials which will be used later in design examples.

TABLE II

COATING MATERIALS

Material	Approximate index of refraction	Useful wavelength region (μ)
NaAlF$_2$	1.35	<0.2–10
MgF$_2$	1.38	<0.2–5
SiO$_2$	1.45	0.2–8
Si$_2$O$_3$	1.55	0.3–8
Al$_2$O$_3$	1.69	0.2–7
SiO	1.85	0.8–7
ZrO$_2$	2.1	0.25–7
CeO$_2$	2.30	0.4–5
ZnS	2.30	0.4–15
TiO$_2$	2.30	0.4–12
Si	3.40	0.9–8
Ge	4.0	1.3–35

5. TYPES OF FILTERS

In the interference filter field it is customary to present the transmittance and reflectance characteristics as functions of the wavelength. Yet the performance of most multilayer interference systems is more easily described as a function of frequency. We will use both presentations: frequency for theoretical studies and wavelength for practical filter examples. We have to remember, though, that a short-wavelength-pass filter is equivalent to a high-frequency-pass filter and a long-wavelength-pass filter to a low-frequency-pass filter.
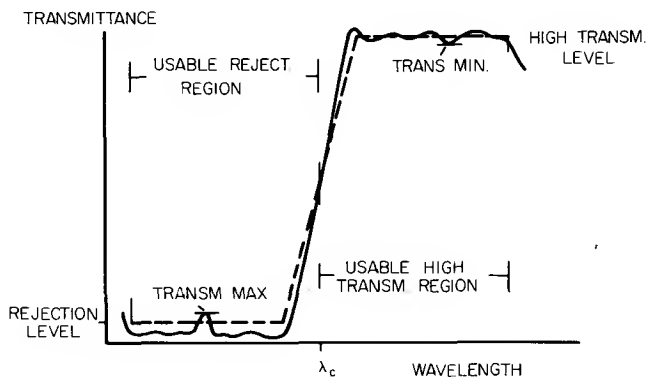
FIG. 2. Typical long-wavelength-pass filter characteristic.

TRANSMITTANCE

HIGH TRANSM.
LEVEL

TRANSM. MIN.

USABLE REJECT.
REGION

USABLE HIGH
TRANSM. REGION

TRANSM. MAX.

REJECTION
LEVEL
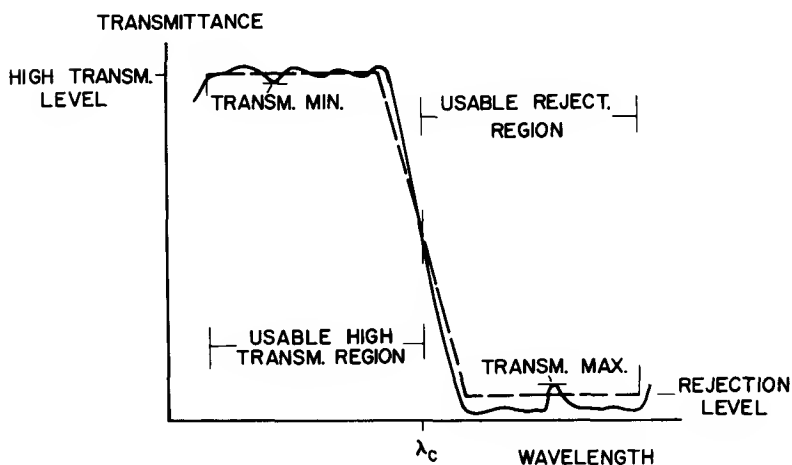
λ_c WAVELENGTH

FIG. 3. Typical short-wavelength-pass filter characteristic.

TRANSMITTANCE

HALF - BANDWIDTH
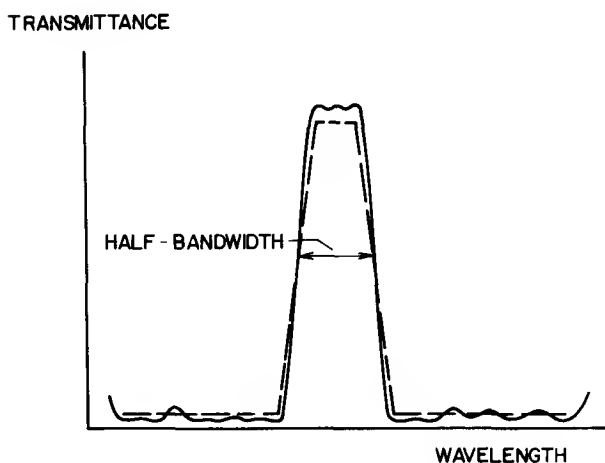
WAVELENGTH

FIG. 4. Typical band-pass filter characteristic.

Figures 2–4 show the idealized filter characteristics of a long-wavelength-pass, short-wavelength-pass, and band-pass filter. In practice, the filter performance is described with the following terms:

1. cut-on and/or cutoff wavelength with allowable slopes;

2. spectral width of the high transmittance region with average transmittance level and allowable transmittance minima;

3. spectral width of the rejection region with low transmittance level and allowable transmittance maxima.

Table III gives a typical specification for an infrared multilayer interference filter.

<div align="center">TABLE III</div>

<div align="center">SPECIFICATION OF AN INFRARED FILTER</div>

Substrate:	Vycor (7905)
Thickness	0.020 in. (nominal)
Size	0.75×1.50 in. $+0.000$ in.
	-0.010 in.
Wavelength of peak transmission:	2.732 μ (nominal)
Peak transmission	40%
Wavelengths within which transmission is 50% of peak:	2.705 and 2.759 μ
Wavelengths within which transmission is 5% of peak:	2.686 and 2.778 μ
Wavelengths within which transmission is 0.01%	
(absolute):	2.650 and 2.814 μ

Transmission is to remain less than 0.01% (outside the pass band defined above) for all other wavelengths less than 4.5 μ.

II. Theoretical Basis

Let us try to generate the previously described filter characteristics with the following model of a multilayer interference filter (Fig. 5).

A layered optical medium or multilayer extends in space from $z = z_a$ to $z = z_b$ $(z_a < z_b)$. The extension in planes perpendicular to the z direction is very large compared to $z_b - z_a$. The index of refraction n varies with z but is constant in the planes perpendicular to the z direction. $n = n(z)$ is given as a real function (no absorption). The optical media in the regions $z < z_a$ and $z > z_b$ can be another multilayer, a substrate, or a surrounding medium (for example, air).

We call the multilayer homogeneous when, except for first order discontinuities, $n = $ const (Fig. 6).

We call the multilayer symmetrical when

$$n(\tfrac{1}{2}(z_a + z_b) + x) = n(\tfrac{1}{2}(z_a + z_b) - x), \qquad z \leq \tfrac{1}{2}(z_b - z_a) \qquad (1)$$

1. THE MULTILAYER MATRIX

If a plane electromagnetic wave propagates in the z direction, through this multilayer the electrical field $E(z_a)$ and the magnetic field $H(z_a)$ are related to the fields $E(z_b)$ and $H(z_b)$ by the following equations (7–9):

$$Q(z_a) = M(z_a - z_b) \cdot Q(z_b)$$

$$\left\{ \begin{matrix} E(z_a) \\ H(z_a) \end{matrix} \right\} = \left\{ \begin{matrix} M_{11} & jM_{12} \\ jM_{21} & M_{22} \end{matrix} \right\} \cdot \left\{ \begin{matrix} E(z_b) \\ H(z_b) \end{matrix} \right\} \tag{2}$$

where the matrix elements are the solutions at the position $z = z_b$ of the following set of four simultaneous differential equations of the first order:

$$\begin{aligned} M'_{11} &= -(2\pi/\lambda)n(z)^2 M_{12} \\ M'_{12} &= (2\pi/\lambda)M_{11} \\ M'_{21} &= (2\pi/\lambda)n(z)^2 M_{22} \\ M'_{22} &= -(2\pi/\lambda)M_{21} \end{aligned} \tag{3}$$

with the initial conditions:

$$M_{11}(z_a) = 1, \qquad M_{12}(z_a) = 0, \qquad M_{21}(z_a) = 0, \qquad M_{22}(z_a) = 1 \tag{4}$$

The very significant feature of these equations is that the multilayer can be represented by a two by two matrix which is completely independent of the optical media at $z < z_a$ and $z > z_b$.
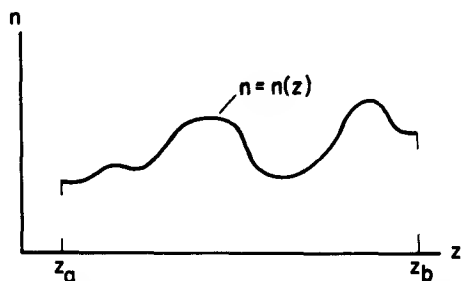
FIG. 5. Refractive index variation of a multilayer filter.
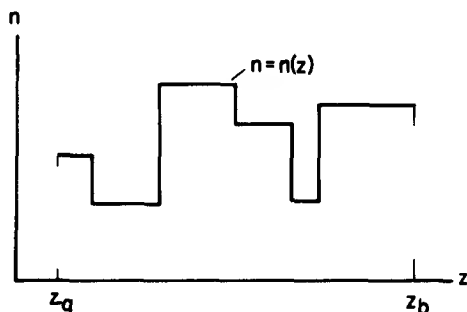
FIG. 6. Refractive index variation of a homogeneous multilayer filter.

2. Rules of Matrix Multiplication

Very little knowledge of matrix theory is required in the design of multi-layer interference filters. In essence, a matrix is an array of numbers consisting of p rows and q columns which obey certain formal rules of addition and multiplication with other matrices and vectors. In our case the matrices all have two rows and two columns; the elements in the leading diagonal are real and purely imaginary elsewhere. Only the operation of multiplication is encountered, which is defined as follows (rows times columns rule):

$$\begin{vmatrix} A_{11} & jA_{12} \\ jA_{21} & A_{22} \end{vmatrix} \begin{vmatrix} B_{11} & jB_{12} \\ jB_{21} & B_{22} \end{vmatrix} = \begin{vmatrix} A_{11}B_{11} - A_{12}B_{21} & j(A_{11}B_{12} + A_{12}B_{22}) \\ j(A_{21}B_{11} + A_{22}B_{21}) & -A_{21}B_{12} + A_{22}B_{22} \end{vmatrix}$$

$$= \begin{vmatrix} C_{11} & jC_{12} \\ jC_{21} & C_{22} \end{vmatrix} \tag{5}$$

the product being again a two by two matrix with the imaginary elements at the same positions. This makes the numerical work in forming a product no greater than that for wholly real matrices. Matrix multiplication is associative:

$$(A \cdot B) \cdot C = A \cdot (B \cdot C)$$

but in general not commutative:

$$A \cdot B \neq B \cdot A$$

3. The Multilayer Matrix as a Product of Component Matrices

It is evident from Eq. (2) that if we would divide the region z_a to z_b into two parts, z_a to x and x to z_b, we would arrive at the following two relations:

$$Q(z_a) = M(z_a - x) Q(x), \qquad Q(x) = M(x - z_b) Q(z_b)$$

$$Q(z_a) = M(z_a - x) \cdot M(x - z_b) \cdot Q(z_b)$$

$$M(z_a - z_b) = M(z_a - x) \cdot M(x - z_b) \tag{6}$$

which means that the matrix of a multilayer can be expressed as the product of the matrices of its parts.

4. Relation between the Elements of a Multilayer Matrix

We can conclude from Eqs. (3) that

$$M'_{12} M_{21} + M_{11} M'_{22} = 0, \qquad M'_{11} M_{22} + M_{12} M'_{21} = 0$$

which means that

$$(d/dz)(M_{11}M_{22} + M_{12}M_{21}) = 0$$

or

$$M_{11}M_{22} + M_{12}M_{21} = \text{const}$$

and with Eqs. (4)

$$M_{11}M_{22} + M_{12}M_{21} = 1. \tag{7}$$

5. Reversing the Order of a Multilayer

Equation (2) relates the fields at the position z_a to the fields at z_b. It is possible to relate the fields at z_b to the fields at z_a without recomputing the multilayer matrix.

We can write Eq. (2) in the following manner:

$$Q(z_b) = M^{-1}(z_a - z_b)\, Q(z_a).$$

In order to evaluate M^{-1} we can write

$$M^{-1} = \begin{Bmatrix} X_{11} & jX_{12} \\ jX_{21} & X_{22} \end{Bmatrix}$$

and

$$\begin{Bmatrix} M_{11} & jM_{12} \\ jM_{21} & M_{22} \end{Bmatrix} \cdot \begin{Bmatrix} X_{11} & jX_{12} \\ jX_{21} & X_{22} \end{Bmatrix} = \begin{Bmatrix} 1 & 0 \\ 0 & 1 \end{Bmatrix}$$

which yields

$$X_{11} = M_{22}; \qquad X_{12} = -M_{12}; \qquad X_{21} = -M_{21}; \qquad X_{22} = M_{11}.$$

Consequently

$$M^{-1}(z_a - z_b) = \begin{Bmatrix} M_{22} & -jM_{12} \\ -jM_{21} & M_{11} \end{Bmatrix}. \tag{8}$$

We can use this relation (8) to relate the matrices of a multilayer used in opposite directions. Replacing z by $-z$ in Eqs. (3) yields:

$$M_{11}(z) = M_{11}(-z); \qquad M_{12}(z) = -M_{12}(-z)$$
$$M_{21}(z) = -M_{21}(-z); \qquad M_{22}(z) = M_{22}(-z);$$

Inserting these relations into Eq. (8) we can establish the following relation:

$$M(z_b - z_a) = \begin{Bmatrix} M_{22} & jM_{12} \\ jM_{21} & M_{11} \end{Bmatrix} \tag{9}$$

which means that by merely exchanging M_{11} with M_{22} we arrive at the matrix of a multilayer arranged in reverse order.

6. Transformation to Optical Thickness

It is often desirable to use optical thicknesses rather than physical thicknesses. We can make this transition with the following transformation:

$$u = (\pi/\lambda_0) \int_0^z n(x)\, dx \qquad (10)$$

which mathematically is a Liouville transformation. Equations (3) assume then the following shape:

$$
\begin{aligned}
M'_{11} &= -(2\lambda_0/\lambda)n(u)\, M_{12} \\
M'_{12} &= (2\lambda_0/\lambda)(1/n(u))M_{11} \\
M'_{21} &= (2\lambda_0/\lambda)n(u)\, M_{22} \\
M'_{22} &= -(2\lambda_0/\lambda)(1/n(u))M_{21}.
\end{aligned}
\qquad (11)
$$

7. Reflectance and Transmittance of a Multilayer

Following Abelès (7) and Born and Wolf (8) the complex reflection and transmission coefficients r and t of a plane electromagnetic wave propagating in the z direction through the multilayer are given by the following relations:

$$r = \frac{n_M M_{11} + jn_M n_S M_{12} - jM_{21} - n_S M_{22}}{n_M M_{11} + jn_M n_S M_{12} + jM_{21} + n_S M_{22}} \qquad (12)$$

$$t = 2n_M(n_M M_{11} + jn_M n_S M_{12} + jM_{21} + n_S M_{22})^{-1}, \qquad (13)$$

where M_{11}, M_{12}, M_{21}, M_{22} are the elements of the multilayer matrix, n_S the constant index of refraction for $z > z_b$, and n_M the index for $z < z_a$.

From relations (12) and (13) we can derive the relation for the energy reflectance and transmittance R and T:

$$T = 1 - R = 4\left(2 + \frac{n_M}{n_S} M_{11}^2 + \frac{n_S}{n_M} M_{22}^2 + n_M n_S M_{12}^2 + \frac{1}{n_S n_M} M_{21}^2\right)^{-1} \qquad (14)$$

and for the phases upon reflection and transmission:

$$\tan \gamma_t = -\frac{M_{21} + n_M n_S M_{12}}{n_M M_{11} + n_S M_{22}}$$

$$\tan \gamma_r = 2\frac{n_S M_{12} M_{22} - (1/n_S)M_{21}M_{11}}{(n_M/n_S)M_{11}^2 - (n_S/n_M)M_{22}^2 + n_M n_S M_{12}^2 - (1/n_M n_S)M_{21}^2} \qquad (15)$$

8. Invariance of Reflectance and Transmittance to Index Changes

The transmittance, reflectance, and phase of transmittance of a nonabsorbing multilayer are invariant to multiplying all indices of refraction (multilayer, substrate, and medium) with a constant factor or replacing all indices of refraction by their reciprocal value.

The phase of reflectance is only invariant to constant factor changes. Replacing all indices by their reciprocal values results in a phase change of π.

Examples. The following multilayers exhibit the same transmittance reflectance, phase of transmittance, and phase of reflectance ($+\pi$ for System III):

System I	System II	System III
$n_S = 2.0$	$n_S = 4.0$	$n_S = 1/2$
$n_H = 2.5$	$n_H = 5.0$	$n_H = 1/2.5$
$n_L = 1.5$	$n_L = 3.0$	$n_L = 2/3$
$n_M = 1.0$	$n_M = 2.0$	$n_M = 1.0$

Proof. Replace $n(u)$ in Eq. (11) by $f(u) = A\, n(u)$ or by $f(u) = 1/n(u)$. Calculate the new matrix elements and insert into Eqs. (12)–(15).

9. Homogeneous Films

If the multilayer consists of homogeneous films only the evaluation of the multilayer matrix can be greatly simplified. For $n = $ const, Eqs. (3) yield the following solutions:

$$M_{11} = M_{22} = \cos[(2\pi/\lambda)nd]$$
$$M_{12} = (1/n)\sin[(2\pi/\lambda)nd] \qquad (16)$$
$$M_{21} = n\sin[(2\pi/\lambda)nd],$$

where d is the physical thickness of the film. Or

$$M_{(\text{single})\text{film}} = \begin{Bmatrix} \cos[(2\pi/\lambda)nd] & j(1/n)\sin[(2\pi/\lambda)nd] \\ jn\sin[(2\pi/\lambda)nd] & \cos[(2\pi/\lambda)nd] \end{Bmatrix}. \qquad (17)$$

In order to evaluate the matrix M of a multilayer which consists of p individual homogeneous films we use Eq. (6):

$$M = M_1 M_2 M_3 \cdots M_p, \qquad (18)$$

where $M_1, \ldots, M_p$ are the matrices of the individual homogeneous films and have the form as given in Eq. (17).

10. Multilayers with Periodic Structures

Let us study a multilayer which consists of a submultilayer repeated p times. If the matrix of the submultilayer is

$$A = \begin{Bmatrix} A_{11} & jA_{12} \\ jA_{21} & A_{22} \end{Bmatrix};$$

then the matrix of the periodic multilayer is according to Eq. (6)

$$M = A^P = \begin{Bmatrix} A_{11} & jA_{12} \\ jA_{21} & A_{22} \end{Bmatrix}^P.$$

According to Abelès (7) this matrix can be written in the following way:

$$M = A^P = \begin{Bmatrix} A_{11} S_{p-1}(x) - S_{p-2}(x) & jA_{12} S_{p-1}(x) \\ jA_{21} S_{p-1}(x) & A_{22} S_{p-1}(x) - S_{p-2}(x) \end{Bmatrix}, \quad (19)$$

where

$$x = A_{11} + A_{22} \quad (20)$$

and the S_p are Chebyshev polynomials defined by the following equations:

$$S_p(x) = \frac{\sin(p+1)\theta}{\sin \theta}; \qquad x = 2\cos\theta, \quad |x| \leq 2$$

$$S_p(x) = \frac{\sinh(p+1)\theta}{\sinh \theta}; \qquad x = 2\cosh\theta, \quad |x| \leq 2. \quad (21)$$

Besides being of great theoretical importance these relations are of significant practical value in the computation of the matrix of a periodic multilayer. Chebyshev polynomials can be easily generated by their recurrence relation

$$S_p(x) - x S_{p-1}(x) + S_{p-2}(x) = 0 \quad (22)$$

and the first two polynomials:

$$S_0(x) = 1; \qquad S_1(x) = x.$$

It is generally easier to calculate the matrix of the periodic element and the associated Chebyshev polynomial than to perform p-matrix calculations.

III. Design Methods

It is obvious from the complexity of Eqs. (14) and (18) that the straightforward approach of inserting the desired spectral transmittance function

and solving for a set of individual film thicknesses and indices of refraction is extremely difficult and in general probably impossible. Even if it were possible, the results would only be of limited value since there are severe practical limitations on the choice of available refractive indices.

The following design methods were proposed in the literature:

1. breaking down a multilayer into groups of symmetrical film combinations, establishing equivalent indices of refraction and thicknesses, and matching the symmetrical film combinations (10);

2. relating the spectral transmittance to certain normalized polynomials (e.g., Chebyshev polynomials) and fitting these polynomials to the desired transmittance characteristic (11, 12) (this method is commonly used in the design of waveguide impedance transformers and filters at microwave frequencies and is, with modifications, applicable to multilayer filters);

3. calculating the partial derivatives of the transmittance to the individual film thicknesses of a design which only moderately approximates the desired characteristic, and solving for the thickness increments which provide a better fit [refining method (13, 14)];

4. adjusting the performance of a given multilayer by evaluating the reflectances of an effective interface inside the multilayer (15);

5. expressing the spectral transmittance as a Fourier series, establishing the required Fourier coefficients, and solving for the thicknesses and refractive indices of the individual films (16, 17);

6. using no particular starting design a proper design is built up step by step evaluating "merit functions" (14, 18);

7. graphical methods using vector charts.

Methods 1, 3, and 4 are used extensively in practice. Method 2 has led to interesting designs and is, due to its systematic approach, of great value. Methods 5 and 6 are very complex and do not appear to be fully developed yet. The graphical method 7 is generally used in the design of antireflection coatings, multilayers with fewer layers, and in the practical analysis of new designs.

IV. Equivalent Layers

According to Eq. (2) the matrix of a general nonabsorbing multilayer has the following form:

$$M = \begin{Bmatrix} M_{11} & jM_{12} \\ jM_{21} & M_{22} \end{Bmatrix}.$$

In the special case when $M_{11} = M_{22}$ we can define the following two quantities (10):

$$\Gamma_E = \text{equivalent thickness} = \arccos M_{11} = \arccos M_{22} \quad (23)$$

$$N_E = \text{equivalent index} = +\left(\frac{M_{21}}{M_{12}}\right)^{1/2}, \tag{24}$$

which transform matrix (2) into

$$M = \left\{ \begin{array}{cc} \cos \Gamma_E & j\left(\frac{M_{12}}{M_{21}}\right)^{1/2}(M_{12}M_{21})^{1/2} \\ j\left(\frac{M_{21}}{M_{12}}\right)^{1/2}(M_{12}M_{21})^{1/2} & \cos \Gamma_E \end{array} \right\}$$

$$= \left\{ \begin{array}{cc} \cos \Gamma_E & j\dfrac{1}{N_E}\sin \Gamma_E \\ jN_E \sin \Gamma_E & \cos \Gamma_E \end{array} \right\} \tag{25}$$

remembering that according to Eq. (7)

$$M_{12}M_{21} = 1 - M_{11}M_{22} = \sin^2 \Gamma_E.$$

With Eq. (8) we can prove that the matrix of a symmetrical multilayer satisfies the condition $M_{11} = M_{22}$. Only in this case is a multilayer invariant to arrangement in reverse order—which is another way of describing a symmetrical multilayer.

With this result and comparing matrices (25) and (18) we can state the following.

A symmetrical multilayer is equivalent to a single homogeneous film with index of refraction N_E and thickness Γ_E as defined by Eqs. (23) and (24).

We have to remember, however, that the matrix elements of Eq. (20) are functions of the wavelength. Consequently, N_E and Γ_E are also functions of the wavelength.

The usual way to compute N_E and Γ_E for homogeneous multilayers is to compute the multilayer matrix as a product of the matrices of the individual homogeneous layers [Eqs. (17) and (18)]. In the case of inhomogeneous layers it is very seldom possible to find closed solutions to Eqs. (3) or (11). But both numerical integration (Runge-Kutta–Gill's and Hamming's method) and approximation by many thin homogeneous layers lead to satisfactory results.

The computational efforts can be greatly reduced by the following set of theorems (19).

Theorem I. The equivalent index N_{E1} of a symmetrical multilayer with an index distribution $n_1 = A \cdot f(u)$ is A times the equivalent index N_{E2} of a multilayer with $n_2 = f(u)$ or

$$N_E(n = A \cdot f(u)) = A \cdot N_E(n = f(u)). \tag{26}$$

Theorem II. The equivalent thickness Γ_{E1} of a symmetrical multilayer with $n_1 = A \cdot f(u)$ is equal to the equivalent thickness Γ_{E2} of a multilayer with $n_2 = f(u)$ or

$$\Gamma_E(n = A \cdot f(u)) = \Gamma_E(n = f(u)). \tag{27}$$

Proof. Substitute n_1 into Eqs. (11) and absorb the constant factor A into M_{12} and M_{21}.

Example. $N_E(\text{Ge–ZnS}) = 1.75 N_E(\text{TiO}_2\text{–CaF}_2)$, $\Gamma_E(\text{Ge–ZnS}) = \Gamma_E(\text{TiO}_2\text{–CaF}_2)$; assuming that $n_{\text{Ge}} = 4.0$, $n_{\text{ZnS}} = 2.2$, $n_{\text{TiO}_2} = 2.3$, and $n_{\text{CaF}_2} = 1.26$.

Theorem III. The equivalent index N_{E1} of a symmetrical multilayer with $n_1 = f(u)$ is equal to the reciprocal value of the equivalent index of a multilayer with $n_2 = 1/f(u)$ or

$$N_E(n = f(u)) = 1/N_E(n = 1/f(u)). \tag{28}$$

Theorem IV. The equivalent thickness Γ_{E1} of a symmetrical multilayer with $n_1 = f(u)$ is equal to the equivalent thickness Γ_{E2} of a multilayer with $n_2 = 1/f(u)$ or

$$\Gamma_E(m = f(u)) = \Gamma_E(n = 1/f(u)). \tag{29}$$

Proof. Theorems III and IV are valid since replacing n by $1/n$ in Eqs. (11) is equivalent to exchanging M_{12} with M_{21} and M_{11} with M_{22}. Equations (11) are invariant to an exchange of M_{11} and M_{22} since the multilayer is assumed to be symmetrical [Eq. (9)]. Exchanging M_{12} with M_{21} leads to $N_{E1} = 1/N_{E2}$.

Example. Applying the four theorems in combination one can show that $N_E(LHL) = n_H n_L/N_E(HLH)$ and $\Gamma_E(LHL) = \Gamma_E(HLH)$. H stands for a high-index (n_H) film which is one-quarter wavelength thick at λ_0 and L for an equally thick low-index (n_L) film.

Theorem V. When the wavelength approaches infinity (or $\lambda_0/\lambda \to 0$), the equivalent index of a symmetrical multilayer is given by the following expression:

$$N_E(\lambda_0/\lambda \to 0) = \left[\int_{u_a}^{u_b} n \, du / \int_{u_a}^{u_b} du/n \right]^{1/2}. \tag{30}$$

Proof. This theorem follows from the expression given by Born and Wolf (*8*) for the matrix of a stratified medium as a pile of thin homogeneous films.

Example.

$$\lambda_0/\lambda \to 0; \qquad N_E((L/2)H(L/2)) = (n_H \cdot n_L)^{1/2}.$$
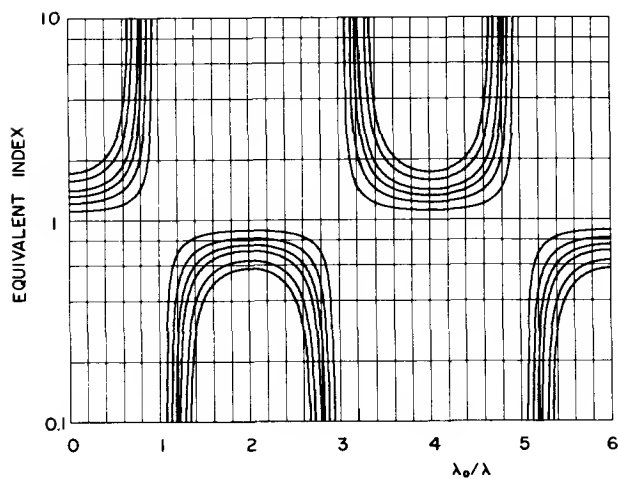
FIG. 7. Equivalent indices for the system $(L/2)H(L/2)$. $n_L = 1$ and n_H/n_L is parameter $n_H/n_L = 1.25, 1.50, 1.75, 2.0, 2.5, 3.0$. The curves with the wider stop band have the higher n_H/n_L values.
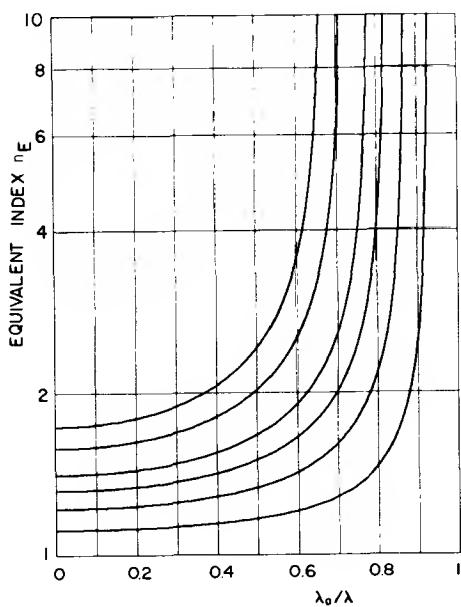
FIG. 8. Enlarged first part of Fig. 7.
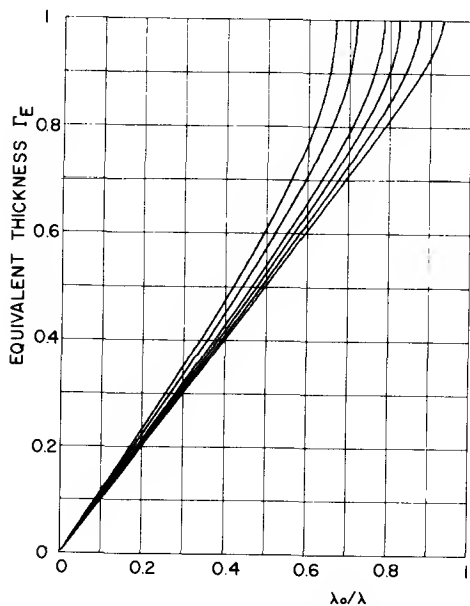
FIG. 9. Equivalent thickness of the system described in Fig. 7.
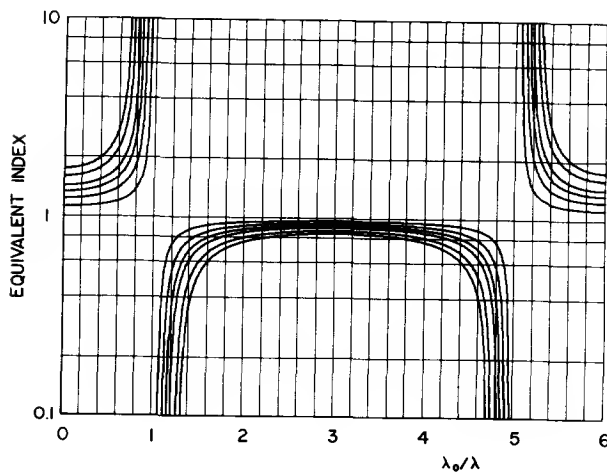
FIG. 10. Equivalent index for the system $LMHHML$. $n_L = 1.0$, $n_M = (n_L n_H)^{1/2}$, and $n_H/n_L = 1.25$, 1.5, 1.75, 2.0, 2.5, 3.0. Again, the curves with the wider stop band have the higher n_H/n_L values.
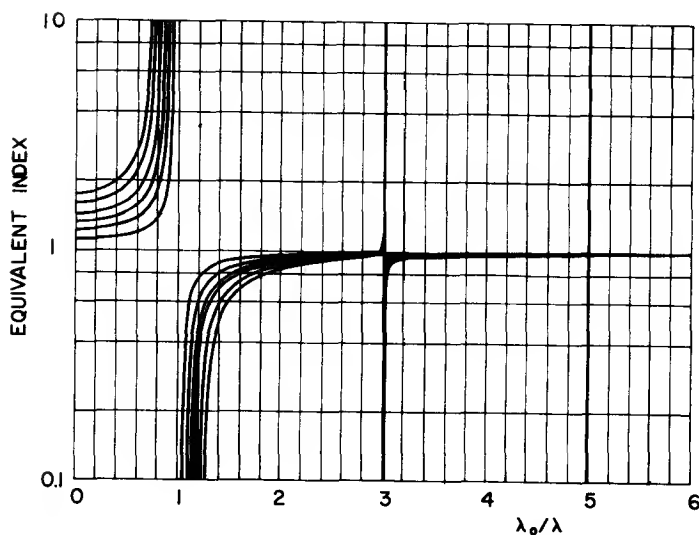
FIG. 11. Equivalent index for an inhomogeneous system where the index varies with the Jacobian elliptic function dn. As before, $n(0) = 1.0$ and $n_{max}/n_{min} = 1.25$, 1.50, 1.75, 2.0, 2.5, 3.0.

It is important to note that these theorems only hold when n is expressed as a function of the optical thickness. Yet they are valid for both homogeneous and inhomogeneous multilayers.

Figures 7–11 give examples of the characteristics of a variety of equivalent layers. The index distribution of all equivalent layers is normalized to $n(u_a) = n(u_b) = 1$. Theorems I and II allow the extension to other starting values. Only equivalent layers with $n(u)/n(0) > 1$ are given. Theorems III and IV allow the extension to $n(u)/n(0) < 1$. The semilogarithmic plot is intended to facilitate the extensions.

The computations for these and the following figures were carried out on an IBM 1620 computer with 20,000 storage locations. All curves are direct traces of an on-line IBM 1627 plotter.

Figures 7–9 apply to an equivalent layer with the homogeneous structure $(L/2) H (L/2)$, where $L/2$ stands for a low-index film which is one-eighth wave thick at λ_0 and H for a high-index film which is one-quarter wave thick at λ_0.

The characteristics are given for $n_L = 1$ and $r = n_H/n_L$ as parameter. Figure 7 gives the equivalent index as function of λ_0/λ. Figure 8 is an enlarged portion of Fig. 1 which, due to symmetries, contains all the information of Fig. 1 [Young (20)]. Figure 9 gives the equivalent thickness. Figure 10 gives the equivalent index of the homogeneous structure (21) $LMHHML$ with $n_M = (n_L \cdot n_H)^{1/2}$, $n_L = 1$, and $r = n_H/n_L$ as parameter. Figure 11 gives the

equivalent index of an inhomogeneous structure where the index of refraction varies according to the Jacobean elliptic function *dn*. Again $n(u_a) = n_{min} = 1$ and $r = n_{max}/n_{min}$ is a parameter. The inhomogeneous profile was approximated by 100 homogeneous layers.

Figures 7–11 contain regions in which no values are given. The equivalent index is then imaginary and the equivalent thickness complex. This region is of particular interest for a periodic multilayer consisting of an equivalent layer repeated *p* times. We can prove that in this case the transmittance of the periodic multilayer steadily decreases when we let *p* increase.

Definition (21) contains two versions for the Chebyshev polynomials. When $|x| \leq 2$, the polynomials are defined by circular functions, which oscillate with increasing *p*. When $|x| > 2$, the polynomials are defined by hyperbolic functions which steadily increase when *p* increases. When the equivalent thickness is complex $|M_{11}|, |M_{22}| > 1$ [Eq. (23)] and $|x| > 2$ [Eq. (20)]. Consequently, the Chebyshev polynomial and the matrix elements of matrix (19) increase steadily with increasing *p*. According to Eq. (14) steadily increasing matrix elements is equivalent to steadily decreasing transmittance, which was to be proven. We call the regions of imaginary equivalent index or complex equivalent thickness stop bands and the other regions pass bands.

Epstein (*10*) has used this concept to develop a powerful method to design multilayer films. A proper equivalent layer configuration is selected so that the stop-band covers the wavelength band in which low transmittance is required. If one equivalent layer system is not enough, several systems with different center wavelengths λ_0 are used. The equivalent layer configurations are repeated until the proper low transmittance level is achieved. In regions where high transmittance is required, the pass bands are placed and the various equivalent indices, the index of the substrate, and the index of the surrounding medium are matched either by making them equal to each other or by using internal antireflection coatings as matching layers.

Figure 12 gives the transmittance curve of a band-pass filter with which Epstein (*10*) demonstrated his design method. He used the following two types of equivalent layers:

I.   (L/2) H (L/2)

II.   (H/2) L (H/2)

with $n_H = 2.30$ and $n_L = 1.38$.

The desired pass band is to extend from 490 to 580 mμ. If we pick $\lambda_c = 672.2$ mμ as the center wavelength of equivalent layer I its stop-band extends from 580 to 803 mμ. If we pick $\lambda_c = 411.9$ mμ for II, its stop-band extends from 354 to 490 mμ. The gap between these two stop bands form the desired pass band.
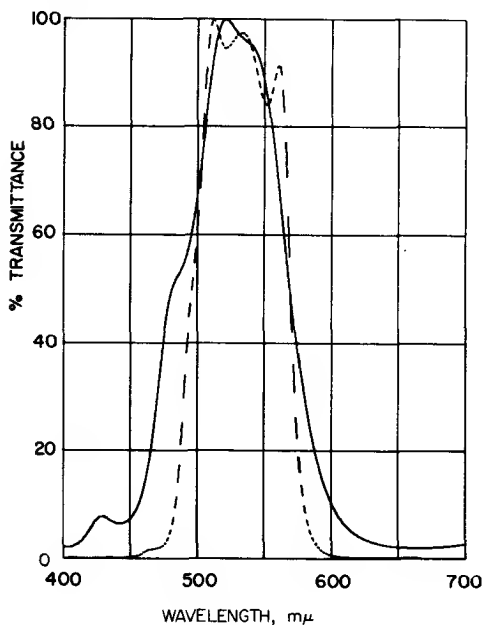
FIG. 12. Transmittance of two band-pass filters [Epstein (*10*)]. The solid curve represents design (31) and the dotted curve the same design with eight instead of four periods each.

The equivalent index of II equals that of air at 540 mμ. At other wavelengths, the mismatch between these two indices varies rapidly, so that a satisfactory antireflection coating would be hard to find. Accordingly, II is placed in contact with air without an intervening antireflection coating. The same arguments apply to the junction between I and II. The indices of these two layers are equal at 516 mμ. Accordingly, the junction between I and II is not antireflection coated either.

Since the equivalent index of I does not even approximately equal that of glass anywhere in the pass band, the use of antireflection coating at the junction of I and glass becomes unavoidable. Since the index of I changes so rapidly with wavelength, a particular value is chosen as a compromise. Let this be 0.595, the equivalent index at 544 mμ. Then the index of the antireflection coating should be $(1.52 \times 0.595)^{1/2} = 0.95$. This is the equivalent index of I at $\lambda_c/\lambda = 1.5$. Consequently, we use as antireflection coating one period of I at $\lambda_c = 816$ mμ.

The only thing left to be determined is the number of periods to be used. This number should be large enough to give a sufficiently high reflectance where required, but it should be small enough for simplicity of manufacture. Epstein (*10*) selected four which resulted in the following design:

$$S|1.495[(L/2) H (L/2)]1.23[(L/2) H (L/2)]^4 0.755[(H/2) L (H/2)]^4|M, \quad (31)$$

with $\lambda_0 = 546$ mμ, $n_H = 2.3$, $n_L = 1.38$, $n_S = 1.52$, and $n_M = 1.0$.

The design description (31) uses the following notation (19):

H stands again for a high-index film and L for a low-index film which is one-quarter wavelength thick at λ_0. The factors associated with L and H in front of the parenthesis change λ_0 into the desired center wavelength. For example, the film next to the substrate is a quarter wave at

$$\lambda_c = 1.495 \cdot 0.5 \cdot \lambda_0 = 408 \text{ m}\mu.$$

All elements belonging to a period are enclosed in parentheses and a power specifies the number of periods in a design. The letter S stands for the substrate of the filter and the letter M for the surrounding medium.

Design (31) has rather high transmittance in the stop-band region. If we increase the number of periods to eight instead of Epstein's four, we arrive at the other design shown in Fig. 12.

V. Refining Methods

The transmittance of a multilayer is a function of the optical thicknesses u_i $(i = 1, \cdots, k)$ and the indices of refraction of the individual films n_i:

$$T = T(u_1, n_1; u_2, n_2; \ldots; u_k, n_k). \quad (32)$$

By partial differentiation with respect to the u_i and n_i we can relate changes of the optical thicknesses and indices of refraction to the resulting change in transmittance:

$$\Delta T \approx \frac{\partial T}{\partial u_1} \Delta u_1 + \frac{\partial T}{\partial u_2} \Delta u_2 + \cdots + \frac{\partial T}{\partial u_k} \Delta u_k$$

$$+ \frac{\partial T}{\partial n_1} \Delta n_1 + \frac{\partial T}{\partial n_2} \Delta n_2 + \cdots + \frac{\partial T}{\partial n_k} \Delta n_k, \quad (33)$$

where T, ΔT, and the partial derivatives are, of course, wavelength dependent.

Let us assume we would like to change the transmittance of a given multi-layer configuration at m wavelength points. Since in practice only discrete values of the indices of refraction are available we limit ourselves to changes in the optical thicknesses. We can then establish the following set of equations:

$$\Delta T(\lambda_1) = \frac{\partial T(\lambda_1)}{\partial u_1} \Delta u_1 + \frac{\partial T(\lambda_1)}{\partial u_2} \Delta u_2 + \cdots + \frac{\partial T(\lambda_1)}{\partial u_k} \Delta u_k$$

$$\Delta T(\lambda_2) = \frac{\partial T(\lambda_2)}{\partial u_1} \Delta u_1 + \frac{\partial T(\lambda_2)}{\partial u_2} \Delta u_2 + \cdots + \frac{\partial T(\lambda_2)}{\partial u_k} \Delta u_k$$

$$\Delta T(\lambda_m) = \frac{\partial T(\lambda_m)}{\partial u_1} \Delta u_1 + \frac{\partial T(\lambda_m)}{\partial u_2} \Delta u_2 + \cdots + \frac{\partial T(\lambda_m)}{\partial u_k} \Delta u_k \qquad (34)$$

or in matrix notation:

$$\Delta T_j = F_{i,j} \cdot \Delta u_i, \qquad \begin{array}{l} i = 1, 2, \ldots, k \\ j = 1, 2, \ldots, m. \end{array} \qquad (35)$$

If we could solve these equations for the Δu_i,

$$\Delta u_i = (F_{i,j})^{-1} \cdot \Delta T_j \qquad (36)$$

we would have the desired solution. Unfortunately, Eq. (36) has a unique solution only when $m = k$ (when the number of change points equals the number of layers). This restriction imposes an unacceptable limitation of flexibility.

Let us first consider the case where the number of layers to be changed is larger than the number of change points ($k > m$):

In this case not all the Δu_i are determined by Eq. (36). Baumeister (13) proposed as a subsidiary condition that the thickness of each layer should be altered only a minimum amount. Using Lagrange multipliers (Λ_j) to solve this extreme value problem with constraints we have:

$$\partial \phi / \partial u_i = 0, \qquad i = 1, 2, \ldots, k \qquad (37)$$

where

$$\phi = \sum_{i=1}^{k} \Delta u_i{}^2 + \sum_{j=1}^{m} \Lambda_j \left(\sum_{i=1}^{k} (\partial T(\lambda_j)/\partial u_i) \Delta u_i - \Delta T(\lambda_j) \right). \qquad (38)$$

Carrying out the partial differentiations in Eq. (37) leads to

$$2 \cdot \Delta u_i + F_{j,i} \cdot \Lambda_j = 0 \qquad (39)$$

where $F_{j,i}$ is the transpose matrix of $F_{i,j}$.

Multiplying with $F_{i,j}$ changes Eq. (39) to

$$2 \cdot F_{i,j} \cdot \Delta u_i + F_{i,j} \cdot F_{j,i} \cdot \Lambda_j = 0$$

and with Eq. (35)

$$2 \cdot \Delta T_j + F_{i,j} \cdot F_{j,i} \cdot \Lambda_j = 0$$

or

$$\Lambda_j = -2(F_{i,j} F_{j,i})^{-1} \Delta T_j.$$

Insertion into Eq. (39) gives us the final solution:

$$\Delta u_i = F_{j,i} \cdot (F_{i,j} \cdot F_{j,i})^{-1} \Delta T_j. \qquad (40)$$

A similar solution can be found for the case where the number of layers to be changed is less than the number of change points ($k < m$).

Here we require that the difference between the requested changes and the possible changes are minimized [Rosen and Eldert (22)]. Using again the method of least squares we require that

$$\sum_{j=1}^{m} \left(\sum_{i=1}^{k} [\partial T(\lambda_j)/\partial u_i] \, \Delta u_i - \Delta T(\lambda_j) \right)^2 = \min$$

or after differentiation with respect to the u_i and setting the derivatives to zero

$$2 \cdot F_{j,i}(F_{i,j} \cdot \Delta u_i - \Delta T(\lambda_j)) = 0,$$

which gives us the final solution for the other case

$$\Delta u_i = (F_{j,i} \cdot F_{i,j})^{-1} \cdot F_{j,i} \cdot \Delta T(\lambda_j). \tag{41}$$

The mathematical problems in carrying out the computations are quite complex but straightforward. The computation of the partial derivatives was discussed by Baumeister (23). The partial derivative of T with respect to the ith layer is with Eq. (14)

$$\frac{\partial T}{\partial u_i} = \frac{T^2}{2} \left(\frac{n_M}{n_S} M_{11} \frac{\partial M_{11}}{\partial \delta_i} + \frac{n_S}{n_M} M_{22} \frac{\partial M_{22}}{\partial \delta_i} \right.$$
$$\left. + n_S n_M M_{12} \frac{\partial M_{12}}{\partial \delta_i} + \frac{1}{n_M n_S} M_{21} \frac{\partial M_{21}}{\partial \delta_i} \right) \frac{\partial \delta_i}{\partial u_i} \tag{42}$$

with

$$\delta_i = 2\pi/\lambda \, u_i.$$

The partial derivatives of the matrix elements are computed by substituting for the matrix of the ith layer the differentiated matrix

$$M_i' = \left\{ \begin{matrix} \dfrac{\partial M_{11}}{\partial \delta_i} & j\dfrac{\partial M_{12}}{\partial \delta_i} \\ j\dfrac{\partial M_{21}}{\partial \delta_i} & \dfrac{\partial M_{22}}{\partial \delta_i} \end{matrix} \right\} = \left\{ \begin{matrix} -\sin \delta_i & j\dfrac{\cos \delta_i}{n_i} \\ jn_i \cos \delta_i & -\sin \delta_i \end{matrix} \right\}, \tag{43}$$

and then multiplying the matrices the same way one would compute the matrix of a multilayer.

After having computed the matrix of the partial derivatives $F_{i,j}$ standard computer routines can be used to perform the matrix multiplications, matrix inversion and matrix–vector multiplication of Eqs. (40) and (41).

From a computer storage point of view it is much easier to work with

Eq. (41) than with (40). Using Eq. (41) the matrix multiplications can be performed while the partial derivatives are calculated and only one square $m \times m$ matrix has to be stored. In the case of Eq. (40) the full rectangular matrix as well as the square $k \times k$ matrix have to be stored. On the other hand, Eq. (41) does not incorporate the underdetermination with minimized thickness changes as does Eq. (40). In fact the practical use of Eq. (41) is rather difficult and requires additional smoothening schemes.

Due to the approximations used in Eq. (33) only small changes are allowable. Consequently Eqs. (40) and (41) have to be used repeatedly to effect a significant change.

The choice between the two methods is not strictly a matter of comparing the number of layers with the number of change points because neither Eq. (40) nor Eq. (41) require that all the layers in a design be opened up for alterations. So, if the total number of layers exceeds the number of change points one can make k smaller than m by holding the thicknesses of some of the layers constant.

On the surface refining appears to be the ideal design technique—all the designer has to do is to find some remotely related starting design and the computer will do the rest. The fallacy in this thinking is that the computer will take the starting design only to its nearest optimum, which might be quite inferior to the optimum derived from another starting design. Consequently, it appears advisable to use the refining methods together with some other design technique which takes the overall relations more into account. This supplementary design technique is then used to come up with the proper starting designs and to monitor the actual refining process. A good supplementary design technique is the use of the equivalent layer concept. As described before, this design technique is a two-step process: in the first step one fits the stop bands of suitable equivalent layers to the rejection region and the pass bands to the high-transmittance region. In the second step the equivalent layers are matched to each other, to the substrate, and to the medium. It is in this second step where refining methods can be used to great advantage: one keeps the thicknesses of the equivalent layers constant and subjects the thicknesses of the matching layers to the refining process. In practice this has proved to be a good synthesis between a design technique based on the understanding of the optical phenomena involved and a purely mathematical optimization technique. This combination of design techniques has the additional advantage that only the few matching layers are opened up for refining. Consequently, a smaller computer suffices and fewer layers have odd thicknesses (which is of significant advantage in the actual manufacture of multilayer filters).

Figure 13 gives the transmittance characteristic of a starting design and the refined design after nine iterations [using Eq. (40)], which Baumeister (*13*)
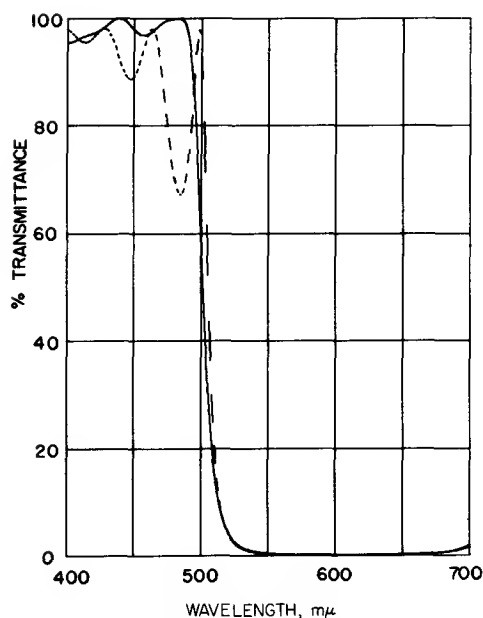
FIG. 13. Transmittance of a refined design [Baumeister (13)]. The dotted curve is the starting design (Column 3 of Table IV) and the solid curve (Column 4) the refined design.

TABLE IV.   OPTICAL DESCRIPTION OF THE DESIGNS SHOWN IN FIGS. 13 AND 14

$(n_M = 1.0$ AND $n_S = 1.52)^a$

Layer	Index	Starting design thickness	1st refined design thickness	2nd refined design thickness
1	1.3800	300.0000	306.0000	278.0000
2	2.3000	599.0000	639.0000	665.0000
3	1.3800	599.0000	620.0000	599.0000
4	2.3000	599.0000	610.0000	599.0000
5	1.3800	599.0000	606.0000	599.0000
6	2.3000	599.0000	597.0000	599.0000
7	1.3800	599.0000	582.0000	599.0000
8	2.3000	599.0000	573.0000	599.0000
9	1.3800	599.0000	577.0000	599.0000
10	2.3000	599.0000	589.0000	599.0000
11	1.3800	599.0000	596.0000	599.0000
12	2.3000	599.0000	590.0000	599.0000
13	1.3800	599.0000	585.0000	599.0000
14	2.3000	599.0000	601.0000	599.0000
15	1.3800	599.0000	646.0000	634.0000
16	2.3000	599.0000	672.0000	744.0000
17	1.3800	599.0000	616.0000	2457.0000

^{a}The layers are counted from the medium.

TABLE V

OPTICAL DESCRIPTION OF THE DESIGNS SHOWN IN FIG. 15 ($n_M = 1.0$ AND $n_S = 4.0$)[a]

Layer	Index	Starting design thickness	Refined design thickness
1	1.9000	64.0000	47.0000
2	4.2000	76.0000	143.0000
3	1.9000	300.0000	111.0000
4	4.2000	150.0000	150.0000
5	1.9000	150.0000	150.0000
6	4.2000	150.0000	150.0000
7	1.9000	150.0000	150.0000
8	4.2000	150.0000	150.0000
9	1.9000	150.0000	150.0000
10	4.2000	150.0000	150.0000
11	1.9000	150.0000	150.0000
12	4.2000	150.0000	150.0000
13	1.9000	150.0000	150.0000
14	4.2000	150.0000	150.0000
15	1.9000	150.0000	150.0000
16	4.2000	150.0000	98.0000
17	1.9000	120.0000	114.0000
18	4.2000	100.0000	100.0000
19	1.9000	100.0000	100.0000
20	4.2000	100.0000	100.0000
21	1.9000	100.0000	100.0000
22	4.2000	100.0000	100.0000
23	1.9000	100.0000	100.0000
24	4.2000	100.0000	100.0000
25	1.9000	100.0000	100.0000
26	4.2000	100.0000	100.0000
27	1.9000	100.0000	100.0000
28	4.2000	100.0000	100.0000
29	1.9000	100.0000	100.0000
30	4.2000	100.0000	100.0000
31	1.9000	100.0000	100.0000
32	4.2000	100.0000	100.0000
33	1.9000	104.0000	104.0000
34	4.2000	109.0000	109.0000
35	1.9000	109.0000	109.0000
36	4.2000	109.0000	109.0000
37	1.9000	218.0000	218.0000

[a]The layers are counted from the medium.

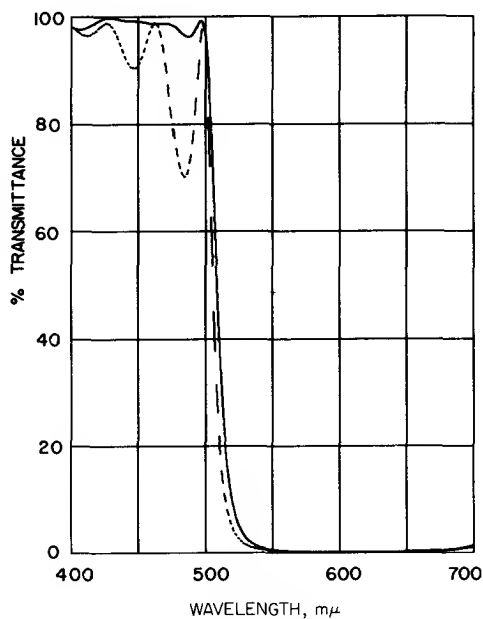FIG. 14. Transmittance of a refined design which originated from the same starting design as the one given in Fig. 13 but was refined by altering the matching layers only. The dotted curve is the starting design (Column 3 of Table IV) and the solid curve (Column 5) the refined design.
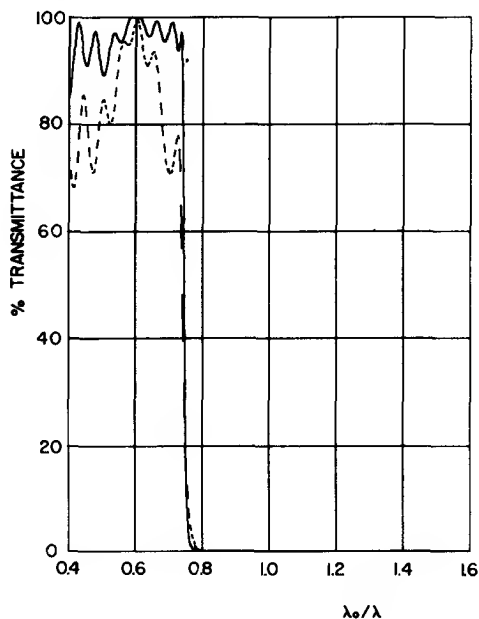

FIG. 15. Transmittance of the refined design given in Table V.

used as an example. The optical description of the two designs is given in Table V. Note that all layers were subjected to the refining process. Figure 14 shows the transmittance of the same starting design compared to the result of refining the matching layers only. The last column of Table I contains the design parameters. Nine refining cycles were used.

Table V and Fig. 15 give the starting design and the refined result of a filter with many layers. Fifteen cycles of Eq. (41) were used. The odd thicknesses of the first two layers and the last five largest in the starting design are the result of a preliminary matching analysis.

VI. Method of Effective Interfaces

The design method of considering effective interfaces was first introduced by Dufour and Herpin (24) and later extended by Smith (15).

Two adjacent interfaces inside a multilayer system (Fig. 15) are selected and the Fabry-Perot formula is applied. One arrives at the following formula:

$$T(\lambda) = \underbrace{\frac{T_1(\lambda)\,T_2(\lambda)}{(1 - R(\lambda))^2}}_{T_0(\lambda)} \times \underbrace{\frac{1}{1 + [4\,R(\lambda)/(1 - R(\lambda))^2]\sin^2[(\phi_1 + \phi_2 - \beta)/2]}}_{F(\lambda)}$$

(44)

with

$T(\lambda)$ = transmission through the total multilayer system;
$T_1(\lambda)$ = transmission through subsystem I (Fig. 1);
$T_2(\lambda)$ = transmission through subsystem II (Fig. 1);
$R(\lambda)$ = $(R_1(\lambda)\,R_2(\lambda))^{1/2}$ with R_1, R_2 being the reflectivities of the sub-systems I, II for light incident from the spacer;
ϕ_1, ϕ_2 = phase changes upon reflection associated with R_1, R_2;
β = $4\pi nd/\lambda$ with n, d being the index of refraction and the physical thickness of the spacer layer.

The important concept about this formula is that the phase and amplitude relations can be considered independently:

$T_0(\lambda)$ depends on the amplitudes of the reflectivities of the subsystems only;

$F(\lambda)$ depends primarily on the phases upon reflection of the two subsystems and the thickness of the spacer.

Both factors are always ≤ 1. For high transmission ($T \approx 1$) the amplitudes have to be adjusted to that $T_0(\lambda) \approx 1$ and the phases so that $F(\lambda) \approx 1$. Since the relations are exact, these are the only possible solutions.

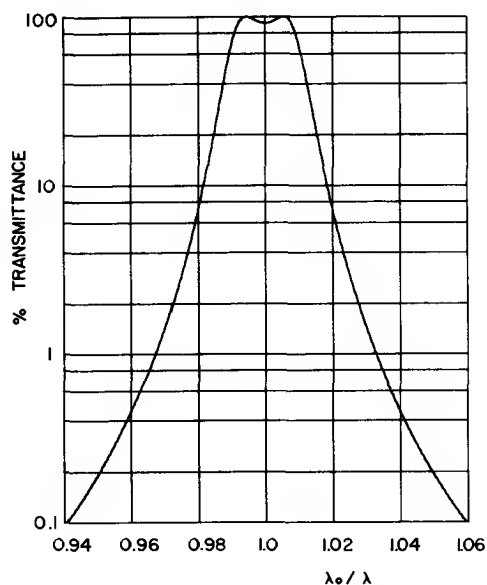Out of the structure of Eq. (44) it can be seen that

FIG. 16. Transmittance of the narrow-band-pass filter [Smith (15)]:1.0|$HLHH$ $LHLHL$ HH LH|1.0 with $n_H = 4.0$, $n_L = 1.35$.
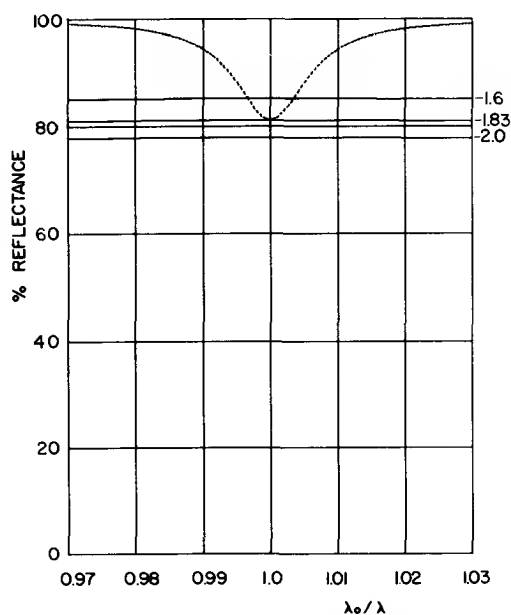

FIG. 17. Reflectance of the subsystems: 4.0|LH LHL HH LH|1.0 (dotted curve) and 4.0|$L'H$|1.0 (solid curves) with $n_H = 4.0$, $n_L = 1.35$, and $n_{L'}$ varying from 1.35 to 2.0.

$$T_0(\lambda) = 1 \qquad \text{only for } R_1(\lambda) = R_2(\lambda) \tag{45}$$

and

$$F(\lambda) = 1 \qquad \text{only for } R(\lambda) = 0 \quad \text{or} \quad \sin^2(\phi_1 + \phi_2 - \beta)/2 \approx 0, \tag{46}$$

and conversely

$$T_0(\lambda) = 0 \qquad \text{the more } R_1(\lambda) \quad \text{and} \quad R_2(\lambda) \text{ differ} \tag{47}$$

and

$$F(\lambda) = 0 \qquad \text{the larger } R_1(\lambda) \quad \text{and} \quad \sin^2(\phi_1 + \phi_2 - \beta)/2 \text{ are.} \tag{48}$$

In the design method of effective interfaces Eqs. (46)–(48) are used as guides to combine two known multilayers into the desired filter.

Figure 16 gives the transmittance characteristic of a narrow-band-pass filter with which Smith (15) demonstrated his method. The configuration of the filter is

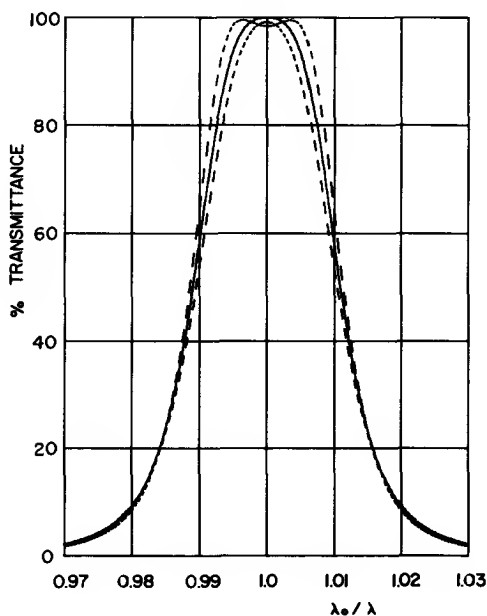$$1.0 \, | \, HL \; HH \; LHLHL \; HH \; LH \, | \, 1.0$$

FIG. 18. Transmittance of three narrow-band-pass filters: $1.0 | HL \; HH \; LHLHL \; HH \; L'H | 1.0$ with $n_H = 4.0$, $n_L = 1.35$, $n_{L'} = 1.6$ (dotted curve, two maxima), $n_{L'} = 1.83$ (solid curve), $n_{L'} = 2.0$ (dotted curve, one maximum).

with $n_H = 4.0$ and $n_L = 1.35$. He arrived at this design by combining the known configuration of a single spacer all dielectric filter (25) with a quarter wave stack. Figure 17 gives the reflectances R_1 and R_2 of the two subsystems:

$$1.0|HL\ HH\ LHLHL|\overset{\curvearrowleft}{4.0} \quad \text{and} \quad \overset{\curvearrowright}{4.0}|LH|1.0.$$

Since the curves for R_1 and R_2 intersect at two points, the resulting filter characteristic has two maxima in the pass band. Should they intersect in only one point, only one maximum would result. Figure 18 gives an example for this case.

In addition to helping to come up with new designs, Eq. (44) can be used to study the effect of changing the thickness inside a multilayer (24) and evaluating the interaction of two multilayers on top of each other.

VII. Long-Wavelength- and Short-Wavelength-Pass Filters

The equivalent-layer method is most commonly used to design long- and short-pass filters. $(L/2)\ H\ (L/2)$ or $(H/2)\ L\ (H/2)$ configurations (Figs. 7–9) are preferred because they give the widest rejection band for a set of available coating materials.

There is normally little difficulty in matching the equivalent index in the flat portion of the curve to the substrate and the surrounding medium. In case the index of the equivalent layer differs substantially from the indices of the substrate and the surrounding medium, antireflection coatings have to be placed in between. There is more difficulty in matching the steep portion without upsetting the match in the flat portion, especially when a large number of layers is involved. Young (20) discussed an approach using a synthesis procedure developed for electrical filters. Thelen (19) reported a simpler approach which does not give as good a result but is quite adequate in practice.

Let us consider a filter which consists of two equivalent-layer systems of the same configuration but of slightly different center wavelengths. In the flat portion of the curve, the equivalent indices remain equal. In the steep portion, we can place the systems in such a way that

$$N_{E1} = (N_{E2}n_S)^{1/2}, \tag{49}$$

which is the condition for a single-layer antireflection coating. We have to make sure, though, that the phase condition is met, too:

$$\Gamma_{E1} = (2v + 1)90°; \quad v = 0, 1, 2, \cdots. \tag{50}$$

Figure 19 compares low-frequency-pass design with and without shifted matching layers. In order to meet condition (50) the shifted layer had to be
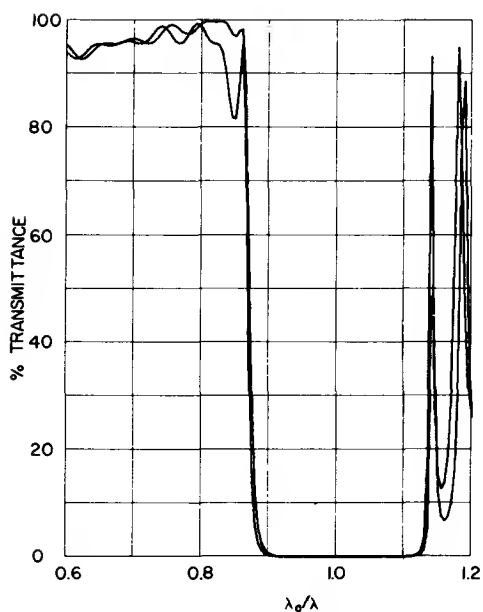
FIG. 19. Comparison of the filters $1.52|[(H/2) L (H/2)]^{15}|1.0$ and $1.52|[1.05(H/2) L (H/2)]^3 [(H/2) L (H/2)]^{12}|1.0$ with $n_H = 2.3$, $n_L = 1.56$.
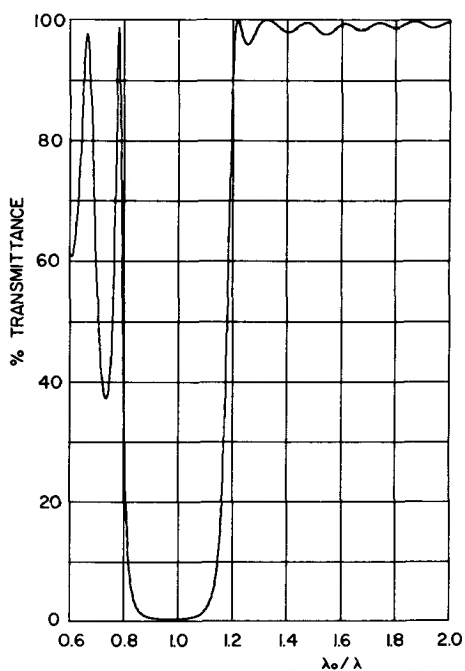

FIG. 20. Transmittance of the filter $1.52|[1.125(\frac{1}{2}LH\frac{1}{2}L)] [\frac{1}{2}LH\frac{1}{2}L]^5[1.1(\frac{1}{2}LH\frac{1}{2}L)]|1.0$ with $n_L = 1.38$, $n_H = 2.30$.
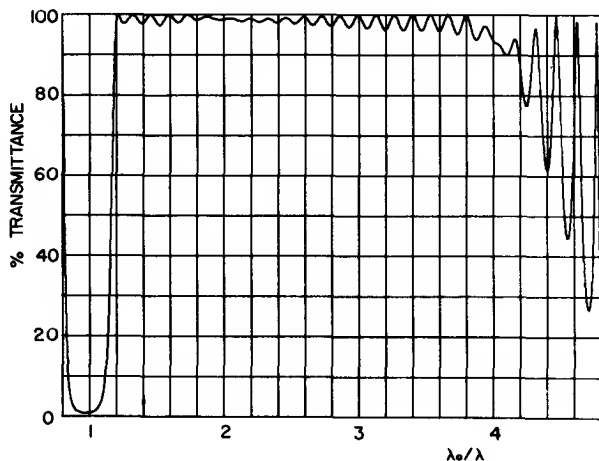
FIG. 21. Transmittance of the filter $1.52|[1.125(\frac{1}{3}L\frac{1}{3}M\frac{2}{3}H\frac{1}{3}M\frac{1}{3}L)][\frac{1}{3}L\frac{1}{3}M\frac{2}{3}H\frac{1}{3}M\frac{1}{3}L]^5[1.1$ $(\frac{1}{3}L\frac{1}{3}M\frac{2}{3}H\frac{1}{3}M\frac{1}{3}L)]|1.0$ with $n_L = 1.38$, $n_M = 1.781$, $n_H = 2.30$.

repeated three times. No match was necessary between the multilayer and the surrounding medium.

Figure 20 gives a design for a high-frequency-pass filter. A shifted equivalent layer had to be used on both sides.

A serious problem in the design of high-frequency-pass filters is the occurrence of secondary low-transmittance bands. If the desired pass band has to extend over a frequency region of close to 3:1 or more, two material homogeneous multilayers can no longer be used (21,26). Designs using equivalent-layer configurations as presented in Fig. 10 or 11 have to be applied then. Figure 21 gives an example.

Most of the time the method of equivalent layers leads to sufficiently good designs. If higher performance is required, the employment of the previously discussed refining methods is necessary.

VIII. Narrow-Band-Pass Filters

Figure 12 gives the transmittance of a fairly wide band-pass filter composed of a short-pass and a long-pass filter. By steepening the slopes and bringing the two films closer together, this same approach could be used to design narrow-band-pass filters.

There are simpler designs, however, which require fewer layers and are easier to control during deposition. They have the following general configuration:

(reflecting stack)   (spacer)   (reflecting stack) . . .

. . . (spacer)   (reflecting stack)   (51)

with the most simple version (25):

(quarter wave stack) (multiple half-wave) (quarter wave stack).   (52)

The bandwidth of the filter is determined by the number of layers in the quarter wave stack and the multiplicity of the half-wave spacer. The maximum transmittance can easily be determined by eliminating half-waves. This is possible since such layers have a unity matrix $\begin{pmatrix} 1 & 0 \\ 0 & 1 \end{pmatrix}$ and contribute therefore nothing to the multilayer matrix. For example, the filter

$$4.0|HLHLHLHHLHLHLHL|1.0 \qquad (53)$$

can be reduced to

$$4.0|HLHLHLLHLHLHL|1.0$$
$$4.0|L|1.0.$$

Consequently, at the maximum the transmittance of this design is the same as that of a single low-index layer. Figure 22 gives the transmittance characteristic of design (53), with $n_H = 4.0$ and $n_L = 1.8$.

The shape of the pass band given by filters of this type (52) is not ideal for a narrow band filter. A more desirable shape would show a more rapid transition from stop band to pass band, a flatter top, and a lower rejection level. These requirements can be fulfilled with less simple versions of the general type (51). The previously discussed double half-wave design by Smith (15) (Fig. 16) is an example.

Although the method of effective interfaces is well suited for designing other versions of the general type (51) the equivalent-layer technique is as effective:

Let us return to the double half-wave design given by Smith (15).

$$\text{substrate} \quad HLHHLHLHLHHLH \quad \text{air}$$
$$n_S \qquad\qquad\qquad\qquad\qquad n_M$$

We can break this design down into the following three equivalent layers:

equivalent layer I:	HLH	
equivalent layer II:	$HLHLHLH$	
equivalent layer III ($= $ I):	HLH	(54)

The transmittance is high when

$$N_{E1} = (n_S N_{E2})^{1/2}; \qquad \Gamma_{E1} = (2v + 1)90^\circ, \qquad v = 0, 1, \ldots$$
$$N_{E3} = (n_M N_{E2})^{1/2}; \qquad \Gamma_{E3} = (2v + 1)90^\circ, \qquad v = 0, 1, \ldots . \qquad (55)$$

Interpretation (54) opens up a wide variety of possible narrow-band-pass designs. Equivalent layer II can be repeated several times without upsetting
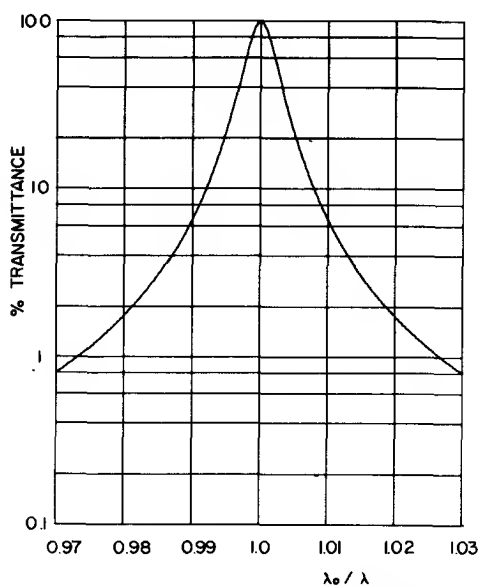
FIG. 22. Transmittance of the narrow-band-pass filter $4.0|LHLHL\ HH\ LHLHLHL|1.0$ with $n_H = 4.0$, $n_L = 1.8$.

FIG. 23. Transmittance of the narrow-band-pass filter $4.0|H\ (LH)^2\ (HLHLHLHLH)^2$ $(HL'H)|1.0$ with $n_H = 4.0$, $n_L = 1.8$, and $n_{L'} = 1.6$.
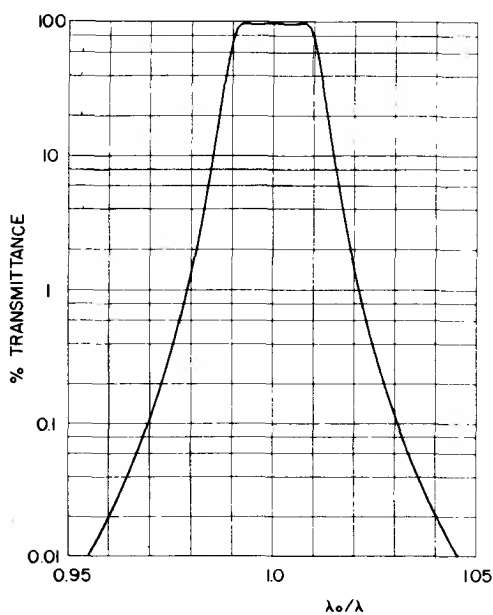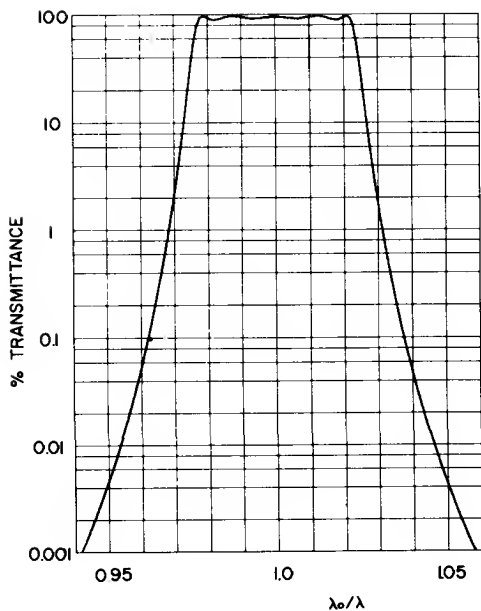
FIG. 24. Transmittance of the narrow-band-pass filter $1.34|(HL'H)(HLHLHLH)^2 HH$ $(HLHLHLH)^2 (HL'H)|1.0$ with $n_H = 4.0$, $n_L = 1.8$, and $n_{L'} = 2.2$
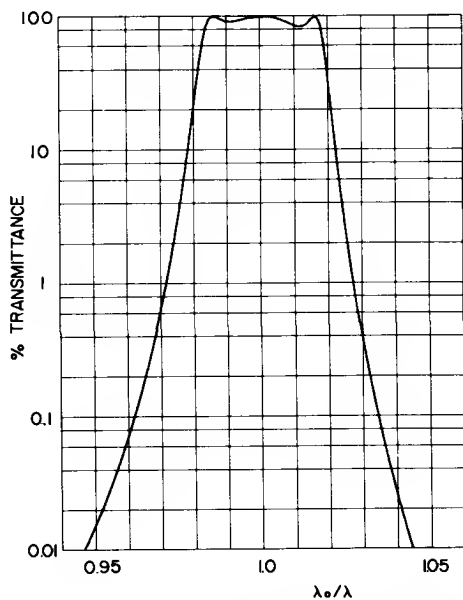

FIG. 25. Transmittance of the narrow-band-pass filter $1.7|(HLH)[(6H/5)(3L5)(6H/5)$ $(3L5)(6H/5)(3L/5)(6H/5)(3L/5)(6H/5)]^3 (HL'H)|1.0$ with $n_H = 4.0$, $n_L = 1.8$, and $n_{L'} = 2.2$.

the matching relations (55). In this way, the transition from pass band to stop band can be sharpened and the rejection level improved without altering the bandwidth and peak transmittance.

Figure 23 shows a design where equivalent layer II is repeated twice. Equivalent layer III uses a lower index for the low-index film in order to provide the proper match to air. Figure 24 gives a design where equivalent layer II is repeated four times. Equivalent layers I and III both use a higher-index material for the low-index film, to achieve a proper match to the substrate and the surrounding medium. This design uses an additional half-wave film in the center. This film can be considered a "decoupling layer" which reduces the ripple in the pass-band.

Finally, Fig. 25 gives a design which uses a 2:1 thickness ratio configuration as equivalent layer II. A filter of this type might be of practical importance since it is less angle sensitive than a comparable design with equally thick layers.

IX. Circular Variable Filters

Recently a practical method was introduced to deposit thin films on a circular substrate disk in such a way that the thicknesses change linearly along concentric circles (27). In one type the thicknesses double around a half circle, and drop back to the original value around the remaining half circle. Figure 26 shows such a disk. Let us assume that we deposited a narrow band interference filter in the described way on the disk. If we now rotate this disk behind a slit we have a monochromator which passes the wavelength $\lambda_p = \lambda_0$ at $\alpha = 0$, $\lambda_p = \lambda_1$ at $\alpha = \alpha_1$, and $\lambda_p = 2\lambda_0$ at $\alpha = x$, or analytically

$$0 \leq \alpha \leq \pi, \qquad \lambda_p = \lambda_0(1 + \alpha/\pi) \qquad (56)$$

$$\pi \leq \alpha \geq 2\pi, \qquad \lambda_p = \lambda_0(3 - \alpha/\pi) \qquad (57)$$
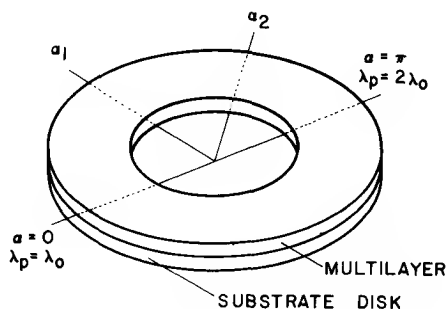

FIG. 26. Construction of a circular variable filter.

A practical example of such a monochromator was described by Apfel (28).

Circular variable filters present no real new design problems. Regular narrow-band-pass designs are used as the basic element. In order to allow maximum light throughput designs which have a minimum angle shift should be selected. Special consideration has to be given to the blocking of the side bands of the narrow-band-pass designs. Since the filter has to cover the complete wavelength region from λ_0 to $2\lambda_0$, no absorption-type blocking filters can be used. This makes the design somewhat difficult because many interference films are needed to cover the 2:1 wavelength range on both sides of the narrow-band-pass.

The development of the circular variable filter did have a significant impact on spectrophotometric instrumentation of moderate resolution (29–32). The circular variable filter permits the construction of extremely simple and hence highly reliable spectrometers with high energy throughput. The entrance and exit slits are one and the same. Hence, no extensive imaging optics are required, and the detector can be located right at the aperture. Since no diagonal reflecting surfaces are required there are no polarizing properties.

The basic limitations of a circular variable filter as a monochromator are: (1) due to the limitations in the manufacture of interference filters it does not appear feasible to match the resolution capabilities of other dispersive elements like gratings; (2) Due to the blocking requirements it is not practical to cover much more than a 2:1 wavelength range with one filter. For example, if one would like to cover the 2–18-μ wavelength range three filters are required: 2–4, 4–8, and 8–16 μ. This is not a serious drawback, however, since these filters can be manufactured in smaller sectors (90°, for example) and then mounted on a single wheel.

REFERENCES

1. L. Holland, "Vacuum Deposition of Thin Films." Wiley, New York, 1956.
2. O. S. Heavens, "Optical Properties of Thin Solid Films." Butterworths, London and Washington, D.C., 1955.
3. H. Mayer, "Physik duenner Schichten." Wissenschaffliche Verlagsgesellschaft, Stuttgart, 1950.
4. Color Filter Glass. Jenaer Glaswerk Schott & Gen, Mainz, West Germany, 1962.
5. Glass Color Filters. Corning Glass Works, Corning, New York.
6. Colour Filters. Chance-Pilkington Optical Works, St. Asaph, Flintshire, Great Britain.
7. F. Abelès, *Ann. Phys.* **5**, 596, 706 (1950).
8. M. Born and E. Wolf, "Principles of Optics," 2nd ed., p. 51. Pergamon Press, Oxford, 1964.
9. P. H. Berning, *in* "Physics of Thin Films." (G. Hass, ed.), Vol. 1, pp. 69–121. Academic Press, New York, 1963.
10. L. I. Epstein, *J. Opt. Soc. Am.* **42**, 806 (1952).
11. H. Pohlack, "Jenaer Jahrbuch," pp. 181–221. Zeiss, Jena, 1952.
12. H. J. Riblet, IRE *Trans. Microwave Theory Tech.* **MIT-5**, 36 (1957).

13. P. W. Baumeister, *J. Opt. Soc. Am.* **48**, 955 (1958).
14. J. A. Dobrowolski, *Appl. Opt.* **4**, 937, (1965).
15. S. D. Smith, *J. Opt. Soc. Am.* **48**, 43 (1958).
16. R. J. Pegis, *J. Opt. Soc. Am.* **51**, 1255 (1961)
17. P. G. Kard, *Opt. Spectry. (USSR) (English Transl.).* **16**, 497 (1964).
18. A. V. Shatilov and L. P. Tyutikova, *Opt. Spectry. (USSR) (English Trans.)* **14**, 227 (1963).
19. A. Thelen, *J. Opt. Soc. Am.* **56**, 1533 (1966).
20. L. Young, *Appl. Opt.* **5**, 77 (1966).
21. A. Thelen, *J. Opt. Soc. Am.* **53**, 1266 (1963).
22. S. Rosen and C. Eldert, *J. Opt. Soc. Am.* **44**, 250 (1954).
23. P. Baumeister, *J. Opt. Soc. Am.* **52**, 1149 (1962).
24. C. Dufour and A. Herpin, *Opt. Acta.* **1**, 1 (1954).
25. H. D. Polster, *J. Opt. Soc. Am.* **42,** 21 (1952).
26. L. I. Epstein, *J. Opt. Soc. Am.* **45**, 360 (1955).
27. A. Thelen, *Appl. Opt.* **4**, 977 (1965).
28. J. H. Apfel, *Appl. Opt.* **4**, 983 (1965).
29. G. T. Keahl, New low cost infrared spectrophotometer, paper presented at the Pittsburgh Conf. Anal. Chem. Appl. Spectry., 17th, February, 1966.
30. G. T. Keahl, Design of an infrared spectrophotometer for use with gas chromatographs, paper presented at the Pittsburgh Conf. Anal. Chem. Appl. Spectry., 17th, February, 1966.
31. W. A. Hovis, Jr., W. A. Kelly, and M. G. Strange, *Appl. Opt.* **6**, 1057 (1967).
32. J. D. Rehnberg, J. R. Yoder, and G. H. Hunt, *Appl. Opt.* **6**, 1111 (1967).

Oxide Layers Deposited from Organic Solutions

H. Schroeder

Jenaer Glaswerk Schott & Genossen
Mainz, West Germany

I. Introduction

Methods to precipitate noble metals such as Ag, Au, and Cu from solutions onto solid substrates in highly reflecting layers have been known since the last century. It was only 30 years ago, however, that experiments to deposit dielectrics as liquid films onto nonmetallic substrates were initiated. The first studies of this kind were stimulated by Langmuir's observation (*1*) that certain insoluble substances of high molecular weight containing polar groups spread over a water surface as a monomolecular layer, and that such films could be deposited onto planar solid surfaces by slowly draining the water or raising the substrate. In 1935, Blodgett (*2*) produced antireflection coatings by this method, but did not pursue this approach any further since these coatings did not seem to offer any practical applications.

Soon thereafter, it was discovered in Germany that clear and stable SiO_2 films could be obtained by spreading colloidal solutions of silicic acid evenly over a glass surface, preferably by spinning the substrate. These studies

became known through a report by Tanner and Lockhart (*3*) and related patents (*4*). In addition to SiO_2, oxides of other Group IV elements were also considered in this work. The SiO_2 process was used industrially in Germany during World War II, but was soon abandoned when vacuum evaporation techniques proved to be more economical. It has been only recently that the production of coatings and films from solutions has found renewed interest, and that more complete studies of the processes involved in the preparation of such layers have been performed.

This review article describes the preparation and characteristics of oxide layers obtained from solutions and discusses their various applications. Coatings of TiO_2 and SiO_2 will be treated with particular thoroughness since these two film materials play an important role in multilayer film combinations consisting of layers with alternately high and low indices of refraction.

II. Formation of Solid Layers from Solutions

1. GENERAL CONDITIONS FOR THE PREPARATION OF HOMOGENEOUS LAYERS

In order to produce dielectric layers with useful optical properties from liquid films, the solutions used must have special physical and chemical characteristics. Their main characteristics are:

1. Adequate solubility of the initial compounds and, at the same time, a minor tendency of the dissolved substances toward crystallization during evaporation of the solvent. These conditions are principally met by those materials which either already dissolve in a colloidal or in a polymeric state, or pass over into such a state by reaction with the solvent, or which, at least, remain after the evaporation of the solvent as a gellike noncrystalline mass.

2. Sufficiently small contact angles between the solution and the substrate to be coated in order to obtain good wetting of the latter. Wettability of a substrate can be improved in some cases by the addition of wetting agents to the solution. For a substrate to be perfectly wetted, the surface of course must be sufficiently clean. This can be obtained by a pretreatment with detergents and working in dust-free rooms. The surface structure of a substrate can also affect the wettability. Scratches or surface roughnesses caused by mechanical treatment (e.g., remainders of grinding structures), having an average depth of more than about 10 μm can cause considerable disturbances in the evenness of the coating when using solutions with a low degree of polymerization.

3. Adequate durability of the solution and constancy of processing conditions. It is often difficult to comply with these requirements because of the

colloidal or polymeric character of solutions to be attained according to paragraph (1). In most cases it is, however, possible to preserve the optimum state by means of stabilizers used in organic and colloid chemistry. This makes processing under sufficiently steady conditions possible for months.

4. Transformability of the deposited gel film into a solid homogeneous (oxide) layer. By drying and heating the films, high bonding strength to the substrate and, at the same time, solidification of film structure should be obtained without the appearance of cracks or haze. Therefore, film components which are released during the solidification should not have an excessive volume content in the gel layer, since the sintering capacity of the thermally transformed layer is frequently limited by the structure of the crystallites.

2. SURVEY OF ATTAINABLE PHYSICAL PROPERTIES

A coating method can obviously be of major interest only if the various layers that can be produced according to this method cover a sufficiently large variety of physical properties and technical requirements. The optical properties of main interest of such films are the index of refraction and the absorption coefficient. They should offer a variation in range as large as possible from the uv to the ir to be useful to the designer of multilayer coatings. Likewise the obtainable electric properties are of interest (e.g., semiconductor properties), thermal expansion, chemical protective properties, etc. It is therefore essential that compounds of numerous elements be available for preparing solutions from which oxides or other stable compounds with different properties can be deposited as layers. Furthermore, in many cases solutions of different substances are miscible with each other, so that layers having any intermediate physical property can be obtained. Thus, for the refractive index n_D, the range between ~ 1.4 and ~ 2.4 can continuously be covered. Due to reactions between components or to physical effects of the resulting solid state structure, however, substantial deviations from the additivity may occur. The admixture of certain activators, such as are known in semiconductor physics, offers further possibilities for creating special effects. On the other hand, the resulting structure and properties of the layers are more or less dependent on the preparation of the solutions, the nature of the substrate, and the ambient conditions during the film formation.

A further extension of the range of properties arises from the possibility of transforming the applied films by subsequent chemical reactions either in the gellike or solid state. Such reactions may be carried out by exposure to gases or liquids and can be used to produce materials such as suboxides or sulfides.

The production of metallic layers, however, seems to be restricted to those metals which can be precipitated in elementary form in the film by thermal

disintegration of the corresponding organometallic compounds. Practical application of layers produced in this manner has not been considered thus far.

3. Coating Apparatus and Techniques

For the deposition of coatings by means of liquid films the following methods can be considered:

1. Dipping processes, in which parts to be coated are withdrawn from the solution and simultaneously covered with a liquid film.

2. Lowering processes, in which the object remains at rest and the liquid level is lowered.

3. Spreading out the liquid film by spinning wetted surfaces, which, however, is only applicable to smaller circular substrates.

4. Spraying processes with fine disperse solutions.

For large surfaces process 1 is the most economic and at the same time the most universally applicable one. The lifting movement of the carrier from which the parts to be coated are suspended, must be completely smooth and shockless, and has to be so slow that the liquid film adhering to the surface of the substrate is left in a flow zone which is as short as possible (see Fig. 2). Its thickness distribution in the vertical direction is then essentially defined only by evaporation of the solvent and remains stationary during the movement, so that the solid film finally takes up a constant thickness along the lifting direction. The film formation on the substrate also develops very uniformly along the horizontal dipping line, provided that the operation is not disturbed by irregularities in the liquid level or by uncontrolled air currents. This can be checked by observing the interference fringes which are formed during the evaporation of the solvent and volatile components on a plane plate during its withdrawal from a dipping container. During movement of the plate, these fringes must run as horizontally as possible and always remain at about the same height (depending on lifting speed) above liquid level.

The thickness (d) of the solid layer thus finally obtained depends mainly on the following parameters:

1. Speed (v) of the lifting movement.

2. Angle of inclination (ϕ) of the coated surface related to the horizontal line.

3. Concentration (c) of the solution.

Further properties that might affect the thickness of the layer, such as viscosity, surface tension, and vapor pressure of the solution, can be summarized in a constant of proportionality (k) which is characteristic of each solution. The temperature dependence of k is to be considered in all appli-
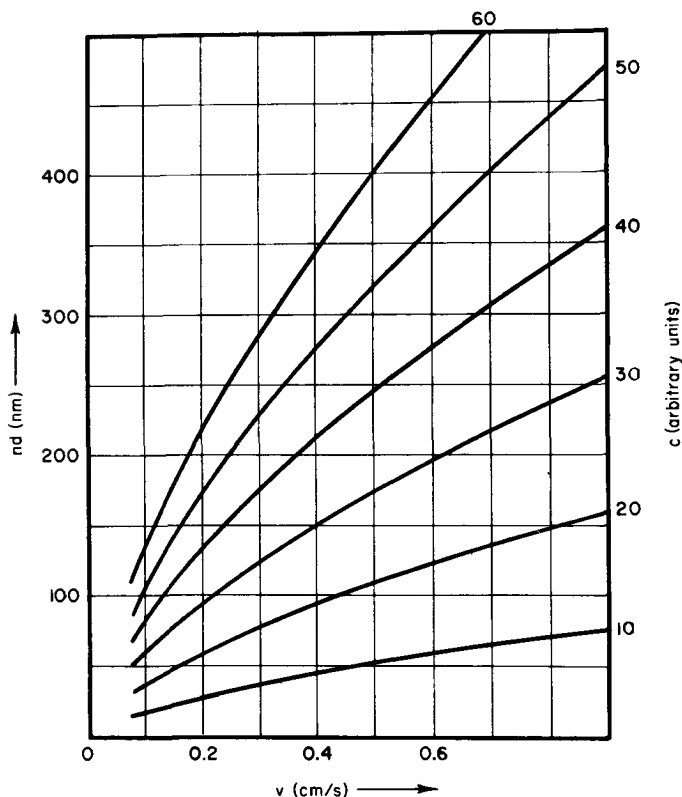
FIG. 1. Optical thickness of films versus lifting speed for different concentrations of solutions.

cations. In cases in which a hydrolytic reaction already has started during the spreading out of the film, a slight influence of air moisture on d has to be taken into consideration.

Thus, if for a given solution the temperature and humidity is kept constant, the thickness is determined only by v and ϕ.

The experimental determination of the influence of v, ϕ, and c on the layer thickness has revealed that all suitable solutions show essentially the same fundamental characteristics which are represented in Figs. 1–3. The dependence on v can be expressed with close approximation by the relation $d \sim v^{2/3}$, which implies the simultaneous effect of gravity as well as viscosity and surface tension of the solution on the formation of the coatings. This becomes even more evident in the unsymmetrical dependence of the coating thickness on ϕ in the case of nonvertical emersion from the solution ($\phi \neq 90°$, Fig. 2).
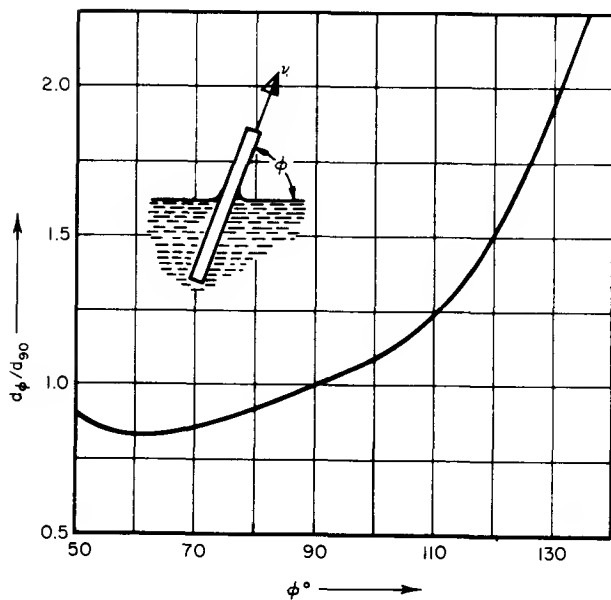
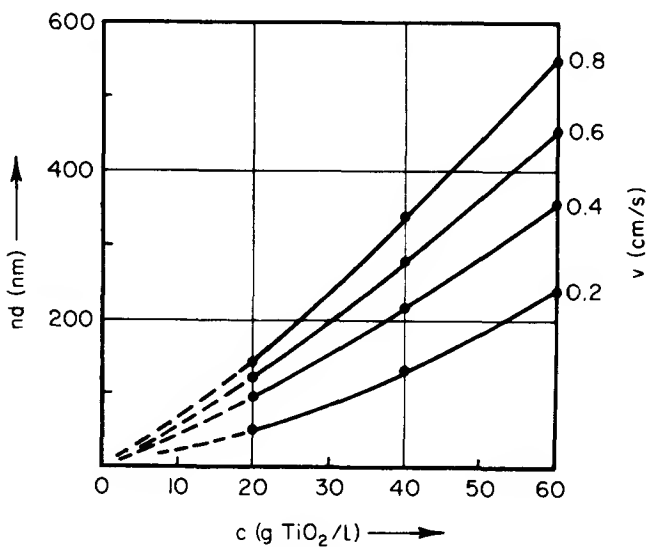Fig. 2. Relative film thickness as a function of angle of inclination of the coated surface to liquid level.

Fig. 3. Resulting optical film thickness versus concentration of TiO_2-forming solutions for different lifting speeds.

The nonlinear relation between d and the concentration c (Fig. 3) is due to an increase of viscosity (η) of solution with c. With solutions of higher concentration and viscosity, a progressive enrichment of dissolved substance in the dipping zone can take place during the lifting process because of the evaporation of the solvent and imperfect mixing of the solution along this zone. This leads to a slight increase in layer thickness from top to bottom. Thorough stirring of the immersion solution, however, would result in liquid surface disturbances and, consequently, in irregularities of evenness of the coating. The above described thickness increase of the coating can be avoided better by continuously changing the lifting speed using a test band for monitoring.

When suspending parts to be immersed, care has to be taken that no solution residues can pass onto the surface to be coated from clamps or other holding devices. If possible, clamps and holding fixtures should, for this reason, not be immersed. It is therefore useful to place small or finished parts on racks and to use clamps only along the lateral edges. However, on the lower edge of parts withdrawn from the solution a certain thickening of the film caused by adhering liquid residues cannot always be completely avoided. The width of this "trouble zone" depends on the shape of the edge, lifting speed, and viscosity of the solution, and is normally between 2 and 8 mm long. In the case of large plates, this marginal band can simply be cut off after the coating process is completed.

The processes discussed under paragraphs 2 and 3 are considered mainly for the coating of small surfaces, where the width of the "trouble zone" must be kept to a minimum. In the lowering process 2 this is preferably achieved by placing the substrates to be coated on a porous and permeable support which forms the top seal of a hollow glass cylinder, and which is open at the bottom. When lowering the liquid below the level of the support, a partial vacuum is generated, which draws off solution residues adhering to the bottom edges of the articles. The required layer thickness can easily be kept under control by measuring the rate of flow with a flowmeter.

In the spinning process 3, which is suitable for small circular disks or lenses only, there are practically no marginal disturbances. The solution poured on a rotating, approximately horizontal substrate spreads out on its surface completely evenly. This process, however, is less economical and, therefore, no longer used today.

Spraying processes 4 are only suitable in general for nonoptical coatings, since it is very difficult to obtain homogeneous films of sufficiently uniform thickness with this technique. Applications of such methods, therefore, have been restricted so far mainly to the production of transparent semiconducting oxide coatings, such as SnO_2 and In_2O_3, on glass surfaces (5). The solution to be sprayed is squirted out of one or several stationary spray guns onto

the preheated glass plate which is moved across the jets at a predetermined speed. The spray guns used should have a high atomizing capacity at pressures of 2–3 atm. In order to obtain a more uniform distribution of the mist droplets, a compressed air nozzle is used to spread the beam of particles perpendicularly to the direction of glass movement. It has been reported that in the Soviet Union machine-drawn sheet glass is coated by such processes with semitransparent Fe_2O_3 and CoO_x films for sun-shielding purposes (6).

Solidification of layers produced according to methods 1–3 can be achieved by heating the coated substrates up to 200–500°C or more. The most suitable maximum temperature depends on the coating materials, as well as on the substrates, and the required mechanical resistance. For the heat treatment, the objects are placed on a continuously running conveyor belt and passed more or less rapidly through a furnace in which they are heated to the required temperature and then cooled down. The speed of the heating and cooling process depends on the thermal shock resistance of the objects. With another technique, the coated substrates are first heated to temperatures of 100–180°C only. This can be achieved with a heating lamp and results in coatings which are sufficiently stabilized so that the final firing process can be performed later on in larger batches in an intermittently heated electric furnace. The influence of the firing temperature and firing period on some of the physical properties of specific layers will be discussed in Section IV.
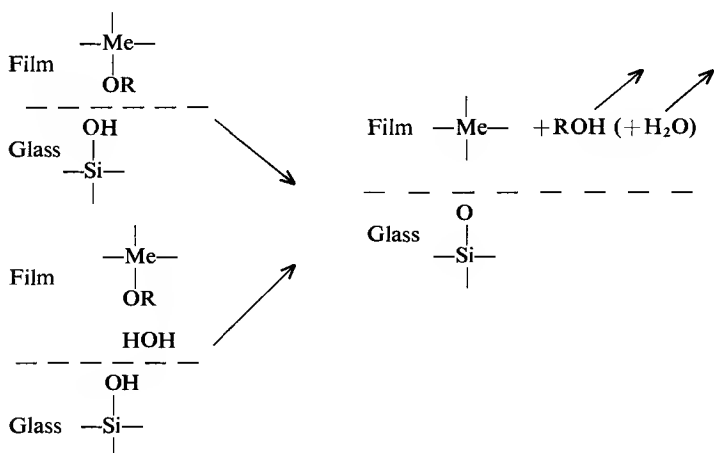
Expenditures for a dip-coating plant depend mainly on the required room air conditioner and on the kiln. For coating smaller samples up to approximately 1 m², expenditures for the air conditioner normally outweigh those for the kiln. For larger sizes, however, the expenses for the kiln rise rapidly with the increasing size of the glass panes to be coated.

III. General Characteristics of Oxide Layers Obtained from Solutions

1. COATING MATERIALS

a. One-Component Coating Materials. The first experiments with film-forming solutions had shown that colloidal SiO_2 hydrate, suitable for the preparation of SiO_2 films, can be produced from silicate solutions by the addition of acids (4). This fact had led to the conclusion that such a method should be applicable with other elements only when these are likewise capable of forming the corresponding colloidal oxide hydrates. Corresponding tests were, therefore, carried out particularly with elements of Group IV of the periodic system (7). Investigations made more recently (8) showed,
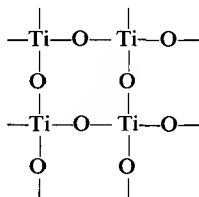
however, that the presence of colloidally precipitated hydroxides or oxide hydrates in a solution is apparently a sufficient, but not necessary, pre-requisite for the production of optically homogeneous inorganic films on solid surfaces. It is basically also possible to start from solutions of any inorganic or organic metallic compounds if these tend to form polymolecules or polysolvated groups in solution which yield gels of poor crystallization tendency while drying. In this case, the hydrolysis method, which is often impracticable, is not necessary. On the other hand, hydrolysis, if feasible, generally contributes to improved hardness and to a higher packing density or "volume factor" of the coatings. According to experience in practice thus far, metallic acid esters and alcoholates which are obtained by treating metallic compounds with the corresponding reactive solvents are particularly suitable. By reaction with the OH groups or H_2O always present on ceramic surfaces they lead to solid chemical bonds between the coating materials and the substrate. On glass, such reactions starting, for example, from an alkyl *ortho*-ester of the acid derived from a quadrivalent metal, can be schematically formulated in the following simplified manner:

$$
\begin{array}{l}
\text{Film} \quad \begin{array}{c} | \\ -\text{Me}- \\ | \\ \text{OR} \end{array} \\
\overline{}\,\overline{}\,\overline{}\,\overline{} \\
\text{Glass} \quad \begin{array}{c} \text{OH} \\ | \\ -\text{Si}- \\ | \end{array}
\end{array}
\qquad\searrow\qquad
\text{Film} \quad \begin{array}{c} | \\ -\text{Me}- \\ | \end{array} \quad +\text{ROH}\ (+H_2O) \nearrow\ \nearrow
$$

Film   —Me—   +ROH (+H₂O)

Glass   O
—Si—

Film   —Me— OR   HOH

Glass   —Si— OH

It will be shown in Section III,3 that it is important for the structural and physical properties of the layers that the strong bond with substrate is normally accomplished in an early phase of solidification.

Whereas such reactions with a vitreous or ceramic surface go on quite readily, hydrolysis or decomposition of the other OR groups seems to start only after increased supply of energy. This can be concluded from the fact that solidification inside the layers occurs only at considerably higher tem-peratures than the development of adhesion to the substrate. However, if a hydrolytic decomposition already has been initiated in solution, or hydrolysis by gaseous H_2O is favored by the presence of readily reacting groups, the

conversion into a stable solid film is possible at much lower temperatures. Thus, to give an example, liquid films containing $TiCl_2(C_2H_5O)_2$ react immediately with gaseous water to form HCl, C_2H_5OH, and a polycondensed Ti compound. When heating such films, the volatile reaction products escape, and the resulting TiO_2 molecules are apparently interlaced with each other in a very regular way:

$$
\begin{array}{c}
| \quad\quad | \\
-Ti-O-Ti-O- \\
| \quad\quad | \\
O \quad\quad O \\
| \quad\quad | \\
-Ti-O-Ti-O- \\
| \quad\quad | \\
O \quad\quad O \\
| \quad\quad |
\end{array}
$$

In the case of TiO_2 and most other oxide films thus obtained, crystalline structures can be observed during this first formation stage of the oxide. A remarkable exception is found with SiO_2 films, which always show an amorphous structure, regardless of the method used. In any case, strong structural interlacing by means of oxygen bridges during the film formation process, as indicated above, is an important characteristic of all oxide layers deposited from the liquid phase. As a consequence, it is in general easier to obtain stable films with substances containing cations of higher valence. Most of the monovalent and some bivalent metals are, as a matter of course, excluded from the application as a one-component coating material because of the instability of their oxides; however, even nobler metals with these valences, such as silver, copper, or mercury, are difficult to deposit as separate oxides.

Although among the metals of higher valence only the more conventional ones have been examined thus far, the results gathered lead to the conclusion that probably all of them are available for this process. In general, however, the methods of preparation, even for substances of chemically related nature, are not identical, and in almost any case extensive investigations are required in order to incorporate an element into a stable solution satisfying all specifications described in Section II,1.

If films are baked in air, they normally pass over into the highest oxidation stage compatible with the given temperature. For polyvalent metals, however, lower oxides can also arise if baking is done under reducing conditions or in a protective gas atmosphere. The admixture of reducing agents to the initial solution likewise can have the same effect.

b. Multicomponent Coating Materials. The possibilities of combining compounds of two or more metals in one solution are numerous. Due to the influence exerted by the molecular structure on the optical properties, coatings produced from such multicomponent solutions normally exhibit

considerably different spectral absorption characteristics from those of the isolated components. As an example, solutions of pure cobalt compounds always produce gray-brown colored layers of cobalt oxide. The spectral transmittance of a glass plate coated on both sides with such layers is represented in Fig. 4, curve a. When adding a cobalt compound to a solution of a hydrolyzed silicic acid ester $Si(OR)_4$ with an OH:R ratio $\sim 1:1$, layers are obtained whose spectral transmittance, calculated for equal quantity of Co per square centimeter, corresponds approximately to curve a, if the difference in refractive index is taken into account. However, in a solution of the same ester hydrolyzed with less water so that two valences of each Si remain occupied with OR groups, an admixture of the same cobalt quantity leads to a slightly blue-colored coating (curve b). If the cobalt oxide is incorporated in a TiO_2 matrix, which is likewise nonabsorbent in the visible region, layers with different colors are observed (Fig. 4, curve c; Fig. 30, curve g). There is obviously no mixture of the original oxides present in the coatings, but binary compounds such as silicates or titanates have been formed which, due to their specific electron configurations, have their own characteristic absorption spectra. This can lead to a large variety of optical properties on which only little research work has been done thus far.

Of course, any given individual solution of different substances cannot be mixed arbitrarily, because reactions might occur which cause precipitations either in the solution or in the film during drying. The preparation of a multicomponent solution, therefore, frequently poses a special problem. Experience has shown that alcoholates or esters of acids of the IIIB, IVA, and IVB elements of the Periodic Table, mainly in the polycondensed OH-rich form described, are particularly capable of accepting other metallic compounds. This makes it feasible to produce an optically homogeneous distribution of various foreign oxides within the Me_2O_3 or MeO_2 layer, respectively (9).

The previously mentioned polyesters are, furthermore, highly suitable for incorporating metal colloids into an oxide layer acting as a matrix. Here again the same metal can cause completely different absorption spectra in different matrices. This is shown by the transmittance curves of Fig. 5 for the case of Au incorporated in (a) SiO_2 and (b) TiO_2 matrices. In both cases, $AuCl_3$ in alcoholic solution had been added to the corresponding esters. When incorporating Ag into SiO_2 layers (by admixture of $AgNO_3$ to a polysilicic acid ester solution), yellow-brown colors are generated similar to the well-known colorations obtained by Ag ions diffusing into glasses. By admixture of $AgNO_3$ to TiO_2, however, color centers are formed which show maximum absorption in the yellow and green region of the spectrum (Fig. 5, curve c). Another matrix which is likewise capable of incorporating
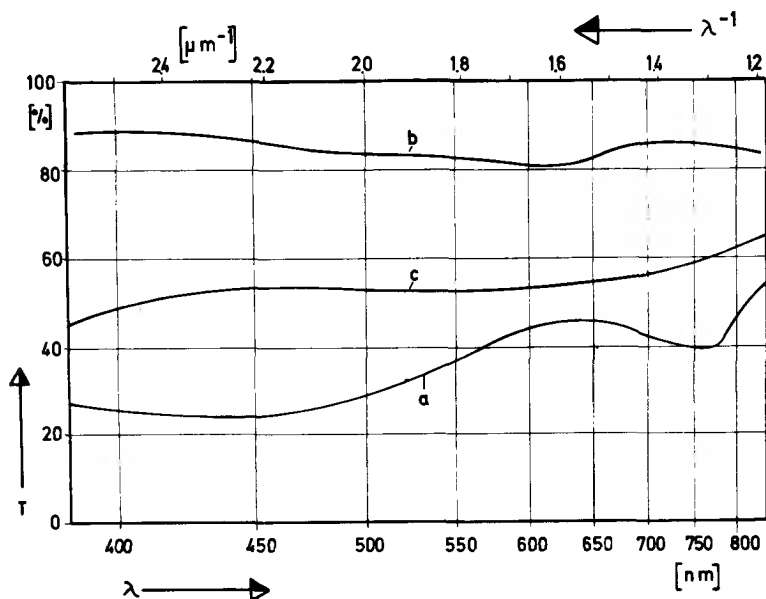
FIG. 4. Spectral transmittance of plate glass coated on both sides with cobalt oxide: (a) without matrix oxide ($d \approx 60$ nm); (b) incorporated in SiO_2 (starting from a solution with OH:R < 1); (c) incorporated in TiO_2 (0.7 mole CoO per 1 mole TiO_2; $d = 70$ nm) (see also Fig. 30, curve g).

various metal colloids or pigments is Al_2O_3, which can be obtained, for example, by depositing a solution of $Al(OC_4H_9)_3$ with subsequent heating. This matrix produces similar spectral absorption curves with embedded coloring substances as does titania. For investigations in solid-state optics, such systems represent interesting specimens for research which by other methods are mostly difficult to prepare.

In a similar way one can also incorporate materials producing other effects. For example there are admixtures of substances which shift the uv absorption edge (10) (see Section V,5,b), and combinations consisting of scattering particles in the form of pyrogenic oxides or pigments, or of organic materials such as silicones, which have sufficient heat resistance. The matrix substances mentioned above are also capable of including compounds of metals whose oxides are not stable per se, such as salts or alcoholates of alkalis or alkaline earths, B_2O_3, H_3PO_4, etc.. Accordingly, for the formation of homogeneous thin films from solutions an almost unlimited number of multicomponent materials is available, which seems to be comparable to the number of glass-forming systems. However, oxide combina-
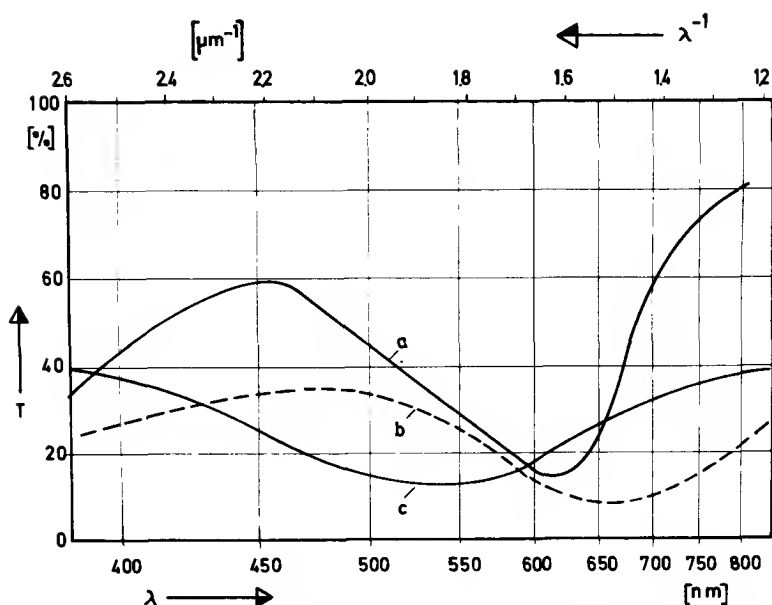
FIG. 5. Spectral transmittance of plate glass coated on both sides with metal colloids incorporated in oxide layers: (a) Au in SiO_2 matrix; (b) Au in TiO_2 matrix; (c) Ag in TiO_2 matrix.

tions suitable for thin film production can be both crystalline and non-crystalline solid state.

2. MULTIPLE LAYERS

In order to obtain specific optical effects, the coating technique must be applicable to combining layers with different optical properties into multi-layer film combinations. Although there seem to be no basic difficulties in repeating the coating process several times using the above described methods, it has been found that this is possible only under certain conditions. Obviously the most important requirement is that the previously deposited layer be insoluble in the following solution and be as wettable as the substrate. Accordingly, the preceding layer must first be converted by thermal aftertreatment to an extent where it contains no more soluble residue of the initial solution. This can be done at lower temperatures if hydrolytic processes are involved to a high degree in the conversion. In the case of SiO_2 layers with which the lowest refractive indices ($n_D \simeq 1.40$–1.45) have been obtained thus far, hydrolysis can already be induced in a solution of silicic acid esters without unduly decreasing their durability. In general it is therefore possible to deposit any further film on SiO_2 layers which have
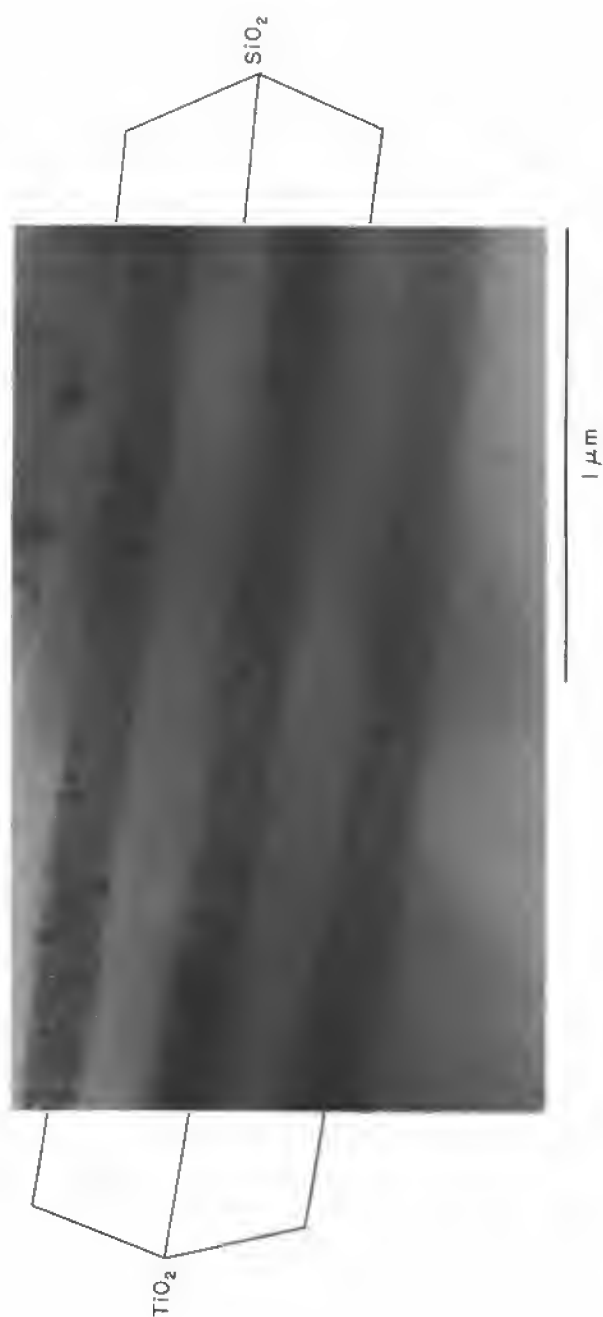
Fig. 6. Electron micrograph of a transverse section through six layers of TiO_2/SiO_2, after baking 1 hr at 550°C. In the TiO_2 films anatase crystallites appear.

been only slightly heated. If each individual layer is sufficiently thin, this procedure can be repeated several times before baking the combined film system.

The bonding strength between different coating materials is usually of the same order as the one between layers and glass substrates, and in some cases even considerably higher. It is therefore sometimes possible to substantially increase the bonding strength to substrates of layers which have poor adhesion to glass surfaces by means of a suitable "priming" with a material such as SiO_2. The wettability of the substrate can sometimes also be improved in this way.

At the most frequently applied baking temperatures the rate of diffusion of the various oxides into each other is imperceptible, apart from a few exceptional cases. Thus, the interfaces between the various layers remain sharply defined. The statistical surface roughness of a film (see Section III,3) is not carried over to the surface of successive layers. Therefore, it does not increase with the number of layers. These features have been demonstrated recently by transmission electron micrographs of thin transverse sections of multiple layers. An example is shown in Fig. 6, which reveals well-defined and remarkably smooth layer interfaces. Such micrographs were obtained by the use of a special ion etching technique which will be described elsewhere (*10a*).

3. STRUCTURE AND MECHANICAL STABILITY OF BAKED OXIDE LAYERS

As indicated above, most oxide layers deposited from solutions show, after heating, polycrystalline structures when examined in the electron microscope. In the diffraction pattern the first diffuse rings normally appear after layers have been heated up to 250–400°C. When the temperature is further increased, the rings become gradually sharper, and the crystallite size increases up to the order of 100 Å. Extended heating at higher temperatures can sometimes favor crystal growth to such an extent that optical scattering occurs.

Adhesion to the substrate and wear resistance of the layers also increase with increasing temperature. Films which have been heat treated at more than 250°C, and which are insoluble in acid and alkaline solutions, can only be removed from glass substrates by polishing. The obtainable maximum mechanical durability of each metal oxide layer depends largely on the type of the initial compound, the preparation of the solution, and the ambient conditions during the film formation. An impairing influence is exerted by the surface roughness which may be measured for example by the average height of the surface irregularities (*11*) or the surface-to-volume ratio (*12*). A high degree of roughness, frequently occurring in connection with a large

porosity of the layers, can be found when solvents, stabilizers, or other
ingredients are applied, which do not escape during the baking process
before the films have been substantially solidified.

The areas of the coated surfaces are limited only by the size of the dip
container and baking furnace. The layer thicknesses, however, are subject
to limitations which are determined by film formation processes of the
substances used, and the degree of "adjustment" of the thermal behavior
of the finished coating to that of the substrate or the previously deposited
films. With single layers it is almost always possible to obtain without diffi-
culties an optical thickness of $\lambda/4$ for visible light. On the other hand, high-
quality single coatings with a thickness exceeding about 0.2 μm can be
obtained only with strongly interlaced polymolecules. A more detailed
examination of these limitations on the thickness has revealed that an
explanation has to be based on the following facts:

1. As has been pointed out in Section III,1,a, film molecules adjoining
the substrate are strongly bound on certain sites of a ceramic or metallic
surface. Therefore, the inner boundary zone of the film can hardly take part
in the subsequent condensation process of the outer zone. If the entire film
thickness is small (e.g., some hundreds of molecular layers), the upper
particles will only have to undergo minor displacements in order to occupy
subjacent vacancies. With increasing film thickness, however, the outer zones
tend to condense irrespective of bonds to the substrate, and consequently
reticular cracks may occur. On the other hand, if a solution of a substance
forming a noncrystalline oxide is deposited on a chemically inert substrate
such as polyethylene which does not exert bonding forces, a gellike mass of
considerable thickness can be condensed, which after a slow increase of
temperature assumes a glasslike appearance. In this process the solvent and
volatile reaction products have to be evaporated with great care.

2. A further reason for the restricted stability of a coating may arise from
differences in the thermal expansion between the film (α_c) and the substrate
(α_s). If α_c is smaller than α_s and the film is fixed on a substrate at relatively
low temperatures, a tensile stress σ_{th} occurs in the film upon heating which
is given by

$$\sigma_{th} = (\alpha_s - \alpha_c)E_c \, \Delta T$$

where E_c is the Young's modulus of the film and ΔT is the temperature
increase.

3. In many kinds of coatings there exists, besides the thermal stress σ_{th},
an intrinsic stress σ_i which sometimes increases with layer thickness d up
to the order of 10^9 dyn/cm^2 (13). Thus, if the resulting tensile stress $\sigma = \sigma_i$
$+\sigma_{th}$ exceeds the tangential strength of the film, cracks appear. The tem-

perature, at which such cracks appear decreases as the thickness of the film that has been made increases.

4. In layers of greater thicknesses ($d > 0.25~\mu$m), surface roughness tends to increase noticeably with the film thickness, particularly when poorly hydrolysable compounds are used. Thus, an optical inhomogeneity, resulting in a decrease of density and refractive index toward the surface, can occur together with an undesired reduction of hardness. In such cases the restriction on layer thickness is determined by the required wear resistance.

The restrictions with respect to the obtainable film thickness are not effective to the same extent, however, if the coating consists of several (N) partial layers and each of them remains below the thickness limit prescribed. Actually, for such coatings the resulting stress σ_N is considerably lower than that of a single layer of the same total thickness. Thus, by repeated deposition of films using the same or an alternating substance, it is possible to obtain coatings of several micrometers thickness, provided the coefficient of thermal expansion does not differ too much from that of the substrate. On window glass ($\alpha_s = 85 \times 10^{-7}/°$C), for example, TiO_2 layers ($\alpha_c \approx 60 \times 10^{-7}/°$C) of approx 100-nm thickness each can be deposited one after another in almost unlimited number, whereas in the case of SiO_2 layers ($\alpha_c \approx 6$–$8 \times 10^{-7}/°$C) a total thickness of more than 1 μm can scarcely be obtained.

In multilayer film combinations with different components, differences in thermal expansion likewise limit the attainable total coating thickness. The thinner the individual layers, the less effective are their expansion properties.

The high intrinsic tensile stress which occurs in various oxide coatings deposited from solutions is obviously a consequence of the incomplete sintering process during firing. Particularly in crystalline structures submicroscopic vacancies are generated which can directly be observed in electron micrographs (see Fig. 9). They lead to a diminution of density and refractive index in comparison with the bulk material. Because of the poor mobility of the molecules in most oxides, the attractive forces exerted between them can not relax at temperatures up to 500°C and more. Such oxide layers are therefore capable of plastically deforming a glass substrate above its softening temperature. An analysis of these phenomena revealed (13, 14) that the following relation exists between the curvature R^{-1} of a glass disk (thickness D, viscosity η) coated on one side by the oxide film, the initial stress σ_0 and the time t:

$$R^{-1} = R_\infty^{-1}[1 - (1 - R_\infty/R_0)\exp - k\sigma_0 R_\infty t], \quad k = \frac{md}{\eta D^2} \quad (m \approx 0.25),$$

where R_0 is the initial, and R_∞ the final value of the radius of curvature ($R = R_\infty$ for $t \to \infty$ and $\sigma \to 0$). Figure 7 shows that this relation is in perfect agreement with experimental results obtained with titania layers of various
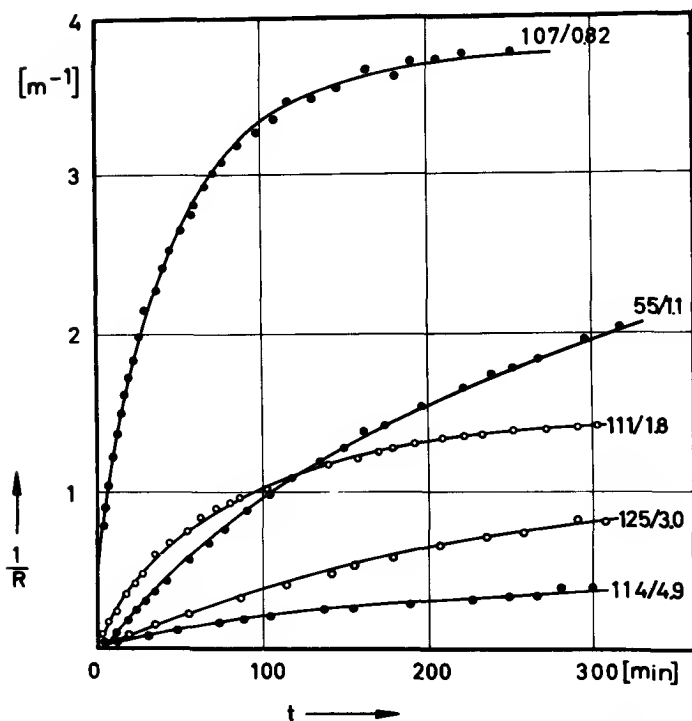
FIG. 7. Curvature versus time for TiO₂-coated glass disks at $\vartheta = 585°C$ (the numbers at the curves indicate film thickness d in nanometers and glass thickness D in millimeters, respectively).

thicknesses d. As can easily be proved, the initial tensile stress σ_0 can be obtained from the initial slope of the curve $1/R_t$ since

$$\sigma_0 = (\eta D^2/md)\ (dR^{-1}/dt|_{t \to 0}).$$

The evaluation of the measurements of Fig. 7 yielded an increase of σ_0 with d up to about 100 nm (13). Above this thickness σ_0 remains approximately constant ($\sim 10^9$ dyn/cm²). σ_0 Values of the same order have been derived from measurements of the elastic curvature of thin coated glass foils just below the softening temperature of the substrate (14). For very small thicknesses d, the measurements reveal a decrease of σ_0 toward zero or toward very low values. The occurrence of a lower tensile stress in thinner films appears conceivable as a consequence of the mechanism suggested above (see Section III,3,a). Another possible reason for this could be the differences in the crystalline structure between thin and thick films of TiO₂, which will be discussed in Section IV,1.

There is another fact which also supports the conclusion that organogenic oxide coatings, when deposited on glass as extremely thin layers (in case of TiO$_2$, $d \lesssim 50$ Å) are particularly free from stresses and flaws. Several observers have found that such layers normally show an even considerably increased hardness and abrasion resistance, as compared with layers of thicknesses in the order of $\lambda/4$. With these thin films an even higher abrasion resistance can be achieved than that shown by uncoated glass. This effect is therefore technologically used to improve the wear resistance of glass containers (15). The oxides most frequently used are TiO$_2$ or SnO$_2$. It is remarkable that the high resistance of extremely thin films can be obtained both by the cold-dipping process and by depositing finely dispersed fluid or evaporated compounds of the same materials on heated glass surfaces.

Although the existence of a tensile stress is particularly striking in coatings exhibiting a crystalline structure, it can be observed also in amorphous oxide layers having a low expansion coefficient compared with that of the substrate. In this case the stress is essentially of thermal origin. The normally small σ_i values, which have been found, for example, in SiO$_2$ coatings, can be enhanced, however, by adding to the solution soluble 'substances, which after baking of the coating are leached out in order to form a slightly porous layer. This method can be applied to create a controlled spherical bending of thin glass discs without the application of pressure.

IV. Special Oxide Layers

1. TITANIA

Of all high index materials, oxide layers obtained from titanium compounds have proved to be of especial practical interest. For this reason, titanium oxide coatings have been investigated with particular thoroughness. The results are, in some respects, also characteristic of the behavior of other coating materials suitable for the preparation of films by liquid coating processes. Therefore, they are treated here in more detail.

A surprising and perhaps specific property of TiO$_2$ films deposited from organic solutions is that their optical properties are dependent on the type of glass substrate. To understand this phenomenon an electron-optical study was made of the structures obtained with layers prepared from identical solutions on various glasses (16). The studies revealed that on alkali-free substrate the anatase structure is always formed (Fig. 8, sector A). However, if the glass substrates used contain sodium ions which can easily migrate (such as are present in window or plate glass), various types of "disturbed" TiO$_2$ structures may appear, the type depending on the rate of heating and to some degree on the initial compound. For example, layers deposited from
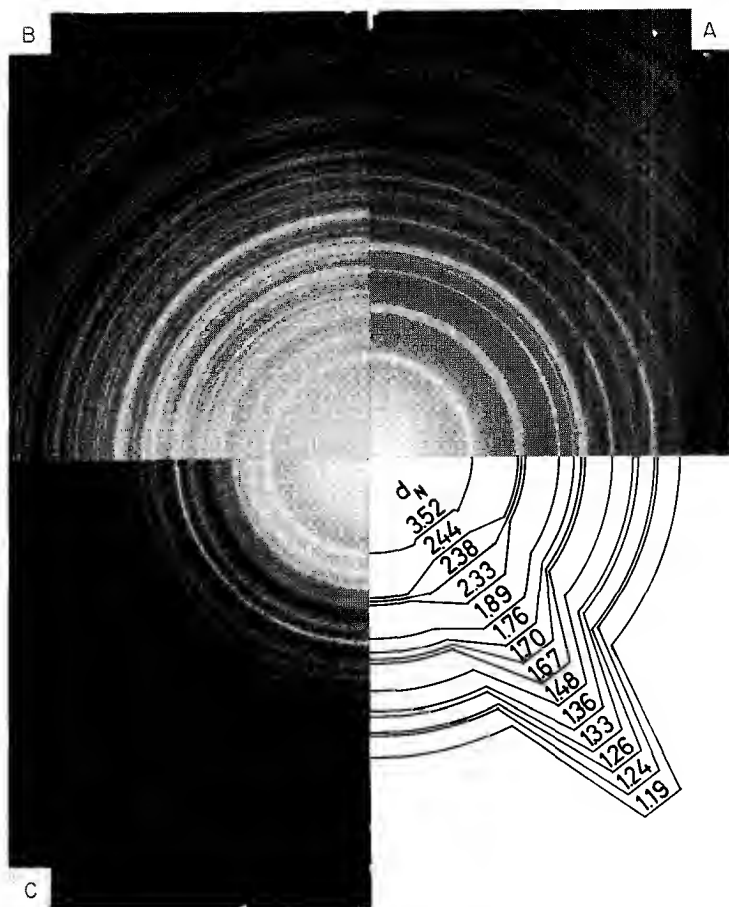
FIG. 8. Electron diffraction pattern of TiO_2 films deposited on: A, silica glass and rapidly or slowly heated; B, window glass and rapidly heated; C, window glass and slowly heated [d_N = spacings between the lattice planes (calculated from the radii of pattern a)].

a $TiCl_2(OC_2H_5)_2$ solution ("T_e films"), begin to form the brookite modification when heated rapidly ($>25°C/min$) to 450°C (Fig. 8, sector B). When, however, T_e films are heated slowly ($<10°C/min$), diffusion of Na^+ out of the glass surface leads to the formation of a crystal phase which exhibits the same diffraction pattern (Fig. 8, sector C) as the ones described in the literature (17) as Na_xTiO_2 or $Na_2O \cdot TiO_x \cdot TiO_2$. Since in our case no indication of the occurrence of a lower oxide of Ti in the solid films has been found, we choose to designate this phase here as "$Na_2O \cdot xTiO_2$." The electron micrographs of the three types of titania films, obtained by means of trans-

mission electron microscopy on samples separated from their substrates, are shown in Fig. 9. They reveal three completely different structures.

If a difficult to hydrolyze Ti compound, such as $Ti(OC_4H_9)_4$ ("T_b films"), is used instead of T_e, a structure of the type shown in Fig. 8c is always observed. In this case crystallization of TiO_2 is delayed so that sodium ions emigrating from the glass substrate are enriched sufficiently in the films to generate the $Na_2O \cdot xTiO_2$-type compound.

The strong influence of sodium ions present in the surface of a substrate on the film structure and composition of titania films can be demonstrated by the following experiment. A silica glass is covered on one side with powdered Na_2CO_3, heated up to 700°C for about 1 hr, and afterwards coated with a T_e or a T_b film. After baking, the coating exhibits the brookite or $Na_2O \cdot xTiO_2$ structure on the side pretreated with soda, and consists of anatase on the untreated side. On the other hand, the alkali influence was found not to be exerted by all types of glass containing sodium. On Schott glasses 2954 and 8405, for example, which contain between 7 and 8 % Na_2O, TiO_2 coatings crystallize only in the anatase form. It may be concluded that in these glasses the diffusion velocity of the alkali ions is so small that it can not compete with the growth rate of the TiO_2 crystallites.

The films with different structures shown in Figs. 8 and 9 also exhibit marked differences in their optical properties. Figure 10 shows the spectral transmission curves of slowly heated T_e films deposited on both sides of (a) silica glass and (b) window glass. The well-known absorption of the latter has been eliminated in this graph by calculation. The evaluation reveals for the various types of films differences in the refractive index n and even more pronounced differences in the position of the uv-absorption edge*. In comparison with pure anatase type coatings, $Na_2O \cdot xTiO_2$ type films formed under slow heating conditions exhibit a lower n and a 14-nm shift of the absorption edge toward shorter wavelengths. On the other hand, brookite type coatings formed from T_e films at sufficiently high heating rates, have a uv cutoff wavelength which is almost identical with that of anatase layers. If T_b or other Ti compounds are used instead of T_e, the refractive index of the baked layers may deviate a little from those prepared from T_e films, since n depends on the packing density in each case. The uv absorption limit λ_s, however, is quite independent of the initial compound but depends on the specific crystal phase formed during baking.

The diffusion of sodium ions into and through a TiO_2 film proceeds rather fast even after the formation of crystals of a certain structure type in the film is terminated. This can be concluded from several observations. First,

---

* This edge is defined here by the intersection λ_s of the tangent at the point of inflection with the abscissa.
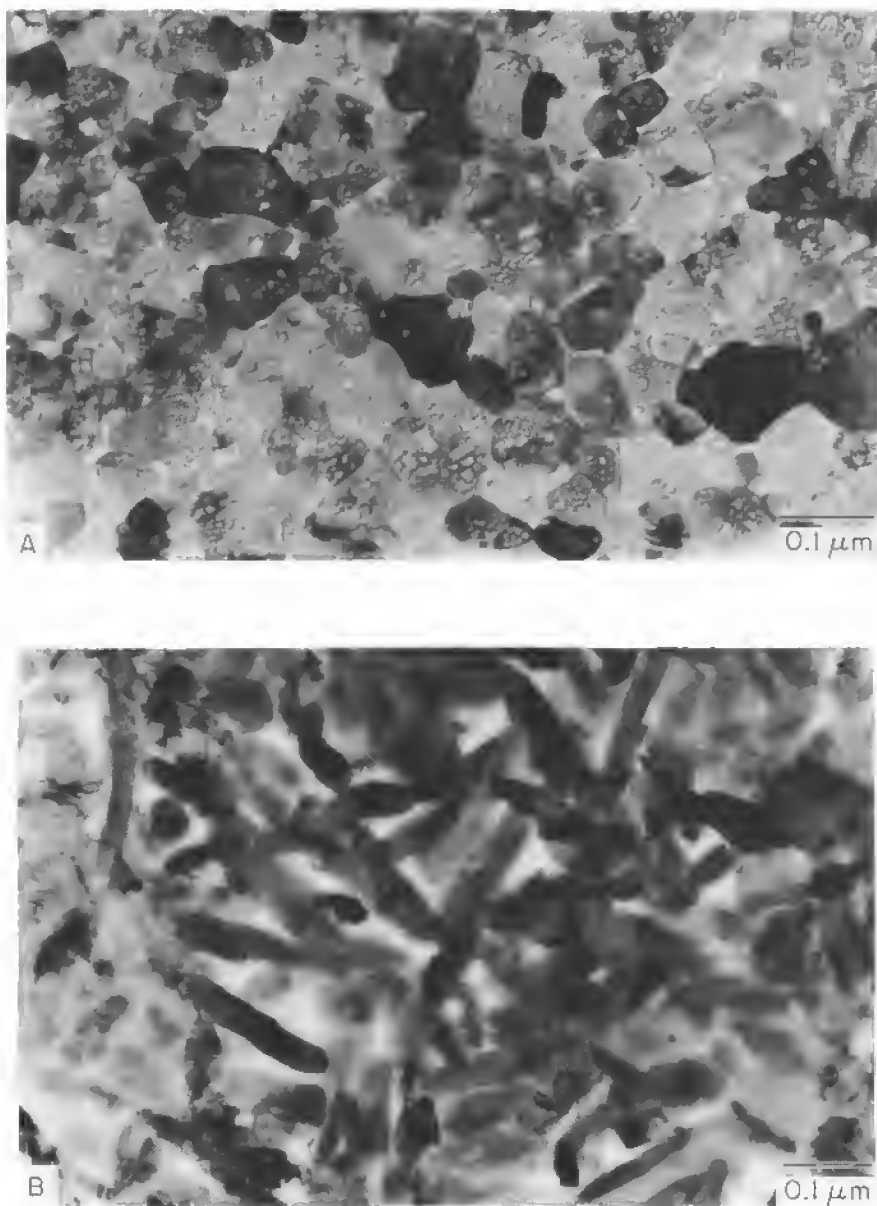
FIG. 9. Electron micrographs of the structures A, B, and C of Fig. 8.
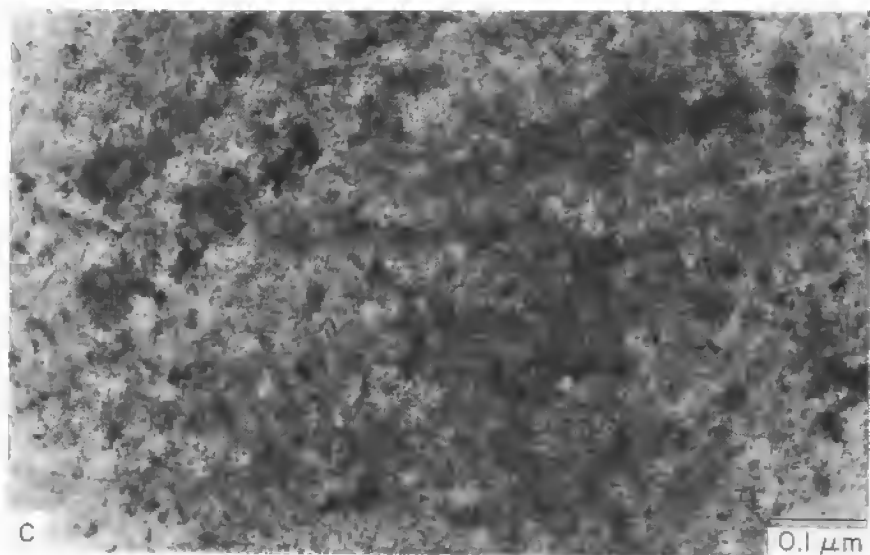
FIGURE 9c.

the "disturbed structures" can also be observed in diffraction patterns generated by electrons reflected at grazing incidence from the layers, unless their thickness is too large. In addition, after baking T_e films, tiny crystallites of NaCl are frequently detected on their surfaces. Remaining traces of Cl on the surface and sodium ions diffused through the film must be responsible for their formation. Finally, it has been found that baked TiO_2 films on soda-containing glasses do not form a substantial diffusion barrier against an ion exchange with silver immigrating from staining pastes at ~500°C. On the other hand, silica layers, produced in a similar way from solutions of silicic acid esters on glass, behave completely differently. They make an excellent diffusion barrier. A 200-Å-thick silica film is already sufficient to prevent, even at high temperatures most of alkali ions at the glass surface from migrating into a subsequently deposited TiO_2 film. Therefore the appearance of the various crystal phases in TiO_2 coatings on soda glasses can be controlled by means of a predeposited SiO_2 layer and by the heating rate. Figure 11 shows the result of deposition parameters on the uv absorption edge of titania films. A more detailed survey of the properties observed with T_e and T_b layers of $\lambda/4$ thickness, which were deposited on SiO_2 precoated window glass and heated up to 500°C, is given in Table 1. This review shows clearly the competition between crystallization of TiO_2 in the anatase form and the Na^+ ions penetrating more or less rapidly into the films. If only small quantities of Na^+ have arrived before crystallization starts, the
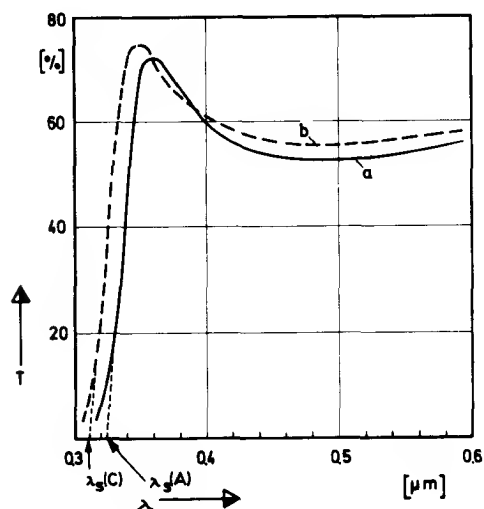
FIG. 10. Spectral transmittance of T_e films deposited on (a) silica glass, (b) window glass (both sides coated).
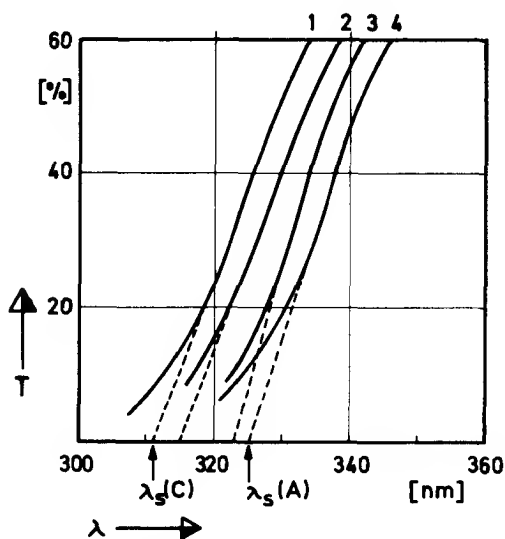

FIG. 11. Ultraviolet absorption edge of T_e films deposited on window glass precoated with SiO_2:

SiO_2 layer thickness d_s (nm)		0	6	12	18
Observed curve, when	rapidly	3	3–4	4	4
heated up	slowly	1	2	2–3	3–4

TABLE I

Structural and Optical Characteristics of TiO_2 Films ($d \approx 60$ nm) on
Window Glass Precoated with SiO_2 Films of Various Thicknesses[a,b]

Thickness of SiO_2 film (nm)	TiO_2 from T_e soln, heated up		TiO_2 from T_b soln, heated up	
	50°/min	10°/min	50°/min	10°m/in
0	B (+ C)[c]	C	C[d]	C (+ A)
	323, 2.25	311, 2.24	315, 2.03	315, 2.03
6	B + A (+ C)	C (+ B)[d]	A (+ C)	A + B
	324, —	315, —	323, —	323, —
12	A	B + C[d]	A	A (+ C)
	325, 2.28	317, —	325, —	325, —
18	A	A + C	A	A
	325, 2.28	324, —	325, —	325, —
24	A	A	A	A
	325, 2.28	325, 2.28	325, 2.20	325, 2.20

[a] Crystal types: A, anatase; B, brookite; C, $Na_2O \cdot xTiO_2$.

[b] Numbers below indicate λ_s (nm) and n measured for $\lambda = 550$ nm.

[c] Structure types in parentheses appear in minor quantities.

[d] Anatase appears in trace amounts only.

brookite type is induced, but as soon as higher quantities have passed over, the sodium is incorporated to form a $Na_2O \cdot xTiO_2$-type structure. In addition, the data listed in Table I allow a comparison of SiO_2 thickness values needed for the exclusion of $Na_2O \cdot xTiO_2$ crystals in T_e and T_b films.

It may be assumed that the emigration of alkali ions from glass substrates into freshly prepared solid films of titania is a phenomenon which might also occur with other film materials produced in a similar way. However, up to now, no publications describing such observations seem to exist.

In order to get further knowledge of the processes occurring during the solidification of titania films, the refractive index n (for $\lambda = 550$ nm) and the geometrical thickness d have been measured as a function of the baking temperature (ϑ_B) and the duration of the baking (t_B). T_e and T_b films of approximately the same thickness (~ 110 nm) were deposited on window glass, slowly heated up to ϑ_B, and tested after baking times of (a) 0.1, (b) 1, and (c) 10 hr. From the curves for T_e and T_b films shown in Fig. 12 it can be concluded immediately that for T_e the formation of the oxide layer is substantially terminated at a rather low temperature of about 250°C. This results obviously from the fact that the hydrolytic reaction of the liquid film with air moisture starts at room temperature and is already finished after moderate heating. With T_b, however, which is much more resistant
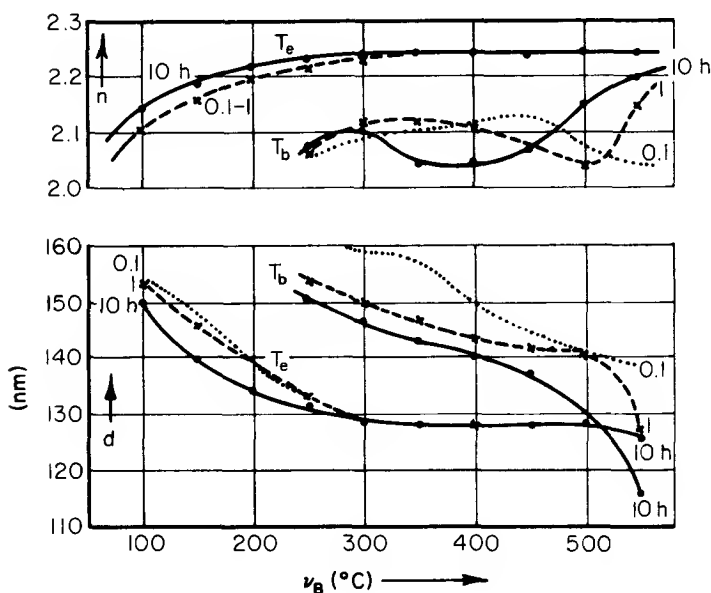
FIG. 12. Refractive index n ($\lambda = 550$ nm) and thickness d vs baking temperature ϑ_B for T_e and T_b films (parameter, baking time t_B).

to hydrolysis, the transformation phenomena produced essentially by pyrolysis extend over the whole temperature rise up to the softening range of the glass. It can further be seen that the n curve, which first rises to a maximum, then drops to a minimum, before showing again a considerable rise, shifts toward a lower temperature when t_B is increased. This means that n can be expressed by a function of the form

$$n = F(\vartheta_B f(t_B)).$$

The d curves of T_b films show a similar displacement of values toward lower temperatures when the baking time is increased from 0.1 to 10 hr.

This behavior can be interpreted as follows. During the first rise of n after the evaporation of the solvent, the T_b film becomes more compact without substantial loss of its mass. At this stage the first crystal nuclei have already formed. When $u = \vartheta_B f(t_B)$ exceeds a certain amount, the organic decomposition products and eventually H_2O, which have been formed during the pyrolysis, are gradually expelled so that despite a further decrease in thickness, the density, and thus also the refractive index both diminish. When u increases further, the porous assemblage of crystallites, consisting in the case under consideration of $Na_2O \cdot xTiO_2$, starts to condense. This
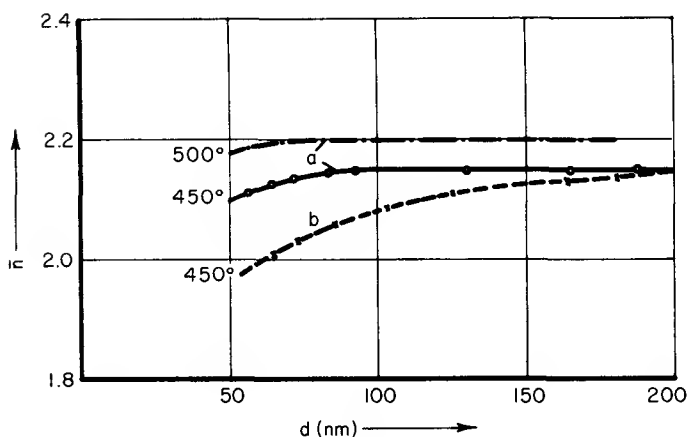
FIG. 13. Mean refractive index $\bar{n}$ ($\lambda = 500$ nm) as a function of layer thickness of T_b films deposited on (a) silica, (b) window glass.

leads to a rise of n to a value which the T_e films have already attained at 250°C, and to a still further decrease of d. It is, however, remarkable that the refractive indices attained are still considerably lower than those of compact titania crystals, so that despite the high degree of hardness of the layers, the volume factor computed from the molar refraction hardly exceeds 0.90.

On the other hand, higher indices can be attained in titania layers if certain heavy metals such as bismuth or lead are incorporated as oxides, and if the influence of alkali is sufficiently suppressed. Under these conditions the increase in refractive index is accompanied by a shift of the uv absorption limit toward longer wavelengths.

An attempt was made to investigate the structure of T_e films containing an admixture of $BiCl_3$ (31 g Bi_2O_3:100 g TiO_2). If the films are deposited on silica glass and fired at temperatures up to ~500°C, the only crystal type observed is anatase. After treatment at higher temperatures, however, the diffraction pattern also reveals the formation of rutile crystallites. This transformation into rutile goes to completion at a temperature of 600–700°C if the silica substrate has been precoated with a SiO_2 film of approx $\lambda/4$ thickness prepared from a silicic acid ester solution. In the case of a precoated window glass this transformation is accomplished only above 850°C, whereas at lower temperatures increasingly higher portions of anatase and $Na_2O \cdot xTiO_2$ are formed. From these observations it can be concluded, first, that the minimum thickness of the diffusion inhibiting SiO_2 layer increases with a higher content of Cl^- ions, and second, that the anatase lattice is stabilized by sodium ions penetrating into the T_{e+Bi} film. The refractive indices n

obtained in such films on silica substrates range from 2.30 to about 2.50 for $\lambda = 550$ nm, depending on the firing temperature and period.

Since the process of alkali emigration from a substrate into a crystallizing film requires a certain time, the influence on the resulting structure type can be expected to decrease more or less from the substrate–film boundary to the film–air boundary, depending on film thickness d. Consequently, since the refractive index of $Na_2O \cdot xTiO_2$-type films was found to be considerably lower than that of anatase-type ones, thin layers deposited on alkali glasses should exhibit lower mean indices $\bar{n}$ than thicker ones. Figure 13 shows the results of measurements of $\bar{n}$ at $\lambda = 500$ nm obtained with T_b films deposited (a) on silica glass and (b) on window glass, both baked 1 hr at 450°C and 500°C, respectively. In the case (a) only a slight drop of $\bar{n}$ occurs at film thicknesses of less than ~ 80 nm, which may be caused by a decreasing packing density near the substrate due to a restriction in the sintering possibility. On window glass (b), however, the alkali diffusion into the T_b films leads to a Na-concentration profile which obviously falls down rapidly at a distance of about 50 nm from the substrate, so that the mean refractive index increases continuously if the film becomes thicker than 50 nm. According to the theory of light reflection at inhomogeneous layers (*18*), it is possible to determine n_a and n_s, the values of n at the film–air and the film–substrate boundaries, from the reflectance values at maximum and minimum. Actually, such measurements carried out for rather thick T_b films on window glass yielded for $\Delta n = n_a - n_s$ values up to $\simeq 0.15$.

Since the refractive index n of TiO_2 layers produced from organic solutions is dependent on a series of parameters during their formation, it is evident that the dispersion, n_λ must likewise exhibit corresponding variations. However, if a reduced dispersion N_λ is introduced by relating the n_λ values of each individual curve to those at $\lambda = 550$ nm, i.e., $N_\lambda = n_\lambda/n_{550}$, all curves for N_λ become nearly identical, no matter which Ti compound, concentration, or substrate has been used and which crystal type appears (see Fig. 14). In addition, this curve coincides largely also with that calculated from dispersion data for bulk TiO_2 (*19*). Deviations from this function N_λ which is characteristic for TiO_2, become noticeable only if oxides are incorporated which have markedly different absorption properties in the uv or visible region, or when suboxides have been formed in the presence of reducing ingredients.

For certain T_b coatings with anatase structure, applied on fused quartz, the optical constants n and k were also determined in the short-wavelength absorption region. The thickness d was first determined from the spectral position of the reflectance maxima and minima in the region where $k = 0$ ($\lambda > 420$ nm). Thereafter were evaluated n_λ and k_λ from measurements of T_λ and R_λ in the region of $\lambda = 200$–1000 nm, using a calculation method
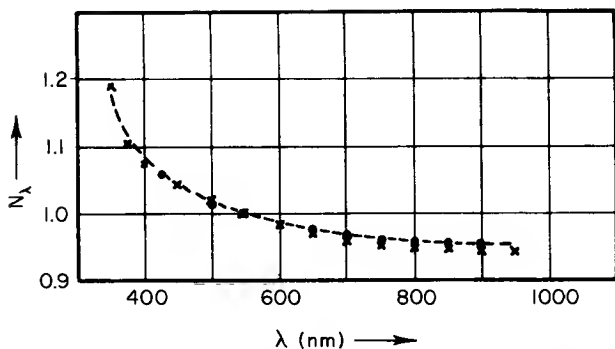
FIG. 14. Reduced dispersion N_λ of various TiO_2 materials in the visible region: ($\times$) films with anatase structure; ($\bullet$) films with C-type structure; (- - -) bulk material (anatase, mean values over the crystallographic axes).
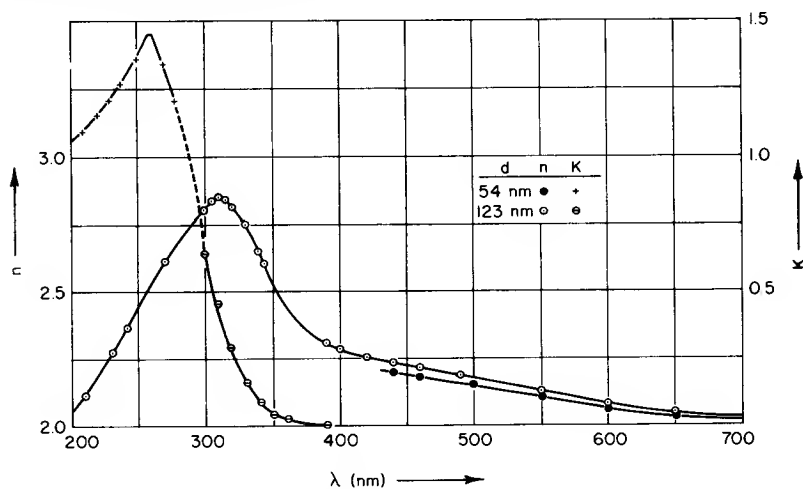

FIG. 15. Optical constants n, k of T_b films ($d = 54$ and 123 nm) on silica glass, calculated from measurements of T_λ and R_λ ($\vartheta_B = 430°C$).

applying to homogeneous layers. The results are recorded in Fig. 15 for two layers of $d = 54$ and 123 nm, respectively. They reveal again a slight dependence on d of the n values as exhibited in Fig. 13.

2. SILICA

SiO_2 has gained its importance for practical applications of the cold-dipping method by the fact that it is the only substance with which hard and stable layers with a refractive index <1.5 can be obtained. Numerous suggestions for the preparation of SiO_2 films are published in the patent
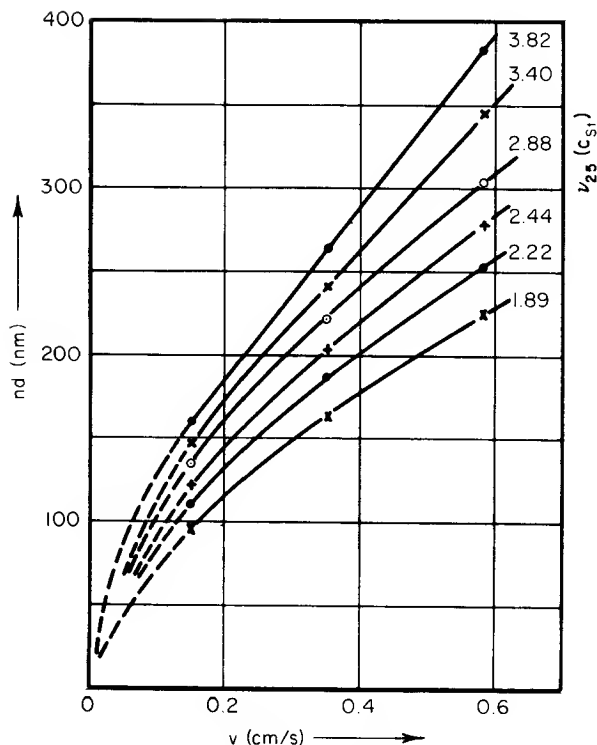
FIG. 16. $nd = f(v)$ for SiO_2 films obtained from methyl silicate solution ($c = 34$ g SiO_2/liter) at different states of polycondensation (measured by kinematic viscosity v at 25°C in cSt).

literature, since silica derivatives for the production of coatings are also applied in other technological fields, such as finishing of textiles. To produce solutions, it is preferable to start from methyl or ethyl orthoesters of silicic acid (20). By adding small amounts of acid, hydrolysis can be started in an alcoholic solution, and, at the same time, precipitation of silicic acid gel can be considerably delayed by using solutions of sufficiently low concentration. Due to polycondensation, there is a gradual rise in viscosity v, starting at very low speed and pursuing with increasing velocity so that, with invariable concentration of the solution, the curve which represents the (optical) layer thickness as a function of the lifting speed v, slowly shifts toward higher values (Fig. 16). The shape of the curves $nd = f(v)$ thus obtained largely resembles that already shown in Fig. 1. It can be used to derive curves representing the lifting speed v, required to obtain a certain layer thickness d, as a function of v (Fig. 17). The value required for v thus can easily be determined from measurements of c and v. If such groups of
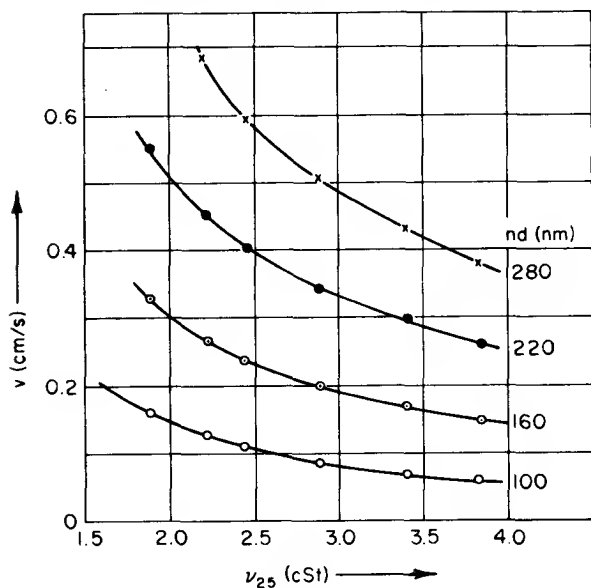
FIG. 17. v required for the production of SiO_2 films of predetermined optical thickness from solutions characterized in Fig. 16.
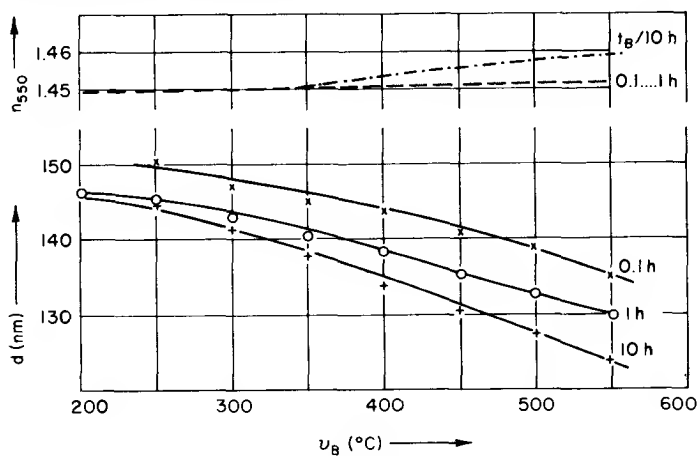

FIG. 18. n ($\lambda = 550$ nm) and d vs ϑ_B for SiO_2 films (parameter, baking time t_B).

curves are present for different concentrations, it is of course also easy to determine the relation occurring between nd and v when any solution is diluted.

The refractive index n_{550} and dispersion of baked SiO_2 layers are almost identical with those of silica glass. As can be seen from Fig. 18, n further

shows only a very slight dependence on the baking temperature ϑ_B. From these observations it can be concluded that the films, due to their amorphous structure, practically attain bulk density at temperatures of approximately 500–550°C. Only in the case of thicker layers ($d \gtrsim 150$ nm) does the refractive index remain, even after extended heating, slightly below that of silica glass. On the other hand, the layer thickness d shows substantial decrease with ϑ_B (Fig. 18), which even considerably surpasses that observed on T_b films (see Fig. 12). Volatile reaction products of hydrolysis are released here only with considerable supply of energy. This applies mainly to physically adsorbed water as well as to H_2O molecules formed during the transition of SiOH groups to Si–O–Si combinations. These reactions take place only at relatively high temperatures, as is known from investigations made on pyrogenic SiO_2 ("Aerosil") (21). During the cooling of baked films, a slight increase in the refractive index ($\Delta n \approx 0.005$) is always observed. This is obviously due to redepositing of H_2O molecules by chemisorption and capillary condensation on pores in the layer.

The uv transmission of SiO_2 layers is, as in the case of silica glass, a function of purity. However, even when using highly purified base materials, the film transmittance in the short wave uv region does not reach the values attained with extremely pure SiO_2 glass, since hydrolytic and pyrolytic decompositions leave behind small residues of organic compounds which, below 205 nm, can produce a measurable absorption (Fig. 19). On extremely
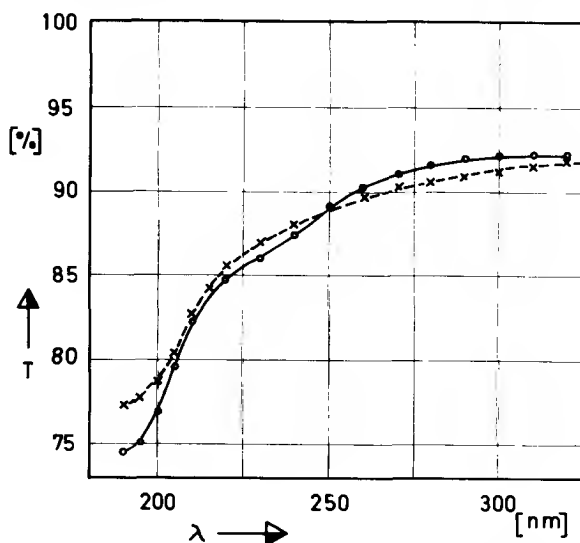

FIG. 19. Ultraviolet transmittance of SiO_2 films ($d = 340$ nm) deposited on both sides of a silica glass substrate of high purity: (——) silica glass uncoated.
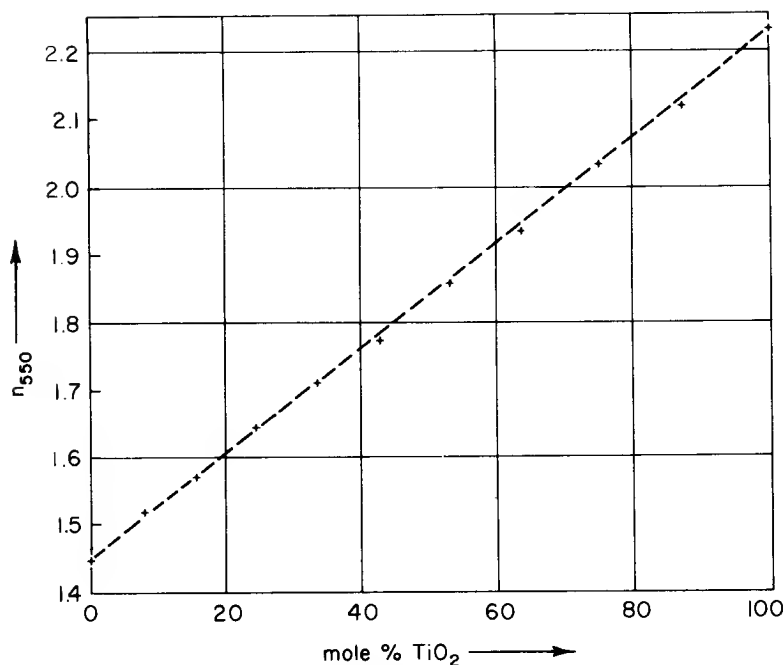
FIG. 20. Refractive index of SiO_2–TiO_2 films as a function of the molar proportion of TiO_2 ($\lambda = 550$ nm).

thick ($d \approx 5$ mm, see p. 102) SiO_2 gels detached from the substrate, an amount of carbon up to 0.1 % could be traced by chemical analysis, even after heat treatments up to 800°C. Nevertheless, these materials are optically entirely clear.

In the infrared region, SiO_2 layers show the strong absorption bands of Si–O vibrations at the same frequencies as pure silica glass, between 7.8 and 11.5 μm. They also exhibit weaker bands between 2.7 and 3.6 μm, suggesting incorporated OH groups, and at 6 μm, bands attributed to adsorbed H_2O.

From measurements of the sputtering yields of layers under bombardment with argon ions and from the optical determination of their range depth, data on their molecular bond energy could be deduced (22). This energy amounts to about 3000 kcal/mole at a thickness of <50 nm, as compared to approx 3200 kcal/mole for the two quartz modifications (23). With the ion-sputtering method the immigration of Na ions into SiO_2 layers could also be verified, as disclosed by Table I (see Section IV,1). By comparing the measured luminescence of the bombarded Na ions to the layer thickness removed, it was confirmed that the diffusion range of the alkali ions attains, under chosen temperature conditions, only just the values at which the "C"

structure of TiO_2 layers deposited on a silica layer of the same thickness recedes behind the "A" structure.

By addition of substances which are volatile at elevated temperatures or which subsequently can be leached out, n can be reduced substantially. However, this is normally possible only at the expense of the mechanical resistance of the layer. An extreme example of this is supplied by alkali silicate solutions which have been used in the past for antireflection coatings of lenses. Here, alkali has been eliminated from these films by water after

TABLE IIA

CHARACTERISTICS OF ORGANOGENIC METAL OXIDE COATINGS
Coatings which are Nonabsorbing in the Visible Region

Oxide	Preferred starting compound	n	Absorbing below (nm)	Structure	Remarks	Ref.
Al_2O_3	$Al(NO_3)_3 \cdot 9H_2O$, Al-*sec*-butylate	1.62	~250	{ Amorph. { Cryst.	a	8
CeO_2	$Ce(NO_3)_3 \cdot 6H_2O$	2.11	400	Cryst.	a	
HfO_2	$HfOCl_2 \cdot 8H_2O$	2.04	~220	Cryst.	b	24
		[$\lambda = 400$]				
In_2O_3	$In(NO_3)_3$	1.95	420	Cryst.	c	8
La_2O_3	$La(NO_3)_3$	1.78	220			
Nd_2O_3	$Nd(NO_3)_3$	(Inhom.)			d	
PbO	$Pb(CH_3COO)_2$	(Inhom.)	~380	Amorph.	e	
Sb_2O_4	$SbCl_5$	1.90	340			8
SiO_2	$Si(OR)_4$	1.455	~205	Amorph.	a	Sect. IV,2
SnO_2	$SnCl_4$	(Inhom.)	350	Cryst.	c	
Ta_2O_5	$TaCl_5$	2.1	310			
ThO_2	$ThCl_4$, $Th(NO_3)_4$	1.93	~220	Cryst.	f	8, 24
TiO_2	$TiCl_4$, $Ti(OR)_4$	~2.3	380	Cryst.	a	Sect. IV,1
Y_2O_3	$Y(NO_3)_3$	1.82	$\lesssim 300$			
ZrO_2	$ZrOCl_2$	1.72	340	Cryst.		8

[a] As a matrix highly suitable for incorporation of other substances (see Section III,1,b).

[b] Uv-absorption limit is a function of ϑ_B; up to $\vartheta_B = 400°C$, Cl residues are traceable in layers (24).

[c] Layers show marked semiconductor properties (see Section V,6,a).

[d] Characteristic absorption bands of Nd^{3+} ions between 500 and 600 nm appear in layers of quarter- or half-wave optical thickness as a very faint attenuation of the transmittance curve.

[e] PbO layers are remarkable because at temperatures of not more than ~500°C a noticeable diffusion of the substance into the glass substrate starts in case of normal plate glass. At the same time a transition zone with decreasing refractive index is being formed, starting from the layer next to the glass, so that optical effects typical of inhomogeneous

depositing the layer, so that a highly porous and mechanically sensitive SiO_2 skeleton with a refractive index of approx 1.3 remained. For technical applications, it is not advisable to reduce by more than approx 2–3% the refractive index of SiO_2 films by means of an artificial formation of pores.

To increase the refractive index of SiO_2 layers, almost all metal oxides suitable for producing durable layers of higher index can be used. The addition of TiO_2 leads to mixed oxides of particularly high resistance and stability. Such layers show already at a molar ratio of approx 30% TiO_2

TABLE IIB

CHARACTERISTICS OF ORGANOGENIC METAL OXIDE COATINGS
Coatings with Pronounced Absorption in the Visible Region

Oxide (of)	Starting compound	n	k	Color (transm. light)	Structure	Remarks	Ref.
Co	$Co(NO_3)_2 \cdot 6H_2O$	~ 2.0	~ 0.16	Brown		g	8 (see Fig. 4)
Cr	$Cr(NO_3)_3 \cdot 9H_2O$, CrOCl			Yellow-orange			8
CuO	$Cu(NO_3)_2 \cdot 3H_2O$			Brown			
Fe_2O_3	$Fe(NO_3)_3 \cdot 9H_2O$	2.38	0.14	Yellow-red	Cryst.	g	8 (see Fig. 22)
Ni	$Ni(NO_3)_2 \cdot 6H_2O$			Grey		h	
Rh	$RhCl_3$		~ 0.2	Grey-brown		c	
Ru	$RuCl_3 \cdot H_2O$			Grey		c, h	
U	$UO_2(COOCH_3)_2$	1.95	0.015	Yellow			(see Fig. 30 h)
V	$VOCl_2$	~ 2.0	0.01	Greenish-yellow		h	8

layers (18) can be observed. When sufficiently heated, so that PbO is completely absorbed by the glass surface, and this surface is treated with dilute nitric acid, the lead will again be eliminated. There then remains on the glass surface a microporous, optically almost homogeneous, low-refractive index layer with $n \approx 1.36$–1.45, depending on the concentration of immigrated Pb. The mechanism of the PbO diffusion into the glasss urface is still not completely understood. Similar phenomena have also been observed between PbO and a subjacent TiO_2 layer. According to investigations by Harris and Cook (25), these phenomena are produced by a counterdiffusion of Pb^{2+} and Ti^{4+} ions and a formation of $PbTiO_3$.

^{f} Ultraviolet absorption limit is a function of ϑ_B; Cl^- and NO_3^- ions act in a different way (24).

^{g} Almost identical optical properties are also observed for layers obtained by spraying chloride or acetate solutions on preheated glasses (6).

^{h} Optical properties being, to a high degree, a function of the preparation conditions of the films.

crystalline structures in the electron diffraction pattern. In Fig. 20 the refractive index of SiO_2–TiO_2 layers is plotted as a function of the molar proportion of TiO_2. The measurements reveal this function to be practically linear.

3. OTHER METAL OXIDES

In Section III,1,a it was pointed out that it is basically possible to deposit oxide films from solutions of all higher-valence metals, if the starting compounds dissolve in organic solvents and show little tendency to crystallize. In most cases, there are numerous possibilities for chemical compositions of a solution suitable for the production of films of a specific metal oxide. Since the type of preparation is crucial both for the deposition conditions (climatic data) to be selected and for the properties of the resulting layers, the optimum composition of the solution has to be determined for the problem posed by means of systematic investigations. The basis for this is of course supplied by the chemical properties of the metal compounds involved. Oxides whose deposition as one-component layers causes difficulties can almost always be deposited as homogeneous mixed oxides by embedding them in a matrix forming high-quality films as, for example, those of SiO_2 or TiO_2.

A compilation of oxides which can be produced as one-component layers of good optical and mechanical quality is given in Table II. Group A comprises coatings which are practically nonabsorbent in the visible region, and group B represents layers which exhibit a pronounced absorption in this region. Whereas the stoichiometric oxygen content of the coatings in group A is hardly questionable, the one in group B is rather uncertain. In some cases, such as with Ni and Ru, the composition is obviously not stoichiometrically defined, but determined by the redox potential existing during layer formation. This becomes apparent by the fact that the degree of extinction can be varied by additives modifying the redox character of the solution, or by the atmosphere during the baking process.

Column 2 of Table IIA and B states the preferred basic compounds from which the alcoholic solutions of the substances are made. Column 3 gives the optical constants of the coatings. If no remarks are made, the numbers listed apply to $\lambda = 550$ nm. The data listed in these columns relate to values which have been obtained after a baking treatment of the films at 480–500°C. Column 4 of Table IIA gives the wavelength at which the coating starts to exhibit noticeable and increasing absorption toward shorter wavelength, and in Table IIB the color is entered which appears in transmitted light for thicknesses, where interference effects are of minor importance. Column 5 indicates whether the electron diffraction pattern—if examined—shows an amorphous or crystalline structure.

V. Applications

The field of application of coating methods by means of solutions results from the manufacturing technique described in Section II,3 and from the layer properties stated in Sections III and IV. The simultaneous deposition of coatings on both sides of a substrate is a particular advantage of the dipping method, since predetermined optical values can be attained by a smaller number of layers or less expenditure. On the other hand, if only one surface has to be coated, the other one must be covered by a lacquer, or two panes of the same size have to be cemented together for dipping and then separated for baking. In the industrial field there are mainly applied coatings in which refraction and absorption properties of the layers are used to obtain specific optical effects. These applications mostly concern glass substrates of large dimensions; however, small parts can also be economically coated if only one or two layers are applied and the layer thickness is not very critical. This holds true mainly for protective coatings, antistatic coatings, and other coatings of minor optical importance.

1. ANTIREFLECTION COATINGS

For an efficient antireflection treatment of sheet or plate glass ($n_G \simeq 1.51$–1.52), the application of monolayers is insufficient, since the refractive index of the lowest index compact film material (SiO_2) is $n = 1.45$. This is much higher than the value required to produce zero reflectance ($n_G^{1/2} \simeq 1.23$). Zero reflectance can of course be obtained with double layers for one or two wavelengths; however, the antireflection degree obtainable with $n \gtrsim 1.45$ for white light is unsatisfactory (26). According to Geffcken (27), an efficient antireflection treatment of glass, with $n_G \approx 1.5$, requires at least three layers of different refractive indices. To build up such systems, it is advisable to start from the design M–2H–L* and to adjust the accurate thicknesses so that residual reflection of white light appears either violet or almost neutral with a slight greenish tan. According to well-known rules, the following relation between the refractive indices n_M, n_L, n_G of bottom layer (M), outer layer (L) and substrate (G), must be satisfied to obtain zero reflectance:

$$n_M = n_L \ n_G^{1/2}.$$

With $n_L = 1.455$ and $n_G = 1.52$, n_M becomes 1.79. This value can easily be obtained by mixing SiO_2 with a high-refractive index oxide such as TiO_2, ZrO_2, CeO_2, etc. (see Fig. 20). The bandwidth, i.e., the spectral distance of the two λ values, between which $R_\lambda < R_0/2$, is determined by n_L and n_H (28). Figure 21 shows R_λ for the two preferred types, the one with violet and the

---

* M, H, and L denote quarter-wave films of medium, high, and low indices of refraction, respectively.
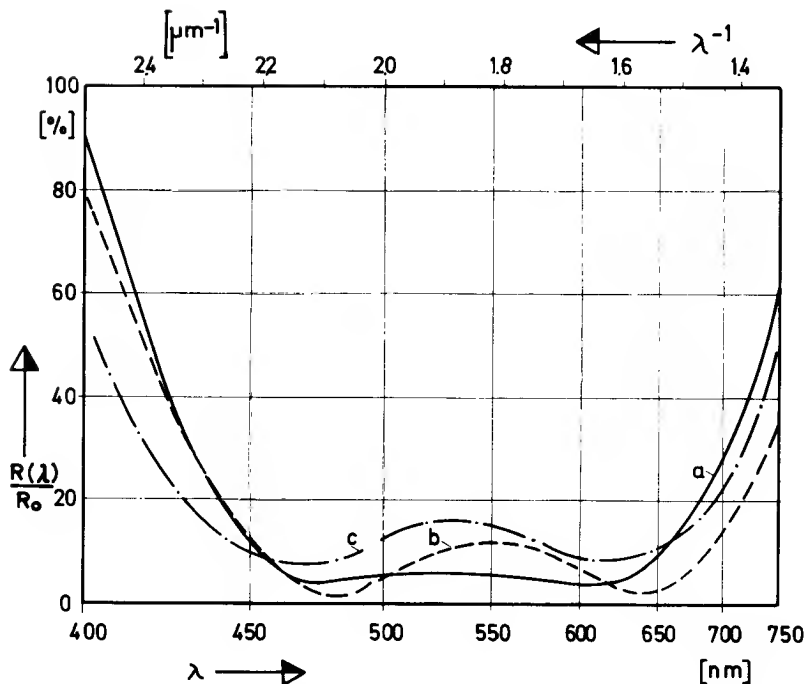
FIG. 21. Spectral reflectance of plate glass coated with three-layer antireflection films (uncoated glass $= 100\%$): (a) type exhibiting violet residual reflection; (b) "achromatic" type; (c) type with absorbing middle layer (see p. 126).

one with greenish residual reflection, using $n_M = 1.79$ ($SiO_2 + TiO_2$), $n_H = 2.20$ (TiO_2), and $n_L = 1.45$ (SiO_2) for $\lambda = 550$ nm. A lower index for n_L would be desirable, but as mentioned in Section IV,2, it is hardly possible to diminish n_L without deteriorating the mechanical and chemical durability of the coating.

Glasses with the three-layer antireflection coating on both sides, as described, are mainly used as cover glasses for instruments, scales and pictures, as well as for glazing showcases, etc. If an antireflected plate glass is silver coated and protected with a lacquer on one surface, according to customary spraying methods, the result is a backside silver mirror which shows practically no double image and whose reflectance surpasses that of a standard mirror of this type by approx 3%.

2. ABSORBING COATINGS WITHOUT ESSENTIAL INTERFERENCE EFFECTS

Most light-absorbing metal oxide coatings have, as compared to ordinary glass, a rather high index of refraction. This leads to superposition of interference and absorption effects. In a number of practical applications, utiliza-

tion of absorption effects only is required, without obtaining at the same time an increased reflectance of the absorbing surface. For this purpose, both metal oxides and metal colloids, as well as very finely dispersed pigments, can be incorporated with homogeneous distribution into a matrix of oxide layers of low or medium refractive index. If the concentration is not too high, the resulting real part of the refractive index of the layer will only slightly differ from that of the substrate. The layers thus formed are free from scattering and show only weak or completely negligible interference effects, whereas their spectral transmittance is more or less strongly reduced by absorption. SiO_2 and Al_2O_3 are particularly suitable as matrix oxides.

To produce "gray" absorption, i.e., absorption which is only insignificantly dependent on the wavelength in the visible range, metals of Group VIII are particularly suitable, either alone or in combination with Au and/or Ag. They can be combined as chlorides, dissolved in organic solvents with silicic acid esters or organic aluminium compounds. Metals of the platinum group, such as Pd or Pt, are, during the heating of the films, normally precipitated in an elementary form as minute microcrystals which can be identified in an electron microscope. They form highly efficient absorption centers which in certain cases also increase the refractive index of the layer (29). Figure 22 (a and b) shows the spectral transmittance of layers containing Pd and Ru, respectively, in an oxide matrix. Absorbing coatings which are practically free of color effects are supplied also by nickel oxide, pure or incorporated into matrix oxides (Fig. 22, c and d). In this case the heat treatment has to
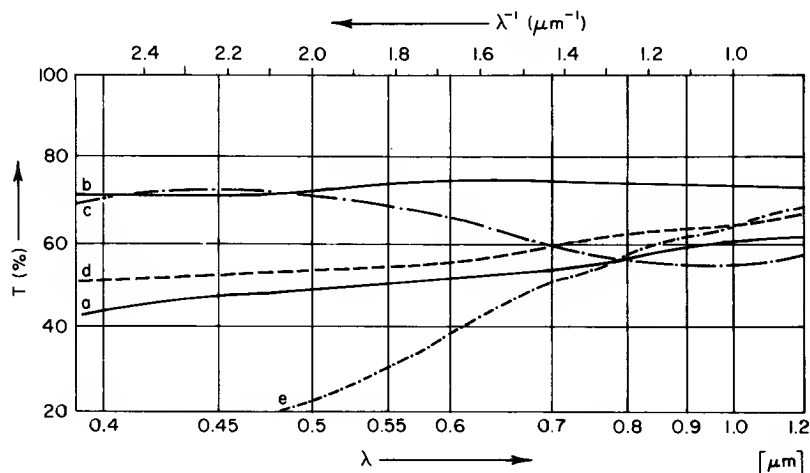
FIG. 22. Spectral transmittance of plate glass coated on both sides with absorbing oxide films of approx 80-nm thickness: (a) Pd in SiO_2/TiO_2 matrix; (b) Ru in SiO_2; (c) NiO; (d) NiO in SiO_2/TiO_2 matrix; (e) Fe_2O_3.

be carried out in a reducing atmosphere or, if the solution contains reducing additives, at least, in an atmosphere free from O_2 (30).

The other coloring metals produce in SiO_2 or Al_2O_3 mostly yellow, brown or greenish shades (see Fig. 4). As already mentioned in Section II, there are possibilities of producing absorption colors in matrix layers also by chemical retreatment of deposited films which are still reactive. Interesting effects are obtained in particular by the action of sulfides (H_2S, (NH_4)$_2$S, rhodanides) on gellike matrix films with embedded metal compounds.

Applications of light-absorbing coatings of low or moderately high refractive index have so far been used mainly as filter or "one-way" glasses, for color temperature conversion, or to obtain antiglare effects. They are also used in multilayer systems to increase the blocking action or to eliminate multiple reflections. Absorbing coatings may also gain practical importance in combination with antireflection layers (see Fig. 21, curve c). This applies in particular to sight glasses in switch and control towers, etc., where double-glazed units are normally used. Here the antireflection effect is even substantially improved by means of the absorption combined in the coating, and the glare is at the same time considerably reduced.

3. Partially Reflecting Coatings ($R/T \lesssim 1$)

Within this group, there are several applications for optical-grade dielectric coatings which are in demand in large quantities and sizes. The number of partial layers required is small (in general $\lesssim 3$), and the application of the dipping method therefore particularly economical. Working operations should be automatic as far as possible.

a. Monolayers. An absorption-free layer of a thickness d and a refractive index $n = 2.25$ gives, on a pane of an absorption-free plate-glass ($n_G = 1.518$) at a wavelength λ_0, for which $nd = \lambda_0/4$, a reflectance of $R_1 = 29\%$. When both surfaces are coated the total reflectance becomes $R_2 = 2R_1/(1 + R_1) = 45\%$. Choosing d so that λ_0 is between 550 and 600 nm, the pane coated on both surfaces gives, for white light, a beam splitting action with an R/T ratio of approx 4:5, which for the human eye is practically free from color effects (see Fig. 23a). With a layer thickness for which $\lambda_0 \approx 1100$ nm, the light transmittance of the pane is, however, related to the relative luminosity curve, 82% (see Fig. 23b). In transmitted light, the pane appears slightly greenish and in reflected light, violet to blue.

These effects, though long known, have recently found considerable practical interest. By virtue of the modern thin film techniques it has become possible to control the solar irradiation through even large window panes by rejecting a portion in the visible and/or infrared region to an extent which is of great importance for room air conditioning. By means of vacuum

deposition techniques mainly metallic films can be deposited for this purpose, which so far can be applied only on the inner surfaces of double-glazed units. The methods described here allow the use of radiation-reflecting and absorbing coatings, which, owing to their high abrasion resistance, can also be applied on single panes (*31a*). Moreover, panes with metal oxide coatings for solar control do not pose problems concerning modifications of color, as will be seen later.

To quantitatively determine the radiation portion transmitted or reflected in a given spectral interval, the spectrophotometrically evaluated T_λ and R_λ data can be plotted to advantage on a λ scale corresponding to a linear energy distribution of the radiation, so that the area between two λ values can serve as a measure for the radiated power pertinent to $\Delta\lambda$. By graphically integrating the area below the curves thus obtained, the average radiation transmittance (T_s) and reflectance (R_s), respectively, in the spectral region considered can be determined. In the case of the terrestrial solar spectrum, a λ scale, recorded in Fig. 23 as an abscissa, will be obtained. By analogy with this, the λ scale for the visible region can be subdivided in a way that the area located below the spectrophotometer curve between two λ values represents a measure of the proportionate brightness pertinent to $\Delta\lambda$, as perceived by the eye. By planimetering the T_λ and R_λ curves in the visible region, values for the physiological light transmittance T_L and light reflectance R_L are obtained.

Figure 23 shows measurements of T_λ and R_λ made on plate glass panes of 4-mm thickness which, in order to realize the above chosen examples, had been coated on both sides with a TiO_2 layer (brookite type) for $\lambda_0 = 580$ (a) and 1.120 nm (b), respectively. As these layers are practically absorption free, the area located between the T_λ and R_λ curves of each coating corresponds
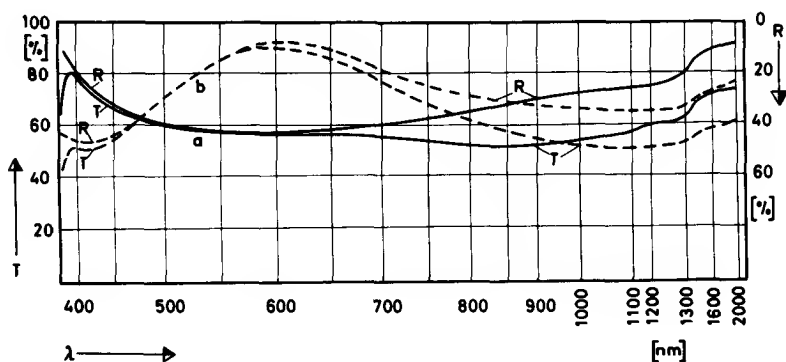
FIG. 23. Spectral characteristics of TiO_2 films on plate glass versus λ plotted in a scale of linear solar energy distribution: optical thickness (a) 145 nm, (b) 280 nm.

TABLE III

TRANSMITTANCE AND REFLECTANCE OF SUN-SHIELDING COATED PLATE GLASSES (THICKNESS 4–5 mm)

Type[a]	Glass substrate	Coating material	Coated surface	nd (nm)	T_s (%)	R_s (%)	T_{eff} (%)	T_L (%)	Locus of chromaticity, x, y	
									Transmittance	Reflectance
a	clear	TiO_2	2	145	58	33	61	58	x 0.298 / y 0.300	0.330 / 0.345
b	Clear	TiO_2	2	280	66	26	69	82	x 0.347 / y 0.362	0.353 / 0.259
c	Clear	$TiO_2 + Pd$	2	140	47	26	53	44	x 0.322 / y 0.327	0.318 / 0.332
d	like c, + 1 pane uncoated	$TiO_2 + Pd$	2	140	41	28	46	40	x 0.320 / y 0.328	0.320 / 0.331
e	Grey glass	Nonabsorbing	1	~130	37	20	51	31	x 0.315 / y 0.320	0.308 / 0.338
f	Clear	SnO_2 + abs. oxides [cf. (32)]	1	~2.000	26	18	~42	33	x 0.287 / y 0.296	0.312 / 0.332

[a] Compare with Fig. 23.

solely to the absorption in the glass. Planimetering of the curves supplies for T_s and R_s, T_L and R_L the data listed in Table III. In addition data are given for the "effective" transmittance, which is composed of the directly transmitted radiation T_s and of a certain percentage of radiation energy absorbed in the glass and the coating and secondarily emitted to the interior from the heated-up pane. This percentage is derived from empirical values and amounts on the average to $\frac{1}{4}$–$\frac{1}{3}$ for single panes and to $\frac{1}{6}$–$\frac{1}{4}$ for double-glazed units. It can be seen from the data of Table III, that the secondary energy portion is relatively insignificant only with coatings of zero or low absorption (a, b, c) and with normal plate glass.

To reduce the cooling load of an air conditioning plant, T_{eff} obviously should be as small as possible. This requirement is of course limited, since T_L should be kept at least at a certain minimum level between approx 30 and 60%, depending on the geographical location and the window area/room volume ratio. If it is therefore desired to obtain lower T_{eff} values with a monolayer than with layers a or b (Table III), such a layer must exhibit, besides a high reflectance, also absorption, and this preferably also in the wavelength region above the maximum eye sensitivity. Unfortunately there are only very few inorganic materials having these properties. Only colloidal gold has proven thus far to have these properties, particularly if embedded in a TiO_2 matrix (31b). This has already been shown in Fig. 5. The relatively high transmittance in the blue region can be compensated by adding metals which cause a predominant absorption of the blue in the layer, as, for example, Co or Pd. It is difficult, however, to render a working solution containing gold sufficiently stable. The materials mentioned in Section V,2, which yield an almost gray tint are therefore preferably used to cause absorption. An example of such a coating is given in Table III,c. By means of double-glazed units the secondary heat transfer into the inside can of course be stopped even more effectively, as is shown by d.

Higher reflectance in the near-infrared region can obviously be attained also with absorbing coatings if they are made accordingly thicker; in this case, however, white light is no longer colorless in reflection. Since in practice a window facade showing conspicuous modifications of color is undesired, panes coated in this manner are rarely used. In general, the color modifications produced by the panes should be so insignificant that the locus of chromaticity, expressed by the coordinates x, y, and related to standard illuminance C (artificial daylight), is located within the following limits:

Transmitted light:
$$\begin{cases} x = 0.29\text{–}0.33 \\ y = 0.29\text{–}0.34 \end{cases}$$

Reflected light:
$$x = 0.30\text{--}0.35$$
$$y = 0.30\text{--}0.36$$

Moreover, the distance of the locus of chromaticity from the black body line should not exceed 0.01, at least for the transmitted light. The x and y values for the different types of coated sun-shielding glasses are recorded in the last column of Table III.

Metal oxide coatings deposited from solutions or dispersed fluids are applied by some producers also for improving the effect of absorbing sun-shielding sheet glass. In this case such glasses are less heated up under solar irradiation, so that both the risk of breaking and secondary heat emission are diminished. An example of the effect of a neutral tinted glass coated with a reflecting dielectric oxide layer on one side is given in Table III by e. The uncomfortable emission of such glasses towards the inside room can be considerably reduced by a coating consisting of a semiconducting oxide with high free charge carrier density ($\gtrsim 10^{20}/\text{cm}^3$). Coatings with these pro-perties are obtained mainly by spraying finely dispersed solutions of Sn or In compounds onto the hot glass surface (see Section V,6,a). Row f of Table III shows the data of such an oxide coating according to statements by Yellott (32).

As already mentioned in Section II,3, spraying processes are also applied for the production of nonconducting sun-shielding coatings made of cobalt and iron oxide (6). These coatings, however, exhibit more or less intensive yellow or brown colors (see Figs. 4 and 22) and therefore do not comply with the above specifications regarding the locus of chromaticity desired.

An easy method to further extend the spectral reflectance band, without additional working expenses, and to simultaneously reduce interference color effects, is particularly offered by the dipping process. If plates emerge with a certain slope angle ϕ, different layer thicknesses will be obtained on both surfaces, according to Fig. 2. This widens the resulting reflectance bands.

b. Multiple Layers. As practical experiences have revealed, multiple layers can also be produced economically and with good reproducibility by means of the dipping process, so that they can be applied to large surfaces and mass-produced industrial articles. For sun-shielding glasses in which increased ir reflection is required with higher light transmission T_L, systems of the designs: $(\alpha H)LH\text{--}G\text{--}HL(\alpha H)$ and $(\beta L)(\alpha H)LH\text{--}G\text{--}HL(\alpha H)(\beta L)$ may be con-sidered. [The definitions for L, H, G are given in Section V,1; α and β are numbers <1 and have to be chosen so that a given T_L value and simul-taneously optimum color neutrality in transparency are obtained (26)].

Combinations of oxide layers from solutions with metallic films deposited

by any other method are likewise feasible, if the metal is not attacked chemically in the solution. Thus it has been proposed to combine partially transmitting silver coatings, which are deposited from sprayed-on solutions by means of reduction, with an SiO_2 or TiO_2 layer in order to produce sun-shielding coatings of high efficiency by a low cost procedure (33). Due to their mechanical sensitivity, they can, however, be applied only on the inner surface of a double-glazed unit. The oxide layer increases the visible light transmittance and eliminates the blue tint of the silver film, due to its anti-reflection effect. To stabilize the oxide layer, a heat treatment at 180–200°C is sufficient in this case.

Widely used are three-layered coatings of the HLH–G–HLH design as nonglaring rear-view mirrors for vehicles. The layer thicknesses are prefer-ably chosen so that maximum reflection (50–60%) is at 450 nm. Shorter-wavelength daylight will then be reflected to a higher extent than the longer-wavelength headlight beams. The coated back side will either be black varnished or frosted in order to attenuate the double image. Three-layered semitransparent mirrors of similar structure are also used as "one-way mirrors" for observation chambers, glass guards for stoves and furnaces, etc. Glasses, provided with such coatings, can even be bent to moderate curvatures after the films are applied, provided they are carefully thermally treated, without damage to the coatings.

For nonabsorbent beam splitters, where the intensity ratio R/T should be equal to unity as closely as possible over a broad spectral region, four-layered systems are suitable. They can be constructed in different ways. Figure 24 shows the relative spectral characteristics of a few designs which are easy to carry out with TiO_2, SiO_2, and mixtures of both of them.
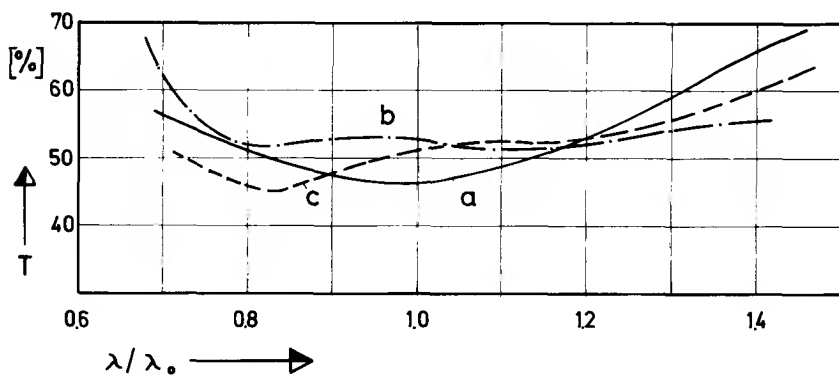
FIG. 24. Transmittance of all-dielectric beam splitters with $R:T \approx 1:1$ as a function of reduced wavelength λ/λ_0, according to design: (a) MHLH (back side antireflected); (b) HLHxL and (c) MH²LH on either side.

If such beam splitters are to be used in optical arrangements at angles of ·
incidence of 40° or more, the angle dependence of the interference phenomena
can be annoying. It can be compensated by varying the layer thickness d
according to beam slope along the intersection with the plane of incidence.
This is achieved by adjusting the lifting speed v during the dip-coating
process to predetermined d values as a function of the lifting height in
accordance with interrelations represented in Fig. 1.

4. Selectively Reflecting Layer Systems $(R/T > 1)$

As already mentioned in Section III,2, multilayers can be obtained by
repeated dippings, the number of which is limited by mutual adhesion,
differences in thermal expansion coefficients, and by the thicknesses of the
partial layers. If λ is within the visible region, approx 10–15 layers of $\lambda/4$
thickness can be combined, for instance, for systems alternately built up
with TiO_2 and SiO_2; accordingly, more layers can be applied with thinner,
and less with thicker partial layers. With ThO_2 and SiO_2, 10 or more $\lambda/4$
layers for the uv and the adjoining visible regions can be obtained. According
to theory (26), 11–15 alternating $\lambda/4$ layers of refractive indices $n_H = 2.25$
and $n_L = 1.45$ yield, when applied on one surface of plate glass, a reflectance
maximum $R = 98.0–99.6\%$, and $R = 99.0–99.8\%$ when applied to both sur-
faces. Thus numerous typical multilayer effects of high efficiency can be
obtained. In the following paragraphs some characteristic examples will be
described.

a. Regular Multilayer Systems. If the bandwidth of R in the first order
(given by the λ difference of the 50% values of R_λ divided by λ_0) does not
have to be larger than ~0.5, systems of the G–$(HL)^N H$ or G–$(HL)^N \alpha H \beta L$
design with uniform λ_0 will be sufficient. The latter design will be chosen
when highest possible transmittance is required in adjoining spectral regions,
in which case adjusted optimum values will have to be calculated for the
α and β factors. Such designs are used, for instance, for dichroic beam
splitters and for reflecting selected uv regions. Examples are given in Fig. 25.
Such plain systems have proved to be successful also for making polarizing
interference beam splitters, cemented between prisms (34).
Similar multilayer stacks are likewise being used for heat reflection filters
(Fig. 26). These filters are particularly suitable for radiation sources of
high blackbody temperatures and high emission power in the near ir, such
as xenon lamps (35). Combined especially with those, such filters can be
used for approximate simulation of terrestrial solar radiation, provided a
uv transmitting material, such as ThO_2, is chosen for the high-index com-
ponent (Fig. 26b).
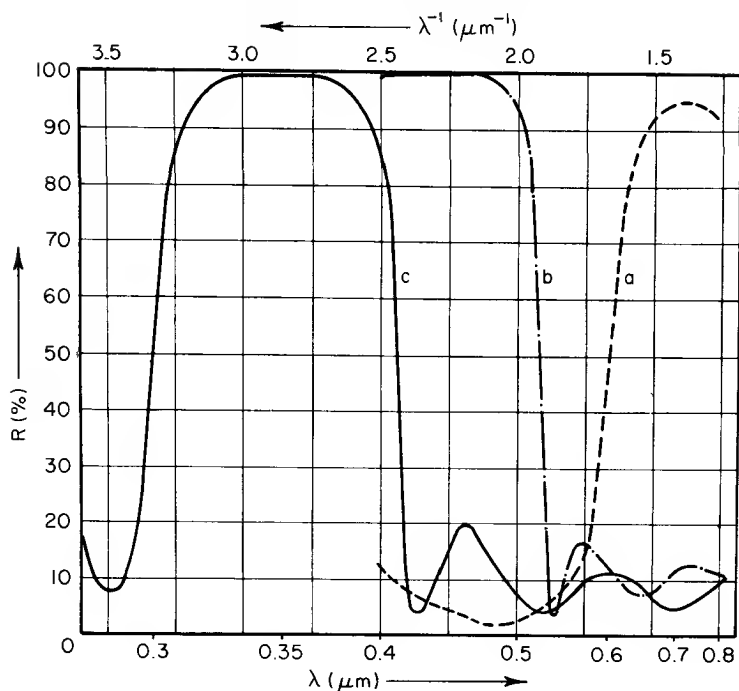
FIG. 25. Spectral reflectance of dichroic beam splitters: (a) red reflecting mirror, design G-$\frac{1}{2}$M(HL)^{4}H$\frac{1}{2}$L; (b) blue reflecting mirror, design G-(HL)^{4}H$\frac{3}{2}$L [substrate for (a) and (b): plate glass, back side antireflected]; (c) uv reflector, R_{max} centered at 350 nm, design $\frac{3}{2}$L(HL)^{5}H-G-(HL)^{5}H$\frac{3}{2}$L (substrate: silica glass, both sides coated).
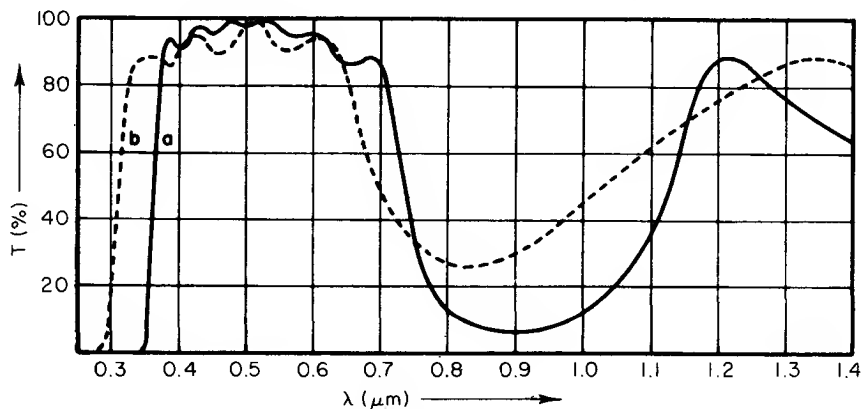

FIG. 26. T_λ of heat reflecting filters on heat resistant Duran glass coated on either side with (a) 8 layers of TiO$_2$ and SiO$_2$; (b) 6 layers of ThO$_2$ and SiO$_2$ for simulating solar radiation by means of xenon lamps.

b. Irregular Multilayer Systems. To obtain spectral reflectance bands of larger widths, several regular systems are superposed, according to well-known theories of thin film optics, or else, a system is built up whose layer thicknesses are varied in a theoretically or experimentally predetermined way (*36, 37*). With two layer components L and H, the latter method offers with a lesser number of layers a smoother run over the bandwidth. Using this method cold mirrors and wide-band uv reflectors are being made by the dipping process (*38*). Figure 27, curve a shows, as an example, a cold mirror
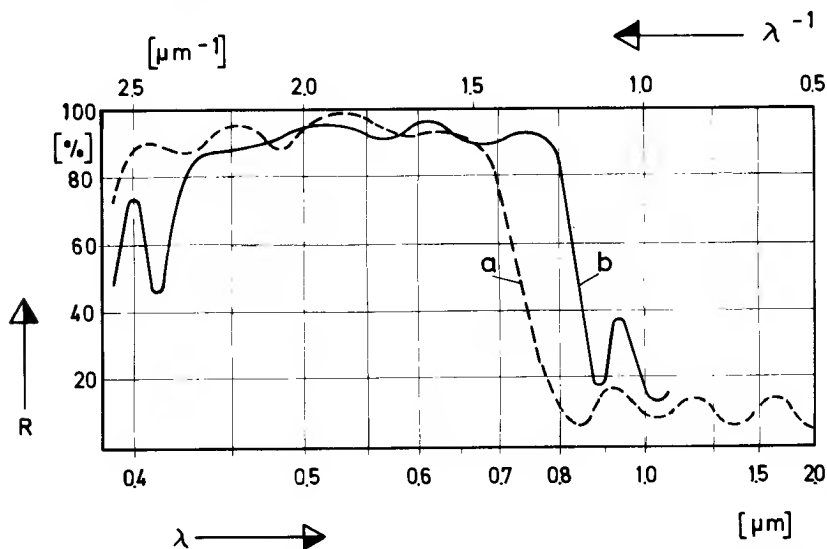
FIG. 27. R_λ of irregular multilayer systems applied on both surfaces of heat resisting substrates: (a) plane cold mirror; (b) elliptically shaped glass cylinder for selective irradiation of neodymium laser glass.

with 14 layers on both surfaces of a heat-resistant plate glass. A variety of cold mirrors consisting of coated elliptically shaped glass cylinders are used as reflectors for solid-state lasers. The exciting light source is fixed in one focal line of the cylinder, and the laser rod in the other one. The reflector projects onto the rod only radiation of the wavelengths required for optical pumping, and transmits the undesired one (Fig. 27, curve b).

5. FILTERS FOR LIGHTING AND OPTICAL PURPOSES

a. Color Filters. Just as with heat-reflecting filters and cold mirrors, there is also a demand for relatively large-sized heat-resisting glasses for use as color filters. This is true mainly in lighting engineering as, for example, for the illumination of stages and studios. The thermal expansion coefficient of
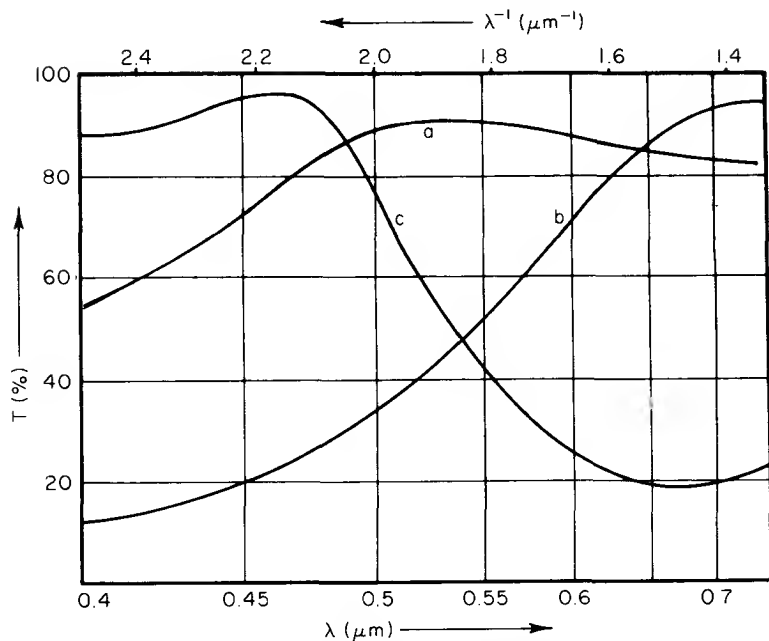
FIG. 28. T_λ of thin film color conversion filters: (a) monolayer coating (approximate composition $2TiO_2 \cdot Fe_2O_3$) applied on one side; (b) three-layer coating for conversion $6000 \rightarrow 3500°K$; (c) nonabsorbing six-layer coating for conversion $3500 \rightarrow 6000°K$ [(b) and (c) applied on both sides].
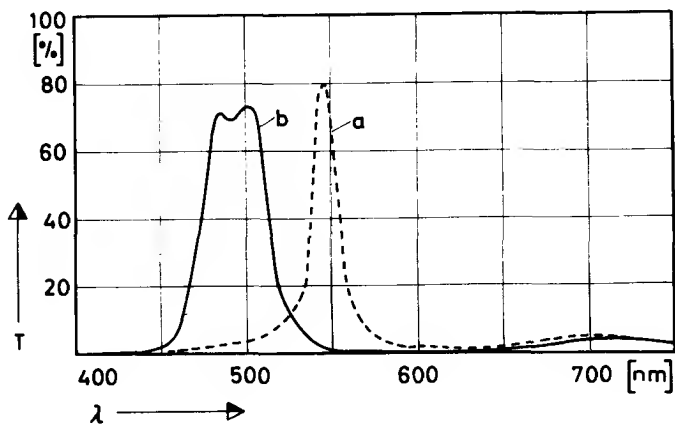
FIG. 29. All-dielectric interference filters: (a) simple narrow-band filter $[(HL)^4(LH)^4]$–$G–[(HL)^4(LH)^4]$; (b) waveband filter, $[(HL)^2(LH)^3L(LH^2]-G-[(HL)^2(LH^3L(LH)^2]$ (each filter combined with a red reflecting filter similar to curve a, Fig. 25).
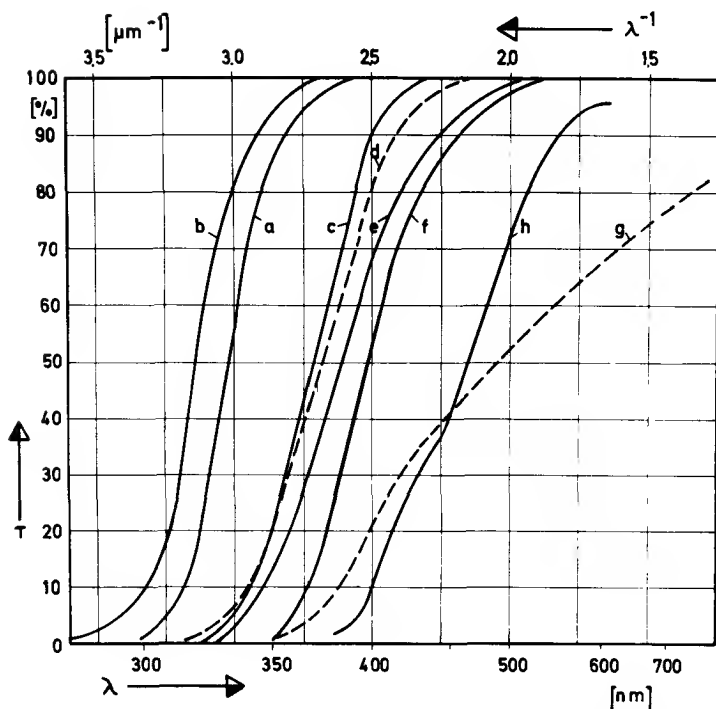
FIG. 30. Intrinsic transmittance of coatings ($d \approx 0.3$ μm) consisting of TiO_2 and incorporated heavy metal oxide (in moles per 1 mole TiO_2): (a) C-type TiO_2 (for comparison); (b) $TiO_2 + 1.5SiO_2$; (c) $TiO_2 + 0.5PbO$; (d) $TiO_2 + 0.15Bi_2O_3$; (e) $TiO_2 + 0.3NiO$; (f) $TiO_2 + 0.15Fe_2O_3$; (g) $TiO_2 + 0.35CoO$; (h) $TiO_2 + 5.7UO_3$.

tinted glasses is normally quite high, consequently they fail to resist high intensity irradiation. The problem can be solved by using heat-resisting sheet glasses, such as Pyrex or Duran, as substrates, and depositing coatings on them which yield the required spectral distribution of the transmitted light. Using the dipping process, this is possible with multilayer systems which, in certain cases, may contain also absorbing layers. A few examples of filters frequently used in practical applications, are shown in Figs. 28 and 29. Figure 28 shows T_λ curves of color conversion filters. Curve a refers to a very simple type, consisting of one $Ti_2Fe_2O_7$ layer of approx 0.12-μm thickness. Coatings of this type are applied, for example, directly on flash light bulbs, in order to attenuate the uv and blue portion of the emitted light. System b is composed of three layers (HLH–G–HLH), H consisting of $TiO_2 + 15$ mole % Fe_2O_3, and L consisting of SiO_2. The absorption of the mixed oxides TiO_2–Fe_2O_3 increases below 500 nm with decreasing wavelength (see Fig. 30), so that T_λ evenly diminishes due to overlapping of

interference and absorption. System c consists of the $\frac{1}{2}$L(HL)^{2}H–G–H(LH)^2-$\frac{1}{2}$L design and is absorption free.

Figure 29 shows two examples of narrow-band filters. The first one consists of two symmetrical multilayer stacks, and the second one is a waveband filter (39) composed of three stacks on either side. The uniformity of these filters can be kept within about 2% of the T_{max} wavelength over an area of at least 50-cm diameter.

It may be assumed, however, that it is also possible to develop less sophisticated color filters by incorporating pigment-forming and, in particular, sulfide-containing layers.

b. *Ultraviolet Cutoff Filters.* A few of the metal oxides to be deposited from organic solutions exhibit an especially steep rise of absorption in the near uv. Among these are TiO_2, CeO_2, Sb_2O_4, and PbO. With these layers efficient cutoff filters for shorter-wave uv radiation can be obtained, at thicknesses as small as 100–200 nm. TiO_2 has the remarkable property that, by admixture of certain other metal oxides, its uv absorption edge can be shifted, without essentially decreasing its steepness (10). Of particular interest are mixtures of TiO_2 and heavy-metal oxides, which shift the absorption edge near or into the visible region. Figure 30 shows in curve a the intrinsic transmittance of TiO_2–(T_b) films of C-type structure (Section IV,1); curve b refers to a mixture of SiO_2 and TiO_2. When PbO (curve c) and Bi_2O_3 (curve d) are added, the absorption limit is at longer wavelengths than in the case of insulated oxides of the components. In combination with the oxides of Ni, Fe, or Co, the characteristic absorption of the pure metal oxide completely vanishes above certain wavelengths, when incorporated into TiO_2 (curves e, f, g). In all these combinations compounds are obviously formed (titanates) whose atomic electron eigenfrequencies, due to the modified bonding forces, are different from those of the insulated oxides.

Ultraviolet absorption properties similar to those exhibited by TiO_2 are observed in cerium oxide layers. The absorption edge of this coating material is normally located at 400 nm. By admixture of SiO_2, however, it can be slightly shifted towards longer wavelengths, thereby gaining a little in steepness (with the amount of cerium oxide per square centimeter remaining constant). This feature has already been observed in evaporated layers of the same composition (40). This effect is not observed, however, when TiO_2 is incorporated into the CeO_2 layer.

Considerable attenuation of uv radiation, with a relatively steep transmittance increase between 400 and 500 nm, is obtained by uranium oxide coatings. In Fig. 30, curve h is related to such a type of coating. For stabilization, a few percent of TiO_2 are contained in the UO_3 coating. Such coatings can be applied, for instance, to shield solid-state lasers against the

destructive action of uv radiation emitted by high-intensity exciting lamps. By the influence of humid air the initially high extinction values in the short-wavelength region are noticeably reduced. They can, however, be restored to their original level by reheating.

6. OTHER APPLICATIONS

a. Semiconducting Coatings. During thermal transformation of gel films into oxides, there are obviously multiple influences opposing perfect crystallization and favoring the occurrence of disordered structures. The incorporation of organic residues, halogen ions, protons, and H_2O molecules, which at rising temperatures partially escape, may cause oxygen ions to be substituted by other ions of different valences or impurity ions to be localized at interstitial sites. In such disordered structures, certain substances can show semiconductor characteristics. This is mainly the case in hydrolytically or pyrolytically decomposable compounds whose cations appear in two or more valence stages. In oxide layers produced from solutions by means of the cold-dipping process, semiconductor characteristics are particularly marked in In_2O_3, SnO_2, rhodium oxide, and ruthenium oxide. According to observations made so far, in all these cases excess (*n*-type) conduction is involved. As in most semiconductors, measured conductivity values are largely a function of the manufacturing conditions and the environmental influences. Minimum resistivity values occurring in layers of about 100-nm thickness are for In_2O_3 $\sim 10^{-1}$, for SnO_2 ~ 10, and for RhO_x and RuO_x $\sim 5 \times 10^{-3}$ Ω cm. Substantially higher degrees of disorder and thus higher conductivity values, are attained, if solutions in extremely fine dispersion or vapors are brought into contact with already preheated substrates, since under these conditions speed of crystallite formation is substantially higher. These methods are being industrially utilized already in numerous variations [see Umblia (5), Wartenberg and Ackermann (41), and Table III, row f].

On the other hand, conductive dip coatings are mainly applied, preferably combined with an additional antireflection layer (42), to obtain antistatic surfaces for cover glasses of sensitive meters and for gauge tubes (such as flowmeters), etc., where coating processes using high temperatures are either not applicable or would yield layers of insufficient optical qualities. In combination with poorly conductive oxide layers (SiO_2, TiO_2), semiconducting dip coatings further show typical boundary layer effects, such as rectifying action, Zener effect, photoconductivity, etc., which so far have not been investigated in detail.

b. Protective Layers. A feature of certain oxide layers which has not much been utilized so far in practical applications, is their ability to lower the rate of chemical attack of surfaces on which they have been deposited.

Coatings which are to be considered for this purpose should meet the following requirements.

1. Insolubility in the attacking medium.

2. Imperviousness to the attacking medium.

3. Solid bond to substrate, preventing penetration of the attacking reagent at edges or flaws in the coating.

The first requirement is met satisfactorily by a few oxides, among which are mainly ThO_2 and Ta_2O_5, provided the attacking media are water, mineral acids and alkalis. TiO_2 likewise exhibits high resistance against water and acids, except in the case of sulfuric acid. For this application, the temperature and time of baking of the layers are of great importance (43). This is shown in Fig. 31 by the example of TiO_2 and SiO_2 layers. As an indication of the durability the time after which the first change in the layer becomes optically perceivable has been plotted.
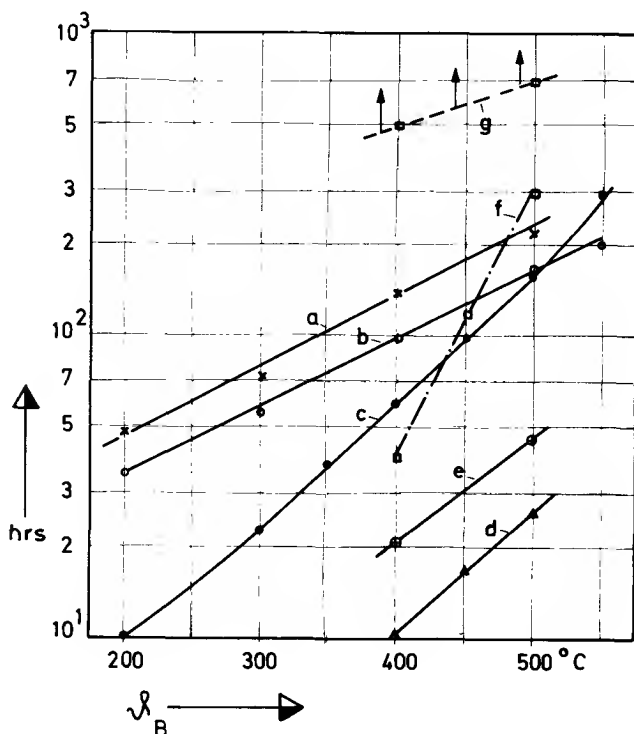
FIG. 31. Chemical durability of $\lambda/4$ TiO_2 and $\lambda/4$ SiO_2 layers on plate glass as a function of baking temperature (baking time 1 hr): (a) TiO_2 (T_b) in NaOH (10%, 20°C); (b) TiO_2 (T_e) in HCl (10%, 20°C); (c) $TiO_2 + SiO_2$ in HCl (10%, 20°C); (d) $TiO_2 + SiO_2$ in NaOH (10%, 20°C); (e) SiO_2; (f) TiO_2 (T_b); (g) TiO_2 (T_e) [(e), (f), and (g) in H_2O dest. (100°C)].

Insoluble oxide layers also normally meet the third requirement very well It appears, however, that effective imperviousness, especially to H^+ ions in solutions, can be obtained only with certain prerequisites. It has, in fact, been discovered that for various glasses subject to severe hydrolytic attack the same type of coating offers excellent protection to certain types, whereas for other glasses it can be almost ineffective. Tests have shown that a high efficiency of protective coatings on glasses is particularly obtained when the glasses contain little or no SiO_2 but a certain minimum amount of alkalis. This suggests two possible mechanisms of protection: either the reagent, gradually diffusing through the protective coating, forms at the boundary layer–glass a reaction product which acts as a barrier against the further advancing attack, or an adequate reaction zone begins to form already during baking of coatings at the boundary layer-glass, due to alkali emigrating from the glass. On alkali-containing phosphate and borate glasses, for instance, the hydrolytic resistance can be increased by several orders using SiO_2 layers to which appropriate amounts of TiO_2 or ThO_2 have been added in order to adjust the refractive index and to increase the durability. In the same manner all customary sorts of sheet or plate glass can be made largely insensitive to the attack of humidity by means of coatings of TiO_2 or mixed oxides. The lifetime of glasses of comparatively high chemical resistance subjected to severe attack can also be substantially increased by oxide coatings of the type described.

At high temperatures, coatings of different metal oxides reveal quite varied behavior to ion diffusion from adjoining solids and melts. Section IV,1 has already described the surprising blocking action which is produced by thin SiO_2 layers against the immigration of Na ions from glasses, whereas TiO_2 layers readily absorb the same. Empirical facts are too scant up to now to get an exact understanding of these phenomena. On the other hand measurements of the diffusion in SiO_2 by means of radioactive tracer substances have already shown that even materials of identical composition, but of different origin, can have extremely different diffusion velocities for alkali ions (44). Obviously we are faced here with an extremely structure-sensitive feature whose further investigation on organogenic oxide films should yield valuable contributions toward clarifying their structures.

REFERENCES

1. J. Langmuir, *J. Am. Chem. Soc.* **39**, 1848 (1917).
2. K. B. Blodgett, *J. Am. Chem. Soc.* **57**, 1007 (1935).
3. H. A. Tanner and L. B. Lockhart, *J. Opt. Soc. Am.* **36**, 701 (1946).
4. German Pat. 736,411 (1939) (U.S. Pat. 2,366,516) (to Schott & Genossen); German Pat. 937,913 (1939) (to Leitz).
5. E. Umblia, *Glass* **32**, 598 (1955); Brit. Pat. 1,119,539 (1964) (to Philips).

6. O. W. Vorob'eva and E. S. Bessonowa, *Glass Ceram. (USSR) (English Transl.)* **21**, 9 (1964).
7. W. Geffcken, *Glastech. Ber.* **24**, 143 (1951).
8. H. Schroeder, *Opt. Acta* **9**, 249 (1962).
9. Brit. Pat. 965,243 (1960) (to Schott & Genossen).
10. H. Schroeder (*Congr. Intern. Verre, 7th*), *Compt. Rend.* **1**, 7.1–7.5 (1965).
10a. H. Bach and H. Schroeder, *Z. Physik* **224**, 122, (1969).
11. P. Bousquet, *J. Phys.* **25**, 50 (1964).
12. H. Mayer, "Physik dünner Schichten," Vol. 1, p. 97. Wiss. Verlagsges., Stuttgart, 1950.
13. H. Schroeder, *Bull. Soc. Belge Phys.* **4**, No. 2, 106 (1964).
14. H. Schroeder and M. Spiller, *in* "Basic Problems in Thin Film Physics" (R. Niedermayer and H. Mayer, eds.), p. 233. Vandenhoeck & Ruprecht, Göttingen, 1966.
15. U.S. Pat. 3,004,863 (1960) and 3,387,994 (1965) (to Du Pont de Nemours & Co.).
16. H. Bach and H. Schroeder, *Thin Solid Films* **1**, 255 (1967/68).
17. G. Bayer, O. W. Flörke, W. Hoffmann, and H. J. Scheel, *Glastech. Ber.* **39**, 242 (1966).
18. H. Schroeder, *Ann. Physik* **39**, 55 (1941); F. Abelès, *in* "Progress in Optical" (E. Wolf, ed.), Vol. II, pp. 249–288. North-Holland Publ., Amsterdam, 1963.
19. A. Schroeder, *Z. Krist.* **67**, 509 (1928).
20. U.S. Pat. 2,474,061 (1943) and 2,466,119 (1944) (to American Optical Co.).
21. H.-P. Boehm, M. Schneider, and F. Arendt, *Z, Anorg. Allgem. Chem.* **320**, 43 (1963).
22. H. Bach, *Naturwissenschaften*, **55**, 439 (1968).
23. A. J. Majumdar, H. A. McKinstry, and R. Roy, *J. Phys. Chem. Solids* **25**, 1487 (1964).
24. A. A. Sviridova and N. V. Suikovskaya, *Opt. Spectry. USSR (English Transl.)* **22**, 509 (1967).
25. N. N. Harris and R. L. Cook, *J. Am. Ceram. Soc.* **51**, 230 (1968).
26. H. Schroeder, *Z. Angew. Phys.* **3**, 53 (1951).
27. W. Geffcken, German Pat. 758,767 (1940).
28. J. T. Cox, G. Hass, and A. Thelen, *J. Opt. Soc. Am.* **52**, 965 (1962).
29. S. Furuuchi, *Symp. Surface Verre et Traitements Modernes, Luxemburg, 1967*, p. 297, Union Scientifique Continentale du Verre, Charleroi (1967).
30. German Pat. 1,063,773 (1957) (to Schott & Genossen).
31a. H. Schroeder, *Vetro Silicati* **10**, N. 60, 10 (1966).
31b. H. Schroeder, *Glastech. Ber.* **39**, 156 (1966).
32. J. I. Yellott, *ASHRAE Trans.* **69**, 418 (1963).
33. R. Jacobi, *Glas-Email-Keramo-Tech.* **19**, 158 (1968).
34. H. Schroeder, *Optik* **13**, 158 (1956).
35. H. Schroeder, *in* "Beiträge zur angew. Glasforschung" (E. Schott, ed.), p. 287. Wiss. Verlagsges., Stuttgart, 1959.
36. A. Thelen, *J. Opt. Soc. Am.* **53**, 1266 (1963).
37. A. F. Turner and P. W. Baumeister, *Appl. Opt.* **5**, 69 (1966).
38. U.S. Pat. 2,852,980 (German priority, 1948) (to H. Schroeder).
39. W. Geffcken, *Z. Angew. Phys.* **6**, 249 (1954).
40. Austrian Pat. 206,202 (1959) (to Balzers AG).
41. E. W. Wartenberg and P. W. Ackermann, *Glastech. Ber.* **41**, 55 (1968).
42. U.S. Pat. 3,094,436 (1957) (to Schott & Genossen).
43. H. Schroeder, *Verres Refr.* **18**, 89 (1964).
44. G. H. Frischat, *Z. Angew. Phys.* **25**, 163 (1968).

The Preparation and Properties of Semiconductor Films

M. H. FRANCOMBE AND J. E. JOHNSON

Westinghouse Research Labratories
Pittsburgh, Pennsylvania

I. Introduction

The purpose of this chapter is to provide what is essentially a status report on recent and current developments in the field of semiconductor films. The recent phenomenal growth of solid state technology has generated a literature in this field which already is beyond the scope of a single review of this type. Certain areas of this literature have been covered by articles dealing with the preparation and utilization of special types of semiconductor films, and where appropriate this work will be cited, but no effort will be made to discuss the subject matter in detail. Emphasis will be placed mainly upon those topics which have not yet been reviewed elsewhere.

In the present section we shall trace briefly some of the earlier applications of semiconductor films, and indicate how new methods of preparation and evaluation have led recently to a proliferation of materials research and device engineering. Subsequent sections will discuss the various techniques

of film preparation, evaluation of structure, and measurement of those properties both of fundamental and practical interest.

TABLE I

Thin Film Semiconductor Materials, Properties, and Applications

Material	Properties	Remarks
Si	$\mu_e \leq 1200$ cm²/V-sec $\mu_h \leq 500$ $E_g = 1.2$ eV	Homoepitaxial material used in all types of integrated circuits and discrete devices Heteroepitaxial material has been realized with near bulk properties Applications include bipolar transistors, diodes, varactors, field effect transistors, solar cells, photocells, and space-charge-limited current devices
Ge	$\mu_e \leq 3900$, $\mu_h \leq 1900$ $E_g = 0.78$	Comments for Si are generally applicable. Applications include tunnel diodes, varactors, thermocouples, etc.
SiC	$\mu_e = 100$, $\mu_h = 25$ $E_g = 3.0$ eV	High-temperature device material—very stable
BN	$E_g = 10$	Dielectric material applications
AlP	$E_g = 2.5$	Electroluminescence applications
AlN	$E_g = 5.9$	Most stable of the Al–V compounds
AlAs	$\mu_e = 180$, $E_g = 2.1$	GaAlAs studied for electroluminescence applications
AlSb	$\mu_e = 200$, $\mu_h = 450$ $E_g = 1.72$	"Best match" to solar spectrum for solar cell application
GaP	$\mu_e = 150$, $E_g = 2.4$	Solar cell applications, electrooptical modulators
GaAs	$\mu_e = 4500$, $\mu_h = 400$ $E_g = 1.53$	Solar cell and electroluminescence applications, optical filters, FET applications, lasers, Gunn effect and other microwave devices
InP	$\mu_e = 4600$, $\mu_h = 700$ $E_g = 1.41$	Solar cells
InAs	$\mu_e = 30,000$, $\mu_h = 240$ $E_g = 0.43$	Hall effect devices, lasers, and thin film transistors
InSb	$\mu_e = 70,000$, $\mu_h = 1000$ $E_g = 0.23$	Hall effect devices, magnetoresistance and Faraday rotation applications, strain transducers, and microwave mixers
ZnS	$E_g = 3.7$	Electroluminescent devices
ZnSe	$E_g = 2.6$	Photoconductors, electroluminescence, metal base transistors
CdS	$\mu_e = 300$ $E_g = 2.4$	Photoconductance, acoustic amplification and transducers, solar cells, thin film transistors, varactors, high-frequency oscillators, piezoelectric devices
CdSe	$E_g = 1.74$	Photoconductors, particle detectors, solar cells
PbS	$\mu_e = 800$, $\mu_h = 1000$ $E_g = 0.37$	Photoconductors
PbSnTe	Variable	Lasers

In Table I we have compiled a partial listing of semiconductors which have been prepared and evaluated in thin film form and the applications for which they have been considered. This listing was derived primarily from the annotated bibliographies of Turnbull (*1*). More detailed discussions of many of these materials are given in later sections.

Semiconductor films have not only figured prominently for many years in a wide variety of commercial electronic applications but have also played an important role in the development of semiconductor device physics. Some basic phenomena, such as rectification, photoconduction, and luminescence, were observed and successfully exploited in films well before the emergence of a semiconductor theory which could explain them. For example, large-scale manufacture of cuprous oxide, and later selenium rectifiers, was begun more than forty years ago and many of these units are still in use today (*2*). Similarly, photocells utilizing cuprous oxide layers or evaporated films of selenium, PbS, PbTe, and PbSe were developed largely on empirical grounds before or during World War II. The devices were simple in concept and depended essentially on recombination effects or rectification occurring at the interface between a metal contact and a thin layer of semiconductor. However, it is evident from reviews such as those of Henisch (*3*), Zworykin and Ramberg (*4*), and Shive (*5*) that the development of optimum device characteristics depended largely upon the black art of film preparation and on the nature of subsequent heat treatments.

To a large extent empiricism has also characterized semiconductor film applications in the radio and cathode-ray tube fields, and in the manufacture of coated fluorescent lamps. Common examples include oxide films used on cathodes to enhance electron emission and sprayed phosphor coatings of the zinc sulfide, oxide, silicate, or germanate type used as display screens. Recent developments in photoconductive layers in the vidicon camera field have been along somewhat systematic lines, and have helped in furthering our understanding of semiconducting, or rather semi-insulating solids. In this case, failure of the semiconductor thin films in the device to provide the anticipated photoconductive gain (*6*) led Rose (*7*) and Lampert (*8*) to the development of new insights into the properties of photoconductors and other semiconductor devices.

Thin film amplifier structures have been of considerable historical significance in the early investigations of transistor concepts, and more recently have formed the basis of many studies aimed at the development of active thin film devices for integrated circuits. The classical germanium thin film amplifier experiments of Shockley and Pearson (*9*) in 1948 played an important role in the evolution of the transistor which triggered the enormous investment of scientific and engineering effort leading during the following decade to the commercial production of a wide variety of semiconductor devices. Later

research on film materials such as CdS more amenable to deposition by vacuum techniques enabled the realization by Weimer (10) in 1961 of a practical thin film transistor, the TFT, compatible with vacuum deposited passive film components used in integrated circuits.

Since about 1960 there has been an especially rapid increase in the volume of engineering effort devoted to semiconductor films. By mid-1961 the deposition of films had become an important industrial process (11), largely due to the feasibility of fabricating junctions by chemical vapor deposition of suitably doped layers. This approach, which was used first with germanium, was soon extended to silicon devices such as transistors and integrated circuits (12) and is now being applied to the III–V compound semiconductors and to many heterojunction systems of the type InAs/GaAs, etc. (13). The need for greater flexibility and improved high-frequency performance in integrated circuits (14) has, within the past 3 or 4 years, prompted interest in the hetero-epitaxial growth of silicon films on refractory insulating substrates such as Al_2O_3 (sapphire), SiO_2 (quartz), and $MgAl_2O_4$ (spinel) (15).

With the more stringent demands now made on device performance and reliability, and with the more general availability of new and improved preparative and analytical techniques, thin film semiconductors and their properties have of late been investigated in far greater detail than was hitherto possible. The basic mechanisms of nucleation and growth and the role of chemical and structural imperfections in influencing transport or optical properties have received increasing attention. These aspects will be discussed in some detail in Sections III and IV of this review. Also, these developments have permitted the growth of pure film products of a wide variety of semi-conductor compounds, possessing well-characterized composition and structure, often in epitaxial form. In several cases films have been grown of compositions for which good-quality single crystals were not readily obtain-able, and at thicknesses suitable for studying the optical absorption spectra over a wide range of energies.

II. Chemical Vapor Deposition

Within the past decade chemical vapor deposition has expanded rapidly in importance to become the main technological method for producing films for semiconductor devices. There are various reasons for this expansion, among which are the basic simplicity and reproducibility of chemical processes and the ease with which they can be adapted to the needs of production. The largest volume of work in this field has been concerned with homoepitaxial growth, whereby a semiconductor such as Si or Ge is deposited upon a single crystal substrate of the same material. But for small differences in the nature and concentration of the impurities in the substrate and grown layer, this

process could be regarded simply as extended growth of a seed crystal from the vapor. A smaller (but rapidly expanding) effort has been directed towards the epitaxial growth of semiconductors on chemically different, crystalline substrates, usually comprising other semiconductors or insulators, but these structures have not yet been exploited commercially.

The chemical vapor deposition of epitaxial semiconductors has formed the subject of several recent review papers, which have covered in particular the growth of silicon and germanium films. Schwartz (16) and Li (17) have provided comprehensive surveys which describe the development of the main experimental techniques as well as the practical problems of controlling crystal quality and composition. Joyce (18), in a more basic treatment, discusses the chemical reactions, growth kinetics, and nucleation effects involved in chemical growth. Miller and Manasevit (19) and, more recently, Filby and Nielsen (20) have reviewed the status of work on heteroepitaxial growth on insulating substrates. For complete discussions of techniques and details of literature in the chemical deposition field the reader is referred to these review papers and to the annotated bibliographic surveys of Turnbull (1).

In this section we shall confine our attention to a brief description of growth methods which have been used for elemental and compound films, referring to some typical applications of these methods and indicating some of the problems now under consideration in the area of heteroepitaxy. Special mention will be made of extensions of the chemical vapor plating methods to the more refractory semiconducting compounds, since these have not yet been reviewed in the literature.

1. Deposition Techniques and Transfer Mechanisms

The basic requirement common to all chemical vapor deposition methods is that they provide a means of conveying a vapor containing the condensate material to a substrate surface, where it is decomposed usually by a heterogeneous process. The nature of the decomposition process varies according to the composition of the volatile transporting species. Reactions so far used in the epitaxial growth of semiconductors are hydrogen reduction of volatile halides, pyrolysis of hydrides, disproportionation of halides, and reactions between volatile metal halides (or oxides) and vaporized elements (usually Group V) leading to the growth of semiconductor compounds. The main features of these methods may be described briefly as follows.

a. Reduction of Halides. This is the most widely used of the chemical growth techniques and is probably best exemplified by the silicon chloride (21) process. Here, hydrogen gas is bubbled through the liquid chloride, $SiCl_4$ (or trichlorosilane, $SiHCl_3$), which is maintained at a fixed temperature so that

the rate of pickup by the gas stream ensures a constant partial pressure of the chloride, usually several Torr. The substrates, normally silicon single-crystal wafers, are mounted on a high-purity silicon or graphite susceptor which is heated by rf induction, to maintain a substrate temperature in the range of 1100–1300°C. As shown by Theurer (22), dopants such as phosphorus and boron can be incorporated by passing the gas stream through a liquid halide such as PCl_3 or BBr_3. It is generally accepted that, except at high super-saturations of the halides, epitaxial growth of the semiconductor is initiated at the substrate surface by a heterogeneous reaction. The same approach can be used with other halides of silicon such as the iodide (16). However, in this case certain practical difficulties arise due to the fact that the iodide is solid at room temperature.

Control of growth rate and of uniformity of layer thickness are very important in the preparation of epitaxial junctions. Joyce (18) and Li (17) have reviewed the literature on factors controlling growth rate. For deposition from $SiCl_4$ it is found that the substrate temperature dependence of growth rate follows an Arhennius-type relation with activation energies variously quoted as lying between 22 and 37 kcal/mole. Theurer (21) found that the rate increased with the flow rate of the $H_2 + SiCl_4$ mixture and also with the partial pressure of $SiCl_4$, peaking at a mole fraction of 0.10 and then decreasing at higher concentrations. When the concentration exceeded a mole fraction of 0.28, etching of the silicon substrate occurred. The temperature dependence of growth rate imposes special problems on heating substrates in such a way as to achieve good temperature uniformity.

b. Pyrolysis of Hydrides. Although developed somewhat later than the methods based on hydrogen reduction of halides, pyrolysis techniques, employing the thermal decomposition of, for example, silane, SiH_4, or germane, GeH_4, appear to offer certain advantages in the preparation of epitaxial films and junctions and in heteroepitaxial growth. Chemical attack of the substrate which occurs in the case of the halides is avoided, while the lower growth temperatures achieved with the hydrides permit sharper electrical junctions to be produced. The SiH_4 or GeH_4 is usually transported by a stream of hydrogen to the heated substrate surface, where a thermally activated heterogeneous reaction occurs as in the case of hydrogen reduction of halides. For the pyrolysis of silane Joyce and Bradley (23) report, for the substrate temperature range 950–1100°C, an activation energy of 37 kcal/mole. At higher temperatures the rate of growth is relatively insensitive to temperature change and appears to be limited primarily by diffusion effects in the vapor or at the substrate surface. Doping of silicon films is achieved by introducing gaseous hydrides such as B_2H_6, PH_3, AsH_3, or SbH_3 into the hydrogen gas flow transporting the silane. Experimental aspects of the

methods for silicon and germanium deposition are covered in some detail in the reviews mentioned above ($17, 18$).

c. *Disproportionation of Halides.* At elevated temperatures an equilibrium condition exists between the tetrahalide and dihalide of silicon or germanium which can be represented by the expression

$$2SiI_2 \rightleftharpoons SiI_4 + Si \tag{1}$$

It was demonstrated by Wajda *et al.* (24) that epitaxial growth of silicon could be achieved by conducting this reaction in a closed tube system containing source silicon at one end and the silicon substrates to be coated in a somewhat cooler zone at the other. Sufficient iodine must be introduced to ensure a pressure in excess of the critical disproportionation pressure of SiI_2. Typically, with the source silicon at a temperature of about 1100°C and with the substrate zone at 800°C, growth rates of up to about 15 μ/hr are obtained (25). The growth rate increases progressively with iodine pressure and with the difference in temperature between the hot and cold zones.

The disproportionation technique has not been adopted as a general method of fabricating epitaxial junctions, primarily for three reasons: (a) *in situ* cleaning of the substrates, e.g., by iodine etching, cannot be achieved without modifying the doping conditions in the system; (b) the controlled incorporation of dopants into the film is more difficult than with open tube flow processes; and (c) the growth rates normally obtained are low for commercial applications. Wajda and Glang (25) have described multiple doped source methods for the growth in sequence of several layers of different resistivity and conductivity type, but these are rather inflexible due to the need for mechanical movement of the entire system or of the sources relative to the hot zone of the furnace.

d. *Transfer Reactions for Compound Film Growth.* Chemical transfer reactions used in the deposition of compound films may be divided into two categories: (1) those in which the compound is used as the source material, and (2) those in which the source comprises the constituent elements (or volatile compounds) of these. Gallium arsenide, GaAs, is the compound which has received most study and may be used to illustrate the principal transfer reactions. In category (1) three methods have been used to transport GaAs from the compound source. The first, described by Pizarello (26), involves disproportionation in a closed-tube system, usually using iodine with a reaction of the form

$$2GaI_3(g) + 4GaAs(s) = 6GaI(g) + As_4(g) \tag{2}$$
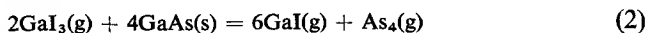
The source material is usually held at about 700°C and the substrate crystal at about 650°C. As in the case of the silicon–iodine reaction, the transfer rate

increases with the difference in source and substrate temperatures. It was found, however, that transport occurred by a combination of diffusion, convective, and laminar flow, each mechanism contributing to a varying extent, depending upon the growth conditions.

A second, more commonly used method where the compound is employed as the source is one in which GaAs (or other III–V compounds) is transported in an open tube flow system by means of a carrier gas comprising a mixture of HCl and H_2. This method has been used for example by Moest and Shupp (27) and by Holloway et al. (28) for depositing GaAs on Ge.

The third method utilizing the compound as a source involves the use of water vapor as the transporting agent. This technique has been applied to the growth of both Ge and GaAs epitaxial films. The transport of GaP has been studied most completely, and Frosch and his co-workers (29, 30) have established that the reaction may be represented as,

$$2GaP + H_2O = Ga_2O + P_2 + H_2 \tag{3}$$
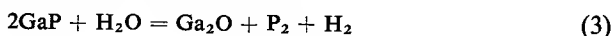
The GaP source temperatures used were typically about 1100°C while the substrate temperatures were about 20–100°C lower. The growth rate is low compared with that obtained with halide carriers. However, good-quality films are obtained by this method, and by using multiple sources it is possible to grow epitaxial solid solutions such as GaP_xAs_{1-x}, with good chemical homogeneity.

We turn now to the second category of transfer reactions in which the source material does not comprise the compound. Figure 1 shows, as a typical example, a system used by Knight et al. (31) for transporting GaAs using high-purity $AsCl_3$ and gallium as the source materials. Purified hydrogen is
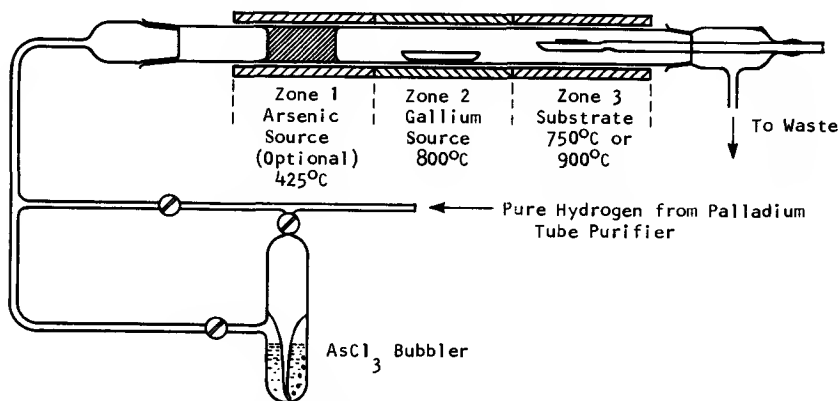
FIG. 1. System for the preparation of GaAs layers using $AsCl_3$ and Ga as reagents. [After Knight et al. (31).]

bubbled through the AsCl$_3$ which is transported to the furnace where it is reduced to arsenic. The arsenic is absorbed (up to saturation at about 2.25 at. %) in the gallium, and once saturation is established the excess arsenic together with gallium in the form of a chloride are transported to the substrate.

In a recent study Manasevit and Simpson (*32*) have discussed the disadvantages of "two-zone" transport methods in which all or part of the source material is held in one temperature zone of the system and the substrate in another. They point out that better control could be attained by transporting the reagents in the form of vapors directly to the substrate so that decomposition can occur *in situ* in a single temperature zone. This is achieved for GaAs by using arsine (AsH$_3$) as the arsenic source and triethylgallium (TEG) or trimethylgallium (TMG) as the gallium source. The reagents are transported by hydrogen to the substrate where they decompose probably by a reaction of the type (for TMG)

$$(CH_3)_3Ga + AsH_3 \rightarrow GaAs + 3CH_4 \tag{4}$$
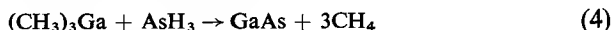
A further advantage of this method over those employing halides for transport lies in the absence of side reactions between the reagents and most common substrate materials. This fact renders the technique very suitable for heteroepitaxial growth on substrates such as sapphire and spinel.

The transfer reactions described thus far do not embrace the complete range of chemical vapor deposition methods which might be applied to the epitaxial growth of semiconductors. Nevertheless, they serve to illustrate the principal types of reaction involved in the vapor transport of most elemental and compound materials. Further reactions specific to refractory compounds will be cited in a later part of this section.

2. Heteroepitaxial Growth

Until recently, the main effort in the epitaxial growth of semiconductors was devoted to the formation of homoepitaxial junctions, mostly in silicon but also in other materials such as Ge and GaAs. But increasing interest in the growth of epitaxial films (mainly by chemical vapor deposition) on foreign substrates has been motivated by three main reasons: (1) the requirements for electrical isolation and compatibility of passive and active devices encountered in the development of integrated circuits, (2) the advantages of growing large single crystals of expensive semiconductor compounds on cheap, readily available substrates, and (3) the increased flexibility and novel *p–p* or *n–n* heterojunction properties obtainable by growing epitaxial layers of one semiconductor on another. The most recent studies of heteroepitaxy have been concerned with the growth of silicon on oxide substrates. A limited but not too successful effort has been made

to grow films of semiconductors on oriented metal surfaces. Successful attempts have been made to form good-quality heterojunctions such as GaAs/Ge and GaAs/GaP, and it seems that this field of research will be pursued further. We shall review briefly some typical studies of the growth of semiconductors (primarily silicon) on insulator crystals and of the formation of semiconductor heterojunctions.

   a. Heteroepitaxy on Insulating Substrates. Work in this area is currently of great interest because of the novel device possibilities offered by such films, especially in the microelectronics field. Much of the work on silicon films prior to 1967 has been reviewed by Filby and Nielsen (*20*). Several workers, e.g., Manasevit *et al.* (*33*) and Joyce *et al.* (*34*), have demonstrated the feasibility of growing epitaxial silicon films on substrates such as quartz (SiO_2), sapphire (Al_2O_3), spinel ($MgAl_2O_4$), and BeO. Both silane and silicon tetrachloride methods have been used, the former having certain advantages in that reactions with the oxide substrate are minimized. Earlier studies of silicon heteroepitaxy placed strong emphasis upon the epitaxial mechanisms involved and the dependence of film perfection upon the epitaxial growth direction. Conflicting results (*20*) were in some cases obtained by different workers using the same substrate materials and the same nominal growth conditions. In general most of the work done subsequently on the electrical properties of such films was confined chiefly to layers grown on the basal (00.1) plane of alumina, giving (111)-oriented Si, the $\{1\bar{1}.2\}$ planes of alumina, giving (100)-oriented Si, or on the low-index planes of spinel which yield layers in parallel orientation.

   Recent studies, in particular by Dumin (*35*), Wang and co-workers (*36*), and others (*37*), have demonstrated the extreme sensitivity of film perfection, composition, and electrical properties to variations in substrate orientation and surface perfection, and to changes in growth temperature and growth rate. Several workers have now been successful in growing epitaxial layers, of structural quality admittedly inferior to that of bulk silicon but with electrical properties perfectly adequate for certain device requirements. However, opinions regarding optimum growth conditions show considerable divergence. Dumin (*35*) reported that the growth from silane of high-mobility films on (00.1) is favored by pretreating the substrate crystals in hydrogen at 1300°C, and that a maximum in mobility versus growth temperature is obtained by depositing (or nucleating) at a substrate temperature of about 1200°C. These results have been queried recently by workers at the Autonetics Laboratories (*37*), who claim that substrate temperature has little influence on mobility. Growth of high-mobility (>200 cm^2/V-sec) *p*-type films appears to present no real problem, although acceptor concentrations are difficult to control due to the strong tendency for autodoping with Al from the alumina substrate.

This tendency makes it extremely difficult to grow n-type films at higher substrate temperatures (where better film perfection and electrical properties would otherwise be favored). Dumin (35) has attempted to overcome this problem by seeding or nucleating the n-type film with a thin layer (approx. 0.2 μ thick) to encourage more perfect growth, and then depositing the remainder of the n-type film at low temperatures (e.g., 1140°C) to reduce autodoping and compensation.

The variability in epitaxial orientations found for Si on alumina and the significant autodoping problem have prompted investigations into alternative substrate materials. Of these, spinel ($MgAl_2O_4$) has received most attention and appears at present to show most promise. Wang et al. (36) have recently reevaluated the suitability of various grades of spinel crystals for the epitaxial growth of silicon from silane. Their preliminary results show that commercial Al-rich spinel crystals of approximate composition $MgO:3.3Al_2O_3$ are thermally unstable at the temperatures required for silicon epitaxy and on heating undergo morphological and compositional changes. The surfaces of such crystals develop severe cracking, and x-ray diffraction studies reveal that precipitates of alumina are formed. Similar results are obtained for Al-rich crystals grown by other methods such as Verneuil flame fusion. Stoichiometric crystals of composition $MgAl_2O_4$ are found to yield the best-quality epitaxial Si crystal growth, and spinel crystals grown at low temperature ($\sim$1250°C) using a PbF_2 flux appear both to be most perfect structurally and best suited for the growth of Si films with good electrical properties. However, to exploit the advantages of the flux-grown crystals, it is important to clean their surfaces prior to deposition using a heat treatment in vacuo at 1200°C.

The potential applications of heteroepitaxial Si films appear at present to be chiefly in the metal oxide semiconductor (MOS) or field effect device structures. Planar diffused devices of good quality are difficult to attain, due to the fact that the films frequently contain crystallographic defects such as stacking faults, twin boundaries, or dislocations. Diffusion occurs more rapidly along these defects, leading typically in transistors to electrical shorts between emitter and collector (37). The inclusion of trapped impurities in the films is difficult to prevent at present and presumably accounts for the low minority carrier lifetimes thus far reported (38). Considerably more work is required before heteroepitaxial silicon films will achieve general application in device production.

A limited amount of heteroepitaxial work using oxide substrates has been performed on other semiconductors, in particular Ge (39) and GaAs (32). Dumin (39) has recently studied the epitaxial growth of Ge from germane, GeH_4, on Al-rich spinel crystals, obtaining mobilities as high as 300 cm^2/ volt-sec in 7-μ-thick films. Optimum mobilities were obtained at a growth temperature of 750°C, above which agglomeration of the film occurred. This temperature is too low to produce autodoping from the spinel substrate, and

at lower temperatures the acceptor concentration in the films is found to increase rather than decrease with decreasing growth temperature. In this case, the rise in the acceptor concentration is attributed to an increase in the defect concentration at lower temperatures. The Ge films grown in this way are found to possess lower residual compressive stress than Si films, due partly to the lower growth temperature used, but also to the closer match in thermal expansion coefficients of film and substrate ($6.19 \times 10^{-6}/°C$ for Ge, $3.8 \times 10^{-6}/°C$ for Si, and $7.45 \times 10^{-6}/°C$ for $MgAl_2O_4$).

One of the problems involved with heteroepitaxial growth of compound films such as the III–V semiconductors arises from the need to use volatile halides of the Group III element which promote side reactions with the substrate. Manasevit (32) has recently overcome such problems for the case of GaAs and GaP by using the trimethylgallium–arsine (or phosphine) reaction mentioned previously, and has obtained epitaxial growth on a wide variety of substrates including Ge, GaAs, alumina, spinel, BeO, and ThO_2. High-mobility films were obtained on both alumina and spinel.

b. Heteroepitaxy on Semiconductor Substrates. Due to the ready availability of high-quality crystals of semiconductors such as Ge, GaAs, and Si, and the greater ease with which the surfaces of these crystals can be cleaned *in situ* in chemical growth systems, many of the best-quality heteroepitaxial films have been grown on semiconductor substrates. Numerous combinations have been tried, e.g., Ge/Si (40), GaAs/Ge (41), GaP/GaAs (42), InAs/GaAs (13), SiC/Si (43), AlP/Si and GaAs (44), AlN/SiC (45), etc. Most of the chemical procedures used are basically those described previously for homoepitaxial growth; however, slightly different reactions and procedures have been applied to the epitaxial growth of the refractory compounds such as AlP, AlN, and SiC. These will be discussed in the following section.

In most cases the semiconductor film–substrate combination is studied directly as a heterojunction, although situations also arise where the substrate (e.g., Ge or Si) plays no active role and merely functions as a cheap readily available support for a compound film or junction structure. In either event structural imperfections at the interface and in the film, as well as autodoping effects, must be kept to a minimum. For a heterojunction, interdiffusion should be suppressed by using reasonably low growth temperatures and rapid growth rates. Factors which are also important in determining film perfection are substrate surface condition, mismatch between the film and substrate lattices, and relative thermal expansion coefficients.

It appears that good-quality epitaxial growth is favored by using semiconductors which are isostructural and mutually completely miscible, e.g., GaP/GaAs. At the start of film growth some interdiffusion occurs, leading to

the formation of a continuous layer with graded composition but with an exposed face closely approximating the composition of the deposit. Unfortunately, this situation with its associated redistribution of dopants between substrate and film can yield a complex multiple junction structure which is not readily amenable to analysis by heterojunction theory (46). By choosing film–substrate combinations which are not mutually miscible one sacrifices the advantages of good structural perfection but achieves a more abrupt electrical junction. A proper understanding of the factors influencing growth in this latter situation is of considerable importance since it is more relevant to the more general problems arising in heteroepitaxy.

A good example of heteroepitaxy on a substrate providing restricted mutual miscibility is GaAs/Ge. This system has been studied by several workers both from the point of view of preparative problems (41) and heterojunction theory (46). Although the materials involved differ in structural symmetry they possess almost identical lattice parameters and thermal expansion coefficients, so that the film/substrate interface should show relatively little structural disturbance. Recent studies by Holloway and his co-workers (41) of the growth of GaAs films on the various low-index planes of Ge have proved highly instructive in identifying some of the key growth factors influencing film perfection.

Bobb *et al.* (41) have performed x-ray rocking curve studies on GaAs films epitaxed on Ge using flow systems in which either a hydrogen–AsCl$_3$ mix is passed over Ga at 900°C or GaAs is transported from a source of the compound using a hydrogen–HCl mix as the carrier (27). They report that film perfection as judged from the width of the rocking curve profiles is sensitive to orientation of the growth plane, growth temperature, presence of impurities, and arsenic deficiency during growth. The orientation effect is felt partly through the anisotropic influence of contamination, but mainly through the polar character of the GaAs structure. The {111} planes of this structure will terminate at a plane of As or Ga atoms, depending upon whether the exposed face is, for example, (111) or ($\bar{1}\bar{1}\bar{1}$). If growth occurs on a polar plane of the {111} type, an ideally perfect film structure would possess a continuous surface terminating in atoms of one type. On a nonpolar surface, however, such as (100) the polar axis can adopt two equivalent orientations with respect to an axis in the film surface, and initial growth centers will be statistically divided between these orientations.

Contamination, arising, for example, from water vapor in the carrier gas, appears to cause local variations in the nucleation conditions over a polar surface, with the result that growth centers of opposite polarity are developed. Associated with this effect is the generation of boundaries between the differently oriented regions, and a loss of crystalline perfection as reflected in broadening of the x-ray rocking curves. If special precautions are taken to

reduce contamination to a minimum, film structures of single orientation with significantly improved perfection are obtained on (111) Ge.

Optimum perfection is obtained at a growth temperature of about 740°C, where for films grown on (311) rocking curves show widths comparable to that observed for a bulk GaAs crystal. Actually, the (311) films are more perfect than (111) films, and it is suggested by the authors (41) that this may be due to the stronger influence of contamination on (111) growth. The enhancement of film perfection at 740°C seems to be related to the presence of excess arsenic when growth is initiated. This exposure to excess arsenic is normally accomplished by flowing the hydrogen–AsCl$_3$ mixture over the substrates for a short period before the Ga source is inserted into the flow. Under these conditions it is likely that a thin liquid As–Ge alloy layer forms at the substrate surface and that the epitaxial film grows via this layer by a VLS mechanism (149). The authors point to strong Ge doping in the films as further evidence for this mechanism.

3. GROWTH OF REFRACTORY COMPOUND FILMS

Recent developments in the space technology field have generated needs for new semiconductor devices capable of withstanding high sustained operating temperatures and prolonged exposure to radiation. In addition, special requirements have emerged which make it desirable to utilize solar energy under conditions of optimum efficiency. Materials such as silicon and germanium are not capable of meeting these needs completely and interest has turned to the more refractory semiconductor compounds possessing greater environmental stability and wider band gaps. In many cases the high melting points of these compounds prohibit the use of conventional growth techniques normally used for preparing bulk crystals. Vacuum sublimation and chemical vapor deposition methods offer means of circumventing these difficulties and also provide possibilities for forming epitaxial junctions analogous to those grown in silicon technology. Although the chemical processes used are essentially those outlined previously, each compound presents its own preparative problems and we shall now discuss some of the experimental approaches devised to overcome these. The compounds referred to are listed in Table I.

Silicon carbide, SiC, has formed the subject of numerous studies aimed at exploiting its unusual combination of semiconducting, optical, and chemical properties. Single crystals of the hexagonal form may be grown by the sublimation technique (47). Depending upon the precise growth conditions, these crystals may adopt a single hexagonal structure or a mixed structure consisting of the various hexagonal and rhombohedral polytypes of SiC. The most commonly occurring form is the 6 H polytype and is that generally used in the preparation of experimental device structures. The cubic β-SiC

form is also of considerable interest since it possesses a lower gap and higher mobilities than the hexagonal form. In general it is of interest to grow epitaxial films of the same polytype as the substrate crystal, although junctions formed from different polytypes are of potential interest for heterojunction applications.

A recent study which resulted in the successful growth of SiC homoepitaxial junctions possessing the 6 H polytype structure is that due to Campbell and Chu (48), who used a reactor system outlined schematically in Fig. 2.
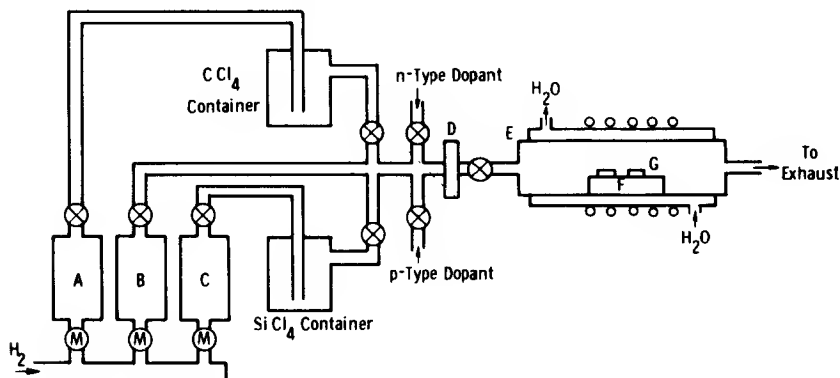
FIG. 2. Schematic diagram of the apparatus for the epitaxial growth of silicon carbide by the thermal reduction technique: (M) metering valve; (⊗) shutoff valve; (A, B, C) flowmeters; (D) filter; (E) water-cooled reaction tube; (F) tantalum silicide coated susceptor; (G) SiC substrates. [After Campbell and Chu (48).]

The substrate crystals used were flat platelets with {00.1} faces, grown previously by the sublimation technique, and were lapped with boron carbide and polished with diamond paste before insertion into the reaction chamber. Prior to growth, the substrates were etched with hydrogen at 1650–1700°C to remove about 10 μ of surface material. During growth the substrate temperature was held between 1700 and 1715°C, and a mixture of silicon and carbon tetrachlorides (0.04–0.1% in hydrogen) was flowed through at about 2.5 liters/min. The results were very sensitive to the concentration of the reactants and to growth temperature; higher concentrations prompted more rapid growth but gave polycrystalline films while low concentrations were accompanied by etching of the substrate. The use of substrate temperatures lower than 1700°C led to epitaxial growth of the cubic β-SiC form. The optimum growth rate for producing films comparable in crystal quality with the substrates was about 0.5 μ/min. Choice of a nonreactive susceptor material presented some problems at the high growth temperatures used, and the most satisfactory susceptor was found to be tantalum coated with tantalum

silicide. Dopants were introduced into the flow mixture, using diborane for p-type doping and nitrogen, arsine, and phosphine for n-type doping. Although the junctions thus far prepared by this method withstand only low applied voltages, mobilities up to 290 cm^2/V-sec were obtained in n-type films.

Chemical vapor deposition has also been applied to growth of films of the Al–V family of compounds. Of the four members of this group (Table I), AlP, AlN, and AlAs have been grown epitaxially on semiconductor substrates. The growth of AlP films provides an especially interesting example which demonstrates the necessity for adjusting the detailed experimental conditions and chemical reactions to meet the characteristics of the reactants and their products. Figure 3 shows the system described by Reid et $al.$ (44), in which iodine is used to transport the Al to the Si or GaAs substrate. Both the iodine and phosphorus are introduced to the quartz reaction chamber by flowing hydrogen over heated external sources. The iodine vapor reacts with the molten Al (held at about 1130°C) to produce AlI, which is transported down the temperature gradient to the substrate (held at about 900°C). Here, the disproportionation reaction

$$3AlI \rightleftharpoons 2Al + AlI_3 \qquad (5)$$

occurs, depositing metallic Al. The metal is free to react with phosphorus vapor at the substrate surface to form AlP.

For the deposition reaction to proceed it is essential that the liquid Al should not be exposed to phosphorus vapor. Otherwise, a stable skin of AlP compound forms on the metal surface, preventing further reaction with iodine, and stopping the deposition process. The alternative approach of transporting the aluminum as a chloride instead of an iodide is not practical, since to produce AlCl rather than $AlCl_3$ would require an Al temperature in excess of 1300°C (see Fig. 4), a condition incompatible with the thermal stability of the quartz reaction tube.

Reid et $al.$ (44) were successful in growing epitaxial films of AlP up to 1000 μ thick and obtained electron mobility values up to 60 cm^2/V-sec. They noted, however, that the film surfaces reacted with moist air.

Whitaker (49) has performed electrical measurements on epitaxial films of AlAs grown an GaAs substrates, using a deposition technique due to Bolger and Berry (50). These latter authors provide few details of the experimental method, but state that the films are grown by an open-tube technique in which the aluminum is transported in the presence of arsenic vapor in a stream of hydrogen. It is claimed that the aluminum is transported by the reversible reaction

$$2Al + AlCl_3 \rightleftharpoons 3AlCl \qquad (6)$$
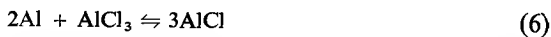
in the temperature region 1150–1000°C. This statement is surprising in view of the fact that thermochemical data (44) suggest that the formation of $AlCl_3$
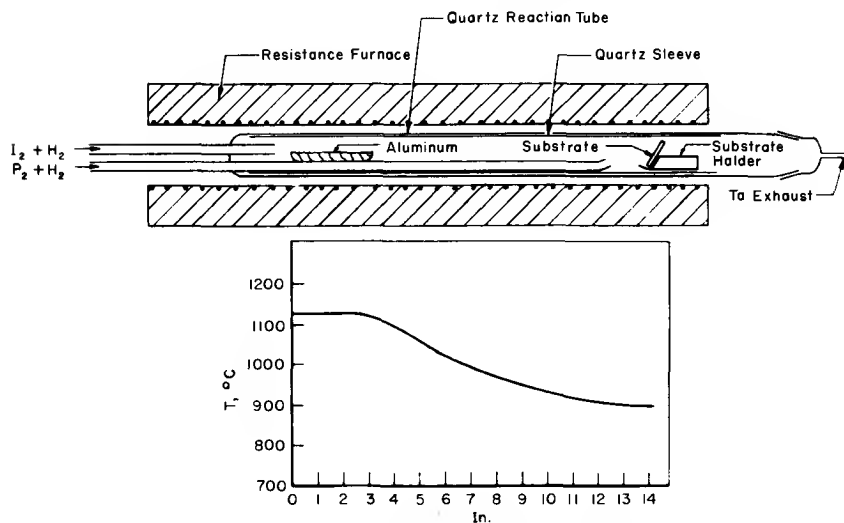
FIG. 3. Vapor growth apparatus for deposition of AlP epitaxial films. [After Reid *et al.* (*44*).]
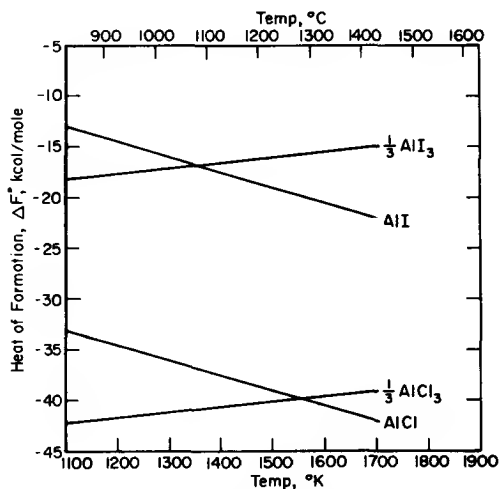
FIG. 4. Heats of formation of aluminum halides as functions of temperature (*44*): $Al + \frac{1}{2}X_2 = AlX$; $\frac{1}{3}Al + \frac{1}{2}X_2 = \frac{1}{3}AlX_3$; $AlX = \frac{2}{3}Al + \frac{1}{3}AlX_3$.

is favored over AlCl until a temperature in excess of 1280°C is achieved. Whitaker's (49) measurements, for thick films subsequently isolated by grinding away the GaAs substrate crystal, indicate that films made in this way attain a maximum mobility of 180 cm²/V-sec at room temperature for a carrier concentration of 8.5×10^{12} cm^{-3}.

Aluminum nitride, AlN, differs significantly in its properties from the other members of the Al–V compound family. It possesses the hexagonal wurtzite structure rather than the cubic sphalerite structure common to AlSb, AlAs, and AlP, and has a much higher band gap (Table I) and far greater chemical stability. Its electrical properties are essentially those of an insulator, resistivity values for the pure material lying typically in the 10^{12} Ω cm range. Crystals have been grown by sublimation, the gas flow comprising either a mixture of aluminum and nitrogen vapors or vaporized AlN. Single crystals produced in this fashion seldom achieve dimensions greater than a few millimeters (51).

Several studies have been reported recently, describing the growth of AlN films by chemical transport methods. In these experiments reactions between pure N_2 or NH_3 and a halide, usually $AlCl_3$, are used. Pastrňak and Součková (52) have grown films of AlN, GaN, and InN using a flow system, in which N_2 is passed over the heated chloride and the gaseous mixture is reacted at the substrate surface in a resistively heated furnace. The reaction is assisted by maintaining a glow discharge in the vicinity of the substrate (see Fig. 5).
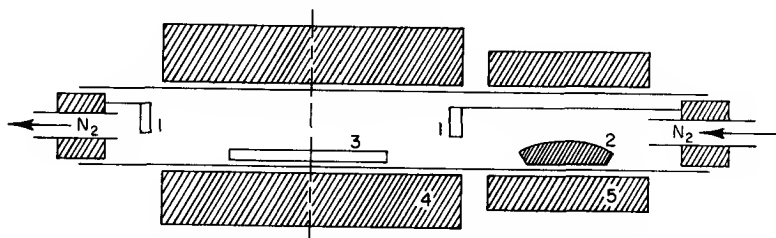
FIG. 5. System for chemical vapor deposition of nitride films: (1) electrodes; (2) boat with chloride; (3) silica substrate; (4) reaction chamber (electrically heated); (5) oven for vaporizing chloride. [After Pastrňak and Součková (52).]

Chu et al. (45) employing an ammonolysis reaction in a flow system were able to grow epitaxial AlN films on single-crystal substrates of AlN and SiC. The basic reaction is

$$AlCl_3(g) + NH_3(g) = AlN(s) + 3HCl(g) \qquad (7)$$
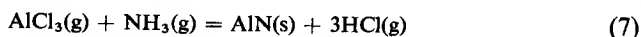
However, it is probable that vapor complexes of the type $AlCl_3 \cdot xNH_3$ (with $1 < x < 3$) are also formed and transported to the substrate, where

they are decomposed pyrolytically. In the experiments of Chu *et al.* the substrates were mounted on an rf heated tantalum susceptor. The optimum temperature for epitaxial growth appeared to lie in the range of 1200–1250°C. Using hydrogen selenide and mercury as dopants it was found possible to grow films which, as judged from hot probe tests, were *n* as well as *p* type.

Noreika and Ing *(53)* have recently extended the studies of Chu *et al. (45)* to growth on silicon substrates and found that the optimum orientation in epitaxial growth occurred at about 1150°C. Their results suggested that these epitaxial films (and probably those grown on AlN and SiC) comprise mosaic arrays of oriented crystallites. The AlN crystallite size was found to decrease systematically with increasing substrate temperature, an observation that conflicts with most other results obtained for both metal and semiconductor film growth. The authors explain this observation on the basis of the "initially incomplete condensation of nuclei" model proposed by Lewis and Campbell *(54)*.

The boron class of III–V compounds has excited considerable interest due to their highly refractory properties, wide band gaps, and potential applications in a variety of high-temperature devices. To date few systematic efforts have been made to prepare good-quality thin films of these materials. Williams and Ruehrwein *(55)* have discussed various reactions which can be used in the preparation of BP and BAs and have shown that films of cubic BP are produced by the vapor phase reaction

$$BCl_3 + PH_3 \xrightarrow{1000°} BP + 3HCl \qquad (8)$$

They state that at 1100°C for BP, and at lower temperatures for BAs, loss of the Group V element occurs to produce the compounds B_6P or B_6As. Vapor transport with iodine, in a sealed tube system, has been achieved for BP and BAs by Armington *(56)*. Ku *(57)* has succeeded in preparing epitaxial films of BAs and BAs–GaAs solid solutions on GaAs substrates, again using iodine transport, with source temperatures of about 740°C and substrate temperatures of about 680°C.

Boron nitride is mainly of interest as a high-temperature insulator, and although chemically deposited films of the hexagonal polymorph and of a vitreous form have been prepared by the ammonolysis of BCl_3 and B_2H_6 *(58)*, the products do not display semiconducting properties.

III. Vacuum Deposition

The recent wide-spread technological development of chemical vapor deposition techniques for the growth of semiconductor junctions has tended to force the older vacuum deposition approaches into a secondary role. Nevertheless, vacuum methods utilizing evaporation and sputtering continue

to receive considerable attention from workers interested in exploring basic formative processes and physical properties. Also, the prospect of ultimately fabricating passive and active components in integrated circuits by compatible techniques continues to excite growing interest in the extended application of newer evaporative or sputtering approaches. The range of potentially useful semiconductor materials is now extremely wide, and their marked differences in physical and chemical properties has made it necessary to devise a variety of vacuum techniques, each suited primarily to the deposition of films of one class of substances. In the following sections we shall describe those vacuum deposition methods which have been applied thus far to the growth of elemental and compound semiconductor films, and discuss their special advantages and, where possible, the prospect of improving them or extending their use to other materials.

1. STANDARD EVAPORATION AND SUBLIMATION

Semiconducting materials display an extremely wide range of vapor pressures, and therefore a corresponding variation in the ease with which they can be vaporized to form thin films. From the treatments of Dushman (59), and more recently Holland (60), the rate of vaporization N_e for an element of atomic weight M_e which possesses a vapor pressure P_e at temperature T_e is given by the expression

$$N_e = 3.513 \times 10^{22} a_1 P_e / (M_e T_e)^{1/2} \quad \text{molecules/cm}^2\text{-sec} \qquad (9)$$

where a_1 is an evaporation coefficient which is equal to unity for a clean evaporant surface. The implications of this expression may be illustrated by comparing the vaporization rates at their melting points of two commonly used semiconducting elements such as Se and Ge. Thus, for sources with similar geometries Se (mp 217°C) would be expected to evaporate at approximately 10^4 the rate of Ge (mp 938°C). The disparity in rates between the constituent elements of certain semiconducting compounds such as the III–V class is even greater, and this poses special problems in the choice of vacuum deposition methods for preparing thin films.

In standard as well as in more complex methods of evaporating semiconducting films the background pressure in the system and the source design play a vital role. These factors not only affect the vaporization rate, but also, through chemical reactions during evaporation or condensation, can modify profoundly the structural and electrical properties of the film. Depending upon the type of pumping system used, the ambient in which evaporation is carried out will contain a variety of gaseous impurities. Mass spectrographic analyses commonly show the residual background gases to comprise H_2O, CO_2, O_2, N_2, H_2, and various organic vapors, e.g., CH_4. These impurities arise from desorption from the chamber walls, decomposition of pump oils,

and outgassing from elastomer or synthetic rubber seals (60). The equation expressing the rate at which such gas molecules strike the substrate surface takes essentially the same form as Eq. (9) above, i.e.,

$$N_g = 3.513 \times 10^{22} P_g / (M_g T_g)^{1/2} \quad \text{molecules/cm}^2 - \text{sec}^1. \qquad (10)$$

The rate N_d at which the evaporant is deposited is related to N_e in Eq. (9) by a geometrical constant. Thus from Eqs. (9) and (10),

$$N_g / N_d = (P_g / P_d) K \qquad (11)$$

where K is a constant whose value depends among other things upon the geometry of the source-substrate arrangement. Holland (60) has used this expression to calculate the value of N_g / N_d for Si evaporated at different gas pressures in a residual gas of the molecular weight of nitrogen, and from his

TABLE II

EVAPORATION OF ELEMENTAL SEMICONDUCTORS

Element	Source	Deposition rate (Å/min)	p (Torr)	Refs.	Remarks
Ge	C or W (R)[a]	100–15,000	10^{-5}–10^{-9}	62, 63	Study of dependence of
	W (EB)[b]	72–4700	10^{-6}–10^{-9}	64, 65	structure and prop-
	C (EB)	20–1000	10^{-8}	66, 67	erties on conditions of deposition
	W (R)	$\sim 10^6$	5×10^{-7}	68	Study of epitaxial devices on Ge
	W (EB)	$\sim 10,000$	5×10^{-8}	69	In situ structure study
	C (R)	~ 600	2×10^{-6}	70	Films etched with iodine vapor during growth
Si	Cu (EB)	Up to 50,000	10^{-6}	71, 72	Epitaxy of Si on Si
	Cu (EB)	400	10^{-7}	73	Structure and prop- erties of epitaxial films on sapphire
	Si (R)	~ 400	10^{-9}–10^{-10}	74, 75	Epitaxy of Si on Si at
	Si (rf)	3000		76	low temperatures
Se	Porcelain/W (R)	200–1000	2×10^{-5}	77	Epitaxial growth study
	Al$_2$O$_3$/W (R)	—	—	78	Rectifier photocells
Te	—	—	—	79	Effect of structure on electrical properties

[a] (R), resistive heating.
[b] (EB), electron bombardment heating.

TABLE III

EVAPORATION OF COMPOUND SEMICONDUCTOR FILMS

Compound	Source	Deposition rate (Å/min)	Refs.	Remarks
CdS	SiO_2/W (R)	100–4000	83	Structure of films for transducers
	SiO_2/W (R)	1000–5000	84, 85	Influence of annealing and composition on electrical properties
ZnS	W filament above charge	600–900	86	Electroluminescent films activated with Cu, Mn, Cl
(Zn, Cd)S	Mo (separate sources)	—	87	Structural and optical properties for entire solid solution range
CdSe	SiO_2/W (R)	1000	88	Dependence of electrical properties on deposition temperature
CdTe	Ta (R)	900	89	Structural and electrical properties
ZnSe	—	—	90	Influence of composition on polymorphic form
ZnTe	Ta (R)	300	91	Epitaxial growth on ionic substrates
PbS PbSe PbTe	SiO_2/Mo (R)	100	92, 93 94, 93 95, 93	Epitaxial film properties
InSb	C (R) Mo (R)	— 6–12×10^4	96 97	Effect on electrical properties of annealing inhomogeneous film products
InSb–GaSb InAs–GaAs InSb–InAs	—	—	98	Alloying and polymorphism in thermally homogenized films
Bi–Te Bi–Se	—	—	99	Structural study
HgTe Ag_2Te	—	300–3600	100	Electrical properties and recrystallization of thermally homogenized films
ZnSb–CdSb	—	—	101	Electrical properties of solid solutions

data it may be shown that at a deposition rate of 450 Å/min in a vacuum of 10^{-5} Torr the arrival rates for the gas and condensate molecules are approximately equal. The extent to which these gas molecules are incorporated into the film depends upon their chemical reactivity, but it is clearly desirable to keep the ratio N_g/N_d negligibly small, and this is only achieved by using low pressures ($<10^{-8}$ Torr) or high evaporation rates.

Earlier experiments in the vacuum evaporation of semiconductor elements and compounds involved the use of resistively heated sources almost exclusively, and these are still in vogue. Some of the more successful source materials, chosen so as to minimize chemical interactions and hence contamination of the film, are indicated in Table II–VI. While such sources may be quite acceptable for the highly volatile elements Se, Te, As, and Sb which can be evaporated or sublimed at low temperatures, they are unsatisfactory when used for Ge and Si, for which high evaporation temperatures are required with the consequent risk of alloying. Although some materials such as Mo, Ta, and W may be relatively stable in good vacuum, the presence of reactive gases, e.g., H_2O or O_2, may lead to the formation of volatile metal oxides so that these are incorporated in the grown film. It is now widely recognized

TABLE IV

EVAPORATION OF COMPOUND SEMICONDUCTOR FILMS
BY MULTISOURCE (THREE-TEMPERATURE) METHOD

Compound A_xB_y	Sources	Refs.	Remarks
InSb	(A, B) SiO_2	102, 103	Condensation model and electrical properties
	(A, B) SiO_2	104	Optical properties
InAs	(A, B) SiO_2	102, 103	Condensation model and electrical properties
InP	—	107	Optical properties
GaAs	(A, B) SiO_2	105, 106	Texture and optical properties
	(A) C (B) SiO_2	107	Optical properties
GaP	—	111	Polymorphism and whisker growth
AlSb	(A, B) SiO_2	108	Electrical and optical properties
	(B) Flash evaporated	109	
CdSe	(A, B) SiO_2	103	Condensation model
CdS	(A, B) SiO_2	110	Oriented films for transducers
Bi_2Te_3	(A, B) SiO_2	103	Condensation model

that an effective solution to this problem is to use crucible-free or cold-crucible sources in which the evaporant is heated by electron bombardment.

If the semiconductor is mechanically stable and attains a reasonably high vapor pressure at temperatures below its melting point, it may be possible to heat it by passing an electric current via chemically inert metal contacts. Simple and clean sources for subliming Si using this principle have been employed by Widmer (74), Jona (61), and by Thomas and Francombe (75), and are found to be compatible with ultrahigh vacuum techniques ($<10^{-9}$ Torr). Alternatively, the Si may be maintained at a temperature below its melting point by means of electron bombardment or rf induction heating.

TABLE V

FLASH EVAPORATION OF SEMICONDUCTOR COMPOUND FILMS

Compound	Source	Deposition rate (Å/min)	Refs.	Remarks
GaP, GaAs, GaSb, InP, InAs, InSb, AlSb	Ta (R)	160–1600	113, 114	Epitaxial growth on Ge and CaF_2; electrical properties of InSb films
Multicomponent system In–Ga–P–As–Sb	Ta (R)	120–600	115	Miscibility of compounds; epitaxy and optical properties
GaSb	—	120,000	116	Epitaxy and electrical properties
GaAs	Ta (R)	—	117	Optical and electrical properties
$Cu_{1.8}S$, $Cu_{1.8}Se$, $Cu_{1.8}Te$	W (R)	—	118	Stoichiometry and electrical properties, flash-evaporation theory
$Cd_xHg_{1-x}Te$ ($0 \leq x \leq 1.0$)	—	50	119	Optical properties of epitaxial films

Using rf heating and close spacing between source and substrate (Fig. 6) Handelman and Povilonis (76) have achieved sublimation rates as high as 0.3 μ/min. The vapor pressure of Ge in its solid form, however, is too low for use of the sublimation method in the growth of Ge films.

To reduce the relative importance of gaseous contaminants and of interdiffusion, and to achieve rapid fabrication of active devices on a competitive commercial scale, it is desirable to deposit films at rates in the micron per minute range. For the elements Ge and Si this implies that the source temperature for reasonable substrate to source separation should be significantly higher than their melting points. If the semiconductor is contained in a wellcooled

TABLE VI

DEPOSITION OF SEMICONDUCTOR FILMS BY SPUTTERING

Semiconductor	Method	Deposition rate (Å/min)	Refs.	Remarks
Ge	Glow discharge	250	125	Epitaxial growth of junctions
	Asymmetric ac	50–250	126	
	Glow discharge	8–100	127, 128	Dependence of structure on growth conditions
	Thermionically supported discharge	3–8	129, 130	Structure and electrical properties
Si	Thermionically supported discharge	50–60	130	Structure and electrical properties
InSb	Glow discharge	—	131	Electrical properties
	Glow discharge	200	132	Epitaxial growth
GaSb	Glow discharge	—	131	Electrical properties
GaAs	Glow discharge	50–200	133	Epitaxial growth on Ge
	Glow discharge (uhv)	200–500	134	Epitaxial growth on NaCl
Bi–Te	Glow discharge	100–1000	135	Oriented growth and stoichiometry
$Cd_xHg_{1-x}Te$ ($0.05 < x < 0.15$)	Glow discharge	1000–2000	136	Optical properties and microprobe analyses
Sulfides of: Pb, Cu, Sn, Mo, Cd, Cd:Cu, Cd:In, Cd:Cu:In	Glow discharge, reactive in H_2S	—	137	Photovoltaic properties of doped CdS films

crucible of high thermal conductivity, it may be melted by means of electron bombardment without the occurrence of chemical interaction at the semiconductor–crucible interface. The various types of electron bombardment sources used for the evaporation of films have been summarized recently by Holland (60), and fall generally into the two categories of (1) line-of-sight systems, in which the electrons travel essentially undeflected from a heated cathode to the evaporant surface, and (2) indirect or deflection systems, in which the evaporant is completely shielded from the electron source. Although direct focusing, line-of-sight systems have been used by Thun and Ramsey (80) and by Reichelt and Mueller (81) for the evaporation of Ge and Si, the fact that decomposition products emitted from the cathode may reach the source renders high purity difficult to maintain. Electrostatic and magnetic deflection systems of the type shown in Fig. 7 have been developed which
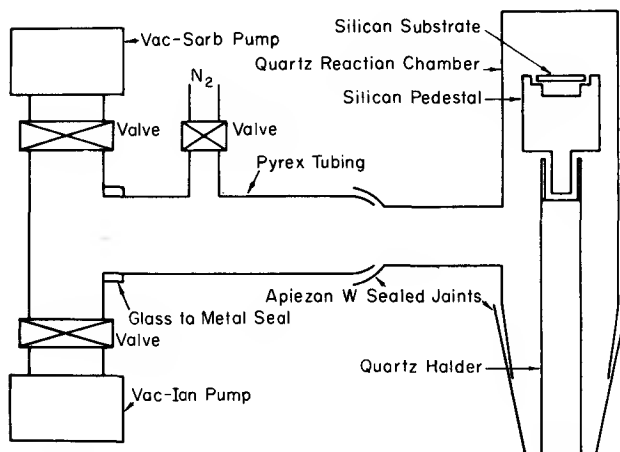
FIG. 6. Schematic diagram of Si sublimation apparatus. [After Handelman and Povilonis (76).]

avoid this problem. The former system has been used successfully by Booker and Unvala (72) to evaporate Si at rates up to 5 μ/min, while the latter E-gun arrangement is now rapidly gaining popularity for the general evaporation of refractory metals and oxides.

a. Deposition of Elements. Of the thin film elemental semiconductors prepared by vacuum evaporation Ge appears to have received by far the greatest attention to date. Numerous papers have appeared in which attempts were made to relate systematically the electrical properties and structure of Ge films to the detailed conditions of their formation. Much of the work prior to 1963 has been summarized by Sloope and Tiller (62), but several important papers discussing in detail electrical and structural properties have appeared since then. These will be referenced in Sections IV and V. As indicated in Table II, a variety of crucible materials has been used, the films being grown in the amorphous and crystalline forms on substrates of polished quartz, and also epitaxially on Ge and CaF_2 crystals. Films prepared for the purpose of studying crystallographic or basic transport properties have in most cases been evaporated from resistively heated tungsten or graphite crucibles at rates of up to about 300 Å/sec. However, in a study of the fabrication of Ge epitaxial junctions Courvoisier *et al.* (68) achieved deposition rates as high as 1–2 μ/sec.

Several authors (62–67) have made detailed studies relating the structure and properties of Ge films to their conditions of formation, partly in an effort to explain the strongly p-type conductivity and the very high acceptor densities ($> 10^{18}$ cm^3) found in evaporated (and in sputtered) deposits. Defect
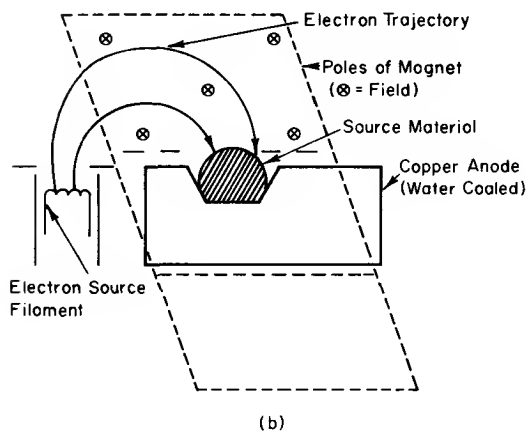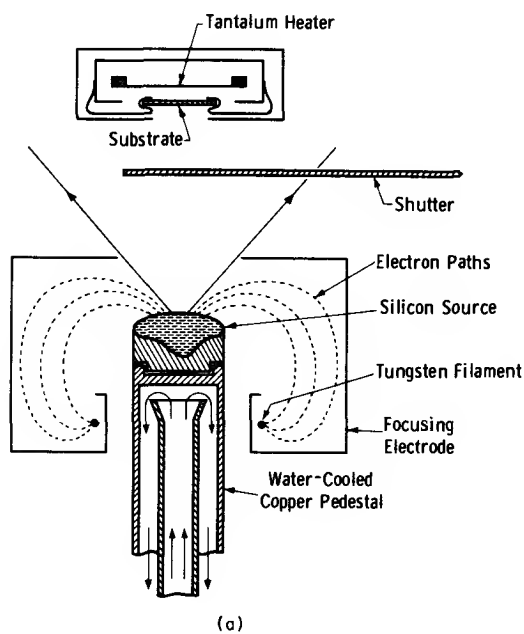
FIG. 7. Electron bombardment sources for evaporation: (a) electrostatic focusing system [after Unvala (71)]; (b) E-gun magnetic focusing system.

concentrations are usually very high in evaporated films on CaF_2 and vary from 10^6 to $5 \times 10^9/cm^2$, depending upon the conditions of growth and the film thickness. Butorina and Tolomasov (70) have suggested that the high densities of faults originate partly in nonequilibrium growth conditions resulting from the use of relatively high vapor supersaturations over the substrate. They have used a novel approach for establishing equilibrium whereby the Ge film is etched with I_2 vapor during growth. The method is in some respects similar to the asymmetric ac sputtering approach applied by Haq (126) to the epitaxial growth of Ge on Ge, and is claimed to produce a marked reduction in the number of crystallographic faults.

Compared to the numerous studies on evaporated Ge films, Si has received little detailed attention, one of the main reasons being its pronounced tendency to react chemically both with crucible materials and, during film growth, with reactive impurities such as O_2 and C in the vacuum chamber. Sublimation from solid sources maintained at temperatures above 1300°C has been shown by Widmer (74) and by Thomas and Francombe (75) to yield clean epitaxial layers of good crystal quality. However, due in part to the low rates obtained ($\sim$400 Å/min) it is essential to maintain ultrahigh vacuum conditions during deposition. The situation can be improved somewhat by reducing severely the source to substrate spacing, thus increasing the rate to about 0.3 μ/min and thereby decreasing the ratio of Eq. (11). The resultant increase in radiation to the substrate, however, imposes restrictions on the possible range of substrate temperatures which can be employed and, by reducing the sticking coefficient, lowers the actual growth rate. Probably the most detailed studies made to date on evaporated silicon films deposited in conventional *vacuo* conditions are those due to Booker and Unvala (72) and more recently to Salama *et al.* (73). Booker and Unvala, using the electron bombardment source shown in Fig. 7a, examined the epitaxial growth of Si on Si and found that by using deposition rates higher than 1 μ/min they could reduce the N_g/N_d ratio to a point where crystalline defects generated by substrate surface impurities essentially vanished. Salama *et al.* (73) studied the considerably more complex problem of epitaxial Si on sapphire (Al_2O_3) and, working with a commercial line-of-sight electron gun, achieved much lower evaporation rates (approx. 400 Å/min). In interpreting their results they had to consider both the defective character of the films and the doping influence of Al which diffused from the substrate.

Selenium films have long been of interest and commercial importance due to their useful photoconductive properties. With its extremely high vapor pressure the element can readily be sublimed *in vacuo* and coatings many microns thick may be produced in a few minutes. The structure and properties of the films are very sensitive to their conditions of preparation. Films deposited at temperatures below 70°C usually possess vitreous structures with

very high dark resistivity, while those made at higher temperatures contain a proportion of the metallic hexagonal modification. The type of spectral response depends critically upon both the amounts and distribution of the hexagonal phase within the vitreous matrix. Attempts have been made to study the kinetics of the transformation from the vitreous to the metallic form (82), and more recently Heavens and Griffiths (77) succeeded in growing epitaxial films of the hexagonal form on the faces of KBr crystals.

Films of tellurium may also be grown at high rates by sublimation, but since the vapor pressure of Te for a given temperature is lower than that of Se, films can be condensed at higher substrate temperatures in a crystalline form. The Hall coefficients of deposits up to 300 μ thick have been measured (79).

b. *Evaporation of Compound Films.* For purposes of the present treatment of standard evaporation, compound semiconductors can be divided into two classes: (1) those such as the II–VI or IV–VI compounds, e.g., CdS, PbS, which can be evaporated without significant change in composition, and (2) those which dissociate during evaporation, yielding very inhomogeneous multiphase film products. Best-known examples of the second class are the compounds comprising elements from Groups III and V of the periodic table, e.g., InSb, GaAs, AlP, etc., although the tendency to dissociate is by no means confined to these and may be displayed strongly by any partly covalent compound containing volatile elements, e.g., Bi_2Te_3, Ag_2Se. Compounds in class (1), when evaporated from a nonreactive crucible, yield film products which without further treatment are structurally (and, to a first approximation, chemically) identifiable with the bulk starting material. Those in class (2), however, usually require thermal annealing in order to homogenize them into structures approaching the single-phase stoichiometric compound.

Examples of semiconductor compound films which have been grown by standard evaporation are shown in Table III. Some of the most detailed studies of the growth and properties of IV–VI compound films have been carried out recently by Zemel and his co-workers on PbS, PbSe, and PbTe (92, 93). Since one of the main objectives was a careful comparison of the properties of bulk crystals and thin films, the deposits were grown epitaxially under conditions favoring optimum perfection, on cleaved alkali halide (usually NaCl) crystals. It was found that the use of metal boats for the evaporation source resulted (for the case of PbS) in the formation of volatile sulfide impurities, and precautions were taken to avoid this by containing the evaporant in chemically inert silica crucibles.

CdS films, which are finding important application in thin film transistors and also high-frequency transducers, have received considerable study. It is found that both their structure and electrical and photoconductive properties are extremely sensitive to conditions of deposition and to subsequent annealing

treatments (*83–85*). As evaporated, the films are nonstoichiometric and contain excess Cd which lowers their resistivity. By codepositing with S vapor (*83*) or by annealing the film in contact with a metal such as Ag (*84*), or in CdS powder (*85*), stoichiometry is regained and significant increases in resistivity are observed. Similar baking treatments are also needed in order to recover mobility values approaching those of the bulk material. Oriented and epitaxial films suitable for transducers have been grown by Foster (*83*) but it is found that the type and degree of orientation depend critically upon the substrate material and angle of incidence of the vapor beam.

Shimizu (*88*) reports that the electrical properties (e.g., conductivity and its temperature dependence) of evaporated CdSe films are sensitive to deposition temperature, but Glang *et al.* (*89*) find that the resistivity of CdTe films is essentially unaffected by their growth temperature. Thus dark resistivities for CdTe always lie in the range 10^7–10^8 Ω cm despite the fact that at substrate temperatures lower than 150°C an excess Te phase is present.

The method of complete evaporation of a compound charge followed by homogenization of the resulting film at elevated temperature has been used for many of the semiconductor compounds. Semiletov and his co-workers (*98, 99*) have applied this approach extensively to structural studies of thin films (<1000 Å) of the III–V compounds and their solid solutions. Optimum homogeneity in the annealed film is favored by several key factors, e.g., a weak tendency for the evaporant to dissociate, the small thickness of the deposited film, a low melting point for the compound, a low dissociation vapor pressure for the more volatile element over the compound, and large diffusion coefficients of the elements in the compound. Of the III–V compounds InSb appears to come nearest to satisfying these requirements, but there has been considerable disagreement between various workers concerning both the conditions for attaining optimum semiconducting behavior and the values of electron mobility and carrier concentration produced (*96, 97*).

Paparoditis (*100*) found that optimum properties for InSb room temperature deposits of about 2.6 μ thickness ($\mu_n = 2000$ cm^2/V-sec) were obtained on annealing at 360°C, while more recently Williamson (*97*) using very high evaporation rates (~1000 Å/sec) and high annealing temperatures (465°C) has attained mobilities as high as 1.3×10^4 cm^2/V-sec. Williamson's results suggest, in agreement with other workers, that the mobility increases with crystallite size and film thickness, but is highest in single-layer films. Attempts to produce thicker multilayer film structures yielded electrically inferior products.

The standard evaporation–annealing method seems best suited to low-melting-point, relatively low-vapor-pressure compounds, e.g., InSb and Bi_2Te_3 in which rather large inhomogeneities can be removed at modest annealing temperatures. However, for more refractory compounds such as

GaAs, GaP, etc., with high vapor pressures and high effective recrystallization temperatures, the prospects of producing thick homogeneous film products are poor.

2. Multisource Evaporation

In the preceding discussion we have shown that the extent to which a compound dissociates and the degree of inhomogeneity in the resulting evaporated deposit increase in severity with the difference in the vapor pressures of its constituent elements. Paradoxically, by suitably adjusting the experimental conditions, this same attribute can be exploited in order to ensure that only the stoichiometric compound grows in the deposited film. It was shown by Günther (102, 103) that this result could be achieved providing that the saturation vapor pressure of the more volatile element (Sb, As) over itself was greater than its vapor pressure over the compound (InSb, InAs). A so-called "stoichiometric interval" in the substrate temperature could then be defined within which the compound only would be stable, while the more volatile Group V element would resublime. Günther has described both the principle of the method and its application to III–V and II–VI compound films in two detailed review articles (102, 103). The summary presented here is based essentially upon the more recent of his papers.

The onset of condensation for a vapor over a substrate surface occurs when the ratio of the actual vapor pressure to its equilibrium pressure exceeds a critical value. In terms of vapor flux this means that the ratio of the incident N_+ to the emitted N_e particles per unit time and area of substrate surface must exceed a critical value. This critical ratio will in general be higher during subsequent equilibrium growth on a like surface. It is the latter condition which determines the final composition of the film in situations where condensation occurs from multicomponent vapors. The condition for condensation, as well as being defined by a critical flux ratio, can also be described, for constant incident flux, in terms of a critical condensation temperature T_c above which nucleation occurs at zero or a very low rate.

The effective critical condensation temperature for an element alone T_{cA} can be raised significantly (to a value T_{cAB}) in the presence of an impinging vapor of a more volatile element B with which it forms a compound. This is demonstrated in Fig. 8, which shows the variation of condensation flux with substrate temperature for constant incident fluxes of components A and B. Lowering of the substrate temperature to a value below T_{cAB} results in nucleation of the compound AB. Further decrease in temperature produces little change in the condensation flux until the temperature T_{cA} is reached at which condensation of the element A is possible. Similarly, a further increase in the net condensation is produced on decreasing the temperature below T_{cB}, when condensation of element B occurs.

The above description, while ignoring some of the details of the nucleation process, e.g., the influence of surface temperature on the rate of compound formation, outlines the essential conditions for the formation of stoichiometric compound films such as InSb and InAs. In accordance with the phase limits indicated in Fig. 8 it is possible to give a "stoichiometric interval" of temperature for InSb and InAs as shown in Fig. 9. These are, for InSb, 400–520°C, and for InAs, 230–680°C.

The control of the incident fluxes and condensation conditions at the substrate is obtained by means of a "three-temperature" evaporation method, whereby the temperatures of the sources for elements A and B (e.g., In and As) and of the substrate are separately adjusted. Different means of achieving optimum experimental conditions have been described, but it seems to be generally agreed that the basic technique is not only effective in controlling film composition but is also capable of producing well-crystallized film products with semiconducting properties approaching those of the bulk. A sampling of the wide range of compounds to which the method has been applied is indicated in Table IV. Simple arrangements using evaporating sources situated side by side in a bell jar have been used, for example, by Günther (103), Potter and Kretschmar (104), and by Johnson (108). In Johnson's experiments on coevaporated AlSb films the fluxes of the elements were monitored by means of quartz-crystal rate monitors. In an alternative system of the type shown in Fig. 10, using concentric sources, Günther claims more effective mixing at the substrate.

Although most earlier studies with the three-temperature technique were directed towards the growth of high-mobility films of InSb and InAs, efforts have been made more recently to extend this approach to other compounds such as GaAs, AlSb, and CdS. Of these, GaAs has received most attention. Davey and Pankey (105, 106), using a thermally enclosed quartz reaction system similar to that in Fig. 10, except that the element sources were in different tubes, made a systematic study of the texture and optical absorption properties of GaAs films deposited at a wide range of substrate temperatures and thicknesses. Similar investigations of the optical properties were carried out by Martinuzzi and his co-workers (109) and by Howson (107). Howson introduced a novel departure from the usual three-temperature approach in which he used a single evaporating source containing a mixture of the elements. He pointed out that since the vapor pressure of arsenic over GaAs was nearer to the vapor pressure of gallium over gallium than to that of arsenic over arsenic, a combined source comprising a small area of GaAs with a large area of gallium could provide the desired vapor mixture. It was found that a source containing approximately 15% by weight of GaAs in gallium yielded the correct film composition.

Johnson (108) and David et al. (109), who used the three-temperature
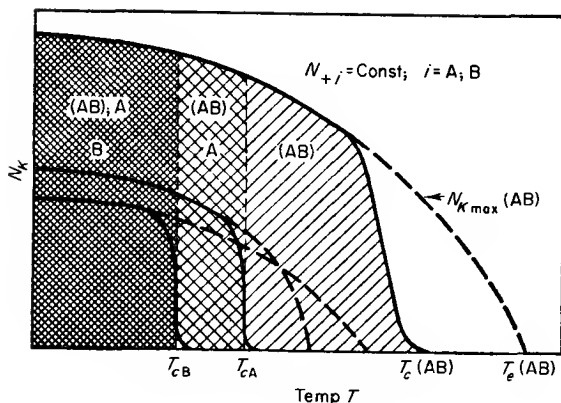
FIG. 8. Condensation flux as a function of temperature with two incident components A and B. [After Günther (103).]
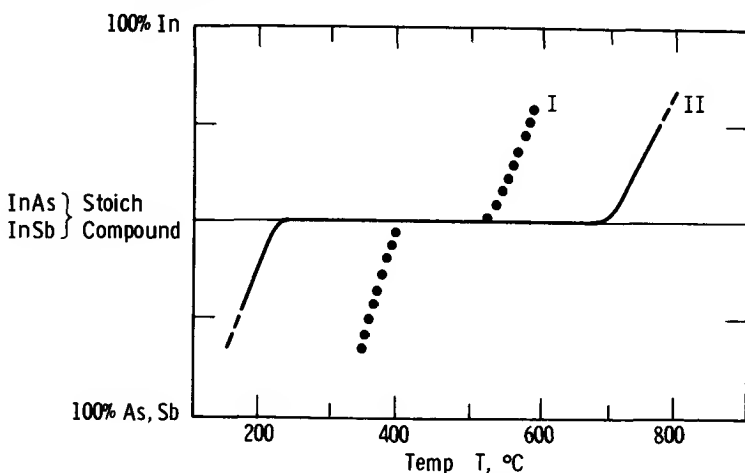
FIG. 9. Composition of condensed InAs or InSb layers as a function of substrate temperature during deposition (103). Curve I (InSb): N_+ (In) $\approx 2 \times 10^{16}/cm^2$-sec; N_+ (Sb) $\approx 6 \times 10^{16}/cm^2$-sec. Curve II (InAs): N_+ (In) $\approx 10^{17}/cm^2$-sec; N_+ (As) $\approx 5 \times 10^{17}/cm^2$-sec.
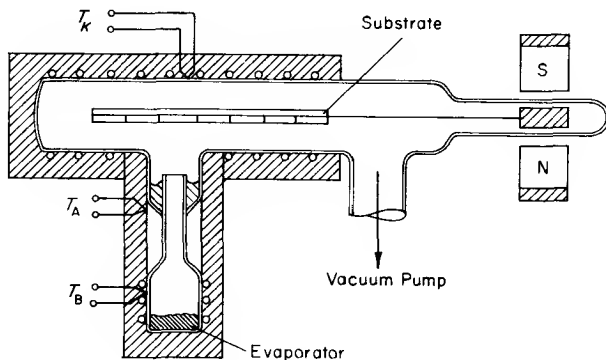
FIG. 10. Technical evaporation system for compound layers consisting of two components (103).

method to grow films of AlSb, report that the properties of the deposited compound are sensitive to exposure to the atmosphere. David *et al.* used a flash-evaporation source to regulate the supply of antimony vapor but made the surprising observation that their films contained free Sb when made at temperatures up to 650°C. This could not be confirmed in unpublished studies by the present authors (*209*). High-resistivity and apparently very stoichiometric deposits of CdS were prepared by de Klerk and Kelly (*110*) using essentially the three-temperature method with slight modifications. In these studies indirect condensation was effected by interposing a baffle between the sources and the substrate. Pure and highly oriented films of CdS were obtained which were ideally suited for use in ultrasonic transducers.

Except for some observations by de Klerk and Kelly (*110*) on their CdS films on sapphire crystals and some recently published studies by Davey and Pankey (*112*) on GaAs on germanium, little effort appears yet to have been made to grow epitaxial films by this method.

3. FLASH EVAPORATION

Although the technique of flash evaporation had been used previously to grow stoichiometric films of metal alloys and mixed oxides, the first attempt to apply this method to the deposition of semiconductor compound films appears to have been made by Richards and his co-workers in 1963 (*114*). In concept, the technique is simple and may be described as follows. For a compound which dissociates on evaporation a given evaporant charge will lose its most volatile components first so that the deposited film will have a layered structure with the high- and low-vapor-pressure ingredients at its bottom and top surfaces, respectively. Assume that the evaporant charge is reduced in size to a point where on complete vaporization it produces a condensed layer at the substrate effectively one compound molecule thick. In principle this monolayer should possess ideal stoichiometry. If a series of such monolayers is built up by sequential and complete evaporation of these small unit charges a stoichiometric film should result.

In practice attempts are made to fulfill this ideal condition by grain-by-grain vaporization of the compound using an arrangement of the type shown in Fig. 11. However, variations in grain size and delivery rate inevitably produce some compositional inhomogeneity in the film and this is removed by heating the substrate. Using mainly single-crystal germanium substrates Richards and co-workers (*113–115*) have succeeded in growing stoichiometric epitaxial films of most of the common III–V compounds (Table V). In a review paper Richards (*113*) has discussed the experimental approach in some detail and shows that to remedy nonstoichiometry resulting from departures from the ideal grain-by-grain condition it may be necessary to add a proportion of excess Group V element to the charge. Providing that the substrate
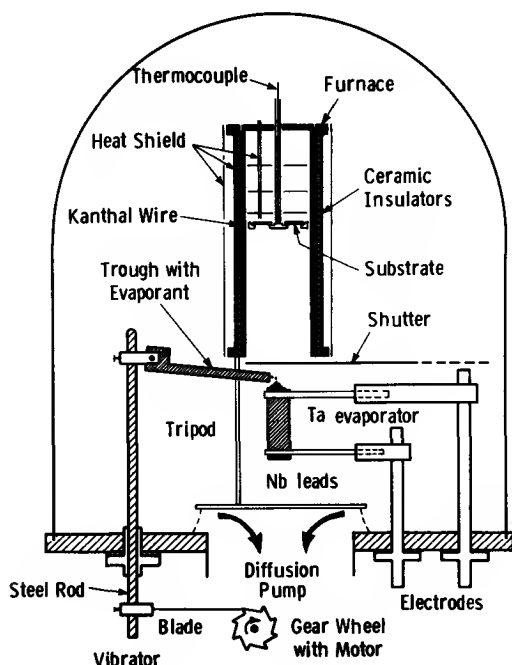
FIG. 11. Flash-evaporation system for compound semiconductors. [After Richards (113).]

temperature is high enough, any excess of the more volatile component is resublimed in the same way as for the three-temperature method. Similarly, impurities required for p- or n-type doping of the films may be introduced into the charge. At higher substrate temperatures there is a tendency for decomposition and loss of the Group V element from the film to occur. Some of the optimum temperatures quoted by Richards et al. for epitaxy on Ge (Table VII) are uncomfortably close to the temperatures at which the Group V element starts to volatilize.

Bourgeois and Moch (117) have made a rather detailed study of optical absorption and doping effects in GaAs films prepared by flash evaporation and describe procedures for producing p- and n-type films by incorporating the dopant during evaporation or by diffusion into the grown film. The growth and electrical properties of flash-evaporated GaSb films were investigated by Aitkozhin and Semiletov (116). Their study dealt with the formation of amorphous and crystalline deposits on amorphous substrates, epitaxial growth on mica, and the evaluation of Hall effect and its temperature dependence. Values of hole mobility were measured which were comparable to those of the starting material used.

Ellis (118) has used the flash-evaporation method to grow films of cuprous

TABLE VII[a]

LIST OF SOME IMPORTANT PARAMETERS IN EPITAXY OF $A^{III}B^V$ COMPOUNDS BY FLASH
EVAPORATION

Compound	Lattice parameters (Å)	Mismatch with Ge (%)	T_1 (°C)[b]	T_2 (°C)[c]	T_3 (°C)[d]	T_4 (°C)[e]	Evaporator temperature (°C)
GaP	5.450	−3.7	400	500	540	560	1500
GaAs	5.653	0	400	400	475	535	1300
				−475	−525	−550	−1800
GaSb	6.095	+7.7	400	450	500	550	1650
InP	5.869	+3.7	100	200	300[f]	300	1400
				250		−400	1650
InAs	6.058	7.1	350	450	500	500	1500
InSb	6.479	14.5	200	250	300	450	1650
				−300	−400		
AlSb	6.135	8.4	625	700	—	—	1400
			−650				−1600

[a] After Richards (113).
[b] T_1, onset of oriented growth.
[c] T_2, epitaxy with twinning.
[d] T_3, untwinned epitaxy.
[e] T_4, onset of reevaporation of Group V element.
[f] Reevaporation of phosphorus also began at this temperature.

sulfide, selenide, and telluride, and has evaluated the experimental factors which may cause the film compositions to depart from those of the charges used. In particular, the effect of particle delivery rate on compositional fluctuations in the films and the departures from stoichiometry due to difference in accommodation coefficients between condensate island surfaces and uncovered substrate during initial growth were examined.

Solid solutions of semiconductor compounds have also been grown successfully by this technique. Müller and Richards (115) have made a comprehensive survey of miscibility in the quasi-binary systems based on several III–V compound films (see Table V). They were able to grow epitaxial films on Ge substrates for most of the systems studied and in several instances observed significant extensions of miscibility in films as compared to equilibrium solid solutions prepared in bulk form. These extensions were favored especially by the use of low substrate temperatures and high deposition rates, and evidently involve the formation of metastable phases analogous to those studied in metal alloy films by Mader (120). Ludeke and Paul (119) flash-evaporated a series of film compositions in the system $Cd_xHg_{1-x}Te$ with $0.2 \leq x \leq 1.0$ and obtained good-quality epitaxial products on cleaved BaF_2

crystals. The fact that the energies of the optical absorption maxima for these films varied linearly with nominal composition of the evaporant indicated that evaporation had produced no significant change in the composition of the charge.

In summary, the studies to date of the flash evaporation of semiconductor compounds show that this is a simple and yet versatile technique for producing films of controlled composition both of compounds and of solid solutions of these. The fact that metastable solid solutions not presently available in bulk form can be obtained is of special interest, since this provides a unique opportunity of studying the optical and electrical properties of new compositions. In general, however, it is necessary to employ granulated charges of the compounds themselves or mixtures of these; the low-melting-point Group-III elements are often not physically amenable to being evaporated as powders. Consequently, only those compositions may be made as thin films for which stoichiometric bulk samples are available. This makes the task of producing high-purity flash-evaporated films of some of the higher-gap compounds, e.g., AlAs, AlP, BP, etc., both difficult and expensive.

4. Sputtering

Sputtering has received far less detailed study than the evaporative techniques, at least in the field of semiconductor films. One reason for this is the fact that the recent reawakening of interest in sputtering, which was probably the oldest vacuum deposition method, was prompted mainly by the requirement to produce films of the highly refractory metals Ta, Nb, Mo, etc., and not by the need of a technique for semiconductor films which could already be deposited by evaporation. However, in addition to growing interest in the processes of formation and the basic properties of sputtered semiconductors, it is rapidly being realized that sputtering may well emerge as a cleaner, more flexible and controllable means of deposition than some of the less satisfactory alternative methods presently available. Three of the key advantages offered by sputtering are: (1) the ability to transfer material from the solid unheated semiconductor source in the absence of possibly reactive crucibles or containers; (2) the fact that with suitable precautions the semiconductor cathode composition is preserved in the growing film; (3) compatibility of sputtering with other nonchemical vacuum techniques used for depositing insulating, resistive, and conductive films. The status of sputtering in relation to vacuum evaporation, as applied to the deposition of films (including semiconducting), has been discussed in recent reviews by Francombe (121, 122), and a complete review of the sputtered film field has been published in Vol. 3 of this series by Maissel (123).

The details of sputtering methods used for thin film deposition have been outlined by several workers, e.g. (60, 78, 121–123), and therefore only those

experimental factors which relate specifically to the more limited field of semi-conductor films will be discussed here. Essentially, three distinguishable types of sputtering have been used thus far for the preparation of semiconductor films: (1) the conventional "diode" or glow discharge arrangement, and also the reactive version of this, (2) asymmetric ac "diode" sputtering, and (3) sputtering in a thermionically supported low-pressure plasma. Method (1) is the most widely used technique for all types of film deposition and involves establishing a glow discharge between the semiconductor cathode (usually in the form of a flat plate) and a nearby parallel and grounded anode plane, which also acts as the substrate support. At inert gas pressures (of argon, krypton, etc.) typically in the range of 30–100 μ and cathode potentials from 1000 to 5000 V the discharge is sustained by the fact that positive ions discharged in bombarding the cathode are replaced by an equal number generated by electrons emitted from the cathode. Shielding with a ground plane of the back surface of the cathode confines sputtering to the front face, and water cooling is desirable especially when using compound cathodes, since otherwise the heat generated by ion bombardment may cause dissociation and sublimation of the more volatile constituents.

Method (2), asymmetric ac sputtering, was originally proposed by Frerichs (124) for improving the purity of sputtered films of superconductors such as Ta, and requires simply that on alternate half-cycles high and low negative potentials be applied, respectively, to the semiconductor cathode and the growing film. The important result is that impurity atoms are back-sputtered (123) from the film surface at a rate considerably higher than for atoms of the semiconductor deposit. In method (3) far lower gas pressures (1–5 μ) are used (121–123) while an electron beam generates enough ions to maintain a plasma around the semiconductor target; usually the ionization process is assisted and the plasma is confined by using additionally a magnetic field.

Examples of the use of these sputtering methods in the preparation of films of Ge and of several of the compound semiconductors are given in Table VI. Probably the first serious attempt made at producing semiconducting films by the diode technique is that of Reizman and Basseches (125) who grew epitaxial junctions of Ge on Ge substrates at temperatures up to 840°C using both p- and n-type cathodes. In all cases the deposited film was p type and could only be converted by prolonged treatment with phosphorus vapor. As in the work on evaporated Ge films (which invariably are p type), the origin of the acceptors could not be positively identified. However, from the large number of faults revealed in the films by chemical etching the authors suggest that the acceptors may be attributed to structural defects. Haq (126), using the asymmetric ac sputtering method in conventional residual *vacuo*, studied the effect of varying the bias potential applied to the epitaxially grown Ge film on its resistivity and conductivity type. He found

that for sufficiently high negative film potentials, or "cleaning" voltages, during the reverse part of the cycle (typically 600 V for a sputtering voltage of 3000 V and substrate temperature of 360°C) it was possible to consistently grow n-type films on Ge substrates. It appears that back-sputtering removes preferentially the acceptor-type impurities from the deposit as it is formed. If outgassing occurred during a run with a reverse voltage applied, the film was found to change from n to p type with increasing thickness. It was concluded that acceptors of chemical origin were therefore being incorporated at a rate higher than they could be removed by back-sputtering.

A detailed study of the growth of Ge on single-crystal Ge and CaF_2 was made by Krikorian and Sneed (127, 128), using a glow–discharge diode sputtering arrangement. They investigated the relationship of the amorphous-polycrystalline and polycrystalline-single-crystal transition temperatures to the growth rate and sputtering conditions. Low-pressure sputtering of Ge on vitreous silica and on single-crystal sapphire and CaF_2 under residual ultrahigh vacuum conditions was studied by Wolsky and his co-workers (129, 130), with the experimental arrangement shown in Fig. 12. The fact that
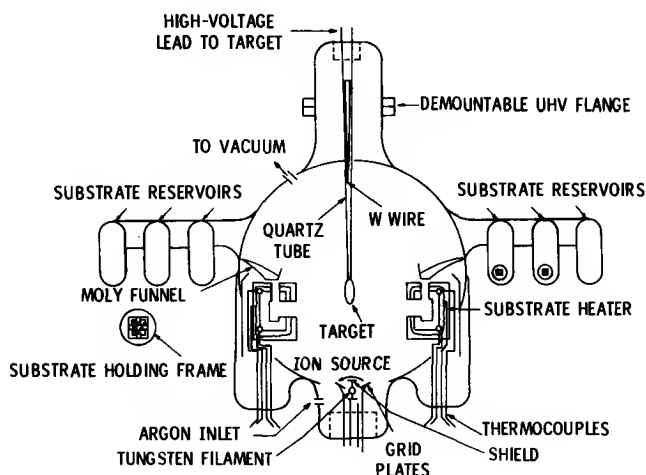
FIG. 12. System for sputtering films of germanium under residual ultrahigh vacuum conditions. [After Wolsky et al. (129).]

low argon pressures (in the 3–4 μ range) were employed limited the deposition rate to considerably lower values than were attained by other workers. The results obtained included data on the amorphous-crystalline transition, the conditions for epitaxial growth, and the variation of electrical properties such as carrier mobility and density with growth conditions, film thickness, and depth within the film. Some preliminary results were also reported for the

sputtering of Si films (Table VI), but neither structural nor electrical studies were made.

Several of the semiconductor compounds have been deposited as thin films by sputtering (Table V). Most of these studies have emphasized structure, and data on electrical properties are thus far rather sparse. In general, for the III–V compounds the composition of the cathode is preserved on transfer to the sputtered film. The use of elevated substrate temperatures, however, or excessive heating of the cathode leads to sublimation of the Group V element, leaving traces of the free Group III metal at the film surface. As with flash-evaporated films, this happens in the case of GaAs when the substrate temperature approaches values of 600°C or higher. Similarly, selective loss of the more volatile Te occurs from Bi_2Te_3 when sputtering onto substrates at temperatures higher than about 300°C. Although it is unsafe to generalize on the basis of one system, the results reported by Kraus *et al.* (*136*) for $Cd_xHg_{1-x}Te$ [cf. (*119*) for flash-evaporated films of this composition] suggest that in sputtering solid solutions of compounds the essential composition of the cathode is preserved in the film.

5. RECRYSTALLIZATION OF FILMS

It is well known that thin films, especially when deposited at relatively low temperatures on foreign nonorienting substrates, contain a very high density of structural defects such as dislocations, twins, stacking faults, or grain boundaries. In semiconductors these defects may modify the electrical properties either by acting themselves as scattering centers or by causing chemical inhomogeneities through the segregation of impurities. Consequently it is not only of basic scientific interest to understand the intrinsic properties of thin films but also of practical value in the fabrication of semiconductor devices to produce films which are as nearly monocrystalline and perfect as possible. Since in many circumstances active devices can be fabricated on comparatively small areas, it is not essential for an entire film to be completely monocrystalline or even for its single-crystal regions to possess identical crystallographic orientations. A desirable aim, particularly in the manufacture of integrated circuits, would be semiconductor films containing large monocrystalline regions with near-bulk properties supported on readily available nonorienting substrates such as glass or glazed ceramics. Several attempts have been made to meet the above requirements by recrystallizing the semiconductor film either after or in some cases during deposition. To complete our present survey some examples of experiments made with vacuum-deposited layers will be discussed.

Several efforts have been made to recrystallize Ge films by electron beam zone heating, and these have met with varying success. Poehler and Gilbert (*138*) were able to grow crystals up to about 0.5 mm in size in films evaporated

on glass, using a scanning electron beam at a voltage of 35 kV and operating current of 50 μA. The beam was swept at a rate of about 10 μsec/cm along a linear zone and the zone moved across the film at velocities from 0.01 to 1 cm/sec. Crystals were grown on tungsten and quartz substrates but the large thermal conductivity in the case of the metal prevented attainment of a narrow zone. Maserjian (139) has made a more detailed study of the zone melting of Ge films on polished sapphire substrates using the electron beam (typically 10 μA at 50 kV) of an RCA-EMU electron microscope. The initial films of thickness 3–10 μ were prepared by rapid evaporation onto substrates held at 800°C and, while scanning, the entire film was heated uniformly to 850°C to minimize thermal gradients between the molten zone and the surrounding film. Maserjian found that best results were obtained with one particular rotating scan pattern.

Considerable improvements in mobility of the films are produced after recrystallization, the values measured approaching those for single-crystal bulk material. In Maserjian's work it was found that although the evaporant charge was n type, both the deposited and recrystallized films were p type. The author suggests that this is caused by the tendency for the more volatile donor impurity to sublime during zone melting. However, in similar circumstances Naber (140) reported that a recrystallized Ge film produced from weakly n-type source material contained both p- and n-type regions, the n type being associated with larger crystals. He cites this as evidence of a correlation between the acceptor centers in the p-type regions and crystal defects.

Nielsen and co-workers (20, 141) have attempted to obtain enhanced crystal growth and lower-temperature epitaxy by exploiting the fact that Ge and Si form low-melting eutectics with many metals. Two approaches were tried. In one, the alloy zone is formed in the semiconductor layer by depositing a metal stripe, typically of Al, and applying a temperature gradient across the film. In the second, the metal (e.g., Au, Ag, Cu, In, Sn) is deposited on a substrate of the semiconductor as a layer about 1–10 μ thick. During deposition of the semiconductor (which in the case of Si is sublimed) the substrate is heated typically to between 550 and 1100°C by radiation from the sublimation source and the metal layer forms a liquid alloy on its surface. The alloy zone is in a temperature gradient region and travels up through the deposited semiconductor during growth, recrystallizing it in the same orientation as the underlying substrate. Epitaxy is thereby achieved at quite low temperatures, e.g., 850, 800, 500, 400, and 300°C for Ag, Cu, Sn, Au, and In alloys, respectively. Unfortunately the recrystallization proceeds in a nonuniform fashion due to the tendency for the alloy to form droplets on the surface.

Considerable work has been done on the recrystallization of semiconductor compound films, in particular with the II–VI compounds such as CdS, CdSe, ZnSe, etc. Much of this research has been reviewed recently by Vecht

in Vol. 3 of this series (142) and will be given only cursory mention here. Probably the best-known method of inducing crystal growth in CdS films is that due to Gilles and Van Cakenberghe (143), in which a thin film of a metal, e.g., Ag, Cu, Pb, In, Bi, Al, or Zn, is evaporated onto the freshly deposited (and preferably near-stoichiometric) sulfide film, and the combination subjected to annealing in the range 500–600°C. At a particular threshold temperature, depending upon the metal used, recrystallization starts and growth proceeds rapidly at a rate of about 0.1 mm/sec. The conditions for recrystallization were reexamined by Addiss (84) and also by Te Velde (144) who studied ZnSe films. Their work indicated that acceptors (activators) such as Group I metals induce, whereas donors (coactivators) inhibit crystal growth. Also atmospheres comprising air or containing S vapor favor growth while Cd vapor suppresses it.

Vecht (142) points out that a disadvantage of the above approach is the relatively large amount of doping involved, and has found that an effective alternative is to immerse the semiconductor film in an inert organic liquid stable up to about 400°C, such as a silicone fluid or ester, in which traces of the active metal are dissolved in the form of an organometallic compound. Recrystallization occurred by this method at temperatures as low as 200°C and yielded films with good photoconductive properties.

Few of the III–V compound films lend themselves to recrystallization at high temperatures, due to the volatility of the Group V element. If a film of nonstoichiometric composition (i.e., containing an excess of the Group III or V elements) is grown, it may be possible to melt this deposit at a temperature below that at which appreciable sublimation of the Group V element occurs. It is preferable that the composition be fairly close to stoichiometry, since on freezing the film will then consist essentially of the compound. Also, as shown by Wieder and Clawson (145) who have applied this method to InSb, excess of In in the recrystallized films modifies significantly the electrical properties by providing short-circuit paths, whereas excess Sb (146) can be sublimed, leaving a dendritic network of InSb crystals behind (Fig. 13). The tendency for surface tension to cause breakup of the liquid film into droplets can be avoided, as shown both by Carroll and Spivak (147), simply by forming a thin retaining skin of In_2O_3 on the film surface before melting it.

As shown in Fig. 13 the structures achieved by this method are not thin films in the usually accepted sense, but rather a partially isolated assemblage of narrow, thin monocrystals having a common (111) plane parallel to the substrate surface. Consistent variations in transport properties with average thickness have been achieved, however, and Wieder (148) has measured Hall mobilities ranging from about 10^4 cm^2/V-sec at 3000 Å to 3.5×10^4 cm^2/V-sec at 30,000 Å.

Extension of this recrystallization approach to other more refractory III–V
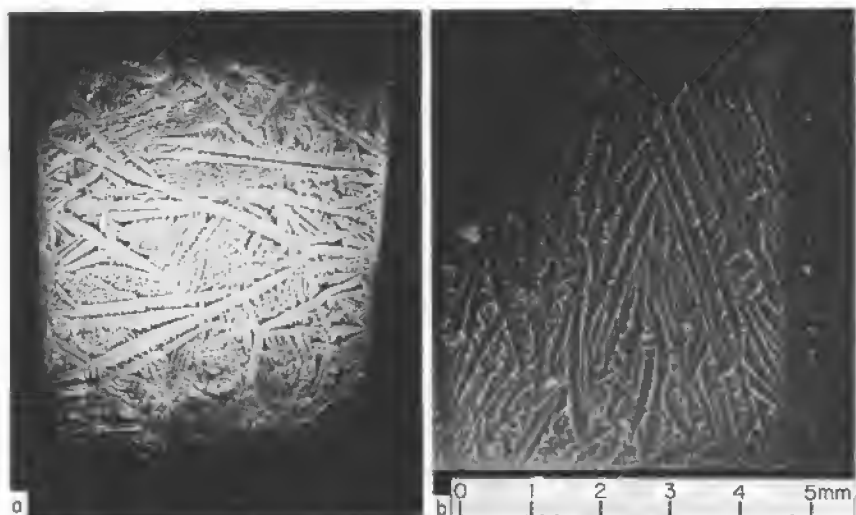
FIG. 13. Dendritic films of InSb: (a) monophase film grown by recrystallization from the liquid phase; (b) electron beam microzone recrystallized film. [Courtesy H. H. Wieder; also Wieder and Clawson (*145*) and Wieder (*146*).]

compounds such as the arsenides and phosphides does not appear feasible since the lowering in melting point for nonstoichiometric compositions (particularly those rich in the Group V element) is not sufficient to avoid rapid loss of As or P during melting. A more promising approach to follow in the case of GaAs and GaP might be a modification of the VLS (vapor–liquid–solid) method, along the lines suggested by Nielsen (*20, 141*). Barns and Ellis (*149*) have succeeded in growing whiskers of these compounds using crystallization from the vapor via a metal and compound liquid solution zone. If a temperature gradient is applied to such a zone, supersaturation, and hence precipitation, of the solid compound occurs at the low-temperature side and the liquid zone moves in the direction of growth.

IV. Structural and Chemical Characterization

1. NATURE OF PROBLEM

The transport properties of semiconductors are known to be highly sensitive both to small changes in their chemical composition and to crystallographic imperfections. Thin films of semiconductors in their various applications to device structures embrace not only a wide range in the common electrical parameters, e.g., resistivity, mobility, lifetime, etc., but also in the acceptable levels of chemical and structural perfection. This is demonstrated,

for example, by the fact that while large-area defect-free epitaxial junctions are needed for optimum performance of silicon power devices, polycrystalline thin films of CdS, InAs, or Te are quite acceptable in the fabrication of miniature transistors. This does not imply that the electrical properties of the latter type of film are insensitive to structure and composition, but only that the scale and type of imperfections which influence device behavior are widely different in the two cases.

In homoepitaxial junctions, e.g., Si on Si, the structural details of interest include the orientation of the film as a whole, the presence of regions of structural disturbance such as polycrystalline inclusions, twins, stacking faults, or dislocations, and the occurrence of chemical inhomogeneities which may be in the form of foreign particulate matter or precipitated dopant-rich aggregates. Stacking faults and dislocations are common defects in epitaxial silicon junctions, and in addition to comprising regions of electrical inhomogeneity they may act as traps or precipitation sites for dopants subsequently diffused into the epitaxial layer. Chemical microinhomogeneities such as noncrystalline aggregates of foreign atoms, e.g., O_2, C, N_2, etc., are far more commonplace in single-crystal semiconductors than is usually realized and vary in size from a few hundred angstroms up to the micron range (*150*).

Heteroepitaxial films, e.g., Si on sapphire, Ge on CaF_2, or GaAs on Ge, vary widely in crystallographic perfection but in general are far more disordered structurally than homoepitaxial films (*33, 34*). In extreme cases the films may only be epitaxial in the sense that they comprise an oriented assemblage of crystallites; however, multiple orientations, grain boundaries, and stacking faults, as well as chemical microdefects, may be present in very high densities. Moreover, where growth temperatures needed for epitaxy are high, as is usually the case with Si on sapphire, chemical interaction with the substrate affects the electrical type and resistivity of the resulting films (*35*).

Polycrystalline films grown on nonorienting substrate, i.e., glass or vitreous silica, present a highly disordered structure, and here it is no longer meaningful to consider isolated imperfections, either structural or chemical. Instead, we are now concerned with overall chemical composition, grain size, and average crystallite orientation.

From these introductory remarks it will be evident that the problem of evaluating the structure and composition of semiconducting films is frequently a complex one requiring several techniques with a wide range of resolving powers. During recent years considerable effort has been directed toward the development of methods for detecting and characterizing imperfections of various types and, with a view to improving quality and reliability of devices, toward the correlation of the analytical data derived with variations in electrical properties. In the following sections we shall describe the application

of the main analytical techniques to the study of semiconductor films and where possible discuss limitations or potential scope of these techniques.

2. ANALYTICAL METHODS

Most of the analytical techniques available for the evaluation of bulk materials have been applied to the problem of characterizing semiconductor films. Since in general the volumes to be analyzed are much smaller in the case of films, those techniques capable of high spatial resolution or sensitivity enjoy a considerable advantage. However, by their nature high-resolution methods are often both selective and destructive, and produce information which may be nonrepresentative. An important attribute of an analytical measurement is that it should yield data that can be correlated in a meaningful way with some physical property of the semiconductor. Unfortunately, too many structural studies have been made in isolation from electrical and optical studies, or vice versa, and attempts to relate the results obtained consequently are of a highly speculative nature. A voluminous literature has developed around the field of structural and analytical studies of semiconductors and complete discussion of this is well beyond the scope of this review. We shall confine the present treatment to describing the key features of each method of evaluation with one or two examples of its application to films.

a. Optical. In this category we consider primarily those methods which utilize radiation of wavelength in the visible or near visible. Direct optical microscope studies of untreated or etched surfaces of both bulk and film semiconductors are probably the commonest and most widely used method available for evaluating structural and chemical homogeneity. Defects, strain fields, or foreign inclusions yield characteristic patterns when the semiconductor is immersed in an etching solution and their distribution can be established in detail. Etches suitable for revealing various types of defects have been reviewed by Faust (*151*). Extensive use of this approach has been made, for example, by Mendelson (*152*), who studied the propagation of dislocations and stacking faults in homoepitaxial Si films.

Standard optical microscopy provides useful information on the surface topography of a grown layer or, in conjunction with etching, establishes the location of those points at which imperfections or inclusions intersect the free surface. To determine the distribution of faults in depth, however, it is necessary to prepare sections of the film as described by Charig *et al.* (*153*), who studied the three-dimensional geometry of stacking faults in Si. Alternatively, the structure can be studied in transmission using infrared radiation. By employing the method proposed by Dash (*154*) for bulk crystals defects can be rendered absorbing by decoration with a metal such as copper.

Another means of viewing electrically active defects in *p–n* junction

structures is through the visible light generated by microplasma effects when the junction is biased near breakdown. Shockley (*155*) has discussed this effect in some detail and related it in silicon to the electric field disturbances associated with oxide precipitates.

b. Electron Optical. Electron microscopy has provided most of the direct structural evidence on which our knowledge of the growth and perfection of films in general is based. Until recently applications of the technique were limited either to transmission studies on films which could readily be isolated by dissolving the substrate, or to the study of electron replicas prepared from the film surface. With the development of special etching techniques, e.g., by Booker and Stickler (*156*), it became possible to examine the various stages of homoepitaxial growth and to some extent the distribution of microinhomogeneities by transmission microscopy. Thus, by jet-etching a region of the supporting substrate away, and when necessary part of the film, it is possible to localize a thin electron-transparent region at any chosen level in the film and to characterize its structure. Remembering that most layers in epitaxial device structures are many microns thick, this approach is obviously highly selective and is best suited for the study of crystal defects of a regular nature such as stacking faults or dislocation networks which extend through the entire film thickness.

The transmission method, used in conjunction with a tilting stage and dark-field attachments, has proven extremely valuable in the detailed analyses of the crystallography of defects such as dislocations, stacking faults, and crystalline precipitates. Information can be obtained as to the type and Burgers vectors of dislocations, whether a stacking fault is intrinsic or extrinsic (*157*), and also concerning the morphology and mutual orientation relationship of a precipitate with reference to the matrix. In particular, from experiments such as those of Booker and Unvala on Si (*72*) and Humphris and Catlin (*66*) on Ge a clearer picture may be established of the growth factors which generate crystal defects and hence which modify the electrical properties of epitaxial films.

Standard electron microscopy makes use of the fact that electrons are absorbed or diffracted differently at inhomogeneities, in order to reveal these as contrast effects. However, in semiconductors the absorption process in the vicinity of a p–n junction may involve the generation and separation of hole–electron pairs. These will recombine more rapidly at defects or inclusions, and if local variations in recombination rate can be measured or displayed, the distribution of electrically active imperfections is obtained. Czaja and co-workers (*158*) have used a scanning electron beam system to accomplish this in the case of diffused junctions about 3–4 μ deep, and were able to reveal dislocations and precipitates. Figure 14 shows an example of a scanning
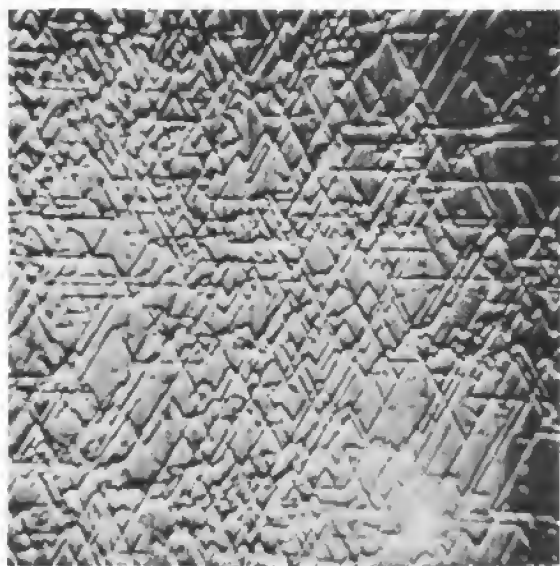
FIG. 14. Scanning electron micrograph showing dislocations in a phosphorus-diffused emitter region ($C_s = 2.9 \times 10^{20}$ cm^{-3}); differentiated signal technique (EBITC); display 0.030 × 0.030 in. [Courtesy C. J. Varker.]

electron micrograph obtained in these laboratories, from the emitter region of a Si device. The method should be readily applicable to epitaxially grown junctions both of Si and of the compound semiconductors.

Similarly, the excitation of characteristic x-radiation from the semiconductor or from foreign inclusions contained in it can be used to reveal compositional variations or the presence of metal precipitates (*159*). This type of analytical display is readily obtainable with commercially available scanning electron microprobe equipment, and, by arranging the crystal optics of the x-ray sensing system to select a characteristic wavelength for one of the impurity elements, its distribution in the film can be mapped. The resolution of this method, and also of the technique used by Czaja for scanning *p–n* junctions, is of the order of a micron, i.e., considerably lower than that of the standard electron microscope.

c. Diffraction Methods. Both electron and x-ray diffraction have been used for structural studies on semiconductor films. Electron diffraction, using accelerating voltages in the range 40–100 kV, forms a natural adjunct to electron microscopy and is performed in the same instrument in connection with orientation determination and dark-field microscopy on twins and stacking faults (*160*). Even for perfect crystals the penetration depth for

electrons in the 100-kV range is limited to about 5000 Å, and thus the volume sampled in transmission diffraction is small. When a nondestructive examination of the film is required, it is frequently studied by low-glancing-angle reflection electron diffraction and in this case, although a relatively large surface area (a narrow strip) is covered by the beam, the depth of penetration is very small ($\sim$100 Å or less). Thus, standard electron diffraction, whether in transmission or reflection, is highly selective and is best used for the evaluation of rather thin films.

The advantages of electron diffraction lie in the ease and rapidity of examination and in the fact that it provides instant and undistorted views of cross sections of the crystal reciprocal lattice. The second feature simplifies considerably the task of evaluating the crystallography of defects, and particularly of twins. This property has been demonstrated recently in reflection studies by Holloway (161), who was able to analyze in detail the multiple twinning effects occurring in epitaxial films of III–V compounds such as GaAs. Unfortunately, the thin surface regions characterized in this way may be completely unrepresentative of the film structure as a whole.

The diffraction of low-energy electrons (LEED) in the voltage range 10–400 eV provides even greater selectivity in that the penetration depth is so small that only the first one or two atomic planes at the crystal surface are sampled. The method must therefore be used in stringently clean uhv conditions ($\sim 10^{-10}$ Torr) which prevent the adsorption of surface contaminants. Since the studies of Farnsworth *et al.* (162) and of Lander and Morrison (163), which showed that the clean surfaces of crystals such as Ge and Si possess structures more complex than the bulk, considerable interest has developed in LEED studies of semiconductor surfaces. The extreme sensitivity of LEED to small traces of surface contaminants means that this technique cannot be used as a general analytical tool for studying surface structure. Nevertheless, as will be demonstrated in our discussion of film growth, surface structure can play a very important role in the mechanism of epitaxial growth at low temperatures. Thus, LEED constitutes a valuable tool for exploration of the basic nucleation and growth processes of semiconductor films.

With the increasing availability of high-intensity x-ray generators, crystal monochromators, and sensitive low-noise diffractometer equipment, far more use is currently being made of x-ray diffraction for studying film structures. It is now possible to examine well-crystallized film samples at thicknesses varying from several microns to as low as a few hundred angstroms. Davey has used the diffractometer method to evaluate texture changes with deposition temperature in Ge (64) and GaAs (105) films. This type of equipment can also be applied to the measurement of compositional changes which cause variations in lattice parameter, and to the determination of crystal size and strain.

An important development in the application of x-rays to the characterization of semiconductors is the recent use of x-ray diffraction microscopy (or topography) in the study of imperfections in single crystals. This technique utilizes the fact that due to extinction effects the diffracting power of a perfect crystal is about two orders of magnitude less than that of a slightly imperfect crystal (*164, 165*). By orienting the crystal in a diffracting position with respect to a finely collimated intense monochromatic x-ray beam, and scanning it across the beam in synchronism with a photographic plate, a composite image or topograph depicting the distribution of imperfections in the crystal is built up. For dislocations the contrast is greatest when the direction of atom displacement (or Burgers vector) is perpendicular to the diffracting planes used, i.e.,

$$\cos < (g \cdot b) = \begin{matrix} 0 & \text{no contrast} \\ 1 & \text{max contrast,} \end{matrix} \qquad (12)$$

where g and b are the diffraction and Burgers vectors, respectively. Hence by following the change in contrast between images formed from different planes, the geometry of the dislocations is established.

To examine the film selectively by suppressing the contribution of the substrate, it is convenient to use the reflection Berg-Barrett arrangement shown in Fig. 15. If the angle of incidence of the x-ray beam to the film surface
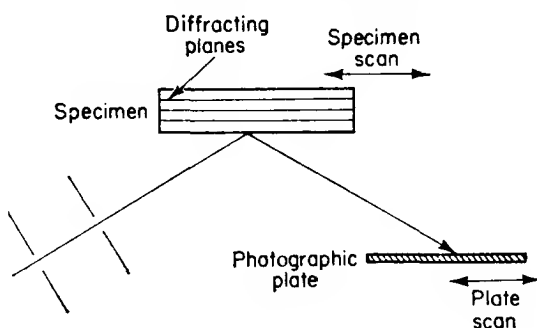
FIG. 15. Reflection arrangement for Berg-Barrett x-ray topography. [After Holloway (*161*).]

is low then absorption occurs entirely in the film. Holloway and Bobb (*166*) have applied this method recently to the study of imperfections in III–V epitaxial films grown by chemical vapor plating and have been able to analyze the formation of surface twins. Figure 16 shows typical images formed from a GaAs film.
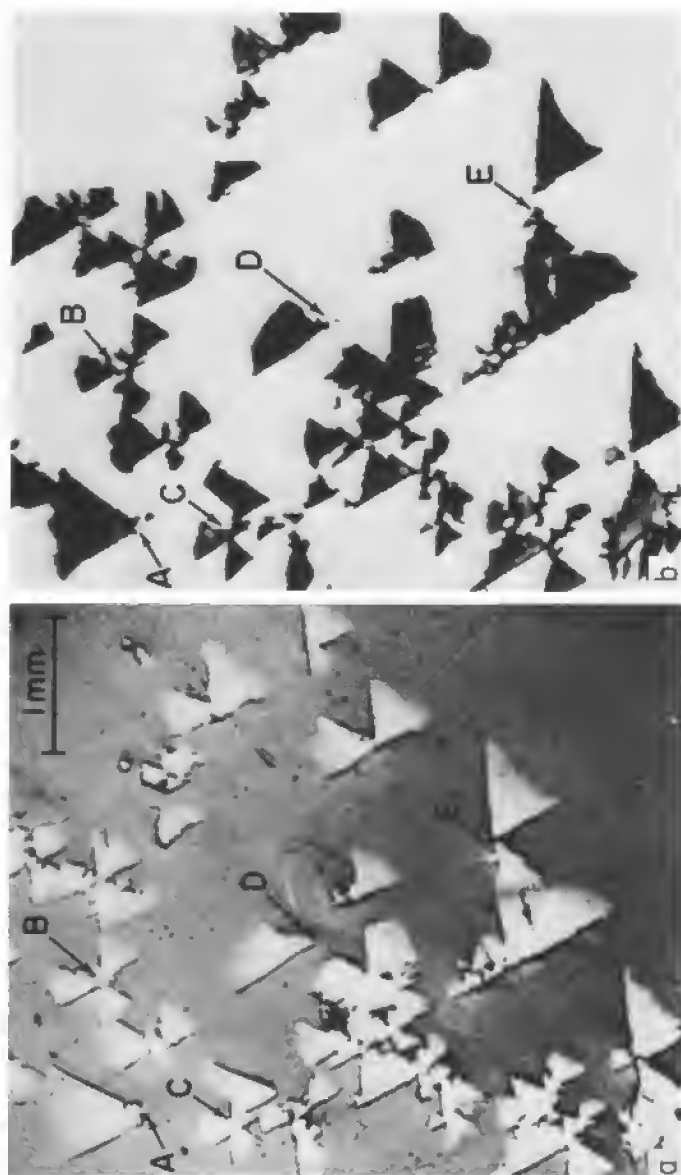
FIG. 16. Berg-Barett reflection topographs of epitaxial GaAs grown on {GaAs} Ga face by chemical transport: (a) topograph of film matrix; (b) topograph of twins about [111]. [Courtesy H. H. Holloway; also Holloway and Bobb (*166*).]

3. FILM GROWTH AND STRUCTURE

a. Nucleation and Growth—General. Most of the semiconductor materials of immediate practical interest possess one of four simple crystal structures: (1) the cubic diamond type, e.g., Ge and Si, (2) the zinc blende type, e.g., InSb, GaAs, (3) the wurtzite type, e.g., CdS, or (4) the NaCl type, e.g., PbS, PbTe. Several of the II–VI and III–V compounds are capable of exhibiting the hexagonal wurtzite-type polymorphic form and, as shown by Semiletov (*98, 99*), this tendency is especially evident in thin films where metastable structures and compositions may be frozen in due to a high degree of crystalline disorder. The materials in the structure classes (1)–(3) possess a strongly covalent character, which is manifested both in their extreme hardness and brittleness and in the tendency for their crystal faces, when clean, to adopt complex surface structures.

When condensed from the vapor phase onto unheated substrates the diamond and zinc blende type semiconductors and certain others, e.g., Se, develop amorphous structures. The temperature up to which the amorphous phase is stable appears to be related to the melting point, being somewhat higher for silicon, approximately 350°C, than for germanium, approximately 200°C. In the case of Ge, comparison of the results of Davey (*64*) on evaporated films and of Krikorian and Sneed (*128*) and Wolsky *et al.* (*129, 130*) on sputtered films suggests that this temperature limit is sensitive also to the level of impurities present and to the deposition technique and rate. Discrepancies have also been reported for GaAs films in that Molnar *et al.* (*133*) observe an amorphous-crystalline transition at about 400°C for sputtered deposits while Davey and Pankey (*105*) find a value of 220°C for films grown by coevaporation of the elements.

At higher temperatures, where the deposited material is crystalline, strong film textures are adopted by the films and these may change abruptly with increasing temperature as shown in Fig. 17 for sputtered films of GaAs. The mechanisms giving rise to these textures are not as yet well investigated or understood. However, studies, for example, by Bauer (*167*) indicate that they arise either during nucleation or growth of the film. Following the general arguments of Rhodin and co-workers (*168*) it may be postulated from nucleation theory that as the deposition temperature or vapor supersaturation is changed so also is the number of atoms in the critical cluster, and therefore the geometry of the cluster. Simple models based on clusters comprising two, three, or more atoms lead to nucleation textures of the type $<100>$, $<110>$, or $<111>$. Such textures may transform as the nominal thickness of the film is increased, due to coalescence, recrystallization, or anisotropic growth effects, and the latter property in particular may generate highly developed growth orientations.

Anisotropy in growth is often more pronounced in materials possessing
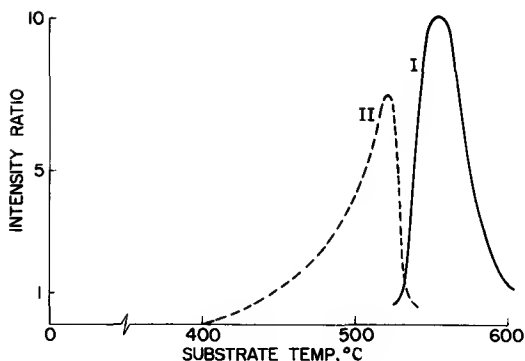
FIG. 17. Texture variation with substrate temperature in GaAs films sputtered without anode glow on vitreous silica substrates, determined from x-ray diffractometer data: curve I, (111)/(220); curve II, (220)/(111). [After Molnar *et al.* (*133*).]

lower symmetry structures, e.g., hexagonal CdS and Bi_2Te_3. At elevated substrate temperatures and large film thickness these structures may display very strong basal plane {00.1} textures in which the <00.1> axes for the constituent crystallites lie essentially parallel to the substrate normal. Studies of sputtered films of bismuth telluride by Francombe (*135*) showed that changes both of texture and of crystal habit occurred with substrate temperature. These changes reflect both the hexagonal symmetry of the unit cell and the pseudocubic packing of the Bi and Te atoms in the Bi_2Te_3 structure. At low substrate temperatures (<250°C) a fiber texture is developed in which the {10.5} planes lie parallel to the substrate surface, the crystallites comprising hexagonal platelets with {00.1} faces inclined to the surface (see Fig. 18). The {10.5} planes correspond to the faces of a primitive pseudocubic (rhombohedral) cell unit which would represent the repeat unit for a lattice in which Bi and Te atoms are randomly distributed. At intermediate temperatures above 300°C a mixed texture comprising both {10.5} and {00.1} fiber orientations appears and the corresponding crystallite habit is mixed tetrahedral and octahedral (Fig. 19a). When the substrate temperature exceeds 350°C the {00.1} orientation predominates and the film comprises hexagonal platelet crystals lying parallel to the substrate (Fig. 19b). A knowledge of the textures and temperature ranges within which they are favored is helpful, at least in the case of bismuth telluride films, for establishing optimum conditions for epitaxial growth.

Few attempts have as yet been made to study systematically the nucleation and early stages of growth of semiconductor films. Those qualitative data that are available, describing, for example, the growth of Ge on CaF_2, Si on Al_2O_3, and Si on Si, suggest that both in chemical and vacuum deposition
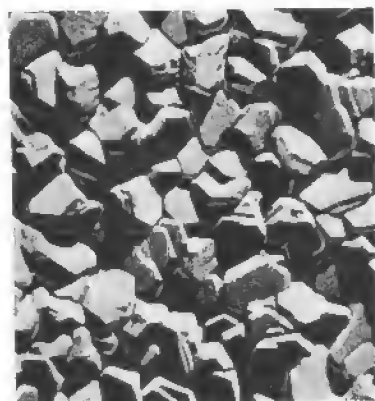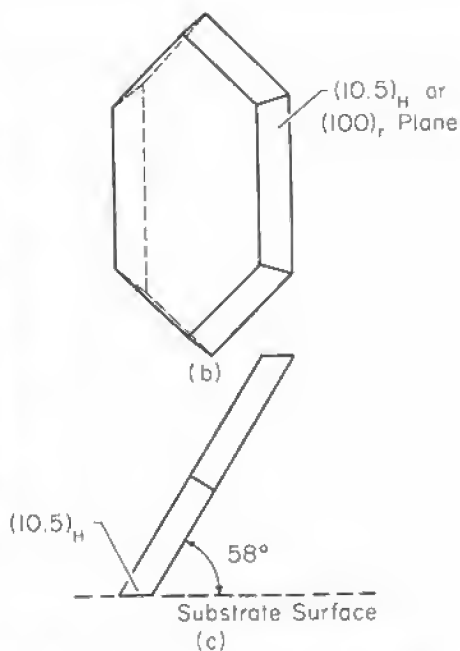
FIG. 18. Orientation in sputtered bismuth telluride film, substrate temperature 200°C, thickness 3 μ: (a) electron micrograph; (b) and (c) sketches of plan and side view, respectively. [After Francombe (135).]

FIG. 19. Electron micrographs of sputtered bismuth telluride films, thickness 3 μ, deposited on glass at different temperatures: (a) 300°C; (b) 400°C. [After Francombe (135).]

the general features of nucleation and growth are essentially the same as those studied in metal deposits on alkali halide crystals. However, quantitative analysis of nucleation of reactive semiconductors such as Si on oxide substrates, and also interpretation of the orientations developed, is difficult due to the unknown effect of chemical interaction with the substrate. At present the most fruitful line to follow appears to be the study of nucleation on a like substrate, e.g., Si on Si.

In investigating the early stages of homoepitaxy of Si on (111) Si using an incident beam of silane molecules, Joyce and his co-workers (169) have successfully interpreted their results on the basis of the nucleation and growth theory developed by Lewis and Campbell (54). They report that after a short induction period, during which it is assumed that a thin SiO_2 film is removed from the Si substrate by the action of the silane beam, a saturation density N_S of uniformly spaced growth centers is rapidly established on the substrate. The regular spacing and size of the growth centers is in agreement with the theory for a case in which the incident atoms are adsorbed. Again in accordance with the model, the saturation density of centers N_S shows an exponential dependence on substrate temperature. A difficulty was encountered in this study, however, viz., why should nucleation occur at all in the situation where Si atoms are incident upon a clean single-crystal Si substrate? Under these conditions one would expect to observe normal equilibrium growth in which epitaxy proceeds by layer completion.

Not only the cleanliness but also the details of atomic order at the substrate surface appear to have an important influence on the growth and perfection of homoepitaxial films. We shall elaborate on this further in our discussion of defects in epitaxial films.

b. Epitaxial Growth. A significant part of the large volume of published studies on epitaxial semiconductor films has dealt with the preparation and electrical properties of homoepitaxial films of Ge and Si. In general, the films were prepared by reduction of the halide or pyrolysis of the hydride using substrate temperatures high enough to ensure rapid growth rates (many microns per min) and good film perfection. Such studies have been aimed primarily at establishing rapid and reproducible methods for making *p–n* junctions for devices, and not at characterizing the basic processes involved in epitaxial growth. Some of the relationships between film structure and properties and conditions of preparation were described briefly in Section II and are discussed more completely in longer reviews of chemical vapor deposition (16, 17). Recently there has been a growing interest in homoepitaxial growth by vacuum deposition methods such as evaporation (71, 72), sublimation (74–76), and sputtering (125–128). In the case of silicon particularly this is prompted partly by the need for compatible vacuum techniques for the

preparation of both active and passive components, and partly by the attractiveness of processing methods which can be used at lower temperatures. If epitaxial growth temperatures could be reduced without sacrificing crystal perfection, important dividends in the areas of the control of junction profile and carrier lifetime would be reaped, and unpleasant chemical side reactions which lead to contamination might be minimized.

If vacuum deposition methods are to be applied successfully to the growth of epitaxial semiconductors, it is of great importance to understand the experimental factors influencing homoepitaxy before the conditions for heteroepitaxy on foreign substrates can be properly evaluated. As we shall demonstrate in the next section, this is especially vital in relation to the generation of defects and their propagation. It is also essential to distinguish between those conditions favoring the growth of epitaxial–polycrystalline films and those which lead to true monocrystalline epitaxial layers, since in the first case the property of "epitaxy" may impart no electrical advantages over a polycrystalline film which displays completely random orientation.

Both Ge and Si films have been grown homoepitaxially by vacuum deposition, and due to the work, for example, of Krikorian and Sneed (127, 128), Booker and Unvala (72), Widmer (74), and Thomas and Francombe (75, 170) dependence of film structure and orientation on growth rate and deposition temperature and vacuum conditions are qualitatively understood. The work of Krikorian and Sneed (128) on sputtered and evaporated films and more recently by Layton and Cross (171) on sputtered films shows that the threshold temperature for epitaxy, T_E, for Ge grown on (111) Ge decreases as the deposition rate is reduced. As reported by Sloope and Tiller (63), and also by Krikorian and Sneed (128), the same behavior is found for Ge films deposited on foreign substrates such as cleaved CaF_2 crystals. Typical data for sputtered Ge films grown under conventional vacuum conditions are shown in Fig. 20. The results of Krikorian and Sneed indicate that not only does T_E fall with decreasing growth rate but that, due to the fact that the amorphous–crystalline transition temperature remains essentially unaltered, a critical growth rate is reached for which, with increasing temperature, *the film structure transforms directly from amorphous to epitaxial.* Films grown at this "triple point" are claimed by Krikorian and Sneed to comprise epitaxial, polycrystalline (meaning randomly oriented), and amorphous components.

The status of this work is still under discussion and some doubts appear to exist as to what extent the results may be influenced by surface contaminants such as oxide (172). Thus, while Krikorian and Sneed measure lower epitaxial temperatures for evaporated than for sputtered films, Layton and Cross (171) obtain epitaxy at temperatures some 100°C lower for triode sputtered than for evaporated films (Fig. 21). The latter workers suggest that their lower
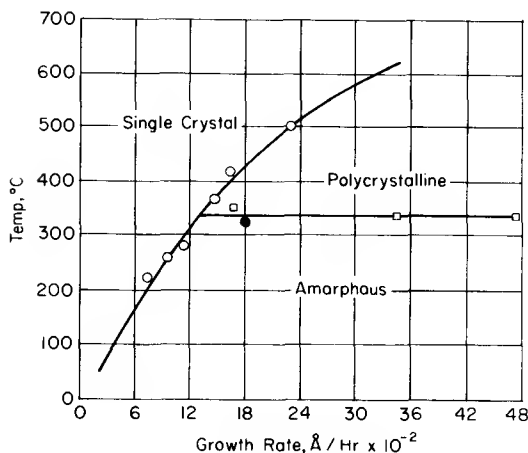
FIG. 20. Effect of growth rate and substrate temperature on film structure for Ge sputtered on to (111) Ge. [After Krikorian (127).]
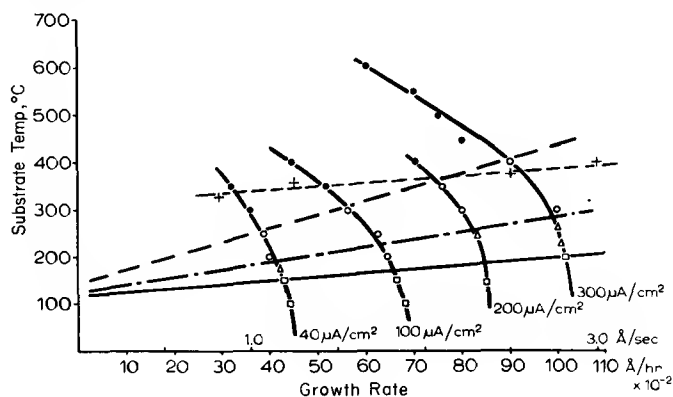
FIG. 21. The growth and orientation dependence on substrate temperature of Ge films grown by triode sputtering onto <111> substrates for various ion-current densities. (●) single crystal untwinned; (○) single crystal twinned; (△) polycrystalline; (□) amorphous. Target potential, 1500 V; target substrate separation, 5 cm; target diameter, 7.5 cm; + data from Krikorian and Sneed (128) for evaporated films. [After Layton and Cross (171).]

epitaxy temperatures may be attributed to the substrate cleaning action of the higher-energy particles sputtered in the triode system.

Booker and Unvala (72) investigated the epitaxial growth of Si on Si using an electron bombardment source of the type shown in Fig. 7a and reported that the epitaxy temperature decreased progressively from about 1210 to 1080°C as the growth rate was reduced from 3.5 μ/min to 0.15 μ/min.

However, under the technical vacuum conditions used ($\sim 10^{-5}$ Torr) they found a marked change in the growth behavior with change in deposition rate. At low rates where the relative rate of contamination was high, imperfect faulted growth centers were formed surrounded by chemical debris—presumably oxide. At high rates gettering by the incident Si vapor removed the surface contamination [as with the silane beam experiments of Joyce et al. (169)] and fault-free growth proceeded on a clean surface at very closely spaced centers ($\sim 10^{12}/cm^2$).

These observations, considered together with the more recent reports of much lower epitaxy temperatures under uhv conditions, suggest that the rate dependence of T_E found by Booker and Unvala was not an intrinsic property of the clean surface but a chemical effect. As shown by Thomas and Francombe (75, 170), epitaxial growth of thick films of Si on Si can be obtained under clean conditions at temperatures as low as 400°C on (111) and 350°C on (100). The results of the LEED and electron microscope studies of these films are summarized in Figs. 22 and 23, and will be discussed further in connection with stacking fault generation in the following section.

Heteroepitaxial growth of Ge and Si has been studied by many workers. In the case of Ge the investigations were aimed mainly at relating detailed electrical properties to the structure and conditions of growth. Sloope and Tiller (62, 63), Krikorian and Sneed (128), and others (66, 67) have studied the conditions for epitaxy of Ge on CaF_2 substrates, while Wolsky et al. (129, 130) have investigated growth on sapphire. In general, there appears to be no difficulty in obtaining epitaxial growth on foreign substrates, but the films produced invariably contain high densities of stacking faults. As discussed in Section III, heteroepitaxy of Si on various refractory oxide substrates and also on SiC, usually by chemical techniques, has recently received considerable attention. In the chemical deposition of Si on foreign substrates Manasevit et al. (33) found that better-quality film growth with less twinning was obtained by using silane rather than $SiCl_4$ and suggested a number of etching mechanisms which in the case of the chloride could cause attack of the oxide substrate and contamination of the silicon deposit. The epitaxial relationships for Si on the principal planes of the hexagonal α-Al_2O_3 (sapphire) structure were analyzed by Nolder and Cadoff (173), who claimed that the orientations observed could be explained by assuming a simple replacement of Al by Si atoms at the growth surface. Similarly Joyce et al. (34) explain the orientations they obtain on quartz on the assumption that the surface oxygen atoms are removed at the start of growth, the Si vapor atoms bonding directly with the Si atoms of the quartz lattice. A more complete discussion of the epitaxial mechanisms is to be found in the review by Filby and Nielsen (20).

In an effort to minimize chemical interaction with the substrate Tallman et al. (174) studied the epitaxial growth of Si (from silane) on the {00.1} faces
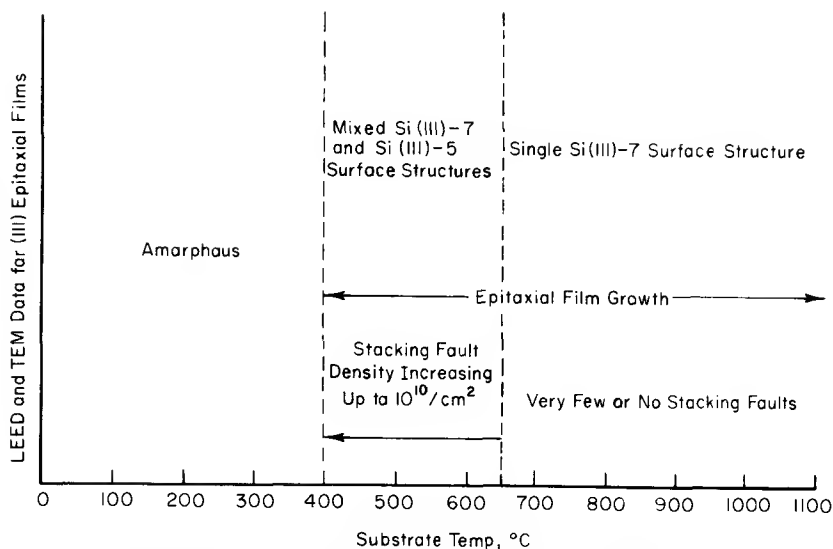
FIG. 22. Structural data for epitaxial silicon films grown by sublimation on clean Si (111) surfaces, in 10^{-10} Torr vacuum. [After Thomas and Francombe (170).]
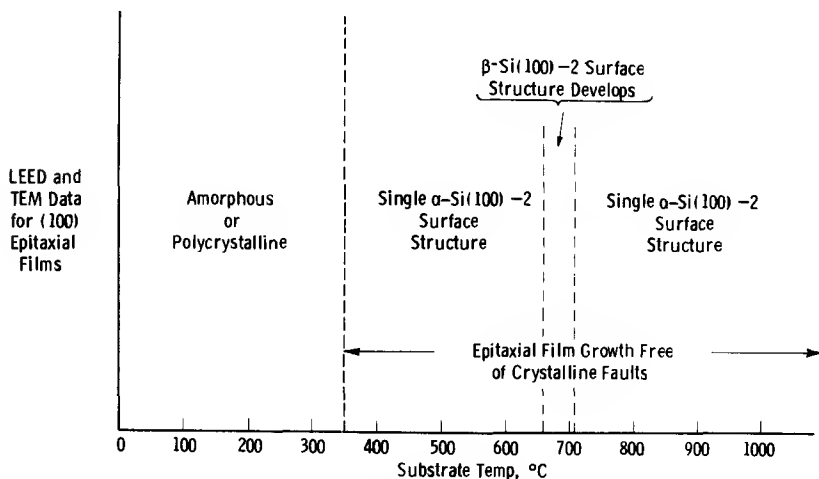
FIG. 23. Structural data for epitaxial silicon films grown by sublimation on clean Si (100) surfaces, in 10^{-10} Torr vacuum. [After Thomas and Francombe (170).]

of SiC crystals (of the 6H polytype). Opposite faces of the SiC crystal terminate, respectively, in Si atoms (A face) and C atoms (B face) and have different chemical etching characteristics and also differing effects on the type of epitaxial growth obtained with Si. This is strikingly demonstrated in Fig. 24 which illustrates that the Si growth centers possess different habits on the two SiC faces. Two orientations were observed, i.e., Si (111) ∥ SiC (00.1) and Si $<1\bar{1}0>$ ∥ SiC $<01.0>$; Si (110) ∥ SiC (00.1) and Si $<1\bar{1}0>$ ∥ SiC $<01.0>$. The second orientation yields a significantly smaller atomic misfit (approx. 2%) than the first orientation (approx. 25%).

Although considerable progress has been made in obtaining heteroepitaxial Si films (see also Section II), even to the extent that experimental devices have been fabricated in these, a number of important materials problems remain to be solved. To ensure high deposition rates with chemical deposition, high substrate temperatures are needed. Consequently, if chemical side reactions are to be minimized, inert refractory substrates must be used; even with sapphire chemical interaction is not avoided completely and sufficient diffusion of Al into the Si films occurs to make them strongly p type. Several of the substrate materials which have been found fairly stable chemically, e.g., sapphire, quartz, BeO, and SiC, possess lower crystal symmetries than Si. Therefore, two or more equivalent epitaxial orientations are permitted, with the result that the film structure is frequently twinned, or contains grain boundaries. Such defects may have a profound influence upon the diffusion profiles and properties of junctions.

We have already referred in Section II to the use of chemical techniques for the epitaxial growth of compound semiconductors, and in particular the III–V compounds such as GaAs. Vacuum deposition methods also have been applied extensively to the growth of epitaxial films of compounds, but many of these studies have been concerned with the standard vacuum evaporation of II–VI or IV–VI compounds, e.g., PbS, PbSe, ZnSe, CdTe (see Table III). The lead salts, which possess cubic NaCl-type structures, are epitaxed without difficulty, and on alkali halide substrates in some cases even at room temperature. Although no detailed quality assessments have been made, the x-ray diffraction, optical, and electrical data suggest that these films possess good crystal perfection. Problems arise in the epitaxial growth of some of those compounds possessing the zinc blende or wurtzite structures, and especially where the condensation coefficient for the constituent elements is low. CdS is a good example of this and when grown by the preferred coevaporation method cannot be formed at temperatures higher than 200°C. Structures for CdS films grown below this temperature, although very strongly fibered are usually not epitaxial.

In principle the vacuum techniques of three-temperature evaporation, flash evaporation, and sputtering, which possess in common the ability to preserve
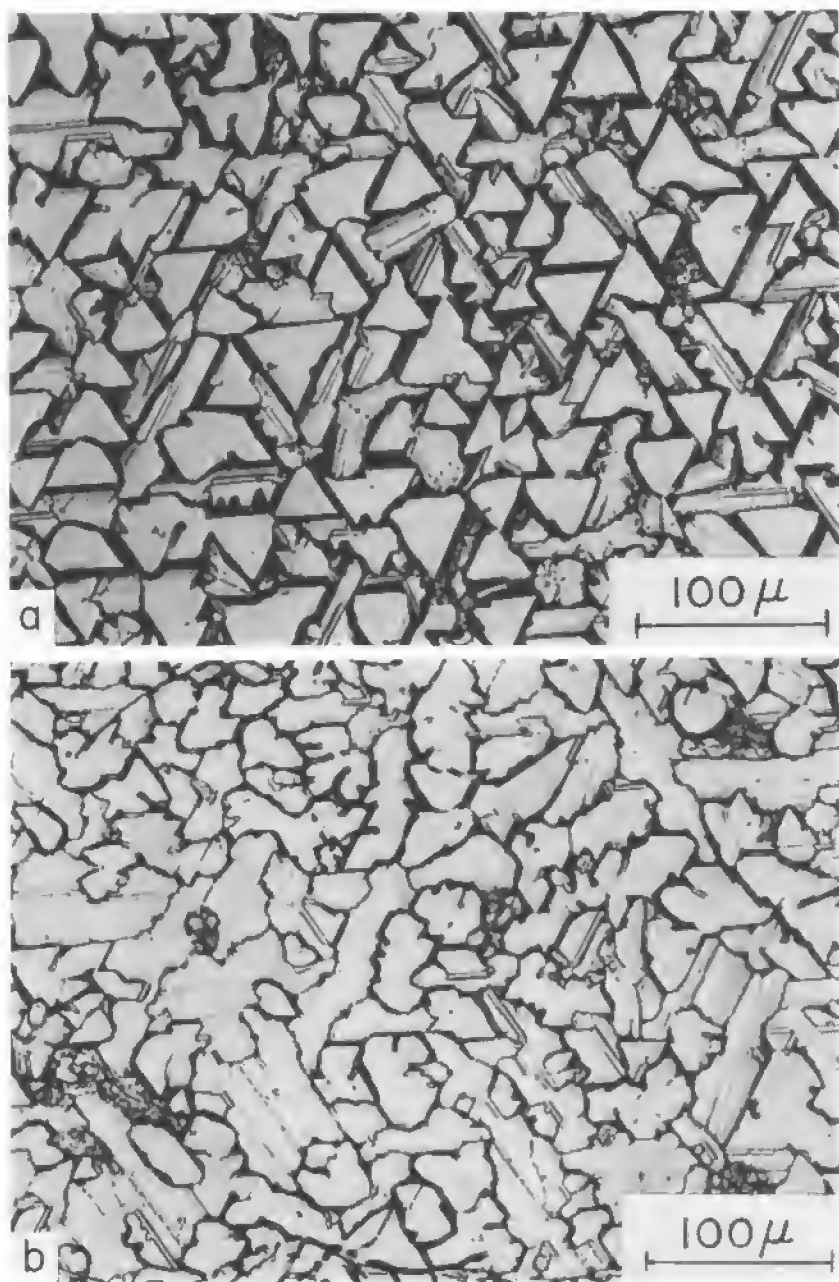
Fɪɢ. 24. As-grown surfaces of silicon films deposited on: (a) face B and (b) face A of hexagonal silicon carbide substrate. These films were prepared at a substrate temperature of 1200°C using hydrogen and silane at flow rates of 10 liters/min and 2 ml/min, respectively The film thickness is approximately 2 μ. [Courtesy R. L. Tallman; also Tallman *et al.* (*174*).]

stoichiometry in the compound film, can be used for epitaxial growth. In a recent paper Davey and Pankey (*112*) were able to demonstrate that the first method can be used to grow epitaxial films of GaAs on GaAs and Ge, and report rather low epitaxy temperatures (425–450°C), compared with the other two techniques (*113–115, 132–135*). Table VII gives a summary of the results obtained by Richards and co-workers on flash-evaporated films of the III–V compounds deposited on Ge substrates. With the exception of AlSb each of the compounds listed could be epitaxed on Ge, free of twinning (as judged from glancing-angle electron diffraction studies), at temperatures lower than the decomposition temperature. The source temperature, i.e., evaporation rate, was found to have a marked influence on the topography of the films, rough surfaces being obtained at low rates and smooth surfaces at high rates. Also, despite the evidence of structural perfection provided by electron diffraction, electron micrographs and diffusion studies indicated that the films contained a large number of crystallographic boundaries.

It was demonstrated by Francombe and co-workers (*132, 133, 135*) that diode sputtering could also be used to grow epitaxial films of semiconductor compounds (Table VI). Molnar *et al.* (*133*) showed that films of GaAs many microns thick, structurally and optically comparable to those grown by flash evaporation, could be deposited epitaxially on Ge substrates, and thinner films on CaF_2. In a later study it was found that epitaxial films of Bi_2Te_3 could be grown on the (111) and (001) faces of NaCl. The hexagonal basal plane orientation was obtained on (111), while double positioning of the crystallites occurred on (001). An analysis of the epitaxial structures in relation to the atom packing of the Bi_2Te_3 structure is contained in the original paper (*135*).

c. Structural and Chemical Defects. From the preceding discussion it will be evident that semiconductor films, depending upon the means by which they are grown, may show an extremely wide variation in crystallographic and chemical perfection. At the one extreme we can consider polycrystalline films of the compound semiconductors such as CdS and InAs used for thin film transistors or the activated II–VI materials used as phosphors or photoconductors. In these films the concentration of crystalline defects is extremely high and the electrical or optical properties of interest are dependent upon the number and distribution of these and on the overall chemical stoichiometry. In epitaxial films which are to be used for fabricating junctions, device properties are sensitive to the type and location of specific defects; therefore, it is important to characterize these and understand how they are generated. Defects may be classed as structural or chemical in origin and we shall consider primarily those commonly arising in epitaxial film growth, e.g., grain

boundaries, twins, stacking faults, dislocations, strains, chemical precipitates, or inhomogeneities.

From numerous theoretical and experimental studies of film growth it is established that, at least in heteroepitaxy, the stage of nucleation from the vapor is succeeded by the enlargement of growth centers which eventually touch one another and coalesce. As shown by the work of Pashley (175), the growing islands are often angularly misoriented with respect to their neighbors. During coalescence this misorientation is removed by a slight relative rotation or may be accommodated by the formation of an edge dislocation. Growth defects of these types are favored by surface disorder or contamination of the substrate. If the misorientation is severe (due perhaps to a competing epitaxial orientation) a grain boundary is formed, while if equivalent or multiple positioning of the islands occurs they may meet at a twin boundary. Also since from nucleation theory the saturation number of growth centers increases with incident vapor flux and with decreasing substrate temperature, growth faults become more numerous at high rates and low temperatures.

Twinning effects about $<111>$ axes are very common in thin film semiconductors of the diamond or zinc-blende structure types. Comparatively few attempts have been made to date to evaluate twinned films in a systematic way or to relate these defects to the conditions of growth. Holloway (161), in studying the structures of III–V films grown epitaxially on (111) Ge, showed that glancing-angle electron diffraction could be used to characterize the twin relationships. Using matrices to transform the original reciprocal lattice to twin orientations, the distribution of reciprocal lattice points lying in a $(1\bar{1}0)$ plane was established and compared with diffraction spot patterns obtained along a $[1\bar{1}0]$ azimuth in the (111) plane of the epitaxial film. In some cases multiple twinning—as high as ninth order—was observed in GaAs films on Ge grown at low substrate temperatures.

Unfortunately, glancing-angle electron diffraction provides data on the twin structure of the film surface only and this can give a misleading impression of the film structure as a whole. Holloway and Bobb (166) have shown that providing the twinned regions are large enough their location may be established by using x-ray topography (Fig. 16). Frequently, if the film structure is less perfect the twins may be more numerous and dispersed as lamellae. In this case a quantitative estimate of the amount of twinned material can be arrived at by using x-ray diffraction and comparing the intensities of reflections from the twinned regions with those from the matrix. This method has been successfully applied by Nolder et al. (176) to epitaxial Si films grown on sapphire, in which electron micrographs of the surface of the Si deposit suggested that it contained many twin lamellae.

Stacking fault defects (Fig. 26b) occur frequently in both homoepitaxial and heteroepitaxial films of the cubic diamond or zinc blende type, and arise

from disturbance in the normal periodicity of the (111) atom layer sequence *abcabcabc* ..., caused by the omission of a layer (intrinsic faults), giving, e.g., *abcacabc* ..., or by the addition of a layer (extrinsic faults), giving, e.g., *abcacbcabc* .... Booker and Stickler (*177*) have proposed a mechanism by which faults are produced. It is suggested that the faults are nucleated at positioning mistakes by atoms which go down in the wrong sequence. Lateral growth occurs, followed eventually by the formation of mismatch boundaries where the faulted area meets surrounding areas which are positioned in the right sequence. Depending upon the shape of the mismatch boundary, a variety of defect geometries are obtained, e.g., triangle, line, prismatic, etc. Stacking faults have been variously attributed to either mechanical damage (*152*) or chemical contamination (*72*) of the substrate surface. Twins appear to be caused mainly by carbon contamination, presumably due to the presence of crystallites of SiC on the surface and in severe cases a multiply twinned star-shaped structure (*178*) may result.

Recently, Thomas and Francombe (*170, 75*), reporting on LEED and electron microscopy studies of homoepitaxial Si films grown in uhv (approx. 10^{-10} Torr), showed that stacking faults may be generated in structures where oxide or carbide impurities are absent, or present only in very small concentrations. It was found from *in situ* LEED observations that on (111) at temperatures above 650°C the Si (111)-7 surface superstructure (Fig. 25a) was retained on the epitaxial film during growth, and that films displaying this structure possessed few or no stacking faults (Fig. 25b). However, in the temperature range 400–650°C the surface structure was found to change rapidly to a mixture of Si (111)-7, Si (111)-5, and the "ideal," nonreconstructed, bulk form (Fig. 26a). Films grown in this temperature range contained very high densities of stacking faults ($>10^8/cm^2$), as shown in Fig. 26b. The correlation of an abrupt change in film perfection with the appearance of these mixed surface structures suggests that the stacking faults originate in a change of the atom packing sequence at those points on the substrate surface where the Si (111)-5 or "ideal" structure nucleates. This explanation is supported also by the observation that the density of faults (and presumably the density of nucleation sites) increases in a regular manner with decreasing temperature, down to about 400°C, below which the structure becomes polycrystalline or amorphous.

Dislocations are often generated during epitaxial growth, especially when the grown layer differs in lattice parameter or thermal expansion coefficient from the substrate. This can happen in homoepitaxial growth of Si junctions due to the small relative lattice volume changes produced by the solution of dopant atoms, e.g., B, As, etc., possessing different tetrahedral radii to Si. Virtually any source of applied stress at the elevated substrate temperatures used in Si epitaxy may generate plastic flow and dislocations. From the theory
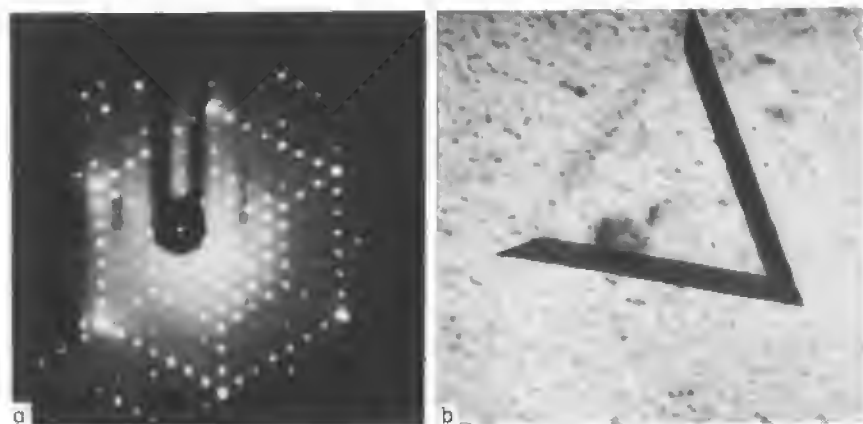
FIG. 25. Structure of homoepitaxial films grown on (111) Si in 10^{-10} Torr vacuum at 650°C: (a) *in situ* LEED pattern at 39 V; (b) transmission electron micrograph showing isolated stacking fault in near-perfect film. [After Thomas and Francombe (*75, 170*).]
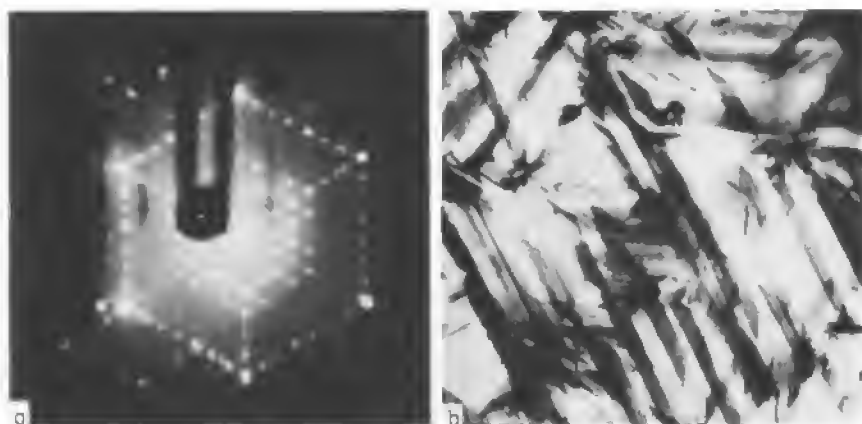
FIG. 26. Structure of homoepitaxial films grown on (111) Si in 10^{-10} Torr vacuum at 500°C: (a) *in situ* LEED pattern at 39 V, (b) transmission electron micrograph. [After Thomas and Francombe (*75, 170*).]

of Van der Merwe (*179*) we might also expect misfit dislocations to be generated in heteroepitaxy, caused by the periodic registry of the mismatched film and substrate lattices. However, these may be masked by interdiffusion effects if epitaxial growth is carried out at high temperatures. Dislocations may be detected, for example, by chemical etching, electron microscopy, or x-ray topography. If high densities are present, it should in principle be

possible to estimate their number by x-ray line broadening measurements using rocking curve techniques. However, these measurements are suspect because of factors such as strain or chemical inhomogeneity which also broaden diffraction lines.

Films grown heteroepitaxially, e.g., Ge on CaF_2 or Si on Al_2O_3, tend to develop large stresses, and in some cases where the film is thick and the bond to the substrate relatively weak, e.g., GaAs on CaF_2, severe peeling occurs. Measurements have been made of the stress in Si films chemically deposited on sapphire by Dumin (180). Applying the beam equation for the case of a disk-shaped substrate he used the curvature induced in the flexible substrate to estimate the compressive stress in the films. For films in the thickness range 2–43 μ grown from $SiCl_4$ at 1100°C, stresses from 8 to 100 × 10^8 dyn/cm^2 were produced, depending upon the thickness of the substrate which governs the extent to which stress could be relieved by bending.

Chemical defects may exhibit several forms and their influence on material properties depends to a large extent on the structure of the film as a whole, e.g., whether polycrystalline with high residual disorder or epitaxial with comparatively few widely dispersed structural defects. Nonstoichiometry in compound films arises from selective loss of one component, e.g., S from CdS or As from GaAs. Due to their large effective surface area, numerous lattice vacancies, and other gross defects, single-phase disordered polycrystalline structures are capable of wider deviations from stochiometry and considerably greater compositional inhomogeneity than defect-free monocrystalline
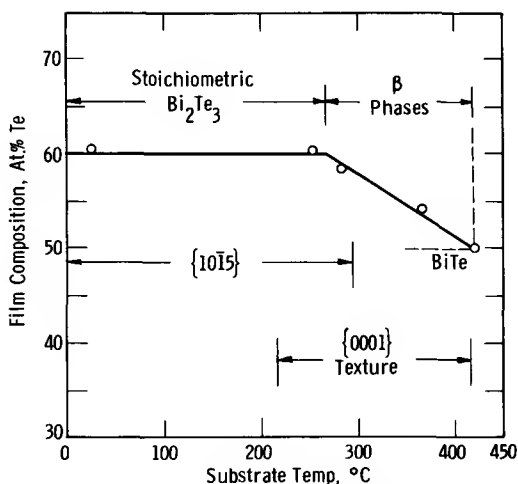
FIG. 27. Composition of sputtered bismuth telluride films as function of substrate temperature, showing temperature ranges for fiber textures. [After Francombe (121, 135).]

structures. This is demonstrated by the nonequilibrium, metastable composi-
tions found in solid solutions of III–V compounds grown by flash evaporation
(*115*) and also in Bi–Te films deposited by sputtering (*121, 135*). In the latter
case it was found that the single-phase hexagonal Bi_2Te_3-type structure could
be retained in Te-deficient films extending in composition to BiTe, a result
which is only paralleled in bulk materials prepared as finely divided sintered
powders or in the mineral form under very high pressures. When the non-
stoichiometric (Te-deficient) β phases (see Fig. 27) are annealed, they decom-
pose into Bi_2Te_3 and metallic Bi.

Complete departure from the single-phase condition results for compounds
at substrate temperatures high enough to volatilize one of the elements,
e.g., As or Sb. The metallic Group III element is then formed on the film
surface.

Chemical inhomogeneities in the form of precipitates or inclusions are
frequently present in high densities both in bulk and thin film semiconductors,
and produce localized variations in electrical properties. Characterization of
these inhomogeneities is very difficult (e.g., by electron microscopy and
diffraction) since in many cases they are in noncrystalline form (*150*). More
detailed information on the role of such defects in influencing junction
diffusion processes and in limiting the minority carrier lifetime of certain
epitaxial devices is badly needed but is exceedingly hard to obtain.

V. Electrical and Optical Characterization

The electrical and optical properties of semiconductor thin films are pro-
foundly influenced by minute quantities of structural and chemical imperfec-
tions, which in turn are controlled by the detailed preparative and growth
conditions. Conversely, electrical and optical measurements can be used to
characterize with great sensitivity the defect structure of a thin film. Many
varieties of behavior are possible, but the measurements by themselves usually
reveal nothing of the qualitative nature of the defects.

In essence, while one may learn that N/cm^3 states lie E eV below the con-
duction band edge in a given sample, it can only be inferred that these states
have a particular origin by tracing their behavior through systematic vari-
ations, for example, in preparative conditions, annealing experiments, or the
gaseous environment. The electrical and optical measurements can provide
no such information directly. Furthermore, the experimental measurements
of a given property can usually be explained by any one of several models.
To establish that a particular model applies uniquely, it is usually necessary
to measure several properties.

Our purpose in this section is not to catalog the numerous, and often
anomalous, experimental trends that have been found, or that can be

anticipated. Rather we will discuss several illustrative examples for which a reasonably clear experimental and theoretical understanding has been achieved.

1. HALL EFFECT STUDIES

a. The Hall Effect at Thermal Equilibrium. Measurement of the Hall effect and resistivity provides data on the density and type, n or p, and mobility μ of free carriers present in a film (*181*). Such data, taken at a single temperature under thermal equilibrium conditions, can provide immediate information on trends in the deposition process. For example, germanium films produced by evaporation (*63*) and chemical vapor deposition (CVD) methods (*39*) are usually p type, no matter what the conductivity type of the source material. Hall effect measurements on Ge films produced or annealed under a variety of conditions have established that crystalline defects are responsible for the observed acceptor densities (*38, 63*).

Silicon films prepared by chemical vapor deposition onto sapphire are now regularly made with good structural perfection (*33*). Hall effect studies show, however, that while nearly optimum hole mobilities can be attained in p-type films, the electron mobility in n-type films is much less than that observed for bulk material with the same free-electron concentration (*35*). Variation of the deposition temperature produces carrier density and mobility values at room temperature that can be reasonably explained by assuming the Si to be doped with Al evolved from the sapphire substrates (*35*).

The most common application of the Hall effect is, indeed, as a "quality factor" in the evaluation of deposition technique. It has been so used in studies of Ge (*63*), Si (*35*), InSb (*182*), InAs (*182*), GaAs–GaP alloys (*183*), CdS (*85*), CdSe (*184*), and others (*185*). Factors in the deposition procedure that have been studied include source material purity, source crucibles, deposition rates, deposition temperatures, source temperatures, substrate material, and vacuum residual pressure. Several of these factors have been examined by Davey *et al.* in a study of Ge film formation problems (*65*).

While Hall effect measurements at a single temperature and with the sample at thermal equilibrium are of great value in following the effects of a process parameter, the trends in a given film series can usually be explained in several ways. Carrier densities may decrease in a series of depositions either because of increasing purity, or because of increasing contamination, manifest as compensation. Mobilities may increase because of reduced impurity content, or increased grain size. Resolution of such ambiguities can be sought in a variety of ways: direct optical or electron microscopic observation of the grain size, x-ray diffractometric linewidth determination of grain size and orientation, or by Hall effect measurements over a range of temperatures. From the latter, knowledge of the temperature dependence of n and μ is

obtained, which can permit a determination of the ionization energy of one or more defect centers, and sometimes also their density.

McCarthy (*186*) has prepared InAs films of very high mobility by a CVD technique. His results illustrate the subtle effects upon mobility that can be observed in even very highly perfect material. By chemical transport of InAs from Te-doped material and its epitaxial deposition onto Cr-doped GaAs substrates, a series of films with electron concentrations ranging from $3 \times 10^{15}/cm^{-3}$ to $4 \times 10^{17}/cm^{-3}$ were prepared. The Hall effect mobility values obtained at 293 and 77°K are plotted in Fig. 28 along with mobility values
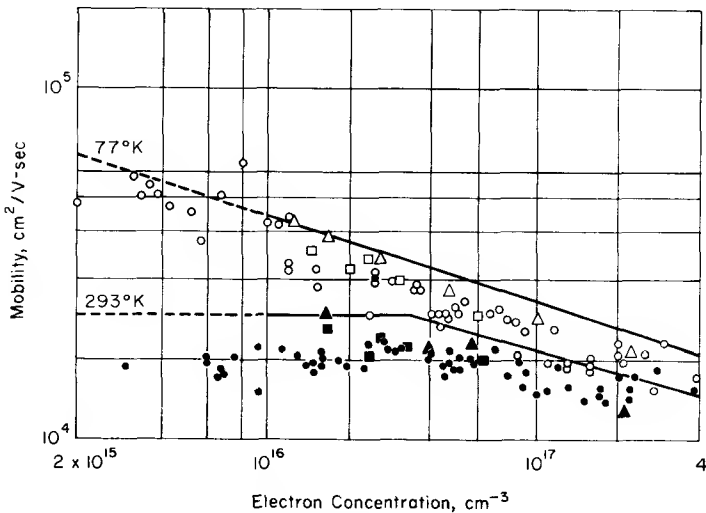
FIG. 28. Electron mobility in InAs as a function of electron concentration: (●) epitaxial InAs at 293°K; (○) epitaxial InAs at 77°K; (■) melt-grown InAs at 293°K; (□) melt-grown InAs at 77°K; (▲) melt-grown InAs at 293°K; (△) melt-grown InAs at 77°K. [After McCarthy (*186*).]

compiled by McCarthy from various melt-grown single-crystal investigations. It can be seen that the epitaxial film μ values compare favorably with the bulk data at 77°K, but fall consistently below the bulk data at 293°K. The latter can indicate either the presence at 293°K of a quantity of ionized scattering centers which are deionized at 77°K, or the presence of dislocation scattering, which also increases with temperature.

Analysis of the mobility-determining features in a given set of semiconducting thin films relies on knowledge of the mobility parameters of the material in bulk single-crystal form to bring out the special features of the thin film configuration. Ramey and McLennan (*187*) illustrated this point by

analyzing their mobility data for polycrystalline, vacuum-deposited, p-type Ge films in terms of the contributions to scattering of the conducting holes by thermal lattice vibrations, ionized impurities, dislocations, and unspecified surface phenomena. Their analysis involved the expression

$$1/\mu_h = 1/\mu_L + 1/\mu_I + 1/\mu_d + 1/\mu_F \tag{13}$$

for the hole mobility, μ_h, where the first three terms on the right-hand side represent the lattice, impurity, and dislocation scattering. The term μ_F is then allowed to represent all deviations of the observed value, μ_h, from the sum of the first three.

Ramey and McLennan obtained values for μ_h from Hall effect measurements of a series of films over a range of temperatures. In their work a value of unity was evidently assumed for the scattering parameter of the Hall coefficient, as is frequently done in thin film studies. Calculation of μ_I, μ_L, and μ_d was made from the theoretical relations given in Table VIII and the measured net acceptor concentrations shown in Fig. 29.

TABLE VIII

Mobility Parameters in Bulk Ge

Limitation	Relationship	Refs.
Lattice scattering	$\mu_L = 1.05 \times 10^9 T^{-2.33}$ (cm²/V-sec)	219
Impurity scattering	$\mu_I = [8.52 \times 10^{13}/N_I \ln(1 + x^2)]T^{3/2}$	220
	$x = 2.86 \times 10^4 T N_I^{-1/3}$	
Dislocation scattering	$\mu_d = T[1.1 \times 10^{11} N m^*/m]^{-1}$	198

These relationships are cited here in order to bring out explicitly the temperature coefficients of the various scattering mechanisms. In practice, reference to experimental data on bulk material, such as given for Si and Ge in engineering texts such as that of Phillips (188), is to be preferred, since the fit of the theoretical expressions to experiment is not exceptionally good.

Ramey and McLennan reduced their raw data by plotting $1/\mu_h - (1/\mu_L + 1/\mu_I)$ versus I/T, as seen in Fig. 30. Included in the figure are their data for films of four thicknesses, and the data of Sloope and Tiller (189) for three thicknesses of single-crystal films. It is evident from the figure that the data can be represented by the sum of a temperature-dependent term, which was identified with μ_d, and a temperature-independent term, μ_F, which was found empirically to have the form

$$1/\mu_F = A \log \delta/a \tag{14}$$
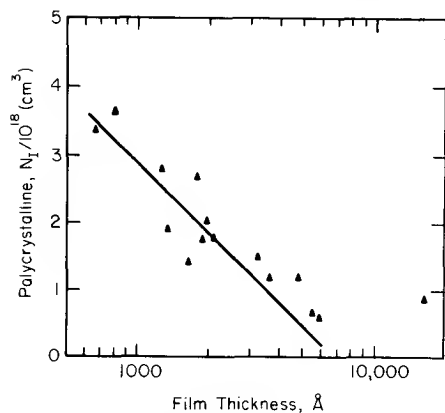
FIG. 29. Ionized acceptor concentration in Ge films as a function of film thickness. [After Ramey and McLennan (*187*).]
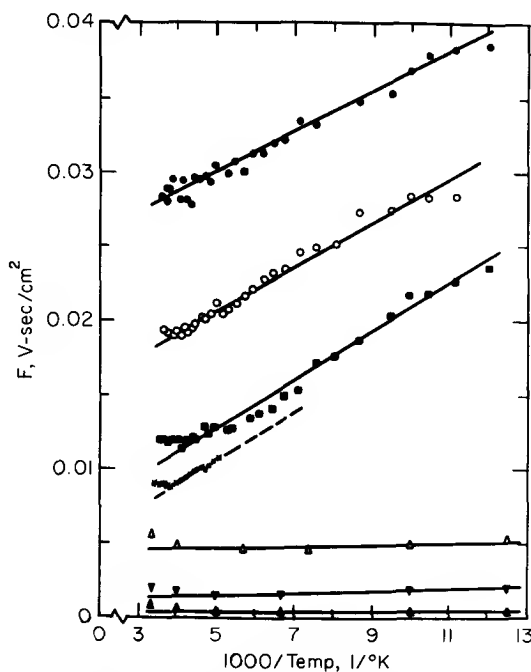
FIG. 30. Separation of lattice and impurity scattering from measured values in Ge films. Film thickness (Å): (●) 665; (○) 1965; (■) 4650; (▲) 19,000; (△) 1150; (▼) 1700; (*) 17,200 [Sloope and Tiller (*189*)]. The function $F = (1/\mu_L + 1/\mu_I)$. [After Ramey and McLennan (*187*).]
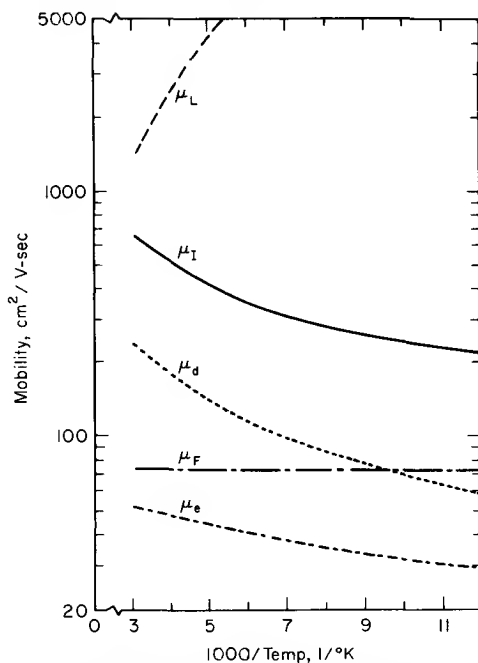
FIG. 31. Variations of μ_L, μ_I, μ_F, and μ_h with reciprocal temperature for a 1965-Å-thick Ge film deposited at 7.5 Å/sec at 500°C. [After Ramey and McLennan (187).]

where a is the film thickness in angstroms, and A and δ are functions of the film structure and deposition technique. Empirical values obtained for the several parameters are listed in Table IX.

TABLE IX

EXPERIMENTAL PARAMETERS FOR GE FILMS

Film type	A (V sec/cm^2)	δ (Å)	N (cm^{-2})
Polycrystalline	0.0219	8000	5×10^{11}
Single crystal	0.0176	2000	1.8×10^{10}

The relative magnitudes of the several contributions to μ_h, from μ_L, μ_I, μ_d, and μ_F, can be judged from Fig. 31. It is evident that, at room temperature, the mobility limitations operative in a bulk single crystal are of little consequence in this particular polycrystalline Ge thin film.

Although the quantitative significance of the μ_F values obtained is not clear,

the μ_d calculation seems quite important in view of the correspondence of the dislocation densities derived from the μ_d fit, and that observed by physical methods by Sloope and Tiller (63).

Decreases in carrier density with increasing film thickness, though not always so clearly defined as in the work of Ramey and McLennan, seen in Fig. 29, are clearly present in the results of many investigators. Similar trends in Ge film preparations have also been noted by Sloope and Tiller (63), Sakai and Takahashi (190), and Davey (191); in Si films by Dumin (35); in InAs films by Günther (102), and Kunig (192), among others. Evidence is available for at least three probable causes for such findings, including the donor or acceptor character of crystal defects, out-diffusion of a dopant from the substrate, and true surface state effects due to chemical and physical effects at the film surface. The various authors cited above have each favored a particular mechanism in their discussions. In fact, there is undoubtedly some contribution from each mechanism present in each case.

Sloope and Tiller (189) noted that the defect density discernible at the surfaces of their films decreased with increasing film thickness, decreasing deposition rate, and increasing substrate temperature during the deposition. In parallel with the surface defect density changes, they later observed corresponding but lesser changes in μ_h (63) as shown in Fig. 32. The film surface defect density, however, was always less than the film–substrate interface defect density, and the μ_p values represented obviously averages over the film thickness. By also averaging the defect density, the authors found reasonable quantitative agreement between both changes and concluded that the crystal defects are the source of the acceptors in their films, and it was surmised that various other factors could be discounted.

Dumin (35), by contrast, has chosen to interpret the acceptor density changes he observes in CVD Si films on sapphire as being due to Al atoms that have diffused into the Si from the substrate during the course of the film deposition. Although Dumin has noted changes in crystallographic defect density with film thickness, his evidence for autodoping effects is quite compelling, and, furthermore, in several instances the trends of acceptor density are opposite to those cited above for Ge deposition onto CaF_2 (63). For example, the Si film acceptor density *increases* with increasing substrate temperature while the Ge film acceptor density *decreases*.

In addition to noting a temperature dependence of the autodoping effect from (00.1) sapphire substrates, Dumin has also found the effect to show a slight dependence on the orientation of the sapphire (35). These latter measurements are in good correspondence with the data of Hart *et al.* (38), also on (1$\bar{1}$.2) material. In more recent work Dumin has noted a lesser degree of Al autodoping when magnesium aluminum spinel was used instead of sapphire, seen in Fig. 33 (15).
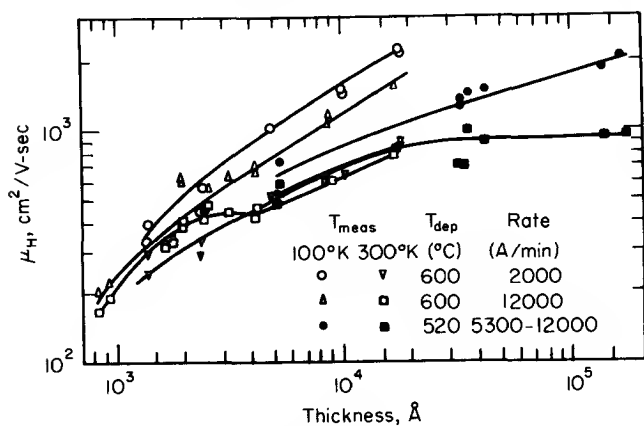
FIG. 32. The Hall mobility at 100 and 300°K as a function of film thickness for single-crystal Ge films. [After Sloope and Tiller (63).]
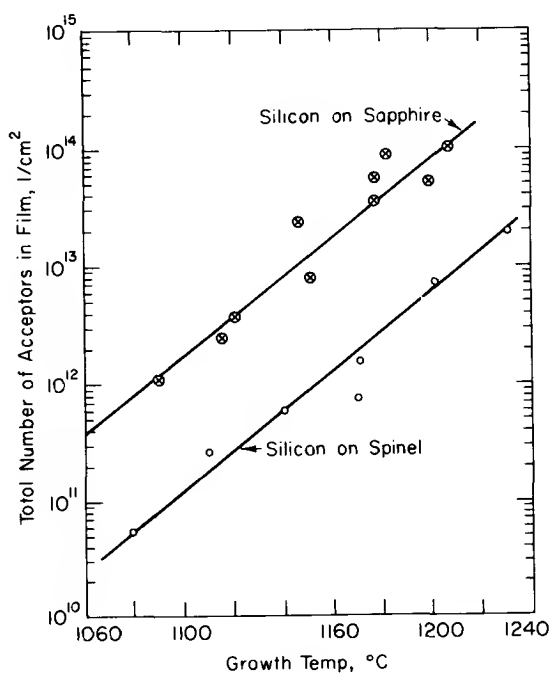
FIG. 33. Comparison of autodoping on silicon films grown epitaxially on sapphire and spinel. [After Dumin (15).]

Somewhat more classical "surface state" effects have also been observed, in which the chemical and physical differences between the semiconductor film surface and its "bulk" give rise to donor or acceptor states. Such effects have been well documented in the course of metal–insulator–semiconductor, MIS, field effect transistor, and varactor studies (193). Particularly detailed bulk data are available in the case of devices fabricated on silicon single crystals (194).

Typically, it is observed that the sheet conductance of a semiconducting thin film is changed when an insulating layer is deposited on top of it in the course of Thin Film Transistor (TFT) preparation. Deposition of SiO on CdS has been found to increase the n-type conductivity, while CaF_2 deposited on CdS causes a reduction of the conductance (10). Other combinations that have been examined include films of the semiconductors CdSe (195) and InAs (192).

Kunig (192), in the course of preparing InAs TFT devices, noted the carrier density variation with thickness seen in Fig. 34. Deposition of SiO on top of the InAs caused a reduction in electron density. Kunig also noted that the field effect mobility in SiO-coated samples exceeded the Hall effect value, measured on uncoated samples, by an amount in general agreement with that expected for the observed reduction in ionized scattering center density.

The silicon and germanium films, discussed previously, represent intermediate cases of film perfection. Dominant factors limiting the observed carrier mobility values are acceptor states arising from structural imperfections and substrate out diffusion. No indication is seen of mobility limitation by the surface scattering phenomena which have been observed in thin films of metals.

Zemel (93) has reviewed surface scattering phenomena, with particular reference to the highly perfect lead salt films that he has investigated. The mobility limitation observed in even such structurally perfect films has, however, evidently been provided by cracks in the films which result from the termal expansion mismatch between the lead salt films and the alkali halide substrates used. True surface scattering phenomena would appear to be most readily observed in semiconductor surface space charge regions (196) —where their observation does not require the semiconductor to be a thin film.

Recrystallized, dendritic InSb films prepared by Wieder (197) emphasized also the effects of dislocation scattering. Sufficiently low impurity levels were attained such that impurity scattering phenomena were of negligible importance. The experimental mobility–temperature data (Fig. 35) exhibit a maximum at a temperature T_0, which can be anticipated from the expression

$$1/\mu = T^{1.68}/(1.09 \times 10^9) + 1/\beta T \qquad (15)$$
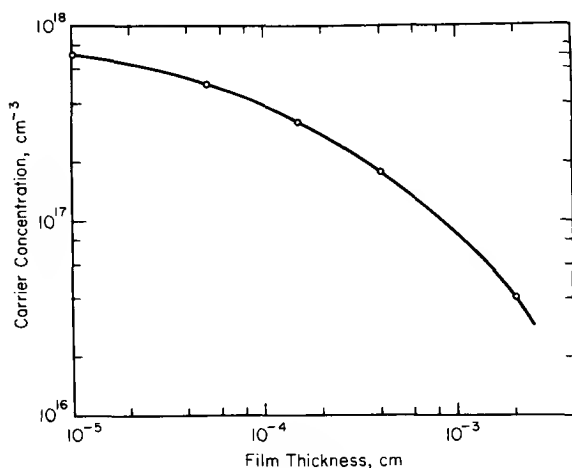
FIG. 34. Doping level of InAs films on glass at various thickness. [After Kunig (*192*).]
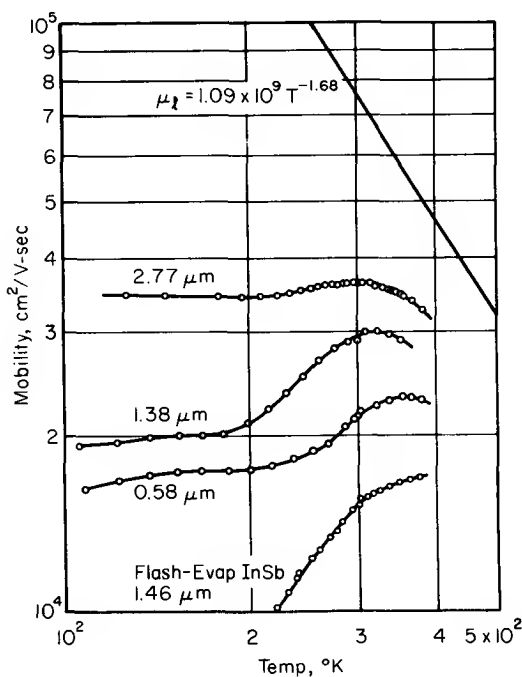
FIG. 35. Temperature dependence of the electron mobility $\mu = R_h\ \sigma$ of three dendritic InSb films of different thickness and of one flash-evaporated film. The bulk InSb μ_L is also shown. [After Wieder (*197*).]

for the combined effects of lattice and dislocation scattering on the observed mobility, the maxium $\mu(T)$ occurring at

$$T_0 = [\beta/(6.49 \times 10^8)]^{+2.68}, \tag{16}$$

where μ is the parameter representing the effects of the dislocation scattering phenomenon.

In fact, Wieder compared μ values obtained by plotting $(1/\mu - 1/\mu_L)$ versus T with those required for the experimental values of T_0. The comparison shows good agreement in the trends of the μ values calculated from the T_0 values, and those calculated from the temperature dependence of the plots of $(1/\mu - 1/\mu_L)$.

Wieder (197), in applying the dislocation scattering model of Dexter and Seitz (198) to his data, stated explicitly the assumptions involved, namely that the charge carrier scattering is assumed to be caused by the deformation potential associated with stationary edge dislocations, that the polar nature of the InSb lattice is neglected, and that a grain boundary is considered as a vertical wall array of edge dislocations oriented in such a way as to minimize the strain field between them. The net scattering power of a grain boundary is then considered to be the sum of the scattering powers of its dislocations. That these assumptions have considerable validity for his data is confirmed by the quality of the fit obtained between theory and experiment. It is evident, however, that an exact fit is not to be expected.

That such a model is valid tacitly implies that the surfaces of individual grains have approximately the same chemical doping density as the "bulk" of the grains, or, stated another way, the grain surfaces are in a "flat-band" condition. Should the grain surfaces and the intergranular contact region have an appreciably different donor or acceptor density, then a rather more severe limitation would be placed upon the mobility, as is noted frequently in CdS films after an air-bake treatment. Detailed analyses of such intergranular contact barrier effects on Hall effect data have been given by Berger (199) and others (85).

b. *Nonequilibrium Hall Effect.* From the discussion in the previous section, it can already be seen that films can exhibit a wide variety of electrical characteristics determined by their content of ionized impurity centers and structural defects in addition to the limitations imposed by the intrinsic carrier mobility which is determined by lattice scattering. Measurement of the Hall effect over a range of temperatures is an effective tool in sorting out these effects since the several mobility-limiting factors have different temperature dependences, and their relative importance can change over a range of temperatures.

Further information on the electronic defects in a film can be obtained by

perturbing the free-carrier density during the Hall measurement through illumination with an appropriate wavelength of light (85), or by application of an electric field in a configuration similar to that of an insulated-gate field-effect transistor (200). The use of light for carrier density perturbation permits one to increase the density at will, either throughout the depth of the film, or only on its surface, simply by varying the wavelength and intensity of the light. Application of an electric field permits one to either increase or decrease the carrier density, but only in the surface regions of the film. There is in general more information available from the use of illumination rather than an electric field.

Nonequilibrium Hall effect measurements are particularly useful in investigations of wide-gap semiconductors, and are frequently necessary in order to make possible any measurements at all, because of the very high resistivities obtained. Variation of the Hall mobility with the perturbation level is chiefly due to two factors: variation of the charge state of ionized scattering centers, and variation of the influence of intergranular contact barriers (200).

Wide-gap semiconductor thin films are generally highly insulating, unless deliberately doped with some easily ionized impurity, such as sulphur in GaP (201). Further, the high resistivity is often due not only to low values of n (or p), but to the simultaneous occurrence of a low value for the mobility (106). Most often, the low mobility is caused by dislocation and grain boundary barrier phenomena as discussed in Section V,1,a, especially in polycrystalline films. In addition, however, there is the probable presence of substantial concentrations of ionized positively charged defects which are very nearly balanced by ionized, negatively charged defects. Each ionized, compensated pair of centers thus contributes no net charge carriers, but does present a pair of ionized scattering centers to the few charge carriers that are present.

The source of the compensation is frequently attributed to a mechanism postulated by Longini and Greene (202) which involves the autogeneration of crystal defects in semiconducting materials. It is the authors' belief, however, that heavy metal contamination, the avoidance of which requires almost fanatic procedures, can be a possible explanation for most published results.

2. Contact Phenomena

Electrical contact phenomena in bulk and thin film semiconductors are identical. A bewildering array of theories is available (3), and almost any results can be explained by one or more of them. Some phenomena, such as the Hall effect, can be measured with any kind of contact, or even with no contact at all. But to obtain an ohmic contact to a particular semiconductor

is at least as vexing an art in thin film semiconductor work as it is in bulk semiconductor studies.

Heuristic arguments regarding the choice of a contact material are available to guide the experimenter. These include: (1) choosing a contact material on the basis of its work function (the work function of In is less than the electron affinity of CdS, hence an ohmic contact is obtained between In and n-type CdS); (2) choosing a contact material by its doping behavior in the bulk semiconductor (In is a donor in CdS, hence an ohmic contact is obtained to n-type CdS); (3) damaging the semiconductor surface, for example, by ion bombardment (in which case the character of the contact does not depend on the nature of the contact metal). In contrast to the example of In on Cds, Al contacts to silicon will be ohmic to n type by reason (1) and ohmic to p type by reason (2), i.e., the results will depend on the application technique.

To permit the widest variety of measurements, the experimenter should have available both an ohmic contact and a blocking contact for each particular semiconductor film. Preliminary evaluation of each particular contacting method is conveniently made through use of a standard multi-armed Hall effect sample, sketched in Fig. 36. If the resistance measured from
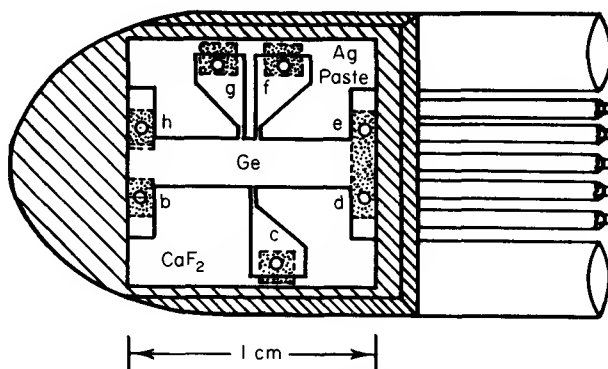
FIG. 36. Substrate holder and film geometry for making electrical measurements on Ge films on CaF_2 substrates. [After Sloope and Tiller (63).]

b to c over a reasonable range of current densities is a proportionate fraction of the resistance from a to d, then the contact is ohmic and the contact resistance is negligible. However, if it is less than proportionate, then the contact has at least partial blocking character. Although it is clearly beyond the scope of this article to discuss carefully the many potential metal thin film semiconductor contact phenomena, an attempt is made in the following paragraphs

to provide a brief introduction to the subject, together with certain key references.

"Ohmic contact" is a term used to describe a contact that is electrically transparent in the sense of exhibiting negligible contact resistance in the measurement described above. Rose (7) has provided a more quantitative discussion of this type of contact, and indicated that one should differentiate among such contacts according to the extent of the mobile space charge produced in the semiconductor. When sufficient mobile space charge is injected to cause a poential minimum to form within the semiconductor, then the ultimate ohmic case of an injecting contact is produced which permits the study of space-charge-limited current phenomena and the fabrication of photoconductors with quantum yields greater than one. It should be noted that photon (203) or electron (204) irradiation of the contact region can be used to cause a blocking contact to become injecting. Important transient space-charge-limited current studies have involved such irradiation techniques (203).

Another important variety of ohmic contact involves a very abrupt transition between metal and heavily doped semiconductor. By very heavy doping of the semiconductor surface, the contact barrier is made so narrow that tunneling of large quantities of carriers is easily possible. Most commercial devices utilize such contacts.

Ohmic contacts facilitate the observation of the "bulk" properties of the semiconducting film, and do not in first order introduce any measurement-dominating phenomena. Nonohmic, or blocking contacts, on the other hand, introduce effects which typically dominate the electrical measurement. Properly interpreted, these contact phenomena can yield a wealth of information about the semiconducting film itself.

Best understood of the several nonohmic contacts is that between electron- and hole-conducting regions of the same crystal; that is, a typical p–n junction (205). Basic p–n junction phenomena have been extensively discussed (205). The most intensive application of junctions in epitaxial material by far is in the manufacture of silicon integrated circuits, which involves exclusively homoepitaxial material.

In any metal–semiconductor contact, the fundamental parameters are the barrier height at the metal–semiconductor interface, and the height of the depletion barrier formed within the semiconductor itself. The former is a function only of the difference between the metal work function and the semiconductor electron affinity, while the latter includes also the influence of the semiconductor doping level. In the case of a blocking contact, both parameters can be obtained from capacitance–voltage data (206), if the semiconductor is in a reasonably conductive state. The metal–semiconductor barrier height can also be obtained by a photoemissive technique (207),

which is applicable over a wide range of resistivities. These measurements, and others have received considerable attention in the recent literature.

Fundamental to experimental investigation of the metal–semiconductor barrier is the achievement of a contaminant-free metal–semiconductor interface. For studies of single-crystal semiconductor material, this condition has been attained by cleaving the crystal inside a uhv system in the presence of a steam of metal vapor which coats the freshly cleaved crystal surface immediately upon its formation (208). In recent studies of AlSb films (209), the present authors obtained comparable metal–semiconductor barrier height results for the deposition of AlSb films onto previously formed Ta contact stripes.

3. Optical Absorption

Optical absorption measurements can provide a wealth of information on the electronic structure of semiconductor thin films. As in the case of electrical measurements, heavy reliance is placed on reference to bulk single crystal studies in the interpretation of the measurements. A concise reference to semiconductor optical absorption phenomena can be found in Vol. 3 of the series edited by Willardson and Beer (210). Absorption measurements on thin films of semiconductors have been used to determine details of the electronic structure of semiconducting materials. More often, however, they have been used to determine the quality of the thin films. Such measurements, of necessity, involve absorption at wavelengths greater than the band edge.

Figure 37 shows Pankey and Davey's measurements (106) of the near-edge absorption in GaAs films. Excess absorption at energies just beyond the edge has been attributed to shallow impurities, and also to structural imperfections in the sense of a perturbation of the band structure which causes a tailing of states into the otherwise forbidden band (106). Discrete absorption thresholds at energies less than E_g can usually be attributed directly to discrete states within the forbidden gap and correlated with particular impurities or imperfections in the same way as electrical data (209).

Imperfection absorption can in principle, and in fact, be observed at all wavelengths greater than the band edge. In the infrared portion of the spectrum, however, additional absorption effects are observed including specific absorptions due to chemical entities such as the Si–O and Si–C bonds of oxygen- or carbon-contaminated silicon, the lattice phonon absorptions, and so-called free carrier absorption caused by the transition of carriers in the conduction and valence bands to adjacent states within the same band. Also observed are various band-to-band transitions of the free carriers. Davey (106) has made particular use of free-carrier absorption to measure the hole concentration in an evaluation of a series of GaAs films in which the mobility was too low to permit Hall effect measurements.
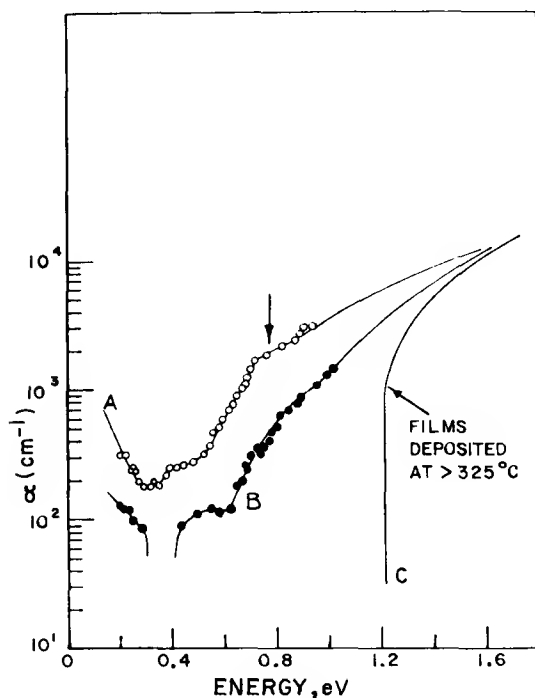
FIG. 37. Optical absorption measurements on GaAs films: (○) film deposited at 250°C, unannealed, 180,000 Å thick; (●) after anneal at 400°C for 1 hr. Curve A: the absorption spectrum of a film deposited at 250°C; the vertical arrow indicates an absorption band at 0.78 ± 0.05 eV, as measured on this and similar films. Curve: B the absorption spectrum of the sample of Curve A after annealing. Curve C: typical absorption spectrum for films deposited above 325°C. The films were deposited on quartz substrates. [After Pankey and Davey (106).]

4. Photoconductance and Related Phenomena

In previous sections we have indicated the effects produced by shining light onto a semiconducting thin film during the measurement of Hall effect and nonohmic contact phenomena. In this section we will briefly examine phenomena involving generation–recombination processes in samples having ohmic or injecting contacts and which are measured in the absence of magnetic fields. Included in this group are photoconductivity, space-charge-limited current, thermally stimulated current (TSC), and noise current.

Bube has termed the application of photoconductance-related phenomena to high-resistivity semiconductor materials "photoelectronic analysis," and has provided several reviews of the subject as well as original studies (211). Because of the existence of these readily available discussions, we will attempt

only a brief description of the phenomena and their use in the investigation of thin films.

Photoelectronic analysis is applicable to semiconductor films of all varieties. The techniques provide information on the density, energy, and capture cross section of electronic states in the material. Similar information is also available from the Hall effect, with the exception of the capture cross section, which is a special feature of the kinetic phenomena, and is not available from thermal equilibrium studies. Interpretation of the Hall effect data is, in general, less complicated than interpretation of photoelectronic data. Measurement of the Hall effect, however, restricts the electrical properties of the sample to a particular range. That is, if the Hall voltage is to be measured, then it must be large enough, and the sample resistance small enough, that available instruments can measure it without unduly affecting its value. The use of sophisticated vibrating-reed electrometers can, of course, considerably extend the range of measurable sample resistivities.

Photoconductance depends upon the density of light-excited free carriers in the conduction or valence bands, and their mobility. The steady-state number of carrier pairs generated, n_0, is simply related to the incident light intensity by

$$n_0 = F\tau, \tag{17}$$

where F is the number of photons absorbed per second per cubic centimeter, and τ is the free carrier pair lifetime before recombination. The number of carriers available to conduct current, n, however, is generally much less than n_0, due to capture of the free carriers by trapping states. The relation between n and n_0 in the presence of a single level of traps is

$$n/(n_0 - n) = n/n_t = N_c/N_t \exp - qE_t/kT, \tag{18}$$

where n_t is the number of trapped carriers, N_c and N_t are the conduction band and trap density of states, and E_t is the energy depth of the trap state in the forbidden gap.

The influence of the trapping centers upon photoconductive performance can be substantial. Indeed trapping effects usually are dominant factors determining the sensitivity and speed of response of experimental and commercial devices. Conversely, photoconductive performance can be used as a sensitive measure of the imperfection or trapping states in a semiconductive material. Again, reference should be made to the reviews by Bube for detailed discussions.

Perhaps the most graphic photoconductive measurement is that known as thermally stimulated current, or TSC. In this measurement the sample is cooled, usually to 77°K, irradiated with light, and then slowly warmed in the absence of light. While the sample is at the low temperature under

illumination, the above-mentioned trapping processes occur, but for those traps for which

$$E_t > k \ (77°\text{K})/e, \tag{19}$$

few carriers are reexcited into the conduction band until higher temperatures are reached. If the current produced by thermal excitation at a temperature T is plotted against T, a graphic representation of the trap levels is produced. A simple analysis has been given which easily relates the TSC measurement to the trap energy and density (211), but a detailed analysis is much more involved (212). Even so, the TSC spectra can be of exceptional value in following the effects of process variations (213).

Noise currents are the least explored of the kinetic evaluation methods. The results, as obtained, for example, by Jordan (214) on InAs films, confirm not only the presence of states revealed by photocurrent measurements (215), but indicate also other states not revealed by the photocurrent decay.

5. DEVICE APPLICATIONS

The role of semiconducting thin films in practical devices should be, if anything, greater than the role of bulk semiconductors, if we include homo-epitaxial films in our definition. Let us, however, exclude such films except for a brief paragraph below. Even so, the role of thin film materials promises to be large, encompassing signal generating, detecting, and amplifying functions. The signals may be electrical, optical, mechanical, or a combination thereof, but the indications at present are that the signals must be small. That is, it does not appear that heteroepitaxial films will play a part in high-power devices. Homoepitaxial silicon high-power devices are, however, already being marketed.

Exclusion of homoepitaxial devices means we will not discuss the many benefits of the "buried collector" technique for integrated circuits, nor will we consider the applications of Ge/Ge, or GaAs/GaAs structures. These exclusions are not based on special device characteristics, since advantages claimed for GaAs on sapphire, such as the advantage of having an insulating substrate for the device, apply also to GaAs on Cr-doped GaAs. Rather, the exclusion has been made because many of the special thin film problems that arise in heteroepitaxial films, that is, the special electrical effects that arise from interfacial dislocations, substrate autodoping, etc., simply do not arise in homoepitaxial films.*

* There are, of course, exceptions to this sweeping statement. For example, homo-epitaxial deposition of high-resistivity silicon onto heavily boron-doped silicon produces autodoping effects due to out-diffusion of the boron, and dislocations due to the gradient of lattice parameter from the heavily to lightly doped regions.

Earlier, in Table I, we listed applications of thin film semiconductors that are noted in a cursory examination of the literature. The typical device applications found are little concerned with details of the properties of the particular semiconductor film. Just as with bulk semiconductors, the important properties are band-gap energy, free carrier mobility and lifetime, etc., for which appropriate values can usually be realized in a number of materials. A few devices, of course, require specific types of band structure, such as Gunn and LSA diodes, or crystal structure, such as piezoelectric transducers.

Most of these applications involve but a single property of the semiconductor film, such as its semiconducting character. A few, however, represent a combination of phenomena, such as the metal insulator piezoelectric semiconductor (MIPS) device of Muller and Conragen (216) which combines piezoelectric activity with metal oxide semiconductor (MOS) transistor action. Muller proposes that a microphone could be made from such devices where the electronic amplifying structure was deposited directly on the microphone diaphragm. Further in this vein, perhaps the ultimate in polyfunctional thin film devices was reported by Hakki (217). He deposited a CdS film over a series of Cu stripes and achieved a scanning electroluminescent device that incorporated, in addition to electroluminescence, the phenomena of piezoelectricity, heterojunctions, and acoustic traveling waves.

In the next, final section of this review, an estimate of the future of semiconductor thin films is given. In large measure, it is based on an extrapolation of the recent history of these materials. That history, in terms of commercial applications, can be summarized as follows: successful applications have come only in areas where a competitive single-crystal device was not available. Only where such features as a particular spectral response, size, shape, weight, location, or other particular property was involved, and for which a bulk single-crystal device had not yet been evolved, have thin film devices successfully been exploited. Often, cost has been cited as an advantage for thin film devices, yet at present the greatest single cost factor in bulk single-crystal devices is the package used to provide the environmental protection, which is also needed by thin film devices. Nevertheless, the list of successful thin film devices, even without including the homoepitaxial variety, is impressive.

VI. Some Important Problem Areas

In this review we have discussed but a part of the extensive literature on semiconductor films, choosing topics which are representative of trends in current technology and recent research. In most instances, if such films are to be used in devices, one is concerned primarily with obtaining and controlling

electrical properties equivalent to those measured in the bulk single-crystal material. The thin film form simply conveys certain geometric advantages in the *in situ* formation of junctions or in permitting novel, small-volume devices to be fabricated rapidly and economically by vapor deposition. Unfortunately, the properties of films usually fall considerably short of those typical of the bulk crystal, and a significant proportion of research in this field has been devoted to explaining these departures. Except for certain well-crystallized homoepitaxial and heteroepitaxial films, such efforts have enjoyed only limited success.

Insofar as it is used in a wide range of devices covering diverse applications, silicon exemplifies most of the key problems encountered in thin film semiconductors. The most perfect silicon films available are those grown homoepitaxially under carefully controlled conditions. It is through more systematic research on homoepitaxial planar junction structures that our main hope lies in determining the true device potential of silicon. High-voltage power devices which require good crystal perfection over large junction areas and tight control of impurity profiles and minority carrier lifetimes present a special challenge in this respect. At present, although the experimental evidence suggests that epitaxial methods should yield better quality junctions than diffusion techniques, quality control problems still arise, due primarily to the high temperatures ($>1200°C$) usually employed for epitaxial growth. It is generally accepted that if these processing temperatures could be lowered to values at which the diffusion coefficients of, in particular, the lifetime-killing heavy metal impurities are low, optimum junction properties could be achieved. Ideally, growth temperatures should be lowered to about 700°C without sacrificing crystal perfection in the epitaxial layer. As shown in this review (75, 170) good-quality epitaxial growth at low temperatures is quite feasible under clean, well-controlled conditions. Indeed, recent studies in the authors' laboratories (218) have demonstrated that excellent diode characteristics can be obtained in junctions grown at 550°C. The potential value of low-temperature processing methods in the high-frequency device field, where abrupt junctions are essential, cannot be overestimated. With new device trends calling for higher power and frequency capability it appears certain that low-temperature epitaxial growth methods will occupy a key place in the field of semiconductor film research.

The above comments might equally well be applied to the problems involved in heteroepitaxial structures, whether they comprise heterojunctions or simply semiconductor films supported on insulating substrates. Thus, lower-temperature growth methods would be of great value in reducing inter-diffusion effects which cause anomalous junction properties in hetero-junctions (46), and which lead to autodoping in heteroepitaxial films on insulator crystals (35). By maintaining very clean chemical growth conditions

or by depositing the films in ultrahigh vacuum it should certainly be possible to improve the perfection of heteroepitaxial films grown on semiconductor substrates (41) and probably to lower the epitaxy temperature. However, it is probable that in the case of growth on insulator substrates, film perfection and epitaxy temperature will be limited more by substrate perfection attainable than by impurities.

Based upon the considerable efforts thus far made with silicon, although considerable improvements may yet be made in the quality of heteroepitaxial films, it seems unlikely that they will achieve the same level of perfection as homoepitaxial films. With silicon on insulating substrates this implies certain limitations in the device structures that can be produced. The higher levels of crystal imperfections in such films have tended to confine their application to unipolar- or MOS-type devices where the junctions are normal to the film surface. Attempts to make bipolar devices by diffusion enjoy limited success due to the fact that the crystal imperfectious act as diffusion pipes and short-circuit paths. It may again be possible to overcome this problem, however, by developing effective low-temperature homoepitaxy techniques and employing these to form subsequent p- or n-doped layers on the heteroepitaxial layer under conditions which minimize interdiffusion effects.

Turning now to the status of polycrystalline semiconductor films (used, for example, as phosphor coatings or in TFT devices), efforts thus far have been devoted primarily to improving reproducibility and uniformity of properties rather than to obtaining optimum bulk-type properties. This is perhaps unfortunate since, as device requirements become more demanding, it is increasingly apparent that systematic experimental and theoretical studies which might permit a controlled improvement in material and device parameters are simply not available. The situation is exemplified by recent and current developments in the TFT device field (10, 192–194). The numerous studies on TFT devices made with films of CdS (10) and InAs (192) have demonstrated that to achieve high gain at high frequencies (in the megacycle range) it is necessary to obtain reproducibly films possessing high mobility with low carrier concentrations. The films should be of uniform thickness with smooth surfaces so as to avoid nonuniformity in the field applied at the gate electrode. Also to dissipate the power generated in high-frequency operation (which might otherwise cause irreversible thermally induced structural and electrical changes) the devices should be deposited on substrates possessing high thermal conductivity.

A clearer understanding of the factor influencing the performance of TFT devices might be obtained by studying structures in which the crystalline perfection and chemical purity of the films are optimized, for example by growing the semiconductor in thin epitaxial form under very clean vacuum

conditions. With such films it should be possible to investigate systematically the role of crystal structure and interface effects in influencing the electrical parameters and to establish clearer objectives for the levels of device performance ultimately attainable.

REFERENCES

1. W. R. Turnbull, Semiconducting thin films—an annotated bibliography, NOLC Rept. 712 (June 1967); 745 (March 1968).
2. W. C. Dunlap, "An Introduction to Semiconductors." Wiley, New York, 1957.
3. H. K. Henisch, "Rectifying Semiconductor Contacts." Oxford Univ. Press, London and New York, 1957.
4. V. K. Zworykin and E. G. Ramberg, "Photoelectricity and Its Applications." Wiley, New York, 1949.
5. J. N. Shive, "Semiconductor Devices." Van Nostrand, Princeton, New Jersey, 1959.
6. R. W. Redington, *J. Appl. Phys.* **29**, 189 (1958).
7. A. Rose, "Concepts in Photoconductivity." Wiley (Interscience), New York, 1963.
8. M. A. Lampert, *Rept. Prog. Phys.* **27**, 329 (1964).
9. W. Shockley and G. L. Pearson, *Phys. Rev.* **74**, 232 (1948).
10. P. K. Weimer, *IRE Trans. Electron Devices* ED-8, 421 (1961); see also P. K. Weimer, "Physics of Thin Films" (G. Haas and R. E. Thun, eds.), Vol. 2, p. 148. Academic Press, New York, 1964.
11. R. Glang and E. S. Wajda, *Conf. AIME Met. Soc.* **15**, 27 (J. B. Schroeder, ed.). Wiley (Interscience), New York, 1961.
12. A. S. Grove, "Physics and Technology of Semiconductor Devices." Wiley, New York, 1967.
13. E. W. Mehal, *Trans. Met. Soc. AIME* **242**, 452 (1968).
14. J. F. Allison, F. P. Heiman, and J. R. Burns, *IEEE. Solid State Circuits* SC-2, 208 (1967).
15. P. H. Robinson and D. J. Dumin, *J. Electrochem. Soc.* **115**, 75 (1968).
16. B. Schwartz, *in* "Vapor Deposition" (C. F. Powell, J. H. Oxley, and J. M. Blocher, Jr., eds.), p. 612. Wiley, New York, 1966.
17. C. H. Li, *Phys. Status Solidi* **15**, 3, 419 (1966).
18. B. A. Joyce, *in* "The Use of Thin Films in Physical Investigations" (J. C. Anderson, ed.), p. 87. Academic Press, London, 1966.
19. A. Miller and H. M. Manasevit, *J. Vacuum Sci. Technol.* **3**, 68 (1966).
20. J. D. Filby and S. Nielsen, *Brit. J. Appl. Phys.* **18**, 1357 (1967).
21. H. C. Theurer, *J. Electrochem. Soc.* **108**, 649 (1961).
22. H. C. Theurer, *J. Electrochem. Soc.* **109**, 742 (1962).
23. B. A. Joyce and R. R. Bradley, *J. Electrochem. Soc.* **110**, 1235 (1963).
24. E. S. Wajda, B. W. Kippenham, and W. H. White, *IBM J. Res. Develop.* **4**, 288 (1960).
25. E. S. Wajda and R. Glang, *Conf. AIME Met. Soc.* **12**, 229 (R. O. Grubel, ed.). Wiley, (Interscience), New York, 1961.
26. F. A. Pizzarello, *J. Electrochem. Soc.* **110**, 1059 (1963).

27. R. R. Moest and B. R. Shupp, *J. Electrochem. Soc.* **109**, 1061 (1962).
28. H. Holloway, K. Wollmann, and A. S. Joseph, *Phil. Mag.* **11**, 110 (1965).
29. C. J. Frosch and C. D. Thurmond, *J. Electrochem. Soc.* **109**, 301C (1962).
30. C. J. Frosch, *J. Electrochem. Soc.* **111**, 180 (1964).
31. J. R. Knight, D. Effer, and P. R. Evans, *Solid State Electron.* **8**, 178 (1965).
32. H. M. Manasevit and W. I. Simpson, Meeting Electrochem. Soc., Extended Abstr. No. *63* (May 1968); H. M. Manasevit, *Appl. Phys. Letters* **12**, 156 (1968).
33. H. M. Manasevit, A. Miller, F. L. Morritz, and R. L. Nolder, *Trans. Met. Soc. AIME* **233**, 540 (1965).
34. B. A. Joyce, R. J. Bennett, R. W. Bicknell, and P. J. Etter, *Trans. Met. Soc. AIME* **233**, 556 (1965).
35. D. J. Dumin, *J. Appl. Phys.* **38**, 1909 (1967).
36. C. C. Wang, G. W. Cullen, E. G. Gottlieb, S. H. McFarlane III, and K. H. Zaininger, Tech. Management Rept. 1–3, F33615–68–C–1025 (1968).
37. Autonetics Final Rept., Single-crystal silicon films on insulating substrates, NOBsr 93145 (May, 1968).
38. P. B. Hart, P. J. Etter, B. W. Jervis, and J. M. Flanders, *Brit. J. Appl. Phys.* **18**, 1389 (1967).
39. D. J. Dumin, *J. Electrochem. Soc.* **114**, 739 (1967).
40. J. Brownson, *Trans. Met. Soc. AIME* **233**, 450 (1965).
41. L. C. Bobb, H. Holloway, K. H. Maxwell, and E. Zimmerman, *J. Appl. Phys.* **37**, 4687 (1966).
42. M. Weinstein, R. O. Bell, and A. A. Menna, *J. Electrochem. Soc.* **111**, 674 (1964).
43. D. M. Jackson, Jr. and R. W. Howard, *Trans. Met. Soc. AIME* **233**, 468 (1965).
44. F. J. Reid, S. E. Miller, and H. L. Goering, *J. Electrochem. Soc.* **113**, 467 (1966).
45. T. L. Chu, D. W. Ing, and A. J. Noreika, *Solid State Electron.* **10**, 1023 (1967).
46. R. L. Longini and D. L. Feucht, *Trans. Met. Soc. AIME* **233**, 443 (1965).
47. D. R. Hamilton, *J. Electrochem. Soc.* **105**, 735 (1958).
48. R. B. Campbell and T. L. Chu, *J. Electrochem. Soc.* **113**, 825 (1966).
49. J. Whitaker, *Solid-State Electron.* **8**, 649 (1965).
50. D. E. Bolger and B. E. Berry, *Nature* **199**, 1287 (1963).
51. G. A. Cox, D. O. Cummins, K. Kawabi, and R. H. Tredgold, *J. Phys. Chem. Solids* **28**, 543 (1967).
52. J. Pastrňak and L. Součková, *Phys. Status Solidi* [2] **3**, K71 (1963).
53. A. J. Noreika and D. W. Ing, Growth characteristics of AlN films pyrolytically deposited on Si, *J. Appl. Phys.* **39**, 5578 (1968).
54. B. Lewis and D. S. Campbell, *J. Vacuum Sci. Technol.* **4**, 209 (1967).
55. F. V. Williams and R. A. Ruehrwein, *J. Am. Chem. Soc.* **82**, 1330 (1960).
56. A. F. Armington, *J. Crystal Growth* **1**, 47 (1967).
57. S. M. Ku, *J. Electrochem. Soc.* **113**, 813 (1967).
58. M. J. Rand and J. F. Roberts, *J. Electrochem. Soc.* **115**, 423 (1968).
59. S. Dushman, "Scientific Foundations of Vacuum Technique" (J. M. Lafferty, ed.), 2nd ed. Wiley, New York, 1962.
60. L. Holland, *in* "Thin Film Microelectronics" (L. Holland, ed.), p. 108. Chapman and Hall, London, 1965.
61. F. Jona, *Appl. Phys. Letters* **1**, 235 (1966).
62. B. W. Sloope and C. O. Tiller, *J. Appl. Phys.* **33**, 3458 (1962); *Trans. Natl. Vacuum Symp.*, *10th* p. 339 (G. H. Bancroft, ed.). Macmillan, New York, 1963.
63. B. W. Sloope and C. O. Tiller, *J. Appl. Phys.* **38**, 140 (1967).
64. J. E. Davey, *J. Appl. Phys.* **32**, 877 (1960).

65. J. E. Davey, R. J. Tiernan, T. Pankey, and M. D. Montgomery, *Solid State Electron.* **6**, 205 (1963).

66. R. R. Humphris and A. Catlin, *Solid State Electron.* **8**, 957 (1965).

67. A. Catlin and R. R. Humphris, *Proc. Intern. Symp. Basic Problems, Thin Film Phys.* p. 175 (R. Niedermayer and H. Mayer, eds.). Vandenhoeck and Rupprecht, Gottingen, 1965.

68. J. C. Courvoisier, W. Haidinger, P. J. W. Jochems, and L. J. Tummers, *Solid State Electron.* **6**, 265 (1963).

69. G. G. Via and R. E. Thun, *Trans. Natl. Vacuum Symp. 8th*, p. 950 (L. E. Preuss, ed.). Pergamon Press, Oxford, 1961.

70. L. N. Butorina and V. A. Tolomasov, *Soviet Phys. Cryst.* (*English Transl.*) **10**, 456 (1966).

71. B. A. Unvala, *Le Vide* **104**, 109 (1963).

72. G. R. Booker and B. A. Unvala, *Phil. Mag.* **11**, 11 (1965).

73. C. A. T. Salama, T. W. Tucker, and L. Young, *Solid State Electron.* **10**, 339 (1967).

74. H. Widmer, *Appl. Phys. Letters* **5**, 105 (1964).

75. R. N. Thomas and M. H. Francombe, *Appl. Phys. Letters* **11**, 134 (1967).

76. E. T. Handelman and E. I. Povilonis, *J. Electrochem. Soc.* **111**, 201 (1964).

77. O. S. Heavens and C. H. Griffiths, *Acta Cryst.* **18**, 532 (1965).

78. L. Holland, "Vacuum Deposition of Thin Films," pp. 112–113, 246, 503. Wiley, New York, 1960.

79. Yin Shih-Duan' and A. R. Regel', *Soviet Phys. Solid State* (*English Transl.*) **3**, 1220 (1961).

80. R. E. Thun and J. B. Ramsey, *Trans. Natl. Vacuum Symp.*, *6th* p. 192. Pergamon Press, Oxford, 1959.

81. W. Reichelt and G. F. P. Mueller, *Trans. Natl. Vacuum Symp.*, *8th* (L. E. Preuss, ed.) Vol. 2, p. 956. Pergamon Press, Oxford, 1961.

82. P. H. Keck, *J. Opt. Soc. Am.* **42**, 221 (1952).

83. N. F. Foster, *J. Appl. Phys.* **38**, 149 (1967).

84. R. R. Addiss, Jr., *Trans. Natl. Vacuum Symp.*, *10th*, p. 354 (G. H. Bancroft, ed.). Macmillan, New York, 1963.

85. J. Dresner and F. V. Shallcross, *J. Appl. Phys.* **34**, 2390 (1963).

86. J. Nickerson and P. Goldberg, *Trans. Natl. Vacuum Symp.*, *10th* (G. H. Bancroft, ed.), p. 475. Macmillan, New York, 1963.

87. W. M. Kane, J. P. Spratt, L. W. Hershinger and I. H. Khan, *J. Electrochem. Soc.* **113**, 136 (1966).

88. K. Shimizu, *Japan. J. Appl. Phys.* **4**, 627 (1965).

89. R. Glang, J. G. Kren, and W. J. Patrick, *J. Electrochem. Soc.* **110**, 407 (1963).

90. K. V. Shalimova, A. F. Andrushko, and I. Dima, *Soviet Phys. Cryst.* (*English Transl.*) **10**, 414 (1966).

91. D. B. Holt, *Brit. J. Appl. Phys.* **17**, 1395 (1966).

92. R. B. Schoolar and J. N. Zemel, *J. Appl. Phys.* **35**, 1848 (1964).

93. J. N. Zemel, *in* "The Use of Thin Films in Physical Investigations" (J. C. Anderson, ed.), p. 319. Academic Press, London, 1966.

94. H. Gobrecht, K. E. Boeters, and H. J. Fleischer, *Z. Phys.* **187**, 232 (1965).

95. L. S. Palatnik, V. K. Sorokin, and M. D. Lebedeva, *Soviet Phys. Solid State* (*English Transl.*), **7**, 1374 (1965).

96. E. B. Dale, G. Senecal, and D. Huebner, *Trans. Natl. Vacuum Symp.*, *10th* p. 348 (G. H. Bancroft, ed.). Macmillan, New York, 1963.

97. W. J. Williamson, *Solid State Electron.* **9**, 213 (1966).

98. S. A. Semiletov and L. I. Man, *Kristallografiya* **5**, 314 (1960).
99. S. A. Semiletov, *Tr. Inst. Kristallogr. Akad. Nauk SSSR* **10**, 76 (1954).
100. C. Paparoditis, *J. Phys.* **25**, 226 (1964).
101. V. E. Schmaevskii and A. G. Mikolaichuk, *Fiz. Metal. Metalloved.* **16**, 941 (1963).
102. K. G. Günther, *in* "Compound Semiconductors" (R. K. Willardson and H. L. Goering, eds.), p. 313. Reinhold, New York, 1962.
103. K. G. Günther, *in* "The Use of Thin Films in Physical Investigations" (J. C. Anderson, ed.), p. 213. Academic Press, London, 1966.
104. R. F. Potter and G. G. Kretschmar, *J. Opt. Soc. Am.* **51**, 693 (1961).
105. J. E. Davey and T. Pankey, *J. Appl. Phys.* **35**, 2203 (1964).
106. T. Pankey and J. E. Davey, *J. Appl. Phys.* **37**, 1507 (1966).
107. R. P. Howson, *J. Phys.* **25**, 212 (1964).
108. J. E. Johnson, *J. Appl. Phys.* **36**, 3193 (1965).
109. J. P. David, L. Capella, L. Laude, and S. Martinuzzi, *Rev. Phys. Appl.* **1**, 172 (1966).
110. J. de Klerk and E. F. Kelly, *Rev. Sci. Instr.* **36**, 506 (1965).
111. J. E. Davey and T. Pankey, *Appl. Phys. Letters* **12**, 38 (1968).
112. J. E. Davey and T. Pankey, *J. Appl. Phys.* **39**, 1941 (1968).
113. J. L. Richards, *in* "The Use of Thin Films in Physical Investigations" (J. C. Anderson, ed.), p. 71. Academic Press, London, 1966.
114. J. L. Richards, P. B. Hart, and L. M. Gallone, *J. Appl. Phys.* **34**, 3418 (1963).
115. E. K. Müller and J. L. Richards, *J. Appl. Phys.* **35**, 1233 (1964).
116. S. A. Aitkozhin and S. A. Semiletov, *Soviet Phys. Cryst. (English Transl.)* **10**, 409 (1966).
117. P. Bourgeois and P. Moch, *Le Vide* **119**, 376 (1965).
118. S. G. Ellis, *J. Appl. Phys.* **38**, 2906 (1967).
119. R. Ludeke and W. Paul, *J. Appl. Phys.* **37**, 3499 (1966).
120. S. Mader, *in* "The Use of Thin Films in Physical Investigations" (J. C. Anderson, ed.), p. 433. Academic Press, London, 1966.
121. M. H. Francombe, *in* "Basic Problems in Thin Film Physics" (R. Niedermayer and H. Mayer, eds.), p. 52. Vandenhoeck and Ruprecht, Gottinger, 1966.
122. M. H. Francombe, *in* "The Use of Thin Films in Physical Investigations" (J. C. Anderson, ed.), p. 29. Academic Press, London, 1966.
123. L. Maissel, *in* "Physics of Thin Films" (G. Haas and R. E. Thun, eds.), Vol. 3, p. 61. Academic Press, New York, 1966.
124. R. Frerichs, *J. Appl. Phys.* **33**, 1898 (1962).
125. F. Reizman and H. Basseches, *in* "Metallurgy of Semiconductor Materials" (J. B. Schroeder, ed.), p. 169. Wiley (Interscience), New York, 1962.
126. K. E. Haq, *J. Electrochem. Soc.* **112**, 500 (1965).
127. E. Krikorian, *in* "Single-Crystal Films" (M. H. Francombe and H. Sato, eds.), p. 113. Pergamon Press, Oxford, 1964.
128. E. Krikorian and R. J. Sneed, *J. Appl. Phys.* **37**, 3665 (1966).
129. S. P. Wolsky, T. R. Piwkowski, and G. Wallis, *J. Vacuum Sci. Technol.* **2**, 97 (1965).
130. G. Wallis, S. P. Wolsky, and E. Pittelli, Investigation of ultra high vacuum sputtered thin films, Contract No. AF 19(628)–3840. Nov. 30 (1965).
131. G. Moulton, *Nature* **195**, 793 (1962).
132. M. H. Francombe, J. J. Flood, and G. L'E. Turner, *Intern. Congr. Electron Microscopy 5th, Philadelphia, 1962*, **1**, DD-8. Academic Press Inc., New York 1962.
133. B. Molnar, J. J. Flood, and M. H. Francombe, *J. Appl. Phys.* **35**, 3554 (1965).
134. T. Evans and A. J. Noreika, *Phil. Mag.* **13**, 717 (1966).
135. M. H. Francombe, *Phil. Mag.* **10**, 989 (1964).

136. H. Kraus, S. G. Parker, and J. P. Smith, *J. Electrochem. Soc.* **114**, 616 (1967).
137. T. K. Lakshmanan and J. M. Mitchell, *Trans. Natl. Vacuum Symp., 10th* (G. H. Bancroft, ed.), p. 335. Macmillan, New York, 1963.
138. T. O. Poehler and G. B. Gilbert, Jr., *in* "Single Crystal Films" (M. H. Francombe and H. Sato, eds.), p. 129. Pergamon Press, Oxford, 1964.
139. J. Maserjian, *Solid State Electron.* **6**, 477 (1963).
140. G. T. Naber, *J. Electrochem. Soc.* **114**, 406 (1967).
141. S. Nielsen, *J. Electrochem. Soc.* **112**, 534 (1965); J. D. Filby and S. Nielsen, *ibid.* **112**, 535 (1965).
142. A. Vecht, *in* "Physics of Thin Films" (G. Hass and R. E. Thun, eds.), Vol. 3. p. 165, Academic Press, New York, 1966.
143. J. M. Gilles and J. Van Cakenberghe, *Solid State Phys. Electron. Telecommun.* **2**, Pt. 2, *Semiconductors* p. 900 (M. Désirant and J. L. Michiels, eds.). Academic Press, New York, 1960.
144. Te Velde, *Electrochem. Abstr. (Luminescence, Toronto Meeting, Electrochem. Soc.)* **13**, 70 (1964).
145. H. H. Wieder and A. R. Clawson, *Solid-State Electron.* **8**, 467 (1965).
146. H. H. Wieder, *Solid-State Commun.* **3**, 159 (1965).
147. J. A. Carroll and J. F. Spivak, *Solid State Electron.* **9**, 383 (1966).
148. H. H. Wieder, *Proc. Intern. Symp. Basic Problems Thin Film Phys.* p. 719 (R. Neidermayer and H. Mayer, eds.). Vandenhoeck and Ruprecht, Gottingen (1966).
149. R. L. Barns and W. C. Ellis, *J. Appl. Phys.* **36**, 2296 (1965).
150. H. F. John, J. W. Faust, Jr., and R. Stickler, *IEEE Trans. Parts, Materials Packaging* **PMP-2**, 51 (1966).
151. J. W. Faust, Jr., *in* "The Surface Chemistry of Metals and Semiconductors" (H. C. Gatos, ed.), p. 151. Wiley, New York, 1960.
152. S. Mendelson, *J. Appl. Phys.* **35**, 1570 (1964).
153. J. M. Charig, B. A. Joyce, D. J. Stirland, and R. W. Bicknell, *Phil. Mag.* **7**, 1847 (1962).
154. W. C. Dash, *J. Appl. Phys.* **27**, 1193 (1956).
155. W. Shockley, *Solid State Electron.* **2**, 35 (1961).
156. G. R. Booker and R. Stickler, *Brit. J. Appl. Phys.* **13**, 446 (1962).
157. G. R. Booker, *J. Appl. Phys.* **37**, 441 (1966).
158. W. Czaja and J. R. Patel, *J. Appl. Phys.* **36**, 1476 (1965).
159. R. B. Ogilvie, *in* "Introduction to Electron Beam Technology" (R. Bakish, ed.), p. 413. Wiley, New York, 1962.
160. M. J. Stowell, *in* "The Use of Thin Films in Physical Investigations" (J. C. Anderson, ed.), p. 131. Academic Press, New York, 1966.
161. H. Holloway, *in* "The Use of Thin Films in Physical Investigations" (J. C. Anderson, ed.), p. 111. Academic Press, New York, 1966.
162. H. E. Farnsworth, R. E. Schlier, T. H. George, and R. M. Burger, *J. Appl. Phys.* **29**, 1150 (1958).
163. J. J. Lander and J. Morrison, *J. Appl. Phys.* **34**, 1403 (1963).
164. A. R. Lang, *J. Appl. Phys.* **30**, 1748 (1959); **29**, 597 (1958).
165. G. H. Schwuttke and V. Sils, *J. Appl. Phys.* **34**, 3127 (1963).
166. H. Holloway and L. C. Bobb, *J. Appl. Phys.* **38**, 2711 (1967).
167. E. Bauer, *in* "Single-Crystal Films" (M. H. Francombe and H. Sato, eds.), p. 43. Pergamon Press, Oxford, 1964.
168. T. N. Rhodin, *in* "The Use of Thin Films in Physical Investigations" (J. C. Anderson, ed.). p. 187. Academic Press, New York, 1966.
169. B. A. Joyce, R. R. Bradley, and G. R. Booker, *Phil. Mag.* **15**, 1167 (1967).

170. R. N. Thomas and M. H. Francombe, Low-temperature epitaxy of silicon junctions by ultrahigh vacuum techniques, F33615–68–C–1058. Techn. Management Rept. 1 and 2 (1968).
171. C. K. Layton and K. B. Cross, *Thin Solid Films* 1, 169(L) (1967).
172. R. F. Adamsky, K. H. Behrndt and W. T. Brogan, *J. Vacuum Sci. Technol.* (in press).
173. R. L. Nolder and I. B. Cadoff, *Trans. Met. Soc. AIME* 233, 549 (1965).
174. R. L. Tallman, T. L. Chu, G. A. Gruber, J. J. Oberly, and E. D. Wolley, *J. Appl. Phys.* 37, 1588 (1966).
175. D. W. Pashley, *in* "Modern Developments in Electron Microscopy" (B. M. Siegel, ed.), p. 149. Academic Press, New York, 1964.
176. R. L. Nolder, D. J. Klein, and D. H. Forbes, *J. Appl. Phys.* 36, 3444 (1965).
177. G. R. Booker and R. Stickler, *J. Appl. Phys.* 33, 3281 (1962).
178. G. R. Booker, *Phil. Mag.* 11, 1007 (1965).
179. J. H. Van der Merwe, *in* "Single-Crystal Films" (M. H. Francombe and H. Sato, eds.), p. 139. Pergamon Press, Oxford, 1964.
180. D. J. Dumin, *J. Appl. Phys.* 36, 2700 (1965).
181. E. H. Putley, "The Hall Effect and Reflected Phenomena." Butterworths, London and Washington, D.C., 1960.
182. K. G. Günther, *Naturwissenschaften* 45, 415 (1958).
183. J. J. Tietjen and L. R. Weisberg, *Appl. Phys. Letters* 7, 261 (1965).
184. F. V. Shallcross, *RCA Rev.* 24, 676 (1963).
185. O. D. Elpat'evskaya, *Soviet Phys. Tech. Phys. (English Transl.)* 3, 2439 (1958).
186. J. P. McCarthy, *Solid State Electron.* 10, 649 (1967).
187. R. L. Ramey and W. D. McLennan, *J. Appl. Phys.* 38, 3491 (1967).
188. A. B. Phillips, "Transistor Engineering." McGraw-Hill, New York, 1962.
189. B. W. Sloope and C. O. Tiller, *J. Appl. Phys.* 37, 887 (1966).
190. Y. Sakai and K. Takahashi, *Japan. J. Appl. Phys.* 2, 629 (1963).
191. J. E. Davey, *Appl. Phys. Letters* 8, 164 (1966).
192. H. E. Kunig, unpublished results; H. E. Kunig and T. P. Brody, *Appl. Phys. Letters* 9, 259 (1966).
193. P. Richman, "Characteristics and Operation of MOS Field-Effect Devices." McGraw-Hill, New York, 1967.
194. J. T. Wallmark and H. Johnson, "Field-Effect Transistors." Prentice-Hall, Englewood Cliffs, New Jersey, 1966.
195. H. L. Wilson and W. A. Gutierrez, *J. Electrochem. Soc.* 112, 85 (1965).
196. F. Fang and S. Triebwasser, *Appl. Phys. Letters* 4, 145 (1964).
197. H. H. Wieder, *Solid State Electron.* 9, 373 (1966).
198. D. L. Dexter and F. Seitz, *Phys. Rev.* 86, 964 (1952).
199. H. Berger, *Phys. Status Solidi*, 1, 739 (1961).
200. A. Waxman, V. E. Henrich, F. V. Shallcross, H. Borkan, and P. K. Weimer, *J. Appl. Phys.* 36, 168 (1965).
201. T. Hara and I. Akasaki, *J. Appl. Phys.* 39, 285 (1968).
202. R. L. Longini and R. F. Greene, *Phys. Rev.* 102, 992 (1956).
203. A. Many, M. Simhony, and Y. Grushkevitz, *J. Phys. Chem. Solids* 26, 1925 (1965).
204. W. Ehrenberg, V. B. Gutan, and L. K. Vodopynov, *Brit. J. Appl. Phys.* 17, 63 (1966).
205. J. L. Moll, "Physics of Semiconductors." McGraw-Hill, New York, 1964.
206. A. M. Goodman and D. M. Perkins, *J. Appl. Phys.* 35, 3351 (1964).
207. A. Waxman, *J. Appl. Phys.* 38, 4763 (1967).
208. C. A. Mead and W. G. Spitzer, *Appl. Phys. Letters* 2, 74 (1963).

209. M. H. Francombe, J. E. Johnson, A. J. Noreika, and S. A. Zeitman, *Quart. Rept.*, Contract NAS 12–568 (1968).
210. R. K. Willardson and A. C. Beer, eds., Optical Properties of III–V Compounds "Semiconductors and Semimetals," Vol. 3. Academic Press, New York, 1967.
211. R. H. Bube, "Photoconductivity of Solids." Wiley, New York, 1960.
212. P. N. Keating, *Proc. Phys. Soc.* **78**, 1408 (1961).
213. J. S. Skarman, *Solid State Electron.* **8**, 17 (1965).
214. N. A. Jordan, *Solid State Electron.* **10**, 503 (1967).
215. N. A. Jordan, *J. Appl. Phys.* **38**, 2710 (1967).
216. R. S. Muller and J. Conragen, *Appl. Phys. Letters* **6**, 83 (1965).
217. B. W. Hakki, *Appl. Phys. Letters* **11**, 153 (1967).
218. R. N. Thomas and M. H. Francombe, *Appl. Phys. Letters* **13**, 270 (1968).
219. F. J. Morin, *Phys. Rev.* **93**, 62 (1954).
220. E. M. Connell and V. F. Weisskopf, *Phys. Rev.* **77**, 388 (1950).

The Preparation of Films by Chemical Vapor Deposition

W. M. FEIST, S. R. STEELE, AND D. W. READEY

Research Division
Raytheon Company
Waltham, Massachusetts

I. Introduction

The increasing interest in thin films of compounds, and in thin films of a highly ordered crystalline structure, has brought about a widespread acceptance of chemical vapor deposition as a means for the formation of thin films. In many instances, this method now competes strongly with the more conventional processes of physical vapor deposition, namely, evaporation and sublimation in a high or a partial vacuum and sputtering in an inert or reactive gaseous atmosphere, and with wet plating. The major impact of chemical vapor deposition on thin film technology took place when it was demonstrated nearly a decade ago that epitaxial layers of silicon and germanium could be grown by this method. Since then it has been successfully used for the formation of a variety of layers: compound semiconductors such as GaAs, GaP, SiC, and others; various insulator, conductor, and resistor materials, particularly those which became important in connection with semiconductor and integrated circuit technology; and ferrites.

Many excellent, more or less specialized surveys of the field of chemical vapor deposition and its applications to the area of thin film or layer

formation do already exist (*1–5*).* The present authors will make an attempt to present as broad a survey as possible of the work that has been abundantly published on this subject, including recent developments not covered in previous surveys. It is intended to provide an introduction to readers less familiar with chemical vapor deposition and its relationship to the field of thin films and layers.

Basically, chemical vapor deposition involves exposure of the substrate to be coated to one or several vaporized compounds, or reagent gases, some or all of which contain constituents of the material to be deposited. A chemical reaction is then initiated, preferably near or on the substrate surface, producing the desired material as a solid-phase reaction product which condenses on the substrate. Activation of the chemical reaction can be accomplished by various means such as the application of heat, an rf field, light or x-ray radiation, an electrical arc, electron bombardment, or catalytic action of the substrate surface. The nature of the chemical reaction and the activation mechanism may greatly influence the morphology of the deposited layer.

Adjusting the deposition conditions so that the reaction takes place near or on the substrate surface (called heterogeneous reaction) is important for avoiding the formation of a powdery deposit, which will result if the reaction takes place in the gas phase (called homogeneous reaction). The latter type of reaction has an important application in the production of pigments (*6*).

Chemical vapor deposition has much in common with the physical vapor deposition processes of condensing a substance after its evaporation by heating or sputtering, since in every case the deposit is formed from a vapor phase. In fact, the boundaries between chemical and physical vapor deposition processes become hard to define if one considers evaporation by heat, or sputtering, in a reactive atmosphere; coevaporation of substances which react with each other; or deposition in vacuum with a subsequent conversion of the deposited material by a chemical reaction activated, e.g., by electron bombardment or any one of the other above-mentioned stimuli. Perhaps the clearest distinction between chemical vapor deposition and physical vapor deposition processes can be made on this basis: in chemical vapor deposition formation of a deposit occurs as a result of a chemical reaction near or on the substrate surface, without involving a mean free path of the gas molecules larger than or comparable with the dimensions of the deposition chamber as a prime necessity for the functioning of the deposition process. However, it should be pointed out that chemical vapor deposition may be carried out at low pressures or in a high vacuum, e.g., for reasons tied to the desired

---

* Reference (*1*) is particularly comprehensive; it covers all aspects of chemical vapor deposition.

structure of the deposit or to the effective transporting of the reactant species to or away from the substrate.

Aside from the special morphological features of the deposit obtainable with chemical vapor deposition, the use of the latter has the following major advantages and disadvantages:

Advantages:

1. No vacuum or pumping facilities are required, in general; because of this, a relatively simple setup and fast recycle times are often possible.

2. Deposition rates are generally much larger than those obtained by physical evaporation.

3. Depositing compounds and controlling their stoichiometry is relatively easy.

4. Doping of the deposit with controlled amounts of impurities is fairly easy.

5. Refractory materials can be deposited without the need to create the very high temperatures which would be necessary for their thermal evaporation.

6. Epitaxial layers of high perfection and small unintentional impurity content can be deposited without much difficulty.

7. Objects of complex shape can be coated (e.g., the inside of a cylinder).

8. An *in situ* chemical vapor etching of substrates prior to their receiving a deposit is possible.

Disadvantages:

1. Frequently, the details of thermodynamics and the reaction kinetics involved in the deposition process are very complex and little understood or unpredictable.

2. Usually, much higher substrate temperatures are required for chemical vapor deposition than for physical vapor deposition.

3. The reactive gases used for the deposition process and their reaction products are often highly toxic, explosive, or corrosive, and have to be properly handled and disposed of.

4. It is often difficult to obtain or store supplies of the reactive source materials.

5. Because of the corrosive nature of the vapors involved in the deposition process, the substrate as well as the deposit may be attacked. Similarly, the materials of which the feeding lines or other parts of the deposition setup are made may also be attacked, and the generation of volatile products in such a reaction may lead to the incorporation of impurities into the growing film.

6. If high deposition temperatures are required in the deposition process undesired diffusion, alloying, or chemical reaction processes may occur on the substrate surface. The doping profile in the substrate may become

affected, or an undesired interface layer may form. The selection of substrates is limited by the high deposition temperature.

7. The uniformity of the deposit is frequently hard to control.

8. The masking of substrate areas from deposition is difficult.

9. By-products of the reaction may settle down in undesirable places, in the deposition apparatus, and their removal may be inconvenient.

Let us look at the historic development of chemical vapor deposition practices. An example of an early use of this method is the refinement and deposition of silicon as carried out in the early part of the nineteenth century; it utilized the reduction of silicon tetrafluoride or silicon tetrachloride with sodium or potassium (7). In the latter part of the nineteenth century, Sawyer and Man (8) deposited pyrolytic carbon, and Aylsworth (9) and deLodyguine (10) strengthened the carbon filaments of incandescent lamps with chemical vapor-deposited metals. In subsequent developments, a great technical impact resulted from the discovery by Mond (11, 12) that nickel could be transported and refined easily by means of nickel carbonyl. The success of this method stimulated further investigations into the refinement and deposition of many other materials, among them the refractory metals such as tantalum, titanium, and zirconium, and into the underlying thermodynamics and reaction kinetics (13). The particular attractiveness of the chemical vapor transport method derives from the fact that the desired material can be preferentially carried away from a contaminated source by means of a chemical vapor, while the temperatures involved in the refinement operation are much below the temperature which would be necessary for distillation by physical evaporation.

Starting in the 1930's, increasing emphasis was also placed on the chemical vapor deposition of refractory compounds, such as metal carbides, nitrides, silicides, borides, and oxides, as well as of sulfides, selenides, tellurides, intermetallic compounds and alloys, and on the production of pigments such as silicon dioxide and titanium oxide. The refractory coatings were primarily of interest for improving the corrosion resistance of the coated material, e.g., nuclear fuel, or crucible material. But in addition, thick coatings were formed from which parts could be machined. Examples are boron nitride and pyrolytic graphite. More recently, much work is being done on forming bodies of complex shapes (e.g., rocket nose cones) of refractory metals or compounds by chemical vapor deposition onto mandrels, frequently made of graphite (14).

In the area of electronics, the earliest application of chemical vapor deposition appears to have been the preparation of highly purified germanium and silicon, and providing a carbon coating for susceptors used in zone refining, e.g., germanium or indium antimonide. When the formation of epitaxial layers of semiconductors became desirable, chemical vapor deposition proved to be the most convenient method for preparing them, offering particular advantages with respect to the deposition rate, the quality of the

deposits, the control of the doping levels, and the deposition of compound semiconductors. It was mainly through this work on epitaxial semiconductors that chemical vapor deposition became widely known as a means for growing thin layers. Its general use has since been extended to the deposition of a variety of films, including insulators, conductors, resistors, varistors, and ferrites.

II. Chemical Processes Used in Chemical Vapor Deposition

Basically, any chemical reaction between one or several reactive vapors which leads to a solid reaction product may be used for chemical vapor deposition. In some cases, the substrate itself purposely takes part in the reaction mechanism if the temperature is sufficiently high. For example, when a silicon or aluminum substrate is exposed to oxygen, the growth of a SiO_2 or Al_2O_3 layer results. A further example is a tungsten substrate exposed to methane, leading to the formation of a WC or W_2C layer. In other cases, such as doping or hardening processes, diffusion of deposited material into the substrate, or alloying with it, may be desired. However, generally the substrate plays only a passive role in a chemical vapor deposition process.

A given elemental or compound deposit may in many cases be obtained by any one of a variety of chemical reactions. In selecting a practical reaction, however, one must also consider the constraints imposed by the substrate and the reaction. First of all, if the substrate is to remain unaffected by the process, the reaction should occur rapidly and at a temperature low enough to prevent melting or appreciable sublimation of the substrate. Second, at the temperature required for the deposition, the substrate should not be chemically attacked, or form an alloy or a solid solution with the deposit, or with any of the primary or secondary species present in the reaction. Third, the desired deposit should be the only solid material settling down on the substrate, and therefore the other reaction products should be sufficiently volatile and nonreactive that they cannot cause contamination of the deposit.

In the following, some typical examples for overall reactions suitable for the chemical vapor deposition of different materials are listed:

$$3SiCl_4 \text{ (g)} + 4NH_3 \text{ (g)} \rightarrow Si_3N_4 \text{ (s)} + 12HCl \text{ (g)}$$
$$2AlCl_3 \text{ (g)} + 3H_2O \text{ (g)} \rightarrow Al_2O_3 \text{ (s)} + 6HCl \text{ (g)}$$
$$2AlCl_3 \text{ (g)} + 3CO_2 \text{ (g)} + 3H_2 \text{ (g)} \rightarrow Al_2O_3 \text{ (s)} + 6HCl \text{ (g)} + 3CO \text{ (g)}$$
$$SiH_4 \text{ (g)} \rightarrow Si \text{ (s)} + 2H_2 \text{ (g)}$$
$$2SiO \text{ (g)} + O_2 \text{ (g)} \rightarrow 2SiO_2 \text{ (s).}$$
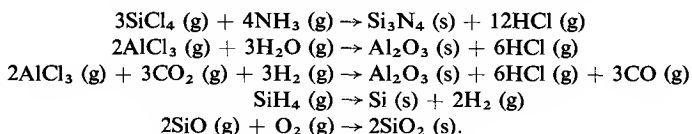
The oxidation state of the metal constituent may be changed as a result of the reaction, as occurs in the last two reactions, or it may remain unchanged, as in the other reactions.

In writing down a chemical reaction linking the initial species and the final products, one should be aware of the fact that the actual course of the reaction may be much more complex because intermediate reaction species may form in accordance with the reaction kinetics. The reaction kinetics are in turn dependent on the environmental conditions under which the reaction takes place, such as flow rates, partial gas pressures, deposition temperature, temperature gradients, and properties of the substrate surface.

Many of the chemical reactions that have been successfully applied to chemical vapor deposition can be put into one of the following categories:

(1) decomposition reactions,
(2) hydrogen or metal reduction of halogens,
(3) polymerization reactions,
(4) transport reactions.

The first three categories combine groups of certain reactions on the basis that a solid phase is derived from reacting vapors regardless of how these vapors have been introduced into the deposition system. In contrast, the fourth category is specified on the basis that at least part of the reactive vapor production is incorporated into the deposition system. The designation "transport reactions" refers to the transport of a solid source material present in the system to the substrate. This is accomplished by chemically attacking the source material by means of a reactive vapor and thus transforming it into a volatile compound. The latter is fed over the substrate and decomposed, resulting in deposition of the source material onto the substrate.

In the following, a brief account of chemical reactions which have become important exponents of the above-mentioned categories will be given. This discussion is mainly a summary of an excellent survey by Powell (15) on this subject.

1. DECOMPOSITION

In the decomposition process, a sufficiently high energy is supplied to the vaporized plating compound streaming over or being adsorbed at the substrate surface that it decomposes and a solid-phase reaction product settles down on the substrate. The general form of this reaction is

$$AB \text{ (g)} \rightleftharpoons A \text{ (s)} + B \text{ (g)}.$$
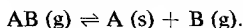
Both organic and inorganic as well as polar and nonpolar plating compounds are suitable for this process. Examples are

$$Ni(CO)_4 \xrightarrow[200\text{-}300°C]{} Ni + 4CO$$

$$SiH_4 \xrightarrow[800\text{-}1300°C]{} Si + 2H_2$$

$$CH_4 \xrightarrow[1000\text{-}2000°C]{} C + 2H_2.$$
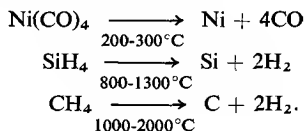
In the case of thermal decomposition, also called pyrolysis, one may distinguish between high-temperature decomposition processes requiring a substrate temperature in excess of about 600°C, and low-temperature processes taking place at temperatures between room temperature and 600°C.

Members of the high-temperature decomposition compounds are primarily the metal halides, in particular the iodides.

Typical examples of low-temperature decomposition compounds include:

(1) metal hydrides,

(2) metal carbonyls and complex carbonyls (such as carbonyl hydrides and nitrosyl carbonyls),

(3) most organometallic compounds,

(4) metal borohydrides,

(5) a few of the more unstable of the metal halides and carbonyl halides (such as gold halides, and platinum group metal halides and carbonyl halides).

However, it should be noted that substantially increased substrate temperatures may be needed for decomposition at small pressures or with a large concentration of decomposition products. Such an increase in substrate temperature may be of advantage for obtaining improved crystalline order, composition, purity, or adhesion of the deposit.

Although the decomposition method is distinguished by its simplicity—it requires only one reactive vapor—certain difficulties may arise from the fact that many compounds after decomposition form more than one nonvolatile residual component. For example, carbon may contaminate deposits derived from carbonyls and organometallic compounds, boron those derived from borohydrides, and oxygen from an oxygen-containing compound may be responsible for forming an oxide layer on the deposit.

Similar difficulties have been observed in activating decompositions with the aid of electron-beam bombardment. The latter converts various silicon oils adsorbed to a substrate surface to deposits resembling SiO or SiO_2, but apparently with the incorporation of some organic constituents (16).

2. REDUCTION

A reduction process can be looked upon as being a decomposition process, as discussed before, aided by the presence of a second reactive species. As a consequence, the deposition takes place at a lower temperature than would be required for pyrolysis of the first component. Reducing agents employed are either hydrogen or metal vapors, while commonly used compounds carrying the material to be deposited are metal halides, carbonyl halides, oxyhalides, or other oxygen-containing compounds. Sometimes a reducing agent is added to a reactive vapor from which the deposit is formed, mainly

by pyrolysis, while the reducing agent serves to prevent the codeposition of oxides or carbides as undesired reaction products. By the proper choice of the reducing agent, in the chemical vapor deposition from metal halides, for example, one can influence the strength of the reducing reaction. The latter increases with the sequence H_2–Cd–Zn–Mg–Na–K ($T < 1000°C$). Therefore, the higher up in this sequence the reducing metal falls, the faster the deposition proceeds, or the lower a deposition temperature is needed. On the other hand, if the reducing reaction is too strong, premature reduction in the gas phase may occur, resulting in a powdery deposit. Examples for chemical vapor deposition by reduction are the deposition of silicon and boron from their halide vapors by using H_2 or Zn as reducing agents, and the deposition of Zr, Ti, or Be from their halides by using Zn or Mg for producing good yields. One advantage of using hydrogen as a less strongly acting reducing agent is that it can usually be premixed with the metal halide without causing a premature reaction before the vapors enter the heated reaction zone. In contrast, reducing metal vapors are usually carried separately from the coating halide to the reaction zone in a stream of carrier gas such as argon, helium, or hydrogen.

One point that needs attention when a metal is used as a reductant is that it may contaminate the deposit. This difficulty can be overcome by using the metal in no more than stoichiometric proportions, and operating at a reduced pressure. In addition, a reductant metal may form a halide in the reaction that is less volatile than the metal, and which therefore may be codeposited. This situation is avoided by working under conditions which keep the pressure of the halide of the reductant metal lower than its saturation pressure at the deposition temperature.

For the above-listed reductant metals, the fluorides, the chlorides, and bromides (except those of zinc), and the iodides (except those of zinc and, perhaps, magnesium) are less volatile than their parent metals; the fluorides are least volatile and the iodides most volatile. As a group, the halides of the alkali metals are least volatile relative to the parent metal. For these reasons, iodides are preferable as deposition media when used with metal vapor reductants, and alkali metals are least suitable as reductants.

In the case of a thermally activated deposition, the substrate temperature has to be raised high enough that the reduction process is sufficiently favored. For the hydrogen reduction of the Pt-group metal carbonyl halides the required temperature may be rather low, on the order of 100°C. However, care should be taken not to apply too high a temperature, since then pyrolysis of a reaction product such as hydrogen halide may occur, which tends to reverse the reaction or produce etching of the substrate.

3. Polymerization

A multitude of organic substances (and, to a less-well-known extent, organic–inorganic composites) form monomers whose molecules can be linked together by a variety of activation processes. (The reverse process, depolymerization upon activation, is also known to occur for certain substances.) Films of the resulting organic or inorganic polymers have electrical properties ranging from semiconducting to insulating, and are distinguished by the completeness with which they can cover surfaces, their good adhesion, their low stress, and their high plasticity. The films may be produced in several ways: by condensing monomer vapor on the substrate and subjecting it simultaneously or sequentially to the activation process, by activating polymerization in the gas phase of the monomer, from which the polymerization products settle onto the substrate, or by coating the substrate with a monomer film by other means (e.g., spraying) and then activating the polymerization. Gregor (5) has presented a detailed survey of polymer films and has classified them according to the activation method:

(1) electron or ion bombardment,

(2) irradiation with light, x-rays, or gamma rays,

(3) electrical discharge in the monomer vapor,

(4) miscellaneous techniques such as surface recombination of monomers having free radicals, surface catalysis, and others.

The first two methods are particularly attractive because they lend themselves readily to the focusing of the activation energy into small areas, and, therefore, to spatially controlled depositions.

The structure of the monomer molecules may be very complex, but not necessarily so. As was pointed out by Bradley and Hammes (17), no functional groups are necessary; solid films may be formed from simple substances such as methane and benzene in a glow discharge.

A discussion of specific substances and the details of the polymerization methods is beyond the scope of this survey; the pertinent information can be found in the work of Gregor (5).

4. Chemical Transport

The term chemical transport refers to the transfer of a material that is relatively nonvolatile from the location of the source material to the location of the substrate by means of a relatively highly volatile chemical vapor. The transport of the material from the source to the substrate occurs in three basic steps:

(1) conversion of the source material into a volatile compound by a chemical reaction,

(2) streaming of the vapor to the substrate,

(3) decomposition of the chemical vapor over or on the substrate, resulting in precipitation of source material onto the substrate.

Usually, chemical transport is performed by shifting the reaction equilibrium to opposite sides in the source and substrate regions. For example, in the reaction

$$\text{Ti (s)} + 2\text{NaCl (g)} \rightleftharpoons \text{TiCl}_2 \text{ (g)} + 2\text{Na (g)}$$
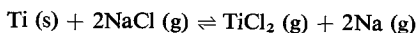
which belongs to the class referred to as an indirect distillation system, a metal is reacted with sodium chloride vapor to form the volatile reaction products appearing on the right side of the equation. Upon reversal of the process, the metal precipitates out again as the only solid phase (18). The direction in which the reaction tends to occur is controlled by properly adjusting the temperature or pressure conditions, or both. Consequently, different conditions of temperature and pressure are maintained at the source and the substrate locations. Of course, the reaction equilibrium may also be shifted by other methods, for example, by introducing an additional chemical vapor to perform a reduction of the transport vapor near the surface, leading to the deposition of the source material, or to perform an oxidation leading to the deposition of a compound. An example of the latter case would be the transport of SiO_2 with the more volatile lower-oxide SiO acting as a transport medium according to the reaction

$$\text{Si (s)} + \text{SiO}_2 \text{ (s)} \rightarrow 2\text{SiO (g)}$$
$$2\text{SiO (g)} + \text{O}_2 \text{ (g)} \rightarrow 2\text{SiO}_2 \text{ (s).}$$
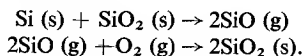
Among the reactions by which chemical transport can be accomplished, the so-called disproportionation reactions are widely used, in particular the halide disproportionation reactions. They are based on the fact that many nonvolatile metals may react at high temperatures to form an unstable, volatile, lower-valent halide rather than the halide of the metal in its highest oxidation state, since generally the stability of the lower-valent halide increases with increasing temperature. Because of this, transfer can be effected by treating the nonvolatile metal with vapor of its own higher-valent halide at a high temperature to produce a lower-valent, volatile halide which after transport into a cooler zone of the system disproportionates back into the higher-valent, volatile halide and a deposit of the nonvolatile metal. Obviously the higher-valent halide can then be fed back to the hotter zone in which the source material is located and the cycle can be continued until all the source material has been carried to the substrate. No vapors need to be fed into or extracted from the system during the deposition process, so the system can be sealed off and operated as a so-called closed system. A famous example of a chemical transport by a halide disproportionation reaction is the transport of silicon in an iodine vapor atmosphere (19):

$$\left. \begin{array}{l} \text{Si (s)} + 2\text{I}_2 \text{ (g)} \rightarrow \text{SiI}_4 \text{ (g)} \\ \text{Si (s)} + \text{SiI}_4 \text{ (g)} \rightarrow 2\text{SiI}_2 \text{ (g)} \end{array} \right\} \text{at } 1100°\text{C}$$
$$2 \text{ SiI}_2 \text{ (g)} \rightarrow \text{Si (s)} + \text{SiI}_4 \text{ (g)} \quad \text{at } 900°\text{C.}$$
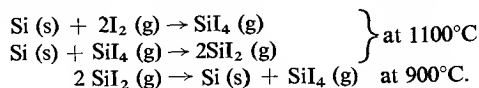
Examples of materials to which the halide disproportionation method has been successfully applied are Al, B, Ga, In, Si, Ge, Ti, Zr, Be, and Cr. Disproportionation reactions similar to those involving the halides occur also with other metal compounds such as oxides and chalcogenides, but the required reaction temperatures are generally higher than those required for the halides.

Transport reactions may serve not only to transport and deposit material, but also to refine it. For example, in the transport of silicon by SiI_4 vapor, refining occurs because the corresponding iodine vapors of the major contaminants of the source material, namely the Group III and V elements B, Al, Ga, In, P, As, and Sb, have vapor pressures sufficiently different from those of the major transporting species SiI_4 (20–23).

Still additional types of transport reactions exist, such as the one responsible for the transport of Ga or Ge in the presence of water vapor, which produces oxidation on one side of the reaction equilibrium and reduction on the other side (24, 25):

$$2\text{Ga (s)} + \text{H}_2\text{O (g)} \rightleftharpoons \text{Ga}_2\text{O (g)} + \text{H}_2 \text{ (g)}$$
$$\text{Ge (s)} + \text{H}_2\text{O (g)} \rightleftharpoons \text{GeO (g)} + \text{H}_2 \text{ (g).}$$
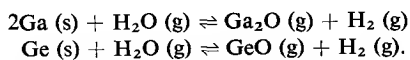
Chemical transport processes have received much theoretical attention. An often referred-to work is that of Schäfer and co-workers (13, 26) who investigated the transport of solids by chemical vapors in a temperature gradient involving gaseous diffusion and heterogeneous equilibrium reactions of the type A (s) + B (g) = R (g). The particular transport reactions studied include the van Arkel-deBoer-type transport system (27, 28) (attack of a metal by halide vapor at a low temperature, and transport of the halide to a hotter surface where decomposition and deposition of the metal occurs), subhalide disproportionation systems, and the indirect distillation systems (18).

An important application of transport reactions is the gaseous etching of substrates, e.g., Ge or Si with HCl (29, 30), Al_2O_3 with fluorinated hydrocarbons (31), to remove contaminants and surface damage prior to the deposition of epitaxial films. Furthermore, it may be of advantage occasionally to form a thin film from a relatively thick deposit, by thinning the latter down by gaseous etching. Sullivan and Kolb (32) have described a method for selected area etching of germanium films exposed to bromine vapor. The etching was activated with visible light which permitted production of a germanium mask duplicating the fine pattern in which the light was focused onto the substrate.

III. Setups for Chemical Vapor Deposition

A chemical vapor deposition system combines the following functions:

(1) generation of reactive chemical vapors,

(2) controlled introduction of chemical vapors into the reaction zone, frequently together with additional inert or reactive vapors serving as diluent or carrier gases,

(3) transport of the chemical vapors to the reaction zone while avoiding premature reaction between them,

(4) supplying activation energy to the reaction which leads to the formation of the desired deposit,

(5) removal and disposal of the reaction by-products.

Depending on how these functions are performed in detail, and how they are combined, a great variety of deposition systems of diverse degrees of complexity can be conceived. Some further factors influencing the design of a chemical vapor deposition system are the pressure at which the reaction is executed, the size and shape of the substrate to be coated, the desired uniformity of the thickness and structure of the deposit, and the attainment of optimum deposition efficiency and speed.

Chemical vapor deposition systems range from extremely simple ones, systems involving a simple decomposition reaction or a disproportionation reaction, to fairly complicated ones in which the deposition of compound semiconductors with a controlled variation of the impurity concentration is performed, after *in situ* etching of the substrate. Two examples of relatively simple systems, one for the deposition of SiO_2 at atmospheric pressure and one for the deposition of BN at a reduced pressure, are shown in Figs. 1 and 2.

1. Closed and Open Systems

As it was pointed out earlier, some transport reactions, among them the halide disproportionation, permit complete recovery during the deposition process of the reagent species used to convert the solid source material into a chemical vapor. This enables one to seal off the deposition apparatus and operate it as a *closed system*, since neither an external supply or extraction of reaction components is required. However, generally it is not possible, or it may not be desired (for reasons to be discussed below), to recover the volatile by-products of the deposition reaction and use them for the generation of further source vapor. Instead, the source vapors are freshly supplied from outside the reaction chamber, and the volatile reaction products are exhausted into the ambient. This kind of deposition system is termed an *open system*.

In the following we will briefly discuss design considerations applying to the functional elements of a chemical vapor deposition system.

2. Generation and Injection of Chemical Source Vapors

The mechanism of feeding the source vapor or vapors into the reaction chamber, and the method of controlling the injection rate, depend on whether the source material is in the gaseous, liquid, or solid state under ambient conditions.

a. Gaseous Source Materials. The simplest case occurs, of course, when the source material is in the gaseous state, provided that it is readily available in storage tanks. The stored gas should be of sufficient purity or it should be possible to purify it by passing it through a suitable flow purification or distillation system. In some cases, it may not be possible to store gases for a long period of time because of their reaction with the cylinder walls and resulting contamination, or because of their decomposition. Therefore, these gases must be produced in the laboratory a short time before their use. The feeding lines and the metering system connecting the storage tank to the reaction chamber and permitting the control of the flow should be made of material that is as inert as possible (or practical) to the corrosive actions of the chemical vapors. Stainless steel, Monel, Teflon, Kel-F, glass, or fused silica are commonly used construction materials. In many cases it is advisable to equip capillary-type flowmeters used for measuring the injection rate with stainless-steel balls instead of the also available sapphire balls, since the latter may be chemically attacked—for example, by halide vapors. Since many of the source vapors react readily with air, it is usually necessary to evacuate the system or to purge it with an inert gas before the reactive vapor is admitted to prevent undesirable deposits and clogging of the flowmeters. Contaminating agents introduced with the source vapors by outgassing of the system walls, or a leak, can cause a significant degradation of the physical, electrical, and structural properties of the deposit, as well as a decrease in the deposition rate. For example, traces of carbon, oxygen, nitrogen, or hydrogen compounds in the source vapor cause brittleness of many metal deposits (*15*). The formation of contaminating carbides or oxides may be responsible for the occurrence of twinned regions or stacking faults in epitaxial layers grown by chemical vapor deposition (*33, 34*). In addition, the purity of the source vapors is of particular importance in the deposition of high-resistivity semiconductor films.

b. Liquid or Solid Source Materials. When the source material is either liquid or solid under ordinary ambient conditions, it is sometimes possible to heat the entire feeding system to a temperature at which the material is

Fig. 1. Setup for chemical vapor deposition at reduced pressures ($<10^{-1}$ Torr). The material deposited is boron nitride.
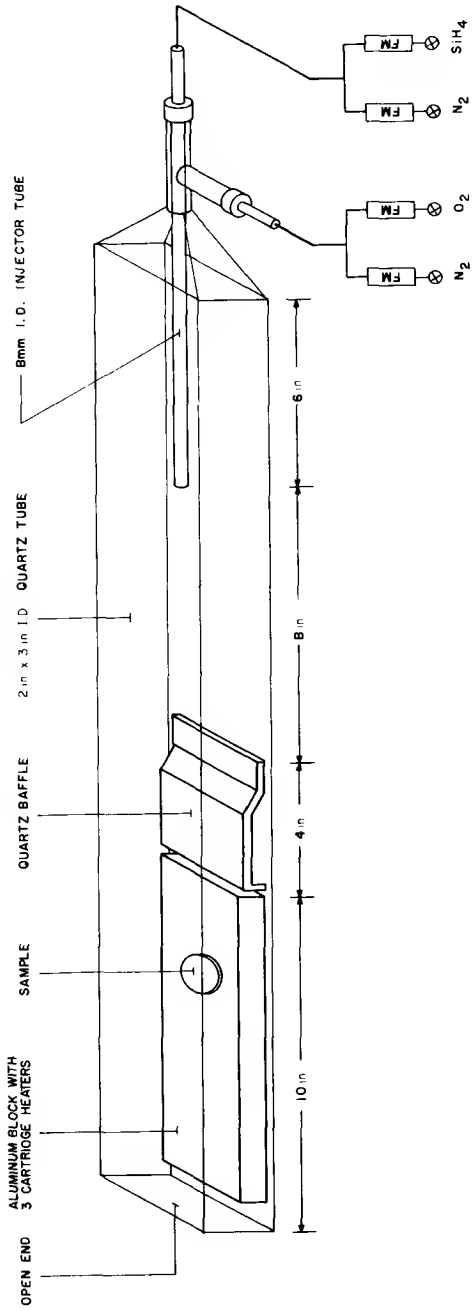
FIG. 2. Setup for chemical vapor deposition at atmospheric pressure. The material deposited is silicon dioxide.

vaporized for easy injection into the reaction chamber. The rate of evaporation can be controlled by measuring the amount of material that has to be added to the vaporizer in order to maintain a constant level of source material in it. However, this method is usually inconvenient, and a chemical transport or a carrier gas method is used instead. The carrier gas can be saturated with the vapor of the liquid or solid source material in several different ways. In the bubble-type vaporizer, the carrier gas is simply bubbled through the liquid source material and becomes saturated with the vapor of the latter. The difficulty with this method is that the bubbling causes a fluctuating flow, which is further accentuated by the formation of droplets which are carried away by the carrier gas. If small vapor concentrations can be tolerated, a more desirable method is to pass the carrier gas over the surface of the source liquid. Under laminar flow conditions, the evaporation rate of the liquid is controlled by diffusion through a vapor film of constant thickness forming on the interface, independent of the flow rate of the carrier gas (35). At high carrier-gas flow rates a constant vapor concentration in the latter can be obtained by passing the gas through a tube filled with an inert wicking material soaked with the liquid whose vapor is to be picked up. In a similar fashion, the surface area of molten metal exposed to a carrier gas may be largely increased by soaking up the molten metal as droplets on an inert and nonvolatile metal screen in a heated vaporizer.

Of special interest is the generation of closely controlled mixtures of source vapors for the deposition of compounds, alloys, or doped materials. These vapors can be obtained by simultaneous evaporation from the appropriate number of individually controlled vaporizers, but in this case the control of the mixing ratio is fairly difficult. Better control is achieved by filling a long tube with the mixture of source materials (which may have quite different vapor pressures), and moving a hot zone gradually from the end nearest to the reaction zone across the tube, evaporating all material that is covered by the hot zone (36). Another method consists of flash evaporation with grain by grain feed of the mixture.

Still another approach is the constant-size pool method. With the latter, evaporation of compound vapors carrying away elements in the proper ratios occurs automatically if a small pool containing the source compound or mixture is heated to the evaporation temperature and the compound or mixture is replenished by just the right amount to keep the pool size constant. However, at the start of the process it is necessary to wait until a steady state mixture in the pool has been established by preferential evaporation of the more volatile component until its mole fraction complies with Raoult's law. A method resembling this is the high surface impedance method, which may be used to generate properly mixed vapors from liquid solutions of compounds. Here the liquid surface is covered by a layer of a solid,

inert, and porous material (e.g., a fritted glass filter) whose function is to prevent mixing of the surface region with the bulk of the liquid by thermal or mechanical agitation. In the process of evaporation, the surface layer becomes enriched with the less-volatile component, and in the steady state the composition of the vapor is again the same as that of the liquid (37). A further method for generating proper vapor ratios from liquid solutions, e.g., of two compounds, utilizes two evaporation chambers in series, the first containing the mixture, and the second a supply of the more volatile compound. Evaporation from the second chamber permits one to compensate for the relative loss of the more volatile component in the first, doped evaporator (38, 39). If P_a is the vapor pressure of the less volatile component, and P_b is the vapor pressure of the more volatile component in the first chamber, and if a pressure $P_b' = P_b - P_a$ is established in the second chamber by properly adjusting its temperature, the mole ratios in the first chamber remain constant. However, this technique has a disadvantage, since knowledge of the volatilities of the components of the solution and a close temperature control of the separate evaporators are required.

In many cases it is convenient to use a chemical transport method, e.g., passing a halogen with or without carrier gas through a heated bed of a metal or a metal compound. If the halogen is a vapor, e.g., chlorine, its flow can be measured directly. On the other hand, use of a carrier technique as discussed before would be indicated if the halogen is a liquid, e.g., bromine or iodine. In using a chemical transport method it is important to note that while the exact conditions of temperature, gas flow, surface area, etc., are not critical when the method is applied to the vaporization of univalent metals, these parameters must be more closely controlled if multivalent metals are involved in order to achieve a nonambiguous oxidation state.

3. Reaction and Exhaust Systems

The reagent vapors obtained as described above are fed into the reaction system, where they stream or diffuse to the zone in which the substrate is located, preferably without any premature reaction. Activation energy is applied to the vapors in such a fashion that the deposition reaction takes place in the substrate zone. The remaining gaseous reaction products are exhausted preferably without impeding the supply of fresh reagent vapor to the growing deposit.

Principal factors influencing the design of the reaction system are:

(1) the method by which activation energy is supplied (e.g., heat, light, x-ray radiation, rf or dc plasma, electron beam);

(2) the shape of the substrate to be coated (particles, the inside of tubing, complex-shaped substrates, or simply flat substrates);

(3) the area of the substrate and the required uniformity of the deposit;

(4) the temperature conditions (e.g., high or low temperature range, one or several different temperature zones);

(5) the operating pressure e.g., (superatmospheric, atmospheric, or sub-atmospheric pressure);

(6) the chemical nature of the gases (requiring special materials to be used for the chamber, perhaps, or special cooling);

(7) the way in which the reagent gases must be injected in order to avoid a premature reaction before they have reached the location of the substrate (e.g., presence of several reactant gases which easily react with each other even at a reduced temperature and therefore could only be combined directly over the substrate).

Further considerations apply to the ease of loading or cleaning the chamber, and to the kind of measurements performed during the deposition (e.g., providing a window which would stay clear of any deposit and through which temperature measurements or measurements of the absorption spectra to identify the species present may be made).

The exhaust system should be designed with the possible toxic or explosive nature of the effluent vapors in mind. Inflammable vapors should be burned off at the end of the exhaust line, and the latter should be sealed off one way against backstreaming of air into the system, e.g., by bubbling the exhaust gases through an inert liquid, or by using a one-way valve. In some cases it may be possible and advantageous to recover or to recirculate exhaust gases. In addition, a dynamic analysis of exhaust gases or certain constituents may be a convenient way of monitoring the deposition reaction—for example, by titration or spectrometric methods.

Some difficulties are experienced if the deposition is performed at a reduced pressure and corrosive exhaust gases have to be passed through a vacuum apparatus. In this case it may be advantageous to remove condensible gases with a liquid-nitrogen trap before they enter the pumping station.

The most frequently used method of supplying energy to the deposition reaction is thermal activation. To this end, the substrate in the reaction chamber is heated by an external furnace, or by internal heating. The latter may be accomplished by passing current through the substrate if it is con-ducting, or by placing it on a resistive heater strip (e.g., heaters made of molybdenum or graphite have been used in the deposition of epitaxial layers on Si or Ge, and GaAs substrates, respectively). In another commonly used method the substrate to be heated is placed on a susceptor which in turn is heated by rf induction. In this fashion the high-current feedthroughs required for resistance heating are eliminated. One widely used susceptor material is graphite preferably with its pores sealed by the application of a layer of pyrolytic graphite (e.g., by thermal decomposition of methane), or silicon

carbide.* The latter coating renders the susceptor oxidation resistant by virtue of a SiO_2 layer that grows on the surface of the SiC. This type of susceptor may be used up to about 1200°C. Another susceptor that can be exposed to an oxidizing atmosphere may be constructed by vacuum sealing a graphite susceptor into a fused silica housing, for example.

In order to avoid contamination of the deposit, it is desirable to fabricate the susceptor of the same material as the substrate. If this happens to be a high-resistivity semiconductor material, some kind of starting mechanism is required to heat the material to a temperature at which it becomes sufficiently conducting and couples well to rf power. Examples of useful starting aids are heating of some portion of the substrate by infrared radiation, placing a small piece of more high-conducting material of the same kind in contact with the susceptor, or imbedding a conductor (e.g., a molybdenum rod) in the susceptor.

Additional means of producing internal heating of a substrate are infrared or visible light radiation, and electron bombardment.

4. Doping Techniques

One of the important aspects of chemical vapor deposition, especially when it is applied to the formation of semiconductor layers, is the relative ease with which controlled amounts of impurities can be introduced. Because the impurities can be implanted into the semiconductor film while it is being grown, arbitrary impurity distribution profiles can be achieved that are not subject to the laws of diffusion theory, in contrast to the process of diffusion from a surface. However, it is also customary to employ chemical vapor deposition techniques in carrying out diffusion of impurities from the substrate surface. In this case, a layer of material containing the dopant as a constituent or in solution is deposited on the semiconductor surface. The release of the dopant from the deposited layer and its driving into the semiconductor is accomplished either by heat treatment alone, or by a combination of heat treatment and chemical reduction of the source layer. The source layer is removed by etching after the diffusion is completed. A familiar example for this process is the doping of silicon with boron, which is derived from B_2O_3 deposited by feeding B_2H_6, O_2, and N_2 carrier gas into the system (40–42).

Depositions of doped semiconductor layers can be accomplished in a very simple fashion by using a chemical vapor transport system, in particular a closed system, in which the source material is doped with the desired impurity, and both the host material and the impurity are chemically transported to the substrate (43). When iodide vapor is used as the transport agent, it turns

* SiC-coated graphite susceptors are commercially available from the Dow Corning Corporation.

out that B, P, As, and Sb are transported at approximately the same rate as the silicon host material, that is, the transfer ratio is nearly 1 : 1 in the doping range 5×10^{16}–2×10^{20} atoms/cm^3. However, for Al, In, and Ga the transfer ratio is only on the order of 10^{-3} because of the relative instability of their triiodides. Unfortunately, this technique is difficult to apply if one wishes to create a given doping profile, or to switch to a different impurity during the deposition process (although a solution to the latter task has been worked out) (44). Greater flexibility in this respect is gained by working with an open system which permits adding of the impurities to the matrix reagent in an independent fashion. The various techniques which have been employed for this purpose are closely related to those discussed above in connection with the chemical vapor deposition of compounds, mixtures, alloys, or solid solutions. Solid, liquid, and gaseous substances may be used for generating vapors carrying the dopant into the deposition zone. Physical vapors from solid dopant sources have been used to some extent for achieving very low doping concentrations because it is sometimes easier to control the vapor pressure of a solid than the very small flow rate of a gaseous doping source, or the amount of carrier gas passing through a bubbler containing a liquid doping source (45). In using physical evaporation from a solid dopant source, it is important that the feeding line connecting the source with the reaction chamber be kept at a temperature higher than that of the dopant source material in order to prevent supersaturation of the vapor and resulting loss of material by precipitation onto the walls of the feeding system. However, if the dopant vapor is diluted by mixing it with a carrier gas or the gas carrying the matrix component, the temperature necessary to avoid supersaturation is correspondingly reduced.

If a liquid dopant source that can form a liquid solution with the liquid matrix source is available, various schemes may be employed for generating a composite vapor that carries the two substances into the reaction chamber with the same mole ratio as prevails in the solution. However, the resulting distribution coefficient in the deposited layer may deviate from this mole ratio, depending on the reagents used, and the deposition conditions. Examples of liquid dopant sources are PCl_3, BCl_3, or BBr_3, added to $SiCl_4$ or $SiBr_4$ as matrix source for the deposition of doped silicon by the halide reduction method. If the vapor pressure of the two compounds is not much different (as is the case with PCl_3 and $SiCl_4$) and a correspondingly large amount of liquid is present, both can be picked up by passing a carrier gas such as hydrogen through the solution in a simple bubbler arrangement. However, if the vapor pressure of the two compounds is very different (as is the case with BCl_3 and $SiCl_4$, or with BBr_3 and $SiBr_4$), fractionation will occur and the solution will alter its composition with time of use. Possible remedies are use of the wick technique according to Theuerer (37) or the

multievaporator technique discussed above (*38, 39*). The first technique prevents any mechanical agitation of the liquid surface by means of a fritted filter and glass beads, so that enrichment of the less-volatile component can occur near the surface. The second technique compensates for the relative loss of the more volatile component by placing a second evaporator containing only the more volatile component in series with the first one which contains the solution.

One limitation of the liquid solution techniques deserves mentioning: the mixed liquids must not react with each other. For example, when BBr_3 is mixed with $SiCl_4$ in order to obtain deposition of *p*-type material, the following reaction has been shown to occur by Miller and Grieco (*46*):

$$3SiCl_4\ (l) + 4BBr_3\ (l) \rightarrow 4BCl_3\ (g) + 3SiBr_4\ (l).$$
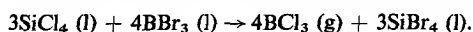
This leads to the production of gaseous BCl_3 (at room temperature) which is a much less effective doping reagent than BBr_3 (particuarly when used in conjunction with germanium at low temperatures). This problem can be avoided by using the same halides for the matrix and the dopant, such as $SiBr_4$ and BBr_3, or $GeBr_4$ and BBr_3.

Another solution to the doping problem is to use gaseous dopant reagents which are chemically similar to the matrix reagent, such as the hydrides PH_3, AsH_3, SbH_3, and B_2H_6 in combination with SiH_4 or GeH_4 for thermal decomposition (*47*). However, some of the hydrides are thermally fairly unstable, and precautions should be taken to prevent decomposition in the feed lines by making the latter short and constructing them of inert material.

IV. Morphology of Deposits Formed by Chemical Vapor Deposition

The structure of coatings of the same material obtained by chemical vapor deposition may range from very porous to impermeable, from amorphous to single crystal, and from powdery to structurally strong, depending upon the nature of the substrate and the condition of its surface, the deposition conditions, and treatments after deposition.

As a rule of thumb it can be stated that, in analogy to physical vapor deposition, chemical vapor deposition at high substrate temperatures and low vapor concentrations results in coarsely crystalline coatings, whereas the use of low substrate temperatures and high vapor concentrations results in amorphous of finely crystalline coatings. Obviously, this rule is modified by the nature of the reacting vapors, the nature of the substrate, the vapor velocities, and the impurities in the system.

The morphology of chemical vapor deposited films is determined to a considerable degree by nucleation processes, particularly in the early growth
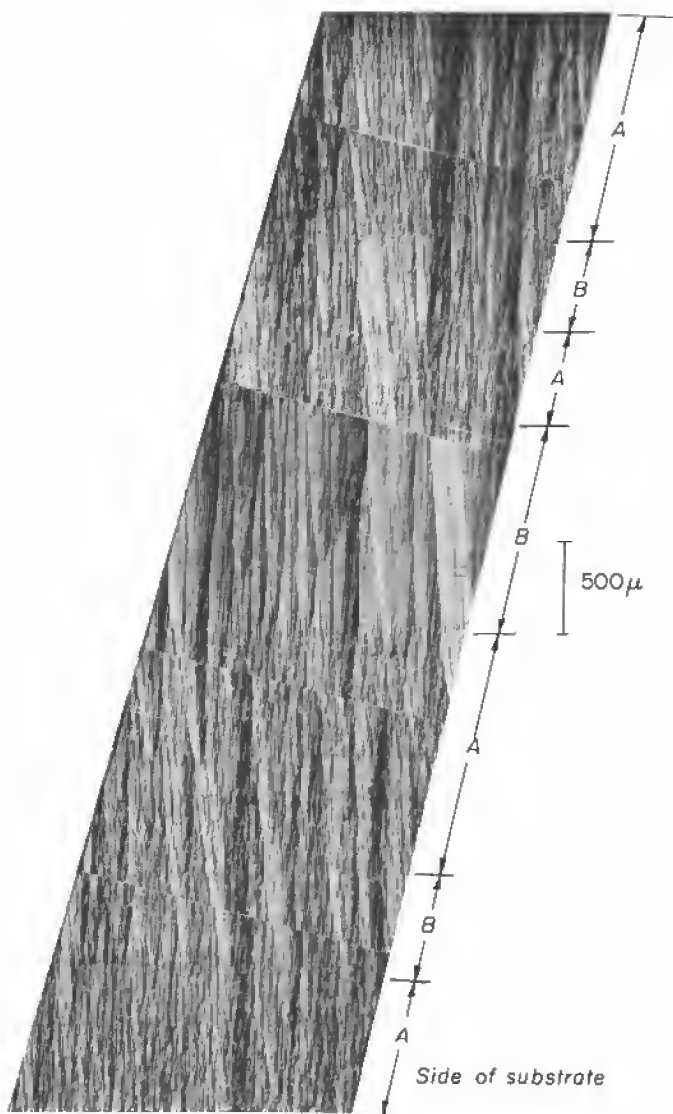
FIG. 3. Cross section of pyrolytic graphite showing changes in morphology due to pressure variations during the deposition process. The total system pressure was alternated between a high value (~ 20 Torr—region A) resulting in considerable gas phase nucleation and a low value (~ 5 Torr—region B) resulting mainly in surface nucleation in the particular deposition system used. Substrate: polished graphite; average deposition rate: 0.25 mm/hr; deposition temperature: ~ 1900°C.

Deposit

100μ
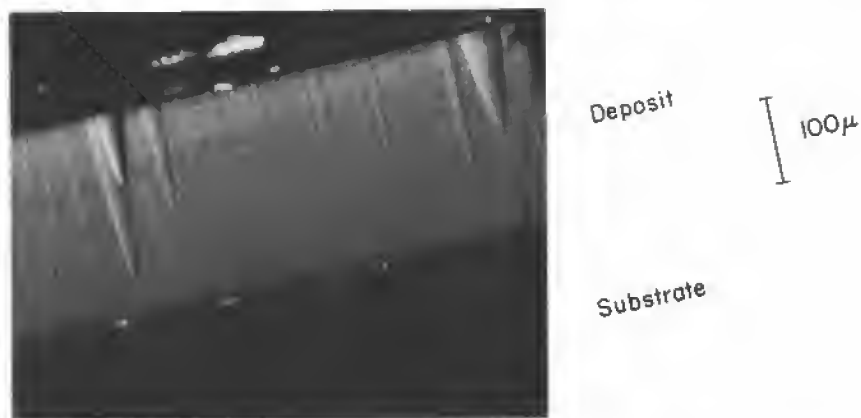
Substrate

FIG. 4. Cross section of pyrolytic graphite exhibiting mostly very narrow columnar grains. The total system pressure during the deposition was 14 Torr. Substrate: polished sapphire; deposition rate: ~0.05 mm/hr; deposition temperature: ~1600°C.

Deposit
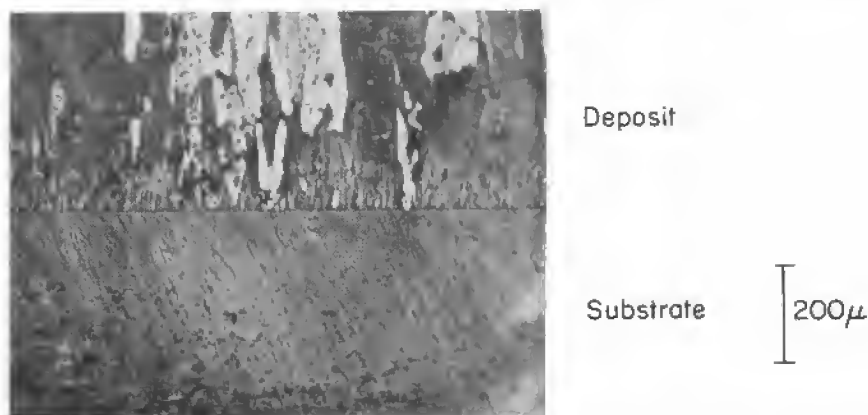
Substrate   200μ

FIG. 5. Cross section showing columnar grains in α-alumina chemically vapor deposited on a polished sapphire substrate. The striations visible in the substrate are polishing marks. (Deposition and photograph by R. C. Ellis, Jr., Raytheon Company, priv. comm.)

stages. A manifestation of this are the frequently observed columnar grains extending from the substrate to the outer surface of the coating. Examples of columnar grains as they appear when looking at a polished cross section of the respective deposits are shown in Figs. 3–5. Although these grains may be individually quite dense, they are often poorly bonded to each other, resulting in a material with little lateral integrity (48). This structural feature may seriously degrade the performance of the coating as an electrical or chemical barrier.

Gretz (49) has concluded that the structure of chemical vapor deposits can be understood, in principle, by an extension of the nucleation and growth theory as developed for physical vapor deposition (50). According to his analysis, much of the difficulty in developing a fully quantitative theory for either chemical or physical vapor deposition is associated with the problems of characterization of the "critical nucleus" and the details of the effects of impurity adsorption on the growth and spreading of the nuclei. He postulates that surface diffusion plays a dominant role in the formation of the deposit, and as a result both "supersaturation" and substrate temperature control the structure of vapor deposits.

Supersaturation, mobility, and impurity adsorption are all functions of the particular lattice plane considered; hence, the key to understanding morphology must be contained in these physical quantities. With the present state of knowledge of surfaces, theoretical understanding is greatest for supersaturation (51) and substantially nonexistent for impurity adsorption. Surface diffusion is only partly understood, in the sense that complete experimental verification of the theoretical ideas is not presently available.

The concentration of defects in a growing film is related to the number of spreading nuclei, determined by the "nucleation rate," that impinge upon each other to form a continuous layer. The most commonly observed defects in the crystalline structure of a thin film are dislocations, stacking faults, and twins. Sloope and Tiller (52) have found that the stacking fault density decreases as the deposition rate decreases. The width of stacking faults increases with film thickness. A high residual gas pressure increases the density of stacking faults and dislocations.

For epitaxial growth it has been stated in the literature [see, for example, Cave and Czorny (87)] that under proper deposition conditions the surface of a deposit is as smooth as that of the substrate and no new imperfections occur in the deposit. Instead, atomic and microscopic defects of the film can be traced to crystal imperfections of the substrate or work damage, or to contamination of the substrate surface. For example: the dislocation density of the film may correspond to that of the substrate; an oxide layer present on a single-crystal silicon substrate may give rise to stacking faults in a deposited silicon film (53); screw dislocations in a (111) germanium substrate mayt be the origin of growth pyramid forming in epitaxial gallium arsenide (54); and work damage of the substrate surface may lead to the formation of polycrystalline instead of epitaxial deposits. Evidence of a more perfect crystalline structure of the deposit than that of the substrate was found by Pulliam et al. (55) in the case of the homoepitaxial growth of MgO under controlled conditions.

Heteroepitaxial films usually exhibit defects resulting from the mismatch of lattice constants and thermal expansion coefficients of the two materials.

According to the experimental findings, the resulting strain energy may be accommodated by the creation of dislocations in a localized zone extending not only into the deposit as predicted by the van der Merwe model but also into the substrate (54).

Filby et al. (56) have discussed the growth features of chemical vapor deposited films (with emphasis on epitaxial silicon) in light of the significance of the nucleation rate responsible for the formation of new growth islands in relation to the rate at which the step-shaped boundary of a growth island spreads out laterally. A relatively high nucleation rate leads to a smooth layer, while a high lateral growth rate gives rise to the formation of facets or steps. The heights of the steps may be greatly increased due to a "bunching mechanism" which has its origin in the retardation of the lateral movement of growth steps by "mobile" impurities adsorbed on the surface. Another factor entering in the above considerations is the mean free path in the vapor phase at the interface. If the latter is <1 μ, diffusion effects at the interface become important.

The smoothness of epitaxial films may be influenced by the substrate orientation. Evidence has been found that deviations of the substrate orientation by a few degrees from a low-order crystal orientation [e.g., (111) or (100)] may be beneficial in reducing the size and density of growth pyramids (57). Relatively little has been published on experimental studies of the dynamics of film growth. We will note here the microscopic measurements by Seltzer et al. (58) of the movement of growth steps as a function of deposition conditions. The medium was germanium deposited by the disproportionation of GeI_2. Further interesting studies were reported by Gabor and Blocher (59) who performed in situ transmission-electron microscopic studies of the growth dynamics of iron and nickel films deposited on (111) gold foils by pyrolysis of the respective carbonyls. For further details on epitaxial growth by chemical vapor deposition the reader is referred to a review by LaChapelle et al. (4).

Of the several factors which influence the general nature of deposits, the substrate temperature is particularly important. At very low temperatures the reactions are slow or incomplete. Under these conditions very finely crystalline, amorphous, or porous coatings often result. For example, in a fluidized bed coating of UO_2 particles from aluminum halide and water vapor, porous coatings of amorphous alumina were deposited at a temperature of 500–700°C. Oxley (60) postulated that either (1) the oxide nucleates in the gas phase and subsequently attaches itself to the substrate, or (2) intermediate products are deposited which are subsequently converted to the oxide with corresponding density changes. As the deposition temperature is increased, the grain size tends to increase and the deposit becomes dense. In the example cited above, alumina coatings of nearly theoretical density are deposited at 1000°C. They are impermeable and consist of small crystallites

of α-alumina with an average size of 3.0 μ dispersed in an amorphous matrix. To explain this Oxley postulates that either (1) the nucleation tendency of the system is reduced as a result of a shift in the reaction equilibrium, (2) the intermediates do not form, or (3) the material recrystallizes rapidly so that dense material is formed.

At still higher temperatures, rapid grain growth occurs, and the deposits are generally weakened and have an integrity inferior to that of coatings deposited at lower temperature. For example, alumina coatings deposited at 1400°C are highly crystalline and have an average crystallite size of about 25 μ, but they exhibit a coating integrity inferior to that of 1000°C coatings.

The structure of a deposit is also strongly influenced by the partial pressure of the reactants in the system. Oxley (60), for example, reports that the morphology of pyrolytic carbon deposited in a fluidized bed on UO_2 particles varies from columnar to laminar to porous as the deposition rate is increased probably as a result of the increase in the methane partial pressure. (See Table I).

TABLE I

SUMMARY OF FLUIDIZED BED DEPOSITION OF PYROLYTIC CARBON

Dep. rate (μ/min)	Morphology	Crystallite size (Å)	Density (g/cm^3)	T_{dep} (°C)
0.1	Columnar	40	1.8	1400
1.0	Laminar	25	1.5	1400
10.00	Porous	—	—	1400

Diefendorf similarly found that the structure of pyrolytic graphite deposited at 1650°C was strongly dependent on system pressure (61). At very low pressures graphite can grow at nucleation sites on the substrate, whereas at slightly higher pressure some nucleation from the gas phase can occur. At still higher pressures poorly formed particles will develop in the gas phase and then be incorporated into the deposit, resulting in a low-density, "continuously nucleated" structure. He found that at high system pressures, the density of the graphite is a minimum at a deposition temperature of about 1650°C and approaches theoretical density as the temperature is either increased or decreased. The density minimum can be eliminated by carrying the deposition out at a sufficiently low pressure. At the lower temperatures the gas is too cool to allow gas phase reactions to occur.

The structural properties of the low-density graphite are considerably different from the high-density graphite. Guentert (62) found that the crystallite size of low-density graphite (ρ = 1.4–1.5) deposited at 1700°C and

15–20 Torr was 25 Å in the c direction, in rough agreement with the results reported by Oxley (60).

The deposited material is surface nucleated at a sufficiently low reactant partial pressure. The resulting microstructure can be explained if it is assumed that the deposition process proceeds normal to the surface and at a rate which is independent of the shape of the surface contour. At any instant of time the surface then forms a contour representing an equal depth of deposit. If the substrate is smooth, and there are no large particles on the surface, smooth parallel layers are formed. If, however, there are asperities on the surface, a nodule or a growth cone is formed. Note from Figs. 3–5 that the nodule grows with each successive layer deposited, and that the irregularity is transmitted to the surface.

Stover (63) has suggested that the growth cones in "continuously nucleated" pyrolytic carbon originate in conical whiskers growing spirally with the deposit rather than in soot particles of equivalent dimensions as postulated by Coffin (64). Whisker growth has been observed in some depositions of isotropic boron nitride, a material which is isomorphous with graphite. The material in this case was invariably rhombohedrally layer ordered, rather than being layer disordered. The particles necessary to initiate a spiral whisker are much smaller and consequently more easily explained than the particles postulated by Coffin.

The addition of small amounts of impurities to the vapor phase can grossly affect the structure and properties of the deposit. For example, Diefendorf (61) reported that traces of oxygen (10–100 ppm) had a profound effect on the deposition of carbon at low temperatures (750–1000°C). While pure hydrocarbons formed dense adherent deposits, the addition of small amounts of oxygen resulted in the formation of whiskers. At higher deposition temperatures the addition of oxygen led to enhanced vapor phase nucleation.

The particular geometric features of the deposit may also be the result of poisoning of certain preferred growth directions. Diefendorf (61), for example, found that when he suspended a pyrolytic graphite bar in methane and heated it to 1600°C, no growth occurred on the a–c faces, although a–b growth occurred. In a second experiment the surfaces of the rod were first etched with hydrogen prior to admission of the methane, and growth occurred on all faces.

The problem of stressed deposits is closely related to the morphology of the coating and has been a major obstacle to the wider use of chemical vapor deposition. Frequently, the deposits are strongly oriented, thus introducing overall anisotropy into deposits of anisotropic substances. Such an anisotropy causes internal stresses to be set up in deposited materials as they are heated or cooled from the deposition temperature. Additional stresses are introduced by differential growth introduced during the deposition process because the

first-deposited material is exposed to a high temperature for a longer time than the last-deposited material. These stresses are often sufficient to cause the deposit to warp or rupture on cool-down or in service (65).

V. Examples of Films Prepared by Chemical Vapor Deposition

1. SEMICONDUCTORS

Chemical vapor deposition, first utilized in the field of semiconductors exclusively for the preparation of high-purity material (66), is recently seeing extensive additional application for growing eptaxial layers of silicon, germanium, gallium arsenide, and other compounds on similar and dissimilar single-crystal semiconductor substrates, as well as on single-crystal or disordered insulator substrates. The successes in depositing layers of device quality were responsible for the rapid development of monolithic large-scale integration (all circuit elements—transistors, diodes, and resistors—grown on the same single-crystal substrate), and for vast improvements in the performance of semiconductor devices.

Epitaxial semiconductor layers are attractive because they enable one to:

(a) grow structures composed of multiple single-crystal layers of different doping levels and conductivity signs without the need for doping compensation;

(b) make these layers very thin without much disturbance from interdiffusion effects;

(c) produce doping profiles at will;

(d) grow single-crystal heterojunctions; and

(e) form semiconductor devices on insulating or semi-insulating substrates.

a. Silicon. Successful processes for producing high-purity silicon deposits include the following ones (66, 67):

(1) reduction of silicon tetrachloride ($SiCl_4$) with zinc or hydrogen,

(2) reduction of disiliconhexachloride (Si_2Cl_6) with hydrogen,

(3) reduction of silicon dichloride ($SiCl_2$) with hydrogen,

(4) reduction of silicon tetraiodide (SiI_4) with hydrogen,

(5) reduction of silicon tetrabromide ($SiBr_4$) with hydrogen,

(6) reduction of trichlorosilane ($SiHCl_3$) with hydrogen,

(7) pyrolytic decomposition of silane (SiH_4), and

(8) pyrolytic decomposition of silicon tetraiodide (SiI_4).

Of these, the processes (1), (6), (7), and (8) have been most widely used, with preference given to the hydrogen reduction systems.

(1) *Reduction of silicon halides.* The reduction of $SiCl_4$ with zinc at about 950°C was developed at DuPont into the first commercial process for the

production of high-purity silicon in the form of dendrites, but later the hydrogen reduction of $SiHCl_3$ came to be preferred in the manufacture of high-purity silicon. The latter follows the gross reaction

$$SiHCl_3 \ (g) + H_2 \ (g) \rightarrow 3HCl \ (g) + Si \ (s).$$
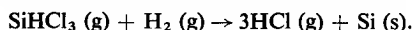
In the course of the actual reaction, a variety of intermediate compounds, long-chain polymers as well as $SiCl_4$ or $SiCl_2$, are also created. Typical temperatures for the deposition of Si by the hydrogen reduction of $SiCl_4$ or $SiHCl_3$ range from 800°C, where mostly a powder deposit develops, to 1100–1300°C, where massive deposits are formed.

In spite of the corrosive nature of the gases involved, hydrogen reduction is the most popular system for depositing silicon. One reason is that the chlorides and bromides of silicon are liquid under ambient conditions and reasonably stable (but $SiHCl_3$ is a flammable gas), and can therefore be conveniently carried into the reaction chamber by the hydrogen. Thus the hydrogen acts simultaneously as a reactant and a carrier gas. In a typical deposition system, the partial pressure of the silicon halide is 1–30 Torr, the total pressure is 1 atm, and the temperature for deposition of single-crystal films falls into the range 1100–1300°C. Typical deposition rates are on the order of 1 μ/min. The underlying kinetics of film growth have received some theoretical consideration, for example by Alexander (*68*). Early descriptions of the above method as applied to the deposition of oriented silicon layers was published in 1957. Sangster *et al.* (*69*) reported at that time deposits, with orientations similar to those of the substrates, obtained from the reaction

$$SiBr_4 \ (g) + H_2 \ (g) \rightarrow Si \ (s) + 4HBr \ (g)$$
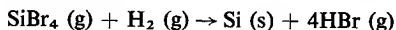
by exposing resistively heated silicon filaments to a mixture of $SiBr_4$ and H_2 at 1100–1200°C. Perhaps the first workers to announce a fully successful deposition of homoepitaxial layers of silicon and likewise germanium were Sheftal *et al.* (*70*), also in 1957. Their depositions were carried out by the hydrogen reduction of $SiCl_4$, or $GeCl_4$. Temperatures for single-crystal growth were 1150°C for silicon, and 850°C for germanium. Layer thicknesses from 1 to 200 μ were obtained in areas up to 2.5 cm². In this work, a sufficiently low supersaturation, a substrate plane parallel to the most densely packed faces, i.e., (111), (110), and (100) for a cubic crystal structure, a sufficiently high temperature to enhance the influence of the substrate on the crystallizing phase, and a clean surface were observed to be essential for achieving single-crystal growth. Among other workers pioneering in the growth of homoepitaxial films of silicon of device quality were Theuerer (*71*), Mark (*72, 73*), Deal (*74*), and Bylander (*75*) who used the hydrogen reduction of $SiCl_4$ bubbled with N_2 or H_2 into systems employing different heating methods (rf induction, external furnace, graphite strip heater).

Allegretti and Shombert (76), Charig and Joyce (77), and Glang and Wajda (78) were among the first workers to perform homoepitaxial depositions by the hydrogen reduction of $SiHCl_3$.

Theuerer et al. (71, 79, 80) grew homoepitaxial films of silicon with controlled thickness, resistivity, and conductivity type by the hydrogen reduction of $SiCl_4$. The films were grown on (111) Si and doped by using either BBr_3 or PCl_3 as doping sources. In the process, $SiHCl_3$ formed with 20% yield and, in addition, high-molecular-weight polymers condensed on the walls of the reaction tube. It was postulated that the reaction of the radical $SiCl_3$ with hydrogen led to the formation of silicon when the radical was adsorbed on the substrate, and to the formation of $SiHCl_3$ when the reaction took place in the gas phase. Miller and Grieco (46) investigated the deposition of p-layers with the aid of a single halide system by employing the simultaneous hydrogen reduction of $SiBr_4$ and BBr_3.

From the temperature dependence of the growth rate of the deposited layer, activation energies were derived as follows:

$SiCl_4$ reduction: 37 kcal/mole [Theuerer (71)], 30 kcal/mole [Kahng et al. (81)].

Si_2Cl_6 reduction in presence of uv light: 37.5 kcal/mole from 600–1000°C [Frieser (82)].

$SiHCl_3$ reduction: 22 kcal/mole from 1110–1200°C [Charig and Joyce (77), Stein (83)].

$SiBr_4$ reduction: 15 kcal/mole from 1050–1300°C [Miller and Grieco (46)].

It appears that the details of the hydrogen reduction reactions are not as straightforward as described by the equations

$$SiCl_4 + 2H_2 \rightarrow Si + 4HCl$$
$$SiHCl_3 + H_2 \rightarrow Si + 3HCl.$$
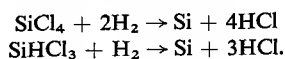
Bylander (75) assumed that the heterogeneous reaction for the $SiCl_4$ reduction in the temperature region 950–1100°C took place in competition with a reaction of the type

$$SiCl_4 + Si \rightarrow 2SiCl_2$$
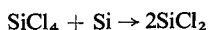
consuming deposited silicon. The formation of $SiCl_2$ is a first step in the formation of the $(SiCl_2)_nH_2$ polymers and $SiHCl_3$ observed in the reaction atmosphere.

According to Bylander, the deposition reaction is controlled by the rate of mass transfer above 1100°C, and by the reaction rate below 1100°C. Steinmeier (84), like Theuerer, observed that as the $SiCl_4:H_2$ ratio increases, the rate of silicon deposition goes through a maximum because an etching

reaction takes over. Monchamp and co-workers (85) found that at 1100°C the deposition rate varies only with the $\frac{1}{2}$ power of the $SiCl_4$ pressure, from which they concluded that the surface is only partially covered by $SiCl_4$ during the reaction, perhaps because the reaction product $SiCl_2$ adheres strongly to the surface. Alstrup and Thomas (86) experienced the same pressure dependence of the deposition, but evaluated a significantly different activation energy.

Regarding the hydrogen reduction of $SiHCl_3$, discrepancies exist among the temperature dependences of the deposition rate reported by different workers. Glang and Wajda (78) found little variation with temperature in the range 1100–1200°C, Stein (83) found a steady increase of the rate according to an activation energy of 22.5 kcal/mole in the temperature range 1100–1300°C with a half-order pressure dependence, while Charig and Joyce (77) observed a maximum in the deposition rate at 1220°C with a rapid falloff at higher temperatures. The latter may be attributed, in part, to a reversal of the direction in which the chemical reaction proceeds, namely favoring etching of the silicon at the higher temperatures. Charig and Joyce stated also that at partial pressures of $SiHCl_3 > 1.3$ Torr, the deposition rate became pressure independent at temperatures of 1220–1235°C. This led to the conclusion that the rate-determining step in the reaction was chemisorption of a radical derived from $SiHCl_3$ on the silicon surface and its subsequent reduction by direct vapor phase impingement of hydrogen. If the rate-controlling step is the reaction between two species chemisorbed on the substrate surface, a maximum in the deposition rate should occur as the partial pressure of one species is increased. Such an effect was indeed observed in the hydrogen reduction of $SiCl_4$; however, the effect may also be due to the favoring of an etching reaction with increasing $SiCl_4$ pressure.

Cave and Czorny (87) reported on the growth of doped silicon homo-epitaxial layers on (111) silicon at temperatures ranging from 1120–1350°C with growth rates of 0.1–3 μ/min. For growing n-type layers, solution doping was successfully employed, that is, PCl_4 or $SbCl_5$ were added to the $SiCl_4$ source. The doping ranges covered were 10^{14}–10^{17} atoms/cm^3 by using PCl_5, and 10^{17}–10^{20} atoms/cm^3 by using $AsCl_3$. According to these authors, chlorides are not satisfactory as doping agents for growing p-type layers since they are too sensitive to moisture which causes a degradation of the dopant. For this reason, B_2H_6 diluted in H_2 introduced as an independent gas stream was used as a dopant source for p-type layers, permitting a dopant concentration from 10^{15}–10^{20} atoms/cm^3. The latter method was also of advantage for producing highly doped n-type layers with 10^{17}–10^{20} atoms/cm^3 by the use of PH_3 diluted with H_2. The crystalline perfection of the deposited layers was a function of the growth rate, the growth temperature, and the quality of the original surface. With appropriate care, no dislocations or

stacking faults were added by the epitaxial growth process to those that had their origin in the substrate surface.

The relationship between the distribution coefficient in the deposited layer and the atomic ratio of dopant to silicon in the initial gas stream as a function of doping agent, deposition temperature, and gas flow was investigated by Shepherd (88). His studies, concerned with the hydrogen reduction of mixtures of $SiCl_4$ and PCl_3, $AsCl_3$, or $SbCl_3$, indicated a decrease in the distribution coefficient as the temperature was increased. At $1200°C$, the distribution coefficient had a value near unity for P and As, and 10^{-2} for Sb.

Ways to reduce the temperature necessary for growing epitaxial silicon films by halide reduction techniques were explored by Nakanuma and Osafune (89), and by Frieser (82). The first two workers obtained high-quality epitaxial films at $850°C$ after they had conditioned the silicon substrate by depositing an epitaxial silicon layer at $1200°C$. Frieser grew highly oriented films at a substrate temperature as low as $700°C$ by the hydrogen reduction of Si_2Cl_6 in the presence of uv light. Without the application of the uv light the deposits were only polycrystalline. The degree of orientation decreased as the wavelength of the light was increased beyond 2300 Å. The presence of the uv light had also the effect of doubling the deposition rate (which was of the order of 1 μ/hr). In contrast, the structure of films deposited by the hydrogen reduction of $SiCl_4$ (undoped and doped), $SiHCl_3$, and the pyrolysis of SiH_4 was scarcely affected by the presence of uv light. In order to explain the low epitaxial deposition temperature, Frieser assumed (1) that Si-atom pairs were deposited from the Si_2Cl_6, and (2) that uv light was effective in creating one "dangling bond" for each atom on the substrate surface, while there is only one for every five surface atoms without illumination. The first factor appears to facilitate oriented growth, while the second increases the number of nucleation sites. Cleaning and preparation of the substrate surface was of greater importance for low-temperature epitaxial depositions than those performed at higher temperatures; the best results were obtained with copper-displacement etching. The formation of an oxide layer prior to the deposition was prevented by treating the surface with an alcohol solution saturated with iodine. The substrate was inserted wet into the reactor in an argon atmosphere, and the I_2 was removed by heating to $\sim 550°C$ in hydrogen.

Epitaxy may also be promoted at reduced temperatures by the presence of a thin or ultrathin alloy layer on the substrate surface. Wagner and Ellis (90) grew whiskers from a single-crystal silicon surface by covering it with gold droplets and then depositing silicon by the hydrogen reduction of $SiCl_4$ at $950°C$ (VLS process). A related effect of trace quantities of gold and certain other metals on the nucleation and growth of evaporated silicon layer was experienced by Filby and Nielsen (91). Traces of gold on the surface of

a single-crystal silicon substrate promoted epitaxial growth at 750°C, while a temperature of 1050°C was required without gold. Substantially reduced temperatures for epitaxial or large grain growth occurred also in the case of single-crystal sapphire or fused silica substrates, respectively.

Epitaxial growth tends to be impeded by the presence of a vitreous SiO_2 layer on a single-crystal silicon substrate. Attempts have been made to exploit this effect for the fabrication of devices, since it permits the selective growth of epitaxial silicon in those areas of an oxide-covered single-crystal silicon substrate from which the oxide was removed. Joyce and Baldrey (92) found that a proper adjustment of the deposition variables, such as $SiCl_4$ flow rate and concentration, deposition time, and deposition temperature, was essential for the minimization of overgrowth from the silicon areas onto the SiO_2 mask, causing lack of definition. The factors responsible for silicon growth on amorphous SiO_2 have also been studied by Alexander and Runyan (93).

The use of the halide reduction method was extended by Miller and Grieco (94) and Oda (95) to mixtures of silicon and germanium halides. Epitaxial films of Si–Ge alloys containing a maximum of 25 % germanium atoms could be grown in this fashion.

Manasevit et al. (96–99) and Joyce et al. (100) have grown epitaxial silicon layers on single-crystal insulating substrates, such as aluminum oxide and beryllium oxide, under conditions similar to those used for homoepitaxial growth (deposition temperature ~ 1150°C, deposition rate ~ 0.3 μ/min or higher). In this work it was observed that the use of $SiCl_4$ may lead to a chemical attack of the substrate by a reaction of the type

$$2Al_2O_3 + 3SiCl_4 \rightarrow 4AlCl_3 + 3SiO_2.$$
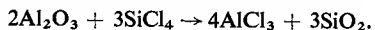
Due to this etching reaction, the surface of the oxide exhibited severe pitting after the grown silicon was removed, and it had to be repolished before it could be used again for the epitaxial deposition of high-quality silicon deposits. The same reaction may also have some bearing on the observation by Blank and Russell (101) that epitaxial growth of silicon on sapphire occurred only in the narrow temperature range extending from about 1050 to 1150°C. Blank and Russell concluded that increased etching of the sapphire surface by $SiCl_4$ at the higher temperature enhances the activity of high-energy adsorption sites located on surface defects. As a result, widely separated growth islands may be formed during the deposition process, depleting silicon and silicon tetrachloride from the ambient gas and thus interfering with uniformly nucleated epitaxial growth. An additional factor impeding epitaxial growth is the production of SiO_2 by the above reaction. Nevertheless various workers obtained high-quality, broad-area heteroepitaxy of silicon on sapphire by the hydrogen reduction of $SiCl_4$ or $SiHCl_3$, provided that

the substrate surface was of high quality (clean and without surface damage) and properly oriented. Hall mobility and minority carrier lifetime were similar to those of bulk material, but the dislocation density of $10^8/cm^2$ was rather large and was probably related to the large dislocation density of the sapphire surface (10^5–$10^6/cm^2$), and to the accommodation of the lattice mismatch between the substrate and the deposit (*102*). However, Schaffer (*103*) has demonstrated that the dislocation density of the sapphire substrate can be greatly reduced (from $10^6/cm^2$ to $10^2/cm^2$) if an epitaxial sapphire film is grown on the substrate under proper conditions. The film defects and the epitaxial relationship between the orientations of the sapphire surface and the silicon deposit were extensively studied by LaChapelle and co-workers (*4*), who have also presented an excellent survey of the results obtained by other workers. They explained the epitaxial relationships by postulating the occupation of metal ion sites by silicon. This arrangement provides for a strong bond of the silicon atoms to the surrounding oxygen atoms. The interface silicon atoms are arranged with optimum spacings for the subsequent growth of the silicon layer.

Epitaxial growth of silicon on single-crystal quartz (β-tridymite) was achieved by Joyce and co-workers (*104, 105*) by the hydrogen reduction of $SiHCl_3$ at temperatures ranging from 950 to 1250°C. Furthermore, Manasevit and co-workers (*99, 106, 107*) deposited single-crystal silicon on single-crystal beryllium oxide and on magnesium aluminate spinel by the hydrogen reduction of $SiCl_4$ at 1175°C.

(2) *Hydride pyrolysis.* The deposition of silicon by the thermal decomposition of silane, SiH_4, affords outstanding simplicity, in view of both the chemical reaction and the apparatus. The only reaction by-product is hydrogen and, therefore, the attacking of the substrate and autodoping that occur with the halide reduction method are greatly reduced. As has been discussed above, dopants can be conveniently introduced as gaseous hydrides such as PH_3 and B_2H_6. Abrupt doping profiles in silicon films can be obtained more easily by hydride pyrolysis than by halide reduction. This is a consequence of both the smaller epitaxial growth temperature and the smaller degree of back-etching afforded by the hydride pyrolysis.

Silane yields silicon at temperatures > 400–600°C by the reaction

$$SiH_4 \ (g) \rightarrow Si \ (s) + 2H_2 \ (g)$$
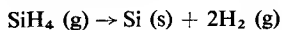
which, to a small extent, is probably accompanied by the formation of polymers (*108*). Decomposition at the lower temperatures is little affected by the presence of Group III and V hydrides, since they tend to decompose less easily than silane. The silane decomposition efficiency improves with increasing temperature and decreasing pressure until a 100% efficiency is reached for temperatures ranging from $\approx$780°C to above the melting point of silicon

provided the pressure is below 8 Torr. However, at temperatures above the melting point of silicon, the efficiency may drop because a reversal in the direction of the reaction may occur.

Perhaps the only drawback of using silane, a gas under ambient conditions, is that it must be handled with caution since it ignites spontaneously on exposure to air. However, silane diluted with hydrogen or a rare gas to a concentration of less than 5 vol% is not pyrophoric and can be stored at a pressure of 1000 psi in a gas cylinder.

Basic work on the deposition of silicon films by silane pyrolysis was performed by Kagdis (109). He obtained epitaxial films of silicon on (111) silicon substrates when the silane decomposition took place at a reduced pressure of 2–11 Torr and at temperatures of 960°C and above. Lewis et al. (110) reported a lower temperature limit of 930°C for epitaxial growth. Mayer and Shea (111) used the pyrolysis of SiH_4 diluted with H_2 and obtained epitaxy over a wide range of $H_2:SiH_4$ ratios and temperatures. The temperature range 1175–1210°C yielded the best-quality films. A deposition rate minimum observed at 1210°C was believed due, in all likelihood, to an adsorption–desorption mechanism which tended to reduce the net reaction rate. Bhola and Mayer (108), also using SiH_4 diluted with H_2, obtained epitaxial films on (111) silicon substrates polished with HCl at 1200–1250°C and fired in H_2 at 1200°C before the run. For a $H_2:SiH_4$ mixture of 0.2 vol % in the deposition zone, the rate of deposition was 0.8 μ/min at 1050–1070°C and 1.12 μ/min at 1100–1140°C. Bhola and Mayer also doped their layers n type and p type with 5×10^{14}–5×10^{19} atoms/cm^3 by using arsine or phosphine, and diborane, respectively. The doping efficiencies in relation to the silane input were: phosphine, 100%; arsine, 25%; and diborane, 10%. At deposition temperatures smaller than 1000°C, the silicon layers tended to be polycrystalline. In contrast to this observation, but in agreement with Kagdis and Lewis et al., Joyce and Bradley (112) obtained homoepitaxial growth over the entire temperature range 920–1260°C. They found that at temperatures >1100°C, the deposition rate varied as $K_1(e^{ap} - 1)$ for a SiH_4 pressure, p, between 0.1 and 1.5 Torr, while the deposition rate was constant for $p > 1.5$ Torr. At temperatures <1100°C the rate varied differently with pressure, namely as $K_2 p^n$, where $n = 1.3$ at 1060°C. The apparent activation energy was determined to be 37 kcal/mole for the temperature range 950–1100°C. Chemisorption, or, more likely, reaction and desorption were assumed to be the rate-controlling steps.

Some of the depositions of epitaxial silicon films on single-crystal sapphire, beryllium oxide, quartz, and spinel ($MgAl_2O_4$) by the hydrogen reduction of $SiCl_4$ or $SiHCl_3$ as described above were duplicated by silane decompositions at similar temperatures and deposition rates. No differences were discovered in the sapphire–silicon epitaxial relationships for silicon layers grown by

either method. However, utilization of the silane decomposition process appeared to be preferable for the following reasons:

(1) The surface of sapphire substrates was not attacked by the silane and could be used over again without refinishing after previously grown epitaxial silicon layers had been stripped off.

(2) The amount of twinning in the silicon layer could be kept much smaller by using the silane process rather than the reduction of $SiCl_4$, apparently because of a faster nucleation rate achieved with the former under comparable reaction conditions and a resulting coalescence of smaller growth islands (4).

The growth rate of silicon films deposited by pyrolysis of SiH_4 at 1150°C was found to depend on the orientation of the film. For example, (111) silicon forming on a (11$\bar{2}$3) sapphire face grew 38% more slowly than (001) silicon forming on a ($\bar{1}$012) face.

Heteroepitaxial growth of silicon on single-crystal quartz using silane pyrolysis at a reduced pressure (≈ 1 Torr) was accomplished by Joyce and co-workers (100) at deposition temperatures of 950–1250°C. Furthermore, Miller and Manasevit (99) achieved the growth of epitaxial silicon on single-crystal beryllium oxide by silane pyrolysis at 1175°C, and Manasevit and Forbes (107) under similar conditions on single-crystal magnesium aluminate spinel. Wang et al. (113) stated that their epitaxial boron-doped or antimony-doped epitaxial silicon films grown on stoichiometric spinel exhibited compressive stress due to the thermal expansion difference between the film and the substrate. They found growth pyramids, microtwins, stacking faults, and dislocations to be the predominant defects.

(3) *Halide disproportionation.* The halide disproportionation method has been used to grow oriented silicon films by either the closed-tube or the open-tube process. The deposition process is based on the reaction:

$$\left. \begin{array}{l} Si + 2I_2 \rightarrow SiI_4 \\ Si + SiI_4 \rightarrow 2SiI_2 \end{array} \right\} \quad \text{at} \quad \approx 1100°C$$
$$2SiI_2 \rightarrow Si + SiI_4 \quad \text{at} \quad \approx 900°C.$$
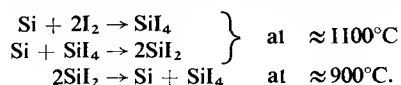
The source silicon, which may also act as a dopant source, is heated to a temperature above 1000°C, typically 1100°C, while the substrate is held at a temperature of 900°C or lower. Deposition of silicon by the hydrogen reduction of SiI_4 has also been suggested. The latter is solid under ambient conditions, can be refined at $\approx 125°C$, and should offer the advantage of a low reduction temperature. However, the heated lines necessary for introducing it into the deposition chamber are inconvenient (67).

The use of chlorine and bromine instead of iodine for silicon deposition by disproportionation has been considered but was found to be less favorable thermodynamically (84). Anderson et al.(114) discovered that tellurium was a suitable transport agent for the deposition of epitaxial silicon layers on

GaAs and GaP at 850°C in a closed system permitting the formation of abrupt heterojunctions.

Iodide disproportionation in a closed tube permitted Wajda *et al.* (*19*) to produce homoepitaxial silicon films on (111) and (100) oriented substrates at a substrate temperature as low as 800°C. Oberly and Adams (*115*) attempted to produce similar results in an open-tube system. In their apparatus, iodine vapors generated from a source at 200°C were swept through the deposition chamber with helium acting as a carrier gas. The silicon source, located in a first temperature zone, was heated to 1300°C while the substrate in a second temperature zone was held at 1000°C. However, only partial success was achieved with this method, since epitaxial growth occurred only in localized areas of the substrate.

Although it appears that the iodide disproportionation method can yield epitaxy at substrate temperatures lower than those usually required in pyrolysis and halide reduction systems, its use has been restricted. The main reasons are: the difficulty in cleaning the substrate surface in the closed system, and in particular, in removing an oxide layer; the difficulty of keeping the gas phase clear of undesired impurities; and the complications arising when switching of the dopant or generation of a specified impurity profile during a run are desired. The substrate surface in the closed system is commonly cleaned merely by initially reversing the role of the substrate and the source by interchanging their temperatures.

b. Germanium. The chemical vapor deposition and doping methods used for silicon apply also to germanium in an analogous fashion. Moreover, in comparison with silicon, the deposition of epitaxial germanium is facilitated by the lower temperature required, and the smaller tendency of germanium to oxidize.

(1) *Reduction of halides.* As in the case of silicon, the hydrogen reduction of halides is the most popular method for producing epitaxial films of germanium. Sheftal *et al.* (*70*) reported, together with their work on silicon, the deposition of homoepitaxial germanium by the hydrogen reduction of GeCl$_4$, obtaining good growth at 850°C. Matovich and Andres (*116*) achieved epitaxial growth at a temperature as low as 575°C, contrary to the finding of Christensen and Teal (*117*) that only etching of the germanium substrates takes place at this low temperature. Miller and Grieco (*46*) investigated the hydrogen reduction of GeBr$_4$ and derived an activation energy of 2.5 kcal/mole from the temperature dependence of the deposition rate. The corresponding value for the reduction of GeCl$_4$ was given as 3 kcal/mole by Kyle and Grossman (*118*). Cave and Czorny (*87*) investigated the preparation of doped epitaxial germanium layers on (111) germanium substrates by GeCl$_4$ reduction. They obtained growth rates of 0.1–8 μ/min at temperatures ranging

from 600 to 920°C. Sources for the dopant were the independently introduced gases phosphine, PH_3, diluted in H_2 for n-type layers, and diborane, B_2H_6, diluted in H_2 for p-type layers. The latitudes of dopant concentrations that could be achieved were $\sim 10^{15}-10^{19}$ atoms/cm^3 for n-type layers, and $\sim 10^{15}-10^{20}$ for p-type layers. Silvestri (*119*) observed that at deposition temperatures ranging from 600 to 850°C the deposition rate was essentially independent of either the temperature or the hydrogen flow rate (over a wide range of flows), but varied linearly with the $GeCl_4$ flux. From this he concluded that the deposition rate was controlled by mass transfer. In contrast, at temperatures smaller than 600°C the deposition reaction was not complete.

(2) *Hydride pyrolysis.* Relatively little attention was given in the past to the thermal decomposition of germane, GeH_4, apparently due to the difficulty of obtaining it with sufficient purity. However, the preparation of germane yielding high-quality germanium layers is possible and has been described by Roth *et al.* (*120*). Early investigations were concerned mainly with the kinetics and mechanism of decomposition, and with depositions on polycrystalline substrates. In 1956, Becker and Lark-Horowitz (*121*) reported on the electrical characteristics of polycrystalline germanium, p type and n type, deposited on quartz substrates by the thermal decomposition of GeH_4 at 600°C. The crystallite size ranged from 0.3 to 0.5 μ. Among the first workers to report homoepitaxial growth were Davis and Lever (*122*). But while they had to heat the substrates to 900°C, Christensen (in *123*) was already able to obtain homoepitaxial growth at 550°C. This lower epitaxial temperature was thought to be related to a higher purity of the germane and a better substrate surface. Tamaru *et al.* (*124, 125*) examined the kinetics of germane pyrolysis and concluded that the decomposition proceeds about one order of magnitude faster on the substrate surface than in the gas phase. They postulated that GeH_x radicals migrate freely on a germanium surface and thus promote high crystalline perfection. The growth of doped homoepitaxial germanium layers was described in detail by Roth *et al.* (*120*). These workers obtained smooth layers on (111) germanium substrates over the temperature range 700–900°C with a typical deposition rate of 0.1 μ/min.

The pyrolysis of germane has also been employed to grow epitaxial Ge layers on foreign substrates. Zanovick (*126*) obtained epitaxial growth of p-type Ge on n-type (111) GaAs substrates at temperatures between 500 and 800°C. The growth rate was on the order of 10 μ/hr at 750°C. Papazian and Reisman (*127*) performed epitaxial deposition of Ge on semiinsulating GaAs at temperatures in the range 650–750°C. At 800°C alloying believed due to a Ge–Ga reaction occurred. The use of undoped GeH_4 resulted in a p-type surface of the deposited layer; but the interior of the layer contained also an n-type region due, presumably, to As diffused into it from the substrate. Light *et al.* (*128*) studied the plastic deformation due to the differential co-

efficient of thermal expansion in epitaxial Ge-layer, 5–10 μ thick, grown on (100) GaAs at 700°C. Spinel of (100) or (111) orientation was used as a substrate by Dumin (129) for growing epitaxial germanium films 5–10 μ thick. The films were p type, 0.1 Ω cm, and exhibited mobilities of 200–300 cm⁹/ sec.

(3) *Halide disproportionation*. The disproportion between germanium and its iodides has particular attraction for the deposition of germanium because it has been demonstrated to yield epitaxial deposits at temperatures as low as 400°C. Both open- and closed-tube deposition systems have been employed. Dunlap *et al.* (130) performed depositions of epitaxial germanium by use of the open-tube process, and Cronemeyer (131) studied the resulting donor and acceptor distributions. Using the closed-tube process, Marinace (132) was able to grow epitaxial layers of germanium on germanium as well as on gallium arsenide by reacting the source material with iodine at 480–700°C and carrying out the deposition on a substrate held at a typical temperature of 400°C. Takabayashi (133) reported that he obtained better crystalline quality and higher resistivity in deposits prepared in a closed- rather than open-tube system, and that the properties of the deposited material were equivalent to those of melt-grown material. The latter two workers investigated the dependence of the growth rate on the substrate orientation and found it to increase in this sequence of orientations: (100); (111), (110). In contrast to this, Tung (134) reported that in the case of hydrogen reduction of $SiCl_4$ the deposition rate increased with the orientations (111), (100), (110). Baker and Compton (135) stated that no correlation between the presence of iodine contamination of 10^{14}–10^{15} atoms/cm³ and the electrical properties of the deposited material could be observed.

In addition to iodine, hydrogen iodide (136), chlorine (137), or, more frequently, water vapor were also successfully used as transfer agents. Working with a closed system, Lever and Jona (25) obtained epitaxial growth of germanium at 828°C with growth rates of 0.2 μ/hr by using water vapor as the transporting agent according to the reaction:

$$Ge \text{ (s)} + H_2O \text{ (g)} \rightleftharpoons GeO \text{ (g)} + H_2 \text{ (g)}.$$
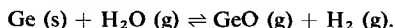
Robinson (24), using an extremely close spacing (0.1–0.5 mm) between the source material [(111) Ge at 805°C] and the substrate [(111) Ge of (100) GaAs at 770°C], and working without a water atmosphere intentionally added to the system, was able to increase the growth rate of the epitaxial layers to 4–6 μ/hr. The close-spaced technique was first suggested by Nicoll (138) for the deposition of a variety of semiconductors.

Among other workers who successfully grew epitaxial layers of germanium on foreign substrates were Anderson (139), using a closed-tube iodide disproportionation system and single-crystal GaAs substrates, and Oldham *et*

al. (*140*) using iodide disproportionation in an open tube and single-crystal silicon substrates. Riben *et al.* (*141*) deposited epitaxial germanium layers at 375–425°C at rates of 5–10 μ/hr on single-crystal Ge, Si, and GaAs, also by the open-tube iodide process. Good results were obtained only on substrates cleaned *in situ* during deposition, in disagreement with the results reported by Takabayaski (*133*) who used gas etching. Marinace (*142*) grew epitaxial Ge films on GaAs to act as a Zn-diffusion mask.

A brief mention shall be given here to the investigations by Tarui and co-workers (*143*) on the effects of an electric field normal to the substrate surface on epitaxial growth of germanium and silicon by disproportionation of GeI_2 and hydrogen reduction of $SiCl_4$, respectively. When the field was varied from zero to about 1.5×10^3 V/cm in magnitude, a steady increase in the growth rate resulted. The increase was largest when the substrate had negative polarity and amounted to over 100% at the maximum applied field. The transfer ratio for dopants was also affected by the electric field, but in a fairly complicated fashion.

c. GaAs, GaP, and Other Compound Semiconductors. Chemical vapor deposition has special appeal for the deposition of epitaxial layers of the III–V compound semiconductors, because of the difficulties arising from decomposition and fractionation in their thermal evaporation in vacuum.

The various approaches taken in the chemical vapor deposition of gallium arsenide fall into two groups, namely (1) those in which a single source of gallium arsenide is used, and (2) those in which the gallium- and the arsenic-carrying vapors are generated from separate sources. Because of its relative simplicity, the first approach has received most attention, in combination with both closed-tube and open-tube techniques. Various transport agents were successfully used: iodine, bromine, hydrochloric acid, metal halides, and water vapor. In the case of the halides, the reaction responsible for the transport of GaAs has been established by total pressure measurements and absorption spectroscopy to proceed as

$$4GaAs\ (s) + 2GaX_3\ (g) \rightleftharpoons 6GaX\ (g) + As_4\ (g) \qquad (X = Cl,\ Br,\ I)$$
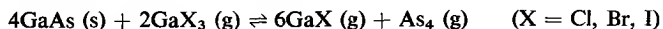
[Lyons and Silvestri (*144*), Richman (*145*)], while

$$2GaAs\ (s) + H_2O\ (g) \rightleftharpoons Ga_2O\ (g) + As_2\ (g) + H_2\ (g)$$

holds in the case of water vapor transport (*146*).

Pioneering work in this area was done by Antell and Effer (*147*), who grew crystals of GaAs in a closed-tube disproportionation system with the vapors of $GaCl_2$ and As acting as transporting species. Among the first workers to deposit homoepitaxial GaAs layers were Pizzarello (*148*), Hagenlocher (*149*), and Okada (*150*), who used the iodine disproportionation, again in a closed-

tube system. The source temperatures ranged from 700 to 770°C, and the respective substrate temperatures from 650 to 720°C. In order to prevent oxide detrimental to epitaxial growth from forming during the deposition process, the reaction tube was pumped out and backfilled with H_2 to 200 Torr before sealing. In addition, the temperature reversal technique mentioned above was used to etch-clean the substrates.

Moest and Shupp (*151*) employed HCl instead of I_2 as a reagent for transporting GaAs and GaP. They found no influence of the substrate orientations (100), (110), (111), and ($\bar{1}\bar{1}\bar{1}$) on the deposition rate of GaAs. On the other hand, Okada *et al.* (*152*) and Pizarello (*148*) were unable to obtain epitaxial growth on a ($\bar{1}\bar{1}\bar{1}$) GaAs substrate with iodine as a transport agent. However, Pizarello found in agreement with Moest and Schupp that no such difficulty existed when he used HCl. In order to explain this phenomenon, Goldsmith (*153*) suggested that the stronger acid, HCl, is more effective in neutralizing the basicity of the ($\bar{1}\bar{1}\bar{1}$) GaAs surface.

A doped GaAs source can be used to grow doped films by a method analogous to that used for silicon or germanium. Silvestri and Fang (*154*), growing zinc-doped films, obtained an efficiency of less than 0.3 for zinc transfer in iodide disproportionation reaction, while Sarace (in *155*) obtained transfer efficiencies ≈ 1 for tin and tellurium with HCl as transport reagent.

There exist still other transport and doping methods for closed systems. For example, Holonyak and co-workers (*156*) grew heavily doped GaAs layers in a closed-tube system by employing the metal halides $ZnCl_2$, $SnCl_2$, $CdCl_2$, $HgCl_2$, and $MgCl_2$ as transfer and doping agents, and Nicoll (*138*) deposited epitaxial GaAs layers in a closed system with a very narrow spacing between source and substrate (≈ 0.25 mm) by using water vapor as transport reagent and oxides as transported species.

Disproportionation techniques were also combined with open-tube techniques in various modifications. Williams and Ruehrwein (*157*) fed HCl gas over a GaAs source held at 750°C in a first chamber of a deposition system, and swept the reagent gases $GaCl_3$, GaCl, and As_4 into a second chamber held at a lower temperature and containing a single-crystal GaAs substrate. Epitaxial growth resulted through the disproportionation of the halide gases. In order to avoid a possible deficiency of the more volatile constituent, As, Newman and Goldsmith (*158*) added some crushed As to the crushed GaAs source material in the first chamber. Using a source temperature of 1000°C, they obtained single-crystal growth at substrate temperatures in the range 750–900°C, and polycrystalline growth below 750°C. A difference in the growth rate on (111) and ($\bar{1}\bar{1}\bar{1}$) was noted. While the undoped growth layers tended to be *p* type, the addition of Sn or Te to the crushed As in the first chamber resulted in *n*-type films.

Frosch and Thurmond (*159*) employed hydrogen saturated with water

vapor as transport reagent for GaAs or GaP source material in a wide-spaced growth apparatus and achieved good-quality epitaxial films at a source temperature of 1050°C and a substrate temperature of about 1000°C. Their finding of the mass transport increasing with increasing water vapor content of the carrier gas was confirmed by Gottlieb and Corboy (*146*) for a close-spaced, open-tube system in which they deposited GaAs on (111) germanium substrates. In the latter system the deposition rate varied with the square root of the partial pressure of the water vapor carried into the system by hydrogen that had flowed over crushed ice. With a source temperature of 800 ± 50°C and a substrate temperature of 700 ± 50°C, and maintaining a temperature difference of 50–100°C, Gottlieb and Corboy were able to produce a growth rate of 0.2–0.8 μ/min. From a plot of log deposition rate versus the inverse absolute temperature, they determined an activation energy of 49 kcal/mole. Under a wide variety of deposition conditions, the outer face of the GaAs layer grown on (111) Ge substrates was always the ($\bar{1}\bar{1}\bar{1}$), arsenic, face. When no water vapor was externally introduced, growth still did occur, but with a rate smaller by about one order of magnitude. The deposition rate decreased with increasing substrate-source distance over the investigated range 0.25–1 mm. It was found difficult to grow p-type layers of GaAs by the water vapor method because of unintentional doping with Ge when a Ge substrate was used, or, in the case of GaAs substrates, because of the low vapor pressure of p-type dopant oxides acting as transporting agents for a p-type GaAs source. The work just described was an extension of work by Nicoll (*138*), and Robinson (*24*), on chemical transport of GaAs in close-spaced systems. Robinson's apparatus is interesting because it permitted the deposition of GaAs without intentionally introducing water vapor into the system. The deposition merely took place in a flow of purified hydrogen, or even in a vacuum of 10^{-6} Torr. GaAs was grown on (111) and (100) Ge held at 725°C, while the temperature of the GaAs source ranged from 825 to 900°C. The deposition rate of about 1–3 μ/min was independent of the spacing if the latter was between 0.25 and 0.75 mm but decreased drastically for smaller spacings, perhaps because of increasing heat transfer from the source to the substrate. Optimum substrate temperatures for obtaining mirror-bright single-crystal deposits fell between 725 and 775°C. At substrate temperatures below 725°C, the layers were polycrystalline, while at temperatures above 775°C hillocks and roughness were observed, apparently due to transport of GaAs away from the substrate. In fair agreement with Gottlieb and Corboy, the activation energy was determined to be 43 kcal/mole. Again, the ($\bar{1}\bar{1}\bar{1}$), arsenic, face was outermost for layers grown on (111) Ge. A noteworthy influence of the face of the GaAs source on the deposition rate and on the structure of the deposit was found: When its ($\bar{1}\bar{1}\bar{1}$) As surface faced the Ge substrate, the deposition was much more rapid than when its

(111), gallium, surface did, but the latter yielded much smoother surfaces of the deposits. In both cases, the surface of the source material became very rough during usage. In contrast, use of (100) GaAs as a source material yielded smooth deposits as well as smooth source surface.

Working on the formation of GaAs–Ge heterojunctions, Jadus et al. (160) succeeded in growing epitaxial layers of n-type GaAs on p-type Ge substrates at temperatures as low as 475°C. This was made possible by the use of a closed-space, open-tube system with HCl of about 20 Torr partial pressure serving as transport agent. The deposition rate was 3 μ/min for substrate temperatures in the range 550–585°C, while temperatures of the GaAs source were higher by 110–125°C. The problem of forming an undesired n layer in the germanium by diffusion of As from the GaAs deposit was alleviated by using either a high uniform doping of the p-type Ge ($\geq 4 \times 10^{19}$/cm^3), or else a dopant gradient (concentration near the surface $\approx 4 \times 10^{18}$/cm^3) which tended to retard As diffusion, a low growth temperature, and a short deposition time.

Among the deposition systems not using GaAs as source material one can find, again, representations of open- and closed-tube systems. Antell and Effer (147) investigated the use of both for the preparation of bulk GaAs, as well as for InAs, InP, and GaP. In the open-tube system, GaCl$_2$ and arsenic vapor were fed into the hot zone containing the substrate, while Ga and AsCl$_3$ served as reagent sources in the closed-tube system. The closed-tube disproportionation system of Lyons and Silvestri (144) was charged with GaCl$_3$ and As in the hot zone. Tausch and Longo (161) grew epitaxial GaAs in an open-tube system from GaCl$_3$ and AsCl$_3$ carried into the system by H$_2$ gas. Ing and Minden (162), instead, used Ga and As as a source material, and HCl and H$_2$ as reagent gases. Frosch and Thurmond (159) arranged an As source upstream from a Ga source and passed wet H$_2$ vapor saturated with arsenic over the Ga on the way into the reaction chamber. Stopek (163) deposited GaAs layers from the combination H$_2$ + AsCl$_3$ + Ga. Rubenstein and Myers (164) preferred using the reaction

$$4GaCl_3 + As_4 + 6H_2 \rightarrow 4GaAs + 12HCl$$
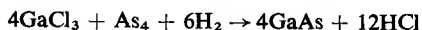
at ≈ 670°C because it permitted a wide latitude in the adjustment of the relative gas flows without an adverse effect on the deposition process.

The selective area deposition of epitaxial GaAs by means of the Ga–AsCl$_3$ reaction system, using SiO$_2$ as a growth-inhibiting mask, has been described by Mehal et al. (165). Planar device structures were formed by etching holes through the SiO$_2$ into the GaAs substrate, and growing epitaxial deposits in the holes.

Goldsmith and Oshinsky (166) built a T-shaped chamber in which one branch of the crossbar of the "T" contained gallium, and the other branch

contained arsenic. Hydrogen was bubbled through zone-refined GaCl₃ at 85°C and fed over the Ga held at 750°C to form GaCl, while another stream of H₂ was fed over the As held at 425°C to carry its vapor into the system. The vapors, combining at the junction of the "T," were directed into the third arm where the deposition took place on (111) or (100) GaAs at a temperature of 725°C. Smooth growth was obtained on the chemically polished (111) surface at a deposition rate of 2.5 μ/hr, but layers grown at a rate of 25 μ/hr on a mechanically polished (111) surface were rough. Smooth layers could also be deposited at a rate of 13.5 μ/hr on chemically polished (100) surfaces. A small leak of 10^{-4} std cm³/sec of air was found to interfere with the reactions sufficiently to reduce the growth rate to virtually zero. In doping experiments, H₂S was introduced together with the H₂ flowing over the As source. By this method, the carrier concentration in the n-type deposit could be varied from a low value of about 5×10^{16}/cm³ (for undoped runs) to a maximum of 4×10^{18}/cm³. The p-type doping was achieved by adding Zn to the Ga source, resulting in a minimum hole concentration of about 10^{19}/cm³. Goldsmith and Oshinsky pointed out that their deposition method was equally applicable to the deposition of GaP, InAs, InP, AlAs, and AlP, as well as to selenides and tellurides of Group III elements.

Amick (54) growing GaAs on Ge, used an arrangement similar to that of Goldsmith and Oshinsky, except that HCl gas diluted with H₂ took the place of the GaCl₃ carried by H₂, and that a provision for *in situ* etching of the Ge substrate with HCl gas at 800°C was made. It was reasoned that the reaction sequence occurred in the following steps:

(a) $4\text{As (s)} \xrightarrow[400-450°C]{} \text{As}_4 \text{ (g)}$

(b) $\text{HCl (g)} + \text{Ga (s)} \xrightarrow[700-800°C]{} \text{GaCl}_3 \text{ (g) } (90\%) + \text{GaCl (g) } (10\%)$

(c) $3\text{GaCl (g)} \xrightarrow[600-700°C]{} 2\text{Ga (s)} + \text{GaCl}_3 \text{ (g)}$

(d) $4\text{Ga (s)} + \text{As}_4 \xrightarrow[600-700°C]{} 4\text{GaAs (s)}.$

A smooth surface on the GaAs deposit was obtained when the substrate temperature was raised to about 750°C. In agreement with the observations by Gottlieb and Corboy (146), the arsenic face was outermost in all cases, and the gallium face adjacent to the Ge substrate. This fact was ascribed to a solubility in Ge that is higher for Ga than for As, and a vapor pressure and diffusion constant in Ge that is higher for As than for Ga. However, other workers found the Ga face outermost on GaAs deposits grown on Ge [Newman and Goldsmith (158), Okada (150)], and this discrepancy may be due to differences in the chemical species present during the deposition process and their concentrations, or in the cleanliness of the substrate. In the same setup, Amick deposited GaAs at about 700°C on (111)-oriented crystal faces of molybdenum as well as tungsten. While the GaAs layer was

polycrystalline on the Mo substrate, it developed a high degree of orientation on the W substrate. Unfortunately, the deposit adhered well only to the Mo substrate. A modification of Amick's system is that reported by Leonhardt (*167*), who replaced the H_2–HCl mixture for transporting the gallium by H_2–HI prepared from elemental iodine and H_2. The gas streams carrying the gallium and the arsenic were mixed at 800°C and the epitaxial depositions carried out at 620°C.

Recently, Manasevit and Simpson (*168*) have pointed out the advantage of using metal–organic compounds for the deposition of III–V gallium compounds: namely, the fact that etching species are absent from the chemical reaction. As a consequence, the usual difficulties with autodoping are largely eliminated. Epitaxial films of GaAs, GaP, and $GaAs_{1-x}P_x$ were produced by the simultaneous thermal decomposition in a hydrogen atmosphere of triethylgallium, or preferably, trimethylgallium, and AsH_3, PH_3, or AsH_3–PH_3, respectively. Single-crystal Ge, GaAs, Al_2O_3, BeO, ThO_2, and spinel served as substrates.

As for the deposition of compound semiconductors other than GaAs, most efforts were concentrated on materials such as GaP, $GaAs_{1-x}P_x$, $GaAs_{1-x}Sb_x$, InAs, ZnS, ZnSe, CdS, and CdSe. These semiconductors derive their attractiveness from applications in electroluminescent and laser devices, photoconductors, Gunn devices, heterojunctions, and others. Below we will list some work on the above materials done in addition to that already mentioned. Kamath and Bowman (*169*) deposited epitaxial GaP layers, claimed to be free of contamination by arsenic, on single-crystal GaAs substrates. Resistivities in excess of 10^{10} Ω cm were obtained when a controlled amount of water vapor was added during the deposition. It was concluded that the deposition proceeded according to the reaction

$$5Ga + 2PCl_3 \rightarrow 2GaP + 3GaCl_2.$$
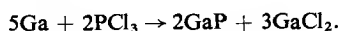
In earlier work by Effer and Antell, the pertinent reaction had been assumed to be

$$2Ga + PCl_3 \rightarrow GaP + GaCl_3.$$
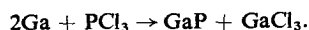
The latter reaction between Ga and PCl_3 prevailed also in the system used by Luther and Roccasecca (*170*) for growing epitaxial zinc- and cadmium-doped GaP on GaAs at 850–900°C. The films deposited at a rate of 0.1 mm/hr exhibited a high density of stacking faults after chemical etching. Furthermore, the GaAs (111)-A face was found to provide a substrate preferable to the (111)-B face since it led to a higher growth rate, a smoother film surface, and a smaller background sulfur doping.

By reacting $AsCl_3$ vapor together with the vapors of PCl_3 and Ga, Akasaki

et al. (*171, 172*) achieved epitaxial growth of $GaAs_{1-x}P_x$ on GaAs substrates. They found that the influence of the substrate orientation on the growth rate decreased as the factor x was increased. These authors also studied the preparation and properties of epitaxial $GaAs_{1-x}P_x$ films heavily doped with sulfur ($>10^{18}/cm^3$). The films were prepared at 790°C at a growth rate on the order of 0.5 μ/min.

Burmeister and Regehr (*173*) obtained epitaxial growth of $GaAs_{1-x}P_x$ ($0 < x < 0.45$) on Ge substrates, of which those with (311) orientation gave the best results. However, the layer contained some Ge carried there by the vapor transport process (rather than by diffusion). Hoss *et al.* (*174*) grew degenerate *p*-type GaAs, GaP, and $GaAs_xP_{1-x}$ for tunnel diode application by using a close-spaced system with $ZnCl_2$ vapor acting as both transporting species and dopant supply.

In the setup devised by Tietjen and Amick (*175*) for growing epitaxial $GaAs_{1-x}P_x$ on GaAs and Ge substrates, the reagent gases were $AsH_3 + H_2$ and $PH_3 + H_2$, mixed in a reaction zone at 850°C with gallium halide vapor derived from passing $HCl + H_2$ over gallium at 775°C. The deposition occurred in an adjacent zone held at 750°C. Both *n*- and *p*-type films were produced, doped with Se and Zn, respectively. The impurities were introduced into the system in the form of H_2Se and $H_2 + Zn$. Replacing the PH_3 with SbH_3 enabled Clough and Tietjen (*176*) to grow epitaxial $GaAs_{1-x}Sb_x$ layers with $0.1 < x < 0.5$, which may permit the construction of Gunn-effect devices with improved characteristics.

The growth and the properties of ZnSe crystals by chemical transport with HCl, HBr, or I_2, and of ZnS and Zn(S, Se) by I_2 transport, were described by Parker and Pinnell (*177*). Luminescent films of ZnS were prepared as early as 1957 by Studer *et al.* (*178, 179*). Zinc vapor was reacted with MnCl and the gas mixture was combined with H_2S over a substrate heated to 400–600°C. Doping of the films was accomplished with phosphorus vapor and with copper or arsenic via their halides. Baczewski (*180*) grew (111) oriented epitaxial layers of ZnSe on the (111) gallium plane of GaAs at rates of 5 μ/hr by using a ZnSe source and a transporting medium of HCl–H_2–A. The transport proceeded according to

$$ZnSe + 2HCl \underset{570-610°C}{\overset{600-740°C}{\rightleftharpoons}} ZnCl_2 + H_2Se.$$
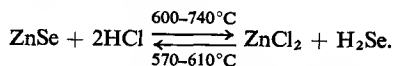
In order to reduce the corrosive effects of the HCl on the substrate, it was found advantageous to add NH_4I to the gas stream. The NH_4I neutralized the excess chlorine by forming NH_4Cl, thus exchanging the less corrosive iodine for the chlorine. Single-crystal growth was attained only in a fairly narrow range of temperatures, 590°C being an optimum. Hovel and Milnes (*181*) produced epitaxial ZnSe layers on (111) Ge with a close-spaced system

(gap $\approx$ 0.3 mm) working with a HCl–H$_2$ atmosphere and adding an n-type dopant. At temperatures of the ZnSe source of 600–800°C, and substrate temperatures of 520–620°C, the deposition rates ranged from 5 to 150 μ/hr.

The equilibrium conditions in the chemical transport of ZnSe in the presence of iodine vapor according to the reaction

$$ZnSe \text{ (s) } + I_2 \text{ (g) } \rightleftharpoons ZnI_2 \text{ (g) } + 1/2Se_2 \text{ (g)}$$
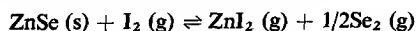
has been studied by Sedgwick and Agule (*182*) by the Bourdon gage technique. The vapor transport becomes effective at temperatures >450°C. Instead of halides, Galli and Morritz (*183*) used hydrogen as a transport medium for depositing ZnSe, CdS, and CdSe on (111) Ge and (111) GaAs. ZnSe grew with the cubic zinc sulfide structure, while CdS and CdSe exhibited the hexagonal wurtzite structure in all cases.

Epitaxial growth of CdS on GaAs and GaP by halide transport was reported by Weinstein and Mena (*184*). CdS films on tantalum substrates were prepared by Belvinger and Smith (*185*). The films were composed of crystallites of 2–75 μ diam which exhibited a preferred orientation such that the c axis was perpendicular to the substrate. The depositions were carried out in a close-spaced system (gap $\approx$ 1.5 mm), with an evaporated CdS layer serving as a source. Highly purified helium was the only medium introduced into the system, and the actual transport agent remained unidentified. Typically, the source temperature was 740°C, and the substrate temperature 60°C lower. Similar systems worked with H$_2$ or I$_2$ as a transport agent [Hegyi (*186*)].

d. Silicon Carbide. Silicon carbide as a film is of importance as both a wide-band gap semiconductor, and protective coating, e.g., for carbon susceptors used to heat single-crystal silicon substrates in epitaxial growth or oxidation furnaces. In the latter function, coatings of about 0.1–1 mm thickness are used. The coating is inert to HCl, HF, and H$_2$SO$_4$ at 300°C and higher temperatures. Its oxidation resistance is due to a protective SiO$_2$ layer that forms on the surface in an oxidizing atmosphere. Upon exposure to oxygen at 1000°C for two weeks the SiO$_2$ layer grows to a thickness of about 1 μ (*187*).

Silicon carbide deposits may be formed indirectly by engaging the substrate in the reaction, or directly by reactions independent of the substrate. Examples for indirect deposition reactions are the hydrogen reduction of SiCl$_4$ in combination with a carbon substrate at 1925–2000°C [Pring and Fielding (*188*)], or the thermal decomposition of CH$_4$ or other hydrocarbons in combination with an SiO$_2$ or Si substrate [Iley and Riley (*189*)]. The direct deposition generally involves processes such as the thermal decomposition of SiC and its subsequent reactive sublimation on a cooler surface [Lely (*190*)], the

hydrogen reduction of $SiCl_4$ in the presence of a hydrocarbon [Pring and Fielding (*188*), Powell (*191*)], e.g.,

$$SiCl_4 + H_2 + C_6H_6 \xrightleftharpoons[1850-2000°C]{} SiC + \ldots \quad (189),$$

$$SiCl_4 + C_6H_6 \xrightleftharpoons[1700°C]{} SiC + \ldots \quad (189),$$

$$SiCl_4 + H_2 + C_7H_8 \xrightleftharpoons[1250°C]{} SiC + \ldots \quad (191),$$
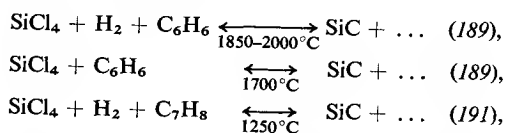
the reaction of $SiCl_4$ with CCl_4 in the presence of hydrogen at $\approx 1700°C$ [Jennings *et al.* (*192*)], or the pyrolysis of compounds such as CH_3SiCl_3 or $(C_2H_5)_2SiCl_2$ at temperatures ranging from about 1300 to above 2400°C [Kendall and Yeo (*193*)].

Common difficulties with SiC deposits are their roughness due to crystallinity, their nonadherence, their polymorphology, their lack of stoichiometry, and their contamination with impurities (*194*). The electronic conduction properties of chemical-vapor-deposited SiC with and without intentional doping were investigated by Kendall (*195*).

The crystalline structure of the deposits obtained by the above methods has been generally cubic β-SiC for deposition temperatures $\lesssim 1700–2000°C$, while at higher temperatures β-SiC or a mixture of hexagonal α-SiC and of β-SiC may form (*192, 196*). However, the 2H polytype of α-SiC (wurtzite structure) has also been detected in some deposits formed at 1400–1600°C [Merz (*197*)]. Unfortunately, only large chunks of polycrystalline SiC have been obtained thus far; the growth of single crystals of reasonable size is not yet possible (*196*).

Epitaxial growth of silicon carbide on both of the opposite {0001} crystal faces (*p* face and *k* face) of several polytype α-SiC crystals has been studied by Brander (*198*). His deposition system consisted of a heated graphite tube in which a temperature gradient was established. A silicon source was placed in the cooler part of the tube ($\approx 1800°C$), and the SiC seed crystal in the hotter part ($\approx 2200°C$). Carbon vapor supplied from the graphite tube (held at $\approx 2500°C$) was swept together with silicon vapor over the substrate by a flow of argon and both vapors recombined at the substrate to yield a SiC growth rate as high as 5 μ/min. However, for obtaining smooth surfaces over areas of several square millimeters and high-quality growth, the deposition rate had to be reduced to 0.1–0.5 μ/min. Substrate temperatures in excess of 1900°C led to perfect homoepitaxy, while lower temperatures led to the nucleation of polycrystalline β-SiC. Under the same deposition conditions, the homoepitaxial growth proceeded twice as fast on the *p* face as on the *k* face.

Campbell *et al.* (*199*) used the simultaneous reduction of $SiCl_4$ and CCl_4 by hydrogen at 1700°C and added gases, such as nitrogen, arsenic, and phosphine, to grow homoepitaxial *n*-type layers of SiC, and diborane to

grow p-type layers. These workers stated that the quality of the epitaxial growth was directly related to the perfection of the substrate surface. Growth defects could always be traced to defects in the substrate. The deposited SiC had the same crystal structure (α- or β-SiC) and orientation as the substrate. For obtaining high-quality epitaxial growth, it was found necessary to work with a sufficiently large excess of hydrogen and to limit the growth rate to a maximum value of 0.7 μ/min.

The growing of hetero epitaxial films of β-SiC on sapphire and silicon was described by Thompson et al. (200). The deposition method used was the pyrolysis of dimethyldichlorosilane at temperatures of 1300–1640°C in the presence of hydrogen (hydrogen excess, 1000:1). The best deposits were obtained at temperatures $>$1625°C on (111) Si and ($\bar{1}$012) sapphire at a rate of about 800 Å/min. The growth of the films proceeded in an epitaxial fashion only to a thickness of about 2 μ; further growth tended to produce a poly-crystalline film structure.

Silicon carbide may also be deposited by chemical vapor transport with hydrogen serving as transport agent. According to Harris et al. (201), α-SiC platelets placed on a graphite susceptor coated with β-SiC gained weight corresponding to a deposition rate of 50 μ/hr at 1800°C in a hydrogen flow, due to transport of SiC from the susceptor coating to the substrate. In the same system, the use of other susceptors made of materials such as Ta, TaSi, Nb, W, and Mo resulted in etching of the SiC substrates, at a rate dependent on the susceptor material. In the temperature range above 1550°C, molyb-denum produced by far the largest etch rate, presumably due to a large hydrogen transport to the sample by surface diffusion along the susceptor in addition to the gas-phase transport. Gaseous etching of SiC may also be accomplished with F_2, HCl, O_2, and Cl_2. The use of the last three gases requires relatively high temperatures in order to avoid the formation of a SiO_2 or carbon residue on the substrate surface. Lamport et al. (202) have stated that ClF_3 may be conveniently used not only for etching Si and Ge, but also SiC at temperatures of only 200–300°C. Etching (111) Si faces of cubic β-SiC by this method produced etch pits, while the C plane did not exhibit a distinctive etch pattern.

2. DIELECTRICS

Dielectric thin films prepared by chemical vapor deposition have recently been receiving a great deal of attention, particularly in conjunction with integrated circuits. Among the functions performed by dielectric films in this application are surface passivation and protection of semiconductors, isolation of circuit elements, gate insulation in insulated gate field-effect transistors, dielectric spacers in capacitors, insulation between leads in multilayer arrangements, and diffusion and photoetching masks. The frequency

region over which the dielectric properties are important ranges from dc to microwaves. Further interest in high-quality dielectric films was stimulated during recent years by the concept of tunnel emission (*203*). Its practicality is contingent upon the fabrication of very thin and uniform dielectric layers, a few tens of angstrom units thick, capable of sustaining electric fields of 10^7 V/cm and currents injected by quantum mechanical tunneling of 1 A/cm^2 and higher. Also to be mentioned is the use of low-leakage dielectric films in charge storage and scan conversion devices. In addition, insulating or semiinsulating films can be used in varistors, coatings of high secondary electron emission yield, optical coatings, corrosion-preventing coatings, high-value resistors, and others. In many cases, chemical vapor deposition produces better dielectric films for these applications than other methods (e.g., wet, thermal, or plasma anodization; reactive or rf sputtering; or direct evaporation in a low-pressure environment), or is more compatible with the overall device-processing procedure.

In the following section we will describe methods for the chemical vapor deposition of some important insulating materials, and typical results which have been achieved with them.

a. Silicon Dioxide. Silicon dioxide is at present the most widely used insulator material in semiconductor and integrated circuit technology, due to its good dielectric and passivating properties, its diffusion blocking capabilities adequate for many cases, and the ease with which it can be selectively etched by using current photolithographic techniques. If the substrate happens to be a silicon wafer, a layer of SiO_2 can be grown by thermal oxidation in dry or wet oxygen. However, use of a deposition method for forming the SiO_2 layer offers the advantage that materials other than silicon can be coated, the thickness and time limitations imposed by thermal oxidation are avoided, and the consumption of substrate material leading to a degradation of the surface or lack of device definition is eliminated. In addition, the SiO_2 layer may be deposited at a reduced temperature over circuit or device structures made of materials that would alloy, react, or diffuse undesirably at the high temperatures required for thermal oxidation (which are on the order of 1000°C or higher). Furthermore, an independent deposition method offers the advantage that doped or composite oxide layers (e.g., alumina borosilicate or silicon oxynitride) can be prepared which offer improved dielectric, diffusion inhibiting, passivating, thermal expansion, or masking properties, or which may act as a dopant source (e.g., phosphorus-doped SiO_2).

The thermally activated chemical vapor deposition of SiO_2 employs either reactions of inorganic compounds such as SiH_4, $SiCl_4$, or $SiBr_4$ with oxygen-containing species, or the pyrolysis of one of the organic silicates which exist in a great variety. Films resembling SiO or SiO_2 have also been formed

by the bombardment of silicon oils or organosilica compounds with an electron beam; this offers the possibility of producing localized deposits [Christy (16), Roberts (204)]. Another deposition method consists of the decomposition of oxysilanes in a low-pressure argon plasma while the substrate is essentially at room temperature [Ing et al. (205, 206)].

(1) *Inorganic deposition media.* Among the deposition methods with thermal activation, the reaction

$$SiH_4 \text{ (g)} + 2O_2 \text{ (g)} \leftrightarrow SiO_2 \text{ (s)} + 2H_2O \text{ (g)}$$
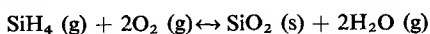
appears to be thermodynamically and kinetically more favorable than other known reactions and lends itself to the deposition of silica films at rather low substrate temperatures. Because of its strong affinity for oxygen, the SiH_4 gas must be adequately diluted—e.g., by argon (207), nitrogen (208), or hydrogen (209)—in order to minimize homogeneous nucleation in the gas phase. Typical flow ratios are $SiH_4:O_2:A = 3:10:500$, $SiH_4:O_2:N_2 = 3.4:88:2500$, or $SiH_4:O_2:H_2 = 1:10:10,000$. At substrate temperatures of 340 and 450°C, deposition rates of 450 and 1000 Å/min have been observed, respectively (207, 209). The same basic reaction with the addition of phosphine, PH_3, has been used to deposit phosphorus-doped silica on single-crystal silicon at substrate temperatures of 375–450°C to act as a diffusion source (210). A deposition rate of 3000 Å/min was reported. In an analogous fashion, a boron diffusion source can be obtained by oxidizing SiH_4 together with B_2H_6 (211).

A different concept has been employed by Chu and Gruber (212) for the chemical vapor deposition of boron-doped silica films containing 10–18% boron: Pyrex glass served as a source material from which silica and boron oxide were simultaneously transported by transport agent consisting of a $HF-H_2O$ mixture. The films were deposited on silicon at a substrate temperature of 400–600°C and were successfullly used as a diffusion source.

Amorphous films of silicon nitride–silicon dioxide mixtures combining the main features of silicon dioxide—good electrical characteristics and good etchability—and silicon nitride—good masking ability against impurities—have been prepared by Chu et al. (213) by the pyrolysis of silane in a mixed ammonia–oxygen atmosphere.

In many cases, the silica films produced by low-temperature processes are not adequate as passivating layers or diffusion barriers as grown. The quality of a deposited oxide layer can be improved by a "densification" procedure which usually consists of exposing the layer to steam at a temperature of 800–900°C for a typical period of 15 min.

Since the diffusion of dopants into silicon is usually carried out at temperatures greater than 900°C, one may also choose to deposit a SiO_2 diffusion barrier to begin with by a higher-temperature process in order to obtain a

better-quality film. An example is the oxidation of $SiCl_4$ according to the reaction

$$SiCl_4 \text{ (g)} + O_2 \text{ (g)} + 2H_2 \text{ (g)} \rightarrow SiO_2 \text{ (s)} + 4HCl \text{ (g)}$$
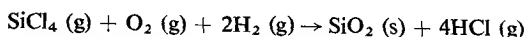
which, at a substrate temperature of 800°C, has permitted Doo and Kerr (209) to obtain deposition rates of 900 Å/min. Typical flow rates are $SiCl_4$: O_2:H_2 = 50:300:30,000. Films prepared by the above methods have been successfully used as masks in etching Si_3N_4 with hot phosphoric acid (214). Additional reactions for forming SiO_2 by the oxidation of $SiCl_4$ are

$$SiCl_4 + 2CO_2 + 2H_2 \rightarrow 2CO + 2H_2O + SiCl_4 \rightarrow 2CO + SiO_2 + 4HCl$$
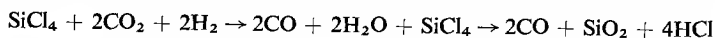
which takes place effectively at temperatures $\gtrsim 1100$°C [Steinmaier and Bloem (215)], or

$$SiCl_4 + nH_2O \rightarrow SiO_2 + \text{gases} \quad (HCl, SiCl_2, H_2, \text{etc.}).$$
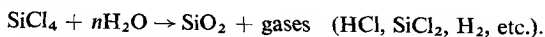
Of these two, the first type of reaction may be preferred because it offers the advantage that the contamination of the deposition system with water vapor is largely avoided.

Tung et al. (216) modified the CO_2–H_2–$SiCl_4$ process by adding various amounts of $AlCl_3$ in order to obtain aluminosilicate films of various compositions. Films deposited at temperatures between 900 and 1200°C varied in their structure from polycrystalline for pure Al_2O_3 to amorphous for pure SiO_2. The composition of the film corresponded very closely to that of the composition of the $AlCl_3$–$SiCl_4$ gas mixture. A film of 50% Al_2O_3:50% SiO_2 exhibited a dielectric strength of $F_b = 1.9 \times 10^7$ V/cm and proved to be an effective sodium barrier.

Swann et al. (217) modified the previously discussed oxidation of silane, replacing the O_2 by CO_2. The reaction was carried out at 1100°C, yielding a deposition rate of 800 Å/min.

For the deposition of SiO_2 onto germanium, Rand and Ashworth (218) chose the reaction

$$SiBr_4 + 2CO_2 + 2H_2 \rightarrow SiO_2 + 2CO + 4HBr$$
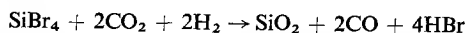
which permits depositions at a temperature as low as 780°C [see also Barnes and Geesner (219)]. Rand (220), employing nitric oxide as agent for oxidizing $SiCl_4$ or $SiBr_4$ according to the reaction

$$SiX_4 + 2H_2 + 2NO \rightarrow SiO_2 + N_2 + 4HX \quad (X = Cl, Br)$$
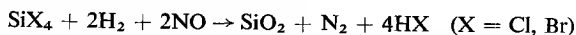
deposited high-quality SiO_2 in this fashion on semiconducting, metallic, and insulating substrates at typical temperatures of 850°C with $SiBr_4$ and of 1150°C with $SiCl_4$. At the same gas flows, and at a deposition temperature of 850°C, the use of NO yielded a deposition rate of $\gtrsim 1000$ Å/min, which is about one order of magnitude larger than that obtainable with CO_2 as

oxidizing reagent. The etch rate of SiO_2 films grown by using $SiCl_4$ at 1100°C was about 2 times faster than that of SiO_2 thermally grown in steam, while the use of $SiBr_4$ at a temperature of 850°C resulted in an etch rate about 4 times faster than that of thermally grown oxide.

The silicon halide process lends itself also to the preparation of doped SiO_2 layers by coreacting the corresponding halide or oxihalide of the dopant. An example is the reaction

$$SiCl_4 + POCl_3 + H_2 + CO_2 \rightarrow SiO_2 \times P_2O_5 + \text{gases}$$
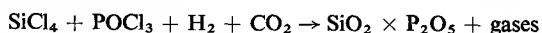
utilized for the preparation of phosphorus-doped SiO_2 [Osafune et al. (221)]. As is well known, a phosphorus-doped SiO_2 layer can serve as a diffusion source; furthermore, the phosphorus tends to impede the motion of charged species (such as sodium ions or oxygen vacancies), which readily occurs in the undoped oxide at high applied electric fields and elevated temperatures producing a drifting of the electrical characteristics of insulated gate field-effect transistors.

(2) *Organic deposition media.* Silicon dioxide deposits can also be obtained by pyrolysis from a large variety of organosilica compounds such as tetra-ethyl orthosilicate (TEOS), and other substituted silanes (222). While the pyrolysis of TEOS according to the reaction (223)

$$Si(OC_2H_5)_4 \xrightarrow{750°C} SiO_2 + 4C_2H_4 + 2H_2O$$
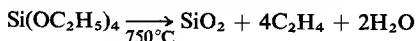
is particularly popular, the pyrolysis of the more complex substituted silanes may result in a larger dielectric strength of the deposited silica films (224).

In 1949, Pensack (225) reported on SiO_2 layers that were formed by decomposing tetraethyl silicate (TES) on a heated tantalum strip in a vacuum chamber. When the substrate temperature exceeded ≈ 1050°C, the films developed a granular structure, while at lower temperatures a microcrystalline electrically very stable structure was obtained. The deposition rates were on the order of 10 Å/sec at 600°C, and 10^4 Å/sec at 1000°C.

While the rate of pyrolytic decomposition decreases to very small levels at substrate temperatures < 700°C if an inert gas is used as a diluent, the process can be considerably speeded up by using oxygen as a carrier gas. In this fashion useful deposition rates (≈ 200 Å/min) can be obtained at temperatures as low as 300°C. Another reason for using oxygen in the reaction is that it avoids carbon contamination of the deposited films which may be responsible for the brownish color of deposits produced at substrate temperatures > 800°C. However, deposits formed in an oxygen atmosphere at > 600°C were found to be cloudy and not well etchable, in contrast to those obtained at 300–400°C which were clear and glassy (5). Oroshnik and Kraitchman (226) recommended the pyrolytic deposition of SiO_2 at a substrate temperature of 750°C in a reduced-pressure (0.3 Torr) TEOS atmosphere. After

densification at 800°C in wet oxygen, the characteristics of the film-breakdown field strength $F_b = 5–7 \times 10^6$/cm, infrared absorption at 9.3 μ, were very similar to those of thermally grown SiO_2, except that an extremely large flat-band voltage (-80 V) of metal oxide semiconductor (MOS) devices resulted after densification. Plishkin and Lehman (*227*) made an extensive investigation of the effect of densification in steam at 800°C on the infrared absorption spectrum, the dielectric constant, the density, and the passivation efficiency of silica layers formed by the TEOS and other methods. The steam treatment increased the refractive index and the density and decreased the etch rate to values near those of high-quality, thermally grown oxide. In addition, it permanently removed hydroxyl groups and moisture from the oxide.

Nakai (*228*) discovered that the pyrolysis of TEOS was catalyzed by the presence of triethylstibine. Reacting a mixture of the two compounds in an oxygen atmosphere permitted him to deposit silica films at 250–500°C at much greater rates than would have been possible using TEOS alone. The films were subsequently annealed at 600–800°C in order to eliminate hysteresis effects in MOS structures.

The TEOS process has also been used to prepare doped oxide layers to act as a diffusion source. For example, Rawa, (*229*) mixed TEOS and $AsCl_3$ vapors and obtained As-doped SiO_2 on a silicon surface heated to 500°C. The subsequent diffusion of the arsenic into the silicon was performed at 1200°C. Doping concentrations approaching the solid solubility limit could be obtained in this fashion. Borosilicate glass for use as a boron diffusion source was formed by Whittle and Vick (*230*) by decomposing a mixture of TEOS and tri-*n*-propylborate vapors carried by argon at 688°C. Phosphosilicate films which proved to be an effective zinc diffusion mask were prepared by Flatley *et al.* (*231*) by the simultaneous pyrolysis of TEOS and trimethyl phosphate (TMP).

When TEOS vapor is mixed with the vapors of triethylaluminum (TEAL) or triisopropyl borate (TIPB), or both, films of complex glasses can be readily deposited (*207*). Of considerable advantage is the fact that pyrolysis of the mixtures takes place effectively at much lower temperatures than the 700°C required for pyrolysis of TEOS alone or in an inert atmosphere. Alumina–silica films containing up to 50% SiO_2 have been deposited at substrate temperatures of about 350°C by the pyrolysis of a TEOS and TEAL mixture. Likewise, films of boroalumina–silicate glass with dielectric properties somewhat superior to those of alumina–silicate glass were deposited by the pyrolysis of a TEOS, TEAL, and TIPB mixture at a substrate temperature of 300–500°C. The optimum film composition contained 7% B_2O_3, 14% SiO_2, and 79% Al_2O_3. Argon served as both carrier gas and diluent in these deposition runs. A sufficiently high vapor pressure of the starting

compounds was produced by heating the TEAL and TEOS sources to 80°C, and keeping the borate at 25°C. At room temperature, the boroalumina-silicate films exhibited a dielectric constant $\varepsilon = 6$, a dissipation factor of $\tan \delta = 2 \times 10^{-3}$ (at 1 kHz), a resistivity of $\rho \approx 10^{16}$ Ω cm, a breakdown strength of $F_b = 10^6-10^7$ V/cm, and a temperature coefficient $(1/\varepsilon)$ $(d\varepsilon/dT)$ ≈ 69 ppm/°C.

(3) *Nonthermal activation methods.* In addition to thermal activation, several other means of energizing the chemical vapor deposition of silica, such as electrical gas discharges or electron-beam bombardment, have been explored. Films which closely resembled amorphous silica and were "quite pinhole free" were deposited on near-room-temperature substrates by Ing *et al.* (205, 206) with the aid of a rf sustained glow discharge. An electrodeless, rf-induced plasma was chosen to avoid the difficulties with sputtering associated with the use of a dc glow discharge. The deposited films were effective as a mask against impurity diffusion into silicon and GaAs at elevated temperatures, and as a protective coating of silicon against chlorine attack at 900–950°C. In order to deposit a film, oxygen was fed into the reaction chamber through a narrow tubulation in which it was ionized in a glow discharge sustained at a pressure on the order of $10^{-2}-10^{-1}$ Torr, and powered by a 500-kHz, 1-kW induction generator. The ionized oxygen emerging from the excitation region was then mixed with TEOS, with which it reacted to form a silica deposit on a substrate positioned close to the mixing region at a deposition rate of up to several thousand angstroms per hour. Upon substitution for the oxygen of argon or hydrogen the deposition rate had to be significantly reduced in order to prevent the incorporation of organic residues into the silica films. But even with the use of an oxygen plasma, films deposited at rates larger than 3000 Å/hr were degraded by organic inclusions. In contrast, films deposited at rates smaller than 2000 Å/hr were of high quality and exhibited breakdown strengths of $F_b = 5-10$ $\times 10^6$ V/cm. As a possible mechanism for the film deposition by the above method, it was postulated that TEOS molecules are decomposed by bombardment with particles emerging from the glow discharge with high energies, and that subsequently a polymerization of the free radicals into silicon dioxide clusters takes place. The latter are then deposited and bonded to the substrate surface. Other decomposition products were thought to be largely prevented from depositing on the substrate by the continuous ion bombardment of the surface.

Performing low-temperature depositions of silicon dioxide and silicon oxynitride by reacting TEOS with oxygen or nitrogen, respectively, in a plasma excited by rf power, Orris and Shiota (232) observed a significant increase in the deposition rate when the rf frequency was raised from 100 kHz to 27 MHz.

Sterling and Swann (*233*) produced films of SiO_2, Si_3N_4, and Si by supplying the energy necessary to sustain the deposition reaction of the mixed gaseous reagents through an rf discharge. The reactions were carried out in a simple fused silica reaction tube which contained the substrate and the rf discharge. Typical operating pressures were in the 0.1 Torr range. The rf energy, supplied by a 500-W, 1-MHz generator, was fed into the system by means of an inductively and capacitatively coupled high-impedance coil. The deposits were formed on cold or heated substrates of silica, glass, Mylar, various metals, and others at a rate of 2–4 μ/hr. For the deposition of SiO_2, silane and nitrous oxide served as reactant gases, and the use of the latter prevented a spontaneous oxidation of the silane. Because of the formation of water as a reaction product, a substrate temperature of 200°C and above was preferred. Films deposited at 25°C exhibited infrared absorption peaks due to hydroxyl groups and absorbed water in the 2.74–3.00-μ region, in addition to the regular silica absorption peaks at 9.5 and 12.4 μ. A substrate temperature of 250°C led to a marked reduction of the irregular absorption peaks, and at a substrate temperature of 500°C they were essentially absent.

Secrist and Mackenzie (*234*) formed films of SiO_2 and other oxides by decomposition of suitable compounds upon their exposure to ionized oxygen or argon. The oxygen or argon was ionized by feeding it through a 1-in. diam Pyrex tube, a section of which was surrounded by a rectangular waveguide. An electrodeless discharge was excited by applying about 100 W of microwave power (2450 MHz) to the waveguide. It was estimated that about 10 % of the molecular oxygen fed into the discharge region entered the deposition zone as atomic oxygen to become chemically combined with the organic compound. The pressure in the deposition zone was held at about 0.25 Torr, and the substrate temperature at 200°C. The purpose of the elevated substrate temperature was again to avoid incorporation of water molecules and other by-products of the reaction such as CO_2, CO, H_2, and traces of CH_4 into the deposit. For the same reason, the deposition rate was kept small (10–80 Å/min). Three different methods were tried for depositing SiO_2 films.:

(1) the decomposition of TEOS via an oxygen plasma,
(2) the decomposition of TEOS via an argon plasma, and
(3) the decomposition of TES via an oxygen plasma.

Methods (1) and (3) resulted in significantly larger deposition rates than method (2). Judged by the measured index of refraction and the infrared absorption spectrum, films obtained by method (1) resembled very closely amorphous silica.

As for the formation of silica films with the aid of electron bombardment, silicalike films were prepared by Christy (*16*), who utilized this method to effect polymerization of DC-704 Silicone pump oil vapor molecules adsorbed

on a substrate. Roberts (*204*) reported recently on attempts to form silicon diffusion barriers by applying electron bombardment to vapors of tetra-ethoxysilane (TEOS), tetramethylcyclotetrasiloxane (TCTS), pentamethyl-cyclopentasiloxane (PCPS), and hexamethylcyclohexasiloxane (HCHS). Roberts asserts that the formation of films from these compounds proceeds with a very low efficiency. In the case of TEOS and a substrate kept at room temperature, only about one out of 20 electrons incident on the substrate was effective in causing the film to grow, and only about one out of 80 adsorbed molecules was incorporated into the film. Local heating of the substrate by the incident electrons was held responsible for this effect. As a consequence, a charge on the order of 1 C/cm^2 was needed to produce a film thickness of 2000 Å. The other compounds mentioned produced from 4 to 6 times better deposition efficiencies on account of the increasing number of silicon atoms in one of their molecules. An improvement in the deposition efficiency, by a factor as large as 10^6 resulted when the substrate was coated, e.g., by dip coating, with less-volatile siloxane polymers containing an increased number of silicon atoms per molecule. This was due to the electron beam's interacting with many layers of molecules at once rather than with one layer after another as adsorbed from the gas phase. Furthermore, re-evaporation of molecules by beam heating was greatly reduced by this procedure.

b. Silicon Nitride. Recently much attention has focused on silicon nitride, Si_3N_4, since it appears to provide remedies for the difficulties encountered with silicon dioxide in applications such as surface passivation, diffusion masking, and gate insulation in field-effect transistors (*209, 235*). Most of the difficulties with amorphous SiO_2 are caused by its "open structure." The latter permits the migration of vacancies (which may be generated through the chemical reduction of a surface layer by a contacting metal film), of metal atoms such as Cu, Zn, and, above all, of Na and other alkali ions in the SiO_2. The migration of electrically charged species under the influence of an applied voltage produces changes in the distribution of the electric field in the SiO_2 and a corresponding instability of the surface potential of the semiconductor substrate. As a result, the reverse characteristics of planar semiconductor junctions, or the operating characteristics of insulated gate field-effect transistors, may be excessively degraded or unstable. Silicon nitride is a considerably denser material than SiO_2 ($\rho_{Si_3N_4} = 3.18$ g/cm^3 vs $\rho_{SiO_2} = 2.2$ g/cm^3) and does not readily permit migration or diffusion to occur through it. Layers of Si_3N_4 only 300 Å thick have proved to be effective diffusion masks, and devices protected with Si_3N_4 were not sensitive to exposure to sodium chloride. Unfortunately, Si_3N_4 does not quite match the favorable dielectric characteristics of SiO_2 due to its smaller band gap (crystalline

$Si_3N_4: E_g = 3.9–4$ eV, amorphous $Si_3N_4: E_g \sim 5$ eV, versus amorphous $SiO_2: E_g \sim 8$ eV). In addition, the relatively low energy barriers towards silicon or metals which Si_3N_4 appears to form facilitate the injection of electrons or holes into the dielectric at fields $F \gtrsim 2 \times 10^6$ V/cm. A consequence of this charge injection is the pronounced hysteresis appearing in the capacitance–voltage curve of metal–insulator–semiconductor structures after the voltage has been swept to large values. For these reasons, it is now customary either to form a thin SiO_2 barrier layer ($\sim$200 Å or thicker) on the silicon surface before the Si_3N_4 layer is deposited, or to form most of the dielectric of SiO_2, and to seal its surface with a protecting layer of Si_3N_4 (a few hundred angstroms thick).

Pure and dense, Si_3N_4 etches at a rather slow rate (the etch rate of amorphous Si_3N_4 in 48% HF is $\sim$100 Å/min). This causes difficulties with conventional photomasking because the latter is destroyed by the etchant during the necessary long etching time. Although techniques using more durable masking (e.g., Cr or SiO_2, permitting the use of hot H_2PO_4 as an etchant) have been worked out, the alternative of using composites of Si_3N_4 and SiO_2 has received attention: These silicon oxynitrides etch faster than Si_3N_4, while retaining much of its favorable masking and passivating properties.

Another interesting feature of silicon oxynitride films was pointed out by Drum and Rand (236): SiO_2 and Si_3N_4 films exhibit stresses of opposite signs. Therefore, by depositing a mixture of the two materials, a more stress-free film can be produced. The stress is zero for films of the composition $Si_3O_4N_2$.

Present schemes for forming Si_3N_4 layers by chemical vapor deposition are based on the nitridation of silane or silicon halides. Direct nitridation of a silicon substrate is not feasible since it requires temperatures in excess of 1150°C and results in granular deposits of crystalline α-Si_3N_4 (237). In contrast, the Si_3N_4 films obtained by chemical vapor deposition are generally amorphous and smooth.

(1) *Nitridation of silane.* One of the first successes in depositing continuous films of silicon nitride was achieved by Doo (238) with the reaction between silane and ammonia:

$$3SiH_4 + 4NH_3 \rightarrow Si_3N_4 + 12H_2.$$
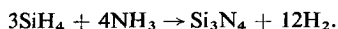
A typical deposition temperature is 900°C, but the latter may be lowered to about 800°C if the substrate contains partially completed devices such as integrated circuits which preferably should not be heated to excessive temperatures (209). Typical flow ratios are $SiH_4:NH_3:N_2 = 1:20:40$, where the nitrogen serves as a diluent carrier gas, and typical growth rates range from 150 to 220 Å/min. The etch rate, which gives some indication of the density and the quality of the deposit, was reported to be 100–120 Å/min in

48 % HF, in contrast to an etch rate of ~1000 Å/min typically found for thermally grown SiO_2. However, a low etch rate may not always be indicative of high-quality Si_3N_4; it could also be caused by departures from stoichiometry with excess silicon. Doo and Kerr (209) investigated the effect of different carrier gases on the properties of the deposited silicon nitride. Originally they used hydrogen as a carrier gas in order to suppress silane decomposition which starts at about 500°C. The use of helium, argon, and nitrogen led to the deposition of silicon powder on the reactor walls unless the carrier gas flow was rather large. The large gas flow held the temperature outside of the reaction zone low enough to prevent premature decomposition. Nitrogen and argon, because of their relatively large molecular weight, produced a more uniform gas mixture and, consequently, a more uniform film growth than hydrogen and helium. In addition, substituting the other gases for hydrogen greatly reduced the operating hazards. Doo and Kerr stated that the electrical characteristics of silicon nitride films grown with nitrogen as a carrier gas were comparable to or better than those resulting from the use of hydrogen. Films grown in a helium environment exhibited the best electrical characteristics, while argon produced inferior results. Unfortunately, films grown in a helium environment were quite nonuniform in thickness, and the large flow rate required made the use of helium impractical.

The growth rate was found to be fairly constant above 850°C, but dropped sharply (exponentially with inverse temperature) at temperatures below 750°C. The etch rate behaved in a corresponding fashion, being fairly constant (~100 Å/min in 48 % HF) for films grown at a substrate temperature $\gtrsim 800$°C, and increasing by approximately five times as the deposition temperature was lowered to 600°C. Silicon substrates that had been cleaned *in situ* by HCl vapor etching or by heating in hydrogen at 1200°C exhibited a rather high flat-band surface charge concentration of $N_{ss} = 2.3$–$8 \times 10^{12}/$ cm^2 after Si_3N_4 deposition. The latter could be reduced to about $N_{ss} = 1.5 \times 10^{12}/cm^2$ by forming a thin SiO_2 layer (~150 Å thick) on the silicon substrate before Si_3N_4 deposition. The presence of a SiO_2 layer (~500 Å) was also beneficial for raising the threshold field for C–V instabilities at room temperature from $F_{th} = 1$–2×10^6 V/cm to $F_{th} = 4 \times 10^6$ V/cm in a typical case.

The flat-band surface charge was not influenced much, in general, by the $NH_3:SiH_4$ ratio (ranging from 1:1 to 20:1) when hydrogen or helium was used as a carrier gas. As a function of deposition temperature, the flat-band charge went through a minimum at about 900°C. In contrast, when argon or nitrogen was used as the carrier gas, the flat-band surface charge tended to decrease steadily as the deposition temperature was increased from 700 to 1000°C and, in the case of nitrogen, as the ammonia flow was increased.

The smallest flat-band surface charge concentration resulted from the use of nitrogen as carrier gas and was on the order of $N_{ss} = 8 \times 10^{11}/cm^2$ for Si_3N_4 deposited onto bare silicon ($SiH_4:NH_3 = 1:20$, 1000°C). A thermally grown oxide layer (~500 Å thick, grown *in situ*) placed between the silicon substrate and the nitride layer, reduced the flat-band charge concentration by a factor of 2 to 6. The latter had the lowest value, $N_{ss} = 7\text{–}8 \times 10^{11}/cm^2$, when helium was used as carrier gas, and the highest value, $N_{ss} = 1.4 \times 10^{12}$, when hydrogen served as carrier.

According to Doo and Kerr (*209*), silicon oxynitride films can be grown by simply adding a small flow of oxygen to the system. Since the oxidation is thermodynamically more favorable than the nitridation over the temperature range of interest (600–1200°C), an oxygen flow ratio in proportion to $SiH_4:NH = 1:10$ leads essentially to the formation of oxide alone.

The deposition of silicon oxynitride on single-crystal silicon (representative deposition conditions: $SiH_4:NH_3:O_2 = 1:10:1$, N_2 carrier, substrate temperature, 850°C) led to a surface charge similar to that of pure Si_3N_4. As in the case of pure Si_3N_4, the surface charge was lowered significantly by placing a thermal oxide layer (~150 Å) under the silicon oxynitride. In addition to an etch rate about one order of magnitude larger than that of amorphous Si_3N_4, the silicon oxynitride exhibited a significantly larger threshold field for C–V instabilities at room temperature than the former ($F_{th} = 5.8\text{–}7.5 \times 10^6$ V/cm vs $F_{th} = 1\text{–}2 \times 10^6$ V/cm). However, when the deposition was carried out onto thermally oxidized silicon, the threshold field was similar in both cases.

Doo and Nichols (*239*) investigated the characteristics of silicon nitride films resulting when the $NH_3:SiH_4$ flow ratio was kept rather small, from 0.5:1 to 5:1, at deposition temperatures of 800–1000°C. At a ratio of 1:1 and lower, the deposit contained polycrystalline silicon. Similarly, the silicon nitride films deposited by Bean *et al.* (*240*) at $NH_3:SiH_4$ ratios smaller than 3:1–8:1 were silicon rich, and exhibited a decreased etch rate and an index of refraction exceeding that of crystalline Si_3N_4 ($n = 2.1$). In addition, the deposition rate increased when the NH_3 flow rate was lowered. Deposits formed at temperatures of about 900°C were mixed amorphous and crystalline while those formed at $\gtrsim 1100°C$ were predominantly crystalline growing as hexagonal rods over the substrate surface. In contrast, Chu *et al.* (*241*) reported that crystallites were only occasionally observed and only when the deposition temperature was above 1200°C.

Dalton and Drobeck (*242*) studied crystalline Si_3N_4 films (~4000 Å thick) of α, β, or mixed $\alpha\beta$ structure deposited on (111) silicon substrates, by different methods. Variations in the deposition and substrate surface conditions led to grain sizes ranging from <10 to 100 Å for different films. Both, thermal diffusion of sodium, and etch rate in diluted buffered HF, increased strongly

with grain size. On the other hand, field enhanced migration of sodium was too small to be observable in any of the films.

Scott and Olmstead (243) went as low as 600°C with the deposition temperature. They stated that the films deposited between 600 and 800°C were the most etchable while the etch rate decreased as the deposition temperature was increased beyond 800°C. A particularly sharp drop in the etch rate occurred for films deposited or annealed at about 1150°C.

Various values were given for the density of chemical vapor deposited silicon nitride films. For example, Lee *et al.* (241) reported $\rho = 2.82$ g/cm^3 for 950°C, and $\rho = 2.92$ g/cm^3 for 1100°C deposition temperatures. In comparison, the density for crystalline β-Si$_3$N$_4$ is $\rho = 3.18$ g/cm^3. Philipp (244) determined a value of $\rho = 3.1$ for films deposited at 1000°C, a value which agrees with that reported by Doo and Kerr (209).

The effect of deposited Si$_3$N$_4$ films on the surface structure of single-crystal substrates was investigated by Comer and Tombs (245). Etch pits (size $\sim$60 Å) revealed on the substrate surface after the deposited Si$_3$N$_4$ was removed were caused, perhaps, by some chemical reaction during the deposition process. However, no evidence was found for dislocations produced by the deposition of the nitride.

(2) *Nitridation of silicon halides.* Silicon nitride can be deposited by nitridation of a variety of silicon halides according to the overall reaction

$$3SiX_4 \text{ (g)} + NH_3 \text{ (g)} \rightarrow Si_3N_4 \text{ (s)} + 12HX \text{ (g)},$$
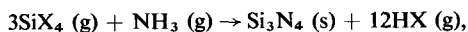
where X stands for Cl, F, or Br. Of these halides, the chloride is probably the most frequently used. Grieco and coworkers (246) used the above reaction with SiCl$_4$ to deposit Si$_3$N$_4$ films at temperatures ranging from 550 to 1250°C, with nitrogen as the carrier gas. When the partial NH$_3$ pressure was set at about 28 Torr, and the SiCl$_4$ partial pressure was varied from 0.01 to 1 Torr the corresponding deposition rates increased linearly with SiCl$_4$ pressure from 10 to 1000 Å/min. Over the temperature range investigated, the deposition rate increased exponentially with $-1/T$, while the etch rate decreased with increasing deposition temperature. The flat-band surface state concentration ($N_{ss} \approx 5$–15×10^{11}/cm^2), the breakdown strength ($F_b \approx 0.5$–1×10^7 V/cm), and the C–V hysteresis effects exhibited by Si$_3$N$_4$ deposited on single-crystal silicon were very similar to those resulting from the silane process.

(3) *Nonthermal activation methods.* Several workers have investigated the activation of reactions by means of a gaseous discharge instead of heating in order to produce Si$_3$N$_4$ films at low substrate temperatures. Perhaps the earliest successes in this direction were achieved by Sterling and Swann (233) by utilizing an rf discharge method identical to that used for the deposition of amorphous silicon and silicon dioxide (which was described above), except

that SiH_4 and NH_3 were introduced as reagent gases. When the films were deposited on cold substrates, they were soluble in HF, but when formed on substrates at temperatures $>300°C$, they were resistant to acid attack. The quality of the films was improved by either depositing them or annealing them at 700–900°C. The dielectric constant (at 1 kHz) had values of $\varepsilon = 6.2$ and $\varepsilon = 9.4$ for films deposited at 200 and 400°C, respectively. Needles growing at the edges of the substrate at 700°C were identified at β-Si_3N_4. Using a similar setup, Swann et al. (247) deposited Si_3N_4 from SiH_4 and NH_3 fed into the system, with flow ratios ranging from 0.03 to 0.5, on substrates held at temperatures of 300–550°C. The deposition rate increased nearly linearly with the $SiH_4:NH_3$ ratio (from <40 to 180 Å/min at 300°C); however, the increasing gas ratio caused also a variation of the dielectric constant from $\varepsilon = 7$ to $\varepsilon = 11$, and of the breakdown strength from $F_b \approx 6 \times 10^6$ V/cm to $F_b \approx 1 \times 10^6$ V/cm, which is an indication that silicon-rich deposits are obtained at the higher gas ratios.

In the apparatus of Erdman and Androshuk (248), a dc discharge through argon at 1 Torr, emerging from a heated cathode, served as a means of activation. Injection of $N_2 + SiH_4$ or $N_2 + SiBr_4$ near the center of the discharge column where the substrate was located resulted in the deposition of a nitride film which exhibited a refractive index of $n = 2$ or 1.93, respectively.

c. Boron Nitride. Boron nitride combines the features of being an excellent dielectric, chemically very inert, and easily machinable. It has exceptionally low dielectric losses at frequencies ranging from dc to microwaves, even at temperatures well above room temperature, and the temperature coefficient of the dielectric constant is extremely small (249). However, attaining of the favorable properties depends on the method of preparation. While various chemical vapor deposition schemes have led to the successful formation of coherent deposits of boron nitride it was also found that the crystalline structure and the density of the deposit could vary considerably, depending on the chemical reaction, the temperature, and other deposition parameters used. The reaction

$$BCl_3 \text{ (g)} + NH_3 \text{ (g)} \rightarrow BN \text{ (s)} + 3HCl \text{ (g)}$$
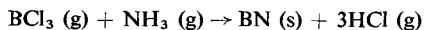
resulted in the formation of a type of boron nitride known as "white graphite" because it resembles the structure of turbostratic graphite (250). Within any one crystallite it is built of layers of B_3N_3 hexagonal atom arrangements forming sheets whose c axes have a tendency to point in the direction normal to the substrate surface. The structure is turbostratic if the hexagonal atom arrangements of two different sheets are randomly oriented with respect to each other in terms of rotation around the c axis. Because of the preferred

orientation of the c axes of all the crystallites, the material has an anisotropic structure and, therefore, anisotropic properties. In order to produce BN of this kind, temperatures on the order of 1300–1900°C and reduced system pressures of 0.10 Torr are usually necessary, depending on the deposition parameters. The density of anisotropic boron nitride deposits is typically $\rho = 2$–2.1 g/cm³, and therefore close to the theoretical density of $\rho = 2.2$ g/cm³.

An isotropic crystal structure (the c axes of the crystallites have no preferred orientation, neither with respect to the substrate, nor with respect to each other; the structure of a crystallite is either turbostratic, hexagonal, or rhombohedral) can be obtained by an as yet undisclosed process (251). It can only be told here that the depositions are usually carried out at temperatures >1500°C. Steele and co-workers (252) have investigated the influence of the deposition temperature on the properties of the isotropic boron nitride. They found that the density of the deposits was significantly smaller than theoretical by a factor of 0.5–0.6. Similar to results reported for pyrolytic graphite (161), a maximum in the density occurred when the deposition temperature was of the order of 1700°C. Due to the small density, and perhaps, the associated porosity, the material was found to be moisture absorbing in contrast to the behavior of dense boron nitride.

The above-mentioned processes were used in the past mainly to produce fairly heavy coatings (on the order of 1 mil to 1 in. thick), or structural parts. Little attention was given to apply them to the formation of continuous thin films, mainly because of the impracticality of the high deposition temperatures involved.

For the deposition of thin films, 0.5–10 μ in thickness, on Mo, W, Ta, graphite, and iron alloy substrates, Patterson et al. (253, 254) employed the static pyrolysis of μ-trichloroborazole, $B_3N_3H_3Cl_3$, at temperatures above 700°C. While depositions carried out at atmospheric pressure in the presence of a diluent gas tended to yield powdery deposits, a reduction of the total pressure below 2.5 Torr yielded continuous films of microcrystalline, turbostratic structure. The dielectric strength of a 0.5-μ-thick film was $F_b \approx 2 \times 10^6$ V/cm, and the resistivity ranged from $\rho \sim 10^{16}$–10^{17} Ω cm at room temperature to $\rho \sim 10^{13}$–10^{14} Ω cm at 250°C. The dielectric constant, $\varepsilon = 4.4$, remained constant up to a temperature of 250°C.

Clear, vitreous films of BN (crystallite size $\approx$10–80 Å) up to 6000 Å thick were deposited by Rand and Roberts (255) from diborane and ammonia according to the reaction

$$B_2H_6 + 2H_3 \rightarrow 2BN + 6H_2.$$
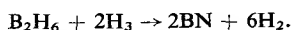
The temperature of the substrates (which included Si, Ta, Mo, Ge, and fused silica) ranged from 600 to 1080°C. The depositions were performed

at atmospheric pressure in the presence of hydrogen, nitrogen, or helium. The use of hydrogen appeared to reduce the moisture sensitivity of the films, perhaps on account of residual bonded hydrogen. Typical deposition rates were 125–600 Å/min in hydrogen or helium, and ≈ 1000 Å/min in nitrogen. The dependence of the deposition rate on temperature and $NH_3:B_2H_6$ ratio was found to be complex: the deposition rate exhibited a maximum at about 800°C, and decreased as the $NH_3:B_2H_6$ ratio was increased from 10:1 to 20:1. Films deposited at 850°C were found to be effective barriers against thermal or field-enhanced sodium diffusion, in contrast to films deposited at 600°C. It also appeared that a smaller crystallite size, < 10 Å, provided a better barrier than a larger crystallite size, ~ 30 Å, in analogy to findings with Si_3N_4 films (242). Rand and Roberts stated that their BN films had a dielectric constant $\varepsilon = 3.7$ (at 1 MHz) and a dielectric strength $F_b = 6 \times 10^6$ V/cm, and behaved similar to Si_3N_4 in metal insulator semiconductor (MIS) capacitors. The films were also useful as localized diffusion sources since they were chemically reduced by the silicon substrate yielding Si_3N_4 and boron, of which the latter would diffuse into the substrate. The lateral spread of the diffusion is minimal if the formation of B_2O_3 (which has a relatively high vapor pressure) is suppressed by excluding oxygen or water vapor from the system. Rand and Roberts also pointed out that the nonlinear high field conductivity characteristics of their BN films were suitable for varistor applications.

The boron nitride films prepared by Steele *et al.* (256) by reacting BCl_3 and NH_3 on a large variety of substrates at temperatures ranging from 800 to 1600°C differed from those of Rand and Roberts in that they were crystalline in all observed cases. Moreover, it was found that the nature of the substrate could greatly influence the degree of preferred orientation of the crystallites. For example, films deposited at 900°C on bare fused silica were composed of crystallites whose c axes were oriented at random. On the other hand, when the fused silica substrates were first coated with an evaporated gold film, a few hundred angstrom units thick, a deposition under identical conditions yielded films whose crystallites were of rhombohedral structure (256a) and had c axes pointing in the direction of the normal to the substrate surface. A manifestation of this orientation effect is the spotty electron diffraction diagram shown in Fig. 6. A surprisingly high degree of crystallinity and relatively high density ($\rho \approx 1.7$ g/cm^3) were obtained with BN films deposited by the BCl_3 method at 800–900°C as opposed to the typical temperature of 1600°C mentioned earlier. These results are attributed to the way in which the deposition system (shown in Fig. 1) was operated, namely at a low total pressure ($10–20 \times 10^{-3}$ Torr, as indicated by a thermocouple gage) and at small deposition rates (~ 100 Å/min). At the low pressure, film growth can proceed without being disturbed much by clusters, formed by
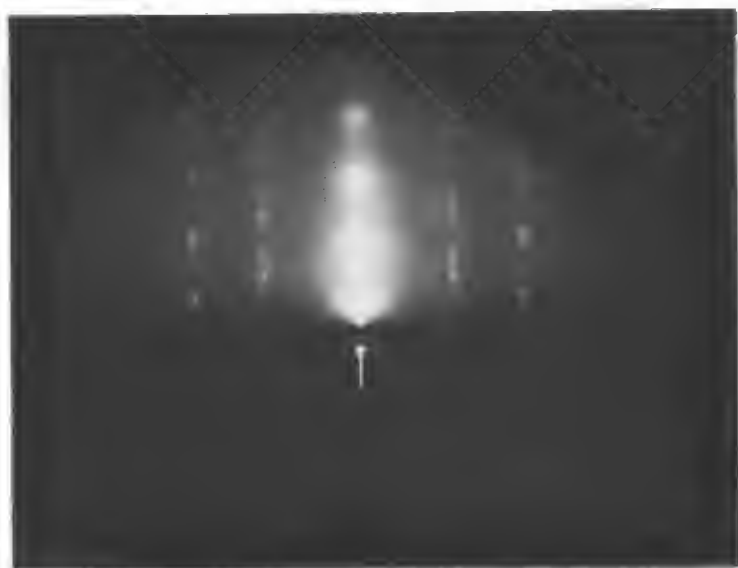
FIG. 6. Electron reflection diffraction diagram obtained from boron nitride film (~ 100 Å) chemically vapor deposited on a polished fused silica substrate coated with a gold film (~ 2000 Å).

homogeneous reactions and settling down on the substrate surface, or by molecules of diluent gas or reaction products adsorbed on the substrate surface. Before the reagent gases are admitted, the reaction chamber (diam $\approx$ 4 cm) shown in Fig. 1 is pumped down into the 10^{-5}–10^{-6}-Torr range and outgassed by heating the graphite susceptor by rf induction. Pumping during outgassing and deposition is performed by an oil diffusion pump in combination with a liquid nitrogen trap. After the outgassing step, the NH_3 flow is turned on (≈ 150 cm^3/min-atm) while the proper BCl_3 flow (≈ 15 cm^3/min-atm) is first adjusted by directing it into a bypass line. In order to perform the deposition, the BCl_3 is quickly admitted to the reaction chamber by means of a toggle valve; this method permits accurate control of the deposition time. A magnet properly arranged under the reaction chamber serves to suppress the electrical gas discharge that otherwise develops at the prevailing low pressure under the influence of the rf field. Two factors were found to be important for proper operation of the system: (1) injection of the BCl_3 rather than the NH_3 gas through the center nozzle shown in Fig. 1, and (2) sealing of the graphite susceptor (e.g., by a coating of pyrolytic graphite). When the injection of the gases was reversed, no deposit was formed in the reaction zone even during prolonged runs. Instead, a heavy NH_4Cl deposit formed in the cooler zones of the reaction tube. Without the sealing, the

pressure during the deposition rose to unduly large values, very likely through an increased rate of reaction or dissociation on the susceptor surface caused by trapping effects in the pores of the graphite.

The above deposition system permitted the formation of continuous BN films as thin as 100 Å or thinner. These films performed well in experiments on quantum mechanical tunneling in metal–insulator–metal structures, and in cold cathodes using the tunneling principle.

d. Aluminum Pentoxide, Aluminum Nitride. A variety of processes may be employed for the chemical vapor deposition of Al_2O_3 (*191*). Examples are the steam hydrolysis of $AlCl_3$:

$$2AlCl_3 + 3H_2O \xrightarrow[>1000°C]{} Al_2O_3 + 6HCl,$$
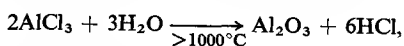
the oxidation of $AlCl_3$ according to

$$2AlCl_3 + 3CO_2 + 3H_2 \xrightarrow[800-1200°C]{} Al_2O_3 + 3CO + 6HCl,$$
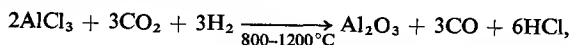
the pyrolytic decomposition of aluminum triethoxide, $Al(OC_2H_5)_3$ (*257*), or of other oxygen-containing organoaluminum compounds (*258, 259*), or the oxidation of lower-molecular-weight aluminum alkyls such as triethyl- or trimethylaluminum (*207*). The latter alkyls offer the advantage of low deposition temperatures (350–450°C). As pointed out by Peterson (*207*), two parallel reactions occur in the process of oxidation of triethylaluminum:

$$2Al(C_2H_5)_3 + 21O_2 \rightarrow Al_2O_3 + 12CO_2 + 15H_2O,$$

and

$$Al(C_2H_5)_3 + 3H_2O \rightarrow Al(OH)_3 + 3C_2H_6.$$
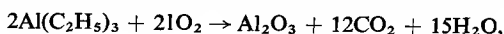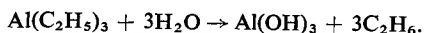
It is desirable to suppress the second reaction by supplying excess oxygen to the reaction zone and quickly sweeping out the reaction products, because the conversion of aluminum hydroxide to aluminum oxide requires substantially higher temperatures than those used in the deposition process.

The alkyl method lends itself readily to the preparation of mixed oxide films such as aluminasilicate or boroalumina silicate films, e.g., by reacting together a mixture of triethylaluminum (TEAL) and tetraethyl orthosilicate (TEOS), or TEAL, TEOS, and trisopropyl borate (*207*). The reaction occurs at 350–450°C, although the deposition of SiO_2 from TEOS alone requires a higher substrate temperature (about 700°C). A boroalumina silicate dielectric ($\varepsilon = 6$) whose composition was 79% Al_2O_3, 14% SiO_2, and 7% B_2O_3 appeared to exhibit a somewhat higher breakdown strength and a 40% smaller temperature coefficient of capacitance than Al_2O_3 ($\varepsilon = 10$–11) deposited alone, at the expense of a smaller dielectric constant.

More recently, Al_2O_3 films came under investigation in connection with a

search for materials not subject to the pitfalls associated with SiO_2 and Si_3N_4 in the passivation and gate insulation applications discussed above.

Matsushita and Koga (257) obtained two different kinds of Al_2O_3 films, depending on the deposition conditions prevailing in their system which used the thermal decomposition of aluminum triethoxide in atmospheric nitrogen at temperatures ranging from 350 to 500°C. The films obtained at the higher deposition temperatures or at low deposition rates ($<0.1 \mu$/hr) were up to 100% Al_2O_3, had a rough surface, were crystalline, and had poor insulating properties. Films obtained at the lower deposition temperatures or at fast deposition rates ($>0.5 \mu$/hr) contained up to 80% Al_2O_3, and for the balance an unidentified component (possibly an inorganic polymer with carbon atoms in a side or a main chain). These films were amorphous, had a smooth surface, and had good insulating properties (resistivity $\sim 10^{13} \Omega$ cm, breakdown field strength $F_B \approx 7 \times 10^6$ V/cm, flat-band surface charge concentration $N_{ss} = 2 \times 10^{12}$/cm^2). Yamamoto *et al.* (260) described a three-layer system: alumina–phosphoric oxide–silica applied to the passivation and surface protection of transistors subsequently encapsulated with epoxy. The alumina was formed either by anodization of an aluminum film, or by chemical vapor deposition as described above.

Krongelb (261) investigated the electrical stability of Al_2O_3 films deposited on germanium by the pyrolysis of aluminum isopropoxide, $Al(OC_3H_7)_3$, at a temperature of 420°C. Shifts in the surface potential of germanium directly under the Al_2O_3 layer, or under an SiO_2 film covered by Al_2O_3, indicated a change in surface charge concentration smaller than $\Delta N_{ss} \approx 10^{12}$/cm^2 after bias-temperature stressing. Krongelb, as well as Aboaf (261a), claimed that the Al_2O_3 layers were superior to SiO_2 formed from TEOS at comparable temperatures.

Aboaf's films, also prepared by the pyrolysis of $Al(OC_3H_7)_3$ at 420° C, were amorphous as deposited but could be converted into a crystalline structure (γ'-Al_2O_3 and γ-Al_2O_3) by heat treatment at 800–1000°C. While the films could be etched with buffered HF at an etch rate of 820 Å/min in their amorphous state, they became insoluble after recrystallization. Cheney *et al.* (262) reported on discrete and integrated field-effect transistors using an Al_2O_3–SiO_2 gate insulation. The Al_2O_3 was formed by the oxidation of $AlCl_3$ with CO_2 and H_2 at 925°C at a deposition rate of about 20 Å/min. For field-effect transistors fabricated on 5 Ω cm, (100)-oriented, n-type silicon, a threshold voltage of -1 V was obtained using 500 Å of deposited Al_2O_3 over 1000 Å of thermally grown SiO_2. Hot H_3PO_4 was used for etching windows into the aluminum oxide while a deposited SiO_2 layer served as a mask.

There has been relatively little work reported thus far on the deposition of thin films of aluminum nitride, AlN. However, Chu and co-workers (263)

were successful in depositing epitaxial layers of this material on the basal plane of hexagonal silicon carbide substrates by the ammonolysis technique, carried out in a flow system.

e. Tantalum Pentoxide, Niobium Pentoxide. Tantalum pentoxide is desirable as a dielectric for capacitor applications because of its relatively large dielectric constant of $\varepsilon \approx 30$. Films can be readily formed by the reaction of tantalum pentaethoxide, $Ta(OC_2H_5)_5$, and oxygen at a substrate temperature of 350–500°C. In the deposition setup described by Peterson (*207*), the $Ta(OC_2H_5)_5$ vaporizor was held at a temperature of about 150°C, and argon was used as a carrier gas. At a substrate temperature of 475°C, deposition rate on the order of 200 Å/min was achieved. The $Ta(OC_2H_5)_5$ may be prepared by a method reported by Bradley *et al.* (*264*) which consists of reacting ethanol and tantalum pentachloride with anhydrous ammonia in dry benzene. A mixture of tantalum pentaethoxide and triethylaluminum resulted in the deposition of a mixed oxide $Ta_2O_5:Al_2O_3$ which exhibited a somewhat lower dissipation factor and temperature coefficient than Ta_2O_5 itself (e.g., $\tan \delta \approx 4 \times 10^{-2}$ vs. 7×10^{-2} at 1 kHz, and $(1/\varepsilon)(d\varepsilon/dT) = 5 \times 10^{-4}/°C$ versus $1 \times 10^{-3}/°C$) at the expense of a slight reduction of the dielectric constant (e.g., $\varepsilon = 27$ vs. 33) (*207*).

Using basically the same deposition scheme, Duffy *et al.* (*265*) formed thin dielectric films of Ta_2O_5 and Nb_2O_5 on silicon and quartz substrates by the pyrolysis of $Ta(OC_2O_5)_5$ and $Nb(OC_2H_5)_5$, respectively, at 450°C in an oxidizing atmosphere. The resulting films had an amorphous structure which could be converted into a polycrystalline structure by a subsequent high-temperature treatment (800°C for Ta_2O_5 and 1200°C for Nb_2O_5). The relative dielectric constants for the two dielectrics were rather small: $\varepsilon = 22$ for Ta_2O_5, and $\varepsilon = 9$ for Nb_2O_5 (instead of $\varepsilon = 40$ usually reported for Nb_2O_5); respective surface charge concentrations for MIS capacitors at flatband were $N_{ss} = 5 \times 10^{11}/cm^2$ and $N_{ss} = 1 \times 10^{11}/cm^2$.

f. Titanium Dioxide. Depending on structure and orientation, TiO_2 can have a dielectric constant as high as $\varepsilon \approx 170$ and is therefore very attractive as a capacitor dielectric, especially since the dielectric constant is relatively frequency insensitive up to the gigahertz range. Several titanium compounds such as tetraisopropyl orthotitanate, $Ti(OiPr)_4$, titanium tetrachloride, $TiCl_4$, or tetraethoxytitanium, $Ti(OEt)_4$, are suitable reagents for depositions at temperatures of 400–500°C. Peterson (*207*) stated that $TiCl_4$, when reacted with water vapor, produced films that were inferior in quality to those produced by using the titanium alkoxides mentioned above. Films deposited at a rate of 300 Å/min at 450°C exhibited dielectric constants in the range $\varepsilon = 22$–42, but showed a high dissipation factor, of the order of 20%, and

a small breakdown voltage (2–5 V for a 1000-Å-thick film). The dielectric constant achieved for these films was rather small compared to that expected for rutile, which is the most stable of the three crystal modifications of TiO_2 (rutile, brookite, and anatase). Pure rutile has a dielectric constant $\varepsilon_a = 86$ in the a direction and $\varepsilon_c = 172$ in the c direction so that for a perfectly isotropic specimen a dielectric constant of $\varepsilon_{ac} \approx \frac{1}{3}(172 + 86 + 86) = 115$ is expected. Because of the presence of impurities, the dielectric constant of ceramic rutile is generally ≈ 90. In contrast to the findings by Peterson, Feuersanger (266) reported successful depositions of TiO_2 films by the hydrolysis of $TiCl_4$ or the pyrolysis of $Ti(OiPr)_4$. Films, 0.1–1 μ thick, formed by the first method at substrate temperatures of 150°C and at rates of ≈ 20 Å/min, had dielectric constants ranging from $\varepsilon = 25$ to $\varepsilon = 82$ and dissipation factors ranging from $\tan \delta \approx 1$–3×10^{-2} (at 1 kHz). The magnitude of the dielectric constant appeared to be related to the chemical resistance of the substrate material to attack by HCl; inert materials such as Pt and stainless steel produced the largest values. The maximum observed breakdown field was $F_b = 1.3 \times 10^6$ V/cm. Films deposited by the second method exhibited constants of up to 178, but also high dielectric losses ($\tan \delta \approx 10^{-1}$).

Lepie and Pucel (267) attempted to grow rutile film both by low- and high-temperature methods. In the low-temperature process, which, again, consisted of reacting $TiCl_4$ with H_2O vapor (nitrogen serving as carrier gas), the gases were mixed in a nozzle heated to 155°C and directed against a heated substrate located out in the atmosphere not far from the nozzle. All deposits were white, powdery, and poorly adherent to the fused silica substrates. For deposition temperatures <300°C, the deposit was amorphous or microcrystalline, while at 300°C it contained anatase with some preference for the <100> direction. A subsequent heat treatment at 1000°C for 10 hr converted most of the anatase to rutile without a preferred direction. The high-temperature process used the reaction

$$TiCl_4 + 2CO_2 + 2H_2 \rightarrow TiO_2 + 2CO + 4HCl$$
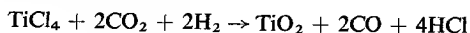
under reduced-pressure conditions (<0.5 atm) and at temperatures on the order of 1000°C. An optimum gas flow ratio was $TiCl_4 : CO_2 : H_2 = 1 : 9 : 90$. Deposits produced below 950°C contained anatase as well as rutile, but temperatures above 950°C resulted only in rutile. Up to 1100°C the deposition rate followed a straight Arrhenius plot with an activation energy of 86 kcal/mole, while at higher temperatures it remained nearly constant. Varying degrees of preferred crystallographic orientation were observed in deposits on fused silica. The appearance of the deposits was distinctly crystalline; in a cross-section view, the deposits were made up of cone-shaped clusters of crystals, typical of many CVD materials. Due to an oxygen deficiency, the deposits generally had a blue-black color which turned white after reheating

in air at 1000°C. Thick deposits caused shattering of the fused silica at the interface due to strong bonding and poor thermal expansion match.

3. METALS AND CONDUCTIVE MATERIALS

a. Metals. Thin films of metals are usually prepared by such methods as evaporation in vacuum, sputtering, or plating in a chemical solution. However, occasionally the use of a chemical vapor deposition method is of advantage. In most cases, the latter consists of pyrolysis or reduction of carbonyls or halides, or of a transport process employing a transporting agent such as iodine.

Among the various metal films that have been deposited by chemical vapor deposition are: tin [Gonser and Slowter (*268*)] by the reduction of stannous chloride at 550°C, niobium tin [Hanak *et al.* (*269*)] by the reduction of $NbCl_5 + SnCl_4$, and iron [Beischer (*270*)] and nickel [Owen (*271*)] by the pyrolysis of the respective carbonyls. The deposition of epitaxial metal films has also received attention. For example, Miller and co-workers (*272*) were able to grow epitaxial films of tungsten on sapphire by the reduction of WF_6 with hydrogen at atmospheric pressure.

More recently, the chemical vapor deposition of metal films has been utilized in the fabrication of Schottky-barrier diodes because of the advantages derived from depositing the metal layer in the same apparatus which is used for growing epitaxial layers of the semiconductor, namely: (1) the transfer of the substrate into a different deposition station is avoided and with it the possible formation of an oxide layer on the substrate; and (2) the deposition of refractory metals can be performed at relatively low temperatures. In addition, the height of the Schottky barrier can be controlled by varying the deposition parameters (partial pressure, flow rate, etc.) of the reagent gases. Sato *et al.* (*273*) formed Schottky-barrier diodes on silicon in this fashion by depositing W, Mo, or V contacts by the hydrogen reduction of WF_6, WCl_6, $MoCl_5$, or VCl_4, respectively; tungsten was also deposited on germanium and gallium arsenide. Furthermore, by adjusting the partial pressure of VCl_4 to an extremely small value, vanadium films could be deposited selectively onto those areas of silicon wafers not covered by an SiO_2 masking layer. The above workers also pointed out that a vanadium silicide layer which formed on the silicon surface was effective in suppressing thickness variations due to island formation in the deposited vanadium film.

Epitaxial vanadium films on (111) silicon surfaces, and vice versa, were formed by Miller *et al.* (*274*) by the hydrogen reduction of VCl_4 at 1300°C (100°C below the eutectic temperature). The resulting Schottky-barriers had a height of ≈ 0.7 eV. Sandler and Zettler (*275*) fabricated Schottky-barrier diodes exhibiting ideal characteristics and barrier heights of 0.59–0.61 eV by chemical vapor deposition of molybdenum onto *n*-type silicon. The method

used was the hydrogen reduction of either molybdenum hexacarbonyl or molybdenum pentachloride at relatively low temperatures that ranged from 300 to 900°C. Hashimoto and Koga (276) investigated the composition and morphology of W, Mo, and Ta deposited on (111), (110), and (100) Si surfaces by the hydrogen reduction of WCl_6, $MoCl_5$, and $TaCl_5$ at temperatures of 650–1250°C, 800–1250°C, and 800–1200°C, respectively. Reflection electron diffraction and x-ray diffraction yielded information about the composition of the deposit near the surface, and in its main body. On the surface polycrystalline Mo and W formed up to higher deposition temperatures than in the interior of the film, where the composition was that of polycrystalline disilicide. Films deposited at temperatures corresponding to the upper end of the temperature range consisted of precipitates of disilicide near the substrate surface, and a thin surface film of oriented disilicide. Deposition of tantalum always produced randomly oriented disilicide of relatively large grain size in the bulk while $TaSi_2$ and, at the lower temperatures, Ta_5Si_3 formed at the surface of the film.

Casey et al. (277) studied the chemical vapor deposition of Mo on Si in connection with hot electron devices, especially the metal base transistor. Two methods of deposition were investigated. The hydrogen reduction of $MoCl_5$, and the hydrogen reduction of MoO_2Cl_2. The surfaces of the substrates, (111) or (100) silicon, were conditioned by depositing an epitaxial silicon layer from $SiCl_4 + H_2$ at 1200°C. The Mo depositions took place at temperatures ranging from 600 to 1350°C. The structure of the deposits ranged from amorphous or polycrystalline molybdenum at low deposition temperatures to polycrystalline or single-crystal Si–Mo alloy phases such as $MoSi_2$ or Mo_3Si at high deposition temperatures. The results depended on the substrate orientation, and on the type of reagent gas. Tucker (278), also working with the hydrogen reduction of $MoCl_5$, reported that he obtained epitaxial molybdenum deposits over areas larger than 1 mil diam on single-crystal silicon at deposition temperatures of 700–800°C.

Investigations into methods for the chemical vapor deposition of thin films of Al, Cu, Au, Ni, W, Cr, Mo, and Ta suitable for use in thin film circuit fabrication have been described in great detail by Peterson (207). The deposition of aluminum was attempted by the thermal decomposition of triisobutylaluminum (TIBA) according to the reactions

$$Al(C_4H_9)_3 \xrightarrow[125°C]{} AlH(C_4H_9)_2 + C_4H_8,$$
$$AlH(C_4H_9)_2 \xrightarrow[260°C]{} Al + \tfrac{3}{2}H_2 + 2C_4H_8.$$
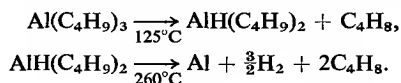
However, there was also an undesirable side reaction possible, proceeding as

$$Al(C_4H_9)_3 \rightarrow Al(CH_3)_3 + 3C_3H_6$$
$$Al_2(CH_3)_3 \rightarrow AlC + \text{other decomposition products.}$$
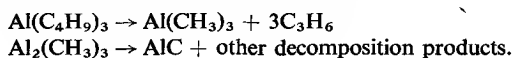
Addition of excess propane, C_3H_6, intended to suppress the undesirable reactions, was possible only up to 420°C; above this temperture, it led to the formation of organic decomposition products. However, the Al films were not satisfactory: a low concentration of TIBA yielded smooth Al films ≈ 1000 Å thick but of unduly high resistivity, and a high concentration produced films with a poor surface.

Copper deposition is possible by the hydrogen reduction of cuprous chloride, Cu_2Cl_2, at 500–700°C if HCl is added to the carrier gas in order to prevent premature decomposition. Unfortunately, this atmosphere is highly corrosive and the decomposition of suitable organometallic compounds is therefore preferred. Copper formate used at 300°C yielded Cu films with resistances in the 0.1 Ω/square range, provided the proper precautions were taken to ensure that decomposition took place only in the vicinity of the substrate. On the other hand, copper acetylacetonate used at temperatures of 300–450°C resulted in poor surfaces, Because it produces only small quantities of organic by-products, cupric formate has been suggested for copper depositions. It decomposes according to the overall reaction

$$Cu(HCO_2)_2 \rightarrow Cu + HCO_2H + CO_2,$$
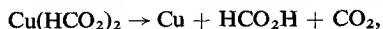
which is accompanied by the side reaction

$$2Cu(HCO_2)_2 \rightarrow 2CuHCO_2 + HCO_2H + 2CO_2.$$

The $CuHCO_2$ decomposes further to yield Cu, H_2, and CO_2, and the HCO_2H decomposes to CO and H_2O; thus, no organic deposits are formed in the reaction.

Continuous gold films were deposited by means of the reaction

$$2AuCl_3 \rightarrow 2Au + 3Cl_2$$
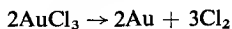
at substrate temperatures of 300–450°C and a total pressure of about 10 Torr, but difficulties were experienced with the adherence of the films to glass, fused silica, or ceramic substrates. The $AuCl_3$ was vaporized by heating it to 150°C.

Smooth nickel films, 1000–4000 Å thick, that were reported to have better adherence, conductivity, and oxidation resistance than films of similar thickness prepared by evaporation in vacuum were deposited by the carbonyl process

$$Ni(CO)_4 \rightarrow Ni + 4CO$$
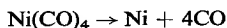
with best results obtained at substrate temperatures of 250–300°C. Films 1000 Å thick were deposited within about 30 min at 190°C. Since the energy required to break a nickel–carbon bond (in the carbonyl) is much smaller than that required to break a C–O bond, the above process should allow only little carbon formation. On the other hand, the reaction

$$2CO \rightarrow C + CO_2$$
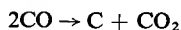
may be catalyzed by the nickel surface, especially at high temperatures, and can become the source of carbon contamination.

Tungsten and tantalum were deposited by the hydrogen reduction of halides. In the case of tungsten, it was found advantageous to use WF_6 instead of WCl_6 as a reagent. The latter tends to decompose prematurely at the required high deposition temperatures of 1000–2000°C, yielding powdery deposits. This difficulty is less apparent in the surface-catalyzed reaction

$$WF_6 + 3H_2 \rightarrow W + 6HF$$
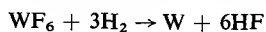
which permits low substrate temperatures of 350–650°C. Care should be taken to exclude any moisture or oxygen from the system, since this will prompt the formation of tungsten oxide and tungsten oxifluoride. The production of HF was held responsible for the poor adherence of films deposited on substrates that are readily etched by HF, such as glass or glazed ceramic.

A useful reaction for the deposition of tantalum films is

$$2TaCl_5 + 5H_2 \rightarrow 2Ta + 10HCl.$$
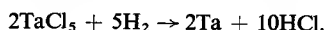
It offers the advantages of producing fewer contaminants and requiring a substantially lower deposition temperature than the straight thermal decomposition of $TaCl_5$. Smooth, adherent tantalum films, 500–2500 Å thick, with resistivities from 10,000 Ω/square to 30 Ω/square, were formed at a substrate temperature of 500°C.

Carbonyl compounds were employed not only for the deposition of nickel but also for the deposition of such metals as tungsten, molybdenum, and chromium. An example is the reaction

$$W(CO)_6 \rightarrow W + 6CO.$$
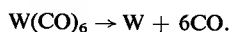
For these three latter metals, the bonding energy to the carbonyl group is larger than it is for nickel. The correspondingly larger deposition temperatures which are therefore required increase the likelihood of premature decomposition, as well as carbon contamination originating from decomposition disproportionation of the CO.

High-purity chromium films may also be deposited by the hydrogen reduction of $CrCl_2$ as was demonstrated by Wakefield (279). He reported that the properties of the resulting films were similar to those of high-purity "iodide" chromium. Boron films were deposited by Peters and Potter (280) on (001). (011), (111), and (112) silicon, as well as on fused SiO_2 substrates by the hydrogen reduction of BCl_3 at about 1000°C. The partial pressure of BCl_3 was ≈ 10 Torr. The films consisted generally of single-crystal, α-rhombohedral boron.

b. Conducting Compounds. Of great importance for thin-film integrated circuits is the deposition of stable low-noise resistors. This application requires materials which combine a high value of film resistance with good stability with respect to temperature variations and aging. At the present time, perhaps most attention is focused on tin oxide, a broad-band-gap semiconductor (*281*). Unfortunately, preparation of resistor films of desirable properties from this material is not a simple matter since its conductivity depends strongly on factors such as crystalline structure, concentration of oxygen vacancies, stresses, film thickness, and dopant concentration. According to Sinclair *et al.* (*282*) amorphous films of SnO_2 obtained by reactive sputtering on unheated substrates are insulating, but the same is true for crystalline tin oxide films containing antimony at a ratio 15% Sb:85% Sn after they were heat treated. Doping of the resistor films with Group V elements has been found to improve the resistor stability and to reduce the temperature dependence. The conventional process of preparation consists of hydrolyzing a spray of tin chloride (with possible additions of antimony or other suitable chlorides), dissolved in an organic compound such as ethanol, on substrates heated to 500–800°C. Basically the deposition takes place according to the reaction $SnCl_4 + 2H_2O \rightarrow SnO_2 + 4HCl$, but, in practice, the atmosphere resulting from the above solution produces a partial reduction of the SnO_2 film which appears to be essential for the conduction mechanism. Chemical vapor deposition, used instead of this process, should offer the advantage of reduced deposition temperatures and improved process control.

Peterson (*207*) has described the deposition of tin oxide from a reaction of vaporized tetraethyl tin with oxygen at 450–600°C. The resulting films had a resistivity of $\rho \approx 10^{-2}$ Ω cm and a temperature coefficient of TCR $\approx$ -10^3 ppm (25–125°C). Addition of tributylantimony to the reaction led to *n*-type doping of the films with antimony which produced a change of the TCR toward positive values at the expense of a lowered resistivity (for example, $a \sim 2000$-Å-thick, Sb-doped film of TCR ≈ 0 exhibited a resistivity of $\rho \approx 2 \times 10^{-3}$ Ω cm). High concentrations of Sb produced metallic conduction of the tin oxide by doping degeneracy and, therefore, a positive TCR. By adding a second dopant, triethylaluminum, to the reaction, the resistivity of tin oxide films could be increased while maintaining a low TCR. The SnO_2 films described by Peterson exhibited resistivity which increased when the crystallinity was increased by raising the deposition temperature or lowering the deposition rate. This effect was ascribed to poor electrical contact between grains due to the fissures observed in thin tin oxide films.

A different method of preparing high-purity tin oxide and tin antimony oxide films, namely reacting a mixture of oxygen, hydrogen, and the respective chlorides, was used by Aronson (*283*). By adjusting the deposition conditions,

the structure of the films could be varied from nearly amorphous to poly-crystalline.

Work on additional resistor materials such as indium oxide and nickel oxide was also described by Peterson (207). In both cases, films were formed by reacting the respective acetyl acetonates with oxygen at substrate temperature >300–$350°C$. Indium oxide films could also be obtained by reacting triethyl indium and oxygen at $300°C$. However, it appeared that the films produced by these methods did not exhibit a useful stability or uniformity.

Examples of further interesting work on conducting compounds are the following:

Films of VO_2, 0.1–1 μ thick, that exhibited a sharp drop in resistance of three orders of magnitude at the transition temperature of $67°C$ were prepared by MacChesney et al. (284). The technique consisted of first forming an amorphous film of V_2O_5 by reacting VCl_3 at temperatures below $127°C$ with CO_2 at atmospheric pressure, and then reducing the V_2O_5 to VO_2 by heating to temperatures between 500 and $550°C$ in a controlled atmosphere containing a partial pressure of oxygen.

Continuous titanium carbide films were obtained by Takahashi et al. (285) by feeding $TiCl_4$ reduced by spongy titanium and carried by argon, or a hydrogen–propane mixture, over the substrate held at 850–$1000°C$. Films of MnO_2 were deposited by McLean and Rocztoczy (286) by the pyrolysis of $Mn(NO_3)_2$ vapor. When these films were used as electrodes in Ta–Ta_2O_5–MnO_2 capacitors they produced self-healing effects.

c. Nonthermal Activation. Some work has been reported on the formation of metal films by the decomposition of chemical compounds induced by electron bombardment. Christy (287) bombarded the substrate with an electron beam of 2 mm diam and 1 mA/cm^9 or less current density; the bombardment voltage was 225 V. In one investigation, $SnCl_2$ vapor, generated from a source heated to $190°C$, was chosen as the chemical compound. Under the prevailing conditions, the electron flux impinging in the substrate (0.1 electron/$Å^2$-sec) was five times larger than the flux of vapor molecules; the resulting deposition of a Sn film occurred at a rate of 0.5 Å/sec. Christy stated that the rate could possibly be increased by a factor of 10^3 by raising the beam current density. When the substrates were at room temperature during deposition, shiny films, 500 Å thick, were obtained. In contrast, 1000-Å-thick films had a rough surface structure. When deposited on substrates cooled to $-60°C$, films of 1000 Å thickness were shiny but full of pinholes. The question whether the decomposition proceeds as the one-step decomposition

$$SnCl_2 \rightarrow Sn + Cl_2$$
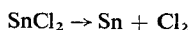
or as the two-step decomposition

$$SnCl_2 \rightarrow SnCl + Cl$$
$$SnCl \rightarrow Sn + Cl$$
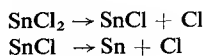
remained open. Tetrabutyltin, $Sn(C_4H_9)_4$, was decomposed under similar flux conditions. However, instead of a metallic film, the process yielded only semiconducting polybutyltin polymer films whose properties depended on the ratio between the electron and the vapor fluxes, and on the substrate temperature. The latter determines the mean time for which the impinging vapor molecules reside on the substrate. A result at variance with these findings was reported by Baker and Morris (288). These workers decomposed tetrabutyltin, tetramethyltin, and tetraethyllead by an electron beam of 5 mA/cm^2 current density at a beam voltage ranging from 50 V to 1 kV, and succeeded in producing highly reflecting tin films of 50–1500 Å thickness and corresponding film resistances of 1000–50 Ω/square.

Metals have also been deposited by decomposition of organic compounds under the influence of uv or x-ray radiation. This mechanism is of great potential importance for the direct deposition of complicated metal patterns without involving laborious photomasking and etching processes.

Leighton and Mortenson (289) discovered that vaporized tetramethyl lead, $Pb(CH_3)_4$, is readily photolized by uv light with a quantum efficiency of 1.1 according to the reaction

$$Pb(CH_3)_4 \underset{uv}{\rightarrow} Pb + 2C_2H_6.$$
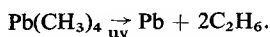
Clouston and Cook (290) assumed that the actual reaction involves the primary reaction

$$Pb(CH_3)_4 \underset{uv}{\rightarrow} Pb(CH_3)_3 + CH_3$$
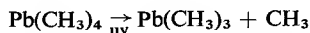
and a subsequent decomposition of the thermally unstable product $Pb(CH_3)_3$. Tetraethyllead, tetraphenyllead, and tetramethyltin were similarly decomposed with the aid of uv light, but less efficiently than the tetramethyllead.

Solid films of tetramethyllead of about 0.1 mm thickness were also successfully decomposed by Mador (291) by irradiation with x-rays. When the films were held at 4°K, CH_4 was produced by the irradiation process. Upon subsequent heating to 40°K, the films became opaque due to the formation of free lead.

4. FERRIMAGNETIC OXIDES

Ferrimagnetic oxide films have potential applications in magnetic and optical memory devices and in microwave integrated circuits. Ferrite films of both spinels and garnets have been produced by a variety of chemical

vapor deposition techniques (*292, 304*), all of which contain the pyrohydro-lysis of the gaseous metal halides as the ultimate deposition reaction. A typical reaction is

$$MgCl_2 \text{ (g)} + 2FeCl_2 \text{ (g)} + 3H_2O \text{ (g)} + \tfrac{1}{2}O_2 \text{ (g)} \rightleftharpoons MgFe_2O_4 \text{ (s)} + 6HCl \text{ (g)}$$
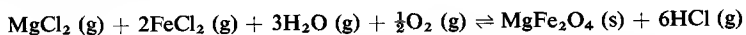
In some cases the metal halides, usually chlorides or bromides, are used as the source materials. These materials have vapor pressures in the Torr range at temperatures between 500 and 1000°C. The reaction takes place on sub-strates at 800–1200°C. Therefore, for the deposition of complex oxides such as the ferrites, multitemperature zone furnaces are required (cf. *293–295, 297–301*). Others have used halide mixtures as a single source, but this leads to compositional variations through the film thickness since the source com-position changes with time (*292*). Another approach that has been successfully utilized is the reverse of the above reaction in a higher temperature region of the furnace to produce the gaseous halides from either single (*303, 304*) or multiple oxide sources (*302*). The pyrohydrolysis then takes place in a lower temperature region of the furnace. Both closed (*302–304*) and flow (*292–301*) systems have been used. In the flow system, an inert carrier gas, such as argon (*293, 294, 296*), helium (*297–302*), or argon–helium mixtures (*297–301*) is usually added to provide a sufficiently high gas velocity over the substrate. Total pressures between 25 Torr (*296*) and 1 atm (*297–301*) have been used. It has been reported that the film composition, particularly the amount of divalent iron, can be controlled by the amount of oxygen in the gas stream (*293–300*). The reported film deposition rates are between 100 Å/hr and 50 μ/hr and can be controlled by such parameters as gas pressures and substrate temperatures. Unfortunately, very little work has been reported on the effect of deposition variables on film properties, structure, and growth rate. No attempt has been made to correlate the deposition variables and resultant film parameters with the possible rate-controlling and growth mechanisms.

In general, most of the reported work has been concerned with epitaxial deposition of single-crystal films with but one exception (*292*). Nickel (*292, 303, 304*), cobalt (*292*), manganese (*300, 302*), nickel–manganese (*295–297*), iron (*292, 296*), and magnesium (*302*) ferrite single-crystal films have been grown on magnesium oxide single-crystal substrates. The ease with which the spinels can be grown on MgO has been attributed to both the substrate and film having close-packed oxygen sublattices and the resultant similarity of the oxygen–oxygen interatomic distances. Spinel films have also been grown epitaxially on single-crystal sapphire and spinel ($MgAl_2O_4$) for apparently the same reason (*300*). Yttrium iron garnet ($Y_3Fe_5O_{12}$) (*293, 294, 298*) and gadolinium iron garnet ($Gd_3Fe_5O_{12}$) (*298*) have been grown epitaxially on yttrium aluminum garnet ($Y_3Al_5O_{12}$). The properties of both the spinel and

garnet films are reported to be essentially the same as those of single crystals of these materials grown by other techniques.

One difficulty that has been experienced with ferrite films is the cracking that occurs in the films or substrates when they are cooled from the deposition temperature (*298, 301*). Since the thermal expansion coefficients of the ferrite and the substrate are usually different, stresses induced on cooling can lead to fracture. Even if the stresses are not sufficiently high to cause fracture, they can alter the magnetic properties of the films via magnetoelastic effects (*300*).

REFERENCES

1. C. F. Powell, J. H. Oxley, and J. M. Blocher, Jr., eds., "Vapor Deposition." Wiley, New York, 1966.
2. D. S. Campbell, *in* "The Use of Thin Films in Physical Investigations" (J. C. Anderson, ed.), p. 11. Academic Press, New York, 1966.
3. B. A. Joyce, *in* "The Use of Thin Films in Physical Investigations" (J. C. Anderson, ed.), p. 87. Academic Press, New York, 1966.
4. T. J. LaChapelle, A. Miller, and F. L. Morritz, *in* "Progress in Solid State Chemistry" (H. Reiss, ed.), Vol. 3, p. 1. Pergamon Press, Oxford, 1967.
5. L. V. Gregor, *in* "Physics of Thin Films" (G. Hass and R. E. Thun, eds.), Vol. 3, p. 131. Academic Press, New York, 1966.
6. E. G. Mezey, *in* "Vapor Deposition" (C. F. Powell, J. H. Oxley, and J. M. Blocher, eds.), p. 423. Wiley, New York, 1966.
7. J. W. Mellor, "A Comprehensive Treatise on Inorganic and Theoretical Chemistry," Vol. 6. Longmans, Green, New York, 1957.
8. W. E. Sawyer and A. Man, U.S. Pat. 229,335 (June 29, 1880).
9. J. W. Aylsworth, U.S. Pat. 553,296 (Jan. 21, 1896).
10. A. deLodyguine, U.S. Pat. 575,002 (Jan. 12, 1897); U.S. Pat. 575,668 (Jan. 19, 1897).
11. L. Mond, U.S. Pat. 455,230 (June 30, 1891).
12. L. Mond, C. Langer, and F. Quincke, *J. Chem. Soc.* **57**, 749 (1890).
13. H. Schaefer, "Chemical Transport Reactions." Academic Press, New York, 1963.
14. J. M. Blocher, *in* "Vapor Deposition" (C. F. Powell, J. H. Oxley, and J. M. Blocher, Jr., eds.), p. 650. Wiley, New York, 1966.
15. C. F. Powell, *in* "Vapor Deposition" (C. F. Powell, J. H. Oxley, and J. M. Blocher, Jr., eds.), p. 249. Wiley, New York, 1966.
16. R. W. Christy, *J. Appl. Phys.* **31**, 1680 (1960).
17. A. Bradley and J. P. Hammes, *J. Electrochem. Soc.* **110**, 15 (1963).
18. P. Gross and D. L. Levi, Symp. Extraction Metallurgy Some Less Common Metals, Inst. Mining Met., London, Paper 19 (March 22–23, 1956).
19. E. S. Wajda, B. W. Kippenham, and W. H. White, *IBM J. Res. Develop.* **4**, 288 (1960).
20. F. B. Litton and H. C. Andersen, *J. Electrochem. Soc.* **101**, 287 (1954).
21. G. Szekely, *J. Electrochem. Soc.* **104**, 663 (1957).

22. C. S. Herrick, U.S. Pat. 3,020,129 (Feb. 6, 1962).
23. C. S. Herrick and J. G. Krieble, *J. Electrochem. Soc.* **107**, 111 (1960).
24. D. H. Robinson, *RCA Rev.* **24**, 574 (1963).
25. R. F. Lever and F. Jona, *J. Appl. Phys.* **34**, 3139 (1963).
26. H. Schaefer, H. Jacob, and K. Etzel, *Z. Anorg. Allgem. Chem.* **286**, 42 (1956).
27. A. E. van Arkel and J. H. deBoer, U.S. Pat. 1,671,213 (May 29, 1928).
28. A. E. van Arkel, "Reine Metalle." Springer, Berlin, 1939.
29. J. A. Amick, E. A. Roth, and H. Gossenberger, *RCA Rev.* **24**, 473 (1963).
30. G. A. Lang and T. Stavish, *RCA Rev.* **24**, 488 (1963).
31. H. M. Manasevit, Meeting Electrochem. Soc., Chicago, Ext. Abstr. 183. (1967).
32. M. V. Sullivan and G. H. Kolb, *J. Electrochem. Soc.* **115**, 62C (1968).
33. R. H. Finch, H. J. Queisser, G. Thomas, and J. Washburn, *J. Appl. Phys.* **34**, 406 (1963).
34. G. R. Booker, *Phil. Mag.* **11**, 1007 (1965).
35. C. H. Li, *J. Electrochem. Soc.* **109**, 952 (1962).
36. A. B. McIntosh and J. S. Broadley, Symp. Extraction Metallurgy Some Less Common Metals, Inst. Mining Met., London, Paper 15, (March 22–23, 1956).
37. H. C. Theuerer, *J. Electrochem. Soc.* **109**, 742 (1962).
38. W. G. Pfann, J. R. Patel, and H. C. Theuerer, *J. Electrochem. Soc.* **109**, 512 (1962).
39. R. Nuttal, *J. Electrochem. Soc.* **111**, 317 (1964).
40. A. M. Smith and R. P. Donovan, Meeting Electrochem. Soc., Toronto, Ext. Abstr. 46 (1964).
41. M. C. Duffy, D. W. Foy, and W. J. Armstrong, Meeting Electrochem. Soc., San Francisco, Ext. Abstr. 125 (1965).
42. K. M. Whittle and G. L. Vick, Meeting Electrochem. Soc., Boston, Ext. Abstr. 94 (1968).
43. R. Orlang and B. W. Kippenham, *IBM J. Res. Develop.* **4**, 229 (1960).
44. E. S. Wajda and R. Orlang, *in* "Metallurgy of Elemental and Compound Semiconductors" (R. O. Grubel, ed.), p. 229. Wiley (Interscience), New York, 1961.
45. J. E. Allegretti, D. J. Shombert, E. Schaarschmidt, and F. Waldman, *in* "Metallurgy of Elemental and Compound Semiconductors" (R. O. Grubel, ed.), p. 255. Wiley (Interscience), New York, 1961.
46. K. J. Miller and M. J. Grieco, *J. Electrochem. Soc.* **110**, 1252 (1963).
47. V. Sils, R. Berkstresser, and P. Wang, *J. Electrochem. Soc.* **109**, 243C (1962).
48. J. J. Gebhardt and R. F. Cree, *J. Am. Ceram. Soc.* **48**, 262 (1965).
49. R. D. Gretz, *in* "Vapor Deposition" (C. F. Powell, J. H. Oxley, and J. M. Blocher, Jr., eds.), p. 149. Wiley, New York, 1966.
50. T. N. Rhodin, *in* "The Use of Thin Films in Physical Investigations" (J. C. Anderson, ed.), p. 187. Academic Press, New York, 1966.
51. G. W. Sears, *Acta Met.* **3**, 362 (1955).
52. B. W. Sloope and C. O. Tiller, *J. Appl. Phys.* **32**, 1331 (1961).
53. H. J. Queisser and R. H. Finch, *J. Appl. Phys.* **33**, 1536 (1962).
54. J. A. Amick, *RCA Rev.* **24**, 555 (1963).
55. G. R. Pulliam, J. E. Mee, and R. G. Warren, Proc. Conf. AIME Southwest Metals, Los Angeles (1964).
56. J. D. Filby, S. Nielsen, and G. J. Rich, *in* "The Use of Thin Films in Physical Investigations" (J. C. Anderson, ed.), p. 233. Academic Press, London and New York, 1966.
57. A. E. Blakeslee, Conf. AIME, Chicago, Abstr. 32 (1968).
58. M. S. Seltzer, N. Albon, B. Paris, and R. C. Himes, Meeting Electrochem. Soc., Buffalo, Ext. Abstr. 122 (1965).

59. T. Gabor and J. M. Blocher, Jr., Meeting Electrochem. Soc., Chicago, Ext. Abstr. 193 (1967).
60. J. H. Oxley, *in* "Vapor Deposition" (C. F. Powell, J. H. Oxley, and J. M. Blocher, Jr., eds.), p. 493. Wiley, New York, 1966.
61. R. J. Diefendorf, *J. Chim. Phys.* **57**, 815 (1960).
62. O. J. Guentert, *J. Chem. Phys.* **27**, 884 (1962).
63. E. T. Stover, G. E. Rept. 64-RL-3609M (March, 1964).
64. L. F. Coffin, *J. Am. Ceram. Soc.* **47**, 473 (1964).
65. J. Pappis, *Electron. Progr.* **11**, 6, Raytheon Co. (1968).
66. W. R. Runyan, *in* "Vapor Deposition" (C. F. Powell, J. H. Oxley, and J. M. Blocher, Jr., eds.), p. 593. Wiley, New York, 1966.
67. B. Schwartz, *in* "Vapor Deposition" (C. F. Powell, J. H. Oxley, and J. M. Blocher, Jr., eds.), p. 612. Wiley, New York, 1966.
68. E. G. Alexander, Meeting Electrochem. Soc., Dallas, Abstr. 105 (1967).
69. R. C. Sangster, E. F. Maverick, and M. L. Croutch, *J. Electrochem. Soc.* **194**, 317 (1957).
70. N. N. Sheftal, N. P. Kokorish, and A. V. Kraselov, *Bull. Acad. Sci. USSR Phys. Ser. (English Transl.)* **21**, 140 (1957).
71. H. C. Theuerer, *J. Electrochem. Soc.* **108**, 649 (1961).
72. A. Mark, *J. Electrochem. Soc.* **107**, 568 (1960).
73. A. Mark, *J. Electrochem. Soc.* **108**, 880 (1961).
74. B. E. Deal, *J. Electrochem. Soc.* **109**, 514 (1962).
75. E. G. Bylander, *J. Electrochem. Soc.* **109**, 1171 (1962).
76. J. E. Allegretti and D. J. Shombert, Meeting Electrochem. Soc., Chicago, 1960.
77. J. M. Charig and B. A. Joyce, *J. Electrochem. Soc.* **109**, 957 (1962).
78. R. Glang and E. S. Wajda, *in* "Metallurgy of Semiconductor Materials" (J. B. Schroeder, ed.), p. 27. Wiley (Interscience), New York, 1962.
79. H. C. Theuerer, H. Loar, J. Kleimack, and H. Christensen, *Proc. IRE* **48**, 1642 (1960).
80. H. C. Theuerer, *J. Electrochem. Soc.* **107**, 29 (1960).
81. D. Kahng, C. O. Thomas, and R. C. Manz, *J. Electrochem. Soc.* **110**, 394 (1963).
82. R. G. Frieser, *J. Electrochem. Soc.* **115**, 401 (1968).
83. A. M. Stein, *J. Electrochem. Soc.* **111**, 483 (1964).
84. W. Steinmeier, *Philips Res. Rep.* **18**, 75 (1963).
85. R. R. Monchamp, W. J. McAleer, and P. I. Pollack, *J. Electrochem. Soc.* **111**, 879 (1964).
86. O. Alstrup and C. O. Thomas, *J. Electrochem. Soc.* **112**, 319 (1965).
87. E. F. Cave and B. R. Czorny, *RCA Rev.* **24**, 523 (1963).
88. W. H. Shepherd, *J. Electrochem. Soc.* **115**, 541 (1968).
89. S. Nakanuma and H. Osafune, Meeting Electrochem. Soc., San Francisco, Ext. Abstr. 75 (1965).
90. R. S. Wagner and W. C. Ellis, *Appl. Phys. Letters,* **4**, 89 (1964).
91. J. D. Filby and S. Nielsen, Conf. AIME, San Francisco, 1965.
92. B. A. Joyce and J. A. Baldrey, *Nature,* **195**, 485 (1962).
93. E. G. Alexander and W. R. Runyan, *Trans. Met. Soc. AIME* **236**, 224 (1966).
94. K. J. Miller and M. J. Grieco, *J. Electrochem. Soc.* **109**, 70 (1962).
95. J. Oda, *Japan. J. Appl. Phys.* **1**, 131 (1962).
96. H. M. Manasevit, A. Miller, F. L. Morritz, and R. L. Nolder, *Trans. Met. Soc. AIME* **233**, 540 (1965).
97. H. M. Manasevit and W. I. Simpson, Meeting, Late News Item Am. Phys. Soc., Edmonton, Alberta, Canada (1963).

98. H. M. Manasevit and W. 1. Simpson, *J. Appl. Phys.* **35**, 1349 (1964).
99. A. Miller and H. M. Manasevit, *J. Vacuum Sci. Technol.* **3**, 68 (1966).
100. B. A. Joyce, R. J. Bennett, R. W. Bicknell, and P. J. Etter, *Trans. Met. Soc. AIME* **233**, 556 (1965).
101. J. M. Blank and V. A. Russell, *Trans. Met. Soc. AIME* **236**, 291 (1966).
102. C. Y. Ang and H. M. Manasevit, *Solid State Electr.* **8**, 994 (1965).
103. P. S. Schaffer, *Proc. Ann. Meeting Am. Ceram. Soc., 66th*, Chicago (1965).
104. B. A. Joyce, R. W. Bicknell, J. M. Charig, and D. J. Stirland, *Solid State Commun.* **1**, 107 (1963).
105. R. W. Bicknell, J. M. Charig, B. A. Joyce, and D. J. Stirland, *Phil. Mag.* **9**, 965 (1964).
106. H. M. Manasevit, D. H. Forbes, and 1. B. Cadoff, Proc. Conf. AIME Tech. Materials, San Francisco (1965).
107. H. M. Manasevit and D. H. Forbes, *J. Appl. Phys.* **37**, 734 (1966).
108. S. R. Bhola and A. Mayer, *RCA Rev.* **24**, 511 (1963).
109. W. Kagdis, *J. Electrochem. Soc.* **109**, 71C (1962).
110. C. H. Lewis, H. C. Kelly, M. B. Giusto and S. Johnson, *J. Electrochem. Soc.* **108**, 114 (1961).
111. S. E. Mayer and D. E. Shea, *J. Electrochem. Soc.* **111**, 550 (1964).
112. B. A. Joyce and R. R. Bradley, *J. Electrochem. Soc.* **110**, 1235 (1963).
113. C. C. Wang, G. E. Gottlieb, G. W. Cullen, S. H. McFarlane III, and K. H. Faininger, Conf. AIME, Chicago, Abstr. 20 (1968).
114. R. L. Anderson, G. Zeidenbergs, and M. Davis, Heterojunction Devices, Final Rept., Contract AF30(602)-3637 (March 1968).
115. J. J. Oberly and A. Adams, *J. Electrochem. Soc.* **109**, 210C (1962).
116. E. Matovich and R. J. Andres, *J. Electrochem. Soc.* **108**, 177C (1961).
117. H. Christensen and G. K. Teal, U.S. Pat. 2,692,839 (Oct. 26, 1954).
118. N. Kyle and J. J. Grossman, *J. Electrochem. Soc.* **110**, 184C (1963).
119. V. J. Silvestri, Meeting Electrochem. Soc., Dallas, Ext. Abstr. 104 (1967); Meeting Electrochem. Soc., Chicago, Ext. Abstr. 163 (1967).
120. E. A. Roth, H. Gossenberger, and J. A. Amick, *RCA Rev.* **24**, 499 (1963).
121. W. M. Becker and K. Lark-Horowitz, *Proc. Natl. Electr. Conf.* **8**, 506 (1952).
122. M. Davis and R. F. Lever, *J. Appl. Phys.* **27**, 835 (1956).
123. C. F. Powell, J. H. Oxley, and J. M. Blocher, Jr., eds., "Vapor Deposition," p. 629. Wiley, New York, 1966.
124. K. Tamaru, M. Boudart, and H. Taylor, *J. Phys. Chem.* **59**, 801 (1955).
125. P. J. Fensham, K. Tamaru, M. Boudart, and H. Taylor, *J. Phys. Chem.* **59**, 806 (1955).
126. R. L. Zanovick, Meeting Electrochem. Soc., Buffalo, Ext. Abstr. 120 (1965).
127. S. A. Papazian and A. Reisman, Meeting Electrochem. Soc., Chicago, Ext. Abstr. 159 (1967).
128. T. B. Light, M. Berkenblit, and A. Reisman, Meeting Electrochem. Soc., Chicago, Ext. Abstr. 161 (1967).
129. D. J. Dumin, Meeting Electrochem. Soc., Dallas, Abstr. 3 (1967).
130. W. C. Dunlap, J. C. Marinace, and R. P. Ruth, *Bull. Am. Physt Soc. Ser. 11*, **1**, 294 (1956).
131. D. C. Cronemeyer, *J. Appl. Phys.* **29**, 1730 (1958).
132. J. C. Marinace, *IBM J. Res. Develop.* **4**, 248 (1960).
133. M. Takabayashi, *Japan. J. Appl. Phys.* **1**, 22 (1962).
134. S. K. Tung, *J. Electrochem. Soc.* **110**, 185C (1963).
135. W. E. Baker and D. J. M. Compton, *IBM J. Res. Develop.* **4**, 269 (1960).

136. A. Reisman and M. Berkenblit, Meeting, Electrochem. Soc., Toronto, Ext. Abstr. 63 (1964).
137. T. O. Sedgwick, Meeting Electrochem. Soc., Toronto, Ext. Abstr. 64 (1964).
138. F. H. Nicoll, *J. Electrochem. Soc.* **110**, 1165 (1963).
139. R. L. Anderson, *IBM J. Res. Develop.* **4**, 283 (1960).
140. W. G. Oldham, A. R. Riben, D. L. Feucht, and A. G. Milnes, *J. Electrochem. Soc.* **110**, 53C (1963).
141. A. R. Riben, D. L. Feucht, and W. G. Oldham, Meeting Electrochem. Soc., San Francisco, Ext. Abstr. 79 (1965).
142. J. C. Marinace, Meeting Electrochem. Soc., San Francisco, Ext. Abstr. 80 (1965).
143. Y. Tarui, H. Teshima, K. Okura, and A. Minamiya, *J. Electrochem. Soc.* **110**, 1167 (1963).
144. V. J. Lyons and V. J. Silvestri, *J. Electrochem. Soc.* **109**, 963 (1962).
145. D. Richman, *RCA Rev.* **24**, 596 (1963).
146. G. E. Gottlieb and J. F. Corboy, *RCA Rev.* **24**, 585 (1963).
147. G. R. Antell and D. Effer, *J. Electrochem. Soc.* **106**, 509 (1969).
148. F. A. Pizzarello, *J. Electrochem. Soc.* **110**, 1059 (1963).
149. A. Hagenlocher, *J. Electrochem. Soc.* **108**, 213C (1961).
150. T. Okada, *Japan. J. Appl. Phys.* **2**, 206 (1963).
151. R. R. Moest and B. R. Shupp, *J. Electrochem. Soc.* **109**, 1061 (1962).
152. T. Okada, T. Kano, and Y. Sasaki, *J. Phys. Soc. Japan*, **16**, 2591 (1961).
153. N. Goldsmith, *J. Electrochem. Soc.* **110**, 558 (1963).
154. V. J. Silvestri and F. Fang, *J. Electrochem. Soc.* **110**, 185C (1963).
155. C. F. Powell, J. H. Oxley, and J. M. Blocher, Jr., eds., "Vapor Deposition," p. 631. Wiley, New York, 1966.
156. N. Holonyak, Jr., D. C. Jillson, and S. R. Bevacqua, *in* "Metallurgy of Semiconductor Materials" (J. B. Schroeder, ed.), p. 49. Wiley (Interscience), New York, (1962).
157. F. V. Williams and R. A. Ruehrwein, *J. Electrochem. Soc.* **108**, 177C (1961).
158. R. L. Newman and N. Goldsmith, *J. Electrochem. Soc.* **108**, 1127 (1961).
159. C. J. Frosch and C. D. Thurmond, *J. Electrochem. Soc.* **109**, 301C (1962).
160. D. K. Jadus, G. O. Ladd, and D. L. Feucht, Meeting Electrochem. Soc., Dallas, Ext. Abstr. 102 (1967).
161. F. W. Tausch and T. A. Longo. *J. Electrochem. Soc.* **109**, 70C (1962).
162. S. W. Ing, Jr., and H. T. Minden, *J. Electrochem. Soc.* **109**, 995 (1962).
163. S. Stopek, Meeting Electrochem. Soc., Pittsburgh, Recent News Item II-2 (1963).
164. M. Rubenstein and E. Myers, Meeting Electrochem. Soc., San Francisco, Ext. Abstr. 101 (1965).
165. E. W. Mehal, R. W. Haisty, and D. W. Shaw, *Trans. Met. Soc. AIME* **236**, 263 (1966).
166. N. Goldsmith and W. Oshinsky, *RCA Rev.* **24**, 546 (1963).
167. H. Leonhardt, Meeting Electrochem. Soc., Toronto, Ext. Abstr. 68 (1964).
168. H. M. Manasevit and W. 1. Simpson, Meeting Electrochem. Soc., Boston, Abstr. 63 (1968).
169. G. S. Kamath and D. Bowman, *J. Electrochem. Soc.* **114**, 192 (1967).
170. L. C. Luther and D. D. Roccasecca, Meeting Electrochem. Soc., Boston, Ext. Abstr. 101 (1968).
171. I. Akasaki and T. Hara, Meeting, Electrochem. Soc., Dallas, Abstr. 4 (1967).
172. I. Akasaki, M. Hashimoto, and T. Hara, Meeting Electrochem. Soc., Dallas, Abstr. 100 (1967).
173. R. A. Burmeister and R. W. Regehr, Conf., AIME, Chicago, Abstr. 30 (1968).
174. P. A. Hoss, L. A. Murray, and J. J. Rivera, *J. Electrochem. Soc.* **115**, 553 (1968).

175. J. J. Tietjen and J. A. Amick, *J. Electrochem. Soc.* **113**, 724 (1966).
176. R. B. Clough and J. J. Tietjen, Conf. AIME, Chicago, Abstr. 33 (1968).
177. S. G. Parker and J. E. Pinnell, Conf. AIME, Chicago, Abstr. 22 (1968).
178. F. J. Studer, D. A. Cusano, and A. H. Young, *J. Opt. Soc. Am.* **41**, 559 (1951).
179. F. J. Studer and D. A. Cusano, *J. Opt. Soc. Am.* **45**, 493 (1955).
180. A. Baczewski, *J. Electrochem. Soc.* **112**, 577 (1965).
181. H. J. Hovel and A. G. Milnes, Meeting Electrochem. Soc., Chicago, Abstr. 165 (1967).
182. T. O. Sedgwick and B. J. Agule, Meeting Electrochem. Soc., Buffalo, Ext. Abstr. 126 (1965).
183. G. Galli and F. L. Morritz, Meeting Electrochem. Soc., Cleveland, Ext. Abstr. 43 (1966).
184. M. Weinstein and A. A. Mena, Meeting Electrochem. Soc., San Francisco, Recent News Item (1965).
185. A. J. Belvinger and M. Smith, Meeting Electrochem. Soc., Buffalo, Ext. Abstr. 125 (1965).
186. I. J. Hegyi, Meeting Electrochem. Soc., Washington D.C., Abstr. 150 (1964).
187. Dow Corning Corp., Preliminary Information Silicon Carbide Epitaxial Susceptors, Hemlock, Mich. (March, 1967)
188. J. N. Pring and W. Fielding, *J. Chem. Soc.* **95**, 1497 (1909).
189. R. Iley and H. L. Riley, *J. Chem. Soc.* **1948**, 1362.
190. J. A. Lely, *Ber. Deut. Keram. Ges.* **32**, 229 (1955).
191. C. F. Powell, "Vapor Deposition" (C. F. Powell, J. H. Oxley, and J. M. Blocher, Jr., eds.), p. 343. Wiley (Interscience), New York, 1966.
192. V. J. Jennings, A. Sommer, and H. C. Chang, *J. Electrochem. Soc.* **113**, 728 (1966).
193. J. T. Kendall and D. Yeo, *Proc. Intern. Congr. Pure Appl. Chem. London, 11th, 1947*, **1**, 171 (1950).
194. D. L. Barrett, Meeting Electrochem. Soc., Buffalo, Ext. Abstr. 123 (1965).
195. J. T. Kendall, *J. Chem. Phys.* **21**, 821 (1953).
196. S. Susman, R. S. Spriggs, and H. S. Weber, *in* "Silicon Carbide" (J. R. O'Connor and J. Smiltens, eds.), p. 94. Pergamon Press, Oxford, 1960.
197. K. M. Merz, *in* "Silicon Carbide" (J. R. O'Connor and J. Smiltens, eds.), p. 1, 73. Pergamon Press, Oxford, 1960.
198. R. W. Brander. *J. Electrochem. Soc.* **111**, 881 (1964).
199. R. B. Campbell, T. L. Chu, and K. C. Liang, *J. Electrochem. Soc.* **113**, 825 (1966).
200. T. L. Thompson, D. W. Hamill, and E. L. Kern, Meeting Electrochem. Soc., Philadelphia, Recent News Item 29 (1966).
201. J. M. Harris, H. C. Gatos, and A. 1. Witt, Meeting Electrochem. Soc., Boston, Ext. Abstr. 68 (1968).
202. C. B. Lamport, E. A. Trickett, and G. A. Wolff, Meeting Electrochem. Soc., Boston, Ext. Abstr. 67 (1968).
203. C. A. Mead, *Proc. IRE* **48**, 359 (1960).
204. E. D. Roberts, Meeting Electochem. Soc., Boston, Ext. Abstr. 160 (1968).
205. S. W. Ing, Jr., and W. Davern, *J. Electrochem. Soc.* **112**, 284 (1965).
206. L. L. Alt, S. W. Ing, Jr., and K. W. Laendle, *J. Electrochem. Soc.* **110**, 465 (1963).
207. D. Peterson, Non-vacuum deposition techniques for use in fabricating thin film circuits, Contract No. NObsr 91336, Final Rept. (Jan. 1967).
208. F. Huber, M. Topfer, M. Witt, W. Laznovsky, and J. Mitchell, Applied research in thick film active devices, Contract NAS1-6285, Final Rept. (Dec. 1966).
209. V. Y. Doo and D. R. Kerr, Investigation of refractory dielectrics for integrated circuits, Contract NAS1 12-105, Final Rept. (July 1967).

210. D. L. Tolliver and D. L. Elgan, Meeting Electrochem. Soc., Philadelphia, Ext. Abstr. 183 (1966).
211. B. M. Mecs, Meeting Electrochem. Soc., Boston, Ext. Abstr. 93 (1968).
212. T. L. Chu and G. A. Gruber, Meeting Electrochem. Soc., Philadelphia, Ext. Abstr. 174 (1966).
213. T. L. Chu, C. H. Lee, and J. R. Szedon, Meeting Electrochem. Soc., Dallas, Ext. Abstr. 83 (1967).
214. W. Van Gelder and V. E. Hauser, *J. Electrochem. Soc.* **114**, 869 (1967).
215. W. Steinmaier and J. Bloem, *J. Electrochem. Soc.* **111**, 206 (1964).
216. S. K. Tung, R. E. Caffrey, and J. Drobek, Meeting Electrochem. Soc., Dallas, Recent News Item (1967).
217. R. C. G. Swann, A. E. Pyne, and T. P. Cauge, Meeting Electrochem. Soc., Boston, Recent News Item 305 (1968).
218. M. J. Rand and J. L. Ashworth, Meeting Electrochem. Soc., San Francisco, Ext. Abstr. 93 (1965).
219. C. R. Barnes and C. R. Geesner, *J. Electrochem. Soc.* **110**, 361 (1963).
220. M. J. Rand, *J. Electrochem. Soc.* **114**, 274 (1967).
221. H. Osafune, Y. Matakura, S. Tanaka, and Y. Miura, Meeting Electrochem. Soc., Buffalo, Ext. Abstr. 110 (1965).
222. E. L. Jordan, *J. Electrochem. Soc.* **108**, 478 (1961).
223. J. E. Sandor, Meeting Electrochem. Soc., Los Angeles, Abstr. 96 (1962).
224. C. F. Powell, J. H. Oxley, and J. M. Blocher, Jr., eds., "Vapor Deposition," p. 605. Wiley (Interscience), New York, 1966.
225. L. Pansack, *Phys. Rev.* **75**, 472 (1949).
226. J. Oroshnik and J. Kraitchman, Meeting Electrochem. Soc., Philadelphia, Recent News Item 7 (1966).
227. W. A. Plishkin and H. S. Lehman, *J. Electrochem. Soc.* **112**, 1013 (1965).
228. Y. Nakai, Meeting Electrochem. Soc., Boston, Ext. Abstr. 84 (1968).
229. R. E Rawa, Meeting Electrochem. Soc., Boston, Recent News Item 303 (1968).
230. K. M. Whittle and G. L. Vick, Meeting Electrochem. Soc., Boston, Ext. Abstr. 94 (1968).
231. D. Flatley, N. Goldsmith, and J. Scott, Meeting Electrochem. Soc., Toronto, Abstr. 69 (1964).
232. E. Orris and P. Shiota, Meeting Electrochem. Soc., Boston, Ext. Abstr. 85 (1968).
233. H. F. Sterling and R. C. G. Swann. *Solid State Electron.* **8**, 653 (1965).
234. D. R. Secrist and J. D. Mackenzie, *Am. Ceram. Soc. Bull.* **45**, 784 (1966).
235. L. V. Gregor, Study of silicon nitride as a dielectric material for microelectronics applications, Contract AF 33(615)-5386, Final Rept. (Sept. 1967).
236. C. M. Drum and M. J. Rand, Meeting Electrochem. Soc., Boston, Recent News Item 313 (1968).
237. W. Kaiser and C. D. Thurmond, *J. Appl. Phys.* **30**, 427 (1959).
238. V. Y. Doo, Meeting Electrochem. Soc., Buffalo, 1965.
239. V. Y. Doo and D. R. Nichols, Meeting Electrochem. Soc., Philadelphia, Ext. Abstr. 146 (1966).
240. K. E. Bean, P. S. Gleim, and W. R. Runyan, Meeting Electrochem. Soc., Philadelphia, Ext. Abstr. 147 (1966).
241. T. L. Chu, C. H. Lee, and G. A. Gruber, *J. Electrochem. Soc.* **114**, 717 (1967).
242. J. V. Dalton and J. Drobek, *J. Electrochem. Soc.* **115**, 865 (1968).
243. J. H. Scott and J. Olmstead, Meeting Electrochem. Soc., Philadelphia, Ext. Abstr. 151 (1966).

244. H. R. Philipp, Meeting Electrochem. Soc., Philadelphia, Ext. Abstr. 155 (1966).
245. J. J. Comer and N. C. Tombs, Meeting Electrochem. Soc., Philadelphia, Ext. Abstr. 153 (1966).
246. M. J. Grieco, F. L. Worthing, and B. Schwartz, *J. Electrochem. Soc.* **115**, 525 (1968).
247. R. C. G. Swann, R. R. Mehta, and T. P. Cuage, *J. Electrochem. Soc.* **114**, 713 (1967).
248. W. C. Erdman and A. Androshuk, Meeting Electrochem. Soc., Philadelphia, Recent News Item 3 (1966).
249. I. Iglesias and W. B. Westphal. Supplementary dielectric constant and loss measurements on high-temperature materials, Contracts Nonr-1841(10), AF 33(615)-2199, p. 40 (Jan. 1967).
250. P. C. Li, A. J. Capriulo, and M. P. Lepie, *Proc. Symp. OSU-RTD Electromagnetic Windows*, **1**, A-1 (June, 2–4 1964).
251. S. R. Steele, Raytheon Co., private communication, 1968.
252. S. R. Steele, J. Pappis, H. Schilling, and J. Simpson, Chemical vapor deposited materials for electron tubes, Contract DAA 1307-68-C-0156, 1st Triann. Rept. (June 1968).
253. R. J. Patterson, R. D. Humphries, and R. R. Haberecht, Meeting Electrochem. Soc., Pittsburgh, Abstr. 103 (1963).
254. R. R. Haberecht, R. J. Patterson, and R. D. Humphries, Conf. Electrical Ins., Natl. Res. Council, Washington, D.C. (1964).
255. M. J. Rand and J. F. Roberts, *J. Electrochem. Soc.* **115**, 423 (1968).
256. S. R. Steele, W. Feist, and W. Getty, Research on thin film tunnel cathodes, recombination cathodes, and similar cold cathodes, Contract No. DA 28-043-AMC-0035(E), Final Rept. (Sept. 1966).
256a. O. J. Guentert, Raytheon Co., private communication, 1968.
257. M. Matsushita and Y. Koga, Meeting Electrochem. Soc., Boston, Ext. Abstr. 90 (1968).
258. P. Robinson, U.S. Pat. 2,805,965 (Sept. 10, 1957).
259. J. V. Hoene, R. G. Charles, and W. M. Hickam, *J. Phys. Chem.* **62**, 1098 (1958).
260. M. Yamamoto, E. Yamada, and Y. Koga, Meeting Electrochem. Soc., Boston, Ext. Abstr. 9 (1968).
261. S. Krongelb, Meeting Electrochem. Soc., Boston, Recent News Item 311 (1968).
261a. J. A. Aboaf, *J. Electrochem. Soc.* **114**, 948 (1967).
262. G. T. Cheney, R. M. Jacobs, H. W. Korb, H. E. Nigh, and J. Stach, Meeting Intern. Electron Devices, Washington, D.C., Abstr. 2.2 (Oct. 1968).
263. T. L. Chu, D. W. Ing, and A. J. Noreika, Meeting Electrochem. Soc., Dallas, Abstr. 84 (1968).
264. D. C. Bradley, B. N. Chakravarti, and W. Wardlow, *J. Chem. Soc.* **1956**, 2381.
265. M. T. Duffy, K. H. Zaininger, and C. C. Wang, Meeting Electrochem. Soc., Boston, Ext. Abstr. 17 (1968).
266. A. E. Feuersanger, *Proc. IEEE* **52**, 1463 (1964).
267. M. P. Lepie and R. A. Pucel, Raytheon Co. Tech. Mem. T-697 (May 1966).
268. B. W. Gonser and E. E. Slowter, Tech. Publ. Intern. Tin Res. Develop. Council, New York (1938).
269. J. J. Hanak, K. Strater, and G. W. Cullen, *RCA Rev.* **25**, 342 (1964).
270. D. Beischer, *Z. Elektrochem.* **45**, 310 (1939).
271. L. W. Owen, *Trans. Intern. Metal Finishing* **37**, 104 (1960).
272. H. M. Manasevit, A. Miller, D. H. Forbes, and I. B. Cadoff, *Bull. Meeting Am. Phys. Soc., Honolulu* (1965).
273. K. Sato, M. Yoshida, and T. Matsui, *Toshiba Rev. (Intern. ed.)* 37 (1967).

274. K. J. Miller, S. M. Sze, and M. J. Grieco, Meeting Electrochem. Soc., San Francisco, Ext. Abstr. 81 (1965).
275. N. P. Sandler and R. A. Zettler, Meeting Electrochem. Soc., Boston, Recent News Item 316 (1968).
276. N. Hashimoto and Y. Koga, Meeting Electrochem. Soc., Boston, Ext. Abstr. 100 (1968).
277. J. J. Casey, R. R. Verderber, and R. R. Garnache, *J. Electrochem. Soc.* **114**, 201 (1967).
278. R. N. Tucker, Meeting Electrochem. Soc., Buffalo, Ext. Abstr. 104 (1965).
279. G. Wakefield, Meeting Electrochem. Soc., Philadelphia, Abstr. 223 (1966).
280. E. T. Peters and W. D. Potter, Conf. AIME, San Francisco, 1965.
281. L. D. Loch, *J. Electrochem. Soc.* **110**, 1081 (1963).
282. W. R. Sinclair, F. G. Peters, D. W. Stillinger, and S. E. Koonce, *J. Electrochem. Soc.* **112**, 1096 (1965).
283. B. S. Aronson, Meeting Electrochem. Soc., Dallas, Recent News Item 23 (1967).
284. J. B. MacChesney, J. F. Potter, and H. J. Guggenheim, Meeting Electrochem. Soc., Dallas, Abstr. 19 (1967).
285. T. Takahashi, K. Sugiyama, and K. Tomita, Meeting Electrochem. Soc., Dallas, Abstr. 213 (1967).
286. D. A. McLean and F. Rocztoczy, Meeting Electrochem. Soc., San Francisco, Abstr. 10A (1965).
287. R. W. Christy, *J. Appl. Phys.* **33**, 1884 (1962).
288. A. G. Baker and W. C. Morris, *Rev. Sci. Instr.* **32**, 458 (1961).
289. P. A. Leighton and R. A. Mortenson, *J. Am. Chem. Soc.* **58**, 448 (1936).
290. J. G. Clouston and C. L. Cook, *Trans. Faraday Soc.* **54**, 1001 (1958).
291. I. L. Mador, *J. Chem. Phys.* **22**, 1617 (1954).
292. H. Takei and S. Takasu, *Japan. J. Appl. Phys.* **3**, 175 (1964).
293. R. C. Linares and R. B. McGraw, *J. Appl. Phys.* **35**, 3630 (1964).
294. R. C. Linares, R. B. McGraw, and J. B. Schroeder, *J. Appl. Phys.* **36**, 2884 (1965).
295. G. R. Pulliam, J. E. Mee, J. L. Archer, and R. G. Warren, *Proc. Natl. Aerospace Conf. IEEE*, 245 (1965).
296. L. B. Robinson, W. B. White, and R. Roy, *J. Mater. Sci.* **1**, 336 (1966).
297. J. L. Archer, G. R. Pulliam, R. G. Warren, and J. E. Mee, *in* "Crystal Growth" (H. S. Peiser, ed.). Pergamon Press, Oxford, 1967.
298. J. E. Mee, J. L. Archer, R. H. Meade, and T. M. Hamilton, *Appl. Phys. Letters* **10**, 289 (1967).
299. G. R. Pulliam, R. G. Warren, R. E. Holmes, and J. L. Archer, *J. Appl. Phys.* **38**, 2192 (1967).
300. G. R. Pulliam, *J. Appl. Phys.* **38**, 1120 (1967).
301. J. E. Mee, *Proc. Trans. IEEE* MAG-3, 190 (1967).
302. J. J. Hanak and D. Johnson, *J. Appl. Phys.* **39**, 1161 (1168).
303. H. Schroeder and E. Glauche, *J. Appl. Phys.* **39**, 1155 (1968).
304. K. Nagasawa, Y. Banda, and T. Takada, *Japan. J. Appl. Phys.* **7**, 174 (1968).

Author Index

Numbers in parentheses are reference numbers and indicate that an author's work is referred to, although his name is not cited in the text. Numbers in italics show the page on which the complete reference is listed.

L

LaChapelle, T. J., 238 (4), 261, 270, 314
Ladd, G. O., 279 (160), 318
Laendle, K. W., 287 (206), 291 (206), 319
Lakshmanan, T. K., 167 (137), 233
Lampert, M. A., 145, 229
Lamport, C. B., 285, 319
Lander, J. J., 190, 233
Lang, A. R., 191 (164), 233
Lang, G. A., 247 (30), 315
Langer, C., 240 (12), 314
Langmuir, J., 87, 140
Lark-Horowitz, K., 274, 317
Laude, L., 165 (109), 174 (109), 232
Layton, C. K., 197, 198, 234
Laznovsky, W., 287 (208), 319
Lebedeva, M. D., 164 (95), 231
Lee, C. H., 287 (213), 298 (241), 297, 320
Lehman, H. S., 290, 320
Leighton, P. A., 312, 322
Lely, J. A., 283, 319
Leonhardt, H., 281, 318
Lepie, M. P., 298 (250), 305, 321
Lever, R. F., 247 (25), 274, 315, 317
Levi, D. L., 246 (18), 247 (18), 314
Lewis, B., 161, 196, 230
Lewis, C. H., 271, 317
Li, C. H., 147, 148, 149 (17), 196 (17), 229, 252 (35), 315
Li, P. C., 298 (250), 321
Liang, K. C., 284 (199), 319
Light, T. B., 274, 317
Linares, R. C., 313 (293, 294), 322
Litton, F. B., 247 (20), 314
Loar, H., 266 (79), 316
Loch, L. D., 310 (281), 322
Lockhart, L. B., 88, 140
Longini, R. L., 155 (46), 219, 227 (46), 230, 234
Longo, T. A., 279, 299 (161), 318
Love, J., 1 (8), 45
Ludeke, R., 166 (119), 178, 232
Luther, L. C., 281, 318
Lye, R., 9 (16), 45
Lyons, V. J., 276, 279, 318

M

McAleer, W. J., 267 (85), 316
McCarthy, J. P., 210, 234
MacChesney, J. B., 311, 322
McFarlane, S. H., 111, 272 (113), 317
McFarlane, S. J., 152 (36), 153 (36), 230
McGraw, R. B., 313 (293, 294), 322
McIntosh, A. B., 252 (36), 315
Mackenzie, J. O., 292, 320
McKinstry, H. A., 119 (23), 141
McLean, D. A., 311, 322
McLennan, W. D., 210, 212, 213, 234
Mader, S., 178, 232
Mador, I. L., 312, 322
Maissel, L., 179 (123), 180 (123), 232
Majumdar, A. J., 119 (23), 141
Man, A., 240 (8), 314
Man, L. I., 164 (98), 172 (98), 193 (98), 232
Manasevit, H. M., 147, 151, 152, 153 (32), 154, 186 (33), 199, 209 (33), 229, 230, 247 (31), 269, 270, 272, 281, 306 (272), 315–318, 321
Many, A., 221 (203), 234
Manz, R. C., 266 (81), 316
Marinace, J. C., 275, 276, 317, 318
Mark, A., 265, 316
Martinuzzi, S., 165 (109), 174 (109), 232
Maserjian, J., 183, 233
Matakura, Y., 289 (221), 320
Matovich, E., 273, 317
Matsui, T., 306 (273), 321
Matsushita, M., 302 (257), 303, 321
Maverick, E. F., 265 (69), 316
Maxwell, K. H., 154 (41), 155 (41), 156 (41), 228 (41), 230
Mayer, A., 270 (108), 271, 317
Mayer, H., 1 (3), 49 (3), 101 (12), 45, 85, 141
Mayer, S. E., 271, 317
Mead, C. A., 222 (208), 234, 286 (203), 319
Meade, R. H., 313 (298), 314 (298), 322
Mecs, B. M., 287 (211), 320
Mee, J. E., 260 (55), 313 (201, 295, 297, 298), 314 (298, 301), 315, 322
Mehal, E. W., 146 (13), 154 (13), 229, 279, 318
Mehta, R. R., 298 (247), 321
Mellor, J. W., 240 (7), 314
Mena, A. A., 283, 319

Patel, J. R., 188 (158), *233*, 253 (38), 257 (38), *315*
Patrick, W. J., 164 (89), 172 (89), *231*
Patterson, R. J., 299, *321*
Paul, W., 166 (119), 178, *232*
Pearson, G. L., 145, *229*
Pegis, R. J., 60 (16), *86*
Perkins, D. M., 221 (206), *234*
Peters, E. T., 309, *322*
Peters, F. G., 310 (282), *322*
Peterson, D., 287 (207), 290, 302, 304, 307, 310, 311, *319*
Pfann, W. G., 253 (38), 257 (38), *315*
Phillips, A. B., 211, *234*
Phillips, H. R., 297, *321*
Pinnell, J. E., 282, *319*
Pittelli, E., 167 (130), 181 (130), 193 (130), 199 (130), *232*
Piwkowski, T. R., 167 (129), 181 (129), 193 (129), 199 (129), *232*
Pizzarello, F. A., 149, *229*, 276, 277, *318*
Plishkin, W. A., 290, *320*
Poehler, T. O., 182, *233*
Pohlack, H., 60 (11), *85*
Pollack, P. l., 267 (85), *316*
Polster, H. D., 78 (25), 81 (25), *86*
Potter, J. F., 311 (284), *322*
Potter, R. F., 165 (104), 174, *232*
Potter, W. D., 309, *322*
Povilonis, E. I., 163 (76), 166, 168, 196 (76), *231*
Powell, C. F., 238 (1), 242, 249 (15), 284, 289 (224), 302 (191), 314, *317–326*
Pring, J. N., 283, 284, *312*
Pucel, R. A., 305, *321*
Pulliam, G. R., 260, 313 (295, 297, 299, 300), 314 (300), *315, 322*
Putley, E. H., 209 (181), *234*
Pyne, A. E., 288 (217), *320*

Q

Queisser, H. J., 249 (33), 260 (53), *315*
Quincke, F., 240 (12), *314*

R

Ramberg, E. G., 145, *229*
Ramey, R. L., 210, 212, 213, *234*
Ramsey, J. B., 167, *231*

Rand, M. J., 161 (58), *230*, 288, 294, 299, 300, *320, 321*
Rawa, R. E., 290, *320*
Redington, R. W., 145 (6), *229*
Regehr, R. W., 282, *318*
Regel', A. R., 163 (79), 171 (79), *231*
Rehnberg, J. D., 85 (32), *86*
Reichelt, W., 167, *231*
Reid, F. J., 154 (44), 158 (44), 159, *230*
Reisman, A., 274, 275 (136), *317, 318*
Reizman, F., 167 (125), 180, 196 (125), *232*
Rhodin, T. N., 193, *233*, 260 (50), *315*
Riben, A. R., 276, *318*
Riblet, H. J., 60 (12), *85*
Rich, G. J., 261 (56), *315*
Richards, J. L., 166 (113, 114, 115), 176, 177, 178, 203 (113, 114, 115), 208 (115), *232*
Richman, D., 276, *318*
Richman, P., 216 (193), 228 (193), *234*
Riley, H. L., 283, *319*
Rivera, J. J., 282 (174), *318*
Roberts, E. D., 287, 293, *319*
Roberts, J. F., 161 (58), *230*, 299, 300, *321*
Robinson, D. H., 247 (24), 278, *315*
Robinson, L. B., 303 (296), *322*
Robinson, P., 302 (258), *321*
Robinson, P. H., 146 (15), *229*
Roccasecca, D. D., 281, *318*
Rocztoczy, F., 311, *322*
Rose, A., 145, 221, *229*
Rosen, S., 70, *86*
Roth, E. A., 247 (29), 274, *315, 317*
Roy, R., 119 (23), *141*, 303 (296), *322*
Rubinstein, M., 279, *318*
Ruehrwein, R. A., 161, *230*, 277, *318*
Runyan, W. R., 264 (66), 269, 296 (40), *316, 320*
Rusch, D., 32 (23), *45*
Russell, V. A., 269, *317*
Ruth, R. P., 275 (130), *317*

S

Sakai, Y., 214, *234*
Salama, C. A. T., 163 (73), 170, *231*
Sandler, N. P., 306, *322*
Sandor, J. E., 289 (223), *320*
Sangster, R. C., 265, *316*
Sasaki, Y., 277 (152), *318*

Subject Index

The letter n following a page number indicates that the cross reference is to the footnote on that page.

Graphite, pyrolytic, in vapor deposition process, 258–259

H

Halide disproportionation, in chemical vapor deposition, 275
Halide reduction
in chemical vapor deposition, 273–274
in semiconductor films, 147–148
Hall effect, in semiconductor films, 209–219, 222–223
Hamming's method, 61
Helium
chemical vapor deposition in, 313
film growth in, 295
in high-power devices, 225
Heteroepitaxial films, *see also* Epitaxial films, Epitaxial growth
vs. homoepitaxial, 228
properties of, 186
Heterojunctions, semiconductor, 152
Homoepitaxial films, growth in, 196–197
Homogeneous films, 58
conditions for, 88–89
Hydride pyrolysis
in chemical vapor deposition, 270, 274–275
in semiconductor films, 148–149
Hydrogen, as transport agent, 285

I

Indium antimonide films, dendritic, 185, 216
Indium arsenate films
doping level of, 217
electron mobility in, 210
Infrared filter, 53
Interference cathodes, 15–43
object of, 43–44
yield and spectral response of, 43–44
Interference effects, absorbing coatings and, 124–126
Interference films, application of, 47–48
Interference filters, multilayer, *see* Multilayer interference filters
Interference photocathodes, 1–44, *see also* Cathode, Photocathode

J

Jacobean elliptic function, 66

L

Lamella, absorption in, 7, 15
Lighting filters, 134–138
Light resonator, 2–8
Light waves, field of, *see* Wave field
Liouville transformation, 57

M

Magnetic field, and multilayer matrix, 53–54
Matrix multiplication, rules of, 55
Metallic layers, physical properties of, 89–90
Metals, chemical vapor deposition of, 306–309
Molybdenum, chemical vapor deposition of, 306–307
Molybdenum hexacarbonyl, reduction of, 307
Monolayers, 126–130
Multialkali cathodes, 12
Multialkali films
first-order RIC and, 26–27
optimum thickness of, 14
reflectance and absorption in, 25, 28–29
RIC principle and, 30
sensitivity of, 44
transmittance and reflectance of, 25
Multilayer(s)
homogeneous, 53, 58
inhomogeneous, 65
irregular, 65
irregular, 134
nonabsorbing, 60
optical thickness in, 57
periodic structures in, 59
reflectance and transmittance in, 57–58
reversing order of, 56
selectively reflecting, 132–133
symmetrical, 53
Multilayer interference filters
absorbing, 50
advantages of, 47–48

". . . this series represents one of the most valuable additions to the practicing engineer's book shelf that can be found at the present time . . . one of the best investments a worker in the field of applied optics and optical engineering can make." —Journal of the Optical Society of America

Applied Optics and Optical Engineering

Edited by RUDOLF KINGSLAKE

Volume V
Optical Instruments: Part 2

Reviews of previously published volumes . . .
"Each of the contributors is a recognized expert in his field, and some of the pages almost seem to sizzle with authenticity!" —*Applied Optics*

". . . should be a welcome and much used addition to the library of any optical engineer." —*Journal of The Optical Society of America*

". . . likely to prove useful, not only for the engineer but also for the physicist generally." —*Journal of the Franklin Institute*

This volume completes a five-volume treatise providing the precise data and information needed by optical engineers for the design, construction, and testing of new optical devices. The books in the treatise also will assist those who use optical equipment in the selection of a suitable instrument for specifically postulated work and in understanding the details of the operation and use of each instrument.

A special feature of Volume 5 is the inclusion of a comprehensive cumulative index covering the contents of all five volumes, designed to provide easy access to the vast amount of information contained within the treatise as a whole.

CONTENTS

Rudolf Kingslake, Dispersing Prisms • David Richardson, Diffraction Gratings • Robert J. Meltzer, Spectrographs and Monochromators • Walter G. Driscoll, Spectrophotometers • Harry K. Hammond III, Colorimeters • A. B. Meinel, Astronomical Telescopes • Francis B. Patrick, Military Optical Instruments • M. S. Dickson, and D. Harkness, Surveying and Tracking Instruments • John H. Hett, Medical Optical Instruments • Henry A. Knoll, Ophthalmic Instruments • Robert M. Corbin, Motion Picture Equipment

Author Index—Subject Index.
Cumulative Index for Volumes 1–5.

°Subscription prices for individual volumes valid on orders for the complete set received before December 31, 1969.

Academic Press
NEW YORK AND LONDON
111 FIFTH AVENUE, NEW YORK 10003
BERKELEY SQUARE HOUSE, LONDON, W1X6BA

12–533005–7

PHYSICS OF THIN FILMS

5

1969